frontiers | Research Topics

New immunotherapy strategies and related therapeutic targets for gastrointestinal malignancies

Edited by
Chi Chun Wong, Yantao Tian, Chenyu Sun,
Qun Zhao and Ganesan Ramamoorthi

Coordinated by
Ping'An Ding

Published in
Frontiers in Immunology
Frontiers in Oncology

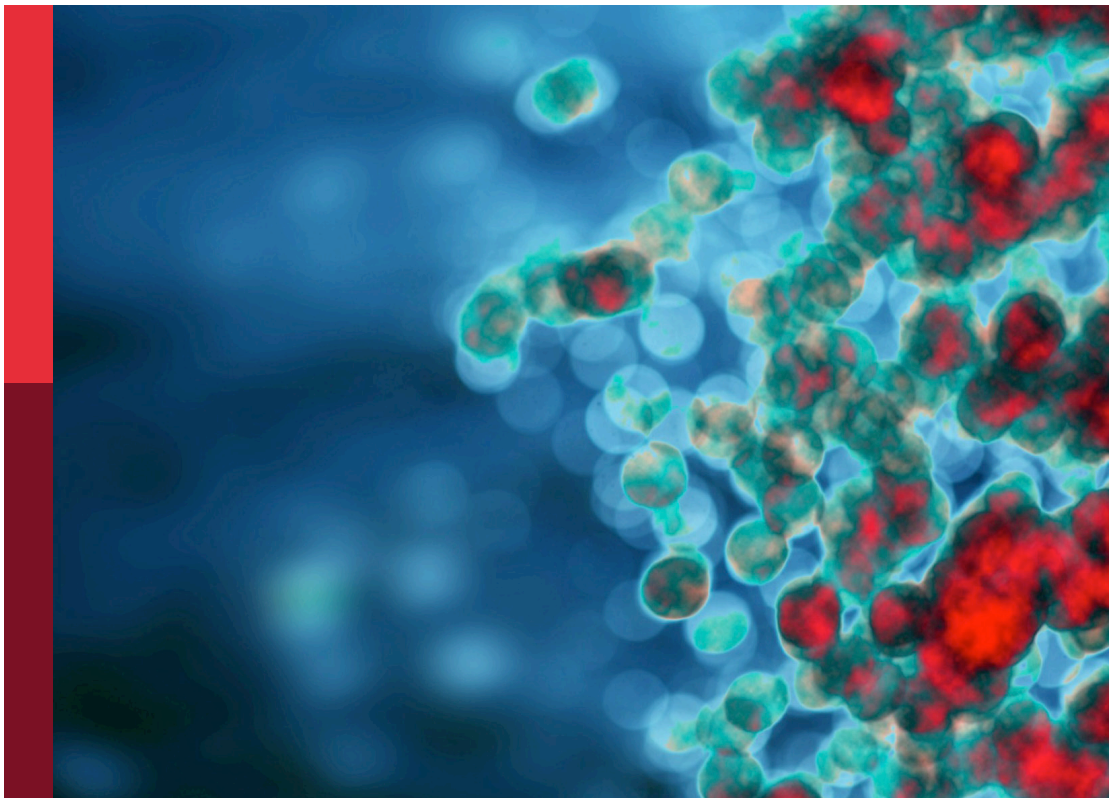

ISSN 1664-8714
ISBN 978-2-8325-4444-0
DOI 10.3389/978-2-8325-4444-0

About Frontiers

Frontiers is more than just an open access publisher of scholarly articles: it is a pioneering approach to the world of academia, radically improving the way scholarly research is managed. The grand vision of Frontiers is a world where all people have an equal opportunity to seek, share and generate knowledge. Frontiers provides immediate and permanent online open access to all its publications, but this alone is not enough to realize our grand goals.

Frontiers journal series

The Frontiers journal series is a multi-tier and interdisciplinary set of open-access, online journals, promising a paradigm shift from the current review, selection and dissemination processes in academic publishing. All Frontiers journals are driven by researchers for researchers; therefore, they constitute a service to the scholarly community. At the same time, the *Frontiers journal series* operates on a revolutionary invention, the tiered publishing system, initially addressing specific communities of scholars, and gradually climbing up to broader public understanding, thus serving the interests of the lay society, too.

Dedication to quality

Each Frontiers article is a landmark of the highest quality, thanks to genuinely collaborative interactions between authors and review editors, who include some of the world's best academicians. Research must be certified by peers before entering a stream of knowledge that may eventually reach the public - and shape society; therefore, Frontiers only applies the most rigorous and unbiased reviews. Frontiers revolutionizes research publishing by freely delivering the most outstanding research, evaluated with no bias from both the academic and social point of view. By applying the most advanced information technologies, Frontiers is catapulting scholarly publishing into a new generation.

What are Frontiers Research Topics?

Frontiers Research Topics are very popular trademarks of the *Frontiers journals series*: they are collections of at least ten articles, all centered on a particular subject. With their unique mix of varied contributions from Original Research to Review Articles, Frontiers Research Topics unify the most influential researchers, the latest key findings and historical advances in a hot research area.

Find out more on how to host your own Frontiers Research Topic or contribute to one as an author by contacting the Frontiers editorial office: frontiersin.org/about/contact

New immunotherapy strategies and related therapeutic targets for gastrointestinal malignancies

Topic editors

Chi Chun Wong — The Chinese University of Hong Kong, China
Yantao Tian — Center for National Cancer, Cancer Hospital, Chinese Academy of Medical Sciences and Peking Union Medical College, China
Chenyu Sun — AMITA Health, United States
Qun Zhao — Fourth Hospital of Hebei Medical University, China
Ganesan Ramamoorthi — Moffitt Cancer Center, United States

Topic Coordinator

Ping'An Ding — Fourth Hospital of Hebei Medical University, China

Citation

Wong, C. C., Tian, Y., Sun, C., Zhao, Q., Ramamoorthi, G., Ding, P., eds. (2024). *New immunotherapy strategies and related therapeutic targets for gastrointestinal malignancies*. Lausanne: Frontiers Media SA. doi: 10.3389/978-2-8325-4444-0

Table of contents

frontiers | Frontiers in Immunology

TYPE Editorial
PUBLISHED 08 March 2024
DOI 10.3389/fimmu.2024.1389781

OPEN ACCESS

EDITED AND REVIEWED BY
Vassiliki A. Boussiotis,
Beth Israel Deaconess Medical Center and Harvard Medical School, United States

*CORRESPONDENCE
Ganesan Ramamoorthi
ganesan.ramamoorthi@moffitt.org

RECEIVED 22 February 2024
ACCEPTED 04 March 2024
PUBLISHED 08 March 2024

CITATION
Ramamoorthi G (2024) Editorial: New immunotherapy strategies and related therapeutic targets for gastrointestinal malignancies.
Front. Immunol. 15:1389781.
doi: 10.3389/fimmu.2024.1389781

Editorial: New immunotherapy strategies and related therapeutic targets for gastrointestinal malignancies

Ganesan Ramamoorthi*

Clinical Science & Immunology Program, H. Lee Moffitt Cancer Center, Tampa, FL, United States

KEYWORDS

cancer immunotherapy, dendritic cells, immune checkpoint inhibitors, gastrointestinal malignancies, prognostic biomarkers

Editorial on the Research Topic
New immunotherapy strategies and related therapeutic targets for gastrointestinal malignancies

Malignancies in the gastrointestinal tract, including esophagus, stomach, colorectum, pancreas and liver, are among the most common cancer types and pose severe health challenges in patients. Current treatment options for gastrointestinal malignancies includes surgery, chemotherapy, radiotherapy, and molecular therapeutic targets. Although chemotherapy combined with molecular therapeutics are typically used for patients with advanced stages of gastrointestinal malignancies, only limited benefits have been observed. Cancer immunotherapy, including immune cell-based therapy, has been emerging as an effective therapeutic approach for treating various cancers including gastrointestinal malignancies. However, the potential targets for developing immunotherapy and prognostic biomarkers that predict treatment response have not been extensively investigated in gastrointestinal malignancies. This Research Topic comprises a series of original research articles and state-of the-art reviews that focused on identifying and summarizing the most promising targets for developing immunotherapies and identifying potential biomarkers that may predict the patients that are likely to respond to immunotherapeutic approaches in gastrointestinal malignancies.

The immunosuppressive tumor microenvironment (TME) can prevent response to conventional therapies and various immunotherapies and lower tumor-infiltrating lymphocytes (TIL) in cancer patients. Wegierek-Ciura et al. have demonstrated that sequential peritumoral delivery of tumor antigen targeting dendritic cells in addition to anti-IL10R antibody with the immunomodulatory methotrexate-hydroxyethyl starch (HES-MTX) nanoconjugate unlocked an effective anti-tumor immune response with inhibition of various immune suppressive cells including T regulatory cells and tumor associated macrophages in a MC38 murine colon carcinoma model. This combination treatment enhanced tumor infiltration of CD4, CD8 and NK cells into the tumors and induced tumor regression. With the help of machine learning and a multiple omics bioinformatics approach, Zhu et al. have attempted to provide a molecular characterization for colon cancer and identified three clinically relevant subtypes and risk-related genes that biologically contributed to tumor aggressiveness, recurrence and metastasis in colon cancer

patients. The authors have also extended their findings and confirmed differential expression status of PPARGC1A and GARBD genes in colon cancer specimens of patients and suggested these genes as potential therapeutic targets. Adaptation of a watch and wait (WW) strategy can be recommended for rectal cancer patients after achieving clinical complete response (cCR) treated with neoadjuvant chemoradiotherapy. This WW strategy can provide survival benefits similar to patients who underwent surgery, but it would prevent surgical trauma and preserve organ function in these patients. A retrospective study from Yang et al. compared the survival outcomes of dMMR/MSI-H locally advanced rectal cancer patients treated with neoadjuvant immunotherapy (anti-PD1 antibodies) who underwent surgery with confirmed as a pathologic complete response (pCR) versus treated patients opted for a WW strategy after achieving a cCR or near-cCR. After a median follow-up for 25 months, patients from both arms were free from local recurrence and distant metastasis with improved survival, suggesting that these patients may benefit from the WW strategy and surgery related complication can be prevented. The findings of this study need to be further validated and confirmed in longer follow-studies and prospective trials.

The reduced or loss of expression of SLC4A4 has been shown to promote cancer cell proliferation and metastasis in renal cancer cell carcinoma. Rui et al. explored the role of SLC4A4 in colorectal cancer and found that SLC4A4 downregulation was positively correlated with microsatellite instability (MSI) and associated with poor prognosis in colorectal cancer. This study suggests that SLC4A4 may be a potential prognostic biomarker with MSI to guide treatment for colorectal cancer. When comparing colorectal patients with dMMR/MSI-H, patients with pMMR/MSS may not achieve satisfactory response to conventional therapies and immune checkpoint inhibitors.

It is well known that combination therapy approach can combat cancer more effectively, reduce side effects and resistance and improve treatment outcomes in patients. Chen et al. in a review, highlighted the molecular aspects and recent advancements of various immunotherapy approaches and their potential synergistic effects with chemotherapy, radiotherapy and preoperative strategies for colorectal cancer. The authors listed various clinical trials that investigated these combination therapy approaches and examined their efficacy and safety in colorectal cancer patients. Immune checkpoint signaling activation can prevent anti-tumor CD4 and CD8T cell mediated immune responses in cancers. Over expression of the immune checkpoint protein CD276 (B7-H3) in cancer cells and tumor vasculature has been associated with tumor aggressiveness in pancreatic, hepatic and gastric cancers. Lutz et al. has developed a novel IgG bispecific antibody CC-3 (B7-H3xCD3 specificity) and confirmed its specific binding to B7-H3 expressed on pancreatic, hepatic and gastric cancer cells. This CC-3 bispecific antibody was able to inhibit cancer cell proliferation and induced CD4 and CD8T cell activation, proliferation, functionality and expansion of memory phenotypes, highlighting the therapeutic applicability of a CC-3 bispecific antibody to be further evaluated in preclinical and clinical studies.

Hepatic arterial infusion chemotherapy (HAIC) has been shown to improve the prognosis of patients with advanced liver cancer which opens a new opportunity to explore the combination strategy of immunotherapy and targeted agents with HAIC. Zhang et al. reported that combination of immunotherapy and molecular targets with HAIC increased tumor regression and surgical conversion rates in primary unresectable liver cancer patients. Lu et al. showed that the combination of the naturally occurring bioactive compounds quercetin, kaempferol, licochalcone A, naringenin, and formaronetin treatment were able to alter various intracellular signaling proteins (PI3K-AKT, p53 and VEGF) in the TME and inhibit progression of colorectal cancer in a mouse model. This treatment also inhibited PD-1 expression on T cells and increased cytotoxic activity of T cells leading to enhanced anti-tumor response in a colorectal cancer mouse model. Wang et al. reported that downregulation of SLCO1B1 as a prognostic signature and predicated overall survival of patients with hepatocellular carcinoma (HCC). Notably, authors have observed that the over expression of SLCO1B1 was able to inhibit the proliferation and migratory and invasive potential of HCC cells.

Oxidative stress and its associated signaling pathways have been explored to contribute to progression of gastric cancer and metastasis. Various oxidative stress-specific therapeutic targets and agents may be a promising strategy in combination with immunotherapy to effectively modulate the anti-tumor immune response and suppress pro-tumorigenic signaling pathways in gastric cancer (Liu et al.). Zhang et al. suggest that the prognostic nutritional index may be used as a prognostic biomarker of treatment outcomes in patients treated with immune checkpoint inhibitors for gastrointestinal malignancies. Immune cell-based therapies directed to target highly immunogenic tumor antigens will be critical for triggering stronger anti-tumor immunity. Ai et al. comprehensively summarized various cancer/testis antigens and their expression status in digestive tract cancers and highlighted potential immune cell-based therapies, targeted antibodies and an oncolytic virus-based therapy approach that can be effectively utilized to harness the anti-tumor immune response. Cancer risk related gene signatures and biomarkers for early esophageal squamous cell cancer (ESCC) diagnosis was explored by Ren et al. and found elevated expression of F2RL2 and reduced expression of SLC4A9, EXPH5, and MAGEC3 in tumors. The findings of this study suggest that these gene signatures may predict response to immunotherapy in patients with ESCC.

In summary, this Research Topic addressed new strategies and tumor specific targets to develop an effective immunotherapy including targeted antibodies, dendritic cell and adaptive cell-based therapies to harness the anti-tumor immune response in gastrointestinal malignancies. I hope that this Research Topic will provide new concepts for readers to further explore the potential role of these biomarkers in predicting treatment outcomes and new immunotherapies to treat gastrointestinal malignancies.

Author contributions

GR: Conceptualization, Data curation, Writing – original draft, Writing – review & editing.

Conflict of interest

The author declares that the research was conducted in the absence of any commercial or financial relationships that could be construed as a potential conflict of interest.

The author declares that he was an editorial board member of Frontiers, at the time of submission. This had no impact on the peer review process and the final decision.

Publisher's note

frontiers | Frontiers in Immunology

TYPE Original Research
PUBLISHED 20 March 2023
DOI 10.3389/fimmu.2023.1142609

OPEN ACCESS

EDITED BY
Qun Zhao,
Fourth Hospital of Hebei Medical University, China

REVIEWED BY
Suxue Tan,
Chongqing Medical University, China
Taohua Yue,
First Hospital, Peking University, China
Hui Li,
Capital Medical University, China

*CORRESPONDENCE
Sujie Zhu
zhusujie@bjmu.edu.cn
Weikaixin Kong
kong.weikaixin@helsinki.fi
Xuelong Jiao
jiaoxuelong@163.com

†These authors have contributed equally to this work

SPECIALTY SECTION
This article was submitted to Cancer Immunity and Immunotherapy, a section of the journal Frontiers in Immunology

RECEIVED 11 January 2023
ACCEPTED 27 February 2023
PUBLISHED 20 March 2023

CITATION
Zhu J, Kong W, Huang L, Bi S, Jiao X and Zhu S (2023) Identification of immunotherapy and chemotherapy-related molecular subtypes in colon cancer by integrated multi-omics data analysis. *Front. Immunol.* 14:1142609. doi: 10.3389/fimmu.2023.1142609

Identification of immunotherapy and chemotherapy-related molecular subtypes in colon cancer by integrated multi-omics data analysis

Jie Zhu[1,2,3,4†], Weikaixin Kong[3,4,5*†], Liting Huang[2], Suzhen Bi[2], Xuelong Jiao[5*] and Sujie Zhu[1,2*]

[1]Key Laboratory of Birth Regulation and Control Technology of National Health Commission of China, Shandong Provincial Maternal and Child Health Care Hospital Affiliated to Qingdao University, Jinan, Shandong, China, [2]Institute of Translational Medicine, The Affiliated Hospital of Qingdao University, College of Medicine, Qingdao University, Qingdao, China, [3]Institute for Molecular Medicine Finland (FIMM), HiLIFE, University of Helsinki, Helsinki, Finland, [4]Department of Molecular and Cellular Pharmacology, School of Pharmaceutical Sciences, Peking University Health Science Center, Beijing, China, [5]Gastrointestinal Surgery Department, The Affiliated Hospital of Qingdao University, College of Medicine, Qingdao University, Qingdao, China

Background: Colon cancer is a highly heterogeneous disease, and identifying molecular subtypes can provide insights into deregulated pathways within tumor subsets, which may lead to personalized treatment options. However, most prognostic models are based on single-pathway genes.

Methods: In this study, we aimed to identify three clinically relevant subtypes of colon cancer based on multiple signaling pathways-related genes. Integrative multi-omics analysis was used to explain the biological processes contributing to colon cancer aggressiveness, recurrence, and progression. Machine learning methods were employed to identify the subtypes and provide medication guidance for distinct subtypes using the L1000 platform. We developed a robust prognostic model (MKPC score) based on gene pairs and validated it in one internal test set and three external test sets. Risk-related genes were extracted and verified by qPCR.

Results: Three clinically relevant subtypes of colon cancer were identified based on multiple signaling pathways-related genes, which had significantly different survival state (Log-Rank test, $p<0.05$). Integrative multi-omics analysis revealed biological processes contributing to colon cancer aggressiveness, recurrence, and progression. The developed MKPC score, based on gene pairs, was robust in predicting prognosis state (Log-Rank test, $p<0.05$), and risk-related genes were successfully verified by qPCR (t test, $p<0.05$). An easy-to-use web tool was created for risk scoring and therapy stratification in colon cancer patients, and the practical nomogram can be extended to other cancer types.

Conclusion: In conclusion, our study identified three clinically relevant subtypes of colon cancer and developed a robust prognostic model based on gene pairs. The developed web tool is a valuable resource for researchers and clinicians in risk scoring and therapy stratification in colon cancer patients, and the practical nomogram can be extended to other cancer types.

KEYWORDS

bioinformatics, colon cancer, machine learning, immune therapy, multiple omics

1 Introduction

Colon cancer is a disease with extensive interpatient heterogeneity, both molecularly and histopathologically, which cannot be resolved by current clinical methods. Despite a continuous refinement to the UICC tumor, node, metastasis (TNM) staging system to measure disease extent and define prognosis, disease outcome still varies considerably even among patients with the same tumor stage. Therefore, new factors that can more precisely stratify patients into different risk categories are clearly warranted (1, 2).

In this age of advanced molecular-profiling technologies, cancer molecular subtype discovery has become one of the more common exercises utilizing transcriptomic data on human tumors. Molecular subtypes can deepen our understanding of cancer as a collection of diseases rather than a single disease. Molecular subtypes can provide insights into the pathways that appear deregulated within tumor subsets, which may suggest therapeutic opportunities, as well as being indicative of which pathways, as characterized in the experimental setting, would appear particularly relevant in the human disease setting (3).

As a highly heterogeneous disease, colon cancer involves DNA repair defects (4, 5), DNA methylation (6, 7), chromosome instability (8), and other molecular pathogeneses during disease development. Biomarkers have been used as common tools for disease detection and prognosis management in colon cancer patients. Therefore, the determination of molecular changes in colon cancer patients has become a hotspot in colon cancer research (9).

Recent attempts to resolve colorectal cancer (CRC) heterogeneity and improve prognosis include molecular subclassification and characterization based on transcriptional profiling (10, 11). The consensus molecular subtype (CMS) classification stratifies CRC into four subtypes CMS 1–4, each with distinct biological and histopathological features. Colorectal cancer is a molecularly heterogeneous disease. Responses to genotoxic chemotherapy in the adjuvant or palliative setting vary greatly between patients, and colorectal cancer cells often resist chemotherapy by evading apoptosis (12, 13). The development of cancer was related to multiple signaling pathways, including the cell cycle, immunity, aging, metabolism, autophagy, and so on. Until recently, most constructed prognostic models were based on single-pathway genes. Herein, we identified three clinically relevant subtypes of colon cancer based on multiple prognostic cancer signaling pathway-related genes. Integrative multi-omics analysis is used to explain the biological processes contributing to colon cancer aggressiveness, recurrence, and progression. We developed a classifier to identify the subtypes of patients and predicted medication guidance for each subtypes using the L1000 platform (14). Finally, we established a prognostic model system based on gene pairs using expression data and further validated it in one internal test set and three external test sets.

2 Methods

2.1 Colon cancer dataset source and preprocessing

The workflow of our study is shown in Supplementary Figure S1A. Public gene-expression data and full clinical annotation were obtained from the Gene-Expression Omnibus (GEO) and The Cancer Genome Atlas (TCGA) databases. Patients without survival information were removed. In total, three colon cancer cohorts (TCGA-COAD, GSE39582, and GSE38832; the data information is in Supplementary Table S1) were gathered in this study for further analysis. TCGA-COAD was downloaded from the Genomic Data Commons (GDC, https://portal.gdc.cancer.gov/). The somatic mutation data were acquired from TCGA database. The genomic instability (GI) and somatic copy-number alterations (SCNAs) of TCGA were downloaded from a previous study (15) (Supplementary Table S3).

2.2 Unsupervised clustering for 66 prognostic genes

Firstly, we searched the articles using the keywords “colon cancer” and “prognosis” to obtain the genes related to the prognosis of colon cancer and then identified 66 prognostic genes using univariate Cox regression. Unsupervised clustering was then used to identify three subtypes of colon cancer patients based on the expression of these 66 prognostic genes. We used the ConsensusClusterPlus package to perform the above steps, and

1,000 repetitions were conducted to guarantee the stability of clustering. Partitioning around medoid (PAM) method and Euclidean distance were used to quantify the similarity of gene expression profiles between the patients, and the area under the curves of the cumulative distribution function (CDF) was used to find the optimal number k of clusters.

2.3 PD1/CTLA4 response prediction

To predict the immunotherapy response of patients with distinct subtypes of breast cancer, we downloaded the immunotherapy prediction information from the TCIA database (https://tcia.at/home), which provides results of comprehensive immunogenomic analyses of next-generation sequencing data (NGS) for 20 solid cancers from TCGA and other data sources. The immunophenoscore (IPS) can be used to predict the response to the immunotherapy agents PD1 and CTLA4 (Supplementary Table S6).

2.4 Gene-set variation analysis and functional annotation

To investigate the differences in biological processes between three subtypes of colon cancer, we performed gene-set variation analysis (GSVA) using "GSVA" R packages. GSVA, a non-parametric and unsupervised method, is commonly used to estimate variation in pathway and biological process activity in expression data. The gene sets of "c2.cp.kegg.v6.2.symbols" were downloaded from the MsigDB database for running GSVA analysis.

2.5 Estimation of TME cell infiltration

We used the single-sample gene-set enrichment analysis (ssGSEA) algorithm to quantify the relative abundance of each cell infiltration in colon cancer tumor microenvironment (TME). The gene set for marking each TME infiltration immune cell type was obtained from the study of Charoentong (15), which stored various human immune cell subtypes including activated CD8 T cell, activated dendritic cell, macrophage, nature killer T cell, regulatory T cell, and so on. The enrichment scores calculated by ssGSEA analysis were utilized to represent the relative abundance of each TME infiltration cell in each sample. We used the limma, GSEABase, ggpubr, and reshape2 packages in R in this step.

2.6 Feature selection of each subtype of colon cancer compared with normal colon and drug analysis

To identify the marker genes for each subtype of colon cancer patients, the empirical Bayesian approach of the limma R package was applied to determine differentially expressed genes (DEGs) between cluster A/B/C and normal colon, respectively. The criteria for determining DEGs were set at an adjusted p-value of< 0.01. At the same time, weighted gene co-expression network analysis (WGCNA) was used to identify the related genes of subtypes of cancer (RG). Next, the protein–protein interaction (PPI) network was further used to screen the hub genes of the intersection of DEGs and RGs using String and Cytoscape software. Maximal Clique Centrality (MCC) was used to screen hub genes (the most connected genes). After obtaining the most connected genes, they were used to perform L1000 to screen drugs for each subtype. The final drug screening criteria of L1000 were set as score< −0.90.

2.7 Prognostic model building

Firstly, TCGA dataset was divided into a training set and an internal test set. Among the 66 prognostic genes, we paired these genes to address the batch effect in the training set. If the expression of gene A > the expression of gene B, then the feature "A|B" is marked as 1, otherwise, it is marked as 0, as shown in Eq. (1).

$$\text{Feature}: \text{"Gene A} \mid \text{Gene B"} = \begin{cases} 1, & \text{Expression}(A) > \text{Expression}(B) \\ 0, & \text{Expression}(A) \leq \text{Expression}(B) \end{cases} \quad (1)$$

In addition, if the expression level of gene A in all the samples is higher than the expression of gene B, then Gene A|Gene B is marked as 1 in all the samples. Such features do not contain classification information, and therefore we delete the gene pairs whose frequency of the "1" label in the training set is less than 0.2 or greater than 0.8. Next, univariate Cox regression and LASSO regression were used to reduce the number of these paired gene features in the training set. Finally, multivariate Cox regression was used to construct the multiple key cancer processes related to gene-pair score (MKPC). The "glmnet," "survival," and "survminer" packages in R were used in the above analysis process.

2.8 Classifier constructing

To make genotyping available to other researchers, we compared two methods based on the expression of the 66 prognostic genes. (1) We used the center points of the three subtypes in the training set (TCGA-COAD) (partitioning around medoid clustering method) to classify the new samples. The label of each new sample depends on the nearest center point of the sample. (2) We use the training set (TCGA-COAD) to build a multi-layer perceptron model (MLP) to label new samples. This MLP model contains three layers, which have 16, 64, and 64 neurons, respectively. We first used 10-fold cross-validation (CV) on the training set to perform a grid search to find the optimal model parameters for accuracy. The parameters in grid search are: "activation" is one of "identity," "logistic," "tanh," or "relu"; "alpha" is one of 0.00001, 0.0001, 0.001, 0.01, and 0.1; "solver" is one of "lbfgs," "sgd," or "adam." The MLP model with the highest accuracy in CV is used to predict the test set.

Accuracy = N(patients predicted correctlty)/N(all patients)

The above methods (1) and (2) were used to make predictions in the test set. We conducted a survival analysis (log-rank test) based on the prediction results. The method with a smaller p-value was used to build a website (https://sujiezhulab.shinyapps.io/coad/) by using the shiny package in R, which can be used by other researchers.

2.9 Prognostic model validation

To investigate the prognostic performance of the MKPC score, we tested it in four colon cancer patient cohorts (three external sets and one internal set). We then calculated the area under the curve (AUC) of the receiver operating characteristic (ROC) for overall survival (OS) time prediction. The models were evealuated using their 1-, 3-, and 5-year AUC values.

2.10 Tumor mutation burden analysis

The mutation data were downloaded from the GDC Data Portal (https://portal.gdc.cancer.gov/) and intersected with the samples with expression data. After that, we obtained 397 patient samples containing both expression data and mutation data. For these patients, we used the "maftools" package in R to plot a waterfall chart and mutation gene cloud chart, obtain differential mutated genes (DMGs) between different subtypes of colon cancer, and calculate the tumor mutation burden (TMB) value by finding out the number of gene mutations per million bases. The Wilcoxon test was used to compare the TMB values of the MKPC high- and low-risk groups.

3 Results

3.1 Construction of three molecular subgroups of colon cancer using prognostic genes

Cancer is a systemic, complex disease related to abnormalities in multiple signaling pathways. In this study, we searched PubMed for studies related to the prognosis of colon cancer and obtained 183 genes from different signaling pathways (Supplementary Table S2). Next, we identified 66 prognostic genes ($p< 0.05$; Supplementary Table S3) using univariate Cox regression in the training set for further analysis.

Based on these 66 prognostic genes, we attempted to classify COAD patients into different subtypes. The R package, ConsensusClusterPlus, was used to classify patients using unsupervised clustering, resulting in 217 cases in cluster A, 188 cases in cluster B, and 43 cases in cluster C (Figures 1A, B). Next, prognostic analysis for the three subtypes revealed a particularly prominent survival advantage in cluster B (Figure 1B). To examine the three subtypes, we also used the GEO dataset (GSE39582) to do clustering. As shown in Figures 1C, D, we could also get similar results based on the 66 prognostic genes. Interestingly, we found that the prognosis of the three subtypes follows the same trend, with cluster B having better survival than the others (Figures 1B, D). This demonstrated that three distinct subtypes did exist in colon cancer.

To explore the survival characteristics of colon cancer, we further examined the characteristics of 66 prognostic genes in different subtypes and found that cluster B was characterized by increased expression of prognostic favorable genes and low expression of adverse prognostic genes. On the contrary, cluster C was characterized by the opposite results of cluster B (Figure 1E, yellow box).

Dysfunction of genes in the DNA mismatch repair pathway reduces the ability of cells to repair DNA replication errors and thereby leads to microsatellite-instable (MSI) subtypes of colon cancer (16). The patients with MSI have a higher somatic mutation burden and immune infiltration in the TME compared to their microsatellite-stable (MSS) counterparts (17). Immune checkpoint genes such as CTLA4 and CD274 are more highly expressed in MSI than in MSS patients (18–20). Apart from high sensitivity to immunotherapy, MSI status itself is a good prognostic marker for CRC patients subject to conventional treatment. MSI patients exhibit less clinical aggressiveness and a longer survival time than MSS patients. Further research showed that tumors with MSI subtype were mainly characterized by clusters B and C, while tumors with the MSS subtype were characterized by cluster A, and that also indicated cluster B/C patients may be suitable for receiving immunotherapy (Figure 1F).

The subtypes based on the 66 prognosis genes were significantly sociated with various clinicopathological parameters; cluster C was enriched for T3 tumors and high-grade tumors (Figure 2A). Analysis of the biological processes associated with distinct subtypes revealed important patterns. Cluster B was associated with cell cycle, DNA replication, mismatch repair, P53 signaling pathway, and apoptosis. Post-translational modifications of the p53 signaling pathway play an important role in cell cycle progression and stress-induced apoptosis (21). P53-mediated apoptosis may account for the favorable prognosis of cluster B (Figure 2A, blue box). By contrast, cluster C tumors were mostly associated with Mapk, Erbb, Wnt, Notch, and Vegf signaling pathways (Figure 2A), and this signaling pathway may play an important role in drug resistance (22–24), which may cause a worse prognosis for cluster C. Additionally, cluster A was intermediate between clusters C and B, which is consistent with the prognosis.

We estimated the presence of immune cells by deconvolution of RNA-Seq data (25). To our surprise, cluster C was prominently related to the immune biological process (Figure 2A, yellow box). The results from GSVA analysis revealed that cluster C was remarkedly enriched in stromal and carcinogenic activation pathways such as ECM receptor interaction and TGF beta signaling pathway, and it was also remarkedly rich in immune cell function activation, such as CD8+ T cell, antigen processing and presentation, inflammation-promoting, and IFN response. Previous studies demonstrated that tumors with immune-excluded phenotypes also showed the presence of abundant immune cells, while these immune cells were retained in the stroma surrounding tumor cell nests rather than penetrating their parenchyma (26).

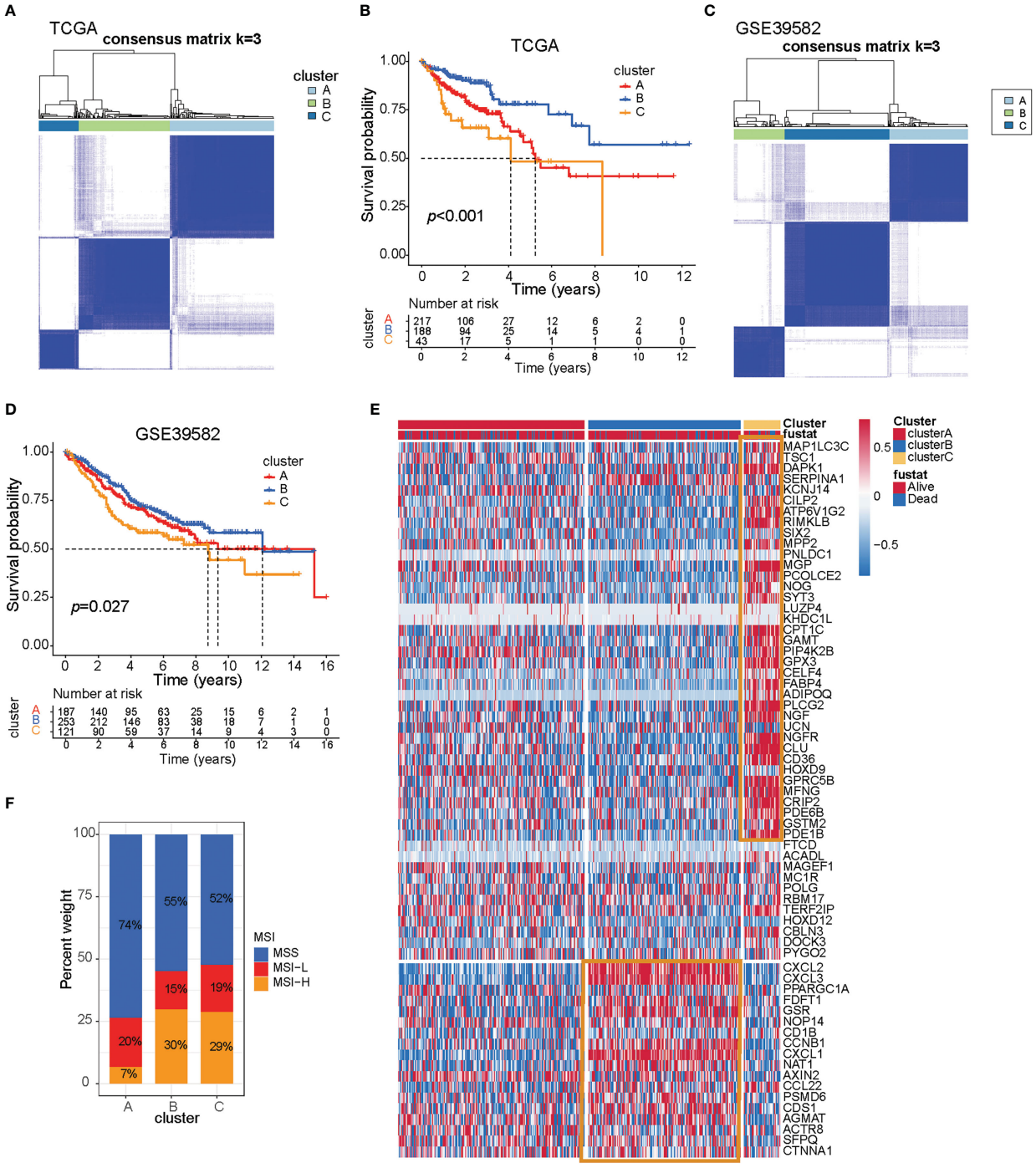

FIGURE 1
Three prognostic molecular subtypes of colon cancer. **(A)** Clustering heat map based on 66 prognosis-related genes in TCGA-COAD cohort. **(B)** Survival curve of TCGA-COAD patients in different clusters. Survival differences were assessed with a log-rank test. **(C)** Clustering heat map based on 66 prognosis-related genes in the GSE39582 cohort. **(D)** Survival curve of GSE39582 patients in different clusters. Survival differences were assessed with a log-rank test. **(E)** Heat map of 66 prognosis-related genes in TCGA-COAD cohort. **(F)** The proportion of microsatellite instable subtypes in A–C subtypes of TCGA-COAD cohort.

Genomic instability (GI) and somatic copy-number alterations (SCNAs) are important in increasing the adaptive potential of the tumor and have been linked with a poor prognosis (27). The SCNA score is a representation of the level of SCNAs occurring in a tumor. For each tumor, the SCNA score was calculated at three different levels: focal, arm, and chromosome level, and the overall score was calculated from the sum of all three levels (15). We found that cluster A tumors were remarkedly enriched with high SCNA and high GI (Figure 2A, red box; Supplementary Table S4).

We then used the CIBERSORT method, a deconvolution algorithm using support vector regression for determining the immune cell type in tumors, to compare the component

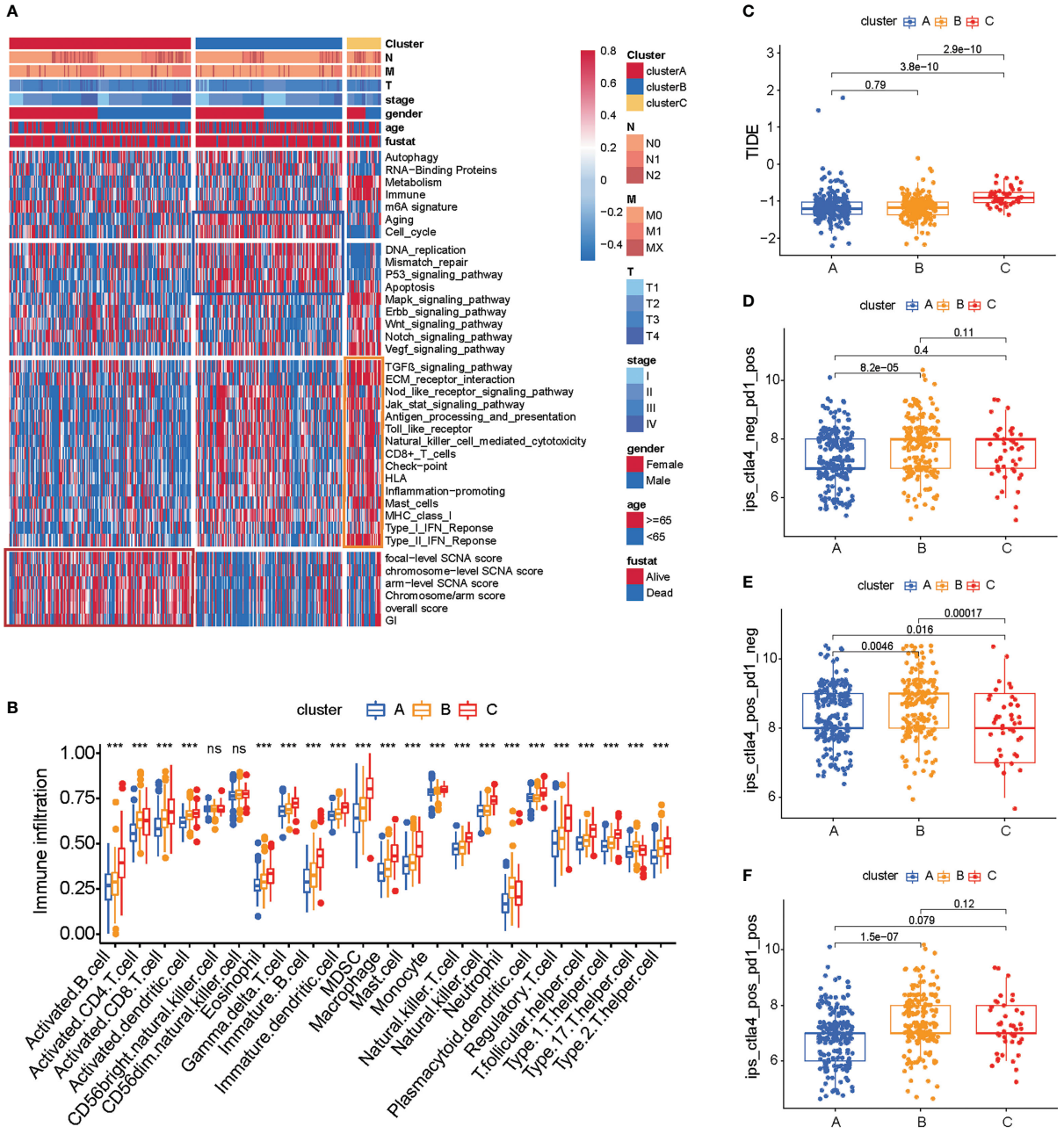

FIGURE 2
TME cell infiltration characteristics and immunotherapy prediction in distinct three subtypes of colon cancer. **(A)** Heat map of molecular characteristics in three clusters in TCGA-COAD cohort. The four regions (rows) of the heat map respectively represent key tumor processes, tumor-related pathways, immune-related processes, chromosome stability, and somatic cell copy number. **(B)** Analysis of immune cell content in TCGA COAD cohort. The one-way ANOVA test was used for comparison between different groups. ***$p < 0.001$, ns $p > 0.05$. **(C)** Heat map of hot or cold tumor marker genes in TCGA-COAD cohort. **(D–F)** The relationship between immunotherapy-related scores and patient subtypes in TCGA-COAD cohort. The Wilcoxon test was used for comparison between different subtypes.

differences of immune cells among the three subtypes of colon cancer. We found that there are significant differences in the composition of TME cell types between the three subtypes of colon cancer (Figure 2B), which suggested that the three subtypes have distinct TME infiltrating-cell types of tumors. Based on the above analyses, we were surprised to find that three subtypes of colon cancer had significantly distinct TME cell infiltration characterization. Cluster A was classified as an immune-desert phenotype, characterized by the suppression of immunity. Cluster B was classified as an immune-inflamed phenotype, characterized by adaptive immune cell infiltration and immune activation. Cluster C was classified as an immune-excluded phenotype, characterized by innate immune cell infiltration and stromal activation (Figure 2B). Interestingly, we found that an immune-excluded state prejudices the survival of colon cancer patients, while immune-inflamed state is a particularly prominent survival

advantage in cluster B. To verify the result in TCGA cohort, we next analyzed the TME cell infiltration in GSE39582 (Supplementary Figures S2A, B). Again, consistent with the result in TCGA cohort, the immune-inflamed phenotype (cluster B) is preferred for survival (Figure 1D).

The above results showed again that three subtypes of colon cancer have distinct TME landscapes. Predicting the response to immunotherapy based on the characterization of TME cell infiltration is a key procedure for increasing the success of existing immunotherapy and exploiting novel immunotherapeutic strategies (28, 29). Therefore, we further predicted the immunotherapy of three subtypes of colon cancer. We found that cluster B had a lower TIDE score and more response to PD1/CTLA4, which indicated that cluster B was more likely to benefit from the immunotherapy. These results indicated that cluster B is suitable for immunotherapy (Figures 2C–F; Supplementary Tables S5, S6).

3.2 Characteristics of three subtypes of colon cancer in tumor somatic mutation

Clinical trials as well as preclinical studies have revealed that patients with high somatic TMB have an enhanced response, long-term survival, and durable clinical benefit when treated with immune checkpoint blockade therapy. We then analyzed the distribution differences of somatic mutation between three subtypes of colon cancer in TCGA-COAD cohort using the maftools package. The TMB quantification analyses confirmed that cluster B was markedly correlated with higher TMB (Figure 3A), which confirmed again that cluster B may be more easily responsive to immune checkpoint blockade therapy.

As shown in Supplementary Figures S3A, B, cluster A presented a lower tumor mutation burden than clusters B and C, with the average rate of the top 15 mutated genes being 28.3% versus 34.6% and 32.9%, respectively. We also found that cluster A was characterized by a high TP53 mutation, cluster B by TTN mutation, and cluster C by APC mutation (Supplementary Figures S3D–F). To further investigate the mutation genes of each subtype of colon cancer, we determined three subtype-related mutations using the maftools package. Given that gene mutation is often related to survival, we analyzed the connection between these mutation genes and survival using the TIMER database (Supplementary Tables S7-S10). Furthermore, seven genes were found to be related to survival (ATXN2L, IGSF3, MYO5B, PTCHD2, SLFN5, ENPEP, and MAP3K2, $p< 0.05$, Figures 3B–H; Supplementary Table S7), and all of these seven genes had a high mutation rate in cluster C. These findings indicated that these adverse prognostic gene mutations may also contribute to cluster C's worse prognosis. Considering that cluster C was characterized by immune activation, we further explore the connection between survival-related gene mutation and CD8+ T-cell infiltration. We found that MAP3K2, ATXN2L, BAZ1B, and PARP14 mutations resulted in high CD8+ T-cell infiltration in tumors (Supplementary Figures S3G–J). Our observation above supported our hypothesis that greater TME cell infiltration may result in the worst prognosis for cluster C patients.

Mutational patterns in DNA are derived from mutational processes that result in distinct biological changes occurring during tumorigenesis. Therefore, we examined the pathways in which the mutation gene was enriched in distinct subtypes. We chose a mutation gene that ranks in the top 200 in each of the subtypes, and then ran a KEGG enrichment analysis on these genes. To our surprise, the mutation genes in cluster C were enriched in signaling pathways related to lipid metabolism compared with clusters A and B, such as ABC transporters and cholesterol metabolism (Figures 3I–K). Based on studies that show that limiting fatty acid availability can control cancer cell proliferation (30), cluster C patients may have lipid disorders, which may result in a poor survival rate.

3.3 Classifier for predicting patient subtypes and drug screening

The above results showed that there are three subtypes of colon cancer patients based on the 66 prognostic genes, and cluster B has a prominent survival advantage over cluster A/C, while cluster C has more TME cell infiltration, indicating that these three subtypes have different transcriptome features. Therefore, we hypothesized that patients of different subtypes should be treated differently. Pursuing this, based on the expression of 66 prognostic genes, we compared two different methods, as described in the Methods section. Method (1) was based on unsupervised learning, and method (2), which is an MLP classifier, was based on supervised learning (Figure 4A). In cross-validation, the MLP model achieves the highest accuracy (0.919; Supplementary Table S11) in the training set when "identity" = "logistic," "alpha" = 0.01, and "solver" = "lbfgs." As a result, we used these parameters to set up the MLP model using the whole training set. In the survival curves of the test set (GSE39582), the labels in method (1) cannot distinguish survival states (p = 0.071, log-rank test, Figure 4B), but the MLP model can distinguish the survival states significantly (p = 0.016, log-rank test, Figure 4C), which is consistent with the result in the training set (Figure 1D). Therefore, this MLP model is used to establish a web app (https://sujiezhulab.shinyapps.io/coad/) that can be used easily by other researchers.

Next, we compared each subtype of colon cancer to normal colon samples and obtained DEGs. We used the WGCNA and PPI to further select hub genes related to each subtype based on these DEGs (Supplementary Figures S4-S6; Supplementary Table S12-S14), and these hub genes were used as L1000 input data (https://clue.io/), a tool used to screen drugs that can reverse gene expression from a disease state to a healthy state. In addition, these drugs were regarded as effective drugs for the special disease. In our research, drugs with CMap connectivity (tau) score of<−0.9 were selected and included in our recommendation list (Figure 4D). Herein, we used up/down gene signatures to obtain a drug list as adjuvant therapy. Furthermore, we observed that there are some drugs with anti-inflammation effects for cluster B/C, which is consistent with the fact that cluster B/C contain more macrophages (Supplementary Tables S15-S17).

To further explore the signaling pathways of the DEGs in cluster A/B/C, we performed KEGG enrichment analysis

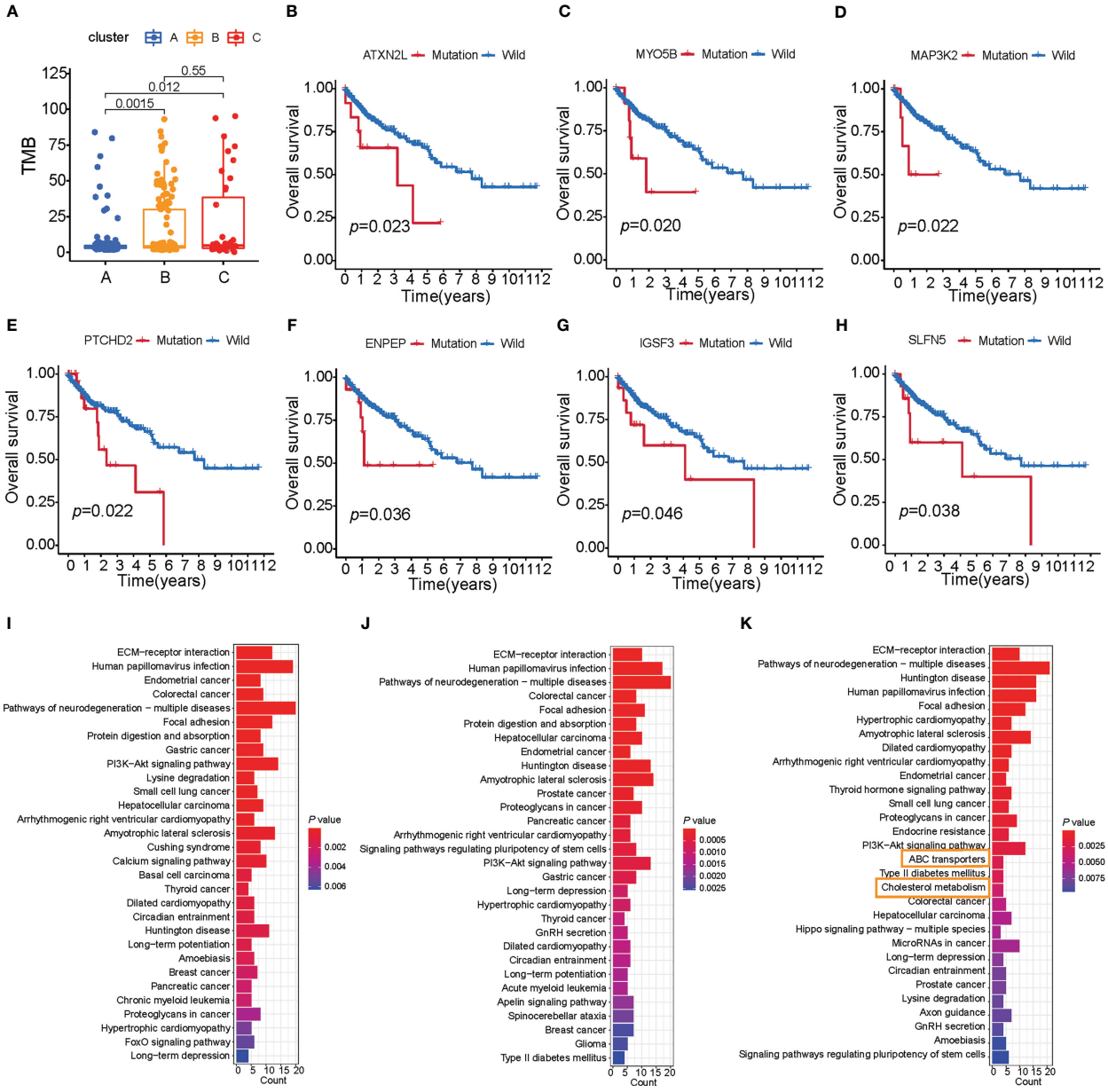

FIGURE 3
Characteristics of three subtypes of colon cancer in tumor somatic mutation. **(A)** TMB analysis (Wilcoxon test) of patient subtypes in TCGA-COAD cohort. **(B–H)** Survival analysis of key gene mutations (log-rank test). **(I–K)** The signaling pathway of the top 200 mutation genes enriched in three distinct subtypes.

(Figure 4E) and found that cluster A/B/C was enriched in some similar signaling pathways, such as the IL-17 signaling pathway and the PPAR signaling pathway. There are also some cluster-specific enriched signaling pathways related to immune and lipid metabolism. Cluster A was associated with the Wnt signaling pathway; cluster B was enriched in tyrosine metabolism; and cluster C was characterized by inflammation signaling pathways such as cell adhesion and ECM–receptor interaction, which supports the results that the drugs for cluster C were anti-inflammatory. Notably, cluster C was also enriched in the Wnt signaling pathway, which indicated that cluster C has a double poorer prognosis feature (Figure 4E). Recalling our observations of drugs for the distinct cluster, drugs related to lipid metabolism all existed in three subtypes, which is consistent with our results that the PPAR signaling pathway was enriched in all subtypes.

3.4 Construction of MKPC score for prognostic classification of colon cancer patients

Given our observation of distinct prognosis of three subtypes based on 66 prognostic genes, it was notable that the expression of 66 prognostic genes differed significantly among the three subtypes.

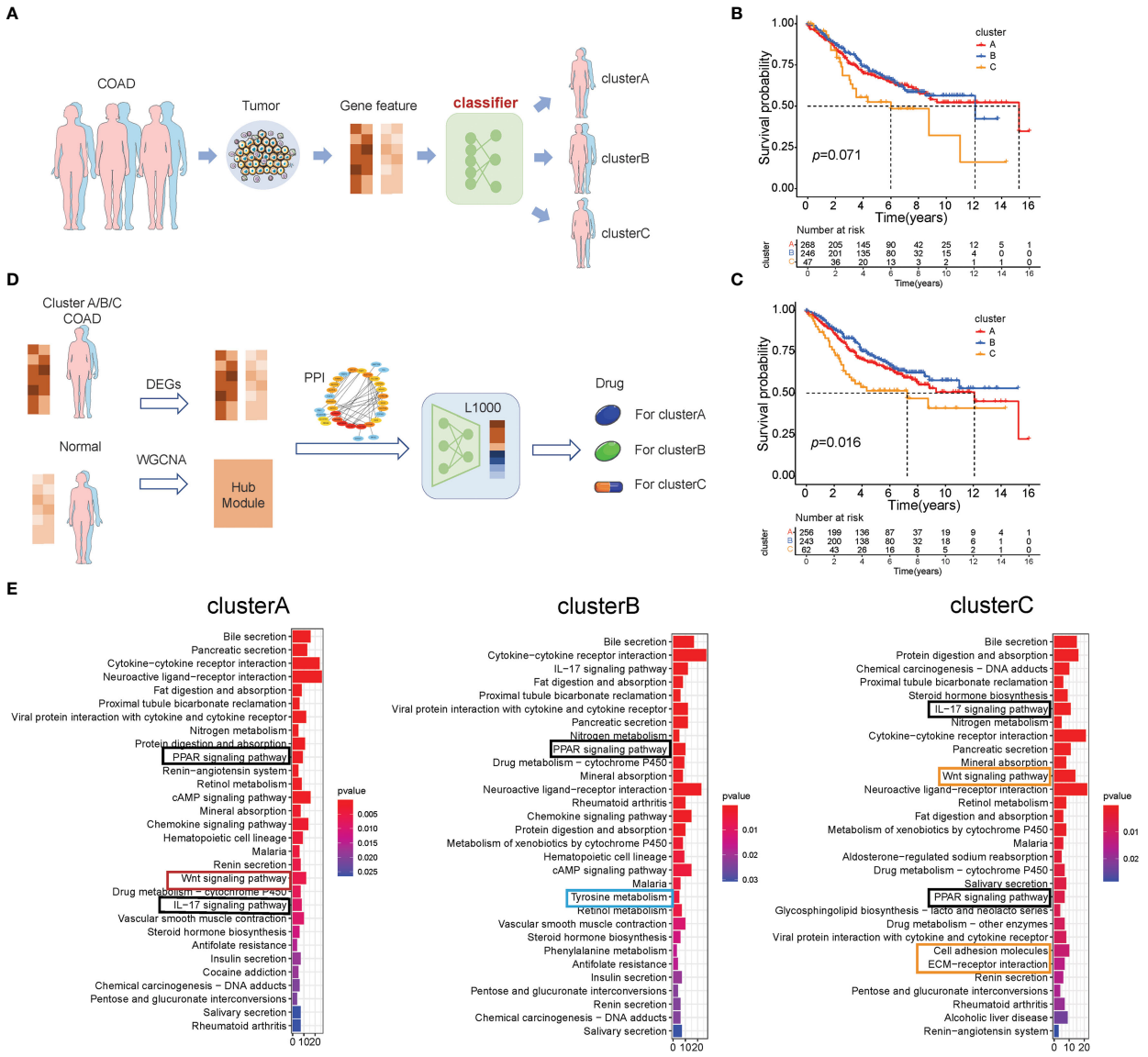

FIGURE 4
Classification-drug-prediction system. **(A)** Flow chart of the COAD subtype prediction. **(B)** For the GSE39582 cohort, if the distance from the centers of the three subtypes in TCGA-COAD was used as a classification standard, then the result of the survival analysis is not significant (log-rank test). **(C)** For the GSE39582 cohort, the MLP model was used to do classification, and the result of the survival analysis is significant (log-rank test). **(D)** Flow chart of drug screening for different molecular subtypes. **(E)** GO analysis of the intersection genes in the WGCNA and DEGs (patients *vs*. controls) of TCGA-COAD clusters A–C, respectively.

Therefore, we explored the ability to distinguish prognosis based on 66 prognostic genes in Pan-cancer. To our surprise, when the cancers were divided into three subtypes, there were 15 kinds of cancer showing distinct prognoses, which indicated that these genes were important for cancer patients' survival ($p< 0.05$, Wilcoxon test, Supplementary Figures S7A–O).

To establish a robust prognostic model and avoid the batch effect, the 66 prognostic genes were used for gene pairing, yielding a total of 2,145 (66 * 65/2) gene pairs, 357 of which have a frequency of "gene A > gene B expression" between 20% and 80% in the training set and are considered to have sufficient information to predict survival state. We then obtained 22 gene pairs using univariate Cox regression (Supplementary Table S18). In multivariate penalized LASSO regression, 13 gene pairs were selected for survival prediction in the training set. Finally, using multivariate Cox regression, eight gene pairs were identified as being associated with survival difference (Supplementary Table S16), and these formed the MKPC score; these eight gene pairs included six risk factors (HR >1) and two protective factors (HR< 1) (Supplementary Figure S8; Supplementary Table S19). Therefore, the MKPC score is calculated as follows:

Sum = 1.028064 * MPP2|CPT1C − 1.09876 * PPARGC1A|CD36 + 0.573201 * NOG|CD1B + 0.661607 * GAMT|CCL22 − 0.57286 * GSR|MAGEF1 + 0.593767 * NGF|CD1B + 0.927301 * CRIP2|ACTR8

$$\text{MKPCscore} = e^{\text{sum}}$$

To investigate the prognostic performance of the MKPC score, we tested it in four colon cancer patient cohorts (three external test sets and one internal test set). We used the median value of the MKPC score in the training set (1.0544) as the cutoff to separate the high- and low-risk groups in these test cohorts. Notably, the MKPC score showed a wide prognostic value in distinguishing the survival status of colon cancer patients across all cohorts (Figures 5A–H), despite differences in patient characteristics and transcriptomic platforms. Consistently, the high-risk group had a worse prognosis in all cohorts (Figures 5A–D). These results suggest that the paired MKPC score is a robust prognostic factor in colon cancer. Interestingly, we tested the model in Pan-cancer and observed that the MKPC score has a good performance in distinguishing the survival status of the READ (Supplementary Figures S8D, E), which indicated that the MKPC score was related to bowel cancer.

To make the MKPC score more easily usable by other researchers, we built an easy-to-use nomogram based on the MKPC score (Supplementary Figure S9). We used the GSE39582 dataset for nomogram construction and validation, which contains various types of clinical information. The GSE39582 cohort was divided into two parts: training set (n = 258) and test set (n = 137). The training set was used for independent prognostic analysis. We further used the training set to establish the nomogram among the independent risk factors and used AUC-ROCs to verify its performance in the test set. To make this nomogram available to other researchers, including those without programming skills, it was deployed on the server using the "shiny" package in R (https://sujiezhulab.shinyapps.io/coad/).

3.5 The clinical and transcriptome characteristics of high- and low-risk patients

An alluvial diagram was used to visualize the connection between the MKPC score and the three subtypes of colon cancer based on the 66 prognostic genes. We found that most cluster C patients are high-risk, whereas most cluster B patients are low-risk (Figure 6A). In clinical practice, patient clinical features, such as age, gender, TNM status, and stage serve as a guide for treating colon cancer. So we looked at how these clinical characteristics differed between the high- and low-risk groups. The higher the grade of the patient, the higher the risk and the lower the chance of survival (Figure 6B). Given our results that three subtypes have distinct TME cell infiltration, we observed that the low-risk group had more immune-activated cells and the high-risk group had more immunosuppressive cells (Figure 6C). To investigate the potential biological behavior of different risk groups, we performed a GSEA analysis. The high-risk group was markedly enriched in stromal and carcinogenic activation pathways such as ECM receptor interaction, cell adhesion, and MAPK signaling pathways, which is consistent with cluster C, whereas the low-risk group presented enrichment in immune activation pathways such as Natural killer cell-mediated cytotoxicity, JAK-STAT signaling pathway, and Toll-like receptor signaling pathway (Supplementary Figure S10).

To obtain risk-related genes, we used the limma packages to obtain DEGs between high- and low-risk groups, and these genes were further selected for risk-related genes (RRGs) using Lasso

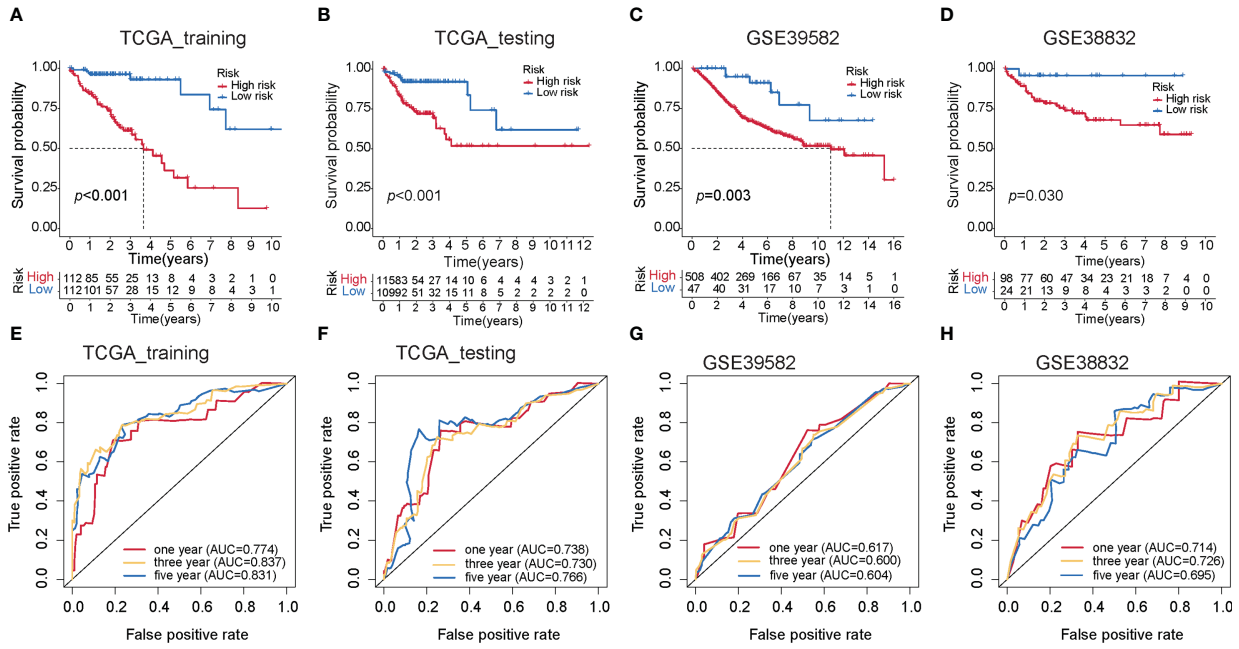

FIGURE 5
Construction of the MKPC score. Survival curves (log-rank test) of MKPC score in **(A)** TCGA training set, **(B)** TCGA test set, **(C)** GSE39582, **(D)** GSE38832, **(E–H)** ROC curves of MKPC score in **(E)** TCGA training set, **(F)** TCGA test set, **(G)** GSE39582, and **(H)** GSE38832.

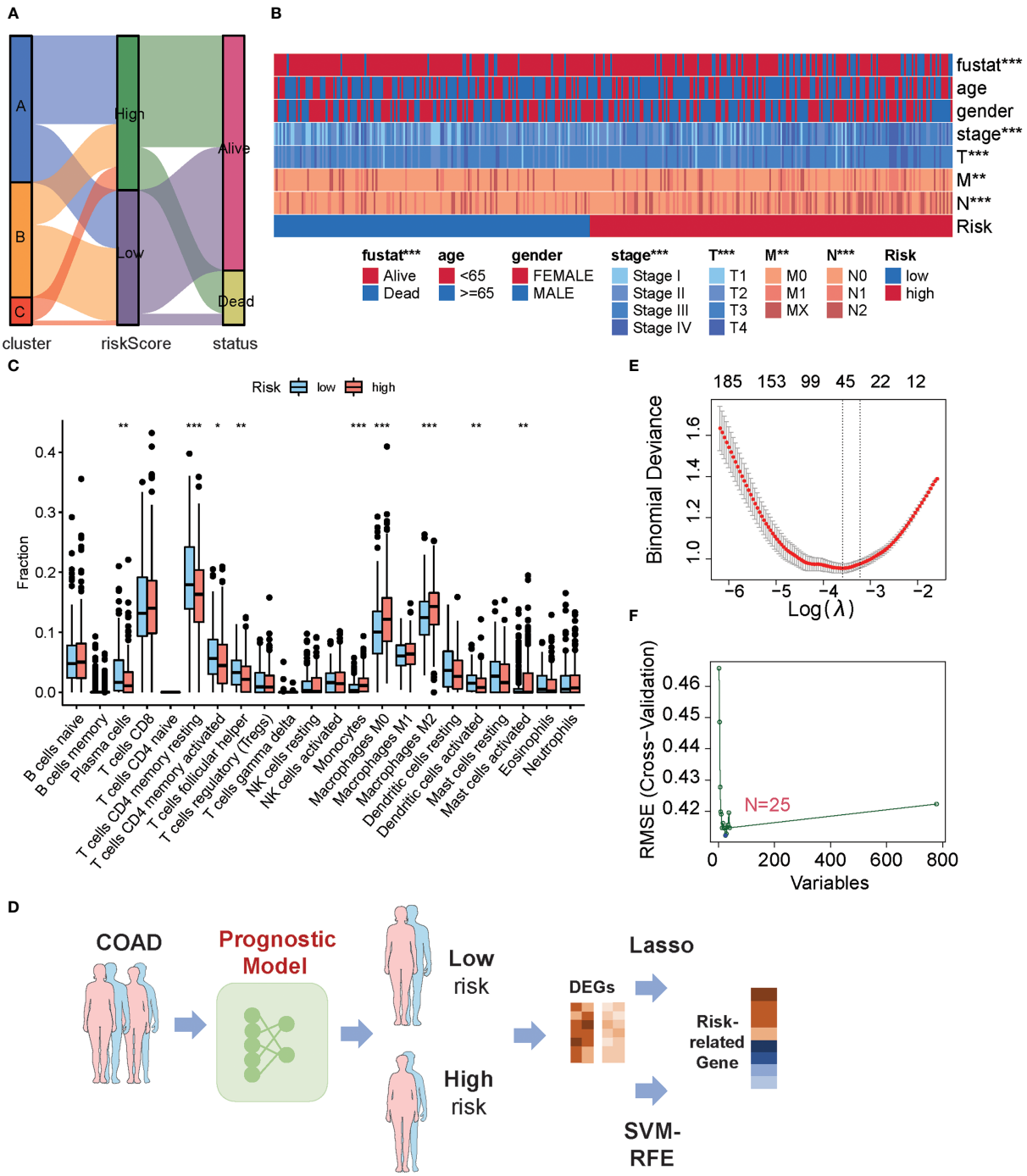

FIGURE 6
Characteristics of low- or high-risk colon cancer patients. **(A)** The relationship among cluster label, MKPC score, and survival state in TCGA-COAD cohort. **(B)** The difference of clinical features in TCGA-COAD cohort in the MKPC risk group by Chi-square test. *$p < 0.05$; **$p < 0.01$; ***$p < 0.001$. **(C)** ssGSEA of immune cell content between different MKPC risk groups in TCGA-COAD cohort (Wilcoxon test). **(D)** Prognosis-related key target analysis process. **(E)** Feature screening based on LASSO regression. **(F)** Feature screening based on Random Forest regression. The blue point corresponds to the smallest RMSE value.

regression and random forest (Figures 6D–F; Supplementary Table S20). In addition, the intersected genes between LASSO regression and random forest were regarded as final risk-related genes, yielding 11 genes (Supplementary Table S20).

3.6 The experiment of risk-related genes

To explore potential colon cancer risk-related genes, we compared the expression of 11 RRGs in normal and tumor

tissues (Supplementary Figures S11A–K) and found that PANX2 and GABRD are highly expressed in tumors, while PPARGC1A is less expressed in tumors. This difference was consistent with the difference between the low- and high-risk groups. To verify whether these three genes were related to the progression of colon cancer, we used qPCR to examine the expression of those genes in one normal colon cell line and four colon cancer cell lines (Figures 7A–C). Among them, PPARGC1A was expressed at a lower level in colon cancer, which is consistent with our previous result that PPARGC1A was expressed at a lower level in a high-risk group, whereas GABRD showed the opposite trend of expression to PPARGC1A in these cell lines, and PANX2 exhibited large expression differences between cell lines. Considering the PPARGC1A and GARBD were consistent in the "tumor *vs.* normal" and "high-risk and low-risk group," we further explored the expression of these two genes in colon cancer patients. There was a lower expression of PPARGC1A and a high expression of GARBD in colon cancer patients (Figures 7D–G). Previous study showed that PGC1-α (PPARGC1A) suppressed melanoma metastasis, and that high PGC1α expression is associated with worse prognosis in metastatic melanomas (31, 32), and that high GARBD expression is associated with poor survival (33). These results indicated that PPARGC1A and GARBD could be potential targets for colon cancer.

4 Discussion

An analysis of the molecular basis of inter-patient heterogeneity is a critical first step in understanding why some patients benefit from specific treatments while others fail to benefit. The molecular subtypes of colon cancer can help guide us with individualized treatment. In this study, our results suggest that three distinct three subtypes are based on the expression of 66 prognostic genes from multiple signaling pathways characterized by diverse prognoses, enabling validation in independent cohorts. Integrating RNA subtype classification, pathway information, clinical signatures, immune infiltrate analyses, and TMB status leads us to find that the model of mRNA-based expression subtypes may be associated with a unique response to therapies. Interestingly, cluster B/C patients were characterized by higher immune infiltration and MSI status, especially cluster B with a lower TIDE score, which is

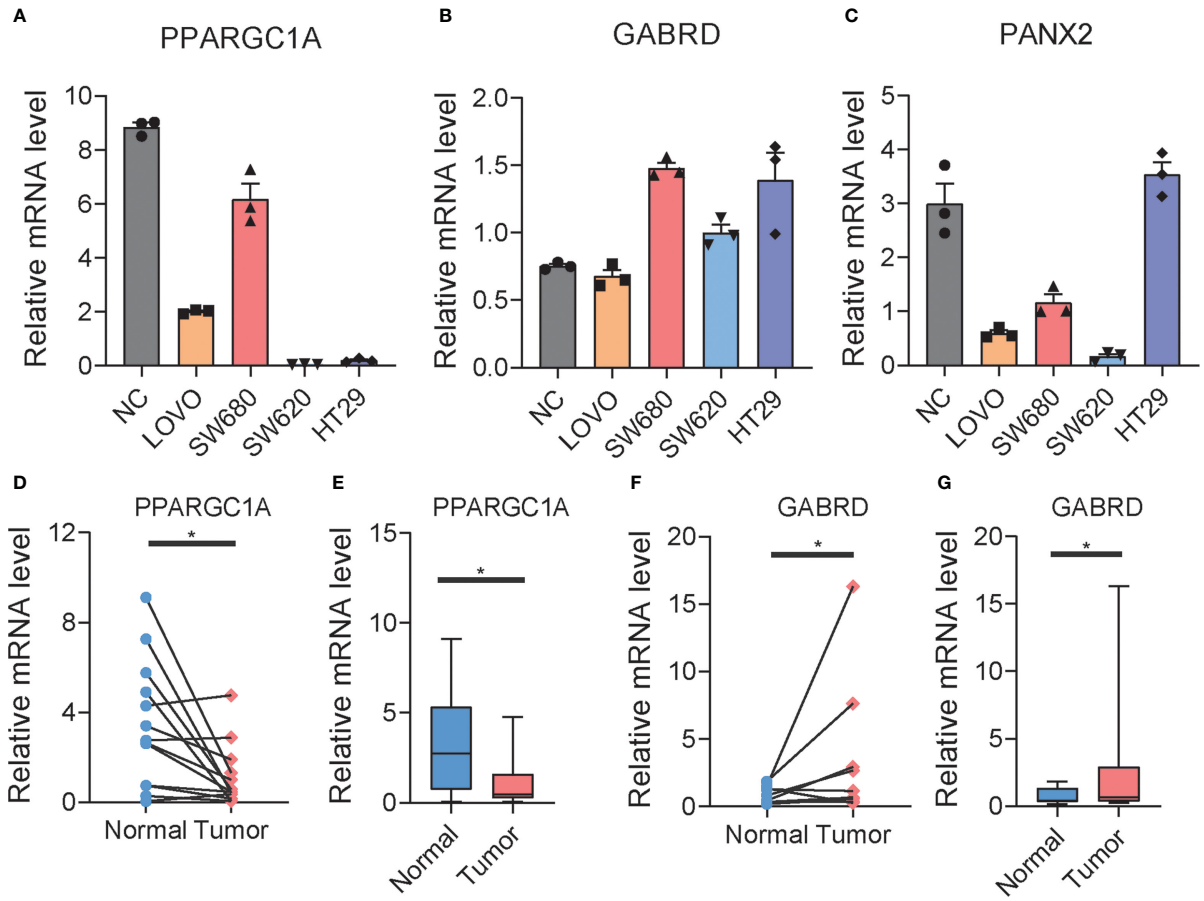

FIGURE 7
The expression of RRGs in colon cancer. **(A–C)** The expression of PPARGC1A, GABRD, and PANX2 in normal colon cell lines and differential colon cancer cell lines. **(D–G)** The expression of PPARGC1A and GABRD in normal colon tissue and tumor colon tissue of patients. *t*-test was used to compare the expression of genes between normal and tumor. *$p < 0.05$.

the candidate for immunotherapy, while cluster A patients were characterized by the suppression of immunity and higher MSS status, indicating cluster A is not suitable for immunotherapy.

We also observed that the three subtypes of colon cancer had distinct TMB statuses and transcriptome expressions, implying that each subtype of patient should be treated in a unique way. Therefore, we used the L1000 platform to predict the drug for these patients. To better assist clinicians with medication, we developed a classifier that can identify which subtypes of colon cancer a patient has. As a result, patients can be treated based on the expression of their unique genes.

Furthermore, using the novel gene pairing approach, we established a new MKPC score. To the best of our knowledge, this is the first COAD prognostic model that considers multiple signaling pathways at the same time. Using three independent COAD cohorts, we have demonstrated that our MKPC score leads to robust and accurate performance, and that the MKCP score is particularly effective in READ. Our web-tool implementation of the MKPC score and nomogram promotes an easy use of the risk score for COAD.

In short, we summarized the differences between the distinct three subtypes of colon cancer from a comprehensive and multi-omics perspective. At the same time, we developed a classification-drug-prognosis-prediction system that can be used to help clinicians in identifying the best drug for a colon cancer patient. The web tool for predicting patient survival also had a great performance in assisting clinicians. However, the current work has some limitations and areas that could be improved in the future. Cancer, for example, is a molecularly heterogeneous disease whose development has been linked to multiple signaling pathways rather than single pathway genes. Our findings provided novel ideas for identifying the subtypes of colon cancer, which can also be used to distinguish subtypes of other cancers; however, the role of these genes in Pan-cancer needs to be further explored to find a new cancer target. Additionally, the drug lists for cluster A/B/C obtained by L1000 need to be verified with more experiments, although the drugs for cluster A/B/C were consistent with the enriched signaling pathway that the gene features of these three clusters share to some degree.

Data availability statement

The datasets presented in this study can be found in online repositories. The names of the repository/repositories and accession number(s) can be found within the article/Supplementary Material.

Author contributions

JZ: conceptualization, formal analysis, methodology, software, and writing—original draft. WK: conceptualization, formal analysis, methodology, software, and writing—original draft. LH: formal analysis. SB: investigation. XJ: supervision and writing—review and editing. SZ: supervision, funding acquisition, writing—review and editing, and project administration. All authors contributed to the article and approved the submitted version.

Acknowledgments

We thank Dr. Tero Aittokallio and Dr. Liye He for participating in the discussion of this project.

Conflict of interest

The authors declare that the research was conducted in the absence of any commercial or financial relationships that could be construed as a potential conflict of interest.

The reviewer TY declared a shared parent affiliation with the authors JZ and WK to the handling editor at the time of review.

Publisher's note

Supplementary material

The Supplementary Material for this article can be found online at: https://www.frontiersin.org/articles/10.3389/fimmu.2023.1142609/full#supplementary-material

SUPPLEMENTARY FIGURE 1
Flow chart of this study.

SUPPLEMENTARY FIGURE 2
The characteristics of three subtypes of colon cancer in GSE39582. **(A)** Heat map of 66 prognostic-related genes in GSE39582. **(B)** Immune cell infiltration among three subtypes of colon cancer in GSE39582. One-way ANOVA was used to analysis the difference of immune cell infiltration among three cluster. "*" means $p<0.05$; "**" means $p<0.01$; "***" means $p<0.001$.

SUPPLEMENTARY FIGURE 3
Mutation analysis of different subtypes in TCGA-COAD cohort. **(A)** Waterfall chart of mutations in Cluster A. **(B)** Word Cloud Analysis of mutations in Cluster A. The character size reflects the number of mutations. **(C)** Waterfall chart of mutations in Cluster B. **(D)** Word Cloud Analysis of mutations in Cluster B. **(E)** Waterfall chart of mutations in Cluster C. **(F)** Word Cloud Analysis of mutations in Cluster C. **(G–J)** The relationship between CD8+ T cell content and gene mutation (Wilcoxon test).

SUPPLEMENTARY FIGURE 4
The gene signature of cluster A. **(A)** The intersection of DEGs (patients *vs* controls) and WGCNA genes in TCGA-COAD Cluster A patients. **(B)** PPI network of intersection genes.

SUPPLEMENTARY FIGURE 5
The gene signature of cluster B. **(A)** The intersection of DEGs (patients *vs* controls) and WGCNA genes in TCGA-COAD Cluster B patients. **(B)** PPI network of intersection genes.

SUPPLEMENTARY FIGURE 6
The gene signature of cluster C. **(A)** The intersection of DEGs (patients *vs* controls) and WGCNA genes in TCGA-COAD Cluster C patients. **(B)** PPI network of intersection genes.

SUPPLEMENTARY FIGURE 7
Prognostic molecular subtypes of Pan cancer landscape based on the expression of 66 genes. In pan-cancer, the survival curves of 15 cancers whose survival status can be distinguished by 66 prognostic-related genes significantly. Log Rank test is used in this process. ACC, Adrenocortical Carcinoma; BRCA, Breast Invasive Carcinoma; CESC, Cervical Squamous Cell carcinoma and Endocervical Adenocarcinoma; KIRC, Kidney Renal Clear Cell Carcinoma; LGG, Brain Lower Grade Glioma; LIHC, Liver Hepatocellular Carcinoma; LUSC, Lung Squamous Cell Carcinoma; MESO, Mesothelioma; OV, Ovarian Serous Cystadenocarcinoma; READ, Rectum Adenocarcinoma; SARC, Sarcomav; SKCM, Skin Cutaneous Melanoma; THYM, Thymoma; UCEC, Uterine Corpus Endometrial Carcinoma; UVM, Uveal Melanoma.

SUPPLEMENTARY FIGURE 8
Construction MKPC score. **(A)** The partial likelihood deviance in cross-validation (CV) as a function of the penalty coefficient lambda. The dotted line shows the lambda value of 0.03 at the minimum partial likelihood deviance level, suggesting 13 genes as optimal predictive features. Standard errors are calculated over 1000 CV rounds. **(B)** The coefficients of the 13 genes as a function of the penalty coefficient (lambda). **(C)** The hazard ratios of the MKPC signature genes based on multivariate Cox regression in the training set. The asterisks indicate the statistical significance: *p<0.05, **p<0.01, ***p<0.001 (Wald's test). **(D)** Survival curves (Log Rank test) of MKPC score in READ. (E) ROC curves (Log Rank test) of MKPC score in READ.

SUPPLEMENTARY FIGURE 9
(A) The idea of web. **(B)**The nomogram based on MKPC score.

SUPPLEMENTARY FIGURE 10
GSEA analysis for TCGA-COAD cohort. **(A)** Enriched KEGG pathways in high risk group. **(B)** Enriched KEGG pathways in low risk group.

SUPPLEMENTARY FIGURE 11
The expression of RRGs in normal colon tissue and colon cancer tissue. **(A–K)** The expression of CCDC151, GAMT, LRFN1, MPP2, NGF, NOG, NXPE1, PANX2, PCOLCE2, PPARGC1A and GABRD in normal colon tissue and colon cancer tissue.

SUPPLEMENTARY TABLE 1
The summary of clinical information of collected cohorts.

SUPPLEMENTARY TABLE 2
The collected 183 genes from multiple signaling pathways.

SUPPLEMENTARY TABLE 3
The significant genes in UniCox regression.

SUPPLEMENTARY TABLE 4
The SCNA and GI sore of the colon cancer patients.

SUPPLEMENTARY TABLE 5
The TIDE score of Cluster A/B/C.

SUPPLEMENTARY TABLE 6
The predicted response to immunotherapy of Cluster A/B/C.

SUPPLEMENTARY TABLE 7
The different mutations between A and C clusters using Fisher test.

SUPPLEMENTARY TABLE 8
The different mutations between B and C clusters using Fisher test.

SUPPLEMENTARY TABLE 9
The intersected mutations between "A *vs* C clusters" and "B *vs* C clusters".

SUPPLEMENTARY TABLE 10
The mutations related to survival (Log-Rank test).

SUPPLEMENTARY TABLE 11
Cross validation of MLP model in TCGA-COAD cohort.

SUPPLEMENTARY TABLE 12
The gene signature of A cluster.

SUPPLEMENTARY TABLE 13
The gene signature of B cluster.

SUPPLEMENTARY TABLE 14
The gene signature of C cluster.

SUPPLEMENTARY TABLE 15
The recommended drugs of A cluster.

SUPPLEMENTARY TABLE 16
The recommended drugs of B cluster.

SUPPLEMENTARY TABLE 17
The recommended drugs of C cluster.

SUPPLEMENTARY TABLE 18
The UniCox regression of gene-pairs.

SUPPLEMENTARY TABLE 19
The parameters of MKPC signature (MultiCox regression).

SUPPLEMENTARY TABLE 20
The risk related genes.

References

1. Mattesen TB, Rasmussen MH, Sandoval J, Ongen H, Arnadottir SS, Gladov J, et al. Publisher correction: MethCORR modelling of methylomes from formalin-fixed paraffin-embedded tissue enables characterization and prognostication of colorectal cancer. *Nat Commun* (2020) 11:2880. doi: 10.1038/s41467-020-16538-5

2. Puppa G, Sonzogni A, Colombari R, Pelosi G. TNM staging system of colorectal carcinoma: A critical appraisal of challenging issues. *Arch Pathol Lab Med* (2010) 134:837–52. doi: 10.5858/134.6.837

3. Chen F, Chandrashekar DS, Varambally S, Creighton CJ. Pan-cancer molecular subtypes revealed by mass-spectrometry-based proteomic characterization of more than 500 human cancers. *Nat Commun* (2019) 10:5679. doi: 10.1038/s41467-019-13528-0

4. Wang XQ, Xu SW, Wang W, Piao SZ, Mao XL, Zhou XB, et al. Identification and validation of a novel DNA damage and DNA repair related genes based signature for colon cancer prognosis. *Front Genet* (2021) 12:635863. doi: 10.3389/fgene.2021.635863

5. Chen S, Dong R, Li Y, Zheng N, Peng G, Lu F, et al. m(7)G-related DNA damage repair genes are potential biomarkers for predicting prognosis and immunotherapy effectiveness in colon cancer patients. *Front Genet* (2022) 13:918159. doi: 10.3389/fgene.2022.918159

6. Huang L, Zhu J, Kong W, Li P, Zhu S. Expression and prognostic characteristics of m6A RNA methylation regulators in colon cancer. *Int J Mol Sci* (2021) 22(4):2134. doi: 10.3390/ijms22042134

7. Yuan S, Gao Y, Xia Y, Wang Z, Wang X. DNA Methylation regulator-mediated modification pattern defines tumor microenvironment immune infiltration landscape in colon cancer. *Front Genet* (2022) 13:1008644. doi: 10.3389/fgene.2022.1008644

8. Mouradov D, Domingo E, Gibbs P, Jorissen RN, Li S, Soo PY, et al. Survival in stage II/III colorectal cancer is independently predicted by chromosomal and

microsatellite instability, but not by specific driver mutations. *Am J Gastroenterol* (2013) 108:1785–93. doi: 10.1038/ajg.2013.292

9. Koberle B, Schoch S. Platinum complexes in colorectal cancer and other solid tumors. *Cancers (Basel)* (2021) 13(9):2073. doi: 10.3390/cancers13092073

10. Guinney J, Dienstmann R, Wang X, de Reynies A, Schlicker A, Soneson C, et al. The consensus molecular subtypes of colorectal cancer. *Nat Med* (2015) 21:1350–6. doi: 10.1038/nm.3967

11. Isella C, Brundu F, Bellomo SE, Galimi F, Zanella E, Porporato R, et al. Selective analysis of cancer-cell intrinsic transcriptional traits defines novel clinically relevant subtypes of colorectal cancer. *Nat Commun* (2017) 8:15107. doi: 10.1038/ncomms15107

12. Hanahan D, Weinberg RA. Hallmarks of cancer: the next generation. *Cell* (2011) 144:646–74. doi: 10.1016/j.cell.2011.02.013

13. Hector S, Prehn JH. Apoptosis signaling proteins as prognostic biomarkers in colorectal cancer: A review. *Biochim Biophys Acta* (2009) 1795:117–29. doi: 10.1016/j.bbcan.2008.12.002

14. Subramanian A, Narayan R, Corsello SM, Peck DD, Natoli TE, Lu X, et al. A next generation connectivity map: L1000 platform and the first 1,000,000 profiles. *Cell* (2017) 171:1437–52.e17. doi: 10.1016/j.cell.2017.10.049

15. Chatsirisupachai K, Lesluyes T, Paraoan L, Van Loo P, de Magalhaes JP. An integrative analysis of the age-associated multi-omic landscape across cancers. *Nat Commun* (2021) 12:2345. doi: 10.1038/s41467-021-22560-y

16. Baretti M, Le DT. DNA Mismatch repair in cancer. *Pharmacol Ther* (2018) 189:45–62. doi: 10.1016/j.pharmthera.2018.04.004

17. De Smedt L, Lemahieu J, Palmans S, Govaere O, Tousseyn T, Van Cutsem E, et al. Microsatellite instable vs stable colon carcinomas: analysis of tumour heterogeneity, inflammation and angiogenesis. *Br J Cancer* (2015) 113:500–9. doi: 10.1038/bjc.2015.213

18. Mandal R, Samstein RM, Lee KW, Havel JJ, Wang H, Krishna C, et al. Genetic diversity of tumors with mismatch repair deficiency influences anti-PD-1 immunotherapy response. *Science* (2019) 364:485–91. doi: 10.1126/science.aau0447

19. Llosa NJ, Cruise M, Tam A, Wicks EC, Hechenbleikner EM, Taube JM, et al. The vigorous immune microenvironment of microsatellite instable colon cancer is balanced by multiple counter-inhibitory checkpoints. *Cancer Discov* (2015) 5:43–51. doi: 10.1158/2159-8290.CD-14-0863

20. Asaoka Y, Ijichi H, Koike K. PD-1 blockade in tumors with mismatch-repair deficiency. *N Engl J Med* (2015) 373:1979. doi: 10.1056/NEJMc1510353

21. Zhang W, Sartori MA, Makhnevych T, Federowicz KE, Dong X, Liu L, et al. Generation and validation of intracellular ubiquitin variant inhibitors for USP7 and USP10. *J Mol Biol* (2017) 429:3546–60. doi: 10.1016/j.jmb.2017.05.025

22. Wang W, Li M, Ponnusamy S, Chi Y, Xue J, Fahmy B, et al. ABL1-dependent OTULIN phosphorylation promotes genotoxic wnt/beta-catenin activation to enhance drug resistance in breast cancers. *Nat Commun* (2020) 11:3965. doi: 10.1038/s41467-020-17770-9

23. Eberl M, Mangelberger D, Swanson JB, Verhaegen ME, Harms PW, Frohm ML, et al. Tumor architecture and notch signaling modulate drug response in basal cell carcinoma. *Cancer Cell* (2018) 33:229–43.e4. doi: 10.1016/j.ccell.2017.12.015

24. Stanton MJ, Dutta S, Zhang H, Polavaram NS, Leontovich AA, Honscheid P, et al. Autophagy control by the VEGF-C/NRP-2 axis in cancer and its implication for treatment resistance. *Cancer Res* (2013) 73:160–71. doi: 10.1158/0008-5472.CAN-11-3635

25. Rosenthal R, Cadieux EL, Salgado R, Bakir MA, Moore DA, Hiley CT, et al. And XXXT. *R consortium Neoantigen-directed Immune escape Lung Cancer evolution Nat* (2019) 567:479–85. doi: 10.1038/s41586-019-1032-7

26. Chen DS, Mellman I. Elements of cancer immunity and the cancer-immune set point. *Nature* (2017) 541:321–30. doi: 10.1038/nature21349

27. McGranahan N, Burrell RA, Endesfelder D, Novelli MR, Swanton C. Cancer chromosomal instability: Therapeutic and diagnostic challenges. *EMBO Rep* (2012) 13:528–38. doi: 10.1038/embor.2012.61

28. Schulz M, Salamero-Boix A, Niesel K, Alekseeva T, Sevenich L. Microenvironmental regulation of tumor progression and therapeutic response in brain metastasis. *Front Immunol* (2019) 10:1713. doi: 10.3389/fimmu.2019.01713

29. Ali HR, Chlon L, Pharoah PD, Markowetz F, Caldas C. Patterns of immune infiltration in breast cancer and their clinical implications: A gene-Expression-Based retrospective study. *PLoS Med* (2016) 13:e1002194. doi: 10.1371/journal.pmed.1002194

30. Ford JH. Saturated fatty acid metabolism is key link between cell division, cancer, and senescence in cellular and whole organism aging. *Age (Dordr)* (2010) 32:231–7. doi: 10.1007/s11357-009-9128-x

31. Vazquez F, Lim JH, Chim H, Bhalla K, Girnun G, Pierce K, et al. PGC1alpha expression defines a subset of human melanoma tumors with increased mitochondrial capacity and resistance to oxidative stress. *Cancer Cell* (2013) 23:287–301. doi: 10.1016/j.ccr.2012.11.020

32. Haq R, Shoag J, Andreu-Perez P, Yokoyama S, Edelman H, Rowe GC, et al. Oncogenic BRAF regulates oxidative metabolism *via* PGC1alpha and MITF. *Cancer Cell* (2013) 23:302–15. doi: 10.1016/j.ccr.2013.02.003

33. Wu M, Kim KY, Park WC, Ryu HS, Choi SC, Kim MS, et al. Enhanced expression of GABRD predicts poor prognosis in patients with colon adenocarcinoma. *Transl Oncol* (2020) 13:100861. doi: 10.1016/j.tranon.2020.100861

frontiers | Frontiers in Immunology

TYPE Original Research
PUBLISHED 14 April 2023
DOI 10.3389/fimmu.2023.1163136

OPEN ACCESS

EDITED BY
Chi Chun Wong,
The Chinese University of Hong Kong, China

REVIEWED BY
Lucia De Monte,
San Raffaele Hospital (IRCCS), Italy
Christian Klein,
Roche Innovation Center Zurich, Switzerland

*CORRESPONDENCE
Helmut R. Salih
helmut.salih@med.uni-tuebingen.de

SPECIALTY SECTION
This article was submitted to Cancer Immunity and Immunotherapy, a section of the journal Frontiers in Immunology

RECEIVED 10 February 2023
ACCEPTED 30 March 2023
PUBLISHED 14 April 2023

CITATION
Lutz MS, Zekri L, Weßling L, Berchtold S, Heitmann JS, Lauer UM, Jung G and Salih HR (2023) IgG-based B7-H3xCD3 bispecific antibody for treatment of pancreatic, hepatic and gastric cancer. *Front. Immunol.* 14:1163136. doi: 10.3389/fimmu.2023.1163136

IgG-based B7-H3xCD3 bispecific antibody for treatment of pancreatic, hepatic and gastric cancer

Martina S. Lutz[1,2], Latifa Zekri[1,2,3], Laura Weßling[1,2], Susanne Berchtold[2,4,5], Jonas S. Heitmann[1,2], Ulrich M. Lauer[2,4,5], Gundram Jung[2,3] and Helmut R. Salih[1,2]*

[1]Department of Internal Medicine, Clinical Collaboration Unit Translational Immunology, German Cancer Consortium (DKTK), University Hospital Tuebingen, Tuebingen, Germany, [2]Cluster of Excellence iFIT (EXC 2180) "Image-Guided and Functionally Instructed Tumor Therapies", University of Tuebingen, Tuebingen, Germany, [3]Department of Immunology, Eberhard Karls Universität Tübingen, Tuebingen, Germany, [4]Department of Internal Medicine VIII, Medical Oncology & Pneumology, University Hospital Tübingen, Tuebingen, Germany, [5]German Cancer Research Center (DKFZ), German Cancer Consortium (DKTK), Tübingen, Germany

T cell-based immunotherapy has significantly improved treatment options for many malignancies. However, despite these and other therapeutic improvements over the last decades, gastrointestinal cancers, in particular pancreatic, hepatic and gastric cancer, are still characterized by high relapse rates and dismal prognosis, with an accordingly high unmet medical need for novel treatment strategies. We here report on the preclinical characterization of a novel bispecific antibody in an IgG-based format termed CC-3 with B7-H3xCD3 specificity. In many cancer entities including pancreatic, hepatic and gastric cancers, B7-H3 (CD276) is overexpressed on tumor cells and also on the tumor vasculature, the latter allowing for improved access of immune effector cells into the tumor site upon therapeutic targeting. We demonstrate that CC-3 induces profound T cell reactivity against various pancreatic, hepatic and gastric cancer cell lines as revealed by analysis of activation, degranulation and secretion of IL2, IFNγ as well as perforin, resulting in potent target cell lysis. Moreover, CC-3 induced efficient T cell proliferation and formation of T cell memory subsets. Together, our results emphasize the potential of CC-3, which is presently being GMP-produced to enable clinical evaluation for treatment of pancreatic, hepatic and gastric cancer.

KEYWORDS

immunotherapy, pancreatic cancer, hepatic cancer, gastric cancer, B7-H3 (CD276), CD3, bispecific antibody, gastrointestinal cancer

Abbreviations: 7-AAD, 7-aminoactinomycin D; bsAb, bispecific antibody; BSA, Bovine Serum Albumin; CAR, chimeric antigen receptor; CD, cluster of differentiation; DAPI, 4,6-Diamidin-2-phenylindol; E:T, effector to target; EU, endotoxin; GI, gastrointestinal; ICI, immune checkpoint inhibition; IFNγ, Interferon γ; IgG1, Immunglobulin G1; mAb, monoclonal antibody; MFI, mean fluorescence intensity; PFA, paraformaldehyde; PBMC, peripheral blood mononuclear cell; PE, phycoerythrin; SD, standard deviation.

Introduction

Malignancies of the gastrointestinal tract belong to the most prevalent cancers, accounting for 26% of global cancer incidence and 35% of all cancer-related deaths (1). Current treatment strategies include chemotherapy, surgery, radiotherapy and targeted therapies. Despite therapeutic improvements over the last decades, among others due to incorporation of antibody-based approaches like monoclonal antibodies (mAbs) targeting e.g. HER2 or VEGF (2, 3), the still high relapse rates and dismal prognosis underline the high medical need for new therapeutic strategies.

In the last decade, immunotherapeutic approaches to mobilize T cells against tumor cells have significantly improved oncological treatment options. In particular, immune checkpoint inhibition (ICI) has become a mainstay of treatment in many solid tumor entities (4, 5). However, long-term remissions are still rare and many patients do not respond to treatment. Chimeric antigen receptor (CAR) T cell therapy and bispecific antibodies (bsAbs) have shown remarkable success in the treatment of hematological malignancies (6, 7) but are so far not effective in solid tumors.

B7-H3 (CD276) is a type I transmembrane protein belonging to the B7 family of immune checkpoint proteins (8). Due to rather specific expression on a wide array of cancer entities, B7-H3 presently receives high interest as target for immunotherapeutic approaches (9, 10). Notably, B7-H3 is not only expressed on tumor cells but also on the tumor vasculature (11). The latter may facilitate improved access of immune effector cells to solid tumors upon therapeutic targeting, thereby overcoming the lacking access of immune effector cells to the tumor site, a major obstacle for T cell-based immunotherapy of solid tumors. Based on previous work including development of bsAbs with FLT3xCD3 (12) and PSMAxCD3 (13, 14) specificity until the stage of clinical evaluation (NCT05143996, NCT04104607 and NCT04496674), we here preclinically evaluated a B7-H3xCD3 bsAb termed CC-3, which is presently undergoing GMP production, for treatment of pancreatic, hepatic und gastric cancer.

Materials and methods

Production and purification of bispecific antibodies

B7-H3xCD3 and its isotype control MOPCxCD3 were generated as described previously (13). In brief, the constructs were produced in ExpiCHO cells (Gibco, Carlsbad, CA, USA) and purified from culture supernatant by affinity chromatography on Mabselect affinity columns (GE Healthcare, Munich, Germany) followed by analytical and preparative size exclusion chromatography using Superdex S200 Increase 10/300GL and HiLoad 16/60 columns (GE Healthcare). Endotoxin levels were measured with EndoZyme II (BioMerieux, Marcy-l'Étoile, France) according to the manufacturer's instructions and < 0.5 EU/ml.

Cells

All cell lines were from ATCC (American Type Culture Collection) and were selected to best reflect the respective cancer entities. Hep3B and SNU387 represent hepatocellular carcinoma, the most common form of liver cancer. The pancreatic cancer cell lines were derived from adenocarcinomas, the most common type of pancreatic cancer. Of these, PANC-1 cells represent pancreatic ductal carcinoma, the most common subtype of pancreatic adenocarcinoma. Adenocarcnimoa also is the most common type of gastric cancer, with NCI-N87 and MKN-45 cells representing well differentiated Lauren intestinal-type gastric adenocarcinoma and poorly differentiated Lauren diffuse-type gastric adenocarcinoma, respectively. Cells were tested routinely for mycoplasma contamination every three months. Authenticity was determined on a regular basis by validating the respective immunophenotype described by the provider using flow cytometry. Peripheral Blood Mononuclear cells (PBMC) of healthy donors were isolated by density gradient centrifugation (Biocoll; Biochrom, Berlin, Germany), and monocytes within the PBMC were depleted for coculture experiments using human CD14 MicroBeads UltraPure kit (Miltenyi Biotec, Bergisch Gladbach, Germany). Where indicated, T cells within PBMC were isolated by using either Pan T cell Isolation Kit, human CD4 Micro Beads or human CD8 Micro Beads (Miltenyi Biotec).

Relative gene expression of CD276 based on TCGA database analysis

Data on relative CD276 expression in tumor tissue of pancreatic, hepatic and gastric cancer patients was obtained from the Cancer Genome Atlas (TCGA) database and the GTEx project utilizing the Gene Expression Profiling Interactive Analysis (GEPIA) web server as described previously. The datasets PAAD LIHC and STAD were downloaded from TCGA (http://www.oncolnc.org/) and analyzed using the online web server GEPIA (http://gepia.cancer-pku.cn/).

Immunofluorescence

Tumor cells were incubated with monocyte-depleted PBMC of healthy donors (E:T 4:1), treated for 3 h and subsequently fixed in 4% paraformaldehyde (PFA) in PBS for 10 min at -20°C. Cells were then blocked using 5% BSA, 0.2% Triton X-100, 0.1% Tween for 60 min, washed three times with PBST (PBS + 0.1% Tween20) and stained using a rabbit anti-human-α-Tubulin antibody (clone 11H10, Cell Signaling, Denvers, MA) and a murine anti-human-Perforin antibody (clone δG9, BD Pharmingen, Heidelberg, Germany), followed by an Alexa-Fluor 488 labelled anti-mouse and Alexa-Fluor 594 labelled anti-rabbit antibody (Invitrogen, Waltham, MA). Slides were mounted in fluorescent mounting medium; DAPI was used for counter-staining. Pictures were

acquired using a Zeiss 800 inverse laser scanning microscope (Zeiss, Oberkochen, Germany) and images were processed using ImageJ (15).

Flow cytometry

For analysis of B7-H3 surface expression and B7-H3xCD3 binding, cells were stained with a parental murine B7-H3 antibody (10 µg/mL) carrying the same B7-H3 binding clone as our construct (7C4), B-H3xCD3 or the corresponding isotype controls followed by a goat anti-mouse-PE conjugate (Dako, Glostrup, Denmark) or a donkey anti-human-PE conjugate (Jackson ImmunoResearch, West Grove, USA), respectively. T cell activation, degranulation and proliferation were determined using CD69-PE, CD107a-PE (BD Pharmingen) as well as CD4-APC, CD8-FITC, CD62L-PB and CD45ro-PeCy7 (BioLegend, San Diego, CA) fluorescence conjugates. For flow cytometric analysis of target cell lysis, tumor cells were loaded with 2.5 µM CellTrace™ Violet (Thermo Fisher Scientific, Waltham, MA) and cultured with monocyte-depleted PBMC (E:T 4:1) in the presence or absence of B7-H3xCD3 or MOPCxCD3 (1 nM each). Standard calibration beads (Sigma-Aldrich, St. Louis, MO) were used to ensure analysis of equal assay volumes and to account for the number of target cells that had vanished from the culture. 7AAD (Biolegend) was used for live- and dead-cell discrimination. Measurements were performed using a FACS Canto II or FACS Fortessa (BD Biosciences, San Diego, CA) and data was analyzed using the software FlowJo (FlowJo LCC, Ashland, OR).

T cell activation and degranulation assays

To determine activation and degranulation in the presence of target cells, tumor cells were cultured with monocyte-depleted PBMC of healthy donors (E:T 4:1) in the presence or absence of B7-H3xCD3 or MOPCxCD3 (1 nM each). For analysis of T cell activation, CD69 expression was determined after 24 h. To compare activation of T cells within PBMC preparations to isolated T cell subpopulations in the absence of target cells, 1 µg/ml recombinant human B7-H3 was coated on 96-well plates overnight. Subsequently, PBMC preparations or isolated T cells and MOPCxCD3 or B7-H3xCD3 (5 nM each) were added, incubated for 72 h and analyzed by flow cytometry for CD69 expression. To analyze T cell degranulation, cells were cultured for 4 h in the presence of CD107a-PE (1:25), BD GolgiStop and BD GolgiPlug (1:1000, both BD Biosciences). Analysis was conducted using flow cytometry.

T cell proliferation assays

For long-term proliferation assays, monocyte-depleted PBMC were loaded with 2.5 µM CellTrace™ Violet cell proliferation dye (Thermo Fisher Scientific) and incubated with tumor cells (E:T 4:1) and the indicated bsAbs (1 nM each). On day 3, cells were reincubated with fresh target cells and treatment was repeated. On day 6, proliferation of $CD4^+$ and $CD8^+$ T cells was analyzed by flow cytometry. For T cell subset analysis, PBMC were incubated with tumor cells (E:T 1:1) and the indicated bsAbs (1 nM each). On day 3, cells were reincubated with fresh target cells and treatment. On day 6, T cell subsets were determined by flow cytometric analysis for expression of CD4, CD8, CD45ro and CD62L.

Analysis of cytokine secretion

Monocyte-depleted PBMC of healthy donors were cultured with tumor cells (E:T ratio 4:1) in the presence or absence of bsAb or control (1 nM each). After 24 h, supernatants were collected and analyzed for IL-2, IFNγ, IL-10 and TNF using Legendplex assays (BioLegend).

Cytotoxicity assays

Monocyte-depleted PBMC of healthy donors were cultured with tumor cells (E:T ratio 4:1) in the presence or absence of bsAb or control (1 nM each). Real-time cytotoxicity analysis was conducted using the xCELLigence RTCA system (Roche Applied Science, Penzberg, Germany).

Statistics

If not otherwise indicated, values depict means ± standard deviation (SD). Student's t test, Mann-Whitney U test, one-way ANOVA and Friedman's test was used for continuous variables. If significant differences by ANOVA were found, group wise comparison was done (Tukey's multiple comparison test). If significant differences were found by Friedman's test, Dunn's multiple comparisons test was used. All statistical tests were considered statistically significant when p was below 0.05. Statistical analysis was performed using GraphPadPrism (v.8.1.0).

Results

Characterization of B7-H3 expression and binding of the B7-H3xCD3 bsAb CC-3 in pancreatic, hepatic and gastric cancer cell lines

As a first step, B7-H3 mRNA expression was studied by analysis of TCGA data sets of 178 pancreatic adenocarcinomas, 368 hepatocellular carcinomas and 408 gastric adenocarcinomas. Highest mRNA expression was observed in pancreatic adenocarcinoma, followed by gastric adenocarcinoma and hepatocellular carcinomas (Figure 1A). Next we characterized whether and to what extent B7-H3 was expressed on the surface of pancreatic, hepatic and gastric cancer cell lines. To this end we used the B7-H3 monoclonal antibody clone 7C4 that also served as

10.3389/fimmu.2023.1163136

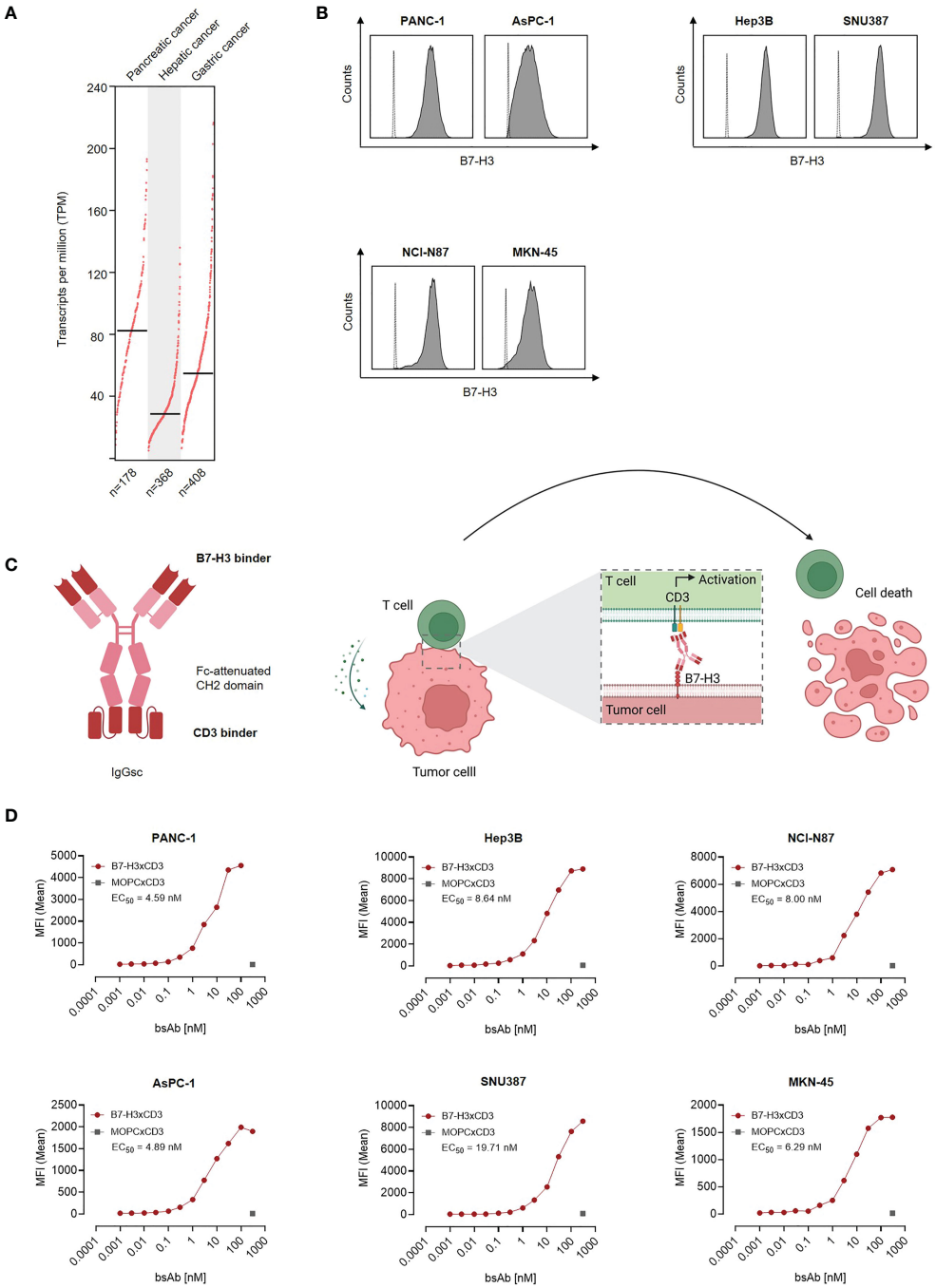

FIGURE 1
Characterization of B7-H3 expression and binding of CC-3 in gastrointestinal cancer cell lines. **(A)** CD276 gene expression profile in pancreatic, hepatic and gastric cancer was analyzed using the online web server GEPIA. **(B)** The indicated cancer cell lines were stained using a murine monoclonal B7-H3 antibody (clone 7C4) followed by an anti-mouse PE conjugate and analyzed using flow cytometry. B7-H3 expression on pancreatic cell lines AsPC-1 and PANC-1, hepatic cell lines Hep3B and SNU-387 and gastric cell lines MKN-45 and NCI-N87 is shown (shaded peaks, anti-B7H3; open peaks, control). **(C)** Schematic illustration and mechanism of action of the B7-H3xCD3 bsAb CC-3. The graphic was created by BioRender (BioRender.com, Toronto, Canada). **(D)** The indicated tumor cells were incubated with increasing concentrations of CC-3 or the respective isotype control MOPCxCD3, followed by an anti-human PE conjugate. Binding of the constructs to the indicated cell lines was analyzed by flow cytometry. MFI, mean fluorescence intensities.

target binder in our B7-H3xCD3 bsAb. Flow cytometric analysis revealed substantial B7-H3 expression in all tested cell lines (Figure 1B). Next we studied binding of our B7-H3xCD3 bsAb CC-3, which contains the variable domain of 7C4 cloned into our previously described IgGsc bsAb format (13), with the single chain sequence of UCHT-1 carrying four mutations in the CDR-H2 and one mutation in the FR-H3 resulting in reduced affinity to CD3 (clone M18) as effector part (Figure 1C) (16). Binding titration experiments using the indicated pancreatic, hepatic and gastric cell lines revealed EC_{50} values between 4.59 nM and 19.71 nM

(Figure 1D), whereas no unspecific binding to B7-H3-negative cells was observed (Figures S1A, B).

Induction of T cell activation

Next, we determined the capacity of CC-3 to induce T cell reactivity against pancreatic, hepatic and gastric cancer cell lines. PBMC of healthy donors were depleted of monocytes that can express substantial levels of B7-H3 upon activation (8, 9) and cultured with the indicated target cells in the presence or absence of increasing concentrations of CC-3 or the isotype control MOPCxCD3. Flow cytometric analysis of CD69 expression revealed maximal activation of $CD4^+$ and $CD8^+$ T cells with CC-3 concentrations as low as 1 nM CC-3 (Figure 2A). Use of the above described PBMC preparations and analysis of the effects of CC-3 on T cells therein served to most closely reflect the physiological situation in patients, where other components of the blood may influence bsAb-induced T cell immunity (17, 18). Analyses evaluating the effect of immobilized CC-3 or isotype control in the absence of tumor targets revealed comparable activation of T cells within PBMC preparations and isolated T cells and excluded potential confounders by the tumor cells. (Figure S2). Analysis of T cell degranulation as determined by analysis of CD107a expression confirmed that CC-3 potently stimulated T cells with maximum effects observed already with doses of 1nM (Figure 2B). No effects were observed when the isotype control MOPCxCD3 or the B7-H3 negative HL-60 cells as targets were used, confirming strictly target antigen-restricted activity of our construct (Figures 2A, B; S1C, D). In line, analysis of culture supernatants by Legendplex assays showed a significant increase in IL-2, IFNγ, IL-10 and TNF secretion after treatment with 1 nM CC-3, but not with the isotype control or when target antigen negative tumor cells were used (Figures 2C, D; S1E, S3). When we used immunofluorescence staining to visualize induction of T cell reactivity against target cells, a significantly higher number of Perforin positive cells within the coculture was observed in samples treated with CC-3 compared to untreated samples. No effect was observed with the isotype control, again confirming target cell restricted activity of our bsAb CC-3 (Figures 3A–C; S4).

Induction of T cell proliferation

As induction of T cell proliferation is an important prerequisite to combat high tumor burden, we next labelled PBMC using CellTrace™ Violet and analyzed induction of $CD4^+$ and $CD8^+$ T cell counts (Figures 4A–C) and cell dye dilution (Figure S5) in cocultures with gastric, hepatic and pancreatic tumor cells upon treatment with 1 nM of CC-3 using flow cytometry. We observed profound T cell proliferation and significantly increased T cell counts in samples treated with CC-3, but not upon application of isotype control or when target cells were negative for B7-H3 (Figures 4A; S1F). As memory T cells constitute the subset most relevant for therapeutic success (19, 20), we next analyzed which T cell subsets were proliferating and found that CC-3 preferentially induced expansion of effector memory and central memory T cells in a target cell restricted manner (Figures 4B, C; Figure S1G).

Induction of target cell lysis

Finally, we analyzed whether induction of T cell activation and proliferation by CC-3 treatment were mirrored by a corresponding effect regarding lysis of pancreatic, hepatic and gastric tumor cells. PBMC were cocultured with target cells and treated with CC-3 or isotype control (1 nM). Flow cytometry-based lysis assays revealed significant induction of cytotoxicity against pancreatic, hepatic and gastric tumor cells by CC-3 after 72 h. Again, isotype control had no effect, and analyses with the B7-H3xCD3 negative HL-60 cells confirmed target antigen-specific efficacy (Figures 5A; S1H, S6). Notably, analyses using the xCELLigence system confirmed the ability of CC-3 to mediate target efficacy of CC-3 over extended time periods, which indicates that CC-3 may induce sustained anti-tumor efficacy (Figure 5B).

Discussion

Although therapeutic options for solid tumors have overall improved over the last decades, treatment of gastrointestinal cancers remains still challenging. Several small molecule inhibitors have been approved by the US Food and Drug Administration (FDA) as therapeutic option for hepatic, gastric and pancreatic cancer, but the benefit of these therapies is limited (21–25). Antibody-based approaches targeting angiogenesis-(e.g., Ramucirumab) or oncogenic signaling pathways (e.g., EGF Cetuximab or HER2 Trastuzumab) likewise show only limited benefit. T cell based-immunotherapy, especially ICI, which has revolutionized oncological treatment e.g. of lung and skin cancer, has also been evaluated for treatment of metastasized GI cancer, but except for the small group with microsatellite instability, achieves only limited efficacy (26–31). Especially in pancreatic cancer, ICI is far from being sufficiently effective, in large part likely due to an immunosuppressive tumor microenvironment (32). Moreover, the dense extracellular matrix of pancreatic cancer may act as physical barrier that prevents tumor infiltration by T and B lymphocytes (33). So far, limited evidence is available that ICI may be effective in some patients with hepatocellular carcinoma, but a reliable predictor for treatment response, e.g. characteristics of the tumor environment, has not been identified yet (34). Overall, new therapeutic concepts to improve treatment options of GI cancer patients are urgently needed. In the present study, we report on the preclinical characterization of a bsAb targeting B7-H3 and CD3 for treatment of gastric, hepatic and pancreatic cancer.

Compared to ICI, bsAbs and CAR T cells induce T cell antitumor immunity in a more targeted manner. Other than CAR T cells, bsAbs constitute readily available 'off the shelf' reagents, avoiding the delay of treatment that is required for the production of CAR T cells and contributes to their vast costs upon clinical application. CAR T cells and bsAbs share the shortcoming that their therapeutic success so far is limited to hematologic malignancies.

10.3389/fimmu.2023.1163136

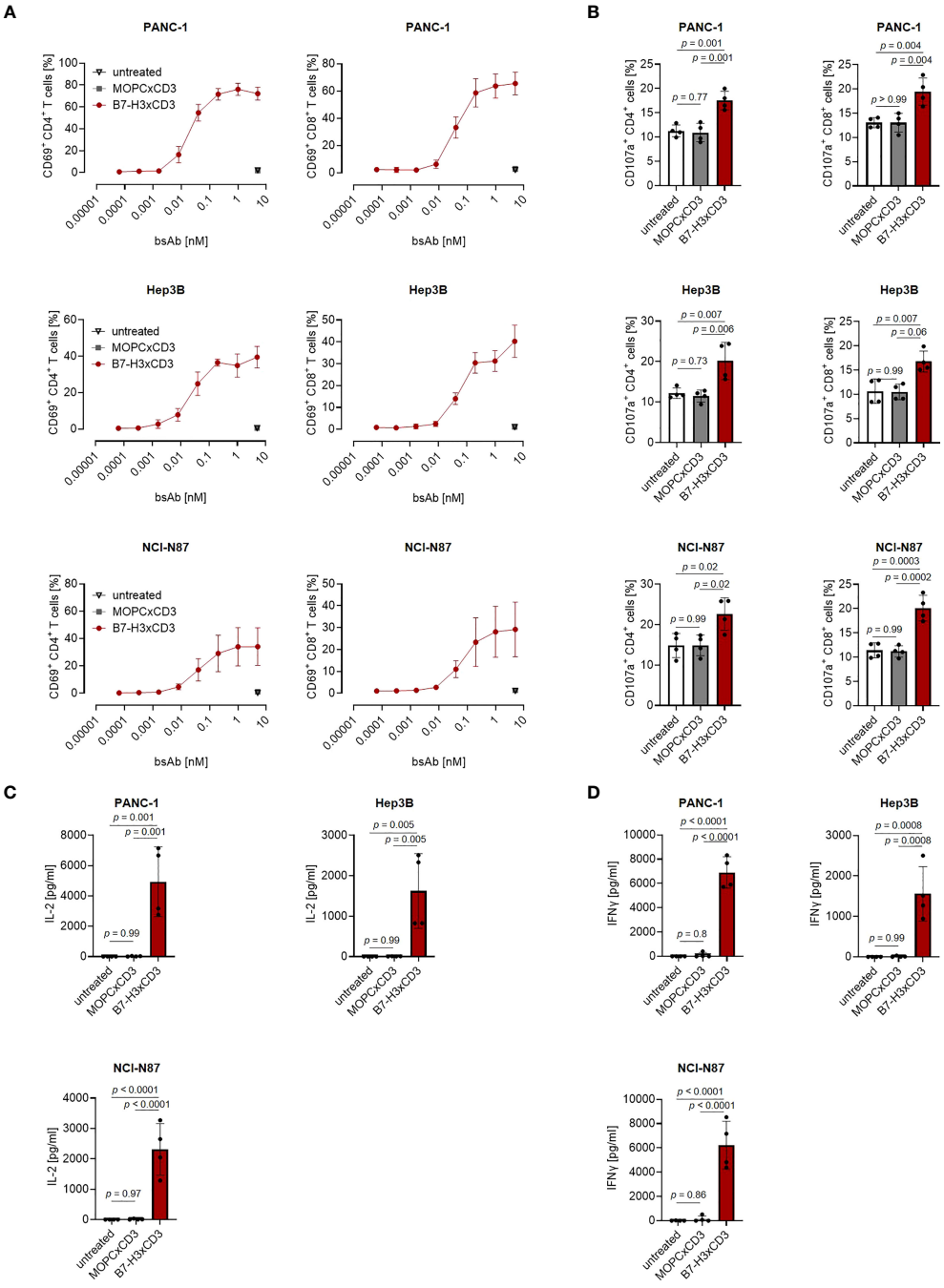

FIGURE 2
Induction of T cell activation against gastrointestinal cancer cell lines by CC-3. Monocyte-depleted PBMC of healthy donors were incubated with the indicated tumor cell lines (E:T 4:1) in the presence or absence of CC-3 or MOPCxCD3. If not stated otherwise, all constructs were used at 1 nM. **(A)** Activation of CD4+ and CD8+ T cells was determined by flow cytometric analysis for CD69 expression after 24 hours. Combined data obtained with PBMC of three independent donors are shown. **(B)** Degranulation of CD4+ and CD8+ T cells was determined by expression of CD107a after 4 h. Combined data obtained with PBMC of four independent donors are shown. **(C)** IL-2 and **(D)** IFNγ levels in culture supernatants were measured after 24 h using LEGENDplex assays. Combined data obtained with PBMC of four independent donors are shown. E:T, effector to target; PBMC, peripheral blood mononuclear cell.

The reasons are not yet fully understood, but limited access of T cells to the tumor site appears to constitute a major obstacle (35, 36). In our view, targeting both tumor cells and tumor vessels thus seems critical, the latter allowing for sufficient influx of immune cells to the tumor site across a damaged or inflamed endothelial barrier. This reasoning is supported by reports demonstrating that even high numbers of tumor-specific T cells fail to induce sufficient antitumor responses unless a proinflammatory tumor environment has been generated (37, 38).

B7-H3 has attracted considerable interest as promising target for cancer immunotherapy because it is not only overexpressed on tumor cells in various types of cancer including GI cancer (9, 39,

40), but also on tumor-associated endothelial and stromal cells (41, 42). High expression of B7-H3 on tumor tissue is associated with poor clinical outcome and lymph node metastasis (43), and several studies report first evidence that B7-H3 positive tumor cell fractions may be enriched for cancer stem cells (44–46). In addition, B7-H3 is reported to act as coinhibitory receptor in the B7-CD28 pathway, suppressing T cell antitumor immunity (47–49). Specifically in pancreatic cancer, B7-H3 was reported to promote tumor progression, and its inhibition reduced cancer metastasis *in vivo* (39). In hepatocellular carcinoma, high B7-H3 expression was associated with adverse clinicopathologic features and poor outcome (50). Another study demonstrated that B7-H3 promotes gastric cancer cell migration and invasion (51). We have recently reported on the preclinical characterization of an optimized B7-H3xCD3 bsAb and showed that targeting a membrane-proximal B7-H3 epitope allows for reduction of CD3 affinity while maintaining therapeutic efficacy. In analyses with colorectal cancer cells, our lead compound CC-3 demonstrated superior tumor cell killing, T cell activation, proliferation, and memory formation, while undesired cytokine release was reduced (16). Based on these characteristics and the aforementioned data on the expression and pathophysiological involvement of B7-H3 we

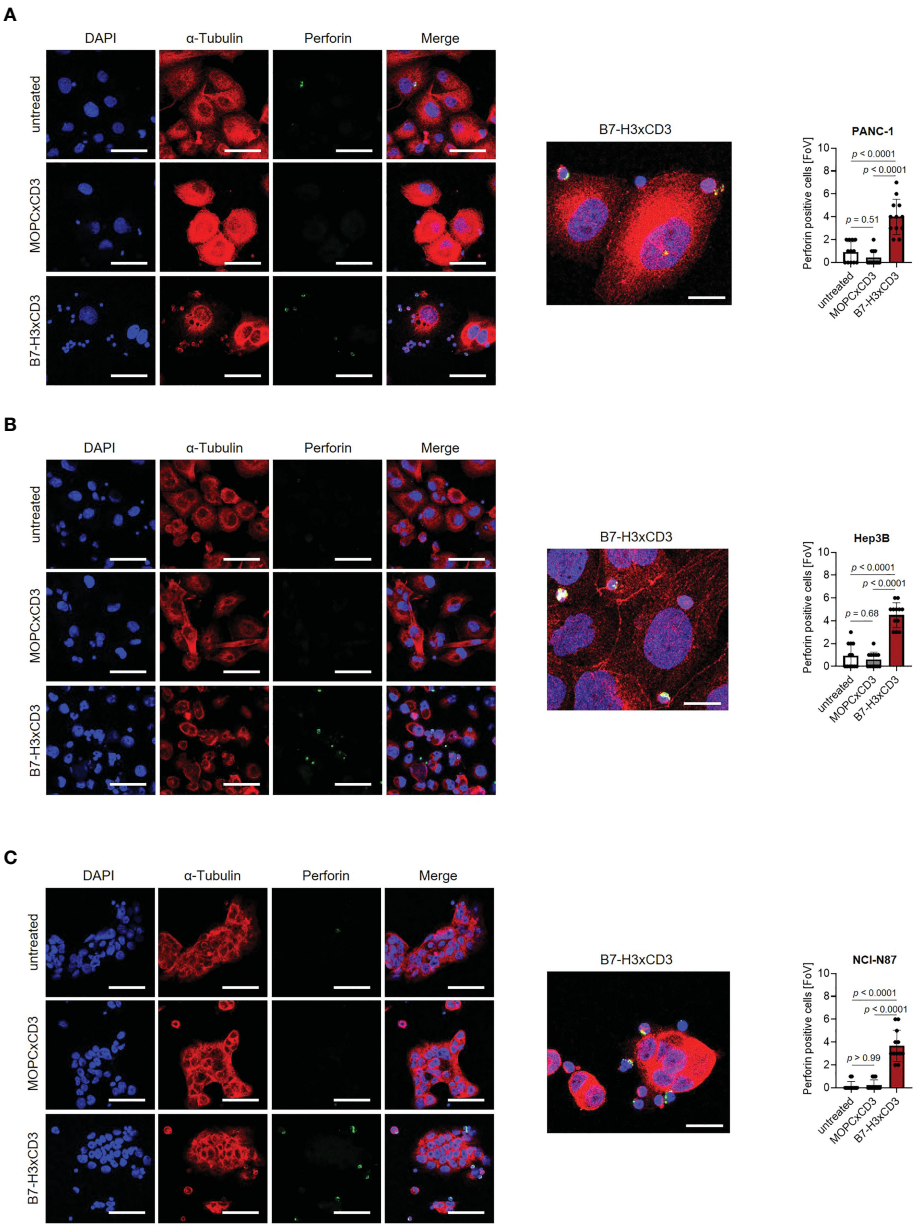

FIGURE 3
Induction of Perforin by CC-3. Monocyte-depleted PBMC of healthy donors were incubated with target cells (E:T 4:1) in the presence or absence of CC-3 or MOPCxCD3 (1 nM each) for 3 hours and subsequently stained for Perforin (green) and α-Tubulin (red). DAPI was used for counterstaining. Scale bars of left panels indicate 50 µM, original magnification x40. Scale bar of exemplary immunofluorescence staining indicates 20 µm, original magnification x63. Perforin positive cells were quantified per FoV (n=12) out of three independent experiments. Results obtained with **(A)** PANC-1, **(B)** Hep3B and **(C)** NCI-N87 cells are shown. DAPI, 4′,6-diamidino-2-phenylindole; E:T, effector to target; FoV, field of view.

10.3389/fimmu.2023.1163136

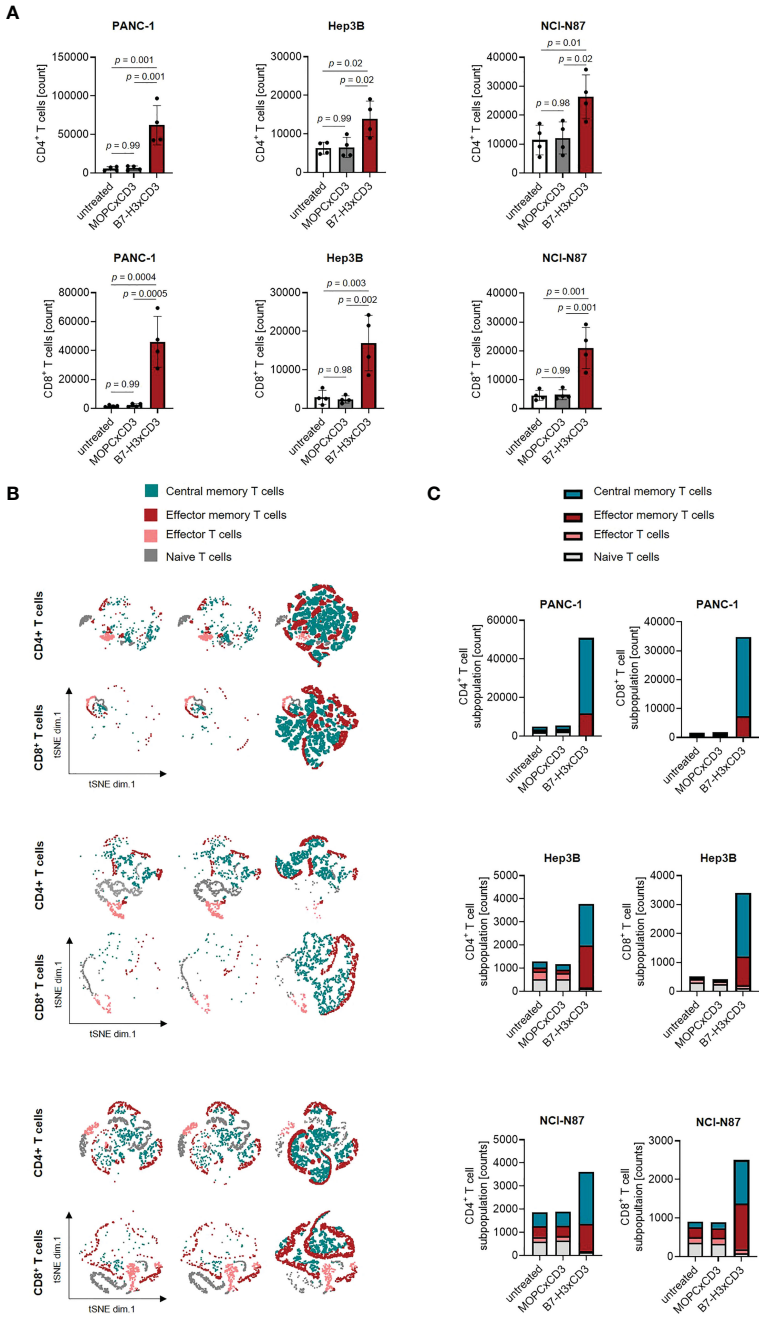

FIGURE 4
Induction of T cell proliferation and memory T cell populations by CC-3. **(A)** Monocyte-depleted PBMC of healthy donors (n=4) were labelled with CellTrace™ Violet cell dye and incubated with or without MOPCxCD3 or CC-3 (1 nM each) in the presence of PANC-1, Hep3B, or NCI-N87 cells (E:T 4:1). After 72 h, PBMC were reexposed to fresh target cells and the respective treatment for additional 72 h. On day 6, proliferation was determined by flow cytometry. **(B, C)** PBMC of healthy donors (n=5) were incubated with or without MOPCxCD3 or CC-3 (1 nM each) in the presence of PANC-1, Hep3B, or NCI-N87 cells (E:T 1:1). After 72 h, cells were reexposed to fresh target cells and the respective treatment. On day 6, subpopulations of $CD4^+$ and $CD8^+$ T cells were determined by flow cytometric analysis. Effector T cells were defined as $CD62L^-CD45ro^-$, naive T cells as $CD62L^+CD45ro^-$, effector memory T cells as $CD62L^-CD45ro^+$ and central memory T cells as $CD62L^+CD45ro^+$. **(B)** representative t-distributed stochastic neighbor embedding (tSNE) plots and **(C)** pooled data are shown. E:T, effector to target. PBMC, peripheral blood mononuclear cell.

reasoned that CC-3 would also constitute a promising compound for other gastrointestinal cancer entities. Initial flow cytometric analyses revealed that indeed high B7-H3 levels were expressed in all tested pancreatic, hepatic and gastric cancer cell lines, confirming suitability as therapeutic target. Subsequent functional characterization documented strong induction of T cell activation, degranulation and secretion of the “antitumor cytokines” like IFNγ and IL-2 as well as potent induction of tumor cell lysis. In addition, we could demonstrate that CC-3 potently induces T cell proliferation, which is a critical prerequisite to enable treatment

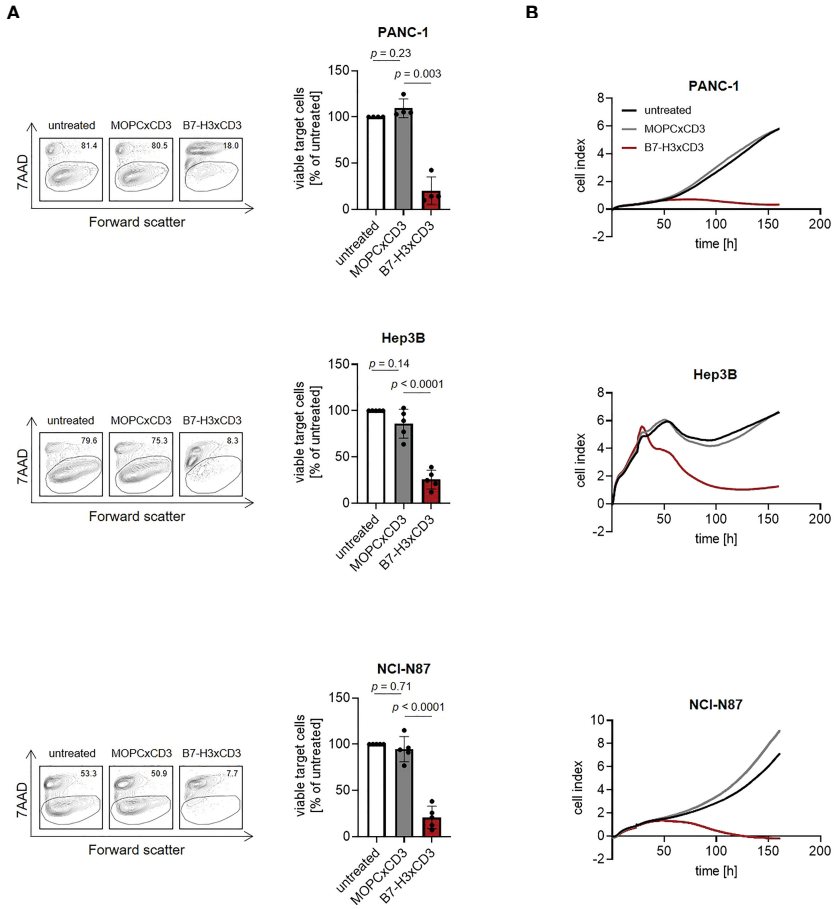

FIGURE 5
Induction of tumor cell lysis mediated by CC-3. Monocyte-depleted PBMC of healthy donors were incubated with the indicated target cells at an E:T ratio of 4:1 in the presence or absence of MOPCxCD3 or CC-3 (1 nM each). **(A)** Lysis of PANC-1, Hep3B and NCI-N87 cells was determined by flow cytometry-based lysis assay after 72 h. Left panels depict exemplary results right panels show combined data obtained with PBMC of five independent donors. **(B)** Long-term cytotoxic effects of PBMC of healthy donors (n=4) against PANC-1, NCI-N87 and Hep3B cells was determined using xCELLigence system. E:T, effector to target.

of patients with higher disease burden. In this context it is particularly noteworthy that CC-3 triggered mainly the proliferation of memory T cells, which are considered to be crucial for therapeutic success (19, 20). These findings support and extend our recently reported data for CC-3 in CRC (16). Of note, various factors like the tumor microenvironment and T cell exhaustion influence the therapeutic success of bsAb treatment and are not accounted for in our experimental systems. Additional preclinical investigations to address the influence of these and other confounders of treatment efficacy are warranted, and eventually could be correlated with findings upon clinical evaluation.

Several approaches targeting B7-H3 are currently under clinical investigation, reflecting the growing interest in this target for antibody-based immunotherapy. This includes among others CAR T cell-based therapies (NCT04897321, NCT05211557, NCT05341492, NCT04483778, NCT05323201, NCT05241392, NCT05474378, NCT03198052, NCT04185038, NCT05366179, NCT04670068, NCT05143151) which are being evaluated in various tumor entities including hepatocellular carcinoma and advanced pancreatic carcinoma.

In conclusion, the preclinical data reported in this study documenting efficacy of CC-3 in pancreatic, hepatic and gastric cancer in our view clearly indicate that this B7-H3xCD3 bsAb constitutes a promising immunotherapeutic compound. GMP compliant production of CC-3 is presently ongoing to enable clinical evaluation.

Data availability statement

The raw data supporting the conclusions of this article will be made available by the authors, without undue reservation.

Ethics statement

The studies involving human participants were reviewed and approved by IRB (ethics committee of the Faculty of Medicine of the Eberhard Karls Universitaet Tuebingen) at the University Hospital Tuebingen and was conducted in accordance with the Declaration of Helsinki; reference number13/2007 V. Human

material was collected after obtaining informed consent. The patients/participants provided their written informed consent to participate in this study.

Author contributions

ML designed and performed the experiments, analyzed and interpreted data, and wrote the manuscript. LZ designed experiments, provided critical reagents and contributed to the study design. LW designed and performed experiments. GJ, SB and UL provided critical reagents. JH wrote and critically revised the manuscript. HS contributed to the study design, critically revised the manuscript, and supervised the study. All authors contributed to the article and approved the submitted version.

Funding

This project was supported by the Deutsche Krebshilfe (70113999), the Wilhelm Sander-Stiftung (2017.100.2), and Deutsche Forschungsgemeinschaft (DFG, German Research Foundation) under Germany's Excellence Strategy - EXC 2180 - 39090067 and DFG, project number SA 1360/9-3.

Acknowledgments

The authors thank Celine Reiß and Michael Beller for excellent technical assistance. Flow cytometry sample acquisition was performed on shared instruments of the Flow Cytometry Core Facility Tuebingen.

Conflict of interest

GJ, HS and LZ are listed as inventors on the patent application "Antibodies targeting, and other modulators of, the CD276 antigen, and uses thereof," EP3822288A1, applicant is German Cancer Research Center, Heidelberg, and Medical Faculty University of Tuebingen, Germany.

The remaining authors declare that the research was conducted in the absence of any commercial or financial relationships that could be constructed as a potential conflict of interest.

Publisher's note

All claims expressed in this article are solely those of the authors and do not necessarily represent those of their affiliated organizations, or those of the publisher, the editors and the reviewers. Any product that may be evaluated in this article, or claim that may be made by its manufacturer, is not guaranteed or endorsed by the publisher.

Supplementary material

The Supplementary Material for this article can be found online at: https://www.frontiersin.org/articles/10.3389/fimmu.2023.1163136/full#supplementary-material

References

1. Arnold M, Abnet CC, Neale RE, Vignat J, Giovannucci EL, McGlynn KA, et al. Global burden of 5 major types of gastrointestinal cancer. *Gastroenterology* (2020) 159 (1):335–349.e15. doi: 10.1053/j.gastro.2020.02.068

2. Janjigian YY, Kawazoe A, Yanez P, Li N, Lonardi S, Kolesnik O, et al. The KEYNOTE-811 trial of dual PD-1 and HER2 blockade in HER2-positive gastric cancer. *Nature* (2021) 600(7890):727–30. doi: 10.1038/s41586-021-04161-3

3. Finn RS, Qin S, Ikeda M, Galle PR, Ducreux M, Kim TY, et al. Atezolizumab plus bevacizumab in unresectable hepatocellular carcinoma. *N Engl J Med* (2020) 382 (20):1894–905. doi: 10.1056/NEJMoa1915745

4. Ishida Y, Agata Y, Shibahara K, Honjo T. Induced expression of PD-1, a novel member of the immunoglobulin gene superfamily, upon programmed cell death. *EMBO J* (1992) 11(11):3887–95. doi: 10.1002/j.1460-2075.1992.tb05481.x

5. Leach DR, Krummel MF, Allison JP. Enhancement of antitumor immunity by CTLA-4 blockade. *Science* (1996) 271(5256):1734–6. doi: 10.1126/science.271.5256.1734

6. Brentjens RJ, Davila ML, Riviere I, Park J, Wang X, Cowell LG, et al. CD19-targeted T cells rapidly induce molecular remissions in adults with chemotherapy-refractory acute lymphoblastic leukemia. *Sci Transl Med* (2013) 5(177):177ra38. doi: 10.1126/scitranslmed.3005930

7. Bargou R, Leo E, Zugmaier G, Klinger M, Goebeler M, Knop S, et al. Tumor regression in cancer patients by very low doses of a T cell-engaging antibody. *Science* (2008) 321(5891):974–7. doi: 10.1126/science.1158545

8. Chapoval AI, Ni J, Lau JS, Wilcox RA, Flies DB, Liu D, et al. B7-H3: a costimulatory molecule for T cell activation and IFN-gamma production. *Nat Immunol* (2001) 2(3):269–74. doi: 10.1038/85339

9. Zhou WT, Jin WL. B7-H3/CD276: An emerging cancer immunotherapy. *Front Immunol* (2021) 12:701006. doi: 10.3389/fimmu.2021.701006

10. Kontos F, Michelakos T, Kurokawa T, Sadagopan A, Schwab JH, Ferrone CR, et al. B7-H3: An attractive target for antibody-based immunotherapy. *Clin Cancer Res* (2021) 27(5):1227–35. doi: 10.1158/1078-0432.CCR-20-2584

11. Crispen PL, Sheinin Y, Roth TJ, Lohse CM, Kuntz SM, Frigola X, et al. Tumor cell and tumor vasculature expression of B7-H3 predict survival in clear cell renal cell carcinoma. *Clin Cancer Res* (2008) 14(16):5150–7. doi: 10.1158/1078-0432.CCR-08-0536

12. Mehta NK, Pfluegler M, Meetze K, Li B, Sindel I, Vogt F, et al. A novel IgG-based FLT3xCD3 bispecific antibody for the treatment of AML and b-ALL. *J Immunother Cancer* (2022) 10(3). doi: 10.1136/jitc-2021-003882

13. Zekri L, Vogt F, Osburg L, Muller S, Kauer J, Manz T, et al. An IgG-based bispecific antibody for improved dual targeting in PSMA-positive cancer. *EMBO Mol Med* (2021) 13(2):e11902. doi: 10.15252/emmm.201911902

14. Heitmann JS, Walz JS, Pflugler M, Kauer J, Schlenk RF, Jung G, et al. Protocol of a prospective, multicentre phase I study to evaluate the safety, tolerability and preliminary efficacy of the bispecific PSMAxCD3 antibody CC-1 in patients with castration-resistant prostate carcinoma. *BMJ Open* (2020) 10(10):e039639. doi: 10.1136/bmjopen-2020-039639

15. Schneider CA, Rasband WS, Eliceiri KW. NIH Image to ImageJ: 25 years of image analysis. *Nat Methods* (2012) 9(7):671–5. doi: 10.1038/nmeth.2089

16. Zekri L, Lutz M, Prakash N, Manz T, Klimovich B, Mueller S, et al. An optimized IgG-based B7-H3xCD3 bispecific antibody for treatment of gastrointestinal cancers. *Mol Ther* (2023). doi: 10.1016/j.ymthe.2023.02.010

17. Gaudino SJ, Kumar P. Cross-talk between antigen presenting cells and T cells impacts intestinal homeostasis, bacterial infections, and tumorigenesis. *Front Immunol* (2019) 10:360. doi: 10.3389/fimmu.2019.00360

18. Schuster IS, Coudert JD, Andoniou CE, Degli-Esposti MA. "Natural regulators": NK cells as modulators of T cell immunity. *Front Immunol* (2016) 7:235. doi: 10.3389/fimmu.2016.00235

19. Ando M, Ito M, Srirat T, Kondo T, Yoshimura A. Memory T cell, exhaustion, and tumor immunity. *Immunol Med* (2020) 43(1):1–9. doi: 10.1080/25785826.2019.1698261

20. Klebanoff CA, Gattinoni L, Restifo NP. CD8+ T-cell memory in tumor immunology and immunotherapy. *Immunol Rev* (2006) 211:214–24. doi: 10.1111/j.0105-2896.2006.00391.x

21. Llovet JM, Ricci S, Mazzaferro V, Hilgard P, Gane E, Blanc JF, et al. Sorafenib in advanced hepatocellular carcinoma. *N Engl J Med* (2008) 359(4):378–90. doi: 10.1056/NEJMoa0708857

22. Kudo M, Finn RS, Qin S, Han KH, Ikeda K, Piscaglia F, et al. Lenvatinib versus sorafenib in first-line treatment of patients with unresectable hepatocellular carcinoma: a randomised phase 3 non-inferiority trial. *Lancet* (2018) 391(10126):1163–73. doi: 10.1016/S0140-6736(18)30207-1

23. Pavlakis N, Sjoquist KM, Martin AJ, Tsobanis E, Yip S, Kang YK, et al. Regorafenib for the treatment of advanced gastric cancer (INTEGRATE): A multinational placebo-controlled phase II trial. *J Clin Oncol* (2016) 34(23):2728–35. doi: 10.1200/JCO.2015.65.1901

24. Shlomai A, Leshno M, Goldstein DA. Regorafenib treatment for patients with hepatocellular carcinoma who progressed on sorafenib-a cost-effectiveness analysis. *PLoS One* (2018) 13(11):e0207132. doi: 10.1371/journal.pone.0207132

25. Moore MJ, Goldstein D, Hamm J, Figer A, Hecht JR, Gallinger S, et al. Erlotinib plus gemcitabine compared with gemcitabine alone in patients with advanced pancreatic cancer: a phase III trial of the national cancer institute of Canada clinical trials group. *J Clin Oncol* (2007) 25(15):1960–6. doi: 10.1200/JCO.2006.07.9525

26. Zhu AX, Kang YK, Yen CJ, Finn RS, Galle PR, Llovet JM, et al. Ramucirumab after sorafenib in patients with advanced hepatocellular carcinoma and increased alpha-fetoprotein concentrations (REACH-2): a randomised, double-blind, placebo-controlled, phase 3 trial. *Lancet Oncol* (2019) 20(2):282–96. doi: 10.1016/S1470-2045(18)30937-9

27. Fuchs CS, Shitara K, Di Bartolomeo M, Lonardi S, Al-Batran SE, Van Cutsem E, et al. Ramucirumab with cisplatin and fluoropyrimidine as first-line therapy in patients with metastatic gastric or junctional adenocarcinoma (RAINFALL): a double-blind, randomised, placebo-controlled, phase 3 trial. *Lancet Oncol* (2019) 20(3):420–35. doi: 10.1016/S1470-2045(18)30791-5

28. Bang YJ, Van Cutsem E, Feyereislova A, Chung HC, Shen L, Sawaki A, et al. Trastuzumab in combination with chemotherapy versus chemotherapy alone for treatment of HER2-positive advanced gastric or gastro-oesophageal junction cancer (ToGA): a phase 3, open-label, randomised controlled trial. *Lancet* (2010) 376 (9742):687–97. doi: 10.1016/S0140-6736(10)61121-X

29. Fuchs CS, Doi T, Jang RW, Muro K, Satoh T, Machado M, et al. Safety and efficacy of pembrolizumab monotherapy in patients with previously treated advanced gastric and gastroesophageal junction cancer: Phase 2 clinical KEYNOTE-059 trial. *JAMA Oncol* (2018) 4(5):e180013. doi: 10.1001/jamaoncol.2018.0013

30. Calderaro J, Rousseau B, Amaddeo G, Mercey M, Charpy C, Costentin C, et al. Programmed death ligand 1 expression in hepatocellular carcinoma: Relationship with clinical and pathological features. *Hepatology* (2016) 64(6):2038–46. doi: 10.1002/hep.28710

31. Ratti M, Lampis A, Hahne JC, Passalacqua R, Valeri N. Microsatellite instability in gastric cancer: molecular bases, clinical perspectives, and new treatment approaches. *Cell Mol Life Sci* (2018) 75(22):4151–62. doi: 10.1007/s00018-018-2906-9

32. Karamitopoulou E. Tumour microenvironment of pancreatic cancer: immune landscape is dictated by molecular and histopathological features. *Br J Cancer* (2019) 121(1):5–14. doi: 10.1038/s41416-019-0479-5

33. Li HB, Yang ZH, Guo QQ. Immune checkpoint inhibition for pancreatic ductal adenocarcinoma: limitations and prospects: a systematic review. *Cell Commun Signal* (2021) 19(1):117. doi: 10.1186/s12964-021-00789-w

34. Mohr R, Jost-Brinkmann F, Ozdirik B, Lambrecht J, Hammerich L, Loosen SH, et al. Lessons from immune checkpoint inhibitor trials in hepatocellular carcinoma. *Front Immunol* (2021) 12:652172. doi: 10.3389/fimmu.2021.652172

35. Pishvaian M, Morse MA, McDevitt J, Norton JD, Ren S, Robbie GJ, et al. Phase 1 dose escalation study of MEDI-565, a bispecific T-cell engager that targets human carcinoembryonic antigen, in patients with advanced gastrointestinal adenocarcinomas. *Clin Colorectal Cancer* (2016) 15(4):345–51. doi: 10.1016/j.clcc.2016.07.009

36. Kebenko M, Goebeler ME, Wolf M, Hasenburg A, Seggewiss-Bernhardt R, Ritter B, et al. A multicenter phase 1 study of solitomab (MT110, AMG 110), a bispecific EpCAM/CD3 T-cell engager (BiTE(R)) antibody construct, in patients with refractory solid tumors. *Oncoimmunology* (2018) 7(8):e1450710. doi: 10.1080/2162402X.2018.1450710

37. Morris ZS, Guy EI, Francis DM, Gressett MM, Werner LR, Carmichael LL, et al. *In situ* tumor vaccination by combining local radiation and tumor-specific antibody or immunocytokine treatments. *Cancer Res* (2016) 76(13):3929–41. doi: 10.1158/0008-5472.CAN-15-2644

38. Ganss R, Ryschich E, Klar E, Arnold B, Hammerling GJ. Combination of T-cell therapy and trigger of inflammation induces remodeling of the vasculature and tumor eradication. *Cancer Res* (2002) 62(5):1462–70. doi: 10.3892/ijmm.2012.1212

39. Zhao X, Li DC, Zhu XG, Gan WJ, Li Z, Xiong F, et al. B7-H3 overexpression in pancreatic cancer promotes tumor progression. *Int J Mol Med* (2013) 31(2):283–91. doi: 10.3892/ijmm.2012.1212

40. Arigami T, Uenosono Y, Hirata M, Yanagita S, Ishigami S, Natsugoe S. B7-H3 expression in gastric cancer: a novel molecular blood marker for detecting circulating tumor cells. *Cancer Sci* (2011) 102(5):1019–24. doi: 10.1111/j.1349-7006.2011.01877.x

41. Seaman S, Zhu Z, Saha S, Zhang XM, Yang MY, Hilton MB, et al. Eradication of tumors through simultaneous ablation of CD276/B7-H3-Positive tumor cells and tumor vasculature. *Cancer Cell* (2017) 31(4):501–515.e8. doi: 10.1016/j.ccell.2017.03.005

42. Qin X, Zhang H, Ye D, Dai B, Zhu Y, Shi G. B7-H3 is a new cancer-specific endothelial marker in clear cell renal cell carcinoma. *Onco Targets Ther* (2013) 6:1667–73. doi: 10.2147/ott.S53565

43. Zang X, Thompson RH, Al-Ahmadie HA, Serio AM, Reuter VE, Eastham JA, et al. B7-H3 and B7x are highly expressed in human prostate cancer and associated with disease spread and poor outcome. *Proc Natl Acad Sci U S A* (2007) 104(49):19458–63. doi: 10.1073/pnas.0709802104

44. Bin Z, Guangbo Z, Yan G, Huan Z, Desheng L, Xueguang Z. Overexpression of B7-H3 in CD133+ colorectal cancer cells is associated with cancer progression and survival in human patients. *J Surg Res* (2014) 188(2):396–403. doi: 10.1016/j.jss.2014.01.014

45. Liu Z, Zhang W, Phillips JB, Arora R, McClellan S, Li J, et al. Immunoregulatory protein B7-H3 regulates cancer stem cell enrichment and drug resistance through MVP-mediated MEK activation. *Oncogene* (2019) 38(1):88–102. doi: 10.1038/s41388-018-0407-9

46. Zhang Y, He L, Sadagopan A, Ma T, Dotti G, Wang Y, et al. Targeting radiation-resistant prostate cancer stem cells by B7-H3 CAR T cells. *Mol Cancer Ther* (2021) 20 (3):577–88. doi: 10.1158/1535-7163.Mct-20-0446

47. Yonesaka K, Haratani K, Takamura S, Sakai H, Kato R, Takegawa N, et al. B7-H3 negatively modulates CTL-mediated cancer immunity. *Clin Cancer Res* (2018) 24 (11):2653–64. doi: 10.1158/1078-0432.Ccr-17-2852

48. Hofmeyer KA, Ray A, Zang X. The contrasting role of B7-H3. *Proc Natl Acad Sci U S A* (2008) 105(30):10277–8. doi: 10.1073/pnas.0805458105

49. Brustmann H, Igaz M, Eder C, Brunner A. Epithelial and tumor-associated endothelial expression of B7-H3 in cervical carcinoma: relation with CD8+ intraepithelial lymphocytes, FIGO stage, and phosphohistone H3 (PHH3) reactivity. *Int J Gynecol Pathol* (2015) 34(2):187–95. doi: 10.1097/pgp.0000000000000116

50. Sun TW, Gao Q, Qiu SJ, Zhou J, Wang XY, Yi Y, et al. B7-H3 is expressed in human hepatocellular carcinoma and is associated with tumor aggressiveness and postoperative recurrence. *Cancer Immunol Immunother* (2012) 61(11):2171–82. doi: 10.1007/s00262-012-1278-5

51. Li Y, Yang X, Wu Y, Zhao K, Ye Z, Zhu J, et al. B7-H3 promotes gastric cancer cell migration and invasion. *Oncotarget* (2017) 8(42):71725–35. doi: 10.18632/oncotarget.17847

frontiers | Frontiers in Immunology

TYPE Review
PUBLISHED 18 April 2023
DOI 10.3389/fimmu.2023.1139589

OPEN ACCESS

EDITED BY
Qun Zhao,
Fourth Hospital of Hebei Medical University, China

REVIEWED BY
Laiping Zhong,
Shanghai Jiao Tong University, China
Sankar Bhattacharyya,
Sidho Kanho Birsha University, India
Chenglin Zhang,
Shenzhen University, China
Yichuan Pang,
Tongji University, China

*CORRESPONDENCE
Renjun Gu
renjungu@hotmail.com
Pengfei Li
lipengfei@njucm.edu.cn
Xiaogang Qin
502693680@qq.com

†These authors have contributed equally to this work

SPECIALTY SECTION
This article was submitted to Cancer Immunity and Immunotherapy, a section of the journal Frontiers in Immunology

RECEIVED 07 January 2023
ACCEPTED 20 March 2023
PUBLISHED 18 April 2023

CITATION
Liu Y, Shi Y, Han R, Liu C, Qin X, Li P and Gu R (2023) Signaling pathways of oxidative stress response: the potential therapeutic targets in gastric cancer. *Front. Immunol.* 14:1139589. doi: 10.3389/fimmu.2023.1139589

Signaling pathways of oxidative stress response: the potential therapeutic targets in gastric cancer

Yingying Liu[1,2†], Yu Shi[3†], Ruiqin Han[4†], Chaoge Liu[5,6], Xiaogang Qin[7*], Pengfei Li[8*] and Renjun Gu[1*]

[1]School of Chinese Medicine & School of Integrated Chinese and Western Medicine, Nanjing University of Chinese Medicine, Nanjing, China, [2]Institute for Immunology and School of Medicine, Tsinghua University, Beijing, China, [3]Shanghai East Hospital, Tongji University School of Medicine, Shanghai, China, [4]State Key Laboratory of Medical Molecular Biology, Department of Biochemistry and Molecular Biology, Institute of Basic Medical Sciences, Chinese Academy of Medical Sciences and Peking Union Medical College, Beijing, China, [5]Department of Oromaxillofacial - Head and Neck Surgery, Tianjin Stomatological Hospital, School of Medicine, Nankai University, Tianjin, China, [6]Tianjin Key Laboratory of Oral and Maxillofacial Function Reconstruction, Tianjin, China, [7]Traditional Chinese Medicine Hospital of Tongzhou District, Nantong, Jiangsu, China, [8]Department of Clinical Laboratory, Jiangsu Province Hospital of Chinese Medicine, Affiliated Hospital of Nanjing University of Chinese Medicine, Nanjing, China

Gastric cancer is one of the top causes of cancer-related death globally. Although novel treatment strategies have been developed, attempts to eradicate gastric cancer have been proven insufficient. Oxidative stress is continually produced and continually present in the human body. Increasing evidences show that oxidative stress contributes significantly to the development of gastric cancer, either through initiation, promotion, and progression of cancer cells or causing cell death. As a result, the purpose of this article is to review the role of oxidative stress response and the subsequent signaling pathways as well as potential oxidative stress-related therapeutic targets in gastric cancer. Understanding the pathophysiology of gastric cancer and developing new therapies for gastric cancer depends on more researches focusing on the potential contributors to oxidative stress and gastric carcinogenesis.

KEYWORDS

gastric cancer, oxidative stress, signaling pathways, pathophysiology, therapeutic targets

1 Introduction

Gastric cancer is the third most frequent cause of cancer-related death, and the fifth most diagnosed malignancy around the world (1). Gastric cancer is the major burden in male, accounting for 20% globally, only to lung and liver cancers (2). Anatomically, true gastric adenocarcinomas (non-cardia gastric tumors) and gastro-oesophageal junction

adenocarcinomas (cardia gastric cancers) are two types of gastric cancer (3). The early stages of gastric cancer are frequently clinically unconscious, and patients are typically diagnosed at an advanced stage. The prognosis is poor once the neoplastic cells invade the muscularis propria, with the 5-year survival is almost 25% in Europe and US (4–6). With the development of economy and living standards, the prevalence of *Helicobacter pylori* (*H. pylori*) which is the key risk factor of non-cardia gastric cancer has decreased (7). Despite a consistent decrease in the rates of morbidity and mortality, more cases of gastric cancer can be seen in the future because of ageing populations (8). The disease's late diagnosis and high mortality rate reveal a lack of knowledge regarding its etiology and pathology, as well as the absence of efficient treatments. Generally, gastric cancer is a consequence of the multifactorial interplay between host genetics, microbial factors, nutrition, and environmental milieu (9), where it is thought that oxidative stress plays a crucial role in the occurrence and development of gastric cancer.

Oxidative stress is the result of an imbalance of reactive oxygen species (ROS) production and natural antioxidant defenses, which can damage biological molecules and cells, with possible effects on the entire organism (10). Numerous studies demonstrate the tight relationship between ROS and cancer, indicating that cancer cells produced more ROS than healthy cells did (11). Increased ROS levels are thought to have an oncogenic effect, inducing DNA damage and chromosomal instability to activate proto-oncogenes and inactivate tumor suppressor genes (12, 13). Additionally, ROS also serve as signaling molecules in cancer, which affect receptor and oncogene activity, as well as alter several signaling pathways or oxidizing enzymes, facilitating tumorigenesis, angiogenesis, cellular proliferation, invasiveness, and metastasis (14). However, excessive intracellular levels of ROS may promote cell death by damaging proteins, lipid bilayers, and chromosomes. Therefore, cancer cells must fight against high level of ROS to strive for progression and develop resistance to apoptosis through antioxidant defense systems, especially at early stages (15). For this reason, both eliminating and elevating ROS production are potentially effective cancer therapies despite the fact that it is a challenging notion.

According to studies, increased levels of oxidative stress are found in individuals with gastric cancer, and this contributes to the development of gastric cancer (16). The significance of the link between oxidative stress and gastric cancer is becoming increasingly clear. This article reviews the current knowledge on the roles of oxidative stress in gastric cancer and the potential therapeutic applications of manipulating related signaling pathways in oxidative stress.

2 ROS production and quench

The human body continuously produces ROS which are oxygen-containing oxidants with reactive properties, represented as oxygen radicals including superoxide anions (O_2^-), hydroxyl (HO·), alkoxyl (RO·), peroxyl (RO_2·), and certain nonradicals either oxidizing agents and/or easily converted to radical including hydrogen peroxide (H_2O_2), hypochlorous acid (HOCl), singlet oxygen ($^1O_2$) and ozone (O_3) (17). Reactive nitrogen species (RNS) are nitrogen-containing chemical species, which can damage cells via nitrosative stress. Reactive nitrogen species (RNS) include nitric oxide (·NO), nonradical compounds, peroxynitrite ($ONOO^-$), nitrogen dioxide ($\cdot NO_2$) and dinitrogen trioxide (N_2O_3) (18) (Table 1). Most of these molecules are produced from oxygen in numerous metabolic processes occurring throughout the body, which primarily take place in the mitochondria, endoplasmic reticulum (ER) and peroxisomes. Approximately 2% of the oxygen consumed by the mitochondria is converted into superoxide, making it one of the largest sources of endogenous ROS (19). Peroxisomes mediate the production of ROS

TABLE 1 Formation of major oxidants.

Oxidant	Formula	Equation
Superoxide anion	$O2\cdot -$	$NADPH + 2O_2 \rightarrow 2O2\cdot - + NADP^+ + H^+$ $Xanthine + 2O_2 + NAD(P)H \rightarrow Uric\ acid + 2O2\cdot - + NAD(P)^+ + H^+$ $Hypoxanthine + 2O_2 + NAD(P)H \rightarrow Xanthine + 2O2\cdot - + NAD(P)^+ + H^+$
Hydrogen peroxide	H_2O_2	$Hypoxantine + H_2O + O_2 \rightarrow Xanthine + H_2O_2$ $Xanthine + H_2O + O_2 \rightarrow Uric\ acid + H_2O_2$
Hydroxyl radical	OH^-	$Fe^{2+} + H_2O_2 \rightarrow Fe^{3+} + OH^- + OH$
Singlet oxygen	$^1O_2$	$HOCl \rightarrow {}^1O_2 + H^+ + Cl^-$
Peroxyl radicals	ROO	$R + O_2 \rightarrow ROO$
Hypochlorous acid	HOCl	$H_2O_2 + Cl^- + H^+ \rightarrow HOCl + H_2O$
Hydroperoxyl radical	HOO·	$O_2^- + H_2O \leftrightarrow HOO\cdot + OH^-$
Nitric oxide	·NO	$L\text{-}arginine + O_2 \rightarrow \cdot NO + citrulline + 2H_2O$
Nitrogen dioxide	$\cdot NO_2$	$RNH2 \rightarrow \cdot NO \rightarrow NO_2^- \rightarrow \cdot NO_2 \rightarrow NO_3^-$
Peroxynitrite anion	$ONOO^-$	$NO\cdot + O_2^- \rightarrow ONOO^-$

via β-oxidation of fatty acid and flavin oxidase reaction and degrading ROS *via* catalase-mediated breakdown of H_2O_2 (20). The ER provides an oxidizing environment, which promotes the protein folding and acts as a source of ROS (21).

Enzymatic and non-enzymatic reactions are both necessary for ROS and RNS production. The main enzymes involved in enzymatic reactions are uncoupled endothelial nitric oxide synthase (eNOS), NADPH oxidase (NOX), xanthine oxidase (XO), arachidonic acid (ARA), peroxidase, and metabolic enzymes such the cytochrome P450 system, cyclooxygenase, and lipoxygenase. The major source of ROS comes from non-enzymatic processes in the mitochondrial respiratory chain (22). Generally, ROS are by-products of biological metabolism in healthy organisms, though at lower amounts, which activate different signaling pathways to promote survival, proliferation, or resistance to oxidative stress (15). However, numerous factors, including hypoxia, ER stress, infection, inflammation, environmental toxins, nutrition, and mitochondrial respiration, all participate in the excessive ROS generation in cells.

Everything has two sides, and it is crucial for cell to regulate ROS levels to avoid oxidative stress. Cells have developed antioxidant defense mechanisms to scavenge ROS in maintaining homeostasis. A number of nonenzymatic and enzymatic antioxidant defense mechanisms are responsible for neutralizing ROS. The nonenzymatic defense system includes glutathione (GSH), flavonoids, dietary antioxidants such as vitamins A, C, and E, selenium and β–carotene (23). The enzymatic antioxidant system includes superoxide dismutase (SOD), glutathione peroxidase (GPX), catalase (CAT), peroxiredoxin (PRX), glutathione S-transferases (GST), glutathione reductase (GSR) and thioredoxin reductase (TRX) (24–26). It is important for cells to use these antioxidant defense mechanisms to regulate ROS levels to avoid oxidative stress. However, oxidative stress happens when the antioxidant defense system of body is overwhelmed by the production of ROS (Figure 1). Oxidative stress is involved in numerous human diseases, such as neurodegenerative disease, cancer, cardiovascular disease, inflammatory disease, immune system dysfunctions, allergy, diabetes, aging. For instance, inflammatory cells release chemical mediators of inflammation, particularly ROS. Due to their high reactivity, ROS typically oxidize targets with or adjacent to the intracellular compartment where they are produced, affecting surrounding neighboring cells.

3 Factors causing oxidative stress in gastric cancer

3.1 *H. pylori* and oxidative stress

A gram-negative, microaerophilic bacteria called *H. pylori* infects over 4.4 billion (or 59% of) people worldwide (7). The human gastric mucosa is selectively colonized by *H. pylori*, which can cause gastroduodenal diseases including chronic gastritis, mucosa-associated lymphoid tissue (MALT) lymphoma, peptic ulcers, and gastric adenocarcinoma (27). Sinus gastritis affects 10%-15% of *H. pylori*-infected patients and may potentially be connected to their own concurrent hypergastrinemia (28). Potential long-term complications for the patients include duodenal ulcers, intestinal metaplasia with dysplasia, gastric adenocarcinoma (non-cardia intestinal-type), and spontaneous diffuse gastric cancer (29). *H. pylori* can cause gastric

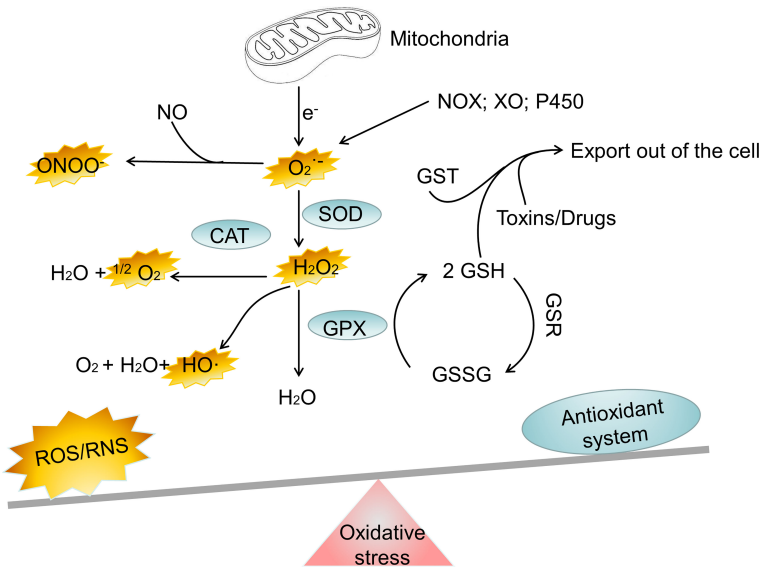

FIGURE 1
The major oxidant and antioxidant systems. NOX, NADPH oxidase; XO, xanthine oxidase; SOD, superoxide dismutase; CAT, catalase; GPX, glutathione peroxidase; GSH, glutathione; GSSG, reduced glutathione; GST, glutathione S-transferase; H_2O_2, hydrogen peroxide; ONOO–, peroxynitrite; HO·, hydroxyl radical; O_2^-, superoxide; $^1O_2$, singlet oxygen; Fe^{2+}, Iron (II); Fe^{3+}, Iron(III); ROS, reactive oxygen species; RNS, reactive nitrogen species.

lymphoma adenocarcinoma or gastric MALT lymphoma when it clings to the underlying epithelium (30, 31).

The principal producers of ROS and RNS in the body are neutrophils, macrophages and gastric epithelial cells (32) (Figure 2). In order to kill bacteria, NOX on the neutrophil membrane catalyzes the production of ROS (33). In an effort to eradicate the infection, phagocytic cells flood the area where *H. pylori* is present. In an effort to eliminate the bacteria, both neutrophils and macrophages phagocytose produce ROS. Additionally, the inducible nitric oxide synthase (iNOS), a crucial enzyme producing Nitric oxide, is expressed in the host neutrophils and epithelial cells (34). Despite the fact that *H. pylori* activates a strong innate and adaptive response, the human immune system is typically unable to completely eliminate the infection (35). DNA damage, oxidative stress, and chronic inflammation are all directly caused by this inadequate immune response (36). Patients with *H. pylori* infections exhibit higher amounts of ROS and NO-derived metabolites, which show that iNOS has been activated (37). Compared with phagocytic cells, the epithelial cells produce ROS at a much lower, which are involved in redox-sensitive signaling pathways but may not directly eradicate *H. pylori* (38). It is also known that the dual oxidases on the gastric epithelial cells produce H_2O_2 in response to infection, which likewise increases the levels of ROS (39). The environment of oxidative stress is available by the interaction of ROS generated by phagocytic and epithelial cell, which result in the growth of gastric cancer. On the one hand, one of the main causes of gastric cancer is oxidative stress by *H. pylori* infection.

The main cause is oxidative stress by *H. pylori* infection in gastric cancer. Tumor forms by *H. pylori* water extract *via* ROS production (40). Reactive oxygen metabolites are terminated by *H. pylori* treatment to eliminate the infections (41). It was feasible to ascertain the impact of bacterial eradication on oxidative stress of mucosal by contrasting the levels of nitrotyrosine and 8-hydroxy-2'-deoxyguanosine (8-oxo-dG) in antral biopsies from patients with peptic ulcer and chronic atrophic gastritis before and after eradication. Human gastric mucosa experiences less oxidative stress when *H. pylori* is removed (42). The infection of *H. pylori* can be cured by prescribed vitamins E and C with antibody therapy (43). According to recent studies, *H. pylori*-infected gastric epithelial cells produce more ROS than healthy cells do. This increased ROS production may contribute to the infection-related apoptosis (44). Furthermore, numerous virulence factors in *H. pylori* strains may lead to oxidative stress in the host. There is a higher risk of gastric carcinogenesis in patients infected with CagA-positive compared to CagA-negative strains (45). Elevated hydrogen peroxide levels and oxidative DNA damage are shown in CagA positive strains (46). IL8 and tumor necrosis factor (TNF), markers of oxidative stress and inflammation, are also increasing (47). Despite the fact that the exact mechanism by which CagA causes carcinogenesis is still unknown, it is evident that these actions can contribute to raising the chance of developing gastric cancer (48). On the other hand, gastric cells can protect themselves against oxidative stress by producing scavenger molecules.

Gastric cells can protect themselves against oxidative stress by producing scavenger molecules. Metallothioneins are important components in preventing *H. pylori*-induced gastric erosive lesions in the animal model (49). Other antioxidant systems include those that control energy metabolism globally, such as AMP-activated protein kinase (AMPK) (50) and the cytoprotective activity of nuclear factor (erythroid-derived 2)-like 2 (Nrf2) (51). At the same time, *H. Pylori* has also developed oxidative stress defense mechanisms that might encourage the acquisition of potentially cancerous traits and accelerate the development of the condition into gastric cancer (52). For example, NO levels and superoxide dismutase activity were found to have a relevant and reverse association in gastric juice of patients suffering from *H. pylori* (53). Isogenic mutants deficient in the activities of thioredoxin (54), catalase (KatA) (55), NADPH quinone reductase (56), and superoxide dismutase (46) are sensitive to host colonization and susceptible to oxidative damage.

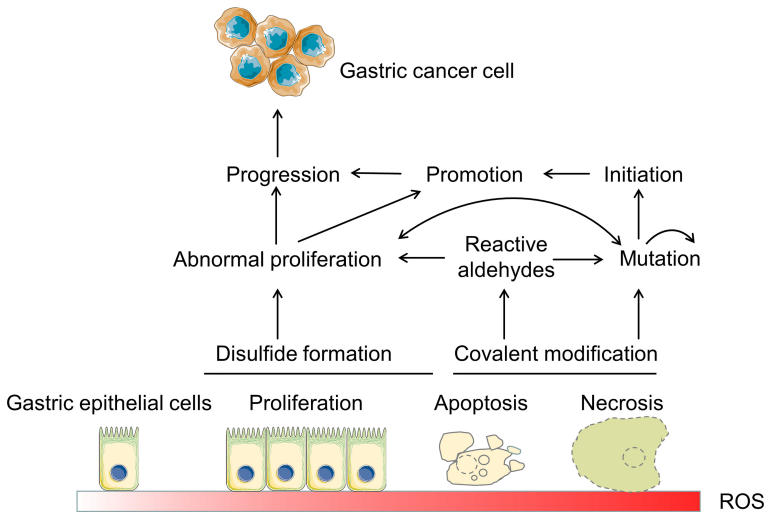

FIGURE 2
The Various pathways of ROS production and DNA damage by the epithelial and immune cells. CagA, cytotoxin-associated gene A; SMO, spermine oxidase; H_2O_2, hydrogen peroxide; VacA, vacuolating cytotoxin A; HO-1, heme oxygenase 1; ROS, reactive oxygen species.

Besides, it is interesting to note that the bacteria also produce ROS (32).

3.2 Smoking and oxidative stress in gastric cancer

Tobacco smoke from tar and gas phases maintain a variety of compounds, including unstable free radicals and ROS, which can harm organism through oxidative stress. The burning of tobacco produces ROS in the gas phase inhaled by smokers, as part of the mainstream smoke (57). Several rather stable free radicals in the tar phase are included in the tarry matrix, such as the quinone/hydroquinone (Q/QH2) complex (58). This Q/QH2 polymer may act as the redox system by converting pulmonary O_2 to O_2^- or additional free radicals like H_2O_2 and ·OH (59). Another crucial point is that, when an individual's antioxidant defense system is weak or saturated, inhaling additional ROS or other reactive metabolites produced by the biotransformation of chemicals in tobacco smoke can increase the amount of oxidative stress caused by the gas-phase and tar-phase derived ROS (60). In addition, tar builds up in the lungs from cigarette smoke particles and processes, producing an aqueous solution that goes through redox cycling to produce different reactive species, causing damage subsequently (61).

Increasing data indicate that the release of ROS from smoking and the subsequent oxidative stress have a substantial impact on inflammation and carcinogenesis. Estimates suggest that tobacco use causes about 80,000 cases of gastric cancer annually (11% of all estimated cases) (62). Despite the decline among population-attributable fractions, smoking remained the main risk factor for men's gastric cancer in 2012, where the incidence is substantially higher in 2020 (63). Healthy smokers may be more susceptible to oxidant-mediated tissue damage and gastric cancer because of their poor antioxidant level. The levels of thiobarbituric acid reactive substances (TBARS) are higher in smokers than in non-smokers with gastric cancer, and smokers have lower levels of SOD, CAT, GPX, GST, GSR and decreased vitamins A, E, and C (64). Low-density lipoprotein cholesterol, high-density lipoprotein cholesterol and total cholesterol all dramatically rise in non-smokers while falling in smokers, whereas these reduced in smokers (65). It has been discovered that antioxidant-rich diet significantly influenced smokers' cellular stress protection (66). Plasma levels of malondialdehyde (MDA) were substantially higher and melatonin levels were substantially lower in smokers than non-smokers, which appears that melatonin can lessen the respiratory system damage caused by free radicals brought on by cigarette smoke (67).

4 Oxidative stress in gastric cancer

4.1 Gastric carcinogenesis

Under oxidative stress, increased ROS in cells may harm tissues and trigger carcinogenesis, especially in the gastrointestinal system (Figure 3). ROS are initiating factor in gastric carcinogenesis in both humans and mice. Serum and tissue samples from the human gastrointestinal have dysregulated ROS levels (41). In mice gastric cancer models induced by *H. pylori* and N-methyl-N'nitro-N'nitrosoguanidine (MNNG), the downstream pathways P53, Wnt, Ras, and mTOR are activated by ROS (70, 71). Proviral insertion in murine lymphomas 2 (PIM2) is reported to act as an

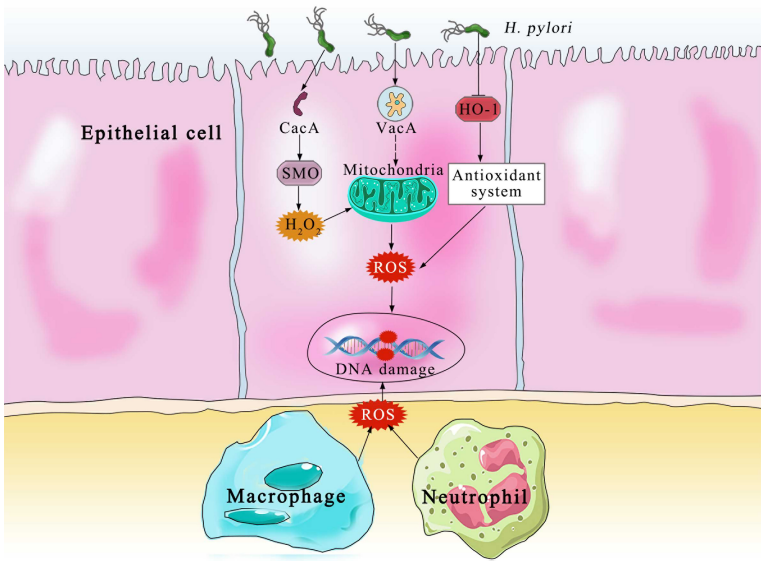

FIGURE 3
ROS and its pathophysiological effects in gastric carcinogenesis. At low to moderate concentrations, ROS function as signaling molecules that support cellular differentiation and proliferation and activate survival pathways in response to stress. Excessive ROS harms lipids, proteins, and DNA, causing mucosal injury and trigger carcinogenesis. Reactive aldehydes include 4-hydroxynonenal and other aldehydes (68). The mutator phenotype is shown by the self-directed arrow at mutation (69).

oncogene in gastric cancer, controlling apoptosis *via* ROS-triggered ER stress, and promoting the development of gastric cancer (72). 13 biomarkers including β-catenin, C-MYC, GATA-4, CXCL13, DAPK1, TIMP3, DC-SIGN, EGFR, PIM2, GRIN2B, SLC5A8, VCAM-1 and CDH1 are related to the development of gastric cancer, and six of them including β-catenin, DC-SIGN, C-MYC, EGFR, CXCL13 and PIM2 have been reported overexpressed in gastric tissue from infected children and gastric cancer patients (73). Moreover, it has been shown that stomach cancer is more likely to develop as a result of the oxidative stress brought on by CagA-positive bacteria (74), in which *H pylori* CagA produces cells with oxidative DNA damage by inducing spermine oxidase (SMO), and a portion of these cells are apoptosis-resistant and therefore highly susceptible to developing cancer (75). Oxidative stress can cause DNA damage caused by *H pylori* infection. *In vitro* investigations have demonstrated that cells infected with *H pylori* that have defective DNA repair systems experience increased oxidative stress and DNA damage (76). *In vivo* studies using mice lacking a component of the base excision repair process revealed significant stomach lesions after *H pylori* infection (46). *H. pylori*'s propensity to generate DNA strand breaks undoubtedly contributes to genomic instability and may aid in carcinogenesis (77). NO can block 8-oxoguanine glycosylase from removing DNA mutations. Research has revealed that *H. pylori* infection increases phosphohistone H2AX, a marker of repair for double-strand DNA breaks (46). It has been reported that 8-hydroxy-2'deoxyguanosine buildup causes DNA damage. The loss of a base following damage would create an abasic site, which could result in a single-strand break in the DNA. Inadequate repair or continuous damage may cause double-strand breaks in the DNA, though DNA strands can be produced in various ways (46). If a cell does not heal enough fractures, it may die.

Tumor hypoxia is well recognized in oncology as a major cause of therapy resistance and poor prognosis. Hypoxia promotes the production of several gene products implicated in tumor development, invasion, and metastasis formation of gastric cancer. Hypoxia causes the production of ROS, which inhibit the degradation of the hypoxia-inducible factor 1 (HIF-1) (78). Subsequently, HIF-1α influences the expression of numerous genes that are crucial for gastric carcinogenesis. For instance, Angiogenesis is promoted by HIF-1 to stimulate the vascular endothelial growth factor (VEGF) pathway in gastric cancer (79). Caveolin-1 (Cav-1) is expressed less while induced by HIF-1, which regulates E-cadherin to cause the epithelial-mesenchymal transition (EMT) in gastric cancer (80). On the other hand, as a signaling molecule, ROS activates vital signaling pathways that are crucial to promote the onset and progression of gastric cancer. ROS, also as a second messenger, can activate tyrosine kinases and MAPK which promote cell development (81), and the protein kinase-B (Akt)/mTOR signaling pathway which promotes cell growth of gastric cancer (82). Additionally, ROS activates nuclear factor-B (NF-κB), facilitating invasion of gastric cancer (83).

Furthermore, *H. pylori*-colonized mucosal cells with deficient DNA repair systems are more vulnerable to oxidative stress and DNA damage (84). Spermine oxidase (SMOX) is activated in *H. pylori* in gastric epithelial cells, leading to oxidative stress (85). DNA damage promotes mutations of suppressor in tumor such as calcium/calmodulin dependent serine protein kinase (CASK), p53, as well as stimulation of the epidermal growth factor receptor (EFGR) signaling pathway, which are important early events in gastric carcinogenesis (86, 87). *H. pylori* colonization also negatively affects the expression of antioxidant proteins, along with epigenetic modifications and DNA methylation, such as GATA-4, GATA-5 and TWIST-1 (88), as well as miRNAs dysregulation, such as mir-21, mir-92a, mir-27a, mir-146a, mir-326, mir-155 and mir-663 (73, 89). It has been demonstrated that the expression of the purine-free/pyrimidine-free nucleic acid endonuclease 1 (APE1) is downregulated in gastric host cells infected with *H. pylori*, which ultimately reduces T-cell capacity for repair, increasing the likelihood of DNA carboxy-terminal genetic alterations. The oxidative stress defensive factors such as FOXO1, are known to be inhibited by miR-27a, which is recognized as an oncogenic miRNA in gastric cancer (90). miR-328 is downregulated in *H. pylori* -infected gastritis (90), and the low level of miR-328 activates CD44 to promote the differentiation of gastric stem cell (68). *H. pylori* increases the expression of miR-210 by controlling its methylation, which in turn suppressed dimethyl adenosine transferase 1 (DIMT1) and oncoprotein 18 or metablastic (STMN1), which promotes the proliferation of gastric epithelial cells (69). Due to the methylation of the gene promoter region by ROS, *H. pylori* infection may change the expression of miRNAs in oxidative stress, interfering with the methylation of miRNAs, which may contribute to the mechanism triggering the onset of gastric carcinogenesis.

4.2 Gastric adenocarcinoma and gastric cancer

The process of developing gastric cancer involves several stages, beginning with the change from normal mucosa to chronic superficial gastritis (non-atrophic gastritis). Atrophic gastritis, intestinal metaplasia, dysplasia and adenocarcinoma, among other conditions can be caused by gastritis (91). Gastritis caused by *H. pylori* is the only condition that always precedes diffuse gastric cancer. According to Correa's idea, a series of events initiating with chronic superficial gastritis and progressing from atrophic gastritis, intestinal metaplasia, and dysplasia to gastric cancer (92). The especially high risk of cancer exists in people who have antibodies to the CagA protein, which is a marker for the more inflammatory and virulent strain of *H. pylori* that carries a pathogenicity island of genes. According to a meta-analysis of research, CagA-positive strains are two times more likely than CagA-negative strains to cause noncardia gastric cancer (93). The cag^+ *H. pylori* strains have a stronger connection to gastric carcinogenesis than strains without cag (94). ROS or RNS production is substantially increased in vascular endothelium, gastric mucosa infected with H. pylori, and neutrophils aggregated in inflammatory mucosa (93). Following *H. pylori* infection, phagocytes that have gathered in the stomach mucosa produce O2·, HO·, and HOCl (95). Rat gastric mucosal

cells have been shown to undergo apoptosis when exposed to NH_2Cl (96).

Epstein-Barr virus (EBV) is recognized as a pathogen that causes stomach cancer. Nearly 10% of cases of gastric cancer are EBV-associated gastric cancer, which is the monoclonal proliferation of epithelial cells infected with EBV that only express a few EBV-latent genes (Latency I program) (97). The production of NH_2Cl by infiltrating neutrophils can convert latent EBV into lytic EBV in the *H. pylori*-infected gastric, which may further contribute to gastric carcinogenesis (98). Although the function of the ROS generated by infected gastric epithelial cells is not fully known, it is thought that these ROS trigger signaling processes that control how *H. pylori* pathogenesis develops.

H. pylori infection directly causes oxidative stress in gastric epithelial cells by the production of ROS, and it also stimulates host responses that result in ROS and controls the production of proinflammatory cytokines, inflammation, and cell death (99). Continuous ROS production results in oncogene and tumor suppressor gene changes, as well as chromosomal abnormalities by oxidative genome damage, which includes the oxidation of guanine to form 8-OhdG and 8-oxo,7,8-dihydroguanosine (8-OHG) in RNA and DNA (100).

When compared to normal mucosa, gastric adenoma and *H. pylori*-infected or uninfected cancer tissues express ROS and APE1/Ref1 more mucosally (101). As a result of *H. pylori* infection, both the gastrointestinal lumen and gastric juice ascorbic acid content decrease. This antioxidant lessens the effects of carcinogens by lowering carcinogenic substances including nitrosamines and ROS. Depleting cellular antioxidants makes ROS more effective at killing cancer cells because this is the traditional treatment strategy for doing so. Perhaps, the disease can be regulated by blocking different antioxidant systems during neoadjuvant treatments.

4.3 Gastric lymphoma

Gastric MALT lymphomas are a slow-growing type of non-Hodgkins lymphoma, developed from the extranodal marginal zone of lymphoid follicles (102). Gastric MALT lymphoma is an illustration of the intimate pathogenetic relationship between chronic inflammation and tumor development. Approximately 92% of gastric MALT lymphomas have a tight connection to *H. pylori* infection which makes *H. pylori* easier to develop and diffuse (103). The *H. pylori* strains linked to gastric MALT lymphoma are less virulent than those linked to gastric adenocarcinoma. The latter strains may have the VacA m2 gene without the CagPAI, which could make *H. pylori* carriers easier to develop diffuse large B-cell lymphoma (104). *H. pylori* infection increased the incidence of low-grade gastric MALT lymphoma by an odds ratio of 2.8 times compared with *H. pylori*-negative individuals (105). Within gastric MALT lymphomas, T lymphocytes activated by *H. pylori* are responsible for B-cell proliferation (106).

Most individuals with early-stage *H. pylori* disease have been in durable remission for more than ten years after completing a single brief course of combination antibiotic therapy. A meta-analysis of more than 30 trials found that the overall remission rate of MALT lymphomas with a low histological grade that is restricted to the perigastric lymph nodes or the gastric wall (stage I or stage IIe_1 illness) was 78% (107). Therefore, preventive removal of *H. pylori* is particularly helpful in reversing MALT lymphoma either in the early MALT stage or in the late bone marrow-involved stage. However, the recurring possibility of MALT lymphoma should not be ignored because it frequently returns several years following surgery, which may due to risk factors for gastric cancer have not been totally blocked.

Gastric MALT lymphoma is regarded as one of the greatest models for understanding how genetic events contribute to oncogenesis, influence tumor biology, govern clinical behavior, and represent feasible treatment targets. Genetic aberrations arise through the release of ROS, *H. pylori*-induced endonucleases, and other effects. Stronger oxidative stress is caused by *H. pylori* strains originating from gastric cancer in the host, and these strains may have suppressive effects on the host's GSH-related defensive mechanisms (108). Surprisingly, the nucleotide-binding oligomerization domain protein 2 (NOD2) functions as a receptor for pattern recognition. *H. pylori* activates NF-κB signaling *via* NOD2. However, the NF-κB signaling is uncontrolled when the R702W gene is mutated, protecting the organism against the harm caused by oxidative stress induced by *H. pylori* (109). Thus, it is essential to consider how the gastric MALT lymphoma is influenced by the NOD2 gene (110) (Table 2).

5 Potential oxidative stress-related therapeutic targets in gastric cancer

Regulation of redox homeostasis is crucial because increasing oxidative stress has a role in all stages of carcinogenesis either initiating/stimulating tumorigenesis and promoting cancer cells transformation/proliferation or leading to cell death. Enhancing antioxidant defense capability decreases ROS as a result of one strategy (Table 3). However, utilizing antioxidants has been shown to change the effectiveness of treatment and, in some cases, even speed up the development of tumors.

According to a recent study, the garlic compound S-allyl cysteine has anti-inflammatory and antioxidant properties, which greatly raises the GSH levels in the liver, gastric tissue, and serum of rat models of gastric cancer, and lowers the risk of developing gastric cancer (156). In experimental settings using AGS cells infected with *H. pylori* strains, GSH levels are lower in individuals with gastric cancer than in those with duodenal ulcers, indicating a more severe oxidative stress response to gastric cancer with *H. pylori* infection (157). The level of GSH and the ratio of GSSG/GSH

TABLE 2 A partial list of signaling pathways linked to oxidative stress in gastric cancer.

Signaling pathways	Reference
Cell cycle regulators: Cyclin D and Cyclin E; p53, $p21^{Waf1/Cip1}$ and $p27^{Kip1}$	(111, 112) (113, 114)
COX-2/PGE2 and LOX/leukotrienes signaling	(115–118)
E-cadherin and Wnt/β-catenin signaling	(119, 120)
EGFR, HER2 and Ras/MAPK signaling	(121, 122)
FAK signaling	(123, 124)
Grb2/HER2 signaling	(125)
Hedgehog signaling	(126)
HIF-1α signaling pathway	(127, 128)
Hippo signaling Pathway	(129, 130)
JAK/STAT signaling	(131)
Matrix metalloproteinase and plasminogen activator system	(132, 133)
MUC1 mucin-mediated signaling pathways	(134)
NF-κB signaling	(135)
Notch signaling	(136)
PI3K/AKT/mTOR signaling	(137, 138)
PGD2/PTGDR2 signaling	(139)
STAT3 pathway	(140, 141)
TLR4 signaling	(142)
TGFβ, bone morphogenetic protein and activin signaling	(143, 144)
VEGFR-3 signaling	(145)
WNT-β-catenin-TCF signaling pathway	(146)

significantly decline in patients of gastric cancer with *H. pylori* infection, and glutamine levels are also low. Additionally, the production of hydrogen peroxide is encouraged, aggravating the effects of oxidative stress. However, GSH therapy is proved successful in alleviating the high ROS buildup (158). In conclusion, intestinalization in the gastric host cells is caused by low GSH levels. Therefore, the risk of *H. pylori*-induced carcinogenesis of gastric mucosal may be ameliorated in rats by raising their GSH levels, which may also prevent oxidative stress damage (108).

Antioxidants, such as vitamin E and selenium, have been the subject of numerous research in this context. In 1993, the first large, randomized, double-blind, primary prevention trial to investigate the potential cancer prevention benefits of supplementing with vitamin E, selenium and β-carotene was conducted, and the cocktail has been found to dramatically lower mortality from gastric cancer (159). Interestingly, the protective effects of these antioxidants can still be noticeable ten years after the end of supplementation (160). Clinical studies have shown that consistent oral dose of β-carotene is advantageous for lowering bacterial colonization by 48% (151). It has been proposed that intake of diet rich in vitamin C, carotenoids, and alpha-lipoic acid (α-LA) may lessen the morbidity of gastric disease linked to *H. pylori* infection. α-LA, a naturally occurring dithiol with antioxidant and anti-inflammatory function, can decrease the interaction between Nrf2 and Keap1, inhibit the pro-inflammatory cytokine IL-8 production and minimize the infection *via* the Nrf2/HO-1 pathway in the AGS cells (161). It is reported that omega-3 fatty acids inhibit the oxidation of polyunsaturated long-chain fatty acids and boost the antioxidant and anti-inflammatory effects of other nutrients (162). However, omega-3 may result in oxidative stress, and the process is associated with the suppression of the production of antioxidant enzymes. Therefore, antibiotics such clarithromycin, metronidazole, quinolones, amoxicillin, and tetracycline to counteract the oxidative effects of omega-3 is recommended (74). The expression of SOD2 (Mn-SOD), superoxide anion scavenger, is elevated, but the expression of SOD1 (copper/zincSOD) is decreased while comparing gastric cancer tissues with their matching normal mucosa. In specifically, the Mn-SOD ratio (levels in normal and malignant tissue) is demonstrated as an independent predictive indicator in patients of gastric cancer, and it appears to be therapeutically relevant for the survival of patients, the higher the ratio, the poorer overall survival (163). MnSOD is elevated in primary tumors with lymph node metastases while comparing gastric cancer patients with and without metastasis, indicating that MnSOD and ROS are involved in metastasis (164).

More importantly, it is necessary to block oxidative stress completely sometimes. For instance, HsrA, the *in vivo* exclusive regulator for epsilon proteobacteria, is involved in altering redox homeostasis and protein expression. Consequently, it may serve as a potential therapeutic target to eradicate *H. pylori* (153, 165). The increased expression of apoptosis-regulated gene in the gastric host cells of patients with *H. pylori* infection, such as BID, ZMAT3, PMAIP1 and FAS, can also be successfully controlled by the combination of curcumin and Res, which causes apoptosis to decline (166, 167).

TABLE 3 Antioxidant therapy.

Compound	Target	Reference
GSK2606414 (GlaxoSmithKline)	PERK	(147)
Statins	Autophagy	(148)
Gastrin	Autophagy	(149)
S-allyl cysteine	GSH	(150)
β-carotene	NADPH oxidase	(151)
Omega-3 fatty acids	Inflammatory and antioxidant	(152)
HsrA	Protein expression and redox homeostasis	(153, 154)
Curcumin and Res	Apoptosis-regulated genes	(155)

6 Conclusion

Gastric cancer is the third leading cause of cancer-related death worldwide. Free radicals and oxidative stress are continuously imposed upon cells in tissues and organs on a regular basis. More and more evidences show that ROS functions an essential role in the gastric cancer. Despite a number of mechanisms have been discussed in this review, most of the ROS-induced signaling targets are yet unknown. The elevated ROS production in gastric cancer can initiate genotoxic consequences, contributing to genetic instability, DNA damage, metabolic adaptation, drug resistance and occasional cell death. However, certain amounts of ROS can be advantageous because they trigger the antioxidant defense system and shield cells. There is an urgent need to find selective and readily available therapeutic therapies for gastric cancer and gastric cancer-predisposed patients. In order to treat and prevent ROS in gastric cancer, it may be crucial to focus on the enhancement of ROS by neutralizing antioxidants to induce cancer cell death, and the inhibition of ROS activity or increase of antioxidant capacity to regulate pro-tumorigenic signaling pathways. Nevertheless, considering that multiple studies have connected some dietary antioxidants with a rise in cancer incidence, it will be crucial to thoroughly investigate all biochemical reactions within cancer cells, including their precise targets and downstream effects while boosting antioxidant capacity. More researches are needed to put on the agenda to explore the function of elevated ROS and identify the exact ROS target pathways that will be most beneficial in treating gastric cancer.

Author contributions

All authors listed have made a substantial, direct, and intellectual contribution to the work and approved it for publication.

Funding

Young Talent Project of Jiangsu Provincial Traditional Chinese Medicine Science and Technology Development Plan (QN202206).

Conflict of interest

The authors declare that the research was conducted in the absence of any commercial or financial relationships that could be construed as a potential conflict of interest.

The reviewer YP declared a shared parent affiliation with the author YS to the handling editor at the time of the review.

Publisher's note

All claims expressed in this article are solely those of the authors and do not necessarily represent those of their affiliated organizations, or those of the publisher, the editors and the reviewers. Any product that may be evaluated in this article, or claim that may be made by its manufacturer, is not guaranteed or endorsed by the publisher.

References

1. Rawla P, Barsouk A. Epidemiology of gastric cancer: Global trends, risk factors and prevention. *Prz Gastroenterol* (2019) 14(1):26–38. doi: 10.5114/pg.2018.80001

2. Thrift AP, El-Serag HB. Burden of gastric cancer. *Clin Gastroenterol Hepatol* (2020) 18(3):534–42. doi: 10.1016/j.cgh.2019.07.045

3. Van Cutsem E, Sagaert X, Topal B, Haustermans K, Prenen H. Gastric cancer. *Lancet* (2016) 388(10060):2654–64. doi: 10.1016/S0140-6736(16)30354-3

4. Karimi P, Islami F, Anandasabapathy S, Freedman ND, Kamangar F. Gastric cancer: Descriptive epidemiology, risk factors, screening, and prevention. *Cancer Epidemiol Biomarkers Prev* (2014) 23(5):700–13. doi: 10.1158/1055-9965.EPI-13-1057

5. Wang JP, Sun YH, Bertagnolli MM. Comparison of gastric cancer survival between Caucasian and Asian patients treated in the united states: Results from the surveillance epidemiology and end results (Seer) database. *Ann Surg Oncol* (2015) 22 (9):2965–71. doi: 10.1245/s10434-015-4388-4

6. Bauer K, Schroeder M, Porzsolt F, Henne-Bruns D. Comparison of international guidelines on the accompanying therapy for advanced gastric cancer: Reasons for the differences. *J Gastric Cancer* (2015) 15(1):10–8. doi: 10.5230/jgc.2015.15.1.10

7. Hooi JKY, Lai WY, Ng WK, Suen MMY, Underwood FE, Tanyingoh D, et al. Global prevalence of helicobacter pylori infection: Systematic review and meta-analysis. *Gastroenterology* (2017) 153(2):420–9. doi: 10.1053/j.gastro.2017.04.022

8. Song Y, Liu X, Cheng W, Li H, Zhang D. The global, regional and national burden of stomach cancer and its attributable risk factors from 1990 to 2019. *Sci Rep* (2022) 12 (1):11542. doi: 10.1038/s41598-022-15839-7

9. Jencks DS, Adam JD, Borum ML, Koh JM, Stephen S, Doman DB. Overview of current concepts in gastric intestinal metaplasia and gastric cancer. *Gastroenterol Hepatol (N Y)* (2018) 14(2):92–101.

10. Habtemariam S. Modulation of reactive oxygen species in health and disease. *Antioxid (Basel Switzerland)* (2019) 8(11):513. doi: 10.3390/antiox8110513

11. Sarmiento-Salinas FL, Perez-Gonzalez A, Acosta-Casique A, Ix-Ballote A, Diaz A, Trevino S, et al. Reactive oxygen species: Role in carcinogenesis, cancer cell signaling and tumor progression. *Life Sci* (2021) 284:119942. doi: 10.1016/j.lfs.2021.119942

12. Barnes RP, Fouquerel E, Opresko PL. The impact of oxidative DNA damage and stress on telomere homeostasis. *Mech Ageing Dev* (2019) 177:37–45. doi: 10.1016/j.mad.2018.03.013

13. Kotsantis P, Petermann E, Boulton SJ. Mechanisms of oncogene-induced replication stress: Jigsaw falling into place. *Cancer Discovery* (2018) 8(5):537–55. doi: 10.1158/2159-8290.cd-17-1461

14. Perillo B, Di Donato M, Pezone A, Di Zazzo E, Giovannelli P, Galasso G, et al. Ros in cancer therapy: The bright side of the moon. *Exp Mol Med* (2020) 52(2):192–203. doi: 10.1038/s12276-020-0384-2

15. Azmanova M, Pitto-Barry A. Oxidative stress in cancer therapy: Friend or enemy? *Chembiochem* (2022) 23(10):e202100641. doi: 10.1002/cbic.202100641

16. Braga-Neto MB, Costa DVS, Queiroz DMM, Maciel FS, de Oliveira MS, Viana-Junior AB, et al. Increased oxidative stress in gastric cancer patients and their first-degree relatives: A prospective study from northeastern Brazil. *Oxid Med Cell Longev* (2021) 2021:6657434. doi: 10.1155/2021/6657434

17. Pisoschi AM, Pop A. The role of antioxidants in the chemistry of oxidative stress: A review. *Eur J Med Chem* (2015) 97:55–74. doi: 10.1016/j.ejmech.2015.04.040

18. Sharaf A, De Michele R, Sharma A, Fakhari S, Obornik M. Transcriptomic analysis reveals the roles of detoxification systems in response to mercury in chromera velia. *Biomolecules* (2019) 9(11):647. doi: 10.3390/biom9110647

19. Kowaltowski AJ, de Souza-Pinto NC, Castilho RF, Vercesi AE. Mitochondria and reactive oxygen species. *Free Radic Biol Med* (2009) 47(4):333–43. doi: 10.1016/j.freeradbiomed.2009.05.004

20. Sandalio LM, Rodríguez-Serrano M, Romero-Puertas MC, del Río LA. Role of peroxisomes as a source of reactive oxygen species (Ros) signaling molecules. *Subcellular Biochem* (2013) 69:231–55. doi: 10.1007/978-94-007-6889-5_13

21. Lin Y, Jiang M, Chen W, Zhao T, Wei Y. Cancer and er stress: Mutual crosstalk between autophagy, oxidative stress and inflammatory response. *BioMed Pharmacother* (2019) 118:109249. doi: 10.1016/j.biopha.2019.109249

22. Zia A, Farkhondeh T, Pourbagher-Shahri AM, Samarghandian S. The roles of mitochondrial dysfunction and reactive oxygen species in aging and senescence. *Curr Mol Med* (2022) 22(1):37–49. doi: 10.2174/1566524021666210218112616

23. Oyewole AO, Birch-Machin MA. Mitochondria-targeted antioxidants. *FASEB J* (2015) 29(12):4766–71. doi: 10.1096/fj.15-275404

24. Veskoukis AS, Tsatsakis AM, Kouretas D. Dietary oxidative stress and antioxidant defense with an emphasis on plant extract administration. *Cell Stress Chaperones* (2012) 17(1):11–21. doi: 10.1007/s12192-011-0293-3

25. Benhar M. Roles of mammalian glutathione peroxidase and thioredoxin reductase enzymes in the cellular response to nitrosative stress. *Free Radic Biol Med* (2018) 127:160–4. doi: 10.1016/j.freeradbiomed.2018.01.028

26. Kirtonia A, Sethi G, Garg M. The multifaceted role of reactive oxygen species in tumorigenesis. *Cell Mol Life Sci* (2020) 77(22):4459–83. doi: 10.1007/s00018-020-03536-5

27. Backert S, Neddermann M, Maubach G, Naumann M. Pathogenesis of helicobacter pylori infection. *Helicobacter* (2016) 21 Suppl 1:19–25. doi: 10.1111/hel.12335

28. Censini S, Stein M, Covacci A. Cellular responses induced after contact with helicobacter pylori. *Curr Opin Microbiol* (2001) 4(1):41–6. doi: 10.1016/s1369-5274(00)00162-4

29. Banks M, Graham D, Jansen M, Gotoda T, Coda S, di Pietro M, et al. British Society of gastroenterology guidelines on the diagnosis and management of patients at risk of gastric adenocarcinoma. *Gut* (2019) 68(9):1545–75. doi: 10.1136/gutjnl-2018-318126

30. Kalisperati P, Spanou E, Pateras IS, Korkolopoulou P, Varvarigou A, Karavokyros I, et al. Inflammation, DNA damage, helicobacter pylori and gastric tumorigenesis. *Front Genet* (2017) 8:20. doi: 10.3389/fgene.2017.00020

31. Zhang XY, Zhang PY, Aboul-Soud MA. From inflammation to gastric cancer: Role of helicobacter pylori. *Oncol Lett* (2017) 13(2):543–8. doi: 10.3892/ol.2016.5506

32. Handa O, Naito Y, Yoshikawa T. Helicobacter pylori: A ros-inducing bacterial species in the stomach. *Inflammation Res* (2010) 59(12):997–1003. doi: 10.1007/s00011-010-0245-x

33. Brown DI, Griendling KK. Nox proteins in signal transduction. *Free Radic Biol Med* (2009) 47(9):1239–53. doi: 10.1016/j.freeradbiomed.2009.07.023

34. Saini R, Singh S. Inducible nitric oxide synthase: An asset to neutrophils. *J Leukoc Biol* (2019) 105(1):49–61. doi: 10.1002/JLB.4RU0418-161R

35. Karkhah A, Ebrahimpour S, Rostamtabar M, Koppolu V, Darvish S, Vasigala VKR, et al. Helicobacter pylori evasion strategies of the host innate and adaptive immune responses to survive and develop gastrointestinal diseases. *Microbiol Res* (2019) 218:49–57. doi: 10.1016/j.micres.2018.09.011

36. Souliotis VL, Vlachogiannis NI, Pappa M, Argyriou A, Ntouros PA, Sfikakis PP. DNA Damage response and oxidative stress in systemic autoimmunity. *Int J Mol Sci* (2019) 21(1):55. doi: 10.3390/ijms21010055

37. Lin TY, Lan WH, Chiu YF, Feng CL, Chiu CH, Kuo CJ, et al. Statins' regulation of the virulence factors of helicobacter pylori and the production of ros may inhibit the development of gastric cancer. *Antioxid (Basel Switzerland)* (2021) 10(8):1293. doi: 10.3390/antiox10081293

38. Jain U, Saxena K, Chauhan N. Helicobacter pylori induced reactive oxygen species: A new and developing platform for detection. *Helicobacter* (2021) 26(3):e12796. doi: 10.1111/hel.12796

39. Grasberger H, El-Zaatari M, Dang DT, Merchant JL. Dual oxidases control release of hydrogen peroxide by the gastric epithelium to prevent helicobacter felis infection and inflammation in mice. *Gastroenterology* (2013) 145(5):1045–54. doi: 10.1053/j.gastro.2013.07.011

40. Ishikawa T, Yoshida N, Tokuda H, Kokura S, Nakabe N, Kuchide M, et al. Role of oxygen-derived free radicals in helicobacter pylori water extract-induced mouse skin carcinogenesis. *Biofactors* (2006) 28(1):1–7. doi: 10.1002/biof.5520280101

41. Mashimo M, Nishikawa M, Higuchi K, Hirose M, Wei Q, Haque A, et al. Production of reactive oxygen species in peripheral blood is increased in individuals with helicobacter pylori infection and decreased after its eradication. *Helicobacter* (2006) 11(4):266–71. doi: 10.1111/j.1523-5378.2006.00410.x

42. Zou Y, Chen X, Sun Y, Li P, Xu M, Fang P, et al. Antibiotics-free nanoparticles eradicate helicobacter pylori biofilms and intracellular bacteria. *J Control Release* (2022) 348:370–85. doi: 10.1016/j.jconrel.2022.05.044

43. Sezikli M, Cetinkaya ZA, Sezikli H, Güzelbulut F, Tiftikçi A, Ince AT, et al. Oxidative stress in helicobacter pylori infection: Does supplementation with vitamins c and e increase the eradication rate? *Helicobacter* (2009) 14(4):280–5. doi: 10.1111/j.1523-5378.2009.00686.x

44. Ding SZ, Minohara Y, Fan XJ, Wang J, Reyes VE, Patel J, et al. Helicobacter pylori infection induces oxidative stress and programmed cell death in human gastric epithelial cells. *Infect Immun* (2007) 75(8):4030–9. doi: 10.1128/IAI.00172-07

45. Tsugawa H, Suzuki H, Saya H, Hatakeyama M, Hirayama T, Hirata K, et al. Reactive oxygen species-induced autophagic degradation of helicobacter pylori caga is specifically suppressed in cancer stem-like cells. *Cell Host Microbe* (2012) 12(6):764–77. doi: 10.1016/j.chom.2012.10.014

46. Butcher LD, den Hartog G, Ernst PB, Crowe SE. Oxidative stress resulting from helicobacter pylori infection contributes to gastric carcinogenesis. *Cell Mol Gastroenterol Hepatol* (2017) 3(3):316–22. doi: 10.1016/j.jcmgh.2017.02.002

47. O'Hara AM, Bhattacharyya A, Bai J, Mifflin RC, Ernst PB, Mitra S, et al. Tumor necrosis factor (Tnf)-Alpha-Induced il-8 expression in gastric epithelial cells: Role of reactive oxygen species and ap endonuclease-1/Redox factor (Ref)-1. *Cytokine* (2009) 46(3):359–69. doi: 10.1016/j.cyto.2009.03.010

48. Amieva M, Peek RMJr. Pathobiology of helicobacter pylori-induced gastric cancer. *Gastroenterology* (2016) 150(1):64–78. doi: 10.1053/j.gastro.2015.09.004

49. Mita M, Satoh M, Shimada A, Okajima M, Azuma S, Suzuki JS, et al. Metallothionein is a crucial protective factor against helicobacter pylori-induced gastric erosive lesions in a mouse model. *Am J Physiol Gastrointestinal liver Physiol* (2008) 294(4):G877–84. doi: 10.1152/ajpgi.00251.2007

50. Zhao H, Zhu H, Lin Z, Lin G, Lv G. Compound 13, an Alpha1-selective small molecule activator of ampk, inhibits helicobacter pylori-induced oxidative stresses and gastric epithelial cell apoptosis. *Biochem Biophys Res Commun* (2015) 463(4):510–7. doi: 10.1016/j.bbrc.2015.05.059

51. Skowron MA, Niegisch G, Albrecht P, van Koeveringe G, Romano A, Albers P, et al. Various mechanisms involve the nuclear factor (Erythroid-derived 2)-like (Nrf2) to achieve cytoprotection in long-term cisplatin-treated urothelial carcinoma cell lines. *Int J Mol Sci* (2017) 18(8):1680. doi: 10.3390/ijms18081680

52. Wang G, Alamuri P, Maier RJ. The diverse antioxidant systems of helicobacter pylori. *Mol Microbiol* (2006) 61(4):847–60. doi: 10.1111/j.1365-2958.2006.05302.x

53. Ansari MR-N M, Dolatkhah H, Fattahi E, Aghazade AM, Mojtabaii-Motlag S. Comparison of levels of nitric oxide, superoxide dismutase and glutathione peroxidase of gastric juice in infected and non-infected patients with helicobacter Pylori. *Acta Medica Iranica* (2006) 44(3):159–66.

54. Lu J, Holmgren A. The thioredoxin antioxidant system. *Free Radic Biol Med* (2014) 66:75–87. doi: 10.1016/j.freeradbiomed.2013.07.036

55. Harris AG, Wilson JE, Danon SJ, Dixon MF, Donegan K, Hazell SL. Catalase (Kata) and kata-associated protein (Kapa) are essential to persistent colonization in the helicobacter pylori Ss1 mouse model. *Microbiol (Reading England)* (2003) 149(Pt 3):665–72. doi: 10.1099/mic.0.26012-0

56. Wang G, Maier RJ. An nadph quinone reductase of helicobacter pylori plays an important role in oxidative stress resistance and host colonization. *Infect Immun* (2004) 72(3):1391–6. doi: 10.1128/IAI.72.3.1391-1396.2004

57. Seyler RWJr., Olson JW, Maier RJ. Superoxide dismutase-deficient mutants of helicobacter pylori are hypersensitive to oxidative stress and defective in host colonization. *Infect Immun* (2001) 69(6):4034–40. doi: 10.1128/iai.69.6.4034-4040.2001

58. Stone KK, Bermudez E, Pryor WA. Aqueous extracts of cigarette tar containing the tar free radical cause DNA nicks in mammalian cells. *Environ Health Perspect* (1994) 102 Suppl 10:173–8. doi: 10.1289/ehp.94102s10173

59. Dizdaroglu M. Oxidatively induced DNA damage and its repair in cancer. *Mutat Res Rev Mutat Res* (2015) 763:212–45. doi: 10.1016/j.mrrev.2014.11.002

60. Birben E, Sahiner UM, Sackesen C, Erzurum S, Kalayci O. Oxidative stress and antioxidant defense. *World Allergy Organ J* (2012) 5(1):9–19. doi: 10.1097/WOX.0b013e3182439613

61. Wang S, Gallimore PJ, Liu-Kang C, Yeung K, Campbell SJ, Utinger B, et al. Dynamic wood smoke aerosol toxicity during oxidative atmospheric aging. *Environ Sci Technol* (2023) 57(3):1246–56. doi: 10.1021/acs.est.2c05929

62. Lyons K, Le LC, Pham YT, Borron C, Park JY, Tran CTD, et al. Gastric cancer: Epidemiology, biology, and prevention: A mini review. *Eur J Cancer Prev* (2019) 28(5):397–412. doi: 10.1097/cej.0000000000000480

63. Peleteiro B, Castro C, Morais S, Ferro A, Lunet N. Worldwide burden of gastric cancer attributable to tobacco smoking in 2012 and predictions for 2020. *Dig Dis Sci* (2015) 60(8):2470–6. doi: 10.1007/s10620-015-3624-x

64. Pasupathi P, Chinnaswamy P, Saravanan G, Kumar US. Effect of chronic smoking on lipid peroxidation and antioxidant status in gastric carcinoma patients. *Bangladesh Med Res Counc Bull* (2009) 35(1):1–6. doi: 10.3329/bmrcb.v35i1.2132

65. Alvarez-Parrilla E, de la Rosa LA, Legarreta P, Saenz L, Rodrigo-Garcia J, Gonzalez-Aguilar GA. Daily consumption of apple, pear and orange juice differently affects plasma lipids and antioxidant capacity of smoking and non-smoking adults. *Int J Food Sci Nutr* (2010) 61(4):369–80. doi: 10.3109/09637480903514041

66. Bøhn SK, Myhrstad MC, Thoresen M, Holden M, Karlsen A, Tunheim SH, et al. Blood cell gene expression associated with cellular stress defense is modulated by antioxidant-rich food in a randomised controlled clinical trial of Male smokers. *BMC Med* (2010) 8:54. doi: 10.1186/1741-7015-8-54

67. Cizmarova B, Tomeckova V, Hubkova B, Hurajtova A, Ohlasova J, Birkova A. Salivary redox homeostasis in human health and disease. *Int J Mol Sci* (2022) 23(17):10076. doi: 10.3390/ijms231710076

68. Ishimoto T, Sugihara H, Watanabe M, Sawayama H, Iwatsuki M, Baba Y, et al. Macrophage-derived reactive oxygen species suppress mir-328 targeting Cd44 in cancer cells and promote redox adaptation. *Carcinogenesis* (2014) 35(5):1003–11. doi: 10.1093/carcin/bgt402

69. Kiga K, Mimuro H, Suzuki M, Shinozaki-Ushiku A, Kobayashi T, Sanada T, et al. Epigenetic silencing of mir-210 increases the proliferation of gastric epithelium during chronic helicobacter pylori infection. *Nat Commun* (2014) 5:4497. doi: 10.1038/ncomms5497

70. Candido MF, Medeiros M, Veronez LC, Bastos D, Oliveira KL, Pezuk JA, et al. Drugging hijacked kinase pathways in pediatric oncology: Opportunities and current scenario. *Pharmaceutics* (2023) 15(2):664. doi: 10.3390/pharmaceutics15020664

71. Tatsuta M, Iishi H, Baba M, Mikuni T, Narahara H, Uedo N, et al. Suppression by iron chelator phenanthroline of sodium chloride-enhanced gastric carcinogenesis induced by n-Methyl-N'-Nitro-N-Nitrosoguanidine in wistar rats. *Cancer Lett* (2003) 191(1):9–16. doi: 10.1016/s0304-3835(01)00797-2

72. Xin H, Deng Y, Cao J. Proviral insertion in murine lymphomas 2 promotes stomach cancer progression by regulating apoptosis *Via* reactive oxygen species-triggered endoplasmic reticulum stress. *Biochem Biophys Res Commun* (2018) 506 (1):145–52. doi: 10.1016/j.bbrc.2018.09.062

73. George S, Lucero Y, Torres JP, Lagomarcino AJ, O'Ryan M. Gastric damage and cancer-associated biomarkers in helicobacter pylori-infected children. *Front Microbiol* (2020) 11:90. doi: 10.3389/fmicb.2020.00090

74. Han L, Shu X, Wang J. Helicobacter pylori-mediated oxidative stress and gastric diseases: A review. *Front Microbiol* (2022) 13:811258. doi: 10.3389/fmicb.2022.811258

75. Chaturvedi R, Asim M, Romero-Gallo J, Barry DP, Hoge S, de Sablet T, et al. Spermine oxidase mediates the gastric cancer risk associated with helicobacter pylori caga. *Gastroenterology* (2011) 141(5):1696–708 e1-2. doi: 10.1053/j.gastro.2011.07.045

76. Bagchi D, McGinn TR, Ye X, Bagchi M, Krohn RL, Chatterjee A, et al. Helicobacter pylori-induced oxidative stress and DNA damage in a primary culture of human gastric mucosal cells. *Dig Dis Sci* (2002) 47(6):1405–12. doi: 10.1023/a:1015399204069

77. Hanada K, Uchida T, Tsukamoto Y, Watada M, Yamaguchi N, Yamamoto K, et al. Helicobacter pylori infection introduces DNA double-strand breaks in host cells. *Infect Immun* (2014) 82(10):4182–9. doi: 10.1128/IAI.02368-14

78. Pan Z, Ma G, Kong L, Du G. Hypoxia-inducible factor-1: Regulatory mechanisms and drug development in stroke. *Pharmacol Res* (2021) 170:105742. doi: 10.1016/j.phrs.2021.105742

79. Rath S, Das L, Kokate SB, Pratheek BM, Chattopadhyay S, Goswami C, et al. Regulation of noxa-mediated apoptosis in helicobacter pylori-infected gastric epithelial cells. *FASEB J* (2015) 29(3):796–806. doi: 10.1096/fj.14-257501

80. Kannan A, Krishnan A, Ali M, Subramaniam S, Halagowder D, Sivasithamparam ND. Caveolin-1 promotes gastric cancer progression by up-regulating epithelial to mesenchymal transition by crosstalk of signalling mechanisms under hypoxic condition. *Eur J Cancer* (2014) 50(1):204–15. doi: 10.1016/j.ejca.2013.08.016

81. Hao W, Yuan X, Yu L, Gao C, Sun X, Wang D, et al. Licochalcone a-induced human gastric cancer bgc-823 cells apoptosis by regulating ros-mediated mapks and Pi3k/Akt signaling pathways. *Sci Rep* (2015) 5:10336. doi: 10.1038/srep10336

82. Lin J, Chen Z, Huang Z, Chen F, Ye Z, Lin S, et al. Effect of T-cadherin on the Akt/Mtor signaling pathway, gastric cancer cell cycle, migration and invasion, and its association with patient survival rate. *Exp Ther Med* (2019) 17(5):3607–13. doi: 10.3892/etm.2019.7350

83. Chaithongyot S, Jantaree P, Sokolova O, Naumann M. Nf-Kb in gastric cancer development and therapy. *Biomedicines* (2021) 9(8):870. doi: 10.3390/biomedicines9080870

84. Kidane D, Murphy DL, Sweasy JB. Accumulation of abasic sites induces genomic instability in normal human gastric epithelial cells during helicobacter pylori infection. *Oncogenesis* (2014) 3(11):e128. doi: 10.1038/oncsis.2014.42

85. Chaturvedi R, Asim M, Piazuelo MB, Yan F, Barry DP, Sierra JC, et al. Activation of egfr and Erbb2 by helicobacter pylori results in survival of gastric epithelial cells with DNA damage. *Gastroenterology* (2014) 146(7):1739–51.e14. doi: 10.1053/j.gastro.2014.02.005

86. Zhou X, Xu G, Yin C, Jin W, Zhang G. Down-regulation of mir-203 induced by helicobacter pylori infection promotes the proliferation and invasion of gastric cancer by targeting cask. *Oncotarget* (2014) 5(22):11631–40. doi: 10.18632/oncotarget.2600

87. Su M, Zhang Z, Zhou L, Han C, Huang C, Nice EC. Proteomics, personalized medicine and cancer. *Cancers (Basel)* (2021) 13(11):2512. doi: 10.3390/cancers13112512

88. Crowe SE. Helicobacter pylori infection. *N Engl J Med* (2019) 380(12):1158–65. doi: 10.1056/NEJMcp1710945

89. Singh N, Baby D, Rajguru JP, Patil PB, Thakkannavar SS, Pujari VB. Inflammation and cancer. *Ann Afr Med* (2019) 18(3):121–6. doi: 10.4103/aam.aam_56_18

90. Furukawa-Hibi Y, Yoshida-Araki K, Ohta T, Ikeda K, Motoyama N. Foxo forkhead transcription factors induce G(2)-m checkpoint in response to oxidative stress. *J Biol Chem* (2002) 277(30):26729–32. doi: 10.1074/jbc.C200256200

91. Piscione M, Mazzone M, Di Marcantonio MC, Muraro R, Mincione G. Eradication of helicobacter pylori and gastric cancer: A controversial relationship. *Front Microbiol* (2021) 12:630852. doi: 10.3389/fmicb.2021.630852

92. Correa P. A human model of gastric carcinogenesis. *Cancer Res* (1988) 48 (13):3554–60.

93. El Hafa F, Wang T, Ndifor VM, Jin G. Association between helicobacter pylori antibodies determined by multiplex serology and gastric cancer risk: A meta-analysis. *Helicobacter* (2022) 27(3):e12881. doi: 10.1111/hel.12881

94. Wroblewski LE, Choi E, Petersen C, Delgado AG, Piazuelo MB, Romero-Gallo J, et al. Targeted mobilization of Lrig1(+) gastric epithelial stem cell populations by a carcinogenic helicobacter pylori type iv secretion system. *Proc Natl Acad Sci U.S.A.* (2019) 116(39):19652–8. doi: 10.1073/pnas.1903798116

95. Toh JWT, Wilson RB. Pathways of gastric carcinogenesis, helicobacter pylori virulence and interactions with antioxidant systems, vitamin c and phytochemicals. *Int J Mol Sci* (2020) 21(17):6451. doi: 10.3390/ijms21176451

96. Naito Y, Yoshikawa T, Fujii T, Boku Y, Yagi N, Dao S, et al. Monochloramine-induced cell growth inhibition and apoptosis in a rat gastric mucosal cell line. *J Clin Gastroenterol* (1997) 25 Suppl 1:S179–85. doi: 10.1097/00004836-199700001-00029

97. Wallaschek N, Reuter S, Silkenat S, Wolf K, Niklas C, Kayisoglu O, et al. Ephrin receptor A2, the epithelial receptor for Epstein-Barr virus entry, is not available for efficient infection in human gastric organoids. *PloS Pathog* (2021) 17(2):e1009210. doi: 10.1371/journal.ppat.1009210

98. Akkus S, Gareayaghi N, Saribas S, Demiryas S, Ozbey D, Kepil N, et al. Co-Infection relationship with Epstein-Barr virus in gastroduodenal diseases with helicobacter pylori. quantitative pcr and ebna-1 gene-based approach. *Acta Gastroenterol Belg* (2022) 85(2):301–8. doi: 10.51821/85.2.9440

99. Yang H, Hu B. Immunological perspective: Helicobacter pylori infection and gastritis. *Mediators Inflammation* (2022) 2022:2944156. doi: 10.1155/2022/2944156

100. Saunders RM, Biddle M, Amrani Y, Brightling CE. Stressed out - the role of oxidative stress in airway smooth muscle dysfunction in asthma and copd. *Free Radic Biol Med* (2022) 185:97–119. doi: 10.1016/j.freeradbiomed.2022.04.011

101. Futagami S, Hiratsuka T, Shindo T, Horie A, Hamamoto T, Suzuki K, et al. Expression of Apurinic/Apyrimidinic endonuclease-1 (Ape-1) in h. pylori-associated gastritis, gastric adenoma, and gastric cancer. *Helicobacter* (2008) 13(3):209–18. doi: 10.1111/j.1523-5378.2008.00605.x

102. Du MQ, Atherton JC. Molecular subtyping of gastric malt lymphomas: Implications for prognosis and management. *Gut* (2006) 55(6):886–93. doi: 10.1136/gut.2004.061663

103. Gong EJ, Ahn JY, Jung HY, Park H, Ko YB, Na HK, et al. Helicobacter pylori eradication therapy is effective as the initial treatment for patients with h. pylori-negative and disseminated gastric mucosa-associated lymphoid tissue lymphoma. *Gut liver* (2016) 10(5):706–13. doi: 10.5009/gnl15510

104. Floch P, Megraud F, Lehours P. Helicobacter pylori strains and gastric malt lymphoma. *Toxins (Basel)* (2017) 9(4):132. doi: 10.3390/toxins9040132

105. Kim SS, Ruiz VE, Carroll JD, Moss SF. Helicobacter pylori in the pathogenesis of gastric cancer and gastric lymphoma. *Cancer Lett* (2011) 305(2):228–38. doi: 10.1016/j.canlet.2010.07.014

106. Della Bella C, Soluri MF, Puccio S, Benagiano M, Grassi A, Bitetti J, et al. The helicobacter pylori cagy protein drives gastric Th1 and Th17 inflammation and b cell proliferation in gastric malt lymphoma. *Int J Mol Sci* (2021) 22(17):9459. doi: 10.3390/ijms22179459

107. Zullo A, Hassan C, Cristofari F, Andriani A, De Francesco V, Ierardi E, et al. Effects of helicobacter pylori eradication on early stage gastric mucosa-associated lymphoid tissue lymphoma. *Clin Gastroenterol Hepatol* (2010) 8(2):105–10. doi: 10.1016/j.cgh.2009.07.017

108. Matsuoka K, Nishiumi S, Yoshida M, Kodama Y. Effects of helicobacter pylori on the glutathione-related pathway in gastric epithelial cells. *Biochem Biophys Res Commun* (2020) 526(4):1118–24. doi: 10.1016/j.bbrc.2020.04.019

109. Poplawski T, Chojnacki C, Czubatka A, Klupinska G, Chojnacki J, Blasiak J. Helicobacter pylori infection and antioxidants can modulate the genotoxic effects of heterocyclic amines in gastric mucosa cells. *Mol Biol Rep* (2013) 40(8):5205–12. doi: 10.1007/s11033-013-2622-3

110. Deng R, Mo F, Chang B, Zhang Q, Ran H, Yang S, et al. Glucose-derived ages enhance human gastric cancer metastasis through Rage/Erk/Sp1/Mmp2 cascade. *Oncotarget* (2017) 8(61):104216–26. doi: 10.18632/oncotarget.22185

111. Ahn MJ, Kim BH, Jang SJ, Hong EK, Lee WM, Baik HK, et al. Expression of cyclin D1 and cyclin e in human gastric carcinoma and its clinicopathologic significance. *J Korean Med Sci* (1998) 13(5):513–8. doi: 10.3346/jkms.1998.13.5.513

112. Aoyagi K, Koufuji K, Yano S, Murakami N, Terasaki Y, Yamasaki Y, et al. Immunohistochemical study on the expression of cyclin D1 and e in gastric cancer. *Kurume Med J* (2000) 47(3):199–203. doi: 10.2739/kurumemedj.47.199

113. Arendt T, Rodel L, Gartner U, Holzer M. Expression of the cyclin-dependent kinase inhibitor P16 in alzheimer's disease. *Neuroreport* (1996) 7(18):3047–9. doi: 10.1097/00001756-199611250-00050

114. Gamboa-Dominguez A, Seidl S, Reyes-Gutierrez E, Hermannstädter C, Quintanilla-Martinez L, Busch R, et al. Prognostic significance of P21waf1/Cip1, P27kip1, P53 and e-cadherin expression in gastric cancer. *J Clin Pathol* (2007) 60 (7):756–61. doi: 10.1136/jcp.2006.038976

115. Shin VY, Wu WK, Chu KM, Wong HP, Lam EK, Tai EK, et al. Nicotine induces cyclooxygenase-2 and vascular endothelial growth factor receptor-2 in association with tumor-associated invasion and angiogenesis in gastric cancer. *Mol Cancer Res* (2005) 3(11):607–15. doi: 10.1158/1541-7786.MCR-05-0106

116. Leung WK, To KF, Go MY, Chan KK, Chan FK, Ng EK, et al. Cyclooxygenase-2 upregulates vascular endothelial growth factor expression and angiogenesis in human gastric carcinoma. *Int J Oncol* (2003) 23(5):1317–22. doi: 10.3892/ijo.23.5.1317

117. Shimakura S, Boland CR. Eicosanoid production by the human gastric cancer cell line ags and its relation to cell growth. *Cancer Res* (1992) 52(7):1744–9.

118. Ji XK, Madhurapantula SV, He G, Wang KY, Song CH, Zhang JY, et al. Genetic variant of cyclooxygenase-2 in gastric cancer: More inflammation and susceptibility. *World J Gastroenterol* (2021) 27(28):4653–66. doi: 10.3748/wjg.v27.i28.4653

119. Li Y, Liu C, Zhang X, Huang X, Liang S, Xing F, et al. Cct5 induces epithelial-mesenchymal transition to promote gastric cancer lymph node metastasis by activating the Wnt/Beta-catenin signalling pathway. *Br J Cancer* (2022) 126(12):1684–94. doi: 10.1038/s41416-022-01747-0

120. Tian S, Peng P, Li J, Deng H, Zhan N, Zeng Z, et al. Serpinh1 regulates emt and gastric cancer metastasis *Via* the Wnt/Beta-catenin signaling pathway. *Aging (Albany NY)* (2020) 12(4):3574–93. doi: 10.18632/aging.102831

121. Lei ZN, Teng QX, Tian Q, Chen W, Xie Y, Wu K, et al. Signaling pathways and therapeutic interventions in gastric cancer. *Signal Transduct Target Ther* (2022) 7 (1):358. doi: 10.1038/s41392-022-01190-w

122. Vitiello PP, Cardone C, Martini G, Ciardiello D, Belli V, Matrone N, et al. Receptor tyrosine kinase-dependent Pi3k activation is an escape mechanism to vertical suppression of the Egfr/Ras/Mapk pathway in kras-mutated human colorectal cancer cell lines. *J Exp Clin Cancer Res* (2019) 38(1):41. doi: 10.1186/s13046-019-1035-0

123. Yan H, Zheng C, Li Z, Bao B, Yang B, Hou K, et al. Nptx1 promotes metastasis *Via* Integrin/Fak signaling in gastric cancer. *Cancer Manag Res* (2019) 11:3237–51. doi: 10.2147/CMAR.S196509

124. Wang X, Zhou Q, Yu Z, Wu X, Chen X, Li J, et al. Cancer-associated fibroblast-derived lumican promotes gastric cancer progression *Via* the integrin B1-fak signaling pathway. *Int J Cancer* (2017) 141(5):998–1010. doi: 10.1002/ijc.30801

125. Yu GZ, Chen Y, Wang JJ. Overexpression of Grb2/Her2 signaling in Chinese gastric cancer: Their relationship with clinicopathological parameters and prognostic significance. *J Cancer Res Clin Oncol* (2009) 135(10):1331–9. doi: 10.1007/s00432-009-0574-8

126. Katoh Y, Katoh M. Hedgehog signaling pathway and gastric cancer. *Cancer Biol Ther* (2005) 4(10):1050–4. doi: 10.4161/cbt.4.10.2184

127. Li H, Jia Y, Wang Y. Targeting hif-1α signaling pathway for gastric cancer treatment. *Die Pharmazie* (2019) 74(1):3–7. doi: 10.1691/ph.2019.8674

128. Wang J, Ni Z, Duan Z, Wang G, Li F. Altered expression of hypoxia-inducible factor-1α (Hif-1α) and its regulatory genes in gastric cancer tissues. *PloS One* (2014) 9 (6):e99835. doi: 10.1371/journal.pone.0099835

129. Zhou GX, Li XY, Zhang Q, Zhao K, Zhang CP, Xue CH, et al. Effects of the hippo signaling pathway in human gastric cancer. *Asian Pac J Cancer Prev* (2013) 14 (9):5199–205. doi: 10.7314/apjcp.2013.14.9.5199

130. Kang W, Cheng AS, Yu J, To KF. Emerging role of hippo pathway in gastric and other gastrointestinal cancers. *World J Gastroenterol* (2016) 22(3):1279–88. doi: 10.3748/wjg.v22.i3.1279

131. Khanna P, Chua PJ, Bay BH, Baeg GH. The Jak/Stat signaling cascade in gastric carcinoma (Review). *Int J Oncol* (2015) 47(5):1617–26. doi: 10.3892/ijo.2015.3160

132. Ji F, Chen YL, Jin EY, Wang WL, Yang ZL, Li YM. Relationship between matrix metalloproteinase-2 mrna expression and clinicopathological and urokinase-type plasminogen activator system parameters and prognosis in human gastric cancer. *World J Gastroenterol* (2005) 11(21):3222–6. doi: 10.3748/wjg.v11.i21.3222

133. Lee KH, Choi EY, Kim MK, Kim KO, Jang BI, Kim SW, et al. Inhibition of histone deacetylase activity down-regulates urokinase plasminogen activator and matrix metalloproteinase-9 expression in gastric cancer. *Mol Cell Biochem* (2010) 343(1-2):163–71. doi: 10.1007/s11010-010-0510-x

134. Ganguly K, Rauth S, Marimuthu S, Kumar S, Batra SK. Unraveling mucin domains in cancer and metastasis: When protectors become predators. *Cancer Metastasis Rev* (2020) 39(3):647–59. doi: 10.1007/s10555-020-09896-5

135. Sokolova O, Naumann M. Nf-Kb signaling in gastric cancer. *Toxins (Basel)* (2017) 9(4):119. doi: 10.3390/toxins9040119

136. Brzozowa M, Mielanczyk L, Michalski M, Malinowski L, Kowalczyk-Ziomek G, Helewski K, et al. Role of notch signaling pathway in gastric cancer pathogenesis. *Contemp Oncol (Pozn)* (2013) 17(1):1–5. doi: 10.5114/wo.2013.33765

137. Matsuoka T, Yashiro M. The role of Pi3k/Akt/Mtor signaling in gastric carcinoma. *Cancers (Basel)* (2014) 6(3):1441–63. doi: 10.3390/cancers6031441

138. Tapia O, Riquelme I, Leal P, Sandoval A, Aedo S, Weber H, et al. The Pi3k/Akt/Mtor pathway is activated in gastric cancer with potential prognostic and predictive significance. *Virchows Arch* (2014) 465(1):25–33. doi: 10.1007/s00428-014-1588-4

139. Zhang B, Bie Q, Wu P, Zhang J, You B, Shi H, et al. Pgd2/Ptgdr2 signaling restricts the self-renewal and tumorigenesis of gastric cancer. *Stem Cells* (2018) 36 (7):990–1003. doi: 10.1002/stem.2821

140. Ashrafizadeh M, Zarrabi A, Orouei S, Zarrin V, Rahmani Moghadam E, Zabolian A, et al. Stat3 pathway in gastric cancer: Signaling, therapeutic targeting and future prospects. *Biol (Basel)* (2020) 9(6):126. doi: 10.3390/biology9060126

141. Giraud AS, Menheniott TR, Judd LM. Targeting Stat3 in gastric cancer. *Expert Opin Ther Targets* (2012) 16(9):889–901. doi: 10.1517/14728222.2012.709238

142. Yuan X, Zhou Y, Wang W, Li J, Xie G, Zhao Y, et al. Activation of Tlr4 signaling promotes gastric cancer progression by inducing mitochondrial ros production. *Cell Death Dis* (2013) 4:e794. doi: 10.1038/cddis.2013.334

143. Zhang J, Ge Y, Sun L, Cao J, Wu Q, Guo L, et al. Effect of bone morphogenetic protein-2 on proliferation and apoptosis of gastric cancer cells. *Int J Med Sci* (2012) 9 (2):184–92. doi: 10.7150/ijms.3859

144. Shirai YT, Ehata S, Yashiro M, Yanagihara K, Hirakawa K, Miyazono K. Bone morphogenetic protein-2 and -4 play tumor suppressive roles in human diffuse-type gastric carcinoma. *Am J Pathol* (2011) 179(6):2920–30. doi: 10.1016/j.ajpath.2011.08.022

145. Hsieh HL, Tsai MM. Tumor progression-dependent angiogenesis in gastric cancer and its potential application. *World J Gastrointest Oncol* (2019) 11(9):686–704. doi: 10.4251/wjgo.v11.i9.686

146. Song L, Guo X, Zhao F, Wang W, Zhao Z, Jin L, et al. Ttc36 inactivation induce malignant properties *Via* wnt-Beta-Catenin pathway in gastric carcinoma. *J Cancer* (2021) 12(9):2598–609. doi: 10.7150/jca.47292

147. Axten JM, Medina JR, Feng Y, Shu A, Romeril SP, Grant SW, et al. Discovery of 7-Methyl-5-(1-[3-(Trifluoromethyl)Phenyl]Acetyl-2,3-Dihydro-1h-Indol-5-Yl)-7h-Pyrrolo[2,3-D]Pyrimidin-4-Amine (Gsk2606414), a potent and selective first-in-Class inhibitor of protein kinase r (Pkr)-like endoplasmic reticulum kinase (Perk). *J Med Chem* (2012) 55(16):7193–207. doi: 10.1021/jm300713s

148. Liao WC, Huang MZ, Wang ML, Lin CJ, Lu TL, Lo HR, et al. Statin decreases helicobacter pylori burden in macrophages by promoting autophagy. *Front Cell Infect Microbiol* (2016) 6:203. doi: 10.3389/fcimb.2016.00203

149. Rao SV, Solum G, Niederdorfer B, Norsett KG, Bjorkoy G, Thommesen L. Gastrin activates autophagy and increases migration and survival of gastric adenocarcinoma cells. *BMC Cancer* (2017) 17(1):68. doi: 10.1186/s12885-017-3055-5

150. Velmurugan B, Bhuvaneswari V, Nagini S. Effect of s-allylcysteine on oxidant-antioxidant status during n-Methyl-N'-Nitro-N-Nitrosoguanidine and saturated sodium chloride-induced gastric carcinogenesis in wistar rats. *Asia Pac J Clin Nutr* (2003) 12(4):488–94.

151. Park Y, Lee H, Lim JW, Kim H. Inhibitory effect of B-carotene on helicobacter pylori-induced traf expression and hyper-proliferation in gastric epithelial cells. *Antioxid (Basel Switzerland)* (2019) 8(12):637. doi: 10.3390/antiox8120637

152. Sepidarkish M, Akbari-Fakhrabadi M, Daneshzad E, Yavari M, Rezaeinejad M, Morvaridzadeh M, et al. Effect of omega-3 fatty acid plus vitamin e Co-supplementation on oxidative stress parameters: A systematic review and meta-analysis. *Clin Nutr* (2020) 39(4):1019–25. doi: 10.1016/j.clnu.2019.05.004

153. Pelliciari S, Pinatel E, Vannini A, Peano C, Puccio S, De Bellis G, et al. Insight into the essential role of the helicobacter pylori Hp1043 orphan response regulator: Genome-wide identification and characterization of the DNA-binding sites. *Sci Rep* (2017) 7:41063. doi: 10.1038/srep41063

154. Gonzalez A, Salillas S, Velazquez-Campoy A, Espinosa Angarica V, Fillat MF, Sancho J, et al. Identifying potential novel drugs against helicobacter pylori by targeting the essential response regulator hsra. *Sci Rep* (2019) 9(1):11294. doi: 10.1038/s41598-019-47746-9

155. Xu XY, Meng X, Li S, Gan RY, Li Y, Li HB. Bioactivity, health benefits, and related molecular mechanisms of curcumin: Current progress, challenges, and perspectives. *Nutrients* (2018) 10(10):1553. doi: 10.3390/nu10101553

156. Velmurugan B, Subapriya R, Nagini S. Chemoprotection against n-Methyl-N'-Nitro-N-Nitrosoguanidine-Induced oxidative stress by s-allylcysteine, a garlic constituent, in wistar rats. *Toxicol Mech Methods* (2003) 13(2):83–7. doi: 10.1080/15376510309844

157. Chitcholtan K, Hampton MB, Keenan JI. Outer membrane vesicles enhance the carcinogenic potential of helicobacter pylori. *Carcinogenesis* (2008) 29(12):2400–5. doi: 10.1093/carcin/bgn218

158. Lee YM, Kim MJ, Kim Y, Kim H. Glutamine deprivation causes hydrogen peroxide-induced interleukin-8 expression *Via* Jak1/Stat3 activation in gastric epithelial ags cells. *J Cancer Prev* (2015) 20(3):179–84. doi: 10.15430/JCP.2015.20.3.179

159. Li JY, Taylor PR, Li B, Dawsey S, Wang GQ, Ershow AG, et al. Nutrition intervention trials in linxian, China: Multiple Vitamin/Mineral supplementation, cancer incidence, and disease-specific mortality among adults with esophageal dysplasia. *J Natl Cancer Inst* (1993) 85(18):1492–8. doi: 10.1093/jnci/85.18.1492

160. Qiao YL, Dawsey SM, Kamangar F, Fan JH, Abnet CC, Sun XD, et al. Total and cancer mortality after supplementation with vitamins and minerals: Follow-up of the linxian general population nutrition intervention trial. *J Natl Cancer Inst* (2009) 101 (7):507–18. doi: 10.1093/jnci/djp037

161. Kyung S, Lim JW, Kim H. A-lipoic acid inhibits il-8 expression by activating Nrf2 signaling in helicobacter pylori-infected gastric epithelial cells. *Nutrients* (2019) 11 (10):2524. doi: 10.3390/nu11102524

162. Sepidarkish M, Morvaridzadeh M, Akbari-Fakhrabadi M, Almasi-Hashiani A, Rezaeinejad M, Heshmati J. Effect of omega-3 fatty acid plus vitamin e Co-supplementation on lipid profile: A systematic review and meta-analysis. *Diabetes Metab Syndr* (2019) 13(2):1649–56. doi: 10.1016/j.dsx.2019.03.018

163. Janssen AM, Bosman CB, van Duijn W, Oostendorp-van de Ruit MM, Kubben FJ, Griffioen G, et al. Superoxide dismutases in gastric and esophageal cancer and the prognostic impact in gastric cancer. *Clin Cancer Res* (2000) 6(8):3183–92.

164. Jelic MD, Mandic AD, Maricic SM, Srdjenovic BU. Oxidative stress and its role in cancer. *J Cancer Res Ther* (2021) 17(1):22–8. doi: 10.4103/jcrt.JCRT_862_16

165. Gonzalez A, Casado J, Chueca E, Salillas S, Velazquez-Campoy A, Espinosa Angarica V, et al. Repurposing dihydropyridines for treatment of helicobacter pylori infection. *Pharmaceutics* (2019) 11(12):681. doi: 10.3390/pharmaceutics11120681

166. Xu H, Yu WB, Gao Y, Zhang MJ, Malhotra A, Yu WH. Modulatory potential of curcumin and resveratrol on P53 post-translational modifications during gastric cancer. *J Environ Pathol Toxicol Oncol* (2018) 37(2):93–101. doi: 10.1615/JEnvironPatholToxicolOncol.2018025547

167. Gavrilas LI, Cruceriu D, Ionescu C, Miere D, Balacescu O. Pro-apoptotic genes as new targets for single and combinatorial treatments with resveratrol and curcumin in colorectal cancer. *Food Funct* (2019) 10(6):3717–26. doi: 10.1039/c9fo01014a

frontiers | Frontiers in Oncology

TYPE Original Research
PUBLISHED 19 April 2023
DOI 10.3389/fonc.2023.1179120

OPEN ACCESS

EDITED BY
Chenyu Sun,
AMITA Health, United States

REVIEWED BY
Zhijia Xia,
Ludwig Maximilian University of Munich, Germany
Shi-Nan Wu,
The First Affiliated Hospital of Nanchang University, China

*CORRESPONDENCE
Hesong Zhang
docz5610033@163.com
Hailang Zhou
zhouhl198779@163.com

†The authors have contributed equally to this work

SPECIALTY SECTION
This article was submitted to Cancer Immunity and Immunotherapy, a section of the journal Frontiers in Oncology

RECEIVED 03 March 2023
ACCEPTED 03 April 2023
PUBLISHED 19 April 2023

CITATION
Rui S, Wang D, Huang Y, Xu J, Zhou H and Zhang H (2023) Prognostic value of *SLC4A4* and its correlation with the microsatellite instability in colorectal cancer.
Front. Oncol. 13:1179120.
doi: 10.3389/fonc.2023.1179120

Prognostic value of *SLC4A4* and its correlation with the microsatellite instability in colorectal cancer

Shaorui Rui[1†], Dong Wang[2†], Yong Huang[1], Jingyun Xu[3], Hailang Zhou[4,5*] and Hesong Zhang[6*]

[1]Department of General Surgery, The Second Affiliated Hospital of Wannan Medical College, Wuhu, China, [2]Department of Hepatobiliary Surgery, The First Affiliated Hospital of Wannan Medical College, Wuhu, China, [3]School of Basic Medicine, Wannan Medical College, Wuhu, China, [4]Department of Gastroenterology, Lianshui People's Hospital Affiliated to Kangda College of Nanjing Medical University, Huai'an, China, [5]The Institute of Life Sciences, Jiangsu College of Nursing, Huai'an, China, [6]Department of Hepatobiliary Surgery, The Second People's Hospital of Wuhu, Wuhu, China

Objective: To explore new biomarkers related to microsatellite instability in order to better predict prognosis and guide medication.

Methods: The "limma" R package was used to identify differentially expressed genes in GSE24514, and then weighted correlation network analysis was used to select key genes. Different cell types in the tumor microenvironment were identified and analyzed by single-cell sequencing, with a Lasso regression model used to screen prognostic variables. Furthermore, the correlation between microsatellite instability and potential prognostic variables was explored, as well as the expression characteristics and clinical characteristics of the prognostic variables in the TCGA, UALCAN, and HPA databases. PCR assay was used to investigate the expression of *SLC4A4* in colorectal cancer cell lines. Finally, we further verified the expression of *SLC4A4* by immunohistochemistry.

Results: First, 844 differentially expressed genes in GSE24514 were identified. Subsequently, weighted co-expression network analysis (WGCNA) of GSE24514 obtained all the genes significantly associated with microsatellite instability (MSI), a total of 1452. Analysis of GSE166555 single cell sequencing data set yielded 1564 differentially expressed genes. The gene sets obtained from the above three analysis processes were intersected, and 174 genes were finally obtained. The Lasso regression model revealed two potential prognostic genes, TIMP1 and *SLC4A4*, of which, there was a stronger correlation between microsatellite instability and *SLC4A4*. The mRNA and protein expression of *SLC4A4* was significantly decreased in tumors, and patients with low *SLC4A4* expression had a poor prognosis. In addition, *SLC4A4* was specifically expressed in epithelial cells. In the microenvironment of colorectal cancer, malignant cells have a strong interaction with different stromal cells. PCR showed that *SLC4A4* was significantly down-regulated in colorectal cancer cell lines Caco-2, HCT116 and HT29 compared with normal control NCM460 cell lines.

Immunohistochemistry also showed low expression of *SLC4A4* in colorectal cancer.

Conclusion: *SLC4A4*, as a tumor suppressor gene, is significantly downregulated and positively correlated with microsatellite instability, thus it may be combined with microsatellite instability to guide colorectal cancer treatment.

KEYWORDS

microsatellite instability, single-cell sequencing, colorectal cancer, biomarker, Slc4a4

Introduction

Colorectal cancer (CRC) is one of the most common gastrointestinal malignancies in the world, which is characterized by its high incidence and recurrence rate (1). The liver is the most common site of metastasis, and the 1-,3-and 5-year survival rates of patients with liver metastasis are far from satisfactory (2). According to statistics, there are more than 1.8 million new cases in the world every year (3). At present, due to the great progress in the pathophysiology of colorectal cancer, the treatment options have also increased, including endoscopic and surgical resection, radiotherapy, immunotherapy, targeted therapy, and local ablation (4–7). However, CRC is still the third most frequently diagnosed cancer and the second leading cause of cancer death worldwide due to imperfect screening programs, treatment strategies, and increased incidence (8). Therefore, identifying predictive biomarkers and revealing supporting mechanisms are urgently needed when predicting and treating CRC. The large-scale sequencing cancer genome project has identified biomarkers with potential clinical and therapeutic value, including microsatellite instability (MSI). In normal cells, the mismatch repair (MMR) system verifies and maintains the repeated count of microsatellites during cell division, which is one of the cellular DNA repair mechanisms. The damage to the MMR system causes cells to be unable to adjust the length of their microsatellite during cell division, known as MSI.

After several cell division cycles, the damaged cells will develop cells with different lengths of microsatellite sequences. MSI is often observed in colorectal cancer, endometrial cancer, and gastric adenocarcinoma and has been used in treating colorectal cancer with an improved prognosis of patients with MSI-H (MSI-high) colorectal cancer compared to patients with MSI-L (MSI-low) tumor. In addition, MSI-H colorectal tumors have been proven to be more susceptible to immune enhancement therapy. In 2019, FDA approved pembrolizumab for the treatment of patients with advanced MSI tumors (9), indicating that a programmed death 1 receptor (PD-1) blockade has become a highly relevant treatment choice for this patient group, regardless of tumor site or histology (10).

The solute carrier (SLC) family is a group of membrane transport proteins that play critical roles in the transportation of various metabolites, nutrients, and drugs across cell membranes. Dysregulation of SLC proteins has been implicated in the development and progression of various cancers, including breast, lung, prostate, and colorectal cancer (11). Studies have shown that alterations in SLC expression and activity can affect tumor cell growth, survival, and metastasis.

For instance, SLC transporters have been found to play a role in the uptake of nutrients such as glucose and amino acids, which are essential for cancer cell metabolism and growth. The upregulation of SLC transporters, such as SLC7A5 and SLC1A5, has been observed in various cancer types and is associated with poor prognosis. In contrast, the downregulation of SLC transporters, such as SLC26A4 and SLC5A8, has been shown to inhibit cancer cell proliferation and migration (12, 13).

The bicarbonate transporter consists of two families, SLC4 and SLC26, which can be further subdivided into acid loaders or acid extruders depending on the orientation of the transporter (14). The acidic extruder absorbs bicarbonate and thus prevents TME acidification by acting on the acidic extruder. The reduced expression of *SLC4A4* can promote cancer cell proliferation and migration traits *in vitro* or under the condition of immunodeficiency, which is mainly dependent on the tumor cell type. In renal clear cell carcinoma, miR-223-3p promotes cell proliferation and metastasis by downregulating *SLC4A4* (15). This study investigated novel biomarkers that are significantly associated with MSI and have significant prognostic implications.

Materials and methods

Data download and processing

The TCGA-COAD cohort data, including gene expression data from 471 tumor tissues, survival data from 454 patients, clinical phenotype data from 478 patients, and tumor mutation data from 399 patients, were obtained from the UCSC Xena website (http://xena.ucsc.edu/). The high-throughput sequencing data GSE24514 was downloaded from the GEO database. There were 49 samples in total, and 44 samples remained after quality control. Single cell sequencing data GSE166555 was downloaded from the GEO database and included 12 tumor tissues and their paracancer controls. All the data was log2 transformed.

Differential gene expression by microarray data mining

The expression data of GSE24514 were downloaded from the GEO database (16) and then, principal component analysis (PCA) and UMAP (Uniform Manifold Approximation and Projection for Dimension Reduction) were used to visualize each sample in groups and remove outliers. The R software package limma (version 3.40.6) was then used to identify the differentially expressed genes. Briefly, the data was log2 transformed and subjected to multiple linear regression using the lmFit function. We set up $|\log2FC| > 1$ and P-value < 0.05. The differentially expressed genes were visualized in volcano maps and thermal maps.

Identification of candidate biomarker gene by WGCNA

WGCNA (Weighted Correlation Network Analysis) is a systematic biological method used to describe gene association patterns between different samples to identify gene sets with highly synergistic changes and candidate biomarker genes or therapeutic targets based on the interconnectivity of gene sets and the association between gene sets and phenotypes. When compared to focusing only on differentially expressed genes, WGCNA identified the gene set of interest using the information regarding thousands or nearly ten thousand of the most varied genes or all genes and performed significant association analysis with phenotypes.

Single-cell sequencing to explore heterogeneity in the tumor microenvironment

The sequencing data from TISCH2 and GSE166555 from the GEO database were used to characterize the tumor microenvironment at the single-cell resolution (17). Several different cell types were identified after dimensionality reduction clustering and annotation of cell markers. Understanding the cell-cell interaction (CCI) is essential to study how these cells and signals coordinate function, therefore CellChat was integrated to infer the cell-cell communications between each cluster (18, 19).

Screening potential biomarkers using the Lasso regression model

The RNAseq data was downloaded from the TCGA database (https://portal.gdc.cancer.gov) for the STAR process of the TCGA project and the data was extracted in TPM format and the clinical data. Additional prognostic data was obtained from the literature (20). The data processing method is log2(value+1) and the cleaned data was analyzed using the "glmnet" R package to obtain the variable lambda value, maximum likelihood number, or C index (21).

The correlation between genes and MSI

MSI occurs due to a functional defect in the DNA mismatch repair of tumor tissue and is an important tumor marker. The unified and standardized pan-cancer data set was downloaded from the UCSC (https://xenabrowser.net/) database, and the expression data of ENSG00000080493 (*SLC4A4*) was extracted. The MSI score for each tumor was obtained from a previous study (22) and integrated with the gene expression data to calculate the Pearson correlation for each tumor.

Identification of expression characteristics and clinical features of *SLC4A4*

First, the difference in genes between the two groups was identified based on the TCGA data using the Wilcoxon rank sum test. They were then visualized using the "ggplot2" package. *SLC4A4* transcription and protein levels, as well as survival curves, were evaluated in the UALCAN database (23). The time-dependent AUC is a polygonal line that shows the area (AUC) under the corresponding curve of different variables at different times and is < 0.5 when the value of the variable (protective factor) is opposite to the trend of the event. The AUC of ROC is often used for the evaluation of diagnostic tests and generally, an AUC within the range of 0.5 and 1, and closer to 1 indicates that the variable has a better diagnostic effect on the predicted outcome. The data was analyzed using the timeROC package and the pROC package, and the results were visualized using ggplot2. The *SLC4A4* transcriptome data was combined with clinical data, and grouping comparisons and survival curves were drawn to describe differences between the clinical groupings. The *SLC4A4* proteomic profile was validated using immunohistochemical images from the HPA database (24).

Cell culture

Suzhou Medical University (Suzhou, China) provided the following human colon cancer cell lines: HT29, Caco-2, and HCT116, as well as the normal colon cell line NCM460. There were cultured in DMEM (HyClone, USA) supplemented with 10% FBS (Gibco, USA) and 100 μg/ml streptomycin/penicillin (Hyclone) in a 5% CO2 humidified environment at 37°C. The cells were passaged every 2–3 days using 0.25% trypsin (Hyclone).

RT-PCR

The expression of *SLC4A4* in different colon cancer cell lines was quantified by qRT-PCR, with at least three biological replicates per sample. The total RNA concentration of each sample was adjusted to be the same before reverse transcription using the ChamQ Universal SYBR qPCR Master Mix and HiScript II Q RT SuperMix for qPCR (Nanjing Novozan Biotechnology Co. ltd). The

relative mRNA expression was calculated using the 2ΔΔCT method and normalized to the internal reference β-actin. The primer sequences were as follows:

SLC4A4: Forward: 5′-TTGCCAACTATGTCTTCTACTGA-3′
Reverse: 5′-ATTACAGTTGTTCCCGACGAG-3′
β-actin: Forward: 5′-GTGGCCGAGGACTTTGATTG-3′
Reverse: 5′-CCTGTAACAACGCATCTCATATT-3′

Immunohistochemistry

Tissue chips are used for Immunohistochemistry (IHC) which was performed as per standard protocols. In summary, the tissue samples were fixed in 4% paraformaldehyde, embedded in paraffin, and sectioned. Following deparaffinization, rehydration, antigen retrieval and blocking, incubation of the slides with primary antibodies was conducted at 4°C. The sections then underwent incubation with an HRP-conjugated anti-rabbit secondary antibody (Servicebio, China). The chromogen used was diaminobenzidine (DAB). To capture the images under white light, a fluorescence microscope from Olympus (Japan) was used.

Statistical analysis

The analysis was conducted using R software (version 4.1.0). The Wilcoxon test was employed to compare the two groups, while the Kruskal-Wallis test was used for comparing multiple groups. A p-value of < 0.05 was considered statistically significant. The Spearman correlation test was utilized to compare the correlations between two continuous variables.

Results

Figure 1 shows the workflow of our study.

Data quality control and identification of differentially expressed genes

First, the spatial features in the PCA map and the UMAP map were used to represent the biological characteristics of each sample and significant inter-group differences were observed after the removal of the lower-quality samples (Figures 2A–D). The sample normalization box plot showed good correction for all samples and

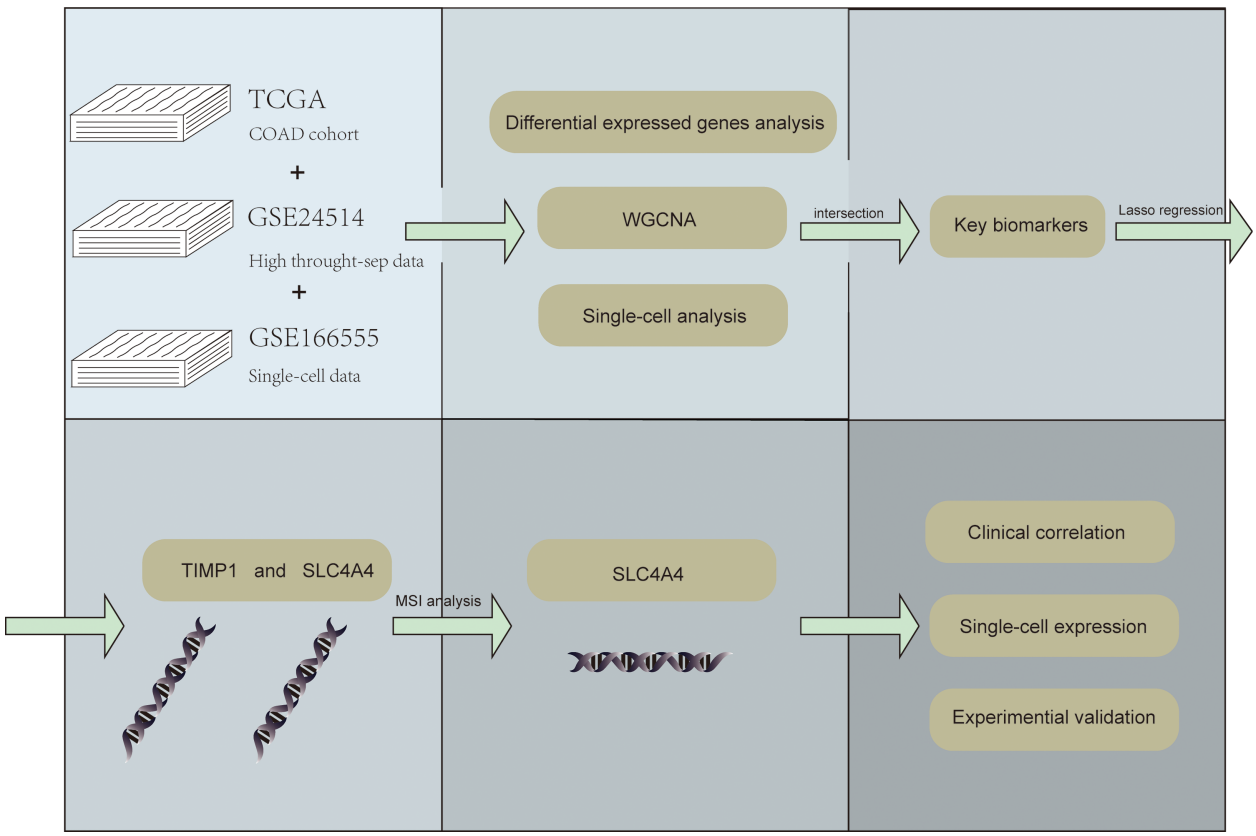

FIGURE 1
The flow chart.

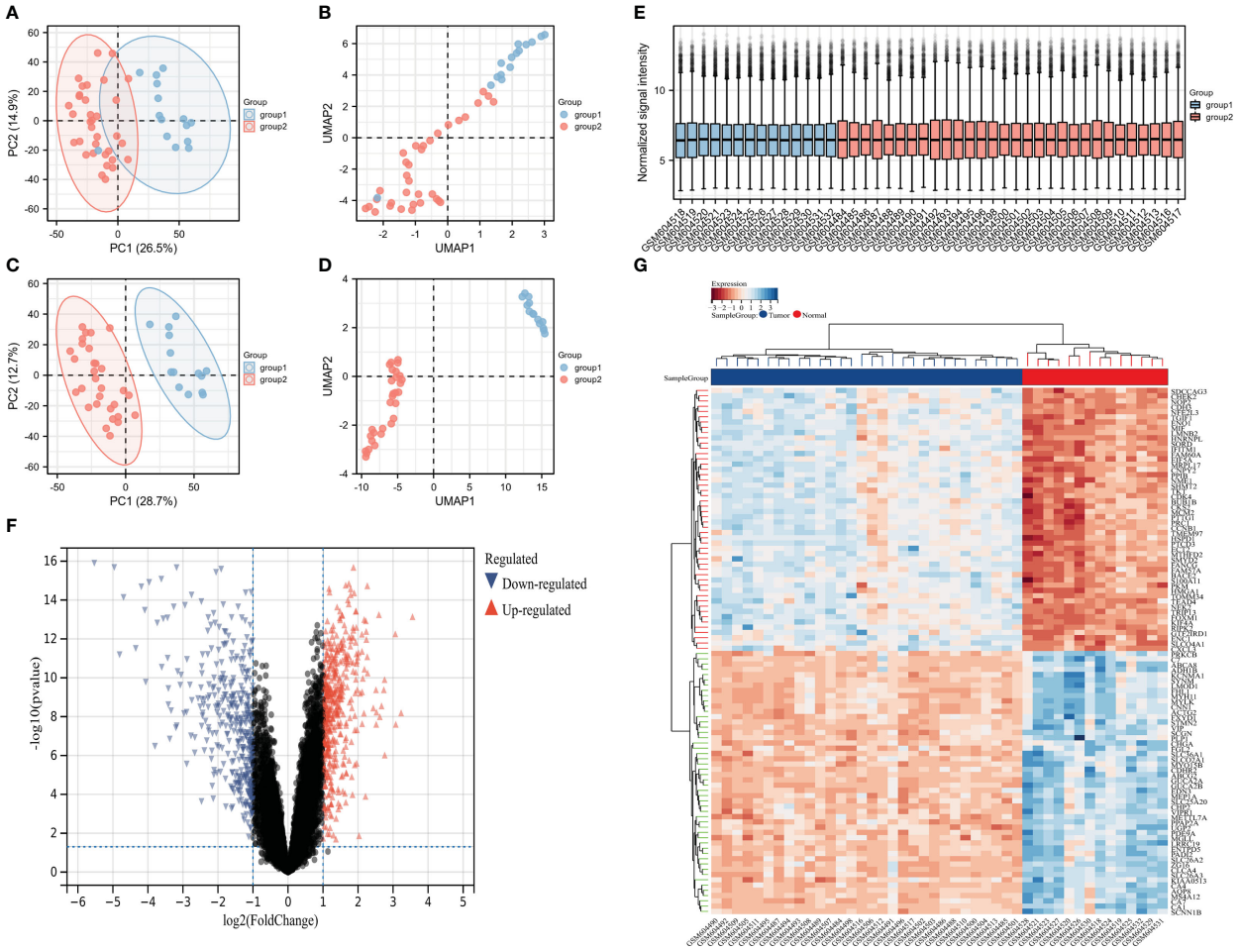

FIGURE 2
The sample quality was acceptable and many differential genes were identified. **(A)** PCA before quality control, **(B)** UMAP before quality control, **(C)** PCA after quality control, **(D)** UMAP after quality control, **(E)** sample normalization box diagram, **(F)** volcanic map, and **(G)** heat map.

no significant batch effects or other rejected samples (Figure 2E). Subsequently, volcanic and thermal maps were used to display the 844 differential genes meeting the threshold, including 648 genes with significantly high expression and 216 genes with significantly low expression (Figures 2F, G).

Identification of MSI-associated candidate biomarker genes in colorectal cancer by WGCNA

A weighted gene network was constructed to identify candidate biomarkers associated with MSI in colorectal cancer. Scale independence and mean connectivity indicated that the soft threshold used to construct the weighted gene network was 24 (Figures 3A, B). Sample clustering revealed significant differences between the two groups, and there were no outliers (Figures 3C, D). The hierarchical clustering diagram identified gene modules with high correlation, with the clustering heat map drawn according to the different vector features of each module, showing the distance between the different modules (Figure 3E). Finally, association analysis was performed on each module and phenotype to identify modules with a high correlation with the phenotype of interest and then the key genes were extracted from the statistically significant modules (Figure 3F).

Single cell sequencing revealed tumor heterogeneity and characteristics of different cell groups in colorectal cancer

Single-cell sequencing revealed 33 different cell clusters (Figure 4A) in the GSE166555 dataset through dimensionality reduction and clustering. The punctiform figures show the cell marker for cell annotation and their expression levels (Figure 4B). Annotating these clusters through cell markers yielded 13 cell types, Including B cells, CD4Tconv cells, CD8T cells, DC cells, endothelial cells, epithelial cells, fibroblasts, malignant cells, mast cells, Mono/

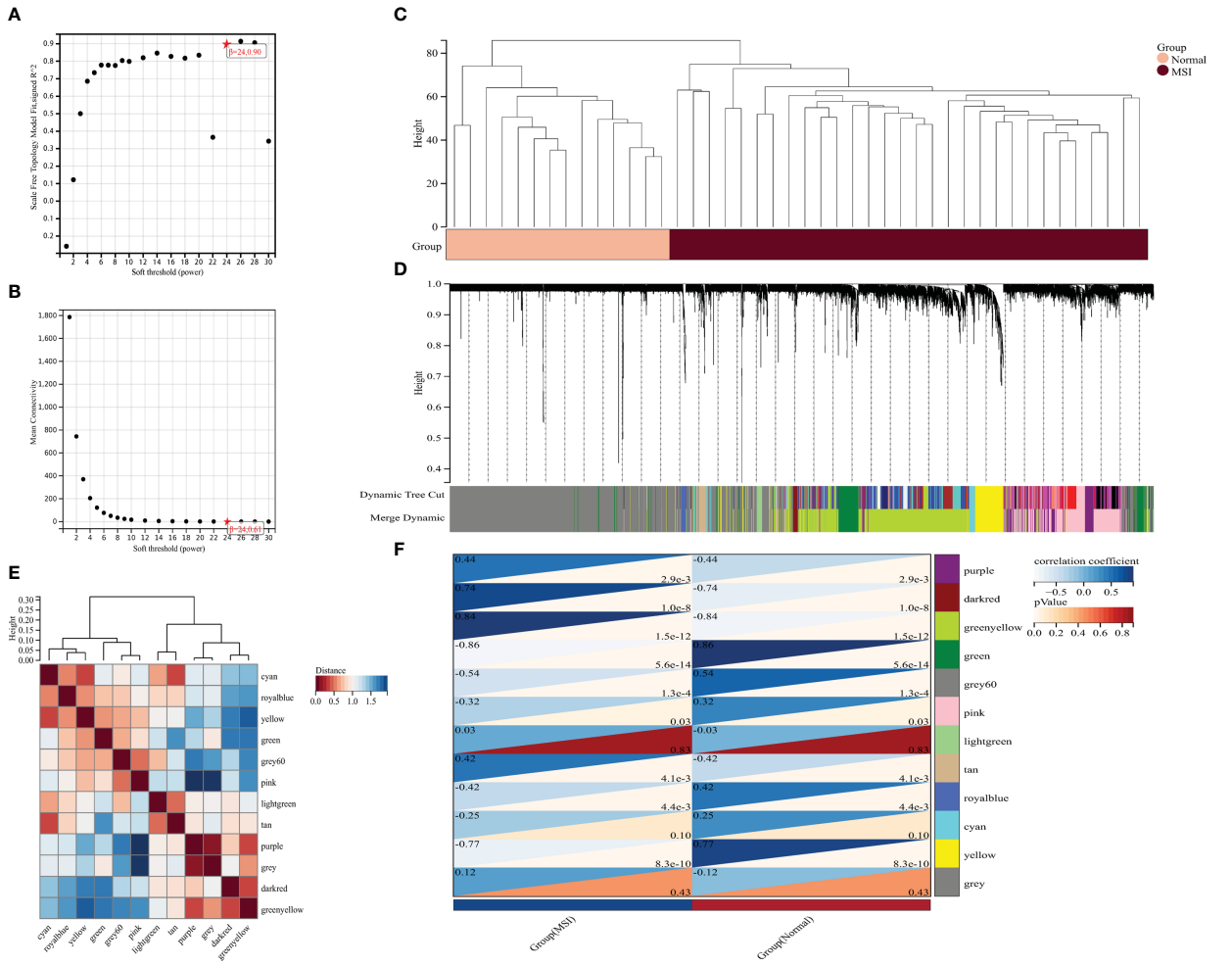

FIGURE 3
Mining potential biomarker genes associated with MSI based on weighted gene networks. **(A)** scale independence, **(B)** average connectivity, **(C)** The sample clustering indicated no outlier samples, **(D)** gene clustering, **(E)** module feature vector clustering, and **(F)** heat map of module and phenotype correlation.

Macro cells, myofibroblasts, plasma tumors, and Tprolif cells (Figure 4C). The pie chart showed the proportion of the different types, and the stacked histogram showed the proportion of the different types in each sample (Figure 4D).

Potential biomarkers identified by Lasso regression

Intersection analysis was performed of the results of the limma difference analysis, WGCNA, and single-cell sequencing difference analysis to construct a Venn diagram to obtain 174 intersection genes (Figure 5A). Subsequently, these 174 crossed genes were further screened using the Lasso regression model, and two potential biomarkers were identified: TIMP1 and *SLC4A4* (Figures 5B, C). To explore which gene had a stronger association with MSI, a lollipop graph of the association between gene expression and MSI was drawn showing that the association between *SLC4A4* and MSI was significantly higher in colorectal cancer than in TIMP1 (Figures 5D, E). According to the risk factor map, when *SLC4A4* expression is decreased, the risk score is significantly increased, and the prognosis is poor (Figure 5F). *SLC4A4* expression and the MSI for each sample were visualized in the correlation scatter plot and the correlation coefficient was 0.268 (Figure 5G).

Expression and clinical characteristics of the MSI-related gene *SLC4A4*

SLC4A4 mRNA and protein expression were significantly downregulated in tumors in both the TCGA and UALCAN databases (Figures 6A–D). The time-dependent AUC suggested that *SLC4A4* might be a protective factor and ROC indicated that *SLC4A4* is highly sensitive and specific (Figures 6E, F). The immunohistochemical results highlighted the decreased *SLC4A4* expression in the tumor (Figures 6G, H). Also, there was lower *SLC4A4* expression in patients with lymphoid metastasis (Figure 6I)

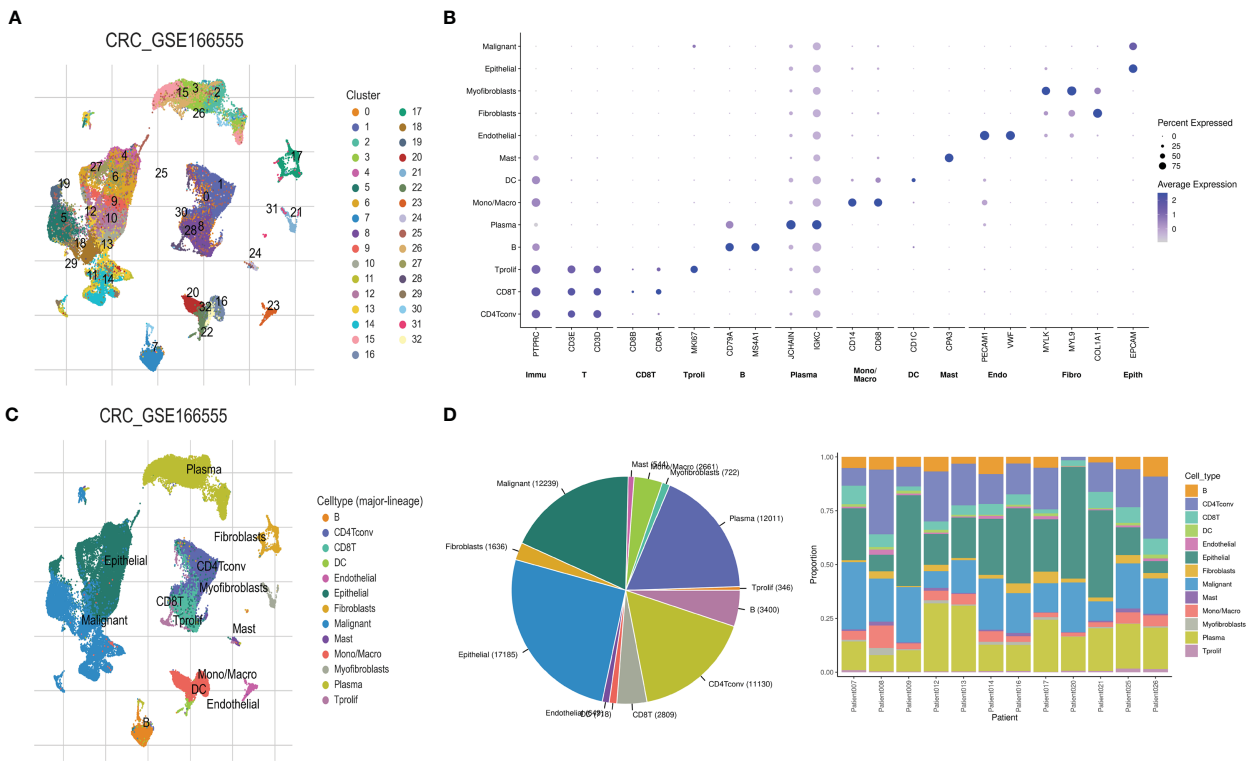

FIGURE 4
Cell heterogeneity in the microenvironment of colorectal cancer revealed by single-cell sequencing. **(A)** The UMAP map revealed 33 different cell clusters, **(B)** cell marker dot pattern, **(C)** 13 cell types were obtained after cell annotation, and **(D)** fan and stacked bar graphs show the proportion of the different cell types.

and low *SLC4A4* expression was associated with poor prognosis (Figures 6J–L).

High *SLC4A4* expression in epithelial cells

Using previous single-cell sequencing data to visualize *SLC4A4* expression in different cells revealed that *SLC4A4* expression was significant in epithelial cells and barely expressed in other cells, including malignant tumor cells (Figures 7A, B). Malignant cells strongly interacted with myofibroblasts, fibroblasts, and endothelial cells (Figure 7C). Also, some pathways were significantly enriched in epithelial cells or malignant tumor cells including fatty acid metabolism, estrogen response late, estrogen response early, apical junction, androgen response, adipogenesis, xenobiotic metabolism, protein secretion, interferon-alpha response, interferon-gamma response, oxidative phosphorylation, and peroxisome (Figure 7D).

PCR and immunohistochemistry to validate the expression of *SLC4A4*

In order to further verify the expression of *SLC4A4*, we first performed PCR experiments on cell lines. The results showed that *SLC4A4* was significantly down-regulated in colorectal cancer cell lines Caco-2, HCT116 and HT29 compared with normal control NCM460 cell lines (Figure 8A, ***P<0.001). Subsequently, clinical samples of colorectal cancer from 3 patients were collected for immunohistochemical experiments. It can be seen that *SLC4A4* expression was downregulated in the tumor tissues of three patients compared with the adjacent normal tissues (Figure 8B).

Discussion

Recently, the relationship between microsatellite instability and the occurrence and development of tumors has become a topic of interest in the study of tumor markers, characteristics, and prognosis. Although there have been many in-depth studies on potential biomarkers of tumors, few biomarkers can be used in combination with MSI to evaluate patient prognosis (25–28). MSI is a feature of many disorders, most of which are neoplastic, with Lynch syndrome being the most well-known non-neoplastic disorder. Protein dysfunction in the MMR family is involved in the occurrence of Lynch syndrome, with most families diagnosed with Lynch syndrome having MLH1 and MSH2 mutations, some families having MSH6 mutations, and a few families having PMS2 mutations (29). The occurrence of Lynch syndrome and partial sporadic colorectal cancer is not related to oncogene activation and tumor suppressor gene inactivation, rather it is caused by MSI due to

10.3389/fonc.2023.1179120

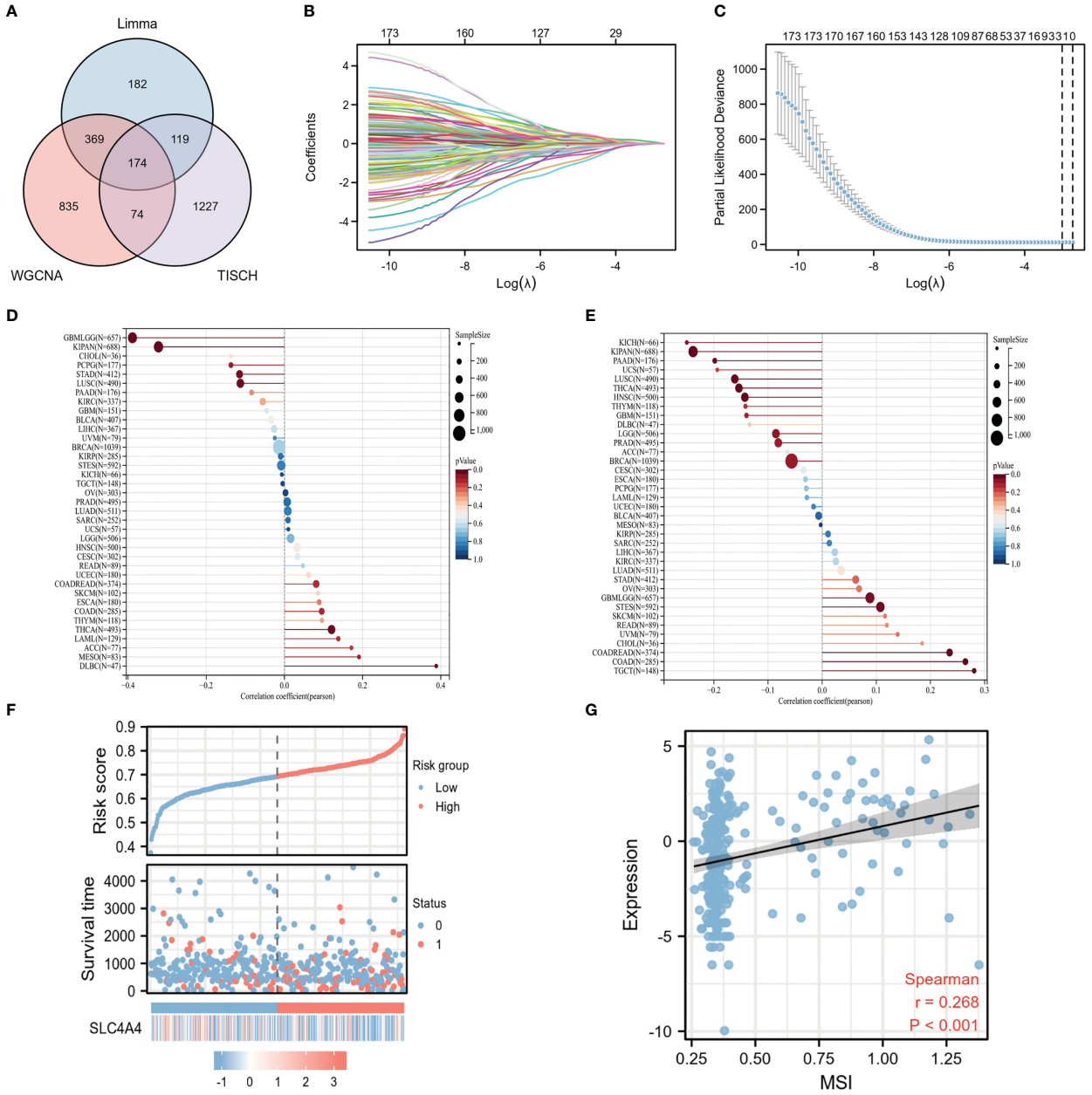

FIGURE 5
The correlation between the potential biomarker *SLC4A4* and MSI is significant. **(A)** The Venn diagram indicates 174 intersecting genes, **(B)** the trace diagram of the different variables in the Lasso regression, **(C)** two undetermined variables were obtained by Lasso regression, **(D)** lollipop plot of the correlation between TIMP1 expression in different tumors and MSI, **(E)** the lollipop plot of correlation between *SLC4A4* expression in different tumors and MSI, **(F)** risk factor diagram, and **(G)** correlation scatter plot.

mutations in mismatch repair genes (30). Currently, MSI/dMMR detection is an important diagnostic indicator for screening patients with Lynch syndrome. In summary, MSI has important clinical implications for Lynch syndrome screening, predicting the prognosis of colorectal cancer, and guiding drug use.

In recent years, significant progress has been made in the field of bioinformatics for CRC research (31, 32). Studies have employed various bioinformatics tools, including transcriptomics, genomics, proteomics, and metabolomics, to investigate the molecular mechanisms underlying CRC development and progression (33). For instance, transcriptomic profiling of CRC tissues has identified gene expression signatures associated with different stages of CRC, providing potential biomarkers for early diagnosis and personalized treatment (34). Additionally, genomic studies have revealed somatic mutations and genetic alterations associated with CRC, including the well-known APC, TP53, and KRAS mutations (35). Other studies have utilized proteomic and metabolomic approaches to identify protein and metabolite biomarkers for CRC diagnosis and

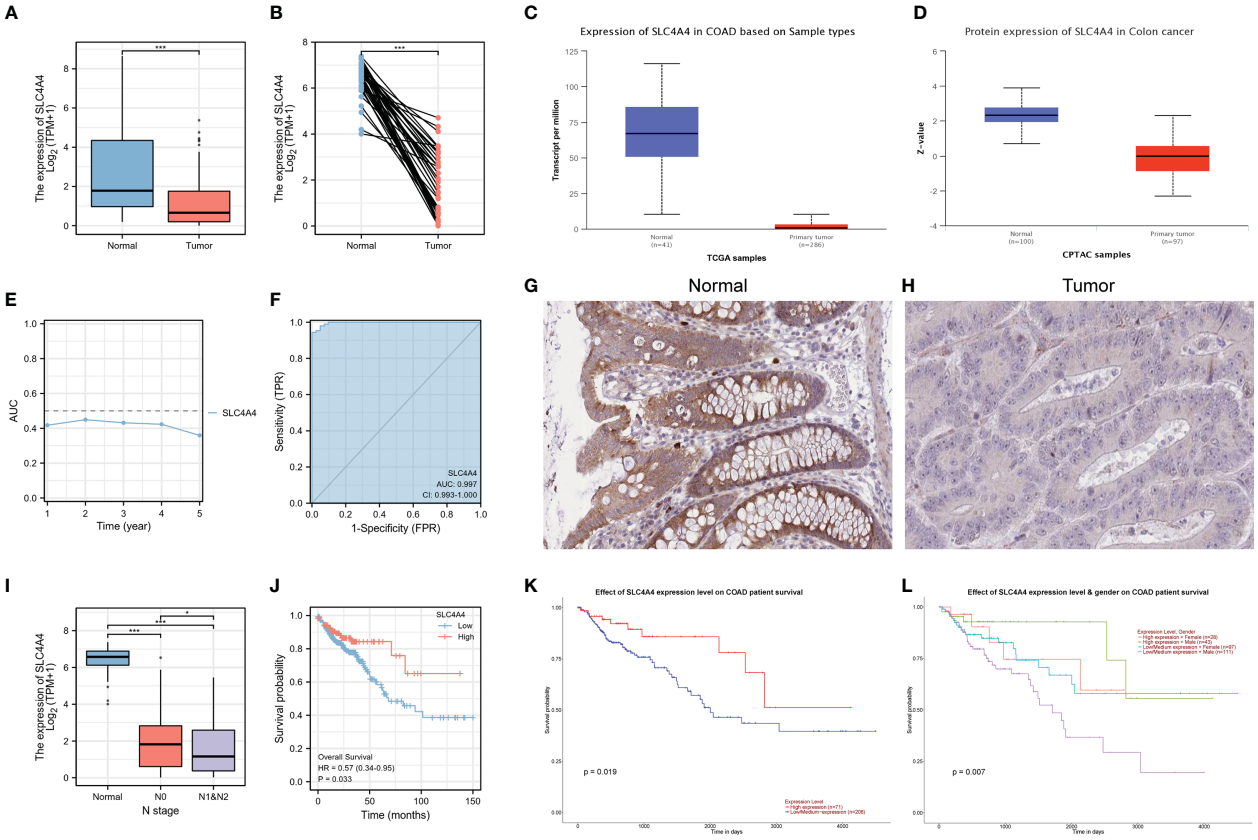

FIGURE 6
SLC4A4 is significantly downregulated in tumors and contributes to poor prognosis. **(A)** Non-paired samples, **(B)** paired samples, **(C)** *SLC4A4* transcriptional levels in UALCAN-TCGA, **(D)** *SLC4A4* protein levels in UALCAN-CPTAC, **(E)** time-dependent AUC, **(F)** ROC tested the stability of *SLC4A4* as a biomarker, **(G)** *SLC4A4* protein expression in normal tissue, **(H)** *SLC4A4* protein expression in tumor tissues, **(I)** the difference in *SLC4A4* expression in different N stages, **(J)** low *SLC4A4* expression is associated with poor prognosis, **(K)** the low *SLC4A4* expression in the UALCAN database contributed to poor prognosis, and **(L)** grouping in combination with gender revealed a significantly poor prognosis for men with low *SLC4A4* expression. *P<0.05; ***P<0.001.

prognosis. The integration of multi-omics data has also been increasingly used to improve the accuracy of CRC diagnosis and prognosis (36).

Here, for the first time, we identified a significant positive correlation between *SLC4A4* and MSI in colorectal cancer. Potential genes were screened using second-generation sequencing data, weighted average co-expression network, and single-cell sequencing data to obtain *SLC4A4* using Lasso regression and MSI correlation calculation. It is well known that patients with MSI-H have a better prognosis than MSS despite a poorer clinical presentation.

We identified a significant positive correlation between MSI and *SLC4A4* expression, the significant downregulation of *SLC4A4* mRNA and protein expression in tumors, and the *SLC4A4* low-expression group had a poorer prognosis which corresponds to MSI. More importantly, *SLC4A4* expression in the N1–N2 group was much lower than that in N0, suggesting that *SLC4A4* might also mediate tumor cell metastasis to lymph nodes. Single-cell sequencing revealed that *SLC4A4* was specifically and highly expressed in epithelial cells. In UMAP, the spatial relative positions of different cell types represent the similarities between biological functions, such as T cells and their subsets, and the close relationship between malignant tumor cells and epithelial cells suggests that malignant tumor cells may evolve from epithelial cells, while *SLC4A4* is rarely expressed in malignant tumor cells. In our analysis, *SLC4A4* was localized on the plasma membrane and involved in the regulation of bicarbonate secretion and absorption as well as intracellular pH. It is hypothesized that the absence of *SLC4A4* may lead to an imbalance between intracellular pH and carcinogenesis.

Conclusion

For the first time, we have identified *SLC4A4* as a potential prognostic biomarker significantly associated with MSI and related to the intracellular pH. The combination of *SLC4A4* and MSI can predict the prognosis and outcomes of colorectal cancer patients and guide clinical medication, providing innovative recommendations for personalized medicine.

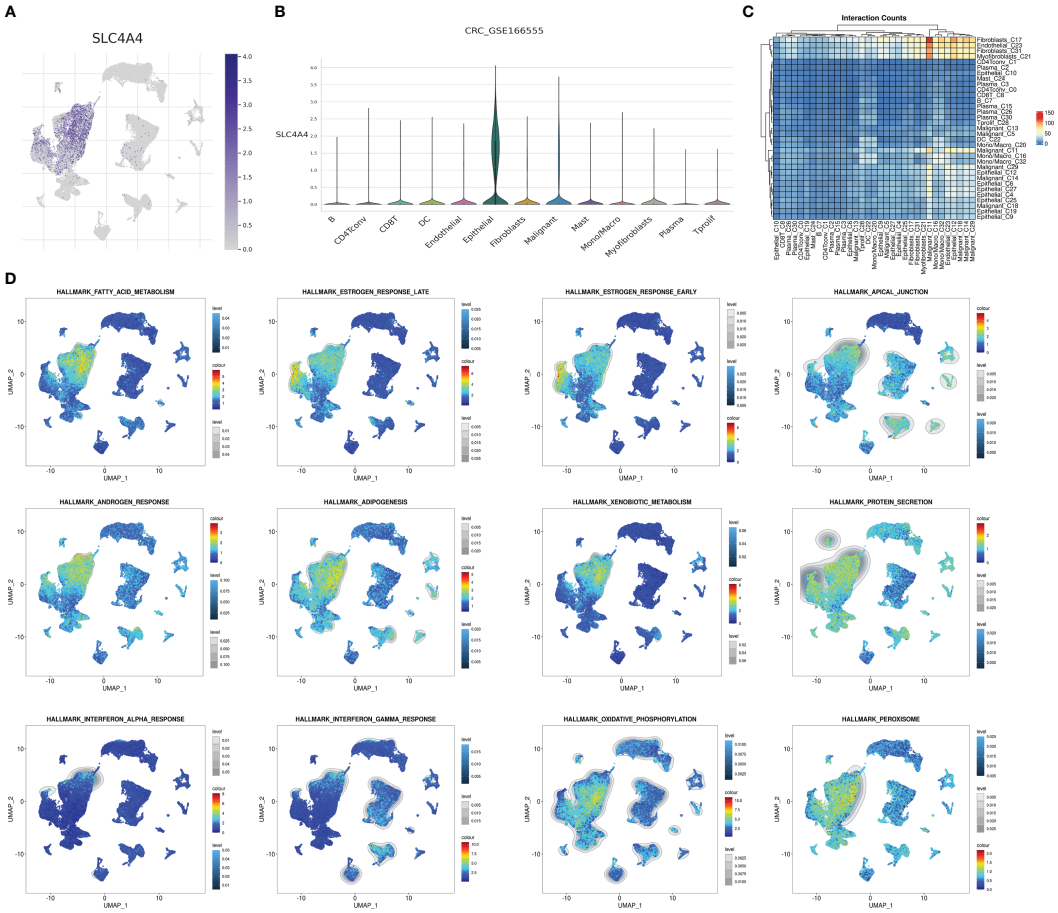

FIGURE 7
SLC4A4 is specifically and highly expressed in epithelial cells. **(A)** The UMAP plot shows *SLC4A4* expression in each cell type, **(B)** the violin diagram shows *SLC4A4* expression in each cell type, **(C)** cell communication heat map, and **(D)** enrichment intensity and the fraction of different hallmark signaling pathways in each cell.

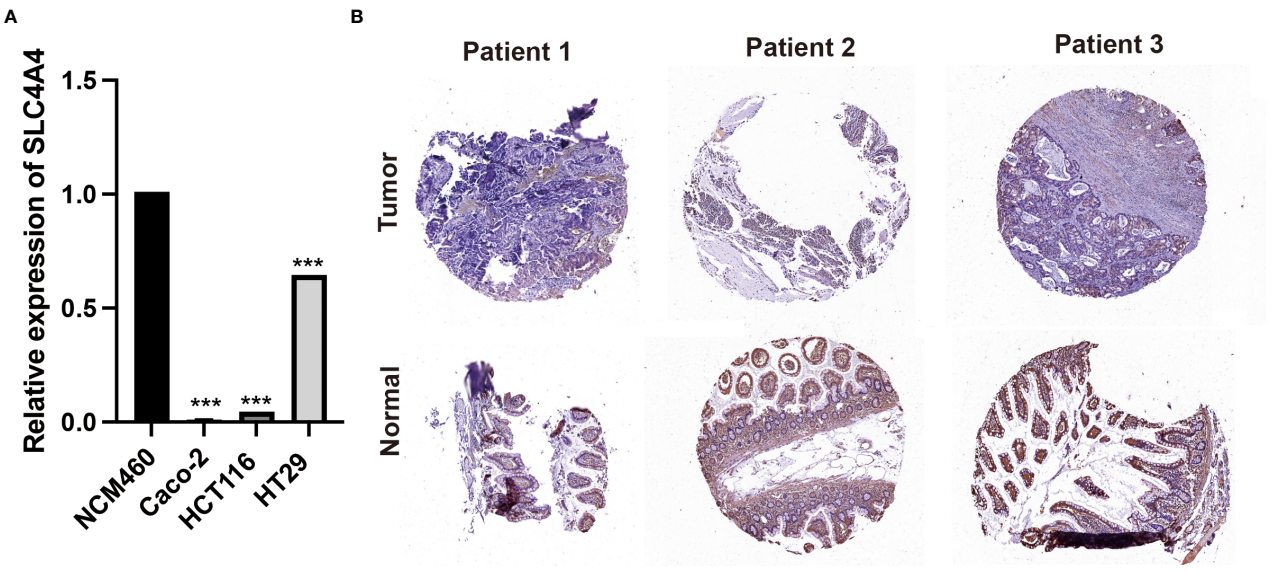

FIGURE 8
Experimental verification of *SLC4A4*. **(A)** PCR experiments in cell lines. *SLC4A4* was significantly down-regulated in colorectal cancer cell lines Caco-2, HCT116 and HT29 (***P<0.001). **(B)** Immunohistochemical examination of 3 clinical samples. The expression of *SLC4A4* is low in tumor tissue.

Data availability statement

The original contributions presented in the study are included in the article/supplementary material. Further inquiries can be directed to the corresponding authors.

Ethics statement

The studies involving human participants were reviewed and approved by The Second Affiliated Hospital of Wannan Medical College. The patients/participants provided their written informed consent to participate in this study.

Author contributions

All authors contributed to the study conception and design. Material preparation, data collection and analysis were performed by YH, JX and HaZ. The first draft of the manuscript was modified by SR, DW and HeZ. The revision draft of the manuscript was written by SR and HeZ. All authors commented on previous versions ofthe manuscript. All authors read and approved the final manuscript.

Funding

This work was funded and supported by Medical Education Integration Research Special Fund in Jiangsu College of Nursing (YJRH202303), Young Science and Technology Talent Support Project of Jiangsu Association for Science and Technology (TJ-2022-063), Natural Science and Research Plan of Huai'an City (HABZ202214) and the clinical research project of the Second Affiliated Hospital of Wannan Medical College (2022YJLC004).

Conflict of interest

The authors declare that the research was conducted in the absence of any commercial or financial relationships that could be construed as a potential conflict of interest.

Publisher's note

References

1. Xia C, Dong X, Li H, Cao M, Sun D, He S, et al. Cancer statistics in China and united states, 2022: profiles, trends, and determinants. *Chin Med J (Engl)* (2022) 135:584–90. doi: 10.1097/CM9.0000000000002108

2. Siegel RL, Miller KD, Fuchs HE, Jemal A. Cancer statistics, 2022. *CA Cancer J Clin* (2022) 72:7–33. doi: 10.3322/caac.21708

3. Sung H, Ferlay J, Siegel RL, Laversanne M, Soerjomataram I, Jemal A, et al. Global cancer statistics 2020: GLOBOCAN estimates of incidence and mortality worldwide for 36 cancers in 185 countries. *CA Cancer J Clin* (2021) 71:209–49. doi: 10.3322/caac.21660

4. Zellweger M, Abdelnour-Berchtold E, Krueger T, Ris HB, Perentes JY, Gonzalez M. Surgical treatment of pulmonary metastasis in colorectal cancer patients: current practice and results. *Crit Rev Oncol Hematol* (2018) 127:105–16. doi: 10.1016/j.critrevonc.2018.05.001

5. Peixoto C, Lopes MB, Martins M, Casimiro S, Sobral D, Grosso AR, et al. Identification of biomarkers predictive of metastasis development in early-stage colorectal cancer using network-based regularization. *BMC Bioinf* (2023) 24:17. doi: 10.1186/s12859-022-05104-z

6. Moslehi J, Salem JE. Immune checkpoint inhibitor myocarditis treatment strategies and future directions. *JACC CardioOncol* (2022) 4:704–7. doi: 10.1016/j.jaccao.2022.11.005

7. Miller ED, Hitchcock KE, Romesser PB. Oligometastatic colorectal cancer: a review of definitions and patient selection for local therapies. *J Gastrointest Cancer* (2023). doi: 10.1007/s12029-022-00900-5

8. Xi Y, Xu P. Global colorectal cancer burden in 2020 and projections to 2040. *Transl Oncol* (2021) 14:101174. doi: 10.1016/j.tranon.2021.101174

9. Marcus L, Lemery SJ, Keegan P, Pazdur R. FDA Approval summary: pembrolizumab for the treatment of microsatellite instability-high solid tumors. *Clin Cancer Res* (2019) 25:3753–8. doi: 10.1158/1078-0432.CCR-18-4070

10. Le DT, Uram JN, Wang H, Bartlett BR, Kemberling H, Eyring AD, et al. PD-1 blockade in tumors with mismatch-repair deficiency. *N Engl J Med* (2015) 372:2509–20. doi: 10.1056/NEJMoa1500596

11. Xue L, Liu J, Xie J, Luo J. Prognostic value of SLC16A3(MCT4) in lung adenocarcinoma and its clinical significance. *Int J Gen Med* (2021) 14:8413–25. doi: 10.2147/IJGM.S337615

12. Yi W, Shen H, Sun D, Xu Y, Feng Y, Li D, et al. Low expression of long noncoding RNA SLC26A4 antisense RNA 1 is an independent prognostic biomarker and correlate of immune infiltrates in breast cancer. *Med Sci Monit* (2021) 27:e934522. doi: 10.12659/MSM.934522

13. Elangovan S, Pathania R, Ramachandran S, Ananth S, Padia RN, Srinivas SR, et al. Molecular mechanism of SLC5A8 inactivation in breast cancer. *Mol Cell Biol* (2013) 33:3920–35. doi: 10.1128/MCB.01702-12

14. Romero MF, Chen AP, Parker MD, Boron WF. The SLC4 family of bicarbonate (HCO(3)(-)) transporters. *Mol Aspects Med* (2013) 34:159–82. doi: 10.1016/j.mam.2012.10.008

15. Xiao W, Wang X, Wang T, Xing J. MiR-223-3p promotes cell proliferation and metastasis by downregulating SLC4A4 in clear cell renal cell carcinoma. *Aging (Albany NY)* (2019) 11:615–33. doi: 10.18632/aging.101763

16. Barrett T, Wilhite SE, Ledoux P, Evangelista C, Kim IF, Tomashevsky M, et al. Archive for functional genomics data sets–update. *Nucleic Acids Res* (2013) 41:D991–5. doi: 10.1093/nar/gks1193

17. Han Y, Wang Y, Dong X, Sun D, Liu Z, Yue J, et al. TISCH2: expanded datasets and new tools for single-cell transcriptome analyses of the tumor microenvironment. *Nucleic Acids Res* (2023) 51:D1425–31. doi: 10.1093/nar/gkac959

18. Jin S, Guerrero-Juarez CF, Zhang L, Chang I, Ramos R, Kuan CH, et al. Inference and analysis of cell-cell communication using CellChat. *Nat Commun* (2021) 12:1088. doi: 10.1038/s41467-021-21246-9

19. Subramanian A, Tamayo P, Mootha VK, Mukherjee S, Ebert BL, Gillette MA, et al. Gene set enrichment analysis: a knowledge-based approach for interpreting genome-wide expression profiles. *Proc Natl Acad Sci U.S.A.* (2005) 102:15545–50. doi: 10.1073/pnas.0506580102

20. Liu J, Lichtenberg T, Hoadley KA, Poisson LM, Lazar AJ, Cherniack AD, et al. An integrated TCGA pan-cancer clinical data resource to drive high-quality survival outcome analytics. *Cell* (2018) 173:400–416 e11. doi: 10.1016/j.cell.2018.02.052

21. Friedman J, Hastie T, Tibshirani R. Regularization paths for generalized linear models via coordinate descent. *J Stat Softw* (2010) 33:1–22. doi: 10.18637/jss.v033.i01

22. Bonneville R, Krook MA, Kautto EA, Miya J, Wing MR, Chen HZ, et al. Landscape of microsatellite instability across 39 cancer types. *JCO Precis Oncol* (2017) 2017. doi: 10.1200/PO.17.00073

23. Chandrashekar DS, Karthikeyan SK, Korla PK, Patel H, Shovon AR, Athar M, et al. UALCAN: an update to the integrated cancer data analysis platform. *Neoplasia* (2022) 25:18–27. doi: 10.1016/j.neo.2022.01.001

24. Zhou X, Du J, Liu C, Zeng H, Chen Y, Liu L, et al. A pan-cancer analysis of CD161, a potential new immune checkpoint. *Front Immunol* (2021) 12:688215. doi: 10.3389/fimmu.2021.688215

25. Xie H, Wu Z, Li Z, Huang Y, Zou J, Zhou H. Significance of ZEB2 in the immune microenvironment of colon cancer. *Front Genet* (2022) 13:995333. doi: 10.3389/fgene.2022.995333

26. Zou J, Li Z, Xie J, Wu Z, Huang Y, Xie H, et al. Methylation drives SLC2A1 transcription and ferroptosis process decreasing autophagy pressure in colon cancer. *J Oncol* (2022) 2022:9077424. doi: 10.1155/2022/9077424

27. Zou J, Zhang H, Huang Y, Xu W, Huang Y, Zuo S, et al. Multi-omics analysis of the tumor microenvironment in liver metastasis of colorectal cancer identified FJX1 as a novel biomarker. *Front Genet* (2022) 13:960954. doi: 10.3389/fgene.2022.960954

28. Chen H, Li Z, Wu F, Ji W, Lu L, Wu Z, et al. BCL10 correlates with bad prognosis and immune infiltration of tumor microenvironment in hepatocellular carcinoma. *IUBMB Life* (2023) 75:207–24. doi: 10.1002/iub.2581

29. Trost H, Merkell A, Lopezcolorado FW, Stark JM. Resolution of sequence divergence for repeat-mediated deletions shows a polarity that is mediated by MLH1. *Nucleic Acids Res* (2023) 51:650–67. doi: 10.1093/nar/gkac1240

30. Amodio V, Lamba S, Chila R, Cattaneo CM, Mussolin B, Corti G, et al. Genetic and pharmacological modulation of DNA mismatch repair heterogeneous tumors promotes immune surveillance. *Cancer Cell* (2023) 41:196–209 e5. doi: 10.1016/j.ccell.2022.12.003

31. Jin W, Yang Q, Chi H, Wei K, Zhang P, Zhao G, et al. Ensemble deep learning enhanced with self-attention for predicting immunotherapeutic responses to cancers. *Front Immunol* (2022) 13:1025330. doi: 10.3389/fimmu.2022.1025330

32. Li C, Sun YD, Yu GY, Cui JR, Lou Z, Zhang H, et al. Integrated omics of metastatic colorectal cancer. *Cancer Cell* (2020) 38:734–747 e9. doi: 10.1016/j.ccell.2020.08.002

33. Chen L, Lu D, Sun K, Xu Y, Hu P, Li X, et al. Identification of biomarkers associated with diagnosis and prognosis of colorectal cancer patients based on integrated bioinformatics analysis. *Gene* (2019) 692:119–25. doi: 10.1016/j.gene.2019.01.001

34. Lin A, Zhang J, Luo P. Crosstalk between the MSI status and tumor microenvironment in colorectal cancer. *Front Immunol* (2020) 11:2039. doi: 10.3389/fimmu.2020.02039

35. Chen H, Yao J, Bao R, Dong Y, Zhang T, Du Y, et al. Cross-talk of four types of RNA modification writers defines tumor microenvironment and pharmacogenomic landscape in colorectal cancer. *Mol Cancer* (2021) 20:29. doi: 10.1186/s12943-021-01322-w

36. Zhao Y, Wei K, Chi H, Xia Z, Li X. IL-7: a promising adjuvant ensuring effective T cell responses and memory in combination with cancer vaccines? *Front Immunol* (2022) 13:1022808. doi: 10.3389/fimmu.2022.1022808

frontiers | Frontiers in Immunology

TYPE Original Research
PUBLISHED 26 April 2023
DOI 10.3389/fimmu.2023.1127349

OPEN ACCESS

EDITED BY
Chenyu Sun,
AMITA Health, United States

REVIEWED BY
Feiling Feng,
Eastern Hepatobiliary Surgery Hospital, China
Xinwei Han,
Zhengzhou University, China

*CORRESPONDENCE
Wenge Xing
xingwenge@tjmuch.com
Haipeng Yu
jieruke@163.com

†These authors have contributed equally to this work and share first authorship

SPECIALTY SECTION
This article was submitted to Cancer Immunity and Immunotherapy, a section of the journal Frontiers in Immunology

RECEIVED 19 December 2022
ACCEPTED 31 March 2023
PUBLISHED 26 April 2023

CITATION
Zhang W, Zhang K, Liu C, Gao W, Si T, Zou Q, Guo Z, Yang X, Li M, Liu D, Mu H, Li H, Yu H and Xing W (2023) Hepatic arterial infusion chemotherapy combined with anti-PD-1/PD-L1 immunotherapy and molecularly targeted agents for advanced hepatocellular carcinoma: a real world study.
Front. Immunol. 14:1127349.
doi: 10.3389/fimmu.2023.1127349

Hepatic arterial infusion chemotherapy combined with anti-PD-1/PD-L1 immunotherapy and molecularly targeted agents for advanced hepatocellular carcinoma: a real world study

Weihao Zhang[1,2,3†], Kai Zhang[1,2,3†], Changfu Liu[1,2,3†], Wei Gao[1,2,3], Tongguo Si[1,2,3], Qiang Zou[1,2,3], Zhi Guo[1,2,3], Xueling Yang[1,2,3], Mei Li[1,2,3], Dongming Liu[2,3,4], Han Mu[2,3,4], Huikai Li[2,3,4], Haipeng Yu[1,2,3*] and Wenge Xing[1,2,3*]

[1]Department of Interventional Therapy, Tianjin Medical University Cancer Institute & Hospital, National Clinical Research Center for Cancer, Tianjin, China, [2]Tianjin's Clinical Research Center for Cancer, Tianjin Medical University Cancer Institute & Hospital, Tianjin, China, [3]Key Laboratory of Cancer Prevention and Therapy, Tianjin Medical University Cancer Institute & Hospital, Tianjin, China, [4]Department of Hepatobiliary, Tianjin Medical University Cancer Institute & Hospital, National Clinical Research Center for Cancer, Tianjin, China

Background: Molecular targeted therapy combined with immunotherapy significantly improves the prognosis of patients with advanced liver cancer. Additionally, hepatic arterial infusion chemotherapy (HAIC) can improve the prognosis of patients with advanced liver cancer. This real-world study aimed to evaluate the clinical efficacy and safety of HAIC combined with molecular targeted therapy and immunotherapy in the treatment of primary unresectable hepatocellular carcinoma (uHCC).

Methods: A total of 135 patients with uHCC were enrolled in this study. Progression-free survival (PFS) was the primary endpoint. The efficacy of the combination therapy was assessed based on the modified Response Evaluation Criteria in Solid Tumors (mRECIST) guidelines. Overall survival (OS), adverse events (AEs) and surgical conversion rate were the secondary endpoints. Univariate and multivariate Cox regression analyses were performed to examine independent prognostic factors. For sensitivity analysis, inverse probability weighting (IPW) was used to balance the influence of the tested confounding factors between groups to verify the robustness of conversion surgery for survival benefits. The E-values were estimated to assess robustness to unmeasured confounders.

Results: The median number of therapies was three. Approximately 60% of the patients had portal vein tumour thrombosis (PVTT). The most common targeted drugs were lenvatinib and bevacizumab, whereas the most common immunotherapy drug was sintilimab. The overall objective response rate (ORR) was 54.1%, and the disease control rate (DCR) was 94.6%. A total of 97 (72%) patients experienced AEs of grades 3–4. Fatigue, pain and fever were the most

common symptoms of grade 3-4 AEs. The median PFS was 28 months and 7 months in the successful and unsuccessful conversion groups, respectively. The median OS was 30 months and 15 months in the successful and unsuccessful conversion groups, respectively. Successful conversion surgery, sex, hapatic vein invasion, BCLC stage, baseline tumour size, AFP levels and maximum therapeutic response were independent prognostic factors for PFS. Successful conversion surgery, number of interventions, hapatic vein invasion and total bilirubin levels were independent prognostic factors for OS. After IPTW, no standardised differences exceeding 0.1 were found. IPW-adjusted Kaplan–Meier curves showed that successful conversion surgery was an independent prognostic factor for both PFS and OS. The E-values of successful conversion surgery were 7.57 and 6.53 for OS and PFS, respectively, which indicated a relatively robust impact of successful conversion surgery on the prognosis of patients.

Conclusion: Patients with primary uHCC undergoing HAIC combined with immunotherapy and molecular targeted therapy have a higher tumour regression rate and the side effects are manageable. Patients undergoing surgery after combination therapy have survival benefits.

KEYWORDS

hepatic arterial infusion chemotherapy, molecularly targeted agents, advanced hepatocellular carcinoma, conversion surgery, survival benefit, anti-PD-1/PD-L1 immunotherapy

Introduction

On a global scale, liver cancer ranks fifth among malignant cancers (1). The most common subtype of primary liver cancer is hepatocellular carcinoma (HCC) (2). The main treatment strategies for early-stage HCC include surgical resection, ablation and liver transplantation (3). However, most patients with HCC are diagnosed at an advanced stage and hence have a poor prognosis. In recent years, the treatment of advanced HCC has rapidly evolved with the introduction of novel systemic therapies. The IMbrave 150 study showed that compared with sorafenib, atezolizumab combined with bevacizumab had better therapeutic effects in patients with unresectable hepatocellular carcinoma (uHCC) (4). After sorafenib, the combination of atezolizumab and bevacizumab was the first therapeutic strategy that demonstrated promising results in a randomised controlled trial. At present, the first-line treatment for advanced liver cancer is a combination of molecular targeted drugs and immune checkpoint inhibitors (5).

As systemic therapy advances, indications for TACE therapy in HCC are narrowing. The Barcelona Clinic Liver Cancer (BCLC) staging system is the most commonly used system for classifying HCC stages (6). In the previous BCLC guidelines, TACE was recommended as the primary treatment method for BCLC B-stage HCC. However, the 2022 BCLC staging system has re-categorised the stratification of risk for patients with B-stage HCC. The recommended first-line treatment for patients with BCLC B-stage HCC with diffuse, infiltrative and extensive bilobar liver involvement has been changed from TACE to systemic therapy (5). We speculate that the reason for this change, in addition to the advancement of systemic therapy, is related to the poor efficacy of TACE therapy in patients with moderate and high tumour burdens (7, 8).

Hepatic arterial infusion chemotherapy (HAIC) is a locoregional therapy that involves the administration of chemotherapeutic agents at higher concentrations directly into tumour sites *via* tumour-associated arterial branches (9). A recent randomised controlled trial showed that compared with TACE, FOLFOX-HAIC significantly improved overall survival (OS) and progression-free survival (PFS) in patients with unresectable large tumours (10). The effectiveness of HAIC has also been confirmed in a real-world study (11). Considering that both HAIC and systemic therapy are effective for patients with moderate and high tumour burdens, the therapeutic efficacy of the combination of these two therapies is currently undergoing investigation. Compared with sorafenib monotherapy, combination therapy with sorafenib and FOLFOX-HAIC can improve the objective response rate (ORR) and OS of patients with HCC (12, 13). In addition, the combination of HAIC, anti-PD-1-based immunotherapy and molecularly targeted agents may improve patient outcomes (14, 15). However, relevant previous studies reporting on the abovementioned combination therapeutic strategies had a limited number of participants, which limits the external validation of the results. To the best of our knowledge, no large-scale, real-world studies have reported the

therapeutic effects of HAIC combined with systemic therapy. Therefore, this study aimed to evaluate the safety and effectiveness of HAIC combined with immunotherapy and molecular targeted therapy in patients with advanced HCC.

Materials and methods

Patients

This retrospective study was conducted in accordance with the principles outlined by the Declaration of Helsinki (16) and was approved by the Tianjin Medical University Cancer Institute and Hospital Review Board (No.: bc2020099). A random number was assigned to each participant, and other information that could reveal the identity of participants was removed.

Patients with uHCC who received triple therapy (HAIC + anti-PD-1-based immunotherapy + molecular targeted therapy) between November 2018 and December 2021 at Tianjin Medical University Cancer Institute and Hospital were enrolled. All patients were evaluated by our multidisciplinary board for surgical resection. The board comprises multidisciplinary specialists, including hepatobiliary surgeons, oncologists, interventionists, radiologists and radiotherapy physicians. To increase the sample size and ensure representativeness, there was no limitation regarding the specific use of immune checkpoint inhibitors and targeted drugs in the included patients. Figure 1 demonstrates a flowchart representing the patient enrolment strategy with detailed inclusion and exclusion criteria.

Treatment protocol

Patients were locally anaesthetised, and the Seldinger technique was used to puncture the femoral artery. To examine blood supply at the tumour site, digital subtraction angiography was used to visualise the anatomical features of the celiac, superior mesenteric and hepatic arteries. HAIC was conducted using a 2.7-F microcatheter placed in the tumour-feeding arteries. The FOLFOX regimen was used as follows: 4-hour infusion of 85-mg/m^2 oxaliplatin, 2–3-hour infusion of 400-mg/m^2 calcium folinate and a bolus injection of 400-mg/m^2 fluorouracil, followed by 23-hour infusion of 1200-mg/m^2 fluorouracil on day 1 of treatment. Drug doses may be adjusted depending on the Child–Pugh grade and chemotherapy tolerance. HAIC was repeated every 4–6 weeks until disease progression or unacceptable toxicity was observed or the treatment plan was changed. Treatment may be interrupted or dose adjustments may be required if toxicity is intolerable. When grade 3 or 4 adverse events occur, oxaliplatin would be reduced to 65 mg/m^2, and 5-fluorouracil to 300 mg per bolus and 1000 mg per cycle respectively.

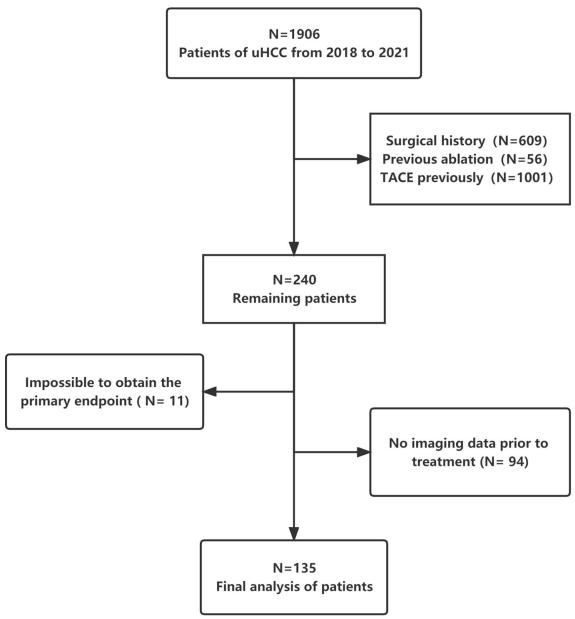

FIGURE 1
Flowchart demonstrating the patient inclusion strategy.

Anti-PD-1-based immunotherapy and molecular targeted therapy

Before or after the first HAIC session, patients were intravenously administered anti-PD-1 antibodies every 3 weeks (200-mg sintilimab, 200-mg tislelizumab, 200-mg camrelizumab, 240-mg toripalimab or 200-mg pembrolizumab). For anti-angiogenesis treatment, the patients were administered 8-mg lenvatinib orally once daily, 200-mg sorafenib orally twice daily and 250-mg apatinib orally once daily. Patients in the T + A group were intravenously administered atezolizumab (1200 mg) plus bevacizumab (15 mg/kg) or sintilimab (200 mg) plus bevacizumab biosimilar (IBI305) every 3 weeks.

Primary endpoints and data collection

PFS was the primary endpoint. Therapeutic efficacy was evaluated based on the modified Response Evaluation Criteria in Solid Tumors (mRECIST) (17). PFS was defined as the time from initiation of treatment to the end of progression or death. The secondary endpoints included OS, ORR (complete response [CR] + partial response [PR]), disease control rate (DCR; ORR + stable disease [SD]), surgical conversion rate and adverse events (AEs) defined by the Common Terminology Criteria for Adverse Events, version 4.0.

Statistical analysis

Categorical variables were analysed *via* the Fisher's exact test and were expressed as numbers (percentages). Data with normal distribution were analysed using the t-test or ANOVA analysis. Data with non-normal distribution were analysed using the rank sum test and were expressed as the median (interquartile range [IQR]). Survival was estimated using the Kaplan–Meier method, and the data were analysed *via* univariate and multivariate Cox proportional risk regression analyses. A p-value of <0.05 was considered significant.

Sensitivity analysis was conducted using two approaches. First, inverse probability weighting (IPW) was employed to manage potential imbalance among covariates between two groups (18). Second, E-values were estimated to examine unmeasured confounders owing to the observational study design (19) and evaluate the impact of unmeasured confounders on the outcomes of patients. Statistical analysis was performed using the R (version 4.2.1) software.

Result

Characteristics of patients and tumors

A total of 2019 patients were screened between November 2018 and December 2021; of which, 135 met the eligibility criteria for inclusion. A flowchart demonstrating the patient selection strategy and inclusion and exclusion criteria is shown in Figure 1. A majority of patients (82.2%) were men. The most prevalent cause of underlying liver disease was chronic hepatitis B virus infection (93.3%). More than half of the patients (58.8%) had portal vein tumour thrombosis. The median tumour size was 8.95 cm (IQR = 6.27–13.0 cm). Lenvatinib and bevacizumab were the most common targeted drugs, whereas sintilimab was the most common immunotherapeutic drug. Patients were divided into two groups based on whether conversion surgery was successful (Table 1). The median number of HAIC sessions was 3 (IQR = 2–3). The median number of HAIC sessions was higher in the successful conversion surgery group than in the unsuccessful conversion surgery group. However, the difference was not significant.

TABLE 1 Baseline information of patients.

	[ALL] *N=135*	No *N=95*	Yes *N=40*	p.overall
Sex				0.848
Female	24 (17.8%)	16 (16.8%)	8 (20.0%)	
Male	111 (82.2%)	79 (83.2%)	32 (80.0%)	
Age	58.0 [51.0;64.5]	57.0 [50.0;64.0]	59.0 [54.0;66.2]	0.240
Number of interventions	3.00 [2.00;3.00]	2.00 [1.00;3.50]	3.00 [2.00;3.00]	0.311
Targeted drug				0.112
Apatinib	5 (3.70%)	2 (2.11%)	3 (7.50%)	
Bevacizumab	57 (42.2%)	36 (37.9%)	21 (52.5%)	
Lenvatinib	67 (49.6%)	52 (54.7%)	15 (37.5%)	
Sorafenib	6 (4.44%)	5 (5.26%)	1 (2.50%)	
ICI				0.460
Atezolizumab	1 (0.74%)	1 (1.05%)	0 (0.00%)	
Camrelizumab	31 (23.0%)	24 (25.3%)	7 (17.5%)	
Pembrolizumab	1 (0.74%)	1 (1.05%)	0 (0.00%)	
Sintilimab	96 (71.1%)	65 (68.4%)	31 (77.5%)	
Tislelizumab	3 (2.22%)	3 (3.16%)	0 (0.00%)	
Toripalimab	3 (2.22%)	1 (1.05%)	2 (5.00%)	
Hypertension				0.853
No	101 (74.8%)	72 (75.8%)	29 (72.5%)	
Yes	34 (25.2%)	23 (24.2%)	11 (27.5%)	
Diabetes				0.777
No	119 (88.1%)	83 (87.4%)	36 (90.0%)	
Yes	16 (11.9%)	12 (12.6%)	4 (10.0%)	
Heart disease				0.669
No	129 (95.6%)	90 (94.7%)	39 (97.5%)	
Yes	6 (4.44%)	5 (5.26%)	1 (2.50%)	

(Continued)

TABLE 1 Continued

	[ALL] N=135	No N=95	Yes N=40	p.overall
Smoking				0.028
No	99 (73.3%)	64 (67.4%)	35 (87.5%)	
Yes	36 (26.7%)	31 (32.6%)	5 (12.5%)	
Liver etiology				0.278
Alcohol	1 (0.74%)	0 (0.00%)	1 (2.50%)	
HBV	126 (93.3%)	90 (94.7%)	36 (90.0%)	
HCV	8 (5.93%)	5 (5.26%)	3 (7.50%)	
Hepatic vein invasion				0.634
No	113 (86.3%)	78 (84.8%)	35 (89.7%)	
Yes	18 (13.7%)	14 (15.2%)	4 (10.3%)	
Portal vein tumor thrombus (vp)				0.489
0	54 (41.2%)	37 (40.2%)	17 (43.6%)	
2	6 (4.58%)	3 (3.26%)	3 (7.69%)	
3	29 (22.1%)	23 (25.0%)	6 (15.4%)	
4	42 (32.1%)	29 (31.5%)	13 (33.3%)	
BCLC				0.204
A	9 (6.92%)	4 (4.40%)	5 (12.8%)	
B	22 (16.9%)	14 (15.4%)	8 (20.5%)	
C	98 (75.4%)	72 (79.1%)	26 (66.7%)	
D	1 (0.77%)	1 (1.10%)	0 (0.00%)	
Baseline tumor size	8.95 [6.27;13.0]	10.0 [7.03;14.0]	7.95 [5.38;10.7]	0.045
Maximum Efficacy Evaluation				0.089
CR	1 (0.90%)	0 (0.00%)	1 (1.37%)	
PR	59 (53.2%)	34 (46.6%)	25 (65.8%)	
SD	45 (40.5%)	32 (43.8%)	13 (34.2%)	
PD	6 (5.41%)	6 (8.22%)	0 (0.00%)	
WBC	5.36 [4.17;6.88]	5.29 [3.96;7.18]	5.59 [4.51;6.39]	0.810
PLT	165 [118;243]	163 [118;230]	170 [117;247]	0.816
PT	12.3 [11.7;13.1]	12.5 [11.7;13.2]	12.1 [11.7;12.8]	0.203
APTT	27.7 [25.6;30.0]	27.9 [25.9;30.3]	27.5 [25.1;29.5]	0.326
GLU	5.12 [4.53;5.93]	5.18 [4.53;6.07]	5.07 [4.58;5.49]	0.874
SCR	64.0 [56.5;76.0]	64.0 [56.5;75.5]	67.0 [56.5;76.0]	0.320
ALB	39.1 [35.6;42.0]	38.4 [35.1;41.8]	40.5 [37.5;42.6]	0.024
ALT	32.0 [20.0;52.0]	33.0 [20.0;52.0]	32.0 [19.2;49.2]	0.544
AST	52.0 [34.0;85.0]	59.0 [35.0;92.0]	45.0 [33.8;65.2]	0.104
TBIL	17.1 [12.1;23.7]	18.2 [12.2;25.2]	15.1 [11.4;21.3]	0.117
AFP team (400ng/ml)				0.092
High	68 (52.3%)	52 (57.8%)	16 (40.0%)	
Low	62 (47.7%)	38 (42.2%)	24 (60.0%)	

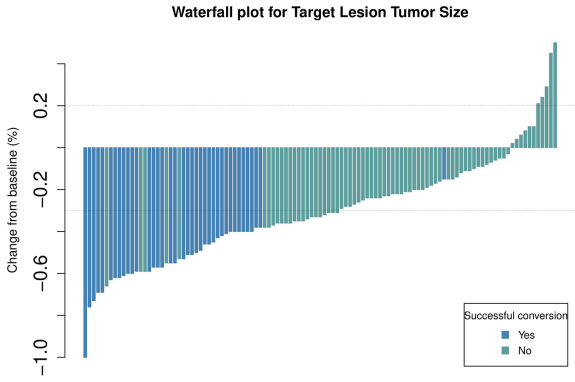

FIGURE 2
Waterfall plot demonstrating the target lesion size estimated using mRECIST guidelines.

Short-term efficacy and side effects

Short-term curative effects evaluated based on the mRECIST guidelines (8, 20, 21). The maximum therapeutic response are significantly correlated with the prognosis (22). Because the patients included in this study had a high tumour burden, we evaluated the maximum tumour response to treatment based on the mRECIST guidelines. Waterfall plots demonstrating the maximum tumour response are depicted in Figure 2. The ORR and DCR of patients were 54.1% and 94.6%, respectively. The ORR was higher in the conversion surgery group (successful vs unsuccessful: 65% versus 36%, p = 0.08).

A total of 280 treatment-related AEs occurred during the follow-up period. The most common grade-1 and -2 AEs were abdominal pain, fatigue and abnormal liver function (Figure 3A). A total of 97 patients experienced at least 1 grade-3 or -4 AE (Figure 3B). The most common grade-3 and -4 AEs were fatigue, pain and fever. Additionally, a patient had gastrointestinal haemorrhage, which was successfully treated *via* endoscopic haemostasis.

Prognostic analysis

The median follow-up duration was 12 months and 11 months in the successful and unsuccessful conversion groups, respectively. The median PFS was 28 months and 7 months in the successful and unsuccessful conversion groups, respectively. The median OS was 30 months and 15 months in the successful and unsuccessful conversion groups, respectively. PFS and OS curves are shown in Figures 4A, B. As shown in the forest plot in Figures 5A, B, successful conversion surgery, sex, hapatic vein invasion, BCLC stage, baseline tumour size, AFP levels and maximum therapeutic response were independent prognostic factors for PFS. Multivariate Cox analysis showed that successful conversion surgery, number of

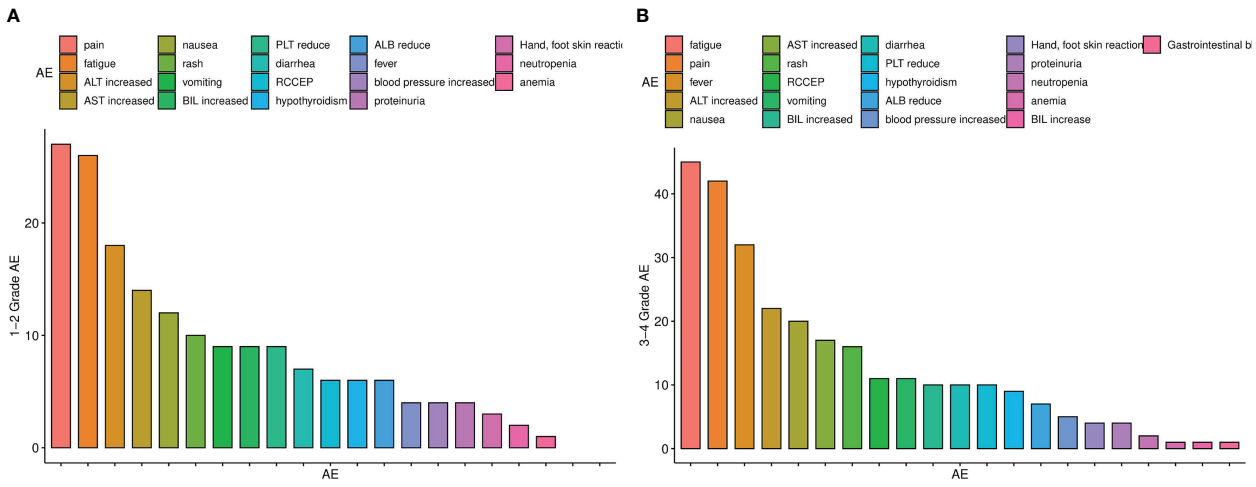

FIGURE 3
(A) Histogram of adverse reactions of grades 1–2, **(B)** Histogram of adverse reactions of grades 3–4.

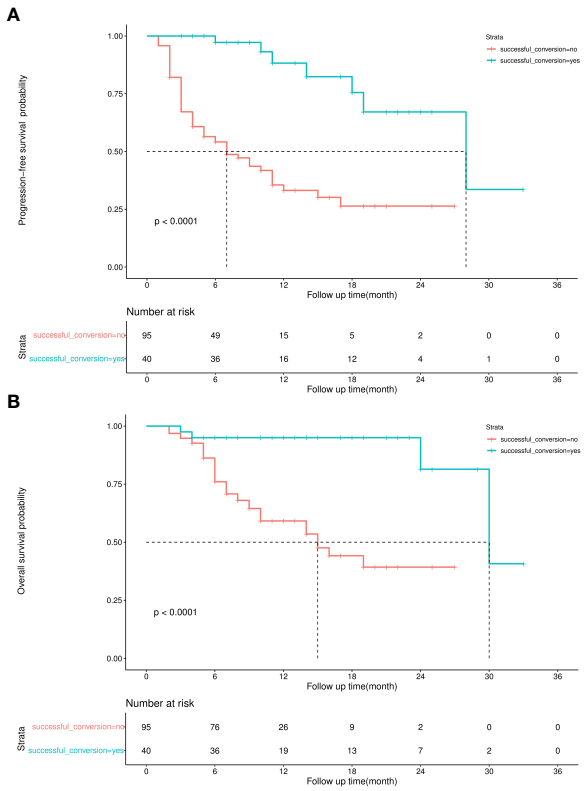

FIGURE 4
(A) Kaplan–Meier curve for progression-free survival, **(B)** Kaplan–Meier curve for overall survival.

interventions, hapatic vein invasion and total bilirubin levels were independent prognostic factors for OS.

Sensitivity analysis

The sample size of this study is small, and the statistical power of multivariate analysis might have been inadequate. Therefore, IPW was used to balance confounding factors between the successful and unsuccessful conversion groups, and weighted survival analysis was subsequently used to examine sensitivity (23). As shown in Figure 6, the factors that may affect the prognosis of patients are incorporated into the IPTW equation. After IPTW analysis, no standardised differences exceeding the threshold were observed. IPW-adjusted survival curves were plotted to demonstrate the effects of successful conversion surgery on PFS and OS (Figures 7A, B). The final results showed that successful conversion surgery was an independent prognostic factor for both PFS and OS.

Because observational analyses have inherent limitations, the E-value was calculated to assess the sensitivity to unmeasured confounders (24). If the effect value of the unmeasured confounding factor reaches the E-value, the result is invalidated. The E-value of successful conversion surgery was 7.57 and 6.53 for OS and PFS, respectively, which indicates a relatively robust impact of successful conversion surgery on the prognosis of patients.

Discussion

In this study, real-world data were used to evaluate the effectiveness of HAIC combined with immunotherapy and molecular targeted therapy in patients with primary uHCC. Patients with high tumour burden had a high tumour regression rate after combination therapy, and successful conversion surgery had strong protective effects on the prognosis. Although the incidence of side effects owing to combination therapy is high, they can be well managed. To adjust for possible confounding factors, the article employs inverse probability weighting. In addition, we calculated E-values, which allow us to assess the effect of unmeasured confounders on the final results in a quantitative manner. The experimental design and methodology of this study will assist us in evaluating the causal relationship between HAIC combined with systemic therapy and patient prognosis, despite the fact that it is a real-world study.

Because most patients with HCC are diagnosed at a middle or advanced stage, they are ineligible for radical local treatment. Before

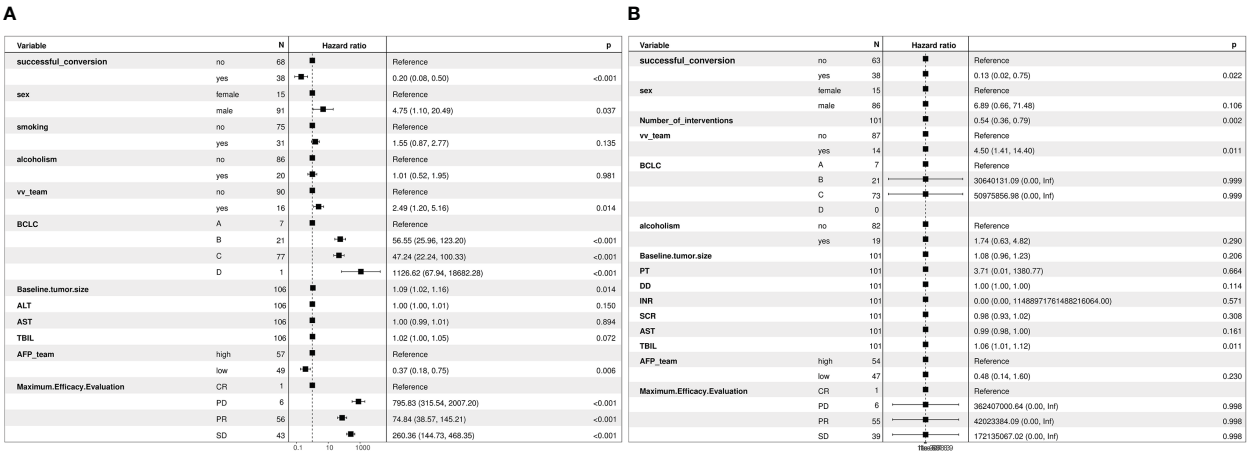

FIGURE 5
(A) Forest plot of multivariate Cox regression analysis of PFS, **(B)** Forest plot of multivariate Cox regression analysis of OS.

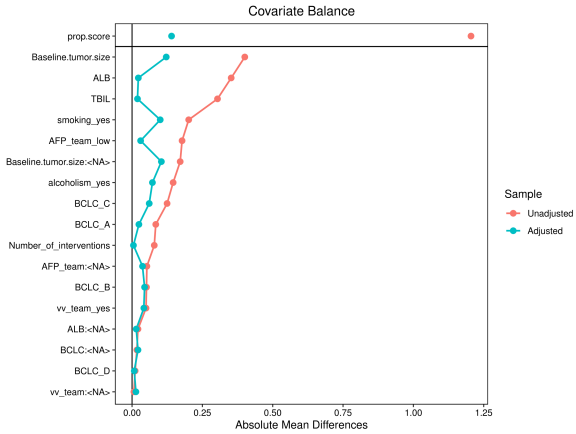

FIGURE 6
Love plot for standardised baseline differences before and after IPTW.

immunotherapy was introduced, TACE was the standard treatment option for middle-stage liver cancer, whereas molecular targeted therapy (sorafenib or lenvatinib) was the standard treatment for advanced HCC (3).

In recent years, several novel systemic therapies have been introduced for the treatment of advanced HCC. In the IMbrave 150 study, combination therapy with atezolizumab and bevacizumab was identified as a better treatment option than sorafenib monotherapy for uHCC (4). In the ORIENT-32 trial, the effectiveness of combination therapy with sintilimab and a bevacizumab biosimilar (IBI305) was found to be superior to that of sorafenib monotherapy, which has been approved by the FDA for the first-line treatment of advanced unresectable liver disease (25). The phase III HIMALAYA trial demonstrated that combined with sorafenib monotherapy, durvalumab plus tremelimumab pre-stimulation treatment significantly improved survival (26). At present, the combination of molecular targeted drugs and immune checkpoint inhibitors is the first-line treatment for advanced liver cancer.

With the advancement of systemic therapy, the use of TACE therapy for treating HCC has reduced. Systemic therapy is recommended for patients with diffuse stage-B liver cancer (BCLC 2022) (27). Before immunotherapy was introduced, significant attempts were made to combine TACE and TKI drugs to improve therapeutic effects and prognosis. However, the results were contradictory (28–30). We speculate that the reason for this phenomenon may be the poor efficacy of TACE therapy in patients with a high tumour burden. However, TKI drugs are only effective in patients with a high tumour burden (7, 8, 31).

HAIC is more effective than TACE in patients with a high tumour burden (10, 32, 33). The combination of HAIC and molecular targeted therapy can increase the tumour regression rate and improve prognosis (13, 14). The findings of this study

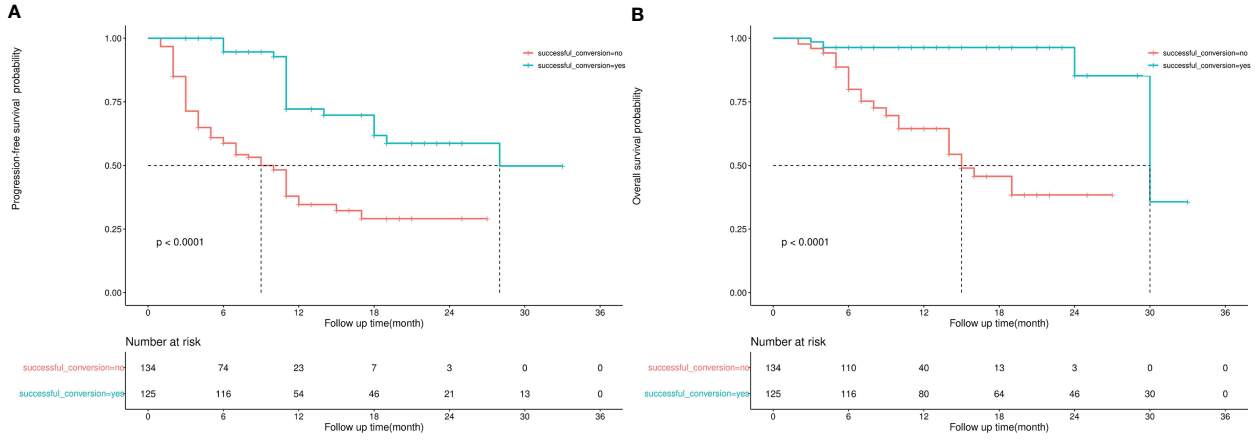

FIGURE 7
(A) IPW-adjusted Kaplan–Meier curve for PFS, **(B)** IPW-adjusted Kaplan–Meier curve for OS.

are similar to those of previous related studies. As evaluated based on the mRECIST guidelines, the overall ORR and DCR were 54.1% and 94.6%, respectively. These rates might have been overestimated because 24 patients had imaging data but cannot be judged. However, the results of survival analysis indicated that combination therapy was associated with a positive outcome. The overall median PFS and OS were 12 months and 30 months, respectively, which are higher than those reported in the IMBRAVE 150 and LEAP-002 studies (4, 34). Therefore, combination therapy may be more effective for patients with a high tumour burden.

At least one side effect was experienced by almost all patients. A total of 97 (72%) patients experienced AEs of grades 3–4. Fatigue, pain and fever were the most common grade-3 and -4 AEs. In addition, a patient had gastrointestinal haemorrhage, which was successfully treated *via* endoscopic haemostasis. The incidence of grade-3 and -4 AEs was significantly higher in this study than in previous studies (14, 35). This increase may be attributed to the inclusion of adverse reactions related to the process of perfusion therapy, such as abdominal pain and fever, in this study. Although these adverse reactions are graded high according to CTCAE 4.0 (36), they are manageable and have a minimal impact on the outcome of patients. No unique adverse effects associated with combination therapy were observed. The common AEs observed in this study are manageable despite their high incidence.

Furthermore, the prognostic impact of successful conversion surgery was assessed. Of the 135 patients with primary uHCC, 40 patients were successfully treated with surgery after the completion of combination therapy. The rate of surgical conversion in patients with uHCC after systemic and local therapy varies widely (35, 37). Owing to the small sample size of previous studies, there is a greater possibility of selection bias. To the best of our knowledge, this study employed the largest cohort to evaluate the efficacy of HAIC combined with immunotherapy and targeted therapy in uHCC. The surgical conversion rate of patients in this study is considered significant for future investigation into this field. Multivariate Cox, IPTW and E-value revealed that successful conversion surgery was an independent prognostic factor in uHCC. This finding indicates that surgical treatment should be administered to eligible patients with primary unresectable liver cancer to improve their prognosis.

This retrospective study has several limitations. First, HAIC combined with immunotherapy and targeted therapy has not been used in clinical practice for a long time, and the overall follow-up period was short. Further follow-up is required to establish long-term efficacy and side effects. Second, this study had a retrospective design with an unavoidable bias, such as selection bias in the inclusion of patients and information bias in the evaluation of imaging data. Due to being a retrospective study and a single-center study, the collected data is somewhat limited. For example, Previous studies showed that the nutritional state of HCC patients has a great impact on prognosis (38). In our study, we did not gather information about these factors. Additionally, because the data were collected from regional cancer centres, the results may not apply to all primary care units. It is necessary to conduct prospective multicentre studies to verify the results of this study. According to our study, the short-term curative effect of patients is greater than that of previous studies and randomized controlled trials. Despite the favorable short-term efficacy of combination therapy, selection bias may have contributed to this high efficacy.

In conclusion, HAIC combined with immunotherapy and molecular targeted therapy has a higher tumour regression rate and surgical conversion rate in patients with primary unresectable liver cancer, and the side effects of this combination therapy are well manageable. Patients undergoing surgery after combination therapy have survival benefits.

Data availability statement

The raw data supporting the conclusions of this article will be made available by the authors, without undue reservation.

Ethics statement

Written informed consent was obtained from the individual(s), and minor(s)' legal guardian/next of kin, for the publication of any potentially identifiable images or data included in this article.

Author contributions

Conception and design: WX and HY; acquisition and analysis of data: WZ and CL; methodology and soft-ware: KZ and ML; formal analysis: XY; data curation and radiological evaluation: QZ and WG; manuscript writing: WZ and KZ; writing – review and editing: DL, HM and HL; supervision: ZG. All authors contributed to the article and approved the submitted version.

Funding

This work was supported by the 2020 pilotage elite special scientific research fund, Grant No.XM2020031029501, China Health Promotion Foundation (No: XM-2018-011-0006-01), Beijing Health Prevention and Therapy Association (No: IZ 2021-1001).

Acknowledgments

Not applicable.

Conflict of interest

The authors declare that the research was conducted in the absence of any commercial or financial relationships that could be construed as a potential conflict of interest.

Publisher's note

All claims expressed in this article are solely those of the authors and do not necessarily represent those of their affiliated organizations, or those of the publisher, the editors and the reviewers. Any product that may be evaluated in this article, or claim that may be made by its manufacturer, is not guaranteed or endorsed by the publisher.

Supplementary material

The Supplementary Material for this article can be found online at: https://www.frontiersin.org/articles/10.3389/fimmu.2023.1127349/full#supplementary-material

References

1. Bray F, Ferlay J, Soerjomataram I, Siegel RL, Torre LA, Jemal A. Global cancer statistics 2018: GLOBOCAN estimates of incidence and mortality worldwide for 36 cancers in 185 countries. *CA Cancer J Clin* (2018) 68(6):394–424. doi: 10.3322/caac.21492

2. McGlynn KA, Petrick JL, El-Serag HB. Epidemiology of hepatocellular carcinoma. *Hepatology* (2021) 73 Suppl 1(Suppl 1):4–13. doi: 10.1002/hep.31288

3. Llovet JM, De Baere T, Kulik L, Haber PK, Greten TF, Meyer T, et al. Locoregional therapies in the era of molecular and immune treatments for hepatocellular carcinoma. *Nat Rev Gastroenterol Hepatol* (2021) 18(5):293–313. doi: 10.1038/s41575-020-00395-0

4. Finn RS, Qin S, Ikeda M, Galle PR, Ducreux M, Kim TY, et al. Atezolizumab plus bevacizumab in unresectable hepatocellular carcinoma. *N Engl J Med* (2020) 382 (20):1894–905. doi: 10.1056/NEJMoa1915745

5. Reig M, Forner A, Rimola J, Ferrer-Fàbrega J, Burrel M, Garcia-Criado Á, et al. BCLC strategy for prognosis prediction and treatment recommendation: The 2022 update. *J Hepatol* (2022) 76(3):681–93. doi: 10.1016/j.jhep.2021.11.018

6. Llovet JM, Villanueva A, Marrero JA, Schwartz M, Meyer T, Galle PR, et al. Trial design and endpoints in hepatocellular carcinoma: AASLD consensus conference. *Hepatology* (2021) 73 Suppl 1:158–91. doi: 10.1002/hep.31327

7. Wang Q, Xia D, Bai W, Wang E, Sun J, Huang M, et al. Development of a prognostic score for recommended TACE candidates with hepatocellular carcinoma: A multicentre observational study. *J Hepatol* (2019) 70(5):893–903. doi: 10.1016/j.jhep.2019.01.013

8. Han G, Berhane S, Toyoda H, Bettinger D, Elshaarawy O, Chan A, et al. Prediction of survival among patients receiving transarterial chemoembolization for hepatocellular carcinoma: A response-based approach. *Hepatology* (2020) 72(1):198–212. doi: 10.1002/hep.31022

9. Li S, Xu J, Zhang H, Hong J, Si Y, Yang T, et al. The role of hepatic arterial infusion chemotherapy in the treatment of hepatocellular carcinoma: A systematic review and meta-analysis. *Chemotherapy* (2021) 66(4):124–33. doi: 10.1159/000518257

10. Li QJ, He MK, Chen HW, Fang WQ, Zhou YM, Xu L, et al. Hepatic arterial infusion of oxaliplatin, fluorouracil, and leucovorin versus transarterial chemoembolization for Large hepatocellular carcinoma: A randomized phase III trial. *J Clin Oncol* (2022) 40(2):150-60. doi: 10.1200/JCO.21.00608

11. Li S, Mei J, Wang Q, Shi F, Liu H, Zhao M, et al. Transarterial infusion chemotherapy with FOLFOX for advanced hepatocellular carcinoma: a multi-center propensity score matched analysis of real-world practice. *Hepatobiliary Surg Nutr* (2021) 10(5):631–45. doi: 10.21037/hbsn.2020.03.14

12. He M, Li Q, Zou R, Shen J, Fang W, Tan G, et al. Sorafenib plus hepatic arterial infusion of oxaliplatin, fluorouracil, and leucovorin vs sorafenib alone for hepatocellular carcinoma with portal vein invasion: A randomized clinical trial. *JAMA Oncol* (2019) 5(7):953–60. doi: 10.1001/jamaoncol.2019.0250

13. Zheng K, Zhu X, Fu S, Cao G, Li WQ, Xu L, et al. Sorafenib plus hepatic arterial infusion chemotherapy versus sorafenib for hepatocellular carcinoma with major portal vein tumor thrombosis: A randomized trial. *Radiology* (2022) 303(2):455-64. doi: 10.1148/radiol.211545

14. Xin Y, Cao F, Yang H, Zhang X, Chen Y, Cao X, et al. Efficacy and safety of atezolizumab plus bevacizumab combined with hepatic arterial infusion chemotherapy for advanced hepatocellular carcinoma. *Front Immunol* (2022) 13:929141. doi: 10.3389/fimmu.2022.929141

15. He MK, Liang RB, Zhao Y, Xu YJ, Chen HW, Zhou YM, et al. Lenvatinib, toripalimab, plus hepatic arterial infusion chemotherapy versus lenvatinib alone for advanced hepatocellular carcinoma. *Ther Adv Med Oncol* (2021) 13:17588359211002720. doi: 10.1177/17588359211002720

16. Malik AY, Foster C. The revised Declaration of Helsinki: cosmetic or real change. *J R Soc Med* (2016) 109(5):184–9. doi: 10.1177/0141076816643332

17. Lencioni R, Llovet JM. Modified RECIST (mRECIST) assessment for hepatocellular carcinoma. *Semin Liver Dis* (2010) 30(1):52–60. doi: 10.1055/s-0030-1247132

18. Austin PC. An Introduction to Propensity Score Methods for Reducing the Effects of Confounding in Observational Studies. *Multivariate Behav Res* (2011) 46 (3):399-424. doi: 10.1080/00273171.2011.568786

19. VanderWeele TJ, Ding P. Sensitivity analysis in observational research: Introducing the e-value. *Ann Intern Med* (2017) 167(4):268–74. doi: 10.7326/M16-2607

20. Llovet JM, Lencioni R. mRECIST for HCC: Performance and novel refinements. *J Hepatol* (2020) 72(2):288–306. doi: 10.1016/j.jhep.2019.09.026

21. Lencioni R, Montal R, Torres F, Park JW, Decaens T, Raoul JL, et al. Objective response by mRECIST as a predictor and potential surrogate end-point of overall survival in advanced HCC. *J Hepatol* (2017) 66(6):1166–72. doi: 10.1016/j.jhep.2017.01.012

22. Xia D, Wang Q, Bai W, Wang E, Wang Z, Mu W, et al. Optimal time point of response assessment for predicting survival is associated with tumor burden in hepatocellular carcinoma receiving repeated transarterial chemoembolization. *Eur Radiol* (2022) 32(9):5799–810. doi: 10.1007/s00330-022-08716-4

23. Huang LL, Wei YY, Chen F. [Confounder adjustment in observational comparative effectiveness researches: (1) statistical adjustment approaches for measured confounder]. *Zhonghua Liu Xing Bing Xue Za Zhi* (2019) 40(10):1304–9. doi: 10.3760/cma.j.issn.0254-6450.2019.10.024

24. Huang LL, Wei YY, Chen F. [Confounder adjustment in observational comparative effectiveness researches: (2) statistical adjustment approaches for unmeasured confounders]. *Zhonghua Liu Xing Bing Xue Za Zhi* (2019) 40(11):1450–5. doi: 10.3760/cma.j.issn.0254-6450.2019.11.020

25. Ren Z, Xu J, Bai Y, Xu A, Cang S, Du C, et al. Sintilimab plus a bevacizumab biosimilar (IBI305) versus sorafenib in unresectable hepatocellular carcinoma (ORIENT-32): a randomised, open-label, phase 2-3 study. *Lancet Oncol* (2021) 22 (7):977–90. doi: 10.1016/S1470-2045(21)00252-7

26. Kudo M. Durvalumab Plus Tremelimumab: A Novel Combination Immunotherapy for Unresectable Hepatocellular Carcinoma. *Liver Cancer* (2022) 11(2):87-93. doi: 10.1159/000523702

27. Reig M, Forner A, Rimola J, Ferrer-Fábrega J, Burrel M, Garcia-Criado A, et al. BCLC strategy for prognosis prediction and treatment recommendation: The 2022 update. *J Hepatol* (2022) 76(3):681-93. doi: 10.1016/j.jhep.2021.11.018

28. Kudo M, Imanaka K, Chida N, Nakachi K, Tak WY, Takayama T, et al. Phase III study of sorafenib after transarterial chemoembolisation in Japanese and Korean patients with unresectable hepatocellular carcinoma. *Eur J Cancer* (2011) 47 (14):2117–27. doi: 10.1016/j.ejca.2011.05.007

29. Park JW, Kim YJ, Kim DY, Bae SH, Paik SW, Lee YJ, et al. Sorafenib with or without concurrent transarterial chemoembolization in patients with advanced hepatocellular carcinoma: The phase III STAH trial. *J Hepatol* (2019) 70(4):684–91. doi: 10.1016/j.jhep.2018.11.029

30. Peng Z, Fan W, Zhu B, Wang G, Sun J, Xiao C, et al. Lenvatinib combined with transarterial chemoembolization as first-line treatment for advanced hepatocellular carcinoma: A phase III, randomized clinical trial (LAUNCH). *J Clin Oncol* (2023) 41 (1):117-27. doi: 10.1200/JCO.22.00392

31. Chen M, Cao J, Hu J, Topatana W, Li S, Juengpanich S, et al. Clinical-radiomic analysis for pretreatment prediction of objective response to first transarterial chemoembolization in hepatocellular carcinoma. *Liver Cancer* (2021) 10(1):38–51. doi: 10.1159/000512028

32. Lyu N, Lin Y, Kong Y, Zhang Z, Liu L, Zheng L, et al. FOXAI: a phase II trial evaluating the efficacy and safety of hepatic arterial infusion of oxaliplatin plus fluorouracil/leucovorin for advanced hepatocellular carcinoma. *Gut* (2018) 67 (2):395–6. doi: 10.1136/gutjnl-2017-314138

33. Ueshima K, Ogasawara S, Ikeda M, Yasui Y, Terashima T, Yamashita T, et al. Hepatic arterial infusion chemotherapy versus sorafenib in patients with advanced hepatocellular carcinoma. *Liver Cancer* (2020) 9(5):583–95. doi: 10.1159/000508724

34. Finn RS, Kudo M, Merle P, Meyer T, Qin S, Ikeda M, et al. LBA34 primary results from the phase III LEAP-002 study: Lenvatinib plus pembrolizumab versus

lenvatinib as first-line (1L) therapy for advanced hepatocellular carcinoma (aHCC). *Ann OF Oncol* (2022) 33:S1401. doi: 10.1016/j.annonc.2022.08.031

35. Zhang J, Zhang X, Mu H, Yu G, Xing W, Wang L, et al. Surgical conversion for initially unresectable locally advanced hepatocellular carcinoma using a triple combination of angiogenesis inhibitors, anti-PD-1 antibodies, and hepatic arterial infusion chemotherapy: A retrospective study. *Front Oncol* (2021) 11:729764. doi: 10.3389/fonc.2021.729764

36. Chen AP, Setser A, Anadkat MJ, Cotliar J, Olsen EA, Garden BC, et al. Grading dermatologic adverse events of cancer treatments: the common terminology criteria for adverse events version 4.0. *J OF THE Am Acad OF Dermatol* (2012) 67(5):1025–39. doi: 10.1016/j.jaad.2012.02.010

37. Zhu XD, Huang C, Shen YH, Ji Y, Ge NL, Qu XD, et al. Downstaging and resection of initially unresectable hepatocellular carcinoma with tyrosine kinase inhibitor and anti-PD-1 antibody combinations. *Liver Cancer* (2021) 10(4):320–9. doi: 10.1159/000514313

38. Rong W, Xia H, Zhang K, Zhang Y, Tao C, Wu F, et al. Serum metabolic effects of corn oligopeptides with 7-day supplementation on early post-surgery primary liver cancer patients: a double-blind randomized controlled trial. *Hepatobiliary Surg Nutr* (2022) 11(6):834–47. doi: 10.21037/hbsn-21-116

frontiers | Frontiers in Immunology

TYPE Original Research
PUBLISHED 29 May 2023
DOI 10.3389/fimmu.2023.1199040

OPEN ACCESS

EDITED BY
Chenyu Sun,
AMITA Health, United States

REVIEWED BY
Guo Huang,
University of South China, China
Xixi Xie,
SWMU, China
Gaoge Peng,
Southwest Medical University, China

*CORRESPONDENCE
Yue Yu
yuyue2014@njmu.edu.cn
Haoran Lin
njlinhaoran@163.com
Long Li
lilong_albert@163.com

†These authors have contributed equally to this work and share first authorship

RECEIVED 02 April 2023
ACCEPTED 19 May 2023
PUBLISHED 29 May 2023

CITATION
Ren Q, Zhang P, Zhang X, Feng Y, Li L, Lin H and Yu Y (2023) A fibroblast-associated signature predicts prognosis and immunotherapy in esophageal squamous cell cancer.
Front. Immunol. 14:1199040.
doi: 10.3389/fimmu.2023.1199040

A fibroblast-associated signature predicts prognosis and immunotherapy in esophageal squamous cell cancer

Qianhe Ren[1†], Pengpeng Zhang[1†], Xiao Zhang[1†], Yanlong Feng[1†], Long Li[2*], Haoran Lin[1*] and Yue Yu[1*]

[1]Department of Thoracic Surgery, The First Affiliated Hospital of Nanjing Medical University, Nanjing, China, [2]Department of Thoracic Surgery, Nanjing Gaochun People's Hospital, Nanjing, China

Background: Current paradigms of anti-tumor therapies are not qualified to evacuate the malignancy ascribing to cancer stroma's functions in accelerating tumor relapse and therapeutic resistance. Cancer-associated fibroblasts (CAFs) has been identified significantly correlated with tumor progression and therapy resistance. Thus, we aimed to probe into the CAFs characteristics in esophageal squamous cancer (ESCC) and construct a risk signature based on CAFs to predict the prognosis of ESCC patients.

Methods: The GEO database provided the single-cell RNA sequencing (scRNA-seq) data. The GEO and TCGA databases were used to obtain bulk RNA-seq data and microarray data of ESCC, respectively. CAF clusters were identified from the scRNA-seq data using the Seurat R package. CAF-related prognostic genes were subsequently identified using univariate Cox regression analysis. A risk signature based on CAF-related prognostic genes was constructed using Lasso regression. Then, a nomogram model based on clinicopathological characteristics and the risk signature was developed. Consensus clustering was conducted to explore the heterogeneity of ESCC. Finally, PCR was utilized to validate the functions that hub genes play on ESCC.

Results: Six CAF clusters were identified in ESCC based on scRNA-seq data, three of which had prognostic associations. A total of 642 genes were found to be significantly correlated with CAF clusters from a pool of 17080 DEGs, and 9 genes were selected to generate a risk signature, which were mainly involved in 10 pathways such as NRF1, MYC, and TGF-Beta. The risk signature was significantly correlated with stromal and immune scores, as well as some immune cells. Multivariate analysis demonstrated that the risk signature was an independent prognostic factor for ESCC, and its potential in predicting immunotherapeutic outcomes was confirmed. A novel nomogram integrating the CAF-based risk signature and clinical stage was developed, which exhibited favorable predictability and reliability for ESCC prognosis prediction. The consensus clustering analysis further confirmed the heterogeneity of ESCC.

Conclusion: The prognosis of ESCC can be effectively predicted by CAF-based risk signatures, and a comprehensive characterization of the CAF signature of ESCC may aid in interpreting the response of ESCC to immunotherapy and offer new strategies for cancer treatment.

KEYWORDS

esophageal squamous cell carcinoma, fibroblasts, risk signature, tumor immune microenvironment, immunotherapy

1 Introduction

Esophageal cancer (EC) is a prevalent form of cancer, ranking eighth among all cancer types, and is also the sixth most common cause of cancer-related deaths globally (1). It primarily consists of two major subtypes: esophageal squamous cell cancer (ESCC) and esophageal adenocarcinoma (EAC). ESCC accounts for the majority of esophageal cancer cases worldwide with a higher incidence in East Asia and Africa. On the other hand, esophageal adenocarcinoma (EAC) is more prevalent in many developed countries (2). Despite the great achievements in the management of ESCC, including surgery, endoscopic resection, chemoradiotherapy, and immunotherapy, this aggressively malignant tumor still extremely threatens patients' health attributed of its heterogeneity (3). Limited understanding of its molecular etiology further makes up for the poor prognosis (4). Thus, exploring the properties and identifying novel biomarkers for ESCC is urgently needed.

Targeted therapies have made remarkable strides in the management of diverse neoplastic conditions, such as esophageal squamous cell carcinoma (ESCC). Immunotherapy, encompassing the utilization of immune checkpoint inhibitors (ICIs)/immunomodulators, therapeutic vaccines, monoclonal antibodies, and adoptive cellular immunotherapy, constitutes a novel approach in the management of esophageal cancer (EC). Of noteworthy importance, ICIs have demonstrated efficacy in the management of melanoma and non-small cell lung cancer, and have exhibited encouraging outcomes in the treatment of advanced ESCC (5). An overarching conclusion that the tumor microenvironment (TME) is a multicellular context containing complex stromal-tumor interactions has been well established (6). The induction of proliferation, angiogenesis, inhibition of apoptosis, immune system suppression, and evasion of immune surveillance are intrinsically linked to TME. The tumor cells and surrounding TME cells constantly adapt to the new conditions and promote tumor growth. TME creates a niche for residing and interacting cancer cells with their surrounding endothelial, and immune cells as well as fibroblasts. The reciprocal communication between cancer cells and stromal cells as well as immune cells induces changes in the cellular components of TME, which predisposes cancer cells to metastasis (7, 8). CAFs are a prominent stromal component in the tumor microenvironment (TME) and are present in varying types of solid tumors, making them an important target for treatment (9). Through various mechanisms, activated CAFs can facilitate tumor growth, angiogenesis, invasion, and metastasis, as well as extracellular matrix (ECM) remodeling and even chemoresistance. CAFs communicate with immune cells that infiltrate the tumor microenvironment (TIME), as well as other immunological constituents, by releasing a plethora of cytokines, growth factors, chemokines, exosomes, and other effectual molecules. This phenomenon leads to the molding of an immunosuppressive TIME, which facilitates cancer cells to elude immune surveillance (10). All cellular and non-cellular constituents of the tumor microenvironment can engage in intricate and tightly regulated reciprocal dialogues, thereby promoting cancer initiation, progression, and resistance to therapy. A comprehensive comprehension of the crosstalk between the microenvironment and cancerous cells is indispensable for devising innovative therapeutic strategies (11). CAFs have been identified in divergent types of tumors, including breast cancers and esophageal squamous cancer (12, 13). Accumulating evidence has confirmed that CAFs-specific signatures can be utilized for prognosis prediction in colon cancer ascribing to several markers expressing in CAFs correlated with prognosis (14). Recently, the interplay between CAFs and the tumor immune microenvironment (TIME) has been recognized as a crucial element in driving tumor progression (10). A study has revealed that primary oral squamous cell carcinoma (OSCC) tumors exhibit a negative correlation between WNT2+ cancer-associated fibroblasts (CAFs) and active CD8+ T cells. The use of anti-WNT2 monoclonal antibody has been shown to significantly restore antitumor T-cell responses within tumors and increase active dendritic cells (DCs) in both mouse OSCC and colorectal cancer (CRC) syngeneic tumor models, thereby enhancing the efficacy of anti-PD-1 treatment. Direct interference with CAFs-derived WNT2 has been found to restore DC differentiation and DC-mediated antitumor T-cell responses. Mechanistic analyses have further demonstrated that CAFs-secreted WNT2 suppresses the DC-mediated antitumor T-cell response through the SOCS3/p-JAK2/p-STAT3 signaling cascades. Targeting WNT2 might enhance the ICI efficacy and represent a new anticancer immunotherapy (15). Thus, CAFs were frequently targeted in anti-tumor immunotherapy (16). Yet, the mechanisms by which CAFs regulate the antitumor immune responses in solid tumors are currently not fully understood.

Recent progresses in single-cell sequencing has shed new light on exploring biological systems with revolutionary solutions (17).

Different from bulk sequencing, which focuses on averaged data, single-cell sequencing, including transcriptomics, epigenomics, genomics, proteomics and metabolomics sequencing, is a splendid tool to illuminate the cellular and molecular landscape at the single-cell level (18). Single-cell sequencing, besides, has become indispensable in decomposing tissues into cell type or cell states and dissecting the cellular heterogeneity (19). Through single-cell sequencing, conventional dendritic cell (cDC) and distinct macrophage subsets were identified exerting enormous impact on mediating cellular cross-talk in the tumor microenvironment, providing myeloid-targeted immunotherapies for colorectal patients (20). One recent research has offered a novel insight complex cellular architecture and potential therapeutic measures for patients diagnosed with breast cancer (21). Breaking down the complexity of several tumors and characterizing heterogeneous phenotypic states in extraordinary detail (20), single-cell sequencing is quite suitable for ESCC analyses.

Numerous studies have been conducted on CAFs in esophageal squamous cancer (ESCC), but the systematic characteristics of CAFs and their correlation with ESCC prognosis and immunotherapy response are not yet fully comprehended. In this study, we obtained single-cell RNA sequencing (scRNA-seq) data and transcriptome data from accessible databases to differentiate CAF subclusters and establish a CAF-based risk signature for ESCC. We evaluated the clinical significance of the CAF-based signature and further analyzed the immune landscape and responsiveness to immunotherapy associated with it. Finally, we developed a novel nomogram that combines the CAF-based risk signature with clinicopathological features to facilitate the clinical use of CAF features in the prognosis of ESCC. Our findings could provide novel insights into the pathophysiology of ESCC, bringing about personalized treatments and improved outcomes for patients with ESCC.

2 Methods

2.1 Data collection and processing

ESCC scRNA-seq data was acquired in Gene Expression Omnibus (GEO) database (accession number GSE191756). We screened out single cells with any gene expressed in fewer than three cells or those expressing fewer than 250 genes. The percentage of rRNA and mitochondria was then calculated with the PercentageFeatureSet function in the Seurat R package (22). Consequently, 12118 cells were totally obtained for subsequent analysis.

We further collected transcript data, single-nucleotide variants (SNV), copy number variants (CNV), and corresponding clinical data of ESCC from The Cancer Genome Atlas (TCGA) database. Samples lacking outcome status or survival data were excluded and 94 ESCC samples were obtained, which were utilized for external validation. GSE53624 data with 119 tumor samples and 119 normal ones was used as the training cohort after abandoning samples without follow-up acquired from Gene Expression Omnibus (GEO) database (The clinical characteristics of both the training cohort and the test cohort were exhibited in Supplementary Tables). Based on the literature, ten cancer-associated pathways (Cell Cycle, NRF1, MYC, NOTCH, HIPPO, PI3K, TP53, PI3K, WNT, and TGF-Beta) were identified and analyzed about their gene expression profiles in our dataset.

2.2 CAF definition

The scRNA-seq data of ESCC was re-analyzed using the Seurat package, with the aim of providing a systematic characterization of the CAF signature. To start the data preprocessing, cells with less than 250 or more than 6000 expressed genes were removed, and the remaining expressed genes were log-normalized. Next, the FindIntegrationAnchors function was utilized. To reduce the dimensionality of the data, the t-distributed Stochastic Neighbor Embedding (tSNE) method was applied, utilizing a resolution of 0.1 and selecting 30 principal components. The tSNE method employed was non-linear in nature. To classify the single cells into various subgroups, we utilized the FindNeighbors and FindClusters functions (dim = 30 and resolution = 0.1). Additionally, we performed tSNE dimensional reduction using the RuntSNE function. Fibroblasts were annotated according to four marker genes, including PDGFRB, ACTA2, FAP, and NOTCH3. Subsequently, the fibroblasts were re-clustered using the FindClusters and FindNeighbors functions. To define the marker genes for each CAF cluster, we used the FindAllMarkers function with a comparison between different clusters (minpct = 0.35, logFC = 0.5, and adjust p-value < 0.05). We utilized the CopyKAT R package to analyze the CNV characteristics of the CAF clusters and distinguish them from tumor cells and normal ones. Finally, Kyoto Encyclopedia of Genes and Genomes (KEGG) enrichment analysis was conducted on the marker genes using the clusterProfiler package (23).

2.3 Identification of hub genes based on CAF

Differentially expressed genes (DEGs) between normal and tumor tissue were identified using the limma package (24, 25), based on criteria of |log2(FoldChange)|>1 and a false discovery rate (FDR)<0.05. Next, the correlations between CAF clusters and DEGs were evaluated, and key CAF-related genes with p<0.01 and cor>0.4 were identified. To identify prognosis-related genes, the survival package was utilized to conduct univariate Cox regression analysis (26). The least absolute shrinkage and selection operator (lasso) was used to reduce the number of genes (27). Multivariate Cox regression analysis was conducted using the stepwise regression method to establish a CAF-based risk signature, which was calculated using the formula: 0.093*ANGPTL7 + 0.15*C6 + 0.121*CSRP1+-0.08*EXPH5 + 0.12*F2RL2 + 0.014*KCNMA1 +-0.373*MAGEC3 + 0.143*MAMDC2+-0.188*SLC4A9. The patients were classified into low- and high-risk groups using zero-mean normalization. The predictive value of the risk signature was evaluated using the timeROC package to perform receiver operating characteristic curve (ROC) analysis. The results demonstrated that the

risk signature had significant predictive value for patient prognosis. In summary, our analysis provides important insights into the molecular mechanisms underlying tumor development and highlights the potential of CAF-related genes as prognostic biomarkers for cancer patients.

2.4 A novel nomogram constructed based on the risk signature

After conducting univariate and multivariate Cox regression analyses based on the risk signature and clinicopathological features (24, 28), a novel nomogram was constructed to predict the prognosis of ESCC using variables with $p<0.05$ in the multivariate Cox model. The predictive accuracy of the model was evaluated by generating a calibration curve.

2.5 Immune landscape analysis

The correlation between the risk signature and the tumor immune microenvironment (TIME) was comprehensively assessed using several algorithms, including CIBERSORT, EPIC, MCPCOUNTER, and TIMER (29). Stromal scores, immune scores, and estimate scores (stromal scores + immune scores) were calculated using the "estimate" R package to evaluate differences in the tumor microenvironment of patients (30, 31). Besides, the proportions of 22 immune cell subtypes were estimated using the CIBERSORT algorithm based on the GSE53624 cohort. The correlation between genes comprising the signature and immune score were further explored to illuminate the great impact those genes exert on immune-related functions.

2.6 Response to immunotherapy

Anti-PD-1 or anti-PD-L1 checkpoint inhibition therapy has gained increasing attention as a crucial component of immunotherapy. Transcriptomic data as well as corresponding clinical data from patients who received anti-PD-L1 therapy from the IMvigor210 cohort were collected to evaluate the performance of the risk signature in predicting responsiveness to immunotherapy (immune checkpoint blocks). Additionally, transcriptomic data from the GSE78220 cohort, which included melanoma patients who received anti-PD-1 checkpoint inhibition therapy before treatment, were downloaded.

2.7 Consensus clustering analysis and immune infiltration

To further probe into the heterogeneity of ESCC, all ESCC patients were separated into different clusters according to the expression of CAF-related genes with the R package 'ConsensusClusterPlus' (22). Differences in survival, TIME, and immune checkpoints were evaluated among subgroups using the same methodology as previously employed. The immune landscape of ESCC patients based on different clusters was demonstrated in the form of heatmap.

2.8 RNA isolation and quantitative RT-PCR assay

Total RNA was isolated from ESCC cells or tissues using TRIzol reagent (Thermo Fisher Scientific, Waltham, MA, USA). The complementary DNA (cDNA) was synthesized as per the manufacturer's instructions, utilizing the RevertAid^{TM} First Strand cDNA Synthesis Kit (Thermo Fisher Scientific). qRT-PCR was performed with SYBR Green PCR kit (Takara Bio, Otsu, Japan) on a StepOne Real-Time PCR system (Thermo Fisher Scientific). The relative gene expression levels were quantified by employing the $2^{-\triangle\triangle CT}$ method.

2.9 Statistical analysis

All statistical analyses were performed using R software (version 4.1.0). The Wilcoxon test was used for comparing two groups, while Spearman or Pearson correlation was used for correlation matrices. Survival differences through K-M curves were assessed using the Log-rank test, where statistical significance was defined as p-value < 0.05.

3 Results

3.1 CAFs screening based on scRNA-seq samples

The flow-process diagram of our study was depicted in Figure 1. After initial screening, 18024 cells were totally obtained based on the scRNA-seq data. As was shown in Figure S1, the details of data preprocessing were demonstrated. After conducting log-normalization and dimensionality reduction, 32 subpopulations were obtained (Figure 2A). As presented in Figure 2B, six CAF populations were further identified with four marker genes (FDGFRB, FAP, ACTA2, and NOTCH3). The proportions of the six clusters in each cohort were then calculated and the results were illustrated in histograms (Figure 2C). Moreover, KEGG analysis illuminated that the DEGs (which were obtained using R package 'FindVariableFeatures') were significantly enriched in various pathways, including tight junction, complement and coagulation, focal adhesion and so on (Figure 2D). Additionally, distributional differences between tumor and normal cells in the six CAF clusters were presented in Figure 2E. In addition, the expression of TOP 5 DEGs were respectively exhibited in heatmap (Figure 2F), bubble diagram (Figure 2G), and volcano plot (Figure 2H).

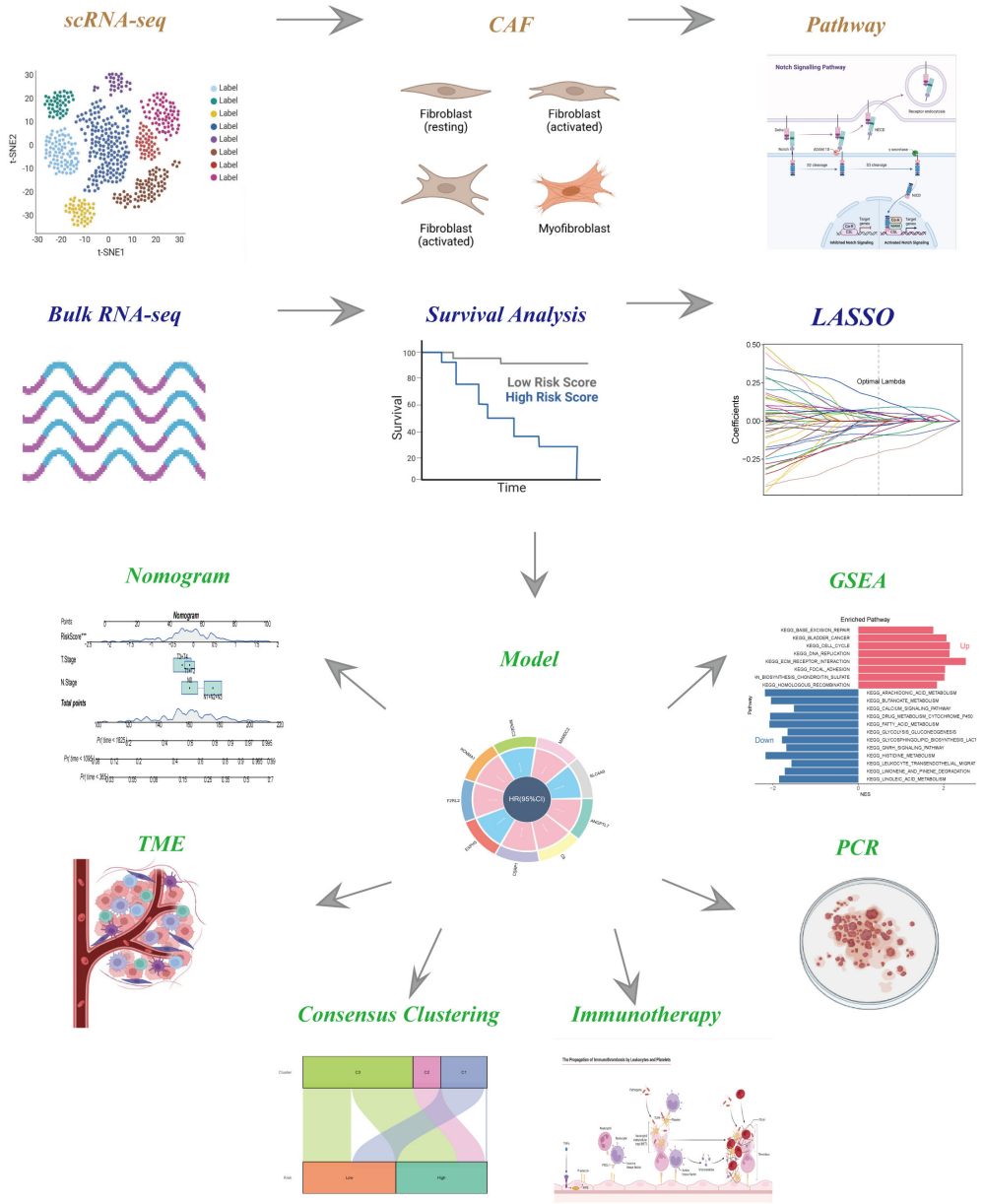

FIGURE 1
The flow chart of this study.

3.2 The exploration of cancer-related pathways in CAF

To probe into the correlations between tumor progression and the CAF clusters, we explored the features of ten tumor-related pathways based on the six CAF clusters. GSVA scores of these divergent pathways were estimated based on various CAF clusters, and the results were depicted in Figure 3A. Significant differences about the ratio of malignant cells were obtained in CAF_0 and CAF_4, where the malignant cells accounted for a few proportions. By contrast, the ratio of malignant cells was remarkably higher among CAF_1, CAF_2, CAF_3, and CAF_5 (Figure 3B). Besides, slight differences were identified after performing the GSVA analysis of these tumor-related pathways between non-malignant and malignant cells in each CAF cluster (Figures 3C-F). (GSVA scores analysis based on CAF_0 CAF_1 was shown in Figures S2A, B)

Furthermore, the ssGSEA score of the marker genes (the TOP 5 DEGs obtained in Figures 2F-H) were analyzed in each CAF cluster based on the GSE53624 cohort to illustrate the relationships between the CAF clusters and crucial clinicopathological characteristics. Interestingly, tumor samples were found having higher scores compared with normal ones only in CAF_0 and CAF_3, while among the other clusters, normal samples gained significantly higher scores (Figure S2C). In addition, ESCC samples of GSE53624 cohort were divided into high-and-low score groups according to the optimal cut-off value with survminer R package. In the CAF_2, CAF_4, and CAF_5 clusters, samples in the low-CAF

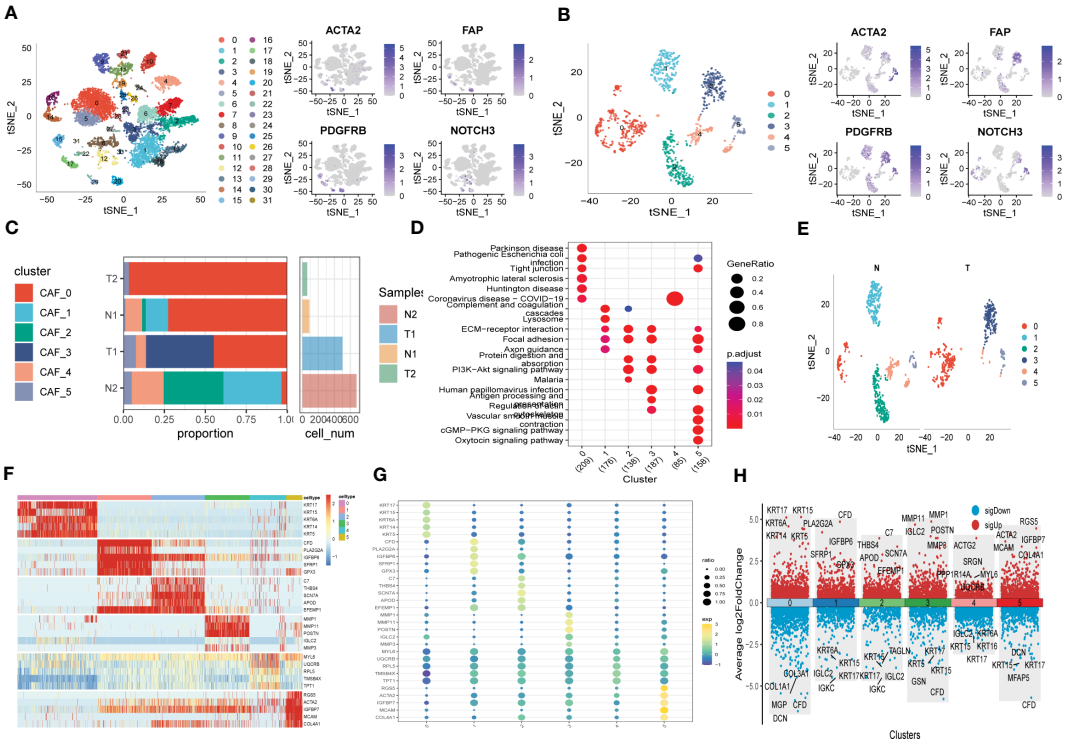

FIGURE 2
The identification of CAF clusters according to scRNA data of ESCC patients. **(A)** tSNE plots of distribution of 32 clusters and fibroblasts-based marker genes expression. **(B)** tSNE plots of distributions of five fibroblasts after clustering. **(C)** Subgroups in cancer and adjacent tissue and proportion as well as cell number calculation. **(D)** KEGG analysis of five fibroblasts subgroups. **(E)** tSNE distribution of malignant and non-malignant cells predicted by copycat package. **(F)** Heatmap of the top5 marker gene expression of subgroups. **(G)** Bubble diagram of the top5 marker gene expression of subgroups. **(H)** Volcano plot of the top5 marker gene expression of subgroups.

score subgroup shared a more favorable prognosis compared with those in high-CAF subgroup. CAF_0, CAF_1, and CAF_3, however, were identified not associated with the prognosis of ESCC (Figure S2D).

3.3 Identification of hub genes correlated with CAF

Firstly, DEGs were screened out between normal and tumor samples to establish a risk signature. As depicted in Figure 4A, 17080 DEGs were totally obtained, with 7556 down-regulated and 9524 up-regulated DEGs. Among them, a total of 642 genes were identified significantly related with those prognosis-related CAF clusters (Figure 4B). After univariate Cox regression analysis, the prognosis of each gene was evaluated, with 8 genes being identified related to protective factors and 18 genes correlated with risk values. Lasso Cox regression analysis was then performed to reduce the number of genes (Figure 4C). Furthermore, the stepwise regression method was utilized to develop the risk signature after performing multivariate Cox regression analysis. The signature was composed with nine genes (Figures 4F, G), namely complement C6, MAM domain containing 2 (MAMDC2), cysteine- and glycine-rich protein 1 (CSRP1), coagulation factor II thrombin receptor like 2 (F2RL2), angiopoietin like 7 (ANGPTL7), potassium calcium-activated channel subfamily M alpha 1 (KCNMA1), exophilin 5 (EXPH5), solute carrier family 4, sodium bicarbonate cotransporter, member 9 (SLC4A9), and MAGE family member C3 (MAGEC3). And the risk model formula is as follows: RiskScore="0.093*ANGPTL7 + 0.15*C6 + 0.121*CSRP1 +-0.08*EXPH5 + 0.12*F2RL2 + 0.014*KCNMA1+-0.373*MAGEC3 + 0.143*MAMDC2+-0.188*SLC4A9". The risk score of each sample was calculated using z-mean normalization, and the patients were then separated into high-and-low-risk groups. The Kaplan-Meier survival analysis exhibited that patients in high-risk groups encountered with worse prognosis compared with those in low-risk groups both in GSE53624 (Figure 4D) and TCGA cohorts (Figure 4E). Additionally, both the GSE53624 and TCGA cohorts exhibited satisfying AUC values of the model, revealing that the predictive power of the signature was excellent. The last, the distribution of patient survival status, risk score, and expression of hub genes in GEO and TCGA cohorts were depicted in Figure S3.

3.4 Independent risk factors recognition and nomogram construction

To improve the accuracy of our predictive model, we incorporated clinicopathological characteristics and the risk score through univariate and multivariate Cox regression analyses. Our multivariate analysis revealed that the risk signature was the most

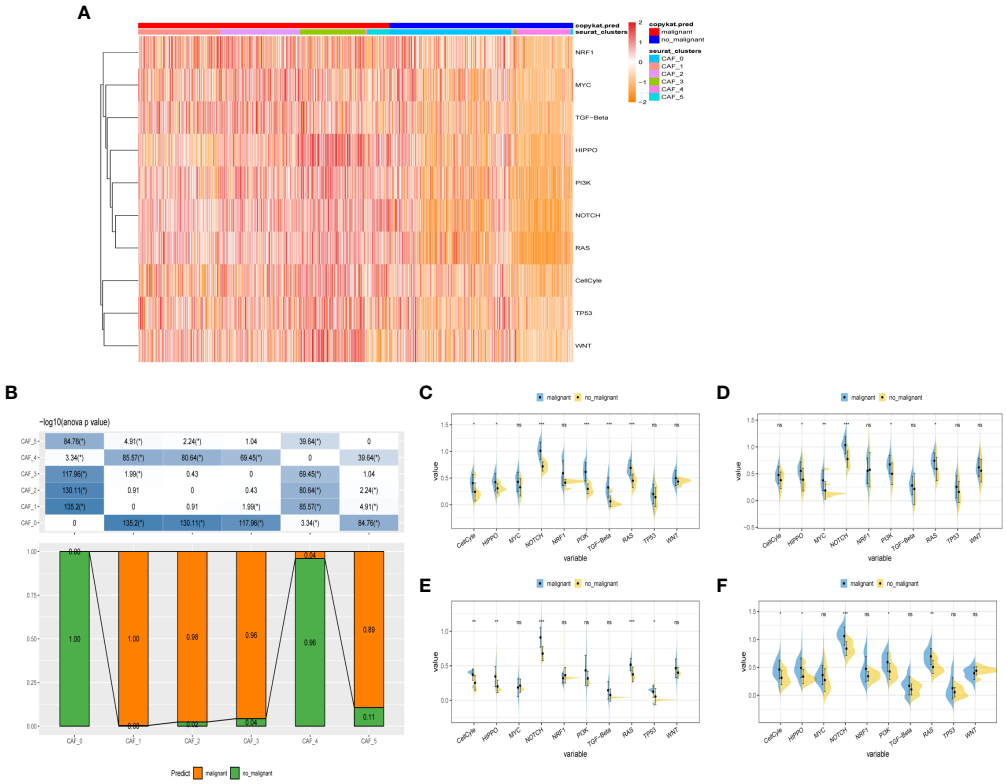

FIGURE 3
The characteristics of tumor-associated pathways in CAF clusters. **(A)** Heatmap of 10 tumor-associated pathways enriched in CAF cells. **(B)** Comparison between each cluster based on proportions of malignant and non-malignant cells. Comparison of each pathway between malignant and non-malignant cells based on GSVA score in CAF_0 (Figure S2A), CAF_1 (Figure S2B), CAF_2 **(C)**, CAF_3 **(D)**, CAF_4 **(E)**, CAF_4 **(F)**. (Wilcox. Test, *P < 0.05; **P < 0.01; ***P < 0.001; ns, not significant.).

significant independent prognostic factor for ESCC, with a p-value of less than 0.001 (Figures 5A, B). We have developed a new nomogram that incorporates T-stage, N-stage, and the risk score (shown in Figure 5C). Through calibration plot analysis, this nomogram was found to have strong predictive power for actual survival outcomes (Figure 5D). The TimeROC analysis in the TCGA cohort has confirmed that the area under the curve (AUC) of both the nomogram and risk score outperformed other indicators (Figure 5E).

3.5 Pathway enrichment analysis

To explore the fundamental functions those DEGs play in initiation and progression of ESCC, Kyoto Encyclopedia of Genes and Genomes (KEGG) and Gene Ontology (GO) analysis were conducted. As shown in Figures 6A–E, the up-regulated genes were most enriched in base excision repair, cell cycle, and DNA replication, while the down-regulated genes were significantly correlated with arachidonic acid metabolism, calcium signaling pathway, and histidine metabolism. Likewise, the results of GO analysis were presented in Figures 6B-D. Furthermore, Gene Set Enrichment Analysis was conducted based on the nine genes involved in the risk signature. The results illustrated that 7 pathways were remarkably associated with these nine genes (Figures 6F, G). Interestingly, olfactory transduction was positively correlated with the genes except for EXPH5, MAGEC3, and SLC4A9, which were identified to have protective values in ESCC, indicating that olfactory transduction might suppress the immigration and progression of ESCC.

3.6 Immune infiltrations landscape and relationship between risk genes and immunity

After conducting an investigation into the landscape of immune and stromal cell infiltrations in both low- and high-risk groups, Figure 7A demonstrated that patients in the high-risk group exhibit higher proportions of immune and stromal cell infiltrations when compared to those in the low-risk group. Besides, the immune cells proportions between the low-and-high-risk groups were estimated using the CIBERSORT algorithm. It was found that the high-risk group had higher proportions of resting memory CD4 T cells, Macrophages (M2), and resting mast cells, while naive B cells were more enriched in low-risk group (Figure 7B). Figure 7C exhibited the results of immune-related functions differences between high-and-low-risk groups.

Additionally, the relationship between risk genes and immunity was probed into. On the one hand, Figures 7D–H demonstrated

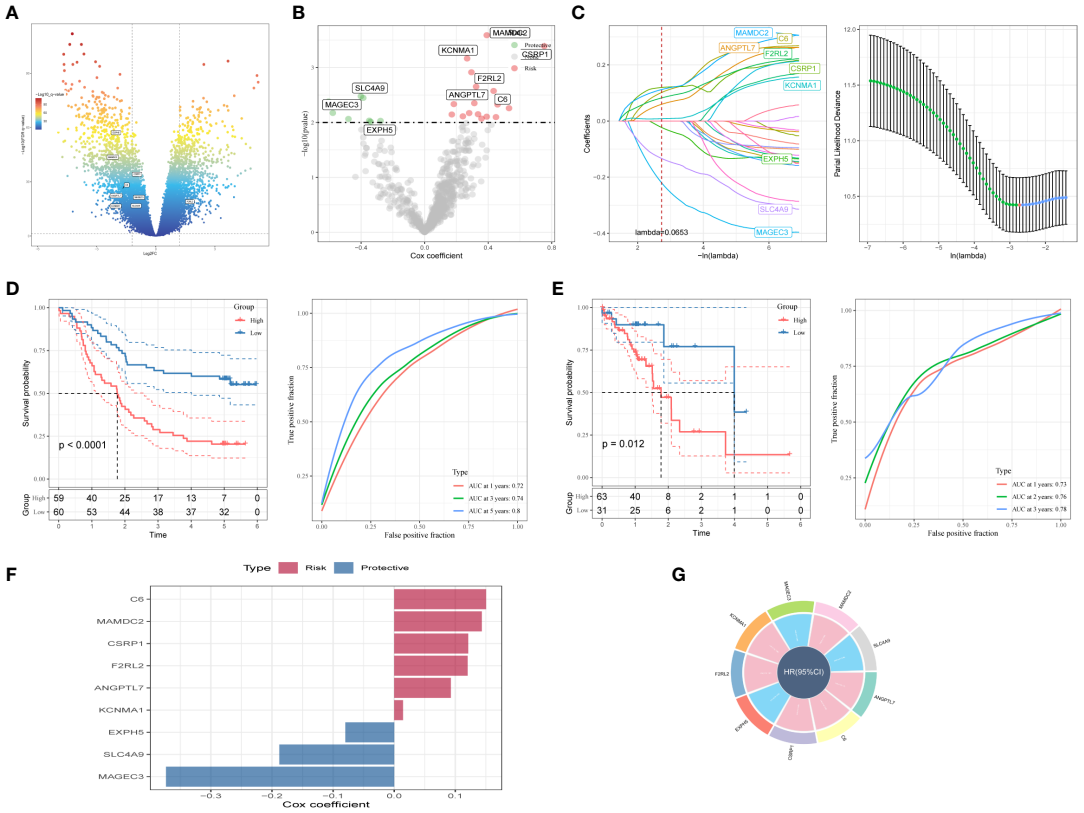

FIGURE 4
A novel risk signature constructed based on several CAF-related genes. **(A)** Volcano plot of differentially expressed genes between tumor and normal samples in GSE53624 cohort. **(B)** Volcano plot of prognosis-correlated genes obtained by univariate Cox regression analysis. **(C)** Each independent variable's trajectory and distributions for the lambda. **(D)** K-M and ROC curves of the risk signature in GSE53624 cohort. **(E)** K-M and ROC curves of the risk signature in TCGA cohort. **(F)** The multivariate Cox coefficients for each gene in the risk signature. **(G)** Circle plot showing the multivariate Cox multivariate Cox.

that the protective genes (including EXPH5, MAGEC3, and SLC4A9) were found negatively correlated with stromal score, immune score, and estimate score. On the other hand, the risk genes (including PR1, F2RL2, KCNMA1, and MAMDC2) were identified positively correlated with divergent immune cells (Figures 7F, I). Finally, the reciprocal communication between the 75 immune-related genes and the nine model genes were displayed in Figure 7G.

3.7 Response prediction of risk signature to immunotherapy

Under the circumstances that T-cell immunotherapy has gained great achievements in recent years, we performed the assessment of prognostic value of our signature for immune-checkpoint therapy in GSE78220 and IMvigor210 cohorts. Divergent degrees of responsiveness of anti-PD-L1 receptor blockers were identified in the 348 patients from the IMvigor210 cohort, including partial response (PR), complete response (CR), progressive disease (PD), and stable disease (SD). As depicted in Figures 8A-C, patients in the high-risk group accounted for more proportions in PD/SD, and had worse prognosis than those in the low-risk group. Besides, SD/PD patients tended to gain higher risk scores than CR/PR patients. However, significant survival differences were identified neither in Stage I+II nor in Stage III+IV patients between the different risk subgroups (Figures 8D, E). To validate our findings, the GSE78220 cohort was enrolled for further analysis. Corresponding with the results from IMvigor210, patients who achieved partial or complete response had lower risk scores and were less likely to be in the high-risk group (Figures 8F-H).

3.8 Consensus clustering and immune infiltrations

Moreover, unsupervised consensus clustering was conducted to explore molecular subtypes based on the expression of CAF-related genes comprising the risk signature. With k = 3 deemed as the optimal clustering stability, patients in GSE53624 cohort were grouped into three clusters (Figure 9A). The ridge plot exhibited the distribution of various clusters (Figure 9B). Besides, as presented in Sankey diagram (Figure 9D), Cluster 1(C1) and Cluster 3(C3) made up the low-risk group while the high-risk group was

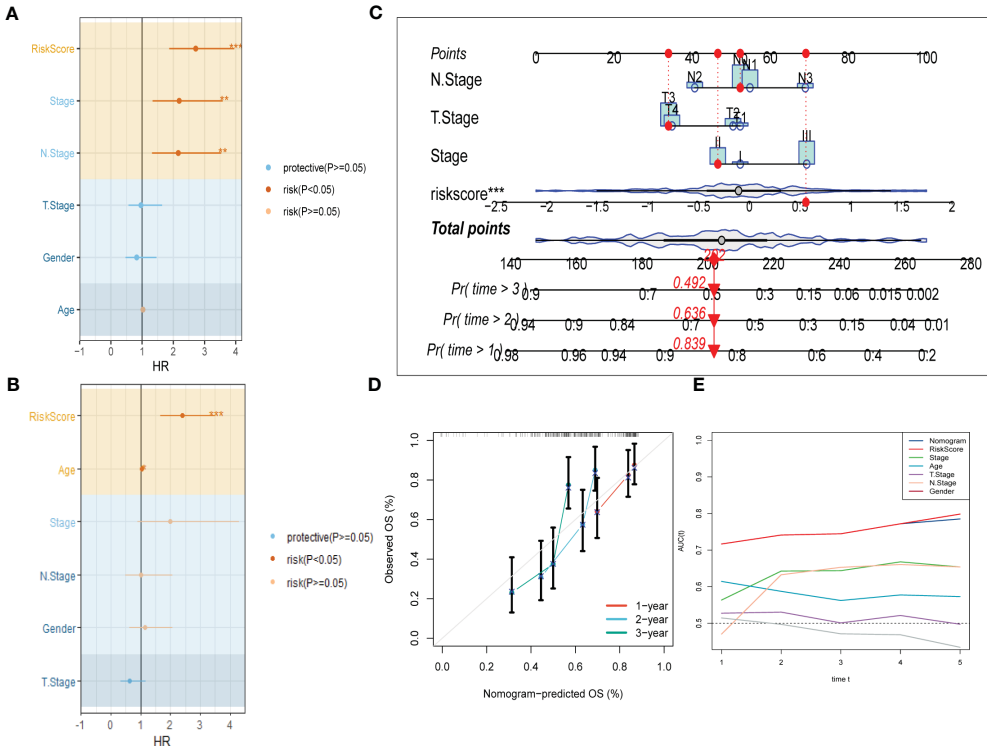

FIGURE 5
Development of a novel nomogram integrating the risk signature and several clinicopathologic features. **(A)** Results of univariate Cox regression analysis based on risk score and clinicopathologic features. **(B)** Results of multivariate Cox regression analysis based on risk score and clinicopathologic features. **(C)** Construction of the nomogram integrating the T,N-stage clinical stage and risk score. **(D)** Calibration curves for 1, 2, and 3 years of nomogram. **(E)** Evaluation of predictive capacity of nomogram and clinicopathologic features by time-ROC analysis. (*P < 0.05; **P < 0.01; ***P < 0.001).

comprised of Cluster 2 (C2) and Cluster 3 (C3). Subsequent survival analysis illustrated those patients in the C1 group had the most favorable prognosis, while patients in the C3 group had the worst clinical outcomes (Figure 9C). The immune landscape based on different clusters were shown in heatmap (Figure 9E), which indicated that C2 cluster beard the highest immune cell infiltrations. The TME scores of varying clusters were then calculated, revealing that C2 cluster had the highest immune, stromal, and estimate score as well as lower tumor purity than the other clusters. (Figures 9F-I). After applying the immune checkpoints inhibitors analysis, it was identified that C2 cluster was significantly correlated with BTLA, CTLA4, CD48, and so on, suggesting that patients involved in the C2 group might benefit from immunotherapy, especially anti-PD-1 receptor blockers.

3.9 Drugs sensitivity

After comparing the efficacy of various chemotherapeutic agents across different clusters, we discovered that patients belonging to cluster 2 (C2) exhibited elevated IC50 values for chemotherapeutic medications such as Bosutinib, Gefitinib, and AICAR. Additionally, patients in cluster 1 (C1) were observed to be more receptive to AMG.706, IPA.3, and the like, while those in cluster 3 (C3) demonstrated poorer response rates to the majority of chemotherapeutic treatments (Figure 10).

3.10 The experiment of genes involved in the risk signature

To explore potential ESCC cancer risk-related genes, four genes involved in the risk signature were selected for further validation in ESCC patients. As demonstrated in Figure 11, F2RL2 exhibited elevated expression levels in tumors, whereas SLC4A9, EXPH5, and MAGEC3 exhibited significantly reduced expression levels in tumors. These distinctions align with our bioinformatic findings, suggesting that these genes may serve as innovative biomarkers for early ESCC diagnosis.

4 Discussion

The tumor microenvironment, as well known, encompasses the non-cancerous cells and components that are found within a tumor, along with the molecules that they produce and release (32).The continuous interactions between tumor cells and the tumor microenvironment are crucial in determining the tumor's

10.3389/fimmu.2023.1199040

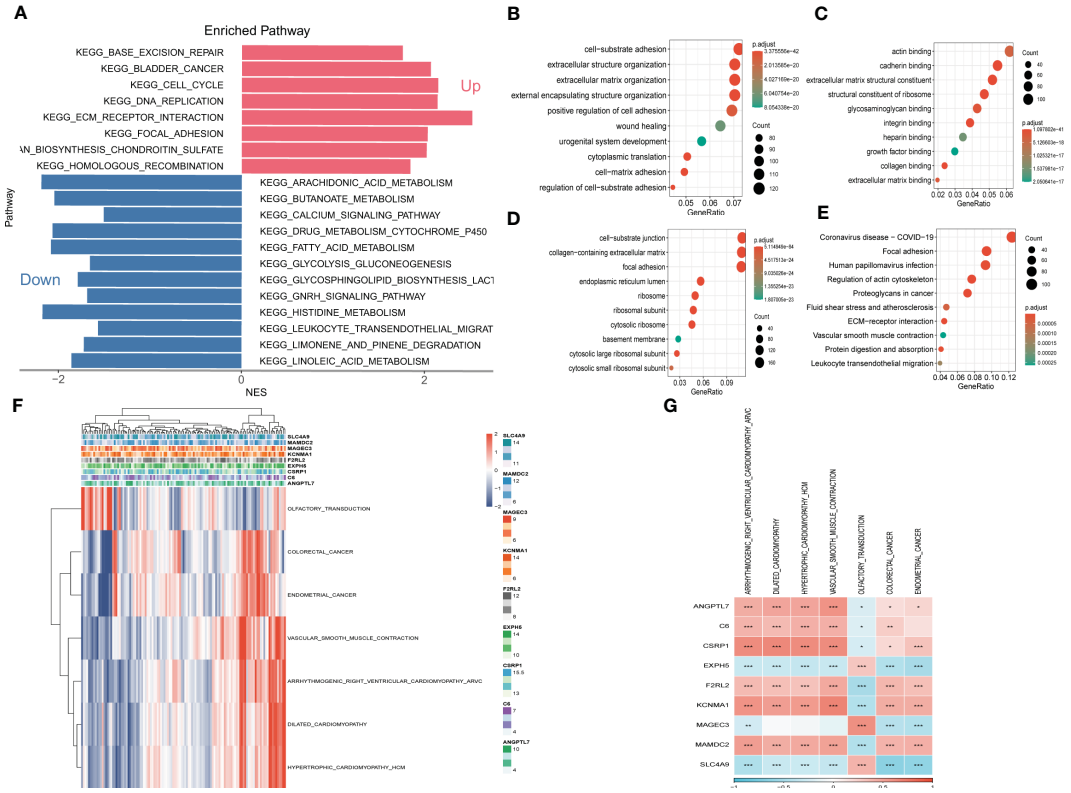

FIGURE 6
Gene Set Enrichment Analysis (GSEA) **(A)** Gene Set Enrichment Analysis of up-regulated and down-regulated genes **(B)** GO-BP analysis **(C)** GO-CC analysis **(D)** GO-MF **(E)** KEGG analysis **(F)** Heatmap exhibiting enrichment score for key pathways based on the hub genes. **(G)** Gene-pathway correlation heatmap.

initiation, progression, metastasis, and response to therapies (33). Numerous studies have provided compelling evidence to support the idea that there is a dynamic crosstalk between tumor cells and stromal cells, which plays a critical role in tumor progression (34). By understanding the mechanism of this interaction, there is an opportunity to develop enhanced therapeutics that target multiple components of the TME simultaneously, ultimately increasing the likelihood of favorable patient outcomes (35). Considering that cancer-associated fibroblasts (CAFs) have been identified linked with tumor initiation and progression (36), a comprehensive exploration on characterization and classification of CAFs of ESCC via scRNA-seq data was performed. Six distinctive CAF clusters were identified, which might exert enormous influence on divergent biological regulation of the TME. Accumulating evidence has confirmed that CAF-related gene signature has great prognostic value in ESCC (37, 38). Correspondingly, three clusters in our data were found significantly associated with ESCC prognosis. After analyzing the tumor-related pathways based on the CAF clusters, HIPPO, NOTCH, and RAS were identified significantly enriched in malignant parts in CAF_2, CAF_3, CAF_4, and CAF_5 clusters. It has been revealed that HIPPO and RAS signaling pathways can impel the tumor proliferation and immigration in ESCC (39, 40). A recent study has illuminated that via Notch signaling pathway METTL3-mediated m6A mRNA modification can propel esophageal cancer initiation and progression (41). Besides, it has been discovered that a depletion of PARK2 promotes the progression of esophageal squamous cell carcinoma (ESCC) via the Hippo/YAP axis, whereas overexpression of PARK2 suppresses tumor progression of ESCC through the Hippo signaling pathway. Consequently, as a newfound regulator of Hippo signaling, the manipulation of PARK2 activity or gene expression levels may prove to be a promising strategy for treating esophageal cancer (39). According to the genes included in the CAF clusters which were identified significantly correlated with ESCC prognosis, a novel risk signature based in CAFs were established. Our model comprised of 6 risk genes (C6, MAMDC2, CSRP1, F2RL2, ANGPTL7, and KCNMA1), and 3 protective genes (EXPH5, SLC4A9, and MAGEC3). It has been revealed that ANGPTL7 had an excellent performance as a surrogate marker of microvascular invasion on hepatocellular carcinoma (42). Besides, several genes (including MAMDC2, F2RL2, and KCNMA1) were enrolled as biomarker for the prognosis of varying cancers (43–45). It has been confirmed that MAGEC3 can stimulate cancer metastasis via intriguing epithelial-mesenchymal and immunosuppression in ESCC (46). The GSEA analysis was then applied, demonstrating that protective genes were enriched in olfactory transduction, while risk genes were remarkably associated with other pathways, such as vascular smooth muscle contraction, dilated cardiomyopathy, colorectal cancer and so on. Interestingly, PLK1 has been confirmed suitable for cancer therapy due to its function in regulating contraction of

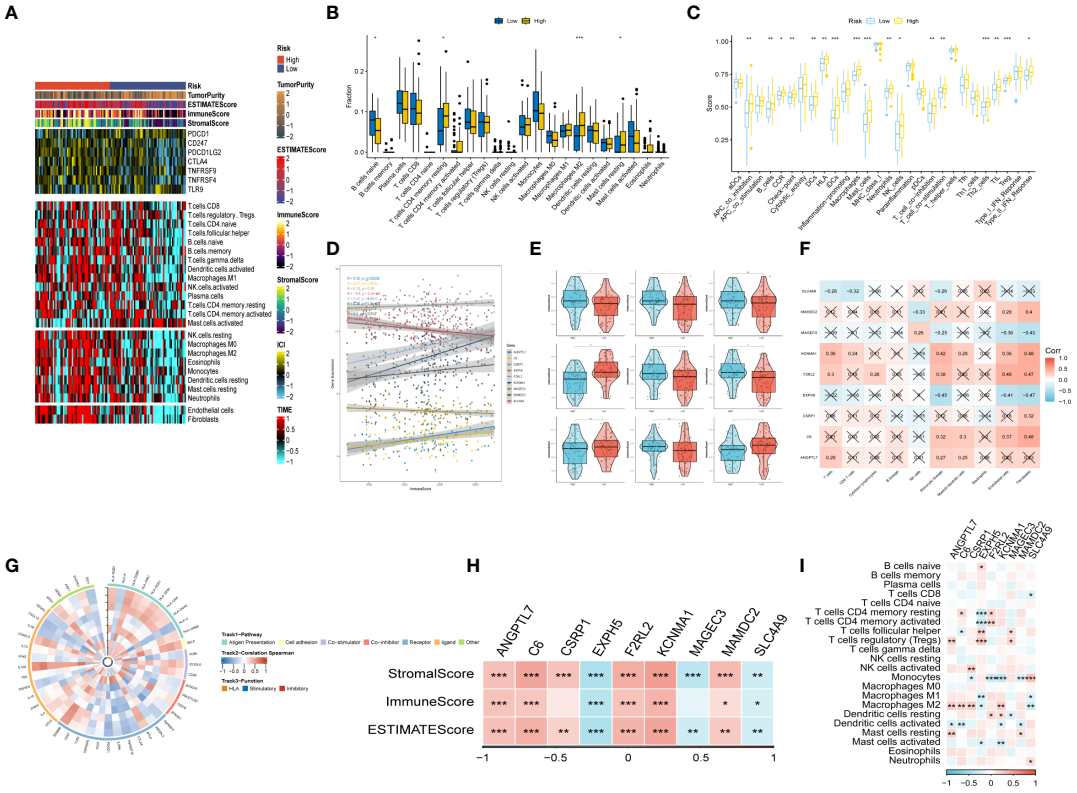

FIGURE 7
The immune infiltrations analysis **(A)** Heatmap of results on immune cells of tumor microenvironment (TME) in ESCC with multialgorithm, including existing data from platform TIMER and MCP-counter. TME-related scores were exhibited in the top bar. **(B)** Comparison of proportions of 22 immune-related cells between high-and-low-risk groups. **(C)** Comparison of proportions of immune-related functions between high-and-low-risk groups. **(D, E)** Correlations between the nine hub genes and immune score. **(F, I)** Correlations between nine hub genes and 22 immune-related cells. **(G)** The correlation analysis between nine hub genes and 75 immune-associated genes. **(H)** Correlations between the four nine genes and immune score, stromal score, estimate score. (*p < 0.05, **p < 0.01, ***p < 0.001).

postmitotic smooth muscle cells (47). Moreover, F2RL2 was identified significantly correlated with initiation and progression of colorectal cancer (48). Several researches suggested that high burden of doxorubicin can threaten cancer patients' health owing to dilated cardiomyopathy (49). Furthermore, the novel signature was confirmed to have excellent prognostic value in ESCC after applying TCGA ESCC cohort for external validation. After categorizing the patients into high- and low-risk groups based on the median risk score, the subsequent analysis revealed that the low-risk group had a significantly better prognosis than the high-risk group. Additionally, both univariate and multivariate Cox regression analyses verified that the risk score was an independent predictor of overall survival (OS). A nomogram was constructed based on the risk signature, which displayed a high degree of consistency between the predicted and observed results for the OS of ESCC patients. Consequently, the study's findings illustrated that the risk signature created was a dependable tool for accurately predicting the prognosis of ESCC patients. With the risk signature, earlier diagnosis and therapy can be received in ESCC patients. The identified CAF-related gene signature provides a potential prognostic tool for predicting patient outcomes and may help guide treatment decisions for ESCC patients. The signature has the potential to improve patient stratification and identify those who may benefit from more aggressive treatment strategies or targeted therapies. In addition, the identification of the specific genes in the CAF signature provides potential targets for therapeutic intervention, such as drugs that target the overexpressed risk genes or enhance the expression of the protective genes.

The vigorous development of cancer immunotherapy has shed a novel light on the cancer treatment, which extremely depended on the comprehensive perception of immune landscape in tumor microenvironment (50). The tumor microenvironment is a complex ecosystem comprised of diverse cell types that significantly impact cancer biology and the effectiveness of therapeutic interventions (51). Considering that such a bunch of ESCC patients still suffer from the unfavorable prognosis in spite of receiving immunotherapy ascribing to immune escape or immune tolerance (52), we explored the immune landscape of ESCC based on the CAF-related risk signature. It was found that the high-risk group had a higher proportion of immune cells infiltration. Nevertheless, macrophages (M2) were identified significantly enriched in high-risk group in the subsequent analysis, which has been confirmed to incite immune tolerance in cancer immunotherapy (53). Taken above results into consideration, we infer that patients in low-risk group are more

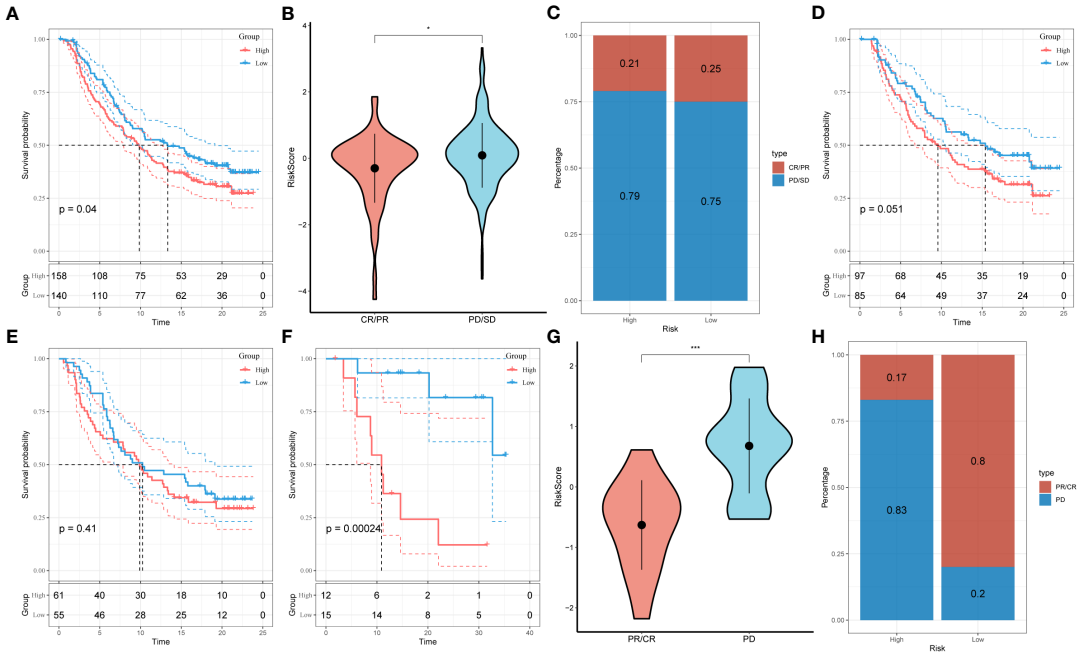

FIGURE 8
Prediction of responsiveness to immunotherapy using our signature based on public database. **(A)** Prognostic differences between risk subgroups in the IMvigor210 cohort. **(B)** Differences among immunotherapy responses based on risk scores in the IMvigor210 cohort. **(C)** Distribution of immunotherapy responses based on risk subgroups in the IMvigor210 cohort. **(D)** Prognostic differences between risk subgroups based on early stage (stage I-II) in the IMvigor210 cohort. **(E)** Prognostic differences between risk subgroups based on advanced patients (stage III-IV) in the IMvigor210 cohort. **(F)** Prognostic differences between risk subgroups in the GSE78220 cohort. **(G)** Differences among immunotherapy responses based on risk scores in the GSE78220 cohort. **(H)** Distribution of immunotherapy responses based on risk subgroups in the GSE78220 cohort.

likely to benefit from immunotherapy. The relationship between immune infiltration and genes composing the risk signature were further analyzed. Risk genes were positively correlated with immune score while protective genes were negatively associated with immune score. In addition, to probe into the response to anti-cancer immunotherapy, IMvigor210 and GSE78220 cohorts were enrolled for analysis. Within the two cohorts, patients belonging to low-risk group account for higher proportions of partial response (PR) and complete response (CR) after immunotherapy of anti-PD-L1 receptor blockers. Consistent with above results, patients in low-risk group benefit more from immunotherapy than those in high-risk group. However, immunotherapy in ESCC is far from anti-PD-1 or anti-PD-L1, further researches are urgently needed to provide precise and comprehensive management for patients diagnosed with ESCC.

An overarching conclusion that esophageal squamous cancer is highly heterogeneous has been well received. Uncovering the heterogeneity of ESCC could revolutionized the management of this malignant cancer and provide patients with more favorable prognosis (51). Thus, we preformed consensus clustering in GSE53624 cohort based on the risk signature. Cluster 2(C2) was found made up by the high-risk group and with the worst prognosis. Besides, C2 had the highest immune score, stromal score, and estimate score and was identified significantly correlated with several immune checkpoints (including BTLA, CD48, CD44, CTLA4, CD28, IDO2, and so on), revealing that patients in Cluster 2 might be suitable for immunotherapy of immune checkpoints inhibitors. Last but not the least, various CAF-associated genes implicated in the risk signature were subsequently subjected to validation using ESCC tissues. In line with our bioinformatic findings, F2RL2 was determined to be highly expressed in tumors; conversely, SLC4A9, EXPH5, and MAGEC3 were observed to be significantly under-expressed in tumors. It has been revealed that F2RL2 can promote the tumorigenesis and immigration of breast cancer (44), indicating that these genes may serve as innovative biomarkers for early ESCC diagnosis. Although our study provides valuable insights, there are some limitations that require attention. Firstly, our risk signature was established based on retrospective data obtained from public databases. Thus, more prospective and multi-center cohorts of ESCC are necessary to mitigate any potential bias. Secondly, our risk signature only predicts the responsiveness to anti-PD-L1 immunotherapy, further research is urgently needed to assess its potential for predicting the response to other precision therapies in the future.

5 Conclusion

In our study, we conducted an extensive investigation into the populations of CAFs in ESCC and identified six distinct CAF clusters. Three of these clusters were significantly associated with ESCC prognosis and were used to establish a prognostic risk

10.3389/fimmu.2023.1199040

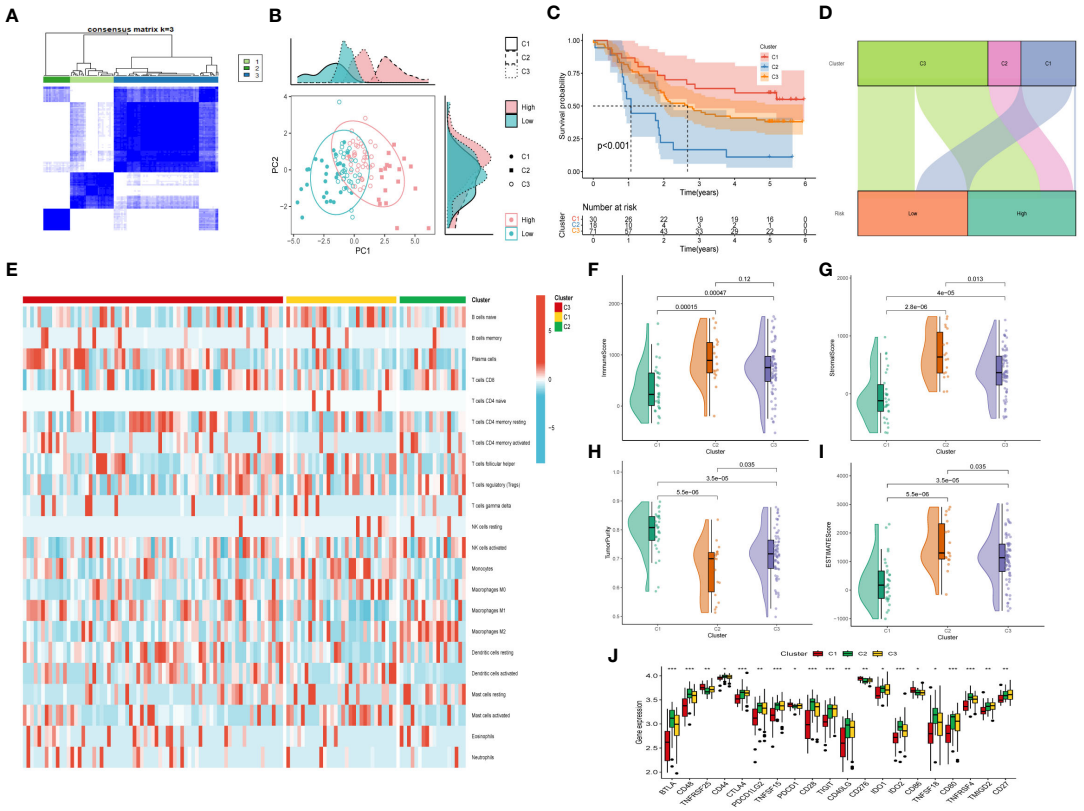

FIGURE 9
Consensus Clustering based on nine prognostic CAF-related genes expression. **(A)** ESCC patients were divided into three clusters (k=3). **(B)** PCA depicted the distribution for clusters. **(C)** Survival analysis based on the three clusters. **(D)** The Sankey diagram of the connection between clusters and high-and low-risk group. **(E)** Immune infiltrations based on three clusters. **(F)** ImmuneScore difference between three clusters. **(G)** SromalScore difference between three clusters. **(H)** TumorPurity difference between three clusters. **(I)** ESTIMATEScore difference between three clusters. **(J)** Expression difference of immune checkpoints between three clusters. (*p < 0.05, ***p < 0.001).

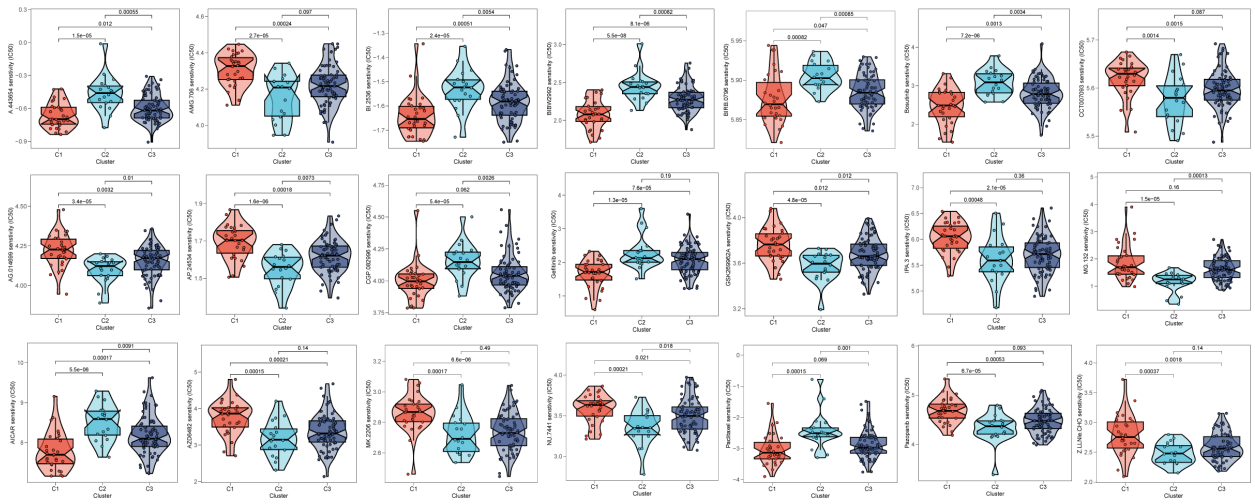

FIGURE 10
Prediction of chemotherapy drug sensitivity in ESCC patients based on different clusters. The experiment of ESCC risk-related genes. (*p < 0.05, **p < 0.01, ***p < 0.001).

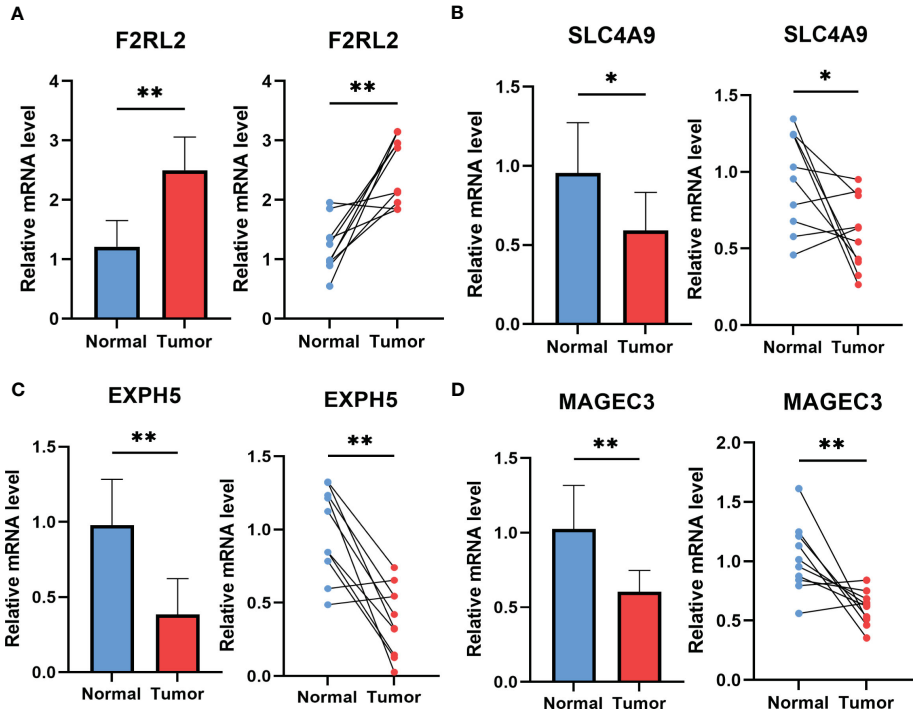

FIGURE 11
The expression of F2RL2 **(A)**, SLC4A9 **(B)**, EXPH5 **(C)** and MAGEC3 **(D)** in normal esophageal tissue and ESCC tissue of patients. t-test was used to compare the expression of genes between normal and tumor. *p < 0.05, **p < 0.01, ***p < 0.001.

signature consisting of nine genes based on the CAFs. Moreover, we developed a novel nomogram that combined the risk signature with clinicopathological characteristics, which exhibited excellent performance in predicting the clinical outcomes of patients with ESCC. We also observed that our risk signature was associated with tumor mutations and immune landscape, and that it is suitable for predicting the responsiveness of ESCC patients to immunotherapy targeting PD-L1 blockade.

Data availability statement

The datasets presented in this study can be found in online repositories. The names of the repository/repositories and accession number(s) can be found within the article/Supplementary Materials.

Ethics statement

All human experiments in this study have been approved by the Ethics Committee of the First Affiliated Hospital of Nanjing Medical University. All subjects gave their informed consent for inclusion before they participated in the study. The study was conducted in accordance with the Declaration of Helsinki, and approved by the Ethics Committee of the First Affiliated Hospital of Nanjing Medical University (protocol code No.2019-SRFA-005; 27 February 2019).

Author contributions

QR, PZ, HL and YY contributed conception and design of the study. XZ finished the dada collection. XZ and YF performed the statistical analysis. QR wrote the first draft of the manuscript. HL and YY revised the manuscript. LL, HL and YY gave the final approval of the version to be submitted. All authors contributed to the article and approved the submitted version.

Funding

This work was supported in part by the National Natural Science Foundation of China (81902453).

Acknowledgments

We are very grateful for data provided by databases such as TCGA, GEO. Thanks to reviewers and editors for their sincere comments.

Conflict of interest

The authors declare that the research was conducted in the absence of any commercial or financial relationships that could be construed as a potential conflict of interest.

Publisher's note

All claims expressed in this article are solely those of the authors and do not necessarily represent those of their affiliated organizations, or those of the publisher, the editors and the reviewers. Any product that may be evaluated in this article, or claim that may be made by its manufacturer, is not guaranteed or endorsed by the publisher.

Supplementary material

The Supplementary Material for this article can be found online at: https://www.frontiersin.org/articles/10.3389/fimmu.2023.1199040/full#supplementary-material

References

1. Wang Y, Cheng J, Xie D, Ding X, Hou H, Chen X, et al. NS1-binding protein radiosensitizes esophageal squamous cell carcinoma by transcriptionally suppressing c-myc. *Cancer Commun (Lond)* (2018) 38:33. doi: 10.1186/s40880-018-0307-y

2. de Gouw D, Klarenbeek BR, Driessen M, Bouwense SAW, van Workum F, Futterer JJ, et al. Detecting pathological complete response in esophageal cancer after neoadjuvant therapy based on imaging techniques: a diagnostic systematic review and meta-analysis. *J Thorac Oncol* (2019) 14:1156–71. doi: 10.1016/j.jtho.2019.04.004

3. Rogers JE, Sewastjanow-Silva M, Waters RE, Ajani JA. Esophageal cancer: emerging therapeutics. *Expert Opin Ther Targets* (2022) 26:107–17. doi: 10.1080/14728222.2022.2036718

4. Cui Y, Chen H, Xi R, Cui H, Zhao Y, Xu E, et al. Whole-genome sequencing of 508 patients identifies key molecular features associated with poor prognosis in esophageal squamous cell carcinoma. *Cell Res* (2020) 30:902–13. doi: 10.1038/s41422-020-0333-6

5. He S, Xu J, Liu X, Zhen Y. Advances and challenges in the treatment of esophageal cancer. *Acta Pharm Sin B* (2021) 11:3379–92. doi: 10.1016/j.apsb.2021.03.008

6. Martinez-Reyes I, Chandel NS. Cancer metabolism: looking forward. *Nat Rev Cancer* (2021) 21:669–80. doi: 10.1038/s41568-021-00378-6

7. Hanahan D, Weinberg RA. Hallmarks of cancer: the next generation. *Cell* (2011) 144:646–74. doi: 10.1016/j.cell.2011.02.013

8. Willumsen N, Thomsen LB, Bager CL, Jensen C, Karsdal MA. Quantification of altered tissue turnover in a liquid biopsy: a proposed precision medicine tool to assess chronic inflammation and desmoplasia associated with a pro-cancerous niche and response to immuno-therapeutic anti-tumor modalities. *Cancer Immunol Immunother* (2018) 67:1–12. doi: 10.1007/s00262-017-2074-z

9. Chen X, Song E. Turning foes to friends: targeting cancer-associated fibroblasts. *Nat Rev Drug Discovery* (2019) 18:99–115. doi: 10.1038/s41573-018-0004-1

10. Mao X, Xu J, Wang W, Liang C, Hua J, Liu J, et al. Crosstalk between cancer-associated fibroblasts and immune cells in the tumor microenvironment: new findings and future perspectives. *Mol Cancer* (2021) 20:131. doi: 10.1186/s12943-021-01428-1

11. Xu M, Zhang T, Xia R, Wei Y, Wei X. Targeting the tumor stroma for cancer therapy. *Mol Cancer* (2022) 21:208. doi: 10.1186/s12943-022-01670-1

12. Musa M. Single-cell analysis on stromal fibroblasts in the microenvironment of solid tumours. *Adv Med Sci* (2020) 65:163–9. doi: 10.1016/j.advms.2019.12.001

13. Qiu L, Yue J, Ding L, Yin Z, Zhang K, Zhang H. Cancer-associated fibroblasts: an emerging target against esophageal squamous cell carcinoma. *Cancer Lett* (2022) 546:215860. doi: 10.1016/j.canlet.2022.215860

14. Herrera M, Berral-Gonzalez A, Lopez-Cade I, Galindo-Pumarino C, Bueno-Fortes S, Martin-Merino M, et al. Cancer-associated fibroblast-derived gene signatures determine prognosis in colon cancer patients. *Mol Cancer* (2021) 20:73. doi: 10.1186/s12943-021-01367-x

15. Huang TX, Tan XY, Huang HS, Li YT, Liu BL, Liu KS, et al. Targeting cancer-associated fibroblast-secreted WNT2 restores dendritic cell-mediated antitumour immunity. *Gut* (2022) 71:333–44. doi: 10.1136/gutjnl-2020-322924

16. Bagaev A, Kotlov N, Nomie K, Svekolkin V, Gafurov A, Isaeva O, et al. Conserved pan-cancer microenvironment subtypes predict response to immunotherapy. *Cancer Cell* (2021) 39:845–865 e7. doi: 10.1016/j.ccell.2021.04.014

17. Grun D, van Oudenaarden A. Design and analysis of single-cell sequencing experiments. *Cell* (2015) 163:799–810. doi: 10.1016/j.cell.2015.10.039

18. Lei Y, Tang R, Xu J, Wang W, Zhang B, Liu J, et al. Applications of single-cell sequencing in cancer research: progress and perspectives. *J Hematol Oncol* (2021) 14:91. doi: 10.1186/s13045-021-01105-2

19. Hedlund E, Deng Q. Single-cell RNA sequencing: technical advancements and biological applications. *Mol Aspects Med* (2018) 59:36–46. doi: 10.1016/j.mam.2017.07.003

20. Zhang L, Li Z, Skrzypczynska KM, Fang Q, Zhang W, O'Brien SA, et al. Single-cell analyses inform mechanisms of myeloid-targeted therapies in colon cancer. *Cell* (2020) 181:442–459 e29. doi: 10.1016/j.cell.2020.03.048

21. Liu SQ, Gao ZJ, Wu J, Zheng HM, Li B, Sun S, et al. Single-cell and spatially resolved analysis uncovers cell heterogeneity of breast cancer. *J Hematol Oncol* (2022) 15:19. doi: 10.1186/s13045-022-01236-0

22. Zhang P, Pei S, Liu J, Zhang X, Feng Y, Gong Z, et al. Cuproptosis-related lncRNA signatures: predicting prognosis and evaluating the tumor immune microenvironment in lung adenocarcinoma. *Front Oncol* (2022) 12:1088931. doi: 10.3389/fonc.2022.1088931

23. Chi H, Peng G, Yang J, Zhang J, Song G, Xie X, et al. Machine learning to construct sphingolipid metabolism genes signature to characterize the immune landscape and prognosis of patients with uveal melanoma. *Front Endocrinol (Lausanne)* (2022) 13:1056310. doi: 10.3389/fendo.2022.1056310

24. Zhang P, Pei S, Gong Z, Feng Y, Zhang X, Yang F, et al. By integrating single-cell RNA-seq and bulk RNA-seq in sphingolipid metabolism, CACYBP was identified as a potential therapeutic target in lung adenocarcinoma. *Front Immunol* (2023) 14:1115272. doi: 10.3389/fimmu.2023.1115272

25. Yuan Q, Ren J, Li L, Li S, Xiang K, Shang D, et al. Development and validation of a novel N6-methyladenosine (m6A)-related multi-long non-coding RNA(lncRNA) prognostic signature in pancreatic adenocarcinoma. *Bioengineered* (2021) 12:2432–48. doi: 10.1080/21655979.2021.1933868

26. Chi H, Peng G, Wang R, Yang F, Xie X, Zhang J, et al. Cuprotosis programmed-Cell-Death-Related lncRNA signature predicts prognosis and immune landscape in PAAD patients. *Cells 11* (2022). doi: 10.3390/cells11213436

27. Peng G, Chi H, Gao X, Zhang J, Song G, Xie X, et al. Identification and validation of neurotrophic factor-related genes signature in HNSCC to predict survival and immune landscapes. *Front Genet* (2022) 13:1010044. doi: 10.3389/fgene.2022.1010044

28. Pei S, Zhang P, Yang L, Kang Y, Chen H, Zhao S, et al. Exploring the role of sphingolipid-related genes in clinical outcomes of breast cancer. *Front Immunol* (2023) 14:1116839. doi: 10.3389/fimmu.2023.1116839

29. Yuan Q, Deng D, Pan C, Ren J, Wei T, Wu Z, et al. Integration of transcriptomics, proteomics, and metabolomics data to reveal HER2-associated metabolic heterogeneity in gastric cancer with response to immunotherapy and neoadjuvant chemotherapy. *Front Immunol* (2022) 13:951137. doi: 10.3389/fimmu.2022.951137

30. Pei S, Zhang P, Chen H, Zhao S, Dai Y, Yang L, et al. Integrating single-cell RNA-seq and bulk RNA-seq to construct prognostic signatures to explore the role of glutamine metabolism in breast cancer. *Front Endocrinol* (2023) 14:1135297. doi: 10.3389/fendo.2023.1135297

31. Zhang P, Pei S, Gong Z, Ren Q, Xie J, Liu H, et al. The integrated single-cell analysis developed a lactate metabolism-driven signature to improve outcomes and immunotherapy in lung adenocarcinoma. *Front Endocrinol (Lausanne)* (2023) 14:1154410. doi: 10.3389/fendo.2023.1154410

32. Joyce JA. Therapeutic targeting of the tumor microenvironment. *Cancer Cell* (2005) 7:513–20. doi: 10.1016/j.ccr.2005.05.024

33. Deepak KGK, Vempati R, Nagaraju GP, Dasari VR, S N, Rao DN, et al. Tumor microenvironment: challenges and opportunities in targeting metastasis of triple negative breast cancer. *Pharmacol Res* (2020) 153:104683. doi: 10.1016/j.phrs.2020.104683

34. Affo S, Yu LX, Schwabe RF. The role of cancer-associated fibroblasts and fibrosis in liver cancer. *Annu Rev Pathol* (2017) 12:153–86. doi: 10.1146/annurev-pathol-052016-100322

35. Hinshaw DC, Shevde LA. The tumor microenvironment innately modulates cancer progression. *Cancer Res* (2019) 79:4557–66. doi: 10.1158/0008-5472.CAN-18-3962

36. Biffi G, Tuveson DA. Diversity and biology of cancer-associated fibroblasts. *Physiol Rev* (2021) 101:147–76. doi: 10.1152/physrev.00048.2019

37. Wang W, Zhang J, Wang Y, Xu Y, Zhang S. Identifies microtubule-binding protein CSPP1 as a novel cancer biomarker associated with ferroptosis and tumor microenvironment. *Comput Struct Biotechnol J* (2022) 20:3322–35. doi: 10.1016/j.csbj.2022.06.046

38. Jin Y, Meng Q, Zhang B, Xie C, Chen X, Tian B, et al. Cancer-associated fibroblasts-derived exosomal miR-3656 promotes the development and progression of esophageal squamous cell carcinoma via the ACAP2/PI3K-AKT signaling pathway. *Int J Biol Sci* (2021) 17:3689–701. doi: 10.7150/ijbs.62571

39. Zhou X, Li Y, Wang W, Wang S, Hou J, Zhang A, et al. Regulation of Hippo/YAP signaling and esophageal squamous carcinoma progression by an E3 ubiquitin ligase PARK2. *Theranostics* (2020) 10:9443–57. doi: 10.7150/thno.46078

40. Wong GS, Zhou J, Liu JB, Wu Z, Xu X, Li T, et al. Targeting wild-type KRAS-amplified gastroesophageal cancer through combined MEK and SHP2 inhibition. *Nat Med* (2018) 24:968–77. doi: 10.1038/s41591-018-0022-x

41. Han H, Yang C, Zhang S, Cheng M, Guo S, Zhu Y, et al. METTL3-mediated m(6)A mRNA modification promotes esophageal cancer initiation and progression via notch signaling pathway. *Mol Ther Nucleic Acids* (2021) 26:333–46. doi: 10.1016/j.omtn.2021.07.007

42. Beaufrere A, Caruso S, Calderaro J, Pote N, Bijot JC, Couchy G, et al. Gene expression signature as a surrogate marker of microvascular invasion on routine hepatocellular carcinoma biopsies. *J Hepatol* (2022) 76:343–52. doi: 10.1016/j.jhep.2021.09.034

43. Zhang J, Ling X, Fang C, Ma J. Identification and validation of an eight-lncRNA signature that predicts prognosis in patients with esophageal squamous cell carcinoma. *Cell Mol Biol Lett* (2022) 27:39. doi: 10.1186/s11658-022-00331-x

44. Liu S, Song A, Wu Y, Yao S, Wang M, Niu T, et al. Analysis of genomics and immune infiltration patterns of epithelial-mesenchymal transition related to metastatic breast cancer to bone. *Transl Oncol* (2021) 14:100993. doi: 10.1016/j.tranon.2020.100993

45. Bloch M, Ousingsawat J, Simon R, Schraml P, Gasser TC, Mihatsch MJ, et al. KCNMA1 gene amplification promotes tumor cell proliferation in human prostate cancer. *Oncogene* (2007) 26:2525–34. doi: 10.1038/sj.onc.1210036

46. Wu Q, Zhang W, Wang Y, Min Q, Zhang H, Dong D, et al. MAGE-C3 promotes cancer metastasis by inducing epithelial-mesenchymal transition and immunosuppression in esophageal squamous cell carcinoma. *Cancer Commun (Lond)* (2021) 41:1354–72. doi: 10.1002/cac2.12203

47. de Carcer G, Wachowicz P, Martinez-Martinez S, Oller J, Mendez-Barbero N, Escobar B, et al. Plk1 regulates contraction of postmitotic smooth muscle cells and is required for vascular homeostasis. *Nat Med* (2017) 23:964–74. doi: 10.1038/nm.4364

48. Supiot S, Gouraud W, Campion L, Jezequel P, Buecher B, Charrier J, et al. Early dynamic transcriptomic changes during preoperative radiotherapy in patients with rectal cancer: a feasibility study. *World J Gastroenterol* (2013) 19:3249–54. doi: 10.3748/wjg.v19.i21.3249

49. Tomczyk MM, Cheung KG, Xiang B, Tamanna N, Fonseca Teixeira AL, Agarwal P, et al. Mitochondrial sirtuin-3 (SIRT3) prevents doxorubicin-induced dilated cardiomyopathy by modulating protein acetylation and oxidative stress. *Circ Heart Fail* (2022) 15:e008547. doi: 10.1161/CIRCHEARTFAILURE.121.008547

50. Zheng Y, Chen Z, Han Y, Han L, Zou X, Zhou B, et al. Immune suppressive landscape in the human esophageal squamous cell carcinoma microenvironment. *Nat Commun* (2020) 11:6268. doi: 10.1038/s41467-020-20019-0

51. Dinh HQ, Pan F, Wang G, Huang QF, Olingy CE, Wu ZY, et al. Integrated single-cell transcriptome analysis reveals heterogeneity of esophageal squamous cell carcinoma microenvironment. *Nat Commun* (2021) 12:7335. doi: 10.1038/s41467-021-27599-5

52. Yang H, Zhang Q, Xu M, Wang L, Chen X, Feng Y, et al. CCL2-CCR2 axis recruits tumor associated macrophages to induce immune evasion through PD-1 signaling in esophageal carcinogenesis. *Mol Cancer* (2020) 19:41. doi: 10.1186/s12943-020-01165-x

53. Li H, Xiao Y, Li Q, Yao J, Yuan X, Zhang Y, et al. The allergy mediator histamine confers resistance to immunotherapy in cancer patients via activation of the macrophage histamine receptor H1. *Cancer Cell* (2022) 40:36–52 e9. doi: 10.1016/j.ccell.2021.11.002

frontiers | Frontiers in Immunology

TYPE Review
PUBLISHED 16 June 2023
DOI 10.3389/fimmu.2023.1190883

OPEN ACCESS

EDITED BY
Ganesan Ramamoorthi,
Moffitt Cancer Center, United States

REVIEWED BY
Olga Gordeeva,
Russian Academy of Sciences, Russia
Erwin Goldberg,
Northwestern University, United States

*CORRESPONDENCE
Kangdong Liu
kdliu@zzu.edu.cn
Zhi Li
zlyylizhi0316@zzu.edu.cn

†These authors share last authorship

RECEIVED 21 March 2023
ACCEPTED 26 May 2023
PUBLISHED 16 June 2023

CITATION
Ai H, Yang H, Li L, Ma J, Liu K and Li Z (2023) Cancer/testis antigens: promising immunotherapy targets for digestive tract cancers.
Front. Immunol. 14:1190883.
doi: 10.3389/fimmu.2023.1190883

Cancer/testis antigens: promising immunotherapy targets for digestive tract cancers

Huihan Ai[1], Hang Yang[1], Liang Li[1], Jie Ma[1], Kangdong Liu[2,3,4*†] and Zhi Li[1*†]

[1]Department of General Surgery, The Affiliated Cancer Hospital of Zhengzhou University & Henan Cancer Hospital, Zhengzhou, Henan, China, [2]Department of Pathophysiology, School of Basic Medical Sciences, Zhengzhou University, Zhengzhou, Henan, China, [3]Department of Molecular and Cellular Biology, China-United States (US) Hormel (Henan) Cancer Institute, Zhengzhou, Henan, China, [4]Research Center of Basic Medicine, Academy of Medical Sciences, Zhengzhou University, Zhengzhou, Henan, China

Digestive tract cancers, including esophageal, gastric, and colorectal cancers, are the major cause of death among cancer patients worldwide due to the heterogeneity of cancer cells, which limits the effectiveness of traditional treatment methods. Immunotherapy represents a promising treatment strategy for improving the prognosis of patients with digestive tract cancers. However, the clinical application of this approach is limited by the absence of optimal targets. Cancer/testis antigens are characterized by low or absent expression in normal tissues, but high expression in tumor tissues, making them an attractive target for antitumor immunotherapy. Recent preclinical trials have shown promising results for cancer/testis antigen-targeted immunotherapy in digestive cancer. However, practical problems and difficulties in clinical application remain. This review presents a comprehensive analysis of cancer/testis antigens in digestive tract cancers, covering their expression, function, and potential as an immunotherapy target. Additionally, the current state of cancer/testis antigens in digestive tract cancer immunotherapy is discussed, and we predict that these antigens hold great promise as an avenue for breakthroughs in the treatment of digestive tract cancers.

KEYWORDS

cancer/testis antigens, digestive tract cancers, immunotherapy, target, esophagus cancer (adenocarcinoma), gastrointestinal carcinoma

1 Introduction

Cancers affecting the digestive tract, such as esophageal cancer, gastric cancer, and colorectal cancer (CRC), continue to be the primary cause of death among cancer patients worldwide (1). Due to application of endoscopic screening, the detection rate of early-stage

digestive tract cancers has increased. However, the mortality is still very high because of the heterogeneity of cancers and little improvement in the standard gold therapy suitable for tumors of the digestive tract. It is therefore essential to search for specific prognostic and predictive molecular signatures to guide targeted, individualized therapy. Immunotherapy, which aims to enhance the body's natural defenses to eliminate malignant cells, represents a monumental breakthrough in cancer treatment and has revolutionized the field of oncology (2). To develop effective immunotherapy treatments, it is crucial to first identify tumor antigens. Cancer/testis antigens (CTAs) are expressed in the testes and various types of cancer but have limited expression in normal adult somatic cells and tissues. These antigens can be recognized by cytolytic T lymphocytes (CTLs) (3, 4). Moreover, CTAs have been reported to be expressed in digestive tract tumors and exhibit specific biological functions. The upregulation of CTAs has been linked to several unfavorable outcomes commonly associated with cancer (5), including promotion of tumor cell stemness (6, 7), elevation of cancer cell tumorigenicity (8), enhancement of mobility (9) and metastasis (10), and conferment of drug resistance (11). These characteristics render CTAs ideal candidates as novel immunotherapeutic targets in digestive tract cancers. The aim of this review is to highlight the latest advances and hypotheses regarding the involvement of CTAs in the pathogenesis of digestive tract cancers and to investigate their potential as targets for cancer immunotherapy.

2 CTAs in the digestive tract cancers

2.1 Discovery and types of CTAs

Melanoma antigen-1 (MAGE-1, MAGE-A1, MA2-E), a member of the MAGE family, was the first CTA discovered by Alexander Knuth and Thierry Boon in 1991 (12). With a new method called serological identification of antigens by recombinant expression cloning (SEREX) (13), many more CTAs were uncovered, such as synovial sarcoma, X breakpoint 2 (HOM-MEL-40/SSX2) (13), New York's esophageal squamous cell carcinoma 1 (CTAG1B, NY-ESO-1) (14, 15), synaptonemal complex protein 1 (SCP1) (16), and CT7 (17). Although the first CTAs was discovered in 1991, the name was defined in 1998 (17). To facilitate the organization of the expanding collection of CTAs, the Cancer-Testis database (CTdatabase, http://www.cta.lncc.br/) was established as a user-friendly interface. Over 730 CTAs belonging to over 100 gene families have been identified in many cancer tissues, where their expression is significantly elevated compared with normal tissues and predominantly restricted to germ cells and trophoblasts. Although not all of them have been demonstrated to induce immune responses, they are collectively referred to as CTAs (18).

Cancer/testis (CT) genes are typically expressed in germ line cells, trophoblasts, and certain cancer cells. CT genes are classified into three groups based on their expression profiles: testis-restricted, testis/brain-restricted, and testis-selective. The majority of CTAs are encoded by CT genes (19). However, due to the lack of a clear and universally applicable definition for CT genes, Oliver Hofmann used multiple *in silico* gene expression analysis technologies to investigate the expression patterns of a set of 153 CTAs in normal and cancer tissues. The CTA genes are further classified into two categories: CT-X and non-X CT genes. CT-X family members are subject to more stringent transcriptional regulation in somatic tissues, making them more suitable for immunotherapy applications (20). The CTdatabase has identified a total of 276 CTA genes, of which 127 (46%) are located on the X chromosome, whereas the remaining are distributed across the autosomes and Y chromosome.

2.2 Expression of CTAs in the digestive tract cancers

Many CTAs were expressed in the human digestive tract cancers. However, the expression profile was diverse in the different digestive tract cancer tissues and cell lines (Figure 1 and Table 1).

2.2.1 Esophagus cancer

In 1995, Masaki Mori found that MAGE-1, -2, -3 were expressed in 26, 18, and 24 of 42 surgical esophageal cancer tissues and 5, 4, and 4 of 12 human esophageal cancer cell lines, respectively. At least one of the them were expressed in 33 of 42 esophageal tumor tissues, and all of them expressed in 12 of 42 esophageal tumor tissues. However, none of them were expressed in the 42 normal esophageal tissues (21). Apart from that, MAGE-A was detected in 38 of 98 (22) and 111 of 213 (23) esophageal cancer patients.

The MAGE gene family consists of several subfamilies, one of which is the MAGE-A subfamily that includes MAGE-A1 to -A12 (24). In esophageal cancer, several members of the MAGE-A

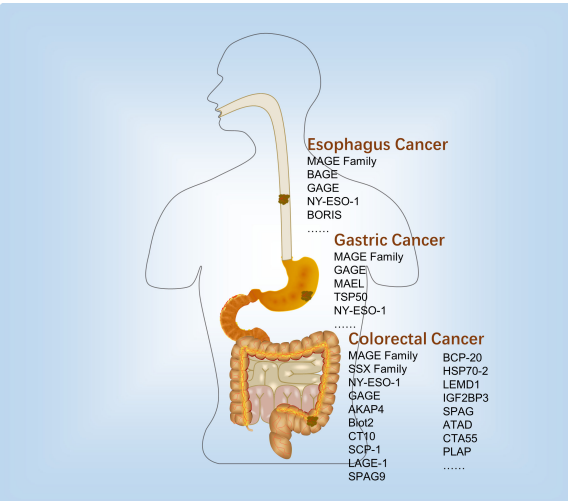

FIGURE 1
Expression and immunological therapy of CTAs in the digestive tract cancers.

10.3389/fimmu.2023.1190883

TABLE 1 The expression of CTA in the digestive tract cancers.

Cancer type	Name	Positive/total	Reference
Esophagus cancer	MAGE-1	26/42	21
	MAGE-2	18/42	21
	MAGE-3	24/42	21
	MAGE-A family	38/98	22
	MAGE-A family	111/213	23
	MAGE-A4	38/41	25
	MAGE-A9	57/103	26
	MAGE-A3	11/12	27
	MAGE-A11	37/96	28
	BAGE	Low/48	29
	GAGE	Low/48	29
	GAGE	42/213	23
	NY-ESO	41/123	31
	NY-ESO	44/213	23
	NY-ESO	17/41	25
	BORIS	28/50	33
	LAGE1	16/41	25
Gastric cancer	MAGE-C2	5/51	36
	MAGE-A1	47/86	37
	MAGE-A1	4/41	38
	GAGE	6/51	36
	MAEL	17/80	39
	TSP50	191/334	41
	CT55	3/14	51
Colorectal cancer	MAGE-A family	None/34	42
	MAGE-A2	87/100	45
	MAGE-A7	83/100	45
	MAGE-A8	75/100	45
	MAGE-A12	71/100	45
	MAGE-B2	75/100	45
	MAGE-B3	79/100	45
	MAGE-D2	75/100	45
	MAGE-F1	79/100	45
	MAGE -H1	70/100	45
	MAGE-1	14/121	44
	MAGE-3	33/121	44
	MAGE-4	27/121	44
	CAGE	31/34	42
	LAGE-1	19/121	44

(Continued)

TABLE 1 Continued

Cancer type	Name	Positive/total	Reference
	NY-ESO-1	2/34	42
	NY-ESO-1	12/121	44
	NY-ESO-1	None/62	5
	SSX-1	6/121	44
	SSX-2	3/121	44
	SSX-2	2/34	42
	SSX-4	3/121	44
	SSX-4	3/34	42
	CT-10	8/121	44
	SCP-1	2/121	44
	SPAG9	41/62	5
	AKAP4	27/62	5
	Biot2	108/147	46
	BCP-20	22/57	47
	HSPA2	156/200	48
	LEMD1	17/18	49
	IGF2BP3	56/110	50
	SPAG1	15/110	50
	ATAD	92/110	50
	CTA55	3/18	51
	PLAP	25/116	52

subfamily, including MAGE-A4 (25), MAGE-A9 (26), MAGE-A3 (27), and MAGE-A11 (28) have been detected. In addition to the MAGE-gene family, B melanoma antigen (BAGE) and G antigen (GAGE) families were also expressed in various tumors of different histological origins, including the esophageal squamous and esophageal adenocarcinoma (29). Similarly, they were not expressed in normal tissues other than testis (30).

Additionally, NY-ESO-1, which is also known as cancer/testis antigen 1B (CTAG1), is a prototypical member of the cancer-testis gene family and was originally identified from esophageal cancer (31). NY-ESO-1 is a major CTA in several studies. A study reported that 33% (41 out of 123) of esophageal squamous specimens showed positive mRNA expression for NY-ESO-1 (31). In two other studies, the proportions are 20.7% (23) and 41.4% (25), respectively. Usually, the expression of CTAs was not independent. A reported strong correlation was observed between the expression of cancer/testis antigen 2 (LAGE-1) and the expression of NY-ESO-1 and MAGE genes in esophageal squamous cancer (25, 32). Yutaka Kawakami discovered a new CTA called brother of the regulator of imprinted sites (BORIS), which is expressed in esophageal cancer and may serve as a novel prognostic indicator for patients with this type of cancer (33). BORIS could bind to the promoter of NY-ESO-1 (34) and MAGE-A1 (35) genes to regulate their expression.

2.2.2 Gastric cancer

There is growing evidence showed that several CTAs were expressed in the gastric cancer. The expression of MAGE-C2, also known as CT10, and GAGE was detected in 5 out of 51 and 6 out of 51 gastrointestinal stromal tumor tissues, respectively (36). MAGE-A1 as an important member of MAGE family was detected positive expression in 47/86 (37) and 4/41 (38) gastric cancer tissues. Another CTA, maelstrom spermatogenic transposon silencer (MAEL), was detected in gastric cancer using RT-PCR to measure its mRNA levels. The results indicated that MAEL over- and underexpressions were 17 and 28 out of 80 gastric cancer patients, respectively (39). A 50-kDa serine protease-like protein called testis-specific protease-like protein 50 (TSP50), which is encoded by a CTA gene, was discovered in human breast cancer cells through the isolation of a hypomethylated DNA fragment (40). According to Rongcheng Luo and his colleagues, a study found that the expression of TSP50 was upregulated in a significant proportion

of human gastric cancer cases, with 57.2% of samples (191 out of 334) showing overexpression (41).

2.2.3 Colorectal cancer

The expression of the MAGE family in CRC tissues is contradictory. The analysis of 34 CRC samples revealed no expression of the MAGE antigen, specifically MAGE-A1, -A2, -1, -A3, -A12, and -C1 (42). Achim A. Jungbluth and his colleagues detected that MAGE antigens were not expressed in CRC (43). However, it was found that MAGE-1 (11.6%), -3 (27.3%), and -4 (22.3%) were detected to have a positive expression in the CRC tumor samples (44). A different study reported significant overexpression of MAGE-A2 (87%), MAGE-A7 (83%), MAGE-A8 (75%), MAGE-A12 (71%), MAGE-B2 (75%), MAGE-B3 (79%), MAGE-D2 (75%), MAGE-F1 (79%), and MAGE-H1 (70%) in CRC tissues (45). Therefore, more research would be required to better understand the expression pattern of the MAGE family in the CRC. In addition to the MAGE family, other cancer/testis antigens (CTAs) have also been identified in CRC, with NY-ESO-1 being one of the most extensively studied. In a cohort of 121 CRC patients, NY-ESO-1 gene expression was detected. The same study reported that several other CTAs, SSX family gene (10%), CT10 (6.6%), SCP-1 (1.7%), and LAGE-1 (15.7%), were overexpressed in CRC tissues compared with matched adjacent non-cancerous tissues (44). Similarly, the researchers analyzed the CTA levels in 34 CRC tissues and found that two of them were NY-ESO-1 positive. The expressions of SSX-2, SSX-4, and CAGE were respectively 2, 3, and 31 (42). However, a study including 62 Iranian CRC samples was not detected the expression of NY-ESO-1. Approximately 66% and 44% of tumors were observed to express the genes encoding for sperm associated antigen 9 (SPAG9) and a-kinase anchoring protein 4 (AKAP4), respectively (5). Other CTAs expressed in CRC include coiled-coil domain containing 7 (Biot2) (46), F-box protein 39 (BCP-20, FBXO39) (47), heat shock protein family A member 1B (HSP70-2) (48), LEM domain containing 1 (LEMD1) (49), insulin-like growth factor 2 mRNA binding protein 3 (IGF2BP3), sperm-associated antigen 1 (SPAG), acute type A aortic dissection (ATAD) (50), CTA55 (51), and recombinant phospholipase A2 activating protein (PLAP) (52). However, due to the small sample size used in these studies, it is necessary to confirm the results in a larger cohort to validate their findings.

2.3 The role of CTAs in the digestive tract cancers

Expressions of CTAs in tumors are perceived as the result of widespread DNA hypomethylation in the carcinogenesis (53). The special expression patterns made them as promising biomarkers and therapeutic targets. There have been numerous clinical research studies and trials conducted to investigate the potential clinical applications of CTAs, but their precise role in cancers is still not well understood.

2.3.1 Prognostic and biomarkers

An increasing body of evidence suggests that CTA expression may have a prognostic role in esophageal, gastric, and colorectal cancers. However, there also a number of CTAs which had no relationship to clinical features of tumors.

2.3.1.1 In esophageal cancer

Studies have found that the presence of MAGE is irrelevant to age, sex, histologic type, depth of wall invasion, lymph-node metastasis, or disease stage (21–23). Additionally, no significant difference was observed between MAGE-A expression and TNM stage, grading, or survival period in patients with the disease (22). A separate study indicated a correlation between tumor progression and the expression levels of MAGE-A4. Specifically, the expression levels of MAGE-A4 were found to be correlated with tumor metastasis to the lymph nodes, and the number of involved lymph nodes was also associated with the level of MAGE-A4 expression (25). Another study found that the expressions of MAGE-A11 (28) and MAGE-A9 (26) in esophageal cancer tissues were significantly correlated with larger tumor size and more advanced tumor stage. Moreover, the expression levels of MAGE-A9 and lymph node metastasis were found to be independent prognostic factors for the overall survival rate of patients with esophageal cancer (26). However, the role of NY-ESO-1 in esophageal cancer is controversial due to conflicting reports on its prognostic value as well as its potential as a target for immunotherapy. One study found that no significant difference was observed in survival rates between NY-ESO-1 protein-positive and -negative cases (31). Nonetheless, co-expression of NY-ESO-1 and MAGE-A4 was significantly correlated with differentiation of esophageal cancer (25). Expressions of MAGE genes have been found to be significantly related to a good prognosis in the absence of BAGE and GAGE expressions. Conversely, the expressions of BAGE or GAGE has been linked to a poor prognosis in cancer patients (29), although there was no significant difference in disease progression, TNM factors, or survival curves with the expression of GAGE (23). BORIS is another biomarker for prognostic diagnosis of esophageal cancer patients. Patients with tumors that tested positive for BORIS had poor overall survival according to one study. Additionally, BORIS expression was identified as an independent poor prognostic factor and was significantly associated with lymph node metastasis (33).

2.3.1.2 In gastric cancer

MAGE-A expression has been linked with lymph node metastasis, poor differentiation, high clinical TNM stage, and inferior patient survival (54). However, MAGE-A expression alone is not deemed an independent prognostic factor in patients with the disease. Conversely, MAGE-A1 expression has been proposed as a predictive marker for resistance to taxane-based chemotherapy in patients with gastric cancer, although it does not directly contribute to drug resistance (38). In high-grade gastrointestinal stromal tumors, MAGE-C2 co-expression with

GAGE was significantly correlated with mitotic rate, tumor size, and neoplasm recurrence (36). Additionally, markers for poor relapse-free survival in gastric cancer include MAGE-A1, MAGE-A3, MAGE-A4, MAGE-C1, and NY-ESO-1 (55). High levels of TSP50 were significantly associated with shorter survival time, later TNM stage, and presence of lymph node metastases in patients with the disease. Furthermore, TSP50 overexpression was identified as a significant independent prognostic factor in gastric cancer patients (41). Moreover, in patients with H. pylori-negative gastric cancer, there was a significant correlation between MAEL expression and tumor stage, tumor grade and depth of invasion (39).

2.3.1.3 In CRC

Who exhibited a high protein expression of MAGE-D4 (56) or MAGE-A9 (57), had significantly shorter overall survival compared with those with a low protein expression. Nevertheless, there was no correlation found between MAGE-D4 expression and clinicopathological parameters (56). In patients with colorectal cancer, a high expression of MAGE-A9 was significantly associated with venous invasion, lymph node metastasis, and poor prognostic (57). Similarly, a study conducted in Taiwanese patients with colorectal cancer revealed that MAGE-B3, MAGE-D2, and MAGE-H1 expressions were correlated with tumor size and stage, whereas MAGE-B3 was also correlated with lymph node metastasis (45). In addition, NY-ESO-1 (44) and AKAP4 (5) were found to be significantly correlated with tumor stages and local lymph node metastasis in CRC patients. Biot2 expression was also found to be associated with poor prognosis in early-stage patients with CRC (58).

However, a high expression of CTAs in digestive tract cancers may have prognostic significance or simply exist as a tumor marker without indicating patient prognosis. Differences in detection methods can lead to different rates of CTA detection in various studies, which may result in biased analysis of patient prognosis. Additionally, some patients' clinical characteristics may be associated with CTA expression, but further research is needed to identify such patients.

2.3.2 Tumorigenesis, development, and metastasis

In addition to being biomarkers for digestive tract cancers, some CTAs also play a key role in the tumorigenesis, development, and metastasis. The absence of BORIS resulted in a decrease of cell proliferation and invasion in the esophageal cancer cell lines (33).Overexpression of MAGE-A1 in the gastric cancer cell lines increased the sensitivity to paclitaxel and docetaxel (38). In a study, SCRN1 was found to be expressed in five of seven gastric cancer patients, and it promoted growth of NIH3T3 cells (59). The knockdown of Biot2 in CRC cell lines has been shown to cause cell cycle arrest in the G1 phase and induce apoptosis by regulating p16 and p21, both *in vitro* and *in vivo* (60). Furthermore, according to research, ablation of HSP70-2 significantly reduced cellular growth, the colony-forming, migratory, and invasive abilities of CRC cells, and tumor growth of human CRC cell line xenograft (48). Additionally, when researchers screened the transcriptome of cancer stem cells (CSC) of human CRC, they found that LEMD1 was preferentially expressed and its presence was essential for the maintenance of CSC (61). Moreover, according to research, CT55 functions as a stimulator of nuclear factor-κB (NF-κB) signaling induced by tumor necrosis factor (TNF)-α by binding to the IκB kinase complex. Deficiency of CT55 suppresses the development of colitis-associated CRC (62).

CTAs can be used as targets for immunotherapy in digestive tract tumors, allowing immune cells or related immune agents to selectively eliminate tumor cells that express CTAs but minimizing side effects on normal cells. Therefore, the application of CTAs to immunotherapy has become an area of active research and a subject of intense interest. These findings suggest that CTAs represent a promising focus for the treatment of digestive tract cancers.

3 CTAs in the immunotherapy of digestive tract tumor therapy

During the course of cancer development, tumor antigens can be identified as aggressor by the immune system, which triggers cellular immune responses. While T-cell-related immunotherapy has received significant attention, research has also demonstrated that other immune cells of both the innate and adaptive immune systems, such as DCs, macrophages, NK cells, and B cells, play a crucial role in facilitating immunotherapy responses. In cancer treatment, the major types of immunotherapies applied are oncolytic virus therapies, cancer vaccines, adoptive cell transfer (ACT), and immune checkpoint inhibitors (ICIs). Due to the limited expression of CTAs in tumors, their high immunogenicity, and their biased expression, CTA-based immunotherapy has emerged as a promising approach in cancer treatment, showing encouraging results in preclinical and early clinical trials (Figure 2).

During cancer development, tumor antigens can be recognized as aggressors by the immune system, triggering cellular immune responses. While T-cell-related immunotherapy has received significant attention, research has demonstrated that other immune cells of both the innate and adaptive immune systems, such as DCs, macrophages, NK cells, and B cells, play a crucial role in facilitating immunotherapy responses. Types of CTA-based immunotherapy applied in digestive tract tumors treatment include oncolytic virus therapies, cancer vaccines, adoptive cell transfer (ACT), and immune checkpoint inhibitors (ICIs). Due to their limited tumor expression, high immunogenicity, and biased expression, CTAs have emerged as a promising strategy in cancer treatment (Table 2), showing encouraging results in preclinical and early clinical trials.

3.1 Oncolytic virus therapies

Oncolytic viruses (OVs) are a unique category of viruses that selectively infect and destroy tumor cells while leaving normal cells unharmed, thanks to their exceptional oncolytic activity and

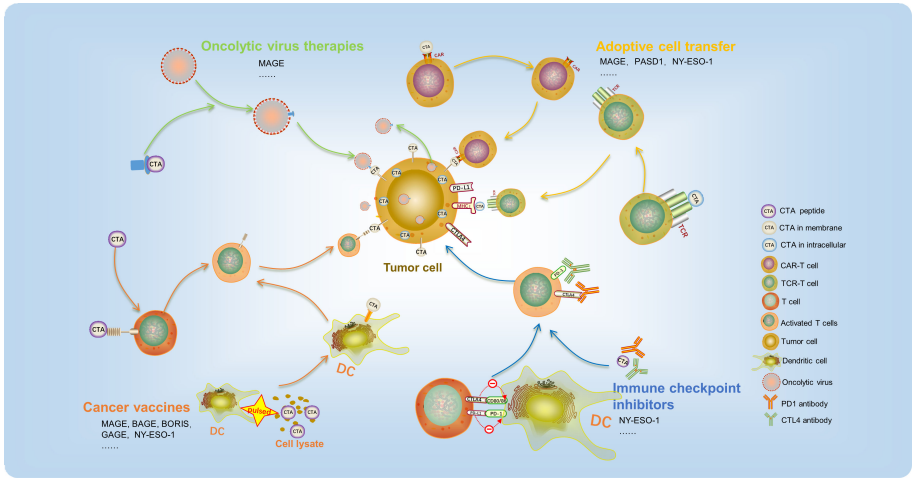

FIGURE 2
CTA-based immunotherapy has recently been used in cancer treatment and achieved promising outcomes. It mainly includes oncolytic virus therapies, cancer vaccines, adoptive cell transfer, and immune checkpoint inhibitors.

TABLE 2 The application of CTA in clinical trials.

Clinical trial number	Number of patients	Types of cancer	Phase	Status	Treatment types	Target	Study year	Reference
NCT02285816	56	Esophagus cancer, gastric cancer	1/2	Active, not recruiting	OVs (MG1MA3, AdMA3)	MAGE-A3	2014-2019	64, 65
NCT00020267	26-56	Colorectal cancer	1	Completed	Peptide vaccine	MAGE-12	2007-2015	Not provided
NCT05130060	15	Colorectal cancer	1	Active, not recruiting	Peptide vaccine (PolyPEPI1018)	Multiple CTAs	2022-2023	72
NCT05243862	28	Colorectal cancer	2	recruiting	Peptide vaccine/ICIs (PolyPEPI1018)	Multiple CTAs	2022-2024	Not provided
NCT01003808	25	Esophagus cancer	1	Completed	Protein vaccine (IMF-001)	NY-ESO-1	2009-2012	70
NCT01522820	18	Esophagus cancer, gastric cancer, colorectal cancer	1	Completed	Protein vaccine (CDX-1401)	NY-ESO-1	2012-2016	Not provided
NCT00291473	9	Esophagus cancer, gastric cancer	1	Completed	Protein vaccine (CHP-NY-ESO-1)	NY-ESO-1	2005-2008	Not provided
NCT00199849	18	Esophagus cancer	1	Completed	Plasmid DNA (pPJV7611)	NY-ESO-1	2004-2006	Not provided
NCT01234012	23	Esophagus cancer	1	Completed	Protein vaccine (IMF-001)	NY-ESO-1	2011-2013	Not provided
NCT00948961	70	Colorectal cancer	1/2	Completed	Protein vaccine (CDX-1401)	NY-ESO-1	2009-2012	71
NCT00106158	9	Esophagus cancer	1	Completed	Protein vaccine	NY-ESO-1	2004-2006	69
NCT00682227	10	Esophagus cancer	1	Unknown	Protein Vaccine	TTK, LY6K, IMP-3	2006-2008	73
NCT00311272	40	Colorectal cancer	2	Completed	Protein vaccine (MelCancerVac)	MAGE	2004-2007	76, 77
NCT05430555	48	Esophagus cancer, gastric cancer	1/2	Recruiting	TCR-T (TK-8001)	MAGE-A1	2022-2024	Not provided

(Continued)

TABLE 2 Continued

Clinical trial number	Number of patients	Types of cancer	Phase	Status	Treatment types	Target	Study year	Reference
NCT03132922	52	Esophagus cancer, gastric cancer	1	Active, not recruiting	TCR-T (MAGE-A4c1032T)	MAGE-A4	2017-2032	89
NCT04752358	45	Esophagus cancer, gastric cancer	2	Active, not recruiting	TCR-T (ADP-A2M4CD8)	MAGE-A4	2021-2023	92
NCT04044859	120	Esophagus cancer, gastric cancer	1	recruiting	TCR-T(ADP-A2M4CD8)	MAGE-A4	2019-2023	91
NCT02096614	18	Esophagus cancer	1	Completed	TCR-T (TBI-1201)	MAGE-A4	2014-2021	Not provided
UMIN000002395	9	Esophagus cancer	Unknown	Completed	TCR-T	MAG4	2009	88
NCT01795976	2	Esophagus cancer	2	Terminated	TCR-T	NY-ESO-1	2014-2017	Not provided
NCT03159585	6	Esophagus cancer, gastric cancer	1	Completed	TCR-T (TAEST16001)	NY-ESO-1	2017-2019	Not provided
NCT02869217	22	Esophagus cancer	1	Active, not recruiting	TCR-T(TBI-1301)	NY-ESO-1	2016-1013	Not provided
NCT05483491	42	Gastric cancer	1	Recruiting	TCR-T	KK-LC-1	2022-2023	Not provided
NCT05035407	100	Gastric cancer	1	Recruiting	TCR-T	KK-LC-1	2022-2025	Not provided
NCT00037817	34	Esophagus cancer	1	Completed	DAC	MY-ESO-1	2002-2008	Not provided
NCT00623831	34	Esophagus cancer	1	Completed	Mixed bacteria vaccine	NY-ESO-1	2007-2013	Not provided

targeting ability. Once inside the tumor cells, OVs can multiply and release new viral particles, which then infect other nearby tumor cells. Additionally, OVs stimulate an antitumor immune response at the local or systemic level, modify the tumor microenvironment, and amplify their antitumor effects. Currently, five types of oncolytic viruses have been approved for clinical use, and many other preclinical studies are underway (63). The application of CTA in oncolytic virus therapy is also currently under investigation. Ad-MAGEA3 (AdMA3) is a replication-deficient adenovirus (E1/E3-deleted) of human serotype 5 that carries a transgene encoding human MAGE-A3 gene. MG1-MAGEA3 (MG1MA3) is an oncolytic rhabdovirus Maraba with replication competency, created by introducing the human MAGE-A3 transgene between the G and L genes of the attenuated MG1 strain. Jonathan G. Pol confirmed the safety of the Ad : MG1 oncolytic vaccination approach in non-human primates (64). Moreover, they initiated clinical trials for solid tumor treatment, including esophageal cancer and gastric cancer (NCT02285816). The Ad : MG1 oncolytic virus has the ability to replicate within the bloodstream and activate an adaptive, antitumor cellular response in cancer patients. In three out of six evaluated patients, antitumor immunity was observed, with over 1% of total circulating CD8+ T cells reacting against MAGE-A3 in one participant (65). This strategy that modified oncolytic viruses with CTAs as target could eliminate the tumor cells specifically and provides an immunotherapy tool for future digestive tract tumor therapy clinical application.

3.2 Cancer vaccines

Cancer vaccines are utilized to deliver tumor antigens into antigen-presenting cells and stimulate T-cell-mediated antitumor immune responses. Vaccines made from a peptide expressed specifically in the tumor may induce the tumor immune response. In patients with digestive tract cancer, specific T-cell responses can be induced by immunogenic epitopes derived from CTAs such as MAGE, BAGE, GAGE, and NY-ESO-1 (66, 67). Up to now, there has been some clinical trial focused on targeting MAGE and NY-ESO-1 that have employed peptide vaccines as a treatment option for digestive tract tumor. (Table 2). Three peptide vaccines, CHP-NY-ESO-1, IMF-001, and CDX-1401, have been constructed targeting NY-ESO-1. CHP-NY-ESO-1 is a recombinant protein that consists of NY-ESO-1 and a polysaccharide-based delivery system. The safety of this peptide vaccine has been demonstrated through *in vitro* and animal experiments, indicating their potential for use in clinical trials (68). A clinical trial (NCT00106158) was conducted using CHP-NY-ESO-1 vaccine for 13 patients with advanced esophageal cancer. The study observed the induction of CHP-NY-ESO-1 immunity and some favorable clinical outcomes in patients, without any major toxicities or adverse events (69). Results from other clinical trials (NCT01003808) have demonstrated that CHP-NY-ESO-1 can trigger an immune response in patients with esophageal cancer, leading to a reduction in tumor size. The degree of reduction was observed to increase with increasing dosage (70).

CDX-1401 is a vaccine that consists of a human monoclonal antibody specific for DEC-205 fused to the full-length tumor antigen NY-ESO-1. CDX-1401 has the capacity to deliver NY-ESO-1 to DCs through DEC-205 and augment the body's immune response. Clinical trial (NCT00948961) results have demonstrated that two out of four patients with colorectal cancer experienced stabilized conditions after treatment (71).

Additionally, PolyPEPI1018 is a readily available, multipeptide vaccine consisting of 12 immunogenic epitopes derived from seven cancer testis antigens (CTAs) that are frequently expressed in patients with colorectal cancer. In clinical trials of metastatic colorectal cancer, PolyPEPI1018 was found to elicit an immune response and T-cell infiltration in MSS-type patients. In comparison with TAS-102 alone, the combination of PolyPEPI1018 plus TAS-102 has demonstrated good tolerability, and it can elicit immune responses in peripheral blood and tumor tissue of patients with a lower likelihood of causing grade 3 adverse events (NCT05130060) (72). A phase I clinical trial (NCT00682227) was conducted to examine the safety, immunogenicity, and antitumor effect of a cancer vaccine targeting TTK protein kinase, lymphocyte antigen 6 family member K (LY6K), and insulin-like growth factor 2 mRNA binding protein 3 (IMP-3) against esophageal squamous cell carcinoma. 50% of the 10 enrolled patients showed favorable clinical responses after receiving the vaccination (73). SCRN1 is another CTA identified in gastric cancer tumor tissue. The CTL clones stimulated by SCRN1 were able to recognize tumor cells that expressed the natural SCRN1 protein endogenously (59).

DCs are considered the most efficient antigen-presenting cells and play critical roles in eliciting antitumor immunity (74). In addition to serving as tumor antigens, CTAs have also been utilized in the development of vaccines delivered by dendritic cells (DCs), which have demonstrated significant clinical outcomes. After 4T1 mammary tumor implantation, mice that were vaccinated with a BORIS-based DC vaccine showed a robust anticancer immune response. The tumor growth was inhibited, and the number of spontaneous clonogenic metastases was also lowered significantly (75). In addition, the effect of DC vaccine on patients with advanced CRC were evaluated. The process of generating MAGE-DCs involves pulsing autologous peripheral blood mononuclear cells with allogeneic tumor cell lysate that contains high levels of MAGE (NCT00311272). The MAGE-DCs can present MAGE antigen to T cells and stimulate an antitumor immune response (76). Moreover, the MAGE-DCs were safe and non-toxic. After treatment with the MAGE-DC vaccine, 24% (4/17) of the patients showed stable disease (77). Taken together, these findings provide compelling evidence for the potential utility of CTAs as vaccines in immunotherapy for digestive tract tumors.

3.3 ICIs

Immune checkpoints are molecules involved in co-inhibitory signaling pathways that help maintain immune tolerance. However, cancer cells often hijack these pathways to evade immunosurveillance (78). To counteract this, ICIs such as programmed cell death 1 (PD-1), programmed cell death 1 ligand 1 (PD-L1), and cytotoxic T lymphocyte-associated antigen-4 (CTLA-4) antibodies have been developed. These drugs aim to reactivate antitumor immune responses by blocking coinhibitory signaling pathways and promoting immune-mediated elimination of cancer cells. However, remarkable efficacy has been observed with ICI only in a subset of patients. The most widely used methods for ICIs was combination with other chemicals to treat cancers. Similarly, combination treatment with ICIs and CTAs can enhance the body's immune response. McAuliffe et al. developed a vaccine consisting of a chimpanzee adenovirus (ChAdOx1) and a modified vaccinia Ankara (MVA) that encodes MAGE-type antigens. In murine tumor models expressing P1A, the combination of ChAdOx1/MVA with anti-PD-1 antibody produced superior tumor clearance and survival when compared with treatment with anti-PD-1 alone (79). Thus far, favorable outcomes have been observed in other types of tumors through the utilization of a combination of CTAs and ICIs (80). Clinical trials are currently underway to investigate the combined treatment of PolyPEPI1018 and atezolizumab for colorectal cancer, and results are pending (NCT05243862). Thus, CTA antibodies are also potentially biomarkers predicting and monitoring response to ICI therapy.

3.4 ACT

ACT therapies refer to the use of autologous immune cells, mainly T cells, that are extracted, modified, and reinfused into patients to target and eliminate cancer cells. These therapies have demonstrated long-lasting clinical efficacy. There are two types of ACT therapies, namely, chimeric antigen receptor-modified T-cell (CAR-T) immunotherapy and T-cell receptor T cell (TCR-T) immunotherapy (81, 82).

While CAR T-cell therapy has demonstrated impressive outcomes in certain types of B-cell cancers, its applicability to other malignancies, including solid tumors is impeded by the absence of appropriate surface antigens (83). An example of the successful application of CAR T-cell therapy in solid tumors is the MAGE-A1-specific CAR, which demonstrated cytotoxic activity *in vitro* and *in vivo*. It was able to infiltrate tumors that express MAGEA1 and specifically inhibit the growth of lung adenocarcinoma xenografts in nude mice (84). Furthermore, PAS domain-containing repressor 1 (PASD1) is another CTA that has been found to be immunogenic in CRC samples. $CD8^+$ T cells, induced by the PASD1 peptide, were shown to be capable of killing HLA-A*24:02$^+$ PASD1$^+$ cells (85). The researchers, led by Vita Golubovskaya, utilized a single-chain Fv fragment from a mouse monoclonal antibody clone specific to alkaline phosphatase, placental (PLAP), to engineer PLAP-CAR-T cells. These humanized PLAP-CAR-T cells were then shown to significantly inhibit tumor growth in a colon cancer xenograft model (52). However, the expression of CTAs is mainly intracellular, which limits their potential as targets for CAR therapy.

Major histocompatibility complexes (MHCs) present intracellular antigens associated with tumors, which can be targeted by T-cell receptors (TCRs). One type of antigenic target

for TCR T cells are cancer-testis antigens (86). The growth of MAGE-A4-expressing esophageal cancer was hindered in NOG mice through the use of genetically engineered T cells that expressed a MAGE-A4-specific TCR designed to target the MAGE-A4 143-151 peptide-NYKRCFPVI, which is restricted to HLA-A24 (87). Furthermore, the use of MAGE-A4-specific TCR in adoptive immunotherapy for patients with recurrent esophageal cancer has been reported as safe (UMIN000002395) (88). In a phase I clinical trial (NCT03132922), Hong et al. evaluated the safety, clinical activity, and translational effects of MAGE-A4-specific TCR (89) in the treatment of solid tumors such as gastric cancer and esophageal cancer. All 38 patients across nine different tumor types experienced grade ≥3 hematologic toxicities; cytokine release syndrome was reported in 55% of patients, with 90% of these being grade ≤2. The objective response rate (ORR) (all partial response) was 24% (9/38). Phase II clinical trials are currently enrolling participants (NCT04044768) (90). In the phase I SURPASS trial (NCT04044859), the safety and efficacy of next-generation ADP-A2M4CD8 SPEAR T-cells that co-express the CD8a coreceptor with an engineered TCR targeting MAGE-A4 were evaluated. In this study which included 18 patients (two with esophageal cancer and four with gastric cancer), the results indicated that the TCR-T cells were safe for use within the human body. The best overall responses observed in the study were one partial response (gastric cancer), four cases of stable disease (two of which were gastric cancer and two were esophageal), and one case of progressive disease (gastric cancer) (91). The phase II clinical trial (NCT04752358) of this TCR-T-cell therapy in esophageal and gastric cancer is currently ongoing, and preliminary results suggest that the clinical outcomes are promising (92).

Furthermore, additional clinical trials have assessed the safety, tolerability, and efficacy of NY-ESO-1 and KK-LC-1-specific TCR gene-transduced T lymphocytes in treating tumors of the digestive tract (Table 2). However, as with the prior studies, only one trial has been completed thus far, and its results are pending publication. These findings form the foundation for future clinical investigations aimed at targeting CTAs with ACT therapies in digestive tract tumors.

4 Opportunity and challenge

Currently, surgery, radiation, and chemotherapy remain the major treatment means of patients with digestive tract tumors. The immune therapeutics have not been used as the first line of digestive tract tumor therapy in the clinical setting. Although recent progresses in cancer immunotherapy therapies have been very rapid, their efficacy is still limited to a very small subset of cancer patients. While CTA-based immunotherapies show great potential, the full therapeutic benefits of CTA-targeted digestive tract tumors have yet to be fully realized. There are also many detours and challenges along the way. To overcome the barriers and increase the efficacy of CTA-targeted digestive tract tumor immunotherapy, new strategies and cutting-edge technology should be applied (Figure 3).

First of all, since the majority of CTA protein targets are intracellular, tumor cells are often not recognized by specific antibodies or active immune cells, thus presenting a major challenge in CTA-targeted therapies (93, 94). Consequently, most CTAs are unable to elicit a robust immune response in cancer patients. With the defect of cytoplasmic localization, TCR mimic antibodies present new opportunities for additional CAR strategies targeting CTAs (82). TCR mimic antibodies have specificities that resemble those of T-cell receptors, targeting peptides presented in complex with MHC or HLA-I (95). This method enabled HLA-A2/NY-ESO-1 peptide-specific CARs to recognize tumors, offering a promising avenue to expand the range of CAR T-cell targets (96). Likewise, there has been considerable interest in bispecific antibody-based therapeutics that aim to target intracellular oncoproteins (97). This approach expands the range of CTAs that can be targeted and enhances the effectiveness of conventional antibody-based therapeutics. Meanwhile, screening more CTAs

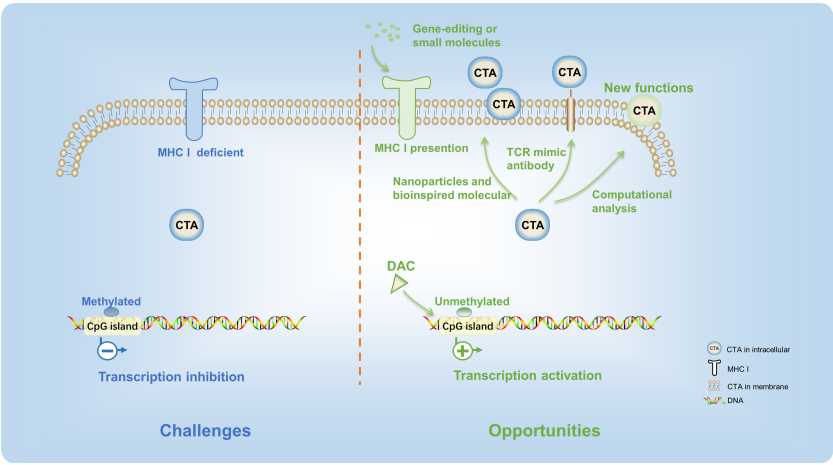

FIGURE 3
There are many detours and challenges in the CTA-based digestive tract tumor immunotherapy. New strategies and cutting-edge technology provided opportunities to overcome these difficulties.

located in the membrane of digestive tract cancer cells is an alternative approach. PRAME, a CTA, was previously recognized as an intracellular protein. In recent years, a computational analysis of transmembrane proteins has predicted that a particular protein has an extracellular region that could be targeted specifically by PRAME-specific antibodies *in vitro* and *in vivo* (98). Therefore, the advances of science and technology could help to find new functions of existing CTAs.

After that, in cancer cells, the MHC-I protein is usually deficient (99), leading to low amounts of CTA epitopes on the cell membrane surface. Therefore, the T cells could not capture tumor antigen. Promoting the transcription of the MHC gene through gene-editing technology or stimulation of small molecules is an effective strategy to improve the efficacy of CTA presentation. Advanced biomaterials, such as nanoparticles and bioinspired molecular (100), could also effectively harness immunotherapies of CTA and improve their potency.

Finally, the inconsistent expression level of CTAs in the digestive tract cancer patients limited their clinical application. Although many CTAs were expressed in digestive tract cancers, only few of CTA-targeted immune therapeutics exhibited high anticancer efficacy. One of the main reasons is that the expression level of CTAs was inhibited by the high DNA methylation level at the promoter regions (101). On account of this, the demethylation agent, such as decitabine (5-aza-2′-deoxycytidine, DAC), was applied to improve antigen-specific T-cell immune responses (102). Expressions of MAGE-A (27, 103), MAGE-3, NY-ESO-1 (104), beta-2-microglobulin, calreticulin, CD58, proteasome 20S subunit beta 8 (PSMB8), and PSMB9 (105) were increased significantly in esophageal cancer and CRC after the treatment of decitabine. Moreover, clinical studies are currently underway to investigate the regulation of CTA expression by DAC (NCT00037817). Furthermore, research has also demonstrated that a mixed bacterial vaccine can activate the body's immune response and serve as an immune modulator, thereby promoting the combination of NY-ESO-1-positive tumor cells with antigen-specific cancer vaccines (NCT00623831) (106). Reports suggest that therapeutic interventions such as radiotherapy may enhance the release of the NY-ESO-1 antigen from the tumor, which could play a critical role in directing tumor immunotherapy (107, 108). Moreover, the overexpression of CTA in the tumor cells not only improved the antitumor efficacy of T cells but also increased sensitivity of tumor cells for immunotherapy in the digestive tract tumors (109). These approaches have the potential to modulate the extent and phenotype of the antitumor immune response, thus increasing the efficacy of CTA-targeted immunotherapy for digestive tract tumors.

In summary, CTA-based immunotherapies provided a new platform and opportunity for the development of therapeutics for digestive tract tumors. It is anticipated that these novel strategies and approaches will bring about significant breakthroughs in the field of digestive tract tumors immunotherapy in the near future.

Author contributions

HA: Conceptualization, Investigation, Writing - review & editing, Writing - original draft. HY: Conceptualization, Investigation, Data curation, Writing - original draft. LL: Conceptualization, Investigation, Data curation, Methodology. JM: Conceptualization, Investigation, Methodology. KL: Conceptualization, Investigation, Funding acquisition. ZL: Conceptualization, Investigation, Methodology, Writing - review & editing. All authors contributed to the article and approved the submitted version.

Funding

This work was supported by the National Natural Science Foundation of China (grant number 81872335), The Central Plains Science and Technology Innovation Leading Talents (No. 224200510015), the Health Commission of Henan Province (grant number 232102311077), and the Health and Family Planning Commission of Henan Province (grant number LHGJ20220198).

Acknowledgments

We would like to thank Guanglong Chen and Weijie Zhao for helpful guidance in data collection, and Ye Kong and Jialin Zhang for technical support.

Conflict of interest

The authors declare that the research was conducted in the absence of any commercial or financial relationships that could be construed as a potential conflict of interest.

Publisher's note

References

1. Siegel RL, KD M, Jemal A. Cancer statistics, 2020. *CA Cancer J Clin* (2020) 70:7–30. doi: 10.3322/caac.21590

2. van Weverwijk A, de Visser KE. Mechanisms driving the immunoregulatory function of cancer cells. *Nat Rev Cancer* (2023) 23:193–215. doi: 10.1038/s41568-022-00544-4

3. Hogan B, Fellous M, Avner P, Jacob F. Isolation of a human teratoma cell line which expresses F9 antigen. *NATURE* (1977) 270:515–8. doi: 10.1038/270515a0

4. Holden S, Bernard O, Artzt K, Whitmore WJ, Bennett D. Human and mouse embryonal carcinoma cells in culture share an embryonic antigen (F9). *NATURE* (1977) 270:518–20. doi: 10.1038/270518a0

5. Tavakoli KA, Mahjoubi B, Mirzaei R, Shabani S, Mahjoubi F. AKAP4, SPAG9 and NY-ESO-1 in Iranian colorectal cancer patients as probable diagnostic and prognostic biomarkers. *Asian Pac J Cancer Prev* (2018) 19:463–9. doi: 10.22034/APJCP.2018.19.2.463

6. Gordeeva O. Cancer-testis antigens: unique cancer stem cell biomarkers and targets for cancer therapy. *Semin Cancer Biol* (2018) 53:75–89. doi: 10.1016/j.semcancer.2018.08.006

7. Costa FF, Le Blanc K, Brodin B. Concise review: cancer/testis antigens, stem cells, and cancer. *Stem Cells* (2007) 25:707–11. doi: 10.1634/stemcells.2006-0469

8. Pan J, Yu H, Guo Z, Liu Q, Ding M, Xu K, et al. Emerging role of sperm-associated antigen 9 in tumorigenesis. *BioMed Pharmacother* (2018) 103:1212–6. doi: 10.1016/j.biopha.2018.04.168

9. Szender JB, Papanicolau-Sengos A, Eng KH, Miliotto AJ, Lugade AA, Gnjatic S, et al. NY-ESO-1 expression predicts an aggressive phenotype of ovarian cancer. *GYNECOL Oncol* (2017) 145:420–5. doi: 10.1016/j.ygyno.2017.03.509

10. Cao QH, Liu F, CZ Li, Liu N, Shu M, Lin Y, et al. Testes-specific protease 50 (TSP50) promotes invasion and metastasis by inducing EMT in gastric cancer. *BMC Cancer* (2018) 18:94. doi: 10.1186/s12885-018-4000-y

11. Kwon Y, Kim Y, HS J, Jeoung D. Role of HDAC3-miRNA-CAGE network in anti-cancer drug-resistance. *Int J Mol Sci* (2018) 20:51. doi: 10.3390/ijms20010051

12. van der Bruggen P, Traversari C, Chomez P, Lurquin C, De Plaen E, Van den Eynde B, et al. A gene encoding an antigen recognized by cytolytic T lymphocytes on a human melanoma. *Science* (1991) 254:1643–7. doi: 10.1126/science.1840703

13. Sahin U, Türeci O, Schmitt H, Cochlovius B, Johannes T, Schmits R, et al. Human neoplasms elicit multiple specific immune responses in the autologous host. *Proc Natl Acad Sci U.S.A.* (1995) 92:11810–3. doi: 10.1073/pnas.92.25.11810

14. Chen YT, MJ S, Sahin U, Türeci O, Gure AO, Tsang S, et al. A testicular antigen aberrantly expressed in human cancers detected by autologous antibody screening. *Proc Natl Acad Sci U.S.A.* (1997) 94:1914–8. doi: 10.1073/pnas.94.5.1914

15. Chen YT, Boyer AD, Viars CS, Tsang S, Old LJ, Arden KC. Genomic cloning and localization of CTAG, a gene encoding an autoimmunogenic cancer-testis antigen NY-ESO-1, to human chromosome Xq28. *Cytogenet Cell Genet* (1997) 79:237–40. doi: 10.1159/000134734

16. Türeci O, Sahin U, Zwick C, Koslowski M, Seitz G, Pfreundschuh M. Identification of a meiosis-specific protein as a member of the class of cancer/testis antigens. *Proc Natl Acad Sci U.S.A.* (1998) 95:5211–6. doi: 10.1073/pnas.95.9.5211

17. Old LJ, Chen YT. New paths in human cancer serology. *J Exp Med* (1998) 187:1163–7. doi: 10.1084/jem.187.8.1163

18. Wang C, Gu Y, Zhang K, Xie K, Zhu M, Dai N, et al. Systematic identification of genes with a cancer-testis expression pattern in 19 cancer types. *Nat Commun* (2016) 7:10499. doi: 10.1038/ncomms10499

19. McFarlane RJ, Feichtinger J, Larcombe L. Cancer germline gene activation: friend or foe? *Cell Cycle* (2014) 13:2151–2. doi: 10.4161/cc.29661

20. Hofmann O, Caballero OL, Stevenson BJ, Chen YT, Cohen T, Chua R, et al. Genome-wide analysis of cancer/testis gene expression. *Proc Natl Acad Sci U.S.A.* (2008) 105:20422–7. doi: 10.1073/pnas.0810777105

21. Inoue H, Mori M, Li J, Mimori K, Honda M, Nakashima H, et al. Human esophageal carcinomas frequently express the tumor-rejection antigens of MAGE genes. *Int J Cancer* (1995) 63:523–6. doi: 10.1002/ijc.2910630411

22. Haier J, Owzcareck M, Guller U, Spagnoli GC, Bürger H, Senninger N, et al. Expression of MAGE-a cancer/testis antigens in esophageal squamous cell carcinomas. *Anticancer Res* (2006) 26:2281–7.

23. Akcakanat A, Kanda T, Tanabe T, Komukai S, Yajima K, Nakagawa S, et al. Heterogeneous expression of GAGE, NY-ESO-1, MAGE-a and SSX proteins in esophageal cancer: implications for immunotherapy. *Int J Cancer* (2006) 118:123–8. doi: 10.1002/ijc.21219

24. Schooten E, Maggio AD, van Bergen En Henegouwen PMP, Kijanka MM. MAGE-a antigens as targets for cancer immunotherapy. *Cancer Treat Rev* (2018) 67:54–62. doi: 10.1016/j.ctrv.2018.04.009

25. Forghanifard MM, Gholamin M, Farshchian M, Moaven O, Memar B, Forghani MN, et al. Cancer-testis gene expression profiling in esophageal squamous cell carcinoma: identification of specific tumor marker and potential targets for immunotherapy. *Cancer Biol Ther* (2011) 12:191–7. doi: 10.4161/cbt.12.3.15949

26. Qi Y, KX C, FC X, CY Z, Huang Q, Wu K, et al. High expression of MAGE-A9 is associated with unfavorable survival in esophageal squamous cell carcinoma. *Oncol Lett* (2017) 14:3415–20. doi: 10.3892/ol.2017.6614

27. Shi X, Chen X, Fang B, Ping Y, Qin G, Yue D, et al. Decitabine enhances tumor recognition by T cells through upregulating the MAGE-A3 expression in esophageal carcinoma. *BioMed Pharmacother* (2019) 112:108632. doi: 10.1016/j.biopha.2019.108632

28. Wu Y, Sang M, Liu F, Zhang J, Li W, Li Z, et al. Epigenetic modulation combined with PD-1/PD-L1 blockade enhances immunotherapy based on MAGE-A11 antigen-specific CD8+T cells against esophageal carcinoma. *Carcinogenesis* (2020) 41:894–903. doi: 10.1093/carcin/bgaa057

29. D AZP DSMP, D APM D BETM, D PZP. MAGE, BAGE, and GAGE gene expression in patients with esophageal squamous cell carcinoma and adenocarcinoma of the gastric cardia. *CANCER-AM Cancer Soc* (2015) 91:1882–8. doi: 10.1002/1097-0142(20010515)91:10<1882::AID-CNCR1210>3.0.CO;2-H

30. Eynde B, Boon T. Tumor antigens recognized by T lymphocytes. *Int J Clin Lab Res* (1997) 27:81–6. doi: 10.1007/BF02912440

31. Fujita S. NY-ESO-1 expression and immunogenicity in esophageal cancer. *Clin Cancer Res Off J Am Assoc Cancer Res* (2004) 10:6551. doi: 10.1158/1078-0432.CCR-04-0819

32. Zhang Y, Zhang Y, Zhang L. Expression of cancer-testis antigens in esophageal cancer and their progress in immunotherapy. *J Cancer Res Clin Oncol* (2019) 145:281–91. doi: 10.1007/s00432-019-02840-3

33. Okabayashi K, Fujita T, Miyazaki J, Okada T, Iwata T, Hirao N, et al. Cancer-testis antigen BORIS is a novel prognostic marker for patients with esophageal cancer. *Cancer Sci* (2012) 103:1617–24. doi: 10.1111/j.1349-7006.2012.02355.x

34. Kang Y, Hong JA, Chen GA, Nguyen DM, Schrump DS. Dynamic transcriptional regulatory complexes including BORIS, CTCF and Sp1 modulate NY-ESO-1 expression in lung cancer cells. *Oncogene* (2007) 26:4394–403. doi: 10.1038/sj.onc.1210218

35. Vatolin S, Abdullaev Z, Pack SD, Flanagan PT, Custer M, Loukinov DI, et al. Conditional expression of the CTCF-paralogous transcriptional factor BORIS in normal cells results in demethylation and derepression of MAGE-A1 and reactivation of other cancer-testis genes. *Cancer Res* (2005) 65:7751–62. doi: 10.1158/0008-5472.CAN-05-0858

36. Ghadban T, Perez DR, Vashist YK, Bockhorn M, Koenig AM, El GA, et al. Expression of cancer testis antigens CT10 (MAGE-C2) and GAGE in gastrointestinal stromal tumors. *Eur J Surg Oncol* (2014) 40:1307–12. doi: 10.1016/j.ejso.2014.03.011

37. Lian Y, Sang M, Gu L, Liu F, Yin D, Liu S, et al. MAGE-a family is involved in gastric cancer progression and indicates poor prognosis of gastric cancer patients. *Pathol Res Pract* (2017) 213:943–8. doi: 10.1016/j.prp.2017.05.007

38. Suzuki T, Yoshida K, Wada Y, Hamai Y, Sentani K, Oue N, et al. Melanoma-associated antigen-A1 expression predicts resistance to docetaxel and paclitaxel in advanced and recurrent gastric cancer. *Oncol Rep* (2007) 18:329–36. doi: 10.3892/or.18.2.329

39. Abbaszadegan MR, Taghehchian N, Aarabi A, Moghbeli M. MAEL cancer-testis antigen as a diagnostic marker in primary stages of gastric cancer with helicobacter pylori infection. *J Gastrointest Cancer* (2020) 51:17–22. doi: 10.1007/s12029-018-0183-3

40. Yuan L, Shan J, De Risi D, Broome J, Lovecchio J, Gal D, et al. Isolation of a novel gene, TSP50, by a hypomethylated DNA fragment in human breast cancer. *Cancer Res* (1999) 59:3215–21.

41. Liu F, Cao Q, Liu N, Li C, You C, Liu C, et al. Overexpression of testes-specific protease 50 (TSP50) predicts poor prognosis in patients with gastric cancer. *Gastroenterol Res Pract* (2014) 2014:498246. doi: 10.1155/2014/498246

42. Dakshinamurthy AG, Ramesar R, Goldberg P, Blackburn JM. Infrequent and low expression of cancer-testis antigens located on the X chromosome in colorectal cancer: implications for immunotherapy in south African populations. *Biotechnol J* (2008) 3:1417–23. doi: 10.1002/biot.200800144

43. Jungbluth AA, Busam KJ, Kolb D, Iversen K, Coplan K, Chen YT, et al. Expression of MAGE-antigens in normal tissues and cancer. *Int J Cancer* (2000) 85:460–5. doi: 10.1002/(SICI)1097-0215(20000215)85:4<460::AID-IJC3>3.0.CO;2-N

44. Li M, Yuan YH, Han Y, YX L, Yan L, Wang Y, et al. Expression profile of cancer-testis genes in 121 human colorectal cancer tissue and adjacent normal tissue. *Clin Cancer Res* (2005) 11:1809–14. doi: 10.1158/1078-0432.CCR-04-1365

45. Chung FY, Cheng TL, Chang HJ, Chiu HH, Huang MY, Chang MS, et al. Differential gene expression profile of MAGE family in taiwanese patients with colorectal cancer. *J Surg Oncol* (2010) 102:148–53. doi: 10.1002/jso.21580

46. Shen YM, Arbman G, Sandstrom P, Gullstrand P, YQ W, Zhang H, et al. Novel gene hBiot2 is an independent prognostic factor in colorectal cancer patients. *Oncol Rep* (2012) 27:376–82. doi: 10.3892/or.2011.1521

47. Song MH, Ha JC, Lee SM, Park YM, Lee SY. Identification of BCP-20 (FBXO39) as a cancer/testis antigen from colon cancer patients by SEREX. *Biochem Biophys Res Commun* (2011) 408:195–201. doi: 10.1016/j.bbrc.2011.02.077

48. Jagadish N, Parashar D, Gupta N, Agarwal S, Suri V, Kumar R, et al. Heat shock protein 70-2 (HSP70-2) is a novel therapeutic target for colorectal cancer and is associated with tumor growth. *BMC Cancer* (2016) 16:561. doi: 10.1186/s12885-016-2592-7

49. Yuki D, YM L, Fujii Y, Nakamura Y, Furukawa Y. Isolation of LEM domain-containing 1, a novel testis-specific gene expressed in colorectal cancers. *Oncol Rep* (2004) 12:275–80. doi: 10.3892/or.12.2.275

50. Vasaikar S, Huang C, Wang X, Petyuk VA, Savage SR, Wen B, et al. Proteogenomic analysis of human colon cancer reveals new therapeutic opportunities. *CELL* (2019) 177:1035–49. doi: 10.1016/j.cell.2019.03.030

51. Dong XY, YY Li, XA Y, Chen WF. BJ-HCC-20, a potential novel cancer-testis antigen. *Biochem Cell Biol* (2004) 82:577–82. doi: 10.1139/o04-056

52. Li X, Berahovich R, Zhou H, Liu X, Li F, Xu S, et al. PLAP -CAR T cells mediate high specific cytotoxicity against colon cancer cells. *Front Biosci (Landmark Ed)* (2020) 25:1765–86. doi: 10.2741/4877

53. Kim R, Kulkarni P, Hannenhalli S. Derepression of Cancer/Testis antigens in cancer is associated with distinct patterns of DNA hypomethylation. *BMC Cancer* (2013) 13:144. doi: 10.1186/1471-2407-13-144

54. Lian Y, Sang M, Gu L, Liu F, Yin D, Liu S, et al. MAGE-a family is involved in gastric cancer progression and indicates poor prognosis of gastric cancer patients. *Pathol - Res Pract* (2017) 213:943–948. doi: 10.1016/j.prp.2017.05.007

55. Perez D, Hauswirth F, Jäger D, Metzger U, Samartzis EP, Went P, et al. Protein expression of cancer testis antigens predicts tumor recurrence and treatment response to imatinib in gastrointestinal stromal tumors. *Int J Cancer* (2011) 128:2947–52. doi: 10.1002/ijc.25836

56. Zhang QM, SJ He, Shen N, Luo B, Fan R, Fu J, et al. Overexpression of MAGE-D4 in colorectal cancer is a potentially prognostic biomarker and immunotherapy target. *Int J Clin Exp Pathol* (2014) 7:3918–27.

57. Zhan W, Zhang Z, Zhang Y, Ma J, Wu T, Gu Y, et al. Prognostic value of MAGE-A9 expression in patients with colorectal cancer. *Clin Res Hepatol Gastroenterol* (2016) 40:239–45. doi: 10.1016/j.clinre.2015.08.005

58. Sun X-F. Novel gene hBiot2 is an independent prognostic factor in colorectal cancer patients. *Oncol Rep* (2012) 27:376–382. doi: 10.3892/or.2011.1521

59. Suda T, Tsunoda T, Uchida N, Watanabe T, Hasegawa S, Satoh S, et al. Identification of secernin 1 as a novel immunotherapy target for gastric cancer using the expression profiles of cDNA microarray. *Cancer Sci* (2006) 97:411–9. doi: 10.1111/j.1349-7006.2006.00194.x

60. Zhou C, Zhang P, GC Xu, DM Wu, RY L, Zeng Q, et al. RNA Interference of Biot2 induces G1 phase arrest and apoptosis in mouse colorectal cancer cell line. *Oncol Res* (2015) 22:93–103. doi: 10.3727/096504014X14146137738583

61. Takeda R, Hirohashi Y, Shen M, Wang L, Ogawa T, Murai A, et al. Identification and functional analysis of variants of a cancer/testis antigen LEMD1 in colorectal cancer stem-like cells. *Biochem Biophys Res Commun* (2017) 485:651–7. doi: 10.1016/j.bbrc.2017.02.081

62. Zhao H, Pan WM, Zhang HH, Song Y, Chen J, Xiang Y, et al. Cancer testis antigen 55 deficiency attenuates colitis-associated colorectal cancer by inhibiting NF-κB signaling. *Cell Death Dis* (2019) 10:304. doi: 10.1038/s41419-019-1537-x

63. Shalhout SZ, Miller DM, Emerick KS, Kaufman HL. Therapy with oncolytic viruses: progress and challenges. *Nat Rev Clin Oncol* (2023) 20:160–77. doi: 10.1038/s41571-022-00719-w

64. Pol JG, Acuna SA, Yadollahi B, Tang N, Stephenson KB, Atherton MJ, et al. Preclinical evaluation of a MAGE-A3 vaccination utilizing the oncolytic maraba virus currently in first-in-human trials. *ONCOIMMUNOLOGY* (2019) 8:e1512329. doi: 10.1080/2162402X.2018.1512329

65. Pol JG, Atherton MJ, Bridle BW, Stephenson KB, Le Boeuf F, Hummel JL, et al. Development and applications of oncolytic maraba virus vaccines. *Oncolytic Virother* (2018) 7:117–28. doi: 10.2147/OV.S154494

66. Yang P, Meng M, Zhou Q. Oncogenic cancer/testis antigens are a hallmarker of cancer and a sensible target for cancer immunotherapy. *Biochim Biophys Acta Rev Cancer* (2021) 1876:188558. doi: 10.1016/j.bbcan.2021.188558

67. Bender A, Karbach J, Neumann A, Jger D, Al-Batran SE, Atmaca A, et al. LUD 00-009: phase 1 study of intensive course immunization with NY-ESO-1 peptides in HLA-A2 positive patients with NY-ESO-1-expressing cancer. *Cancer Immun A J Acad Cancer Immunol* (2007) 7:16.

68. Harada N, Hoshiai K, Takahashi Y, Sakaguchi Y, Kuno T, Hishida T, et al. Preclinical safety pharmacology study of a novel protein-based cancer vaccine CHP-NY-ESO-1. *Kobe J Med Sci* (2008) 54:E23–34.

69. Wada H, Sato E, Uenaka A, Isobe M, Kawabata R, Nakamura Y, et al. Analysis of peripheral and local anti-tumor immune response in esophageal cancer patients after NY-ESO-1 protein vaccination. *Int J Cancer* (2008) 123:2362–9. doi: 10.1002/ijc.23810

70. Kageyama S, Wada H, Muro K, Niwa Y, Ueda S, Miyata H, et al. Dose-dependent effects of NY-ESO-1 protein vaccine complexed with cholesteryl pullulan (CHP-NY-ESO-1) on immune responses and survival benefits of esophageal cancer patients. *J Transl Med* (2013) 11:246. doi: 10.1186/1479-5876-11-246

71. Dhodapkar MV, Sznol M, Zhao B, Wang D, Carvajal RD, Keohan ML, et al. Induction of antigen-specific immunity with a vaccine targeting NY-ESO-1 to the dendritic cell receptor DEC-205. *Sci Transl Med* (2014) 6:232r–51r. doi: 10.1126/scitranslmed.3008068

72. Hubbard JM, Zemla TJ, Graham RP, Jin Z, Zhu M, Mitchell JL, et al. Phase ib open-label study to evaluate safety, tolerability, immunogenicity, and efficacy of multiple subcutaneous injections of PolyPEPI1018 vaccine as an add-on immunotherapy to TAS-102 in participants with late-stage microsatellite-stable metastatic colorectal cancer (MSS mCRC; OBERTO-201). *J Clin Oncol* (2023) 41:147. doi: 10.1200/JCO.2023.41.4_suppl.147

73. Kono K, Mizukami Y, Daigo Y, Takano A, Masuda K, Yoshida K, et al. Vaccination with multiple peptides derived from novel cancer-testis antigens can induce specific T-cell responses and clinical responses in advanced esophageal cancer. *Cancer Sci* (2009) 100:1502–9. doi: 10.1111/j.1349-7006.2009.01200.x

74. Verneau J, Sautes-Fridman C, Sun CM. Dendritic cells in the tumor microenvironment: prognostic and theranostic impact. *Semin Immunol* (2020) 48:101410. doi: 10.1016/j.smim.2020.101410

75. Mkrtichyan M, Ghochikyan A, Davtyan H, Movsesyan N, Loukinov D, Lobanenkov V, et al. Cancer-testis antigen, BORIS based vaccine delivered by dendritic cells is extremely effective against a very aggressive and highly metastatic mouse mammary carcinoma. *Cell Immunol* (2011) 270:188–97. doi: 10.1016/j.cellimm.2011.05.007

76. Burgdorf SK, Claesson MH, Nielsen HJ, Rosenberg J. Changes in cytokine and biomarker blood levels in patients with colorectal cancer during dendritic cell-based vaccination. *Acta Oncol* (2009) 48:1157–64. doi: 10.3109/02841860903099964

77. Burgdorf SK, Fischer A, Myschetzky PS, Munksgaard SB, Zocca MB, Claesson MH, et al. Clinical responses in patients with advanced colorectal cancer to a dendritic cell based vaccine. *Oncol Rep* (2008) 20:1305–11. doi: 10.3892/or_00000145

78. Zhang Y, Zhang Z. The history and advances in cancer immunotherapy: understanding the characteristics of tumor-infiltrating immune cells and their therapeutic implications. *Cell Mol Immunol* (2020) 17:807–21. doi: 10.1038/s41423-020-0488-6

79. McAuliffe J, HF C, Noblecourt L, Ramirez-Valdez RA, Pereira-Almeida V, Zhou Y, et al. Heterologous prime-boost vaccination targeting MAGE-type antigens promotes tumor T-cell infiltration and improves checkpoint blockade therapy. *J Immunother Cancer* (2021) 9:e003218. doi: 10.1136/jitc-2021-003218

80. Haag GM, Zoernig I, JC H, Halama N, Dick J, Lang N, et al. Phase II trial of ipilimumab in melanoma patients with preexisting humoural immune response to NY-ESO-1. *Eur J Cancer* (2018) 90:122–9. doi: 10.1016/j.ejca.2017.12.001

81. Fesnak AD, June CH, Levine BL. Engineered T cells: the promise and challenges of cancer immunotherapy. *Nat Rev Cancer* (2016) 16:566–81. doi: 10.1038/nrc.2016.97

82. Jakobsen MK, Gjerstorff MF. CAR T-cell cancer therapy targeting surface Cancer/Testis antigens. *Front Immunol* (2020) 11:1568. doi: 10.3389/fimmu.2020.01568

83. Sadelain M, Riviere I, Riddell S. Therapeutic T cell engineering. *Nature* (2017) 545:423–31. doi: 10.1038/nature22395

84. Mao Y, Fan W, Hu H, Zhang L, Michel J, Wu Y, et al. MAGE-A1 in lung adenocarcinoma as a promising target of chimeric antigen receptor T cells. *J Hematol Oncol* (2019) 12:106. doi: 10.1186/s13045-019-0793-7

85. Soh JE, Abu N, Sagap I, Mazlan L, Yahaya A, Mustangin M, et al. Validation of immunogenic PASD1 peptides against HLA-A*24:02 colorectal cancer. *Immunotherapy-UK* (2019) 11:1205–19. doi: 10.2217/imt-2019-0073

86. Linnemann C, Heemskerk B, Kvistborg P, Kluin RJ, Bolotin DA, Chen X, et al. High-throughput identification of antigen-specific TCRs by TCR gene capture. *Nat Med* (2013) 19:1534–41. doi: 10.1038/nm.3359

87. Ottaviani S, Colau D, van der Bruggen P, van der Bruggen P. A new MAGE-4 antigenic peptide recognized by cytolytic T lymphocytes on HLA-A24 carcinoma cells. *Cancer Immunol Immunother* (2006) 55:867–72. doi: 10.1007/s00262-005-0053-2

88. Kageyama S, Ikeda H, Miyahara Y, Imai N, Ishihara M, Saito K, et al. Adoptive transfer of MAGE-A4 T-cell receptor gene-transduced lymphocytes in patients with recurrent esophageal cancer. *Clin Cancer Res* (2015) 21:2268–77. doi: 10.1158/1078-0432.CCR-14-1559

89. Sanderson JP, Crowley DJ, Wiedermann GE, Quinn LL, Crossland KL, Tunbridge HM, et al. Preclinical evaluation of an affinity-enhanced MAGE-A4-specific T-cell receptor for adoptive T-cell therapy. *ONCOIMMUNOLOGY* (2020) 9:1682381. doi: 10.1080/2162402X.2019.1682381

90. Hong DS, Van Tine BA, Biswas S, McAlpine C, Johnson ML, Olszanski AJ, et al. Autologous T cell therapy for MAGE-A4(+) solid cancers in HLA-A*02(+) patients: a phase 1 trial. *Nat Med* (2023) 29:104–14. doi: 10.1038/s41591-022-02128-z

91. Hong DS, Clarke JM, Asch A, Charlson J, Johanns TM, Calvo E, et al. 540P safety and efficacy from the SURPASS trial with ADP-A2M4CD8, a SPEAR T-cell therapy incorporating a CD8α co-receptor and an affinity optimized TCR targeting MAGE-A4. *Ann Oncol* (2021) 32:S604–5. doi: 10.1016/j.annonc.2021.08.1062

92. Hong DS, Jalal SI, Elimova E, Ajani JA, Blum Murphy MA, Cervantes A, et al. SURPASS-2 trial design: a phase 2, open-label study of ADP-A2M4CD8 SPEAR T cells in advanced esophageal or esophagogastric junction cancers. *J Clin Oncol* (2022) 40:S363. doi: 10.1200/JCO.2022.40.4_suppl.TPS363

93. Zajac P, Schultz-Thater E, Tornillo L, Sadowski C, Trella E, Mengus C, et al. MAGE-a antigens and cancer immunotherapy. *Front Med (Lausanne)* (2017) 4:18. doi: 10.3389/fmed.2017.00018

94. Schultz-Thater E, Noppen C, Gudat F, Durmuller U, Zajac P, Kocher T, et al. NY-ESO-1 tumour associated antigen is a cytoplasmic protein detectable by specific

monoclonal antibodies in cell lines and clinical specimens. *Br J Cancer* (2000) 83:204–8. doi: 10.1054/bjoc.2000.1251

95. Chang AY, Dao T, Gejman RS, Jarvis CA, Scott A, Dubrovsky L, et al. A therapeutic T cell receptor mimic antibody targets tumor-associated PRAME peptide/HLA-I antigens. *J Clin Invest* (2017) 127:3557. doi: 10.1172/JCI96860

96. Maruta M, Ochi T, Tanimoto K, Asai H, Saitou T, Fujiwara H, et al. Direct comparison of target-reactivity and cross-reactivity induced by CAR- and BiTE-redirected T cells for the development of antibody-based T-cell therapy. *Sci Rep* (2019) 9:13293. doi: 10.1038/s41598-019-49834-2

97. Xu G, Luo Y, Wang H, Wang Y, Liu B, Wei J. Therapeutic bispecific antibodies against intracellular tumor antigens. *Cancer Lett* (2022) 538:215699. doi: 10.1016/j.canlet.2022.215699

98. Pankov D, Sjostrom L, Kalidindi T, SG L, Sjostrom K, Gardner R, et al. *In vivo* immuno-targeting of an extracellular epitope of membrane bound preferentially expressed antigen in melanoma (PRAME). *Oncotarget* (2017) 8:65917–31. doi: 10.18632/oncotarget.19579

99. Garrido F, Romero I, Aptsiauri N, Garcia-Lora AM. Generation of MHC class I diversity in primary tumors and selection of the malignant phenotype. *Int J Cancer* (2016) 138:271–80. doi: 10.1002/ijc.29375

100. Riley RS, June CH, Langer R, Mitchell MJ. Delivery technologies for cancer immunotherapy. *Nat Rev Drug Discovery* (2019) 18:175–96. doi: 10.1038/s41573-018-0006-z

101. Ziller MJ, Gu H, Muller F, Donaghey J, Tsai LT, Kohlbacher O, et al. Charting a dynamic DNA methylation landscape of the human genome. *Nature* (2013) 500:477–81. doi: 10.1038/nature12433

102. Chou J, Voong LN, Mortales CL, Towlerton AM, Pollack SM, Chen X, et al. Epigenetic modulation to enable antigen-specific T-cell therapy of colorectal cancer. *J Immunother* (2012) 35:131–41. doi: 10.1097/CJI.0b013e31824300c7

103. Weinert BT, Krishnadath KK, Milano F, Pedersen AW, Claesson MH, Zocca MB. Real-time PCR analysis of genes encoding tumor antigens in esophageal tumors and a cancer vaccine. *Cancer Immun* (2009) 9:9.

104. Schrump DS, Fischette MR, Nguyen DM, Zhao M, Li X, Kunst TF, et al. Phase I study of decitabine-mediated gene expression in patients with cancers involving the lungs, esophagus, or pleura. *Clin Cancer Res* (2006) 12:5777–85. doi: 10.1158/1078-0432.CCR-06-0669

105. Siebenkas C, Chiappinelli KB, Guzzetta AA, Sharma A, Jeschke J, Vatapalli R, et al. Inhibiting DNA methylation activates cancer testis antigens and expression of the antigen processing and presentation machinery in colon and ovarian cancer cells. *PloS One* (2017) 12:e179501. doi: 10.1371/journal.pone.0179501

106. Karbach J, Neumann A, Brand K, Wahle C, Siegel E, Maeurer M, et al. Phase I clinical trial of mixed bacterial vaccine (Coley's toxins) in patients with NY-ESO-1 expressing cancers: immunological effects and clinical activity. *Clin Cancer Res* (2012) 18:5449–59. doi: 10.1158/1078-0432.CCR-12-1116

107. Klein O, Davis ID, McArthur GA, Chen L, Haydon A, Parente P, et al. Low-dose cyclophosphamide enhances antigen-specific CD4(+) T cell responses to NY-ESO-1/ISCOMATRIX vaccine in patients with advanced melanoma. *Cancer Immunol Immunother* (2015) 64:507–18. doi: 10.1007/s00262-015-1656-x

108. Klar AS, Gopinadh J, Kleber S, Wadle A, Renner C. Treatment with 5-Aza-2'-Deoxycytidine induces expression of NY-ESO-1 and facilitates cytotoxic T lymphocyte-mediated tumor cell killing. *PloS One* (2015) 10:e139221. doi: 10.1371/journal.pone.0139221

109. Kim VM, Pan X, Soares KC, Azad NS, Ahuja N, Gamper CJ, et al. Neoantigen-based EpiGVAX vaccine initiates antitumor immunity in colorectal cancer. *JCI Insight* (2020) 5:e136368. doi: 10.1172/jci.insight.136368

frontiers | Frontiers in Immunology

TYPE Original Research
PUBLISHED 27 June 2023
DOI 10.3389/fimmu.2023.1182299

OPEN ACCESS

EDITED BY
Ganesan Ramamoorthi
Moffitt Cancer Center,
United States

REVIEWED BY
Zhaohui Jin,
Mayo Clinic, United States
Weiwei Xiao,
Sun Yat-sen University Cancer Center (SYSUCC), China
Wenjun Meng,
Sichuan University, China

*CORRESPONDENCE
Yunfeng Li
liyunfeng@kmmu.edu.cn
Xuan Zhang
1025415085@qq.com
Peirong Ding
dingpr@sysucc.org.cn

†These authors contributed equally to this work and share first authorship

RECEIVED 08 March 2023
ACCEPTED 13 June 2023
PUBLISHED 27 June 2023

CITATION
Yang R, Wu T, Yu J, Cai X, Li G, Li X, Huang W, Zhang Y, Wang Y, Yang X, Ren Y, Hu R, Feng Q, Ding P, Zhang X and Li YF (2023) Locally advanced rectal cancer with dMMR/MSI-H may be excused from surgery after neoadjuvant anti-PD-1 monotherapy: a multiple-center, cohort study. *Front. Immunol.* 14:1182299. doi: 10.3389/fimmu.2023.1182299

Locally advanced rectal cancer with dMMR/MSI-H may be excused from surgery after neoadjuvant anti-PD-1 monotherapy: a multiple-center, cohort study

Renfang Yang[1†], Tao Wu[1†], Jiehai Yu[2†], Xinyi Cai[1], Guoyu Li[1], Xiangshu Li[3], Weixin Huang[4], Ya Zhang[5], Yuqin Wang[6], Xudong Yang[1], Yongping Ren[1], Ruixi Hu[1], Qing Feng[1], Peirong Ding[2*], Xuan Zhang[1*] and Yunfeng Li[1*]

[1]Department of Colorectal Surgery, Yunnan Cancer Hospital, The Third Affiliated Hospital of Kunming Medical University, Kunming, China, [2]Department of Colorectal Surgery, Sun Yat-sen University Cancer Center, State Key Laboratory of Oncology in South China, Collaborative Innovation Center for Cancer Medicine, Guangzhou, China, [3]Department of Gastrointestinal Surgery, The First Affiliated Hospital of Chongqing Medical University, Chongqing, China, [4]Department of Gastrointestinal Surgery, Honghe Prefecture Third People's Hospital, Honghe Cancer Hospital, Gejiu, China, [5]Department of Imaging, Yunnan Cancer Hospital, The Third Affiliated Hospital of Kunming Medical University, Kunming, China, [6]Department of Pathology, Yunnan Cancer Hospital, The Third Affiliated Hospital of Kunming Medical University, Kunming, China

Objective: Examine patients with locally advanced rectal cancer (LARC) with deficient mismatch repair (dMMR) or microsatellite instability-high (MSI-H) who received neoadjuvant immunotherapy (nIT), and compare the outcomes of those who chose a watch-and-wait (WW) approach after achieving clinical complete response (cCR) or near-cCR with those who underwent surgery and were confirmed as pathological complete response (pCR).

Methods: LARC patients with dMMR/MSI-H who received nIT were retrospectively examined. The endpoints were 2-year overall survival (OS), 2-year disease-free survival (DFS), local recurrence (LR), and distant metastasis (DM). The efficacy of programmed cell death protein-1 (PD-1) inhibitor, immune-related adverse events (irAEs), surgery-related adverse events (srAEs), and enterostomy were also recorded.

Results: Twenty patients who received a PD-1 inhibitor as initial nIT were examined. Eighteen patients (90%) achieved complete response (CR) after a median of 7 nIT cycles, including 11 with pCR after surgery (pCR group), and 7 chose a WW strategy after evaluation as cCR or near-cCR (WW group). Both groups had median follow-up times of 25.0 months. Neither group had a case of LR or DM, and the 2-year DFS and OS in each group was 100%. The two groups had similar incidences of irAEs (P=0.627). In the pCR group, however, 2 patients (18.2%) had permanent colostomy, 3 (27.3%) had temporary ileostomy, and 2 (18.2%) had srAEs.

Conclusion: Neoadjuvant PD-1 blockade had high efficacy and led to a high rate of CR in LARC patients with dMMR/MSI-H. A WW strategy appears to be a safe and reliable option for these patients who achieve cCR or near-cCR after nIT.

KEYWORDS

locally advanced rectal cancer, neoadjuvant immunotherapy, programmed cell death protein-1 inhibitor, mismatch repair-deficient, clinical complete response, watch-and-wait strategy

Introduction

Colorectal cancer (CRC) is the most common malignancy of the digestive system, and global cancer statistics for 2020 indicated it had the third-highest incidence and the second-highest mortality rate among all cancers (1). About 60% of patients with CRC have locally advanced disease upon diagnosis (2), defined as CRC stage II (clinical T3–T4, N0) or stage III (any clinical T, N1–N2). Neoadjuvant fluorouracil-based chemotherapy and radiotherapy followed by total mesorectal excision (TME), with or without postoperative chemotherapy, is the standard treatment regimen for patients with locally advanced rectal cancer (LARC) (3, 4), and this regimen enables approximately 20% of these patients to achieve a pathological complete response (pCR) (5, 6). Nevertheless, the short- and long-term toxicities from this treatment, including defecation disorders, urinary and sexual dysfunction, surgical complications, and temporary or permanent enterostomy, can seriously reduce a patient's quality of life (7, 8). Data from a large number of studies have confirmed that adoption of a watch-and-wait (WW) strategy by patients with rectal cancer who achieved a clinical complete response (cCR) after neoadjuvant chemoradiotherapy (nCRT) prevented surgical trauma, preserved organ function, and provided a survival benefit similar to surgery (9, 10). Even for patients with near-cCR, a previous study demonstrated that more than half of them achieved organ preservation within 3 years after a WW strategy, and their local recurrence-free survival and metastasis-free survival rates were not significantly different from those who had cCR (11). However, with the increasing availability of neoadjuvant treatment options, it is uncertain whether patients with rectal cancer who achieve a cCR or near-cCR after treatment with other neoadjuvant modalities should also adopt a WW strategy.

There is evidence that CRC patients with deficient mismatch repair (dMMR) or microsatellite instability-high (MSI-H) receive little benefit from fluorouracil-based chemotherapy (12, 13). However, these patients typically have high sensitivity to immunotherapies, such as anti-program death-1 (PD-1) antibodies, and their responses are often long-lasting (14, 15). In addition, higher rates of pathological response were achieved when immune checkpoint inhibitors (ICIs) were used with the first-line or neoadjuvant application rather than at a later time (16–18). Although there is only no more than 10% of rectal cancers are classified as dMMR/MSI-H (19–21), a complete response (CR) rate more than 60% can be achieved from neoadjuvant immunotherapy (nIT), significantly higher than from nCRT (21–23). In addition, immunotherapy leads to fewer adverse effects and almost no damage to the sphincter, reproductive organs, sexual function, or bladder (21–23). These advantages of nIT suggest that LARC patients with dMMR/MSI-H who achieved a cCR or near-cCR after nIT might benefit from a WW strategy.

Current data regarding the effect of a WW strategy after nIT for CRC are very rare. As far as we know, this is the first study to compare the survival outcomes of MSI-H/dMMR LARC patients receiving nIT treatment who opted for a WW strategy after achieving a cCR or near-cCR with those who underwent surgery and confirmed as pCR. The present study is a preliminary evaluation of the safety and feasibility of the WW strategy after nIT in these patients using data from multiple centers.

Materials and methods

Patient selection

This study was a retrospective, multicenter, case series study. We reviewed patients with LARC (clinical stage T3–4/N0–2/M0) and dMMR/MSI-H who received a PD-1 inhibitor (no type limitations) alone as an initial neoadjuvant treatment from January 2019 to May 2020 at the Yunnan Cancer Hospital (Third Affiliated Hospital of Kunming Medical University), Sun Yat-sen University Cancer Center, First Affifiliated Hospital of Chongqing Medical University, or Honghe Cancer Hospital (Honghe Prefecture Third People's Hospital). All eligible patients were 18 to 75 years-old, had an Eastern Cooperative Oncology Group (ECOG) performance score of 0 to 1, and received 4 or more doses of a PD-1 inhibitor. The exclusion criteria were: suspected metastatic disease; dMMR based on immunohistochemical staining (IHC), but no evidence of MSI-H based polymerase chain reaction (PCR) testing or next-generation sequencing (NGS); active autoimmune disease or history of autoimmune disease or previous receipt of systemic biological immunotherapy.

Data collection

Standardized electronic forms were sent to physicians in each center. Complete demographic and clinicopathological information of patients were collected, including ECOG status, family and personal history of malignant tumors, serum carcinoembryonic antigen (CEA) level, clinical and pathological stage, pathological type of CRC, degree of differentiation, mismatch repair (MMR) or microsatellite status, treatment regimen, treatment response, tumor regression grade (TRG), immune-related adverse events (irAEs), surgery-related adverse events (srAEs), follow-up, and survival.

All staging was performed according to the eighth edition of the American Joint Committee on Cancer (AJCC) (24). MMR status was determined by IHC staining for mismatch repair proteins (MLH1, MSH2, MSH6, and PMS2) in biopsy tissues before treatment. Microsatellite status was determined by PCR or NGS technology. Among them, PCR was used as the "gold standard" to determine microsatellite status by analyzing the five consensus tumor microsatellite loci: two mononucleotides (*BAT25* and *BAT26*) and three dinucleotides (*D5S346*, *D2S123*, and *D17S250*), and NGS was recommended as a second-line method for microsatellite status detection (25). Studies have shown that the sensitivity and specificity of IHC for MMR or PCR for MSI were both above 90%, and the concordance between the two methods is approximately 90% (26, 27). In addition, NGS-based MSI testing results to be up to 99% concordant with conventional PCR and 92.4% concordant with double confirmed IHC staining (28).

Treatment methods

All eligible patients started neoadjuvant anti-PD-1 monotherapy after diagnosis, and none of them were treated with combined radiotherapy, chemotherapy, targeted therapy, or an additional ICI. Each patient received 200 mg of a PD-1 inhibitor by intravenous infusion every 3 weeks until tumor regression to feasible R0 resection, cCR, or near-cCR. There were no limits on the type of PD-1 inhibitors, and these included pembrolizumab, sintilimab, and tislelizumab.

The timing and procedure of the operation, need for adjuvant immunotherapy (aIT), and treatment course were determined by the head surgeon after a comprehensive evaluation of the patient's response to treatment and general condition. Patients who achieved a cCR or near-cCR after nIT were informed of the benefits and risks of the therapeutic alternatives, and most of them expressed a strong desire for the preservation of organ function and avoidance of enterostomy. Given the long-lasting response of immunotherapy and the inconsistency between imaging and pathological evaluation (for example, some patients with imaging evaluation of PR were pathologically confirmed as pCR in our previous study (22)), doctors agreed on their request for exemption from surgery. Before undergoing the WW strategy, they were informed that a WW strategy after cCR, especially after near-cCR following nIT is not currently a standard therapy and signed informed consent documents. All of them were vigilant about regular follow-up and adherence to the recommended surveillance, with consent for radical resection once the disease progresses.

Treatment response and survival outcomes

Response to treatment was assessed by magnetic resonance imaging (MRI) of the pelvic region, transrectal ultrasound (TRUS), enhanced CT examination of chest and abdomen, digital rectal examination (DRE), serum carcinoembryonic antigen (CEA), endoscopy, and selective biopsy of any residual mass or scar. The standard of efficacy evaluation was based on the Response Evaluation Criteria in Solid Tumors RECIST Version 1.1 (RECIST 1.1) (29). Because there is currently no unified international diagnostic standard for cCR and near-cCR, the standards in our study were based on the Sao Paulo criteria (30), the criteria in ESMO guidelines (4), and the Memorial Sloan Kettering Regression Schema (31), with fine-tuning according to the actual situation. The specific diagnostic criteria for cCR and near-cCR are in Supplementary Table S1.

The indicators of pathological efficacy after nIT were ypTNM stage and TRG. According to the AJCC system, TRG-0 refers to no residual tumor cells, TRG-1 refers to a single tumor cell or a small group of tumor cells, TRG-2 refers to residual cancer with desmoplastic response, and TRG-3 refers to minimal or no evidence of tumor response (24). The pCR was defined as tumor regression induced by neoadjuvant therapy, with no viable tumor cells in the resected primary tumor sample and all sampled regional lymph nodes (pCR = TRG-0 = ypT0N0M0) (24). Major pathological response (MPR) was considered to be tumor regression with 10% or less pathological residual tumor (MPR = TRG-0 + TRG-1) (24).

The primary survival outcomes were 2-year overall survival (OS), 2-year disease-free survival (DFS), local relapse (LR), and distant metastasis (DM). For DFS, the date of the last nIT treatment in the WW group and the date of surgery in the surgery group was the start date; the date of the last follow-up or the first recurrence, metastasis, or death from any cause was the termination date. OS was measured from the date of the first nIT treatment to the date of death. LR was defined as the presence of rectal adenocarcinoma inside the pelvis at the anastomosis site, presacral area, or pelvic lymph node. DM was defined by rectal adenocarcinoma recurrence that spread to an area or organ outside the pelvis (liver, lung, ovary, distant lymph node, etc.).

Treatment-related adverse events were also recorded. Immune-related adverse events (irAEs) refer to adverse events related to immunotherapy that occurred from the beginning of nIT until 90 days after the last dose of the PD-1 inhibitor, and were graded using the Common Terminology Criteria for Adverse Events (CTCAE) version 5.0 (32). Surgery-related adverse events (srAEs) refer to complications directly or indirectly related to surgery from the day of surgery to 30 days after surgery, and were graded using the Clavien-Dindo grading evaluation standard (33).

Follow-up methods

For patients who underwent TME, follow-up was performed according to international guidelines (3). For patients managed by the WW strategy, a more intensive follow-up protocol was used due to the lack of uniform standards. This follow-up consisted of measurements of serum CEA and DRE every 2 to 3 months during the first two years; T2-weighted and diffusion-weighted MRI of the pelvis, TRUS, and complete colonoscopy every 3 months during the first year, and every 6 months during the subsequent 4 years; and enhanced CT examination of chest and abdomen every 6 months. Biopsy was performed selectively to examine residual nodularity or scarring from the colonoscopy examination, and abnormalities were identified on the cross-sectional imaging. The duration of follow-up was calculated as the time from the last day of the last treatment (last nIT, or aIT, or surgery) until the event of interest or the last follow-up date.

Statistical analysis

Continuous numerical variables were presented as medians and ranges, and compared using an independent samples *t*-test. Categorical variables were presented as numbers and percentages, and compared using the Chi-square test or Fisher's exact test. Cumulative DFS, OS, LR, DM were presented using Kaplan-Meier curves, and the WW and pCR groups were compared using the Wilcoxon test. All statistical tests were two-sided, and results were considered statistically significant when the *P* value was less than 0.05. Statistical analyses were performed using the Statistical Package for the Social Sciences Program (SPSS Inc. Chicago, IL, version 26.0 for Mac).

Results

Characteristics of patients

We identified 20 LARC patients with dMMR/MSI-H who received nIT in one of the four participating institutions from January 2019 to May 2020 (Figure 1). Three patients who achieved cCR and 4 patients who achieved near-cCR were in the WW group and the other 13 patients received TME. Among the 13 patients who underwent TME surgery, 11 patients achieved pCR and were in the pCR group, the other 2 patients had TRG-1 and were excluded from the comparative analysis of LR, DM, 2-year DFS, and 2-year OS.

We compared the baseline demographic and clinicopathological characteristics of all 20 patients, the 11 patients in the pCR group, and the 7 patients in the WW group (Table 1). We also recorded the individual details of each patient in the TME group (Table 2) and the WW group (Table 3). Patients in the pCR and WW groups were similar in terms of age, gender, ECOG performance status, personal or family history of cancer, distance of tumor from the anal verge before nIT, cT stage, cN stage, cTNM stage, maximum diameter of the primary tumor on MRI, serum CEA level before nIT, anal complex invasion, mesorectal fascia invasion (MRF+), extramural vascular invasion (EMVI+), and degree of tissue differentiation (all $P > 0.05$). The median age of all 20 patients was 55 years old (range: 23–74), and the median distance of the tumor from the anal verge before nIT was 6.5 cm. Patients in the WW group were slightly older (55 *vs.* 44 years, $P = 0.347$) and had tumors that were located closer to the anal verge (5 *vs.* 7 cm, $P = 0.052$), although these differences were not significant.

Among all 20 patients, 7 had a family or personal history of malignancy. In the latter group, the 3 patients with a personal and family history of cancer and the 2 with only a family history of

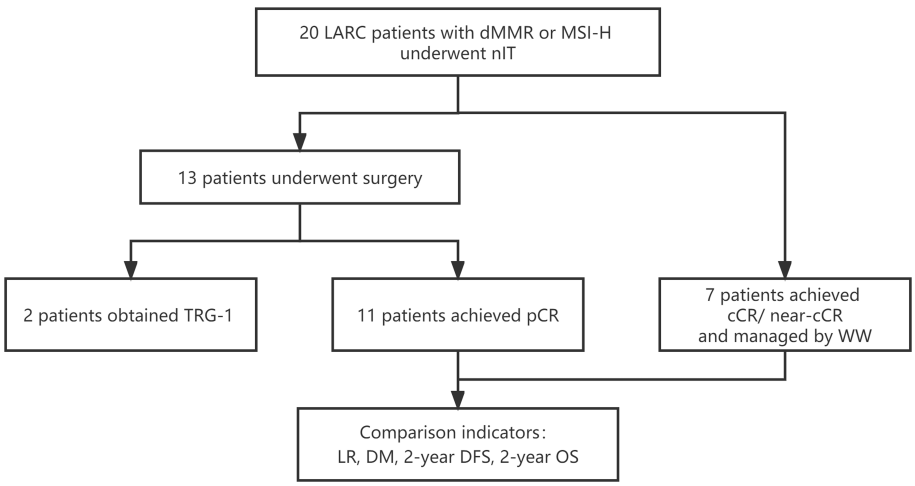

FIGURE 1
Study profile of nIT in LARC patients with dMMR/MSI-H. cCR, clinical complete response; DFS, disease-free survival; DM, distant metastasis; dMMR, mismatch repair-deficient; LARC, locally advanced rectal cancer; LR, local recurrence; MSI-H, microsatellite instability-high; nIT, neoadjuvant immunotherapy; near-cCR, near clinical complete response; OS, overall survival; pCR, pathological complete response; TRG, tumor regression grade; WW, watch-and-wait.

10.3389/fimmu.2023.1182299

TABLE 1 Baseline demographic and clinical characteristics of patients with dMMR/MSI-H LARC.

Characteristics	Total (n=20)	pCR group (n=11)	WW group (n=7)	P-Value
Age, years				0.347
Median (range)	55 (23–74)	44(23-69)	55(43-62)	
Sex				0.141
Female	7/20(35.0%)	2/11(18.2%)	4/7(57.1%)	
Male	13/20(65.0%)	9/11(81.8%)	3/7(42.9%)	
ECOG performance status				0.627
0	11/20(55.0%)	3/11(27.3%)	3/7(42.9%)	
1	9/20(45.0%)	8/11(72.7%)	4/7(57.1%)	
Personal or family history of cancer				
Personal history of gastrointestinal Cancer	2/20(10.0%)	0	2/7(28.6%)	0.263
Personal history of extra-intestinal cancer	2/20(10.0%)	1/11(9.1%)	1/7(14.3%)	
Family history of gastrointestinal Cancer	3/20(15.0%)	2/11(18.2%)	1/7(14.3%)	0.232
Family history of extra-intestinal cancer	3/20(15.0%)	0	2/7(28.6%)	
Distance from the anal verge before nIT (cm)				
Median (range)	6.5(1-15)	7(3-15)	5(1-8)	0.052
0-5 (including 5)	8/20(40.0%)	3/11(27.3%)	4/7(57.1%)	0.304
5-10 (including 10)	9/20(45.0%)	5/11(45.5%)	3/7(42.9%)	
10-15 (including 15)	3/20(15.0%)	3/11(27.3%)	0	
cT stage				0.627
T3	7/20(35.0%)	3/11(27.3%)	3/7(42.9%)	
T4	13/20(65.0%)	8/11(72.7%)	4/7(57.1%)	
cN stage				0.205
N0	6/20(30.0%)	2/11(18.2%)	2/7(28.6%)	
N1	4/20(20.0%)	1/11(9.1%)	3/7(42.9%)	
N2	10/20(50.0%)	8/11(72.7%)	2/7(28.6%)	
cTNM stage				>0.999
II	6/20(30.0%)	2/11(18.2%)	2/7(28.6%)	
III	14/20(70.0%)	9/11(81.8%)	5/7(71.4%)	
Anal sphincter complex				0.528
Involved	4/20(20.0%)	1/11(9.1%)	2/7(28.6%)	
Uninvolved	16/20(80.0%)	10/11(90.9%)	5/7(71.4%)	
MRF				0.627
Positive	8/20(40.0%)	3/11(27.3%)	3/7(42.9%)	
Negative	12/20(60.0%)	8/11(72.7%)	4/7(57.1%)	
EMVI				0.596
Positive	6/20(30.0%)	4/11(36.4%)	1/7(14.3%)	
Negative	14/20(70.0%)	7/11(63.6%)	6/7(85.7%)	

(Continued)

TABLE 1 Continued

Characteristics	Total (n=20)	pCR group (n=11)	WW group (n=7)	P-Value
LLNM				0.316
Yes	8/20(40.0%)	5/11(45.5%)	1/7(14.3%)	
No	12/20(60.0%)	6/11(54.5%)	6/7(85.7%)	
Maximum diameter of primary tumor on MRI before nIT (cm)				
Median (range)	5.5(2.5-15)	6.2(2.6-15)	4.5(2.5-6.9)	0.060
Serum CEA level before nIT (ug/L)				0.449
Median (range)	4.50 (1.07-272.10)	5.05 (2.42-272.10)	3.05 (1.07-48.56)	
Histological appearance				0.593
Well differentiated	7/20(35.0%)	5/11(45.5%)	2/7(28.6%)	
Moderately differentiated	5/20(25.0%)	2/11(18.2%)	3/7(42.9%)	
Poorly differentiated	8/20(40.0%)	4/11(36.4%)	2/7(28.6%)	
Loss of expression of MMR proteins				0.819
MLH1 only	2/20(10.0%)	1/11(9.1%)	1/7(14.3%)	
MSH2 only	3/20(15.0%)	2/11(18.2%)	1/7(14.3%)	
MSH6 only	0	0	0	
PMS2 only	1/20(5.0%)	0	1/7(14.3%)	
MLH1 and PMS2	4/20(20.0%)	2/11(18.2%)	0	
MSH2 and MSH6	3/20(15.0%)	2/11(18.2%)	1/7(14.3%)	
MSH2, MSH6 and PMS2	1/20(5.0%)	0	1/7(14.3%)	
Not tested	6/20(30.0%)	4/11(36.4%)	2/7(28.6%)	
MSI status				
MSI-H	10/20(50.0%)	6/11(54.5%)	4/7(57.1%)	
Not tested	10/20(50.0%)	5/11(45.5%)	3/7(42.9%)	
LS				0.596
Yes	2/20(10.0%)	1/11(9.1%)	1/7(14.3%)	
Suspected	3/20(15.0%)	1/11(9.1%)	2/7(28.6%)	
Unknown	15/20(75.0%)	9/11(81.8%)	4/7(57.1%)	
Types of PD-1 inhibitors				0.566
Tislelizumab	8/20(40.0%)	6/11(54.5%)	2/7(28.6%)	
Sintilimab	9/20(45.0%)	3/11(27.3%)	4/7(57.1%)	
Pembrolizumab	3/20(15.0%)	2/11(18.2%)	1/7(14.3%)	
Course of nIT				
Median (range)	6(4-10)	6(6-10)	8(6-10)	0.408
Efficacy evaluation after nIT				
cCR	3/20(15.0%)	0	3/7(42.9%)	
near-cCR	8/20(40.0%)	4/11(36.4%)	4/7(57.1%)	
PR	9/20(45.0%)	7/11(63.6%)	0	

(Continued)

TABLE 1 Continued

Characteristics	Total (n=20)	pCR group (n=11)	WW group (n=7)	P-Value
Percentage of primary tumor regression after nIT (%)				0.028
Median (range)	77.53 (40-100)	69.09 (40-100)	88.89 (77.27-100)	
Adjuvant immunotherapy (aIT)				
Yes	9/20(45.0%)	7/11(63.6%)	/	
No	4/20(20.0%)	4/11(36.4%)	/	
Course of immunotherapy (nIT+aIT)				0.527
Median (range)	8(6-12)	8(6-12)	8(6-10)	

aIT, adjuvant immunotherapy; cTNM: clinical tumor node metastasis; cCR, clinical complete response; CEA, carcinoembryonic antigen; CR, complete response; CRC, colorectal cancer; dMMR, mismatch repair-deficient; ECOG, eastern cooperative oncology group; EMVI, extramural vascular invasion; LARC, locally advanced rectal cancer; LLNM, lateral lymph node metastasis; MMR, mismatch repair; MRF, mesorectal fascia; MRI, magnetic resonance imaging; MSI-H, microsatellite instability-high; near-cCR, near clinical complete response; nIT, neoadjuvant immunotherapy; pCR, pathological complete response; PR, partial response; RECIST v1.1, response evaluation criteria in solid tumors version 1.1; WW, watch-and-wait.

gastrointestinal malignancy were suspected to have Lynch syndrome, but only 2 of them received tests for the relevant germline genes and had confirmed Lynch syndrome: patient III in the WW group (Table 3) and patient 1 in the pCR group (Table 3). Patient III in the WW group received surgery and chemotherapy for jejunal well-differentiated adenocarcinoma at the age of 30s and ovarian clear cell carcinoma at the age of 40s, and the mother of this patient died from ovarian cancer; genetic testing results indicated this patient had an exon 1 germline mutation in the *MLH1* gene. Patient 1 in the pCR group had a grandmother who died from gastric cancer, and the father of this patient had rectal cancer at the time of this study; genetic testing identified a germline mutation in exon 7 of *MSH2* gene.

Analysis of microsatellite status indicated 1 patient had MSI-H based on PCR, and 5 patients had MSI-H based on NGS. IHC results on pre-treatment tumor specimens in 10 patients confirmed dMMR status, and the remaining 4 patients had both dMMR (by IHC) and MSI-H (by NGS or PCR). Among the 14 patients identified as dMMR, one had losses of MSH2, MSH6, and PMS2; 4 had losses of MLH1 and PMS2; 3 had losses of MSH2 and MSH6; 2 had a loss of MLH1; 1 had a loss of PMS2; and 3 had a loss of MSH2. The pCR and WW groups had no statistically significant difference in MMR protein deletions ($P = 0.819$).

Efficacy of nIT with PD-1 inhibitors and adjuvant therapy

All 20 patients received PD-1 inhibitor monotherapy as the initial treatment (8 patients with tislelizumab, 9 with sintilimab, and 3 with pembrolizumab) and there were no significant differences in the type of drug used in the WW and the pCR groups (Table 1). After completing a median of 6 cycles (range: 4–10) of nIT, the objective response rate (ORR) was 100% (20/20), the cCR rate was 15% (3/20), the near-cCR rate was 40.0% (8/20), and the partial response (PR) rate was 45.0% (9/20) (Table 1). Representative MRI, endoscopic and pathological images of patients with dMMR/MSI-H LARC who achieved cCR and near-cCR after nIT are shown in Figures 2, 3.

The pCR and WW groups had no significant difference in the median number of cycles of nIT (6 *vs.* 8, $P = 0.408$), however, patients in the WW group exhibited greater radiographic regression in the primary lesion ($P = 0.028$; Table 1 and Figure 4). For all 20 patients, the WW group, and the pCR group, there was a median of 3 cycles of nIT (range: 2–6) from treatment initiation to PR, corresponding to 2.25 months (range: 1.5–4.5); and there was a median of 8 cycles of nIT (range: 6–10) needed to achieve cCR or near-cCR.

For the 13 patients who underwent TME after nIT (9 with PR, 1 with cCR, 3 with near-cCR), the ORR, pathological response rate, and MPR were all 100% (13/13), and the pCR was 84.6% (11/13). Typical images from MRI, post-nIT resection specimens, and pathologic response of patients with dMMR/MSI-H LARC who achieved a pCR are shown in Figure 5. The two patients who did not achieve pCR had TRG-1 and pathological stage of ypT1N0M0 (Table 4). Notably, 3 patients achieved a pCR after 6 to 10 cycles of nIT, despite their very large tumors (>10 cm) and very late clinical stage (cT4N2M0) (Table 2).

Adjuvant anti-PD-1 monotherapy was administered to 69.2% (9/13) of patients with surgery, including 7 patients with pCR and 2 with TRG-1. Most of them received 2 cycles, only 1 patient with TRG-1 who completed just 4 cycles of nIT received 4 cycles of aIT. None of the patients in the WW group continued to use PD-1 inhibitors after achieving cCR or near-cCR. There was a median of 8 cycles (6 months) of immunotherapy (nIT + aIT) in all 20 patients, in the pCR group, and in the WW group (Table 1).

Treatment-related adverse events and enterostomy

We evaluated treatment-related adverse events (including those related to immunotherapy and surgery) and enterostomy (Tables 2, 3). During the neoadjuvant and adjuvant phases, the incidence of

TABLE 2 Details of dMMR/MSI-H LARC patients treated with nIT and surgery.

Patient No. (Sex, Age, years)	cTNM stage,	MRF, EMVI	Distance from the anal verge (cm)	Personal or family history of cancer	LS	Loss of MMR protein expressions	MS	Maximum diameter of primary tumor on MRI pre- and post- nIT (cm)	Regimen of nIT	Courses of nIT	Serum CEA level pre- and post- nIT (ug/L)	Response on DRE	Response on endoscopic, and biopsy	Response on MRI, and TRUS	Response evaluation based on the RECIST v1.1	Surgical approach	ypTNM stage, TRG	Courses of aIT
1 (M, 23y)	cT4aN2M0	Positive, Positive	5	Yes	Yes	MSH2, MSH6	MSI-H	11.0, 3.4	Tislelizumab 200mg, q3w	10	8.82, 2.88	Scar	CR, Negative for tumor cell	PR, PR	PR	LAR with a temporary ileostomy	ypT0N0M0, 0	0
2 (M, 55y)	cT4aN2M0	Negative, Positive	2	No	Unknown	MLH1	MSI-H	7.2, 2.7	Tislelizumab 200mg, q3w	6	2.68, 3.43	Palpable tumor	PR, Not tested	PR, Not tested	PR	APR	ypT0N0M0, 0	0
3 (F, 37y)	cT4bN2M0	Negative, Negative	7	Yes	Suspected	Not tested	MSI-H	15.0, 2.0	Sintilimab 200mg, q3w	10	272.1, 2.88	Palpable tumor	PR, Negative for tumor cell	PR, PR	PR	AR	ypT0N0M0, 0	2
4 (M, 40y)	cT4bN2M0	Negative, Negative	14	No	Unknown	Not tested	MSI-H	6.2, 0	Sintilimab 200mg, q3w	10	6.08, 3.29	Scar	CR, Negative for tumor cell	CR, Not tested	cCR	AR	ypT0N0M0, 0	0
5 (M, 62y)	cT3N1M0	Negative, Negative	5	No	Unknown	Not tested	MSI-H	7.6, 0.9	Tislelizumab 200mg, q3w	8	5.05, 1.89	Scar	CR, Negative for tumor cell	near-CR, near-CR	near-cCR	LAR with a temporary ileostomy	ypT0N0M0, 0	2
6 (M, 35y)	cT4bN2M0	Negative, Negative	15	No	Unknown	MLH1, PMS2	Not tested	13.6, 1.1	Pembrolizumab 200mg, q3w	6	3.72, 2.17	Smooth mucosa	CR, Negative for tumor cell	near-cCR, Not tested	near-cCR	AR	ypT0N0M0, 0	2
7 (F, 44y)	cT4aN2M0	Positive, Negative	10	No	Unknown	MLH1, PMS2	Not tested	6.1, 2.3	Sintilimab 200mg, q3w	6	3.16, 0.91	Scar	CR, Negative for tumor cell	near-cCR, near-cCR	near-cCR	AR	ypT0N0M0, 0	2
8 (M, 67y)	cT4bN2M0	Negative, Negative	12	No	Unknown	MSH2, MSH6	Not tested	7.5, 3.7	Pembrolizumab 200mg, q3w	6	39.0, 1.76	Palpable tumor	PR, Not tested	PR, Not tested	PR	AR	ypT0N0M0, 0	0
9 (M, 69y)	cT4bN0M0	Negative, Positive	5	No	Unknown	Not tested	MSI-H	5.0, 1.3	Tislelizumab 200mg, q3w	6	28.02, 3.12	Palpable tumor	PR, Negative for tumor cell	PR, PR	PR	LAR with a temporary ileostomy	ypT0N0M0, 0	2
10 (M, 40y)	cT3N0M0	Negative, Negative	3	No	Unknown	MSH2	Not tested	3.0, 1.8	Tislelizumab 200mg, q3w	6	4.99, 4.6	Palpable tumor	PR, Negative for tumor cell	PR, PR	PR	APR	ypT0N0M0, 0	2
11 (M, 59y)	cT3N2M0	Positive, Positive	7	Yes	Unknown	MSH2	Not tested	5.7, 1.9	Tislelizumab 200mg, q3w	6	2.42, 0.71	Palpable tumor	PR, Negative for tumor cell	PR, PR	PR	AR	ypT0N0M0, 0	2

(Continued)

10.3389/fimmu.2023.1182299

10.3389/fimmu.2023.1182299

TABLE 2 Continued

Patient No. (Sex, Age, years)	cTNM stage,	MRF, EMVI	Distance from the anal verge (cm)	Personal or family history of cancer	LS	Loss of MMR protein expressions	MS	Maximum diameter of primary tumor on MRI pre- and post- nIT (cm)	Regimen of nIT	Courses of nIT	Serum CEA level pre- and post- nIT (ug/L)	Response on DRE	Response on endoscopic, and biopsy	Response on MRI, and TRUS	Response evaluation based on the RECIST V1.1	Surgical approach	ypTNM stage, TRG	Courses of aIT
① (M, 74y)	cT3N0M0	Positive, Positive	8	No	Unknown	MLH1, PMS2	Not tested	5.5, 2.8	Sintilimab 200mg, q3w	4	2.23, 1.57	Palpable tumor	PR, Negative for tumor cell	PR, PR	PR	AR	ypT1N0M0, I	4
② (F, 57y)	cT4bN0M0	Negative, Positive	10	Yes	Unknown	MLH1, PMS2	Not tested	9.2, 3.6	Sintilimab 200mg, q3w	6	4.00, 3.47	Palpable tumor	PR, Adenocarcinoma	PR, PR	PR	AR	ypT1N0M0, I	2

Patient No. 1-11, the patients in the pCR group; ①-②, the patients who did not achieved pCR.
aIT, adjuvant immunotherapy; AR, anterior resection; APR, abdominoperineal resection; cCR, clinical complete response; CEA, carcinoembryonic antigen; CR, complete response; dMMR, mismatch repair-deficient; DRE, digital rectal examination; EMVI, extramural vascular invasion; LAR, low anterior resection; LARC, locally advanced rectal cancer; LS, lynch syndrome; MMR, mismatch repair; MRF, mesorectal fascia; MRI, magnetic resonance imaging; MS, Microsatellite status; MSI-H, microsatellite instability-high; nIT, neoadjuvant immunotherapy; PR, partial response; RECIST v1.1, response evaluation criteria in solid tumors version 1.1; TNM, tumor Node Metastasis; TRG, tumor regression grade; TRUS, transrectal ultrasound; ypTNM stage, pathological tumor node metastasis staging after neoadjuvant therapy.

irAEs was 35.0% (7/20) for all 20 patients, 45.5% (4/11) in the pCR group, and 28.6% (2/7) in the WW group ($P = 0.627$). Most of the irAEs were grade 1, but one patient developed a grade 2 hypothyroidism that was significantly relieved by low-dose thyroxine supplementation. There were no grade 3 or higher irAEs (Table 5).

Among the 13 patients who received TME, the median time from the last nIT to surgery was 25 days (18–42), and none of these patients had a delay of surgery due to an irAE. All 13 of these patients achieved R0 resection: 2 (15.4%) received abdominoperineal resection (APR) and 11 (84.6%) received sphincter-saving surgery. In the latter group, 3 (23.1%) patients received low anterior resection (LAR) with a temporary ileostomy. There were srAEs in 3 (23.1%) of these patients: a grade 1 surgical incision with poor healing, a grade 1 postoperative anastomotic bleeding, and a grade 2 anastomotic leak. No patient experienced perioperative mortality or severe surgery-related morbidity requiring re-operation (Table 6).

Recurrence and survival outcomes

The median follow-up time was 24.35 months (range: 16.4–29.9) in all 20 patients, 24.5 months (range: 16.4–29.9) in the pCR group, and 25.0 months (range: 20.5–29.0) in the WW group (P = 0.633; Table 7). None of the 20 patients (including the 2 with TRG-1) experienced LR, DM, or death as of the last follow-up date (June 15, 2022). Thus, the pCR group and WW group had 2-year DFS rates and 2-year OS rates of 100%, and LR rates and DM rates of 0% (Table 7 and Figure 6). Remarkably, 4 patients who adopted a WW strategy after achieving near-cCR and did not continue anti-PD-1 therapy did not experience LR or DM, even though some of them had high-risk factors at baseline, such as EMVI+, MRF+, and T4 stage (Table 3).

Discussion

Our real-world study examined a multicenter cohort of LARC patients with dMMR/MSI-H who were treated with neoadjuvant PD-1 inhibitor monotherapy. During the 2-year follow-up period, 100% (7/7) of patients who were managed with a WW strategy after achieving a cCR or near-cCR had a comparable oncological safety profile as those who accepted TME surgery. More importantly, patients in the WW group did not experience a reduced quality of life associated with surgical complications, enterostomies, or deterioration of the bowel, urinary system, or sexual function. Moreover, in the WW group, the 4 patients with near-cCR achieved the same rate of organ sparing and oncological safety as the other 3 patients with cCR (Table 3), similar to the results of the OPERA study (11). Thus, for LARC patients with dMMR/MSI-H who achieve cCR or near-cCR after nIT, the WW strategy is a safe and beneficial option.

Previous studies indicated that the 2-year LR rate of LARC patients who achieved cCR and adopted a WW strategy after nCRT was 19 to 25% (9, 34). In our study, a WW approach, even for

TABLE 3 Details of dMMR/MSI-H LARC patients treated with nIT and WW strategy.

Patient No. (Sex, Age, years)	cTNM stage	MRF, EMVI,	Distance from the anal verge (cm)	Personal or family history of cancer	LS	Loss of MMR protein expression	MS	Maximum diameter of primary tumor on MRI pre- and post- nIT (cm)	Regimen of nIT	Courses of nIT before taking WW	Serum CEA level pre- and post- nIT (ug/L)	Response on DRE	Response on endoscopic, and biopsy	Response on rectal MRI, and TRUS	Response evaluated based on the RECIST v1.1
I (M, 58y)	cT4bN0M0	Negative, Negative	8	No	Unknown	MSH2, MSH6, PMS2	Not tested	8.1, 0	Sintilimab 200mg, q3w	10	8.8, 1.28	Scar	CR, Negative for tumor cell	CR, CR	cCR
II (M, 62y)	cT3N1M0	Positive, Negative	2	No	Unknown	Not tested	MSI-H	4.3, 0	Sintilimab 200mg, q3w	8	1.37, 0.86	Scar	CR, Negative for tumor cell	CR, CR	cCR
III (F, 50y)	cT4aN1M0	Negative, Negative	8	Yes	Yes	Not tested	MSI-H	2.7, 0	Tislelizumab 200mg, q3w	8	1.07, 1.03	Smooth mucosa	CR, Negative for tumor cell	CR, CR	cCR
IV (F, 61y)	cT3N1M0	Negative, Negative	1	No	Unknown	PMS2	Not tested	2.2, 0.5	Sintilimab 200mg, q3w	8	3.05, 1.94	Scar	CR, Negative for tumor cell	near-CR, CR	near-cCR
V (F, 55y)	cT3N0M0	Negative, Negative	6	Yes	Suspected	MSH2	MSI-H	6.1, 0.7	Pembrolizumab 200mg, q3w	6	1.47, 0.98	Scar	CR, Negative for tumor cell	near-CR, near-CR	near-cCR
VI (M, 43y)	cT4bN2M0	Positive, Positive	2	Yes	Suspected	MSH2, MSH6	MSI-H	9.4, 0.9	Tislelizumab 200mg, q3w	6	48.56, 0.74	Smooth mucosa	near-CR, Negative for tumor cell	near-CR, near-CR	near-cCR
VII (F, 50y)	cT4bN2M0	Positive, Negative	5	No	Unknown	MLH1	Not tested	4.5, 1.0	Sintilimab 200mg, q3w	10	7.00, 2.58	Scar	CR, Negative for tumor cell	near-CR, near-CR	near-cCR

cCR, clinical complete response; cTNM, clinical tumor node metastasis; CEA, carcinoembryonic antigen; CR, complete response; dMMR, mismatch repair-deficient; DRE, digital rectal examination; EMVI, extramural vascular invasion; LARC, locally advanced rectal cancer; LS, lynch syndrome; MMR, mismatch repair; MRF, mesorectal fascia; MRI, magnetic resonance imaging; MS, Microsatellite status; MSI-H, microsatellite instability-high; nIT, neoadjuvant immunotherapy; PR, partial response; RECIST v1.1, response evaluation criteria in solid tumors version 1.1; TRG, tumor regression grade; TRUS, transrectal ultrasound.

10.3389/fimmu.2023.1182299

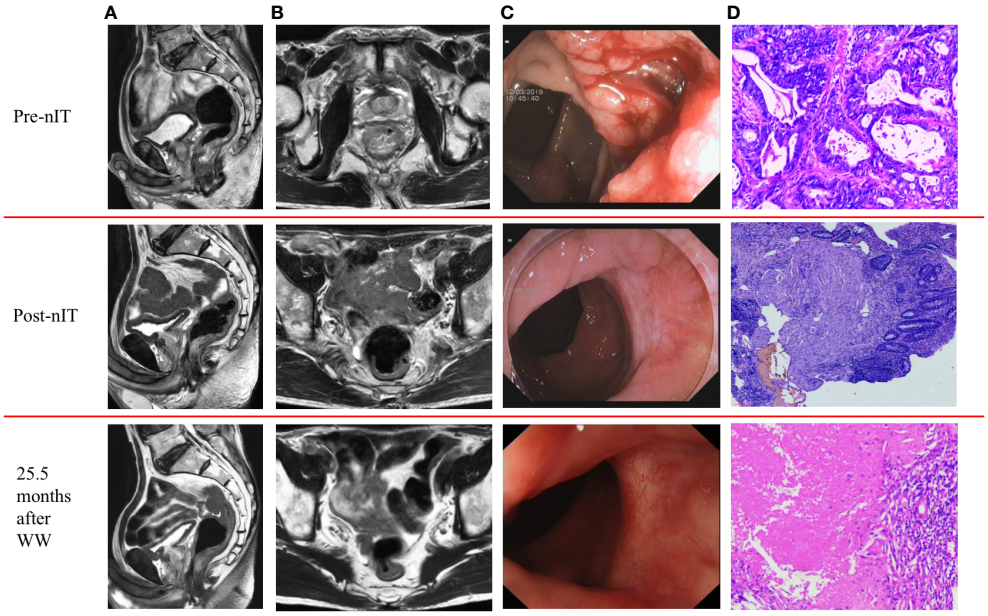

FIGURE 2
Representative radiologic, colonoscopic and pathological response to nIT in one patient with cCR (patient II in Table 3). **(A)** Sagittal plane MR views of the pelvis: pre-nIT VS post-nIT VS 25.5 months after WW; **(B)** Axial plane MR views of the pelvis: pre-nIT VS post-nIT VS 25.5 months after WW; **(C)** Colonoscopy: pre-nIT VS post-nIT VS 25.5 months after WW; **(D)** Pathology: tumor biospy of pre-nIT (HE x40) VS re-biospy of post-nIT (HE x40) VS re-biospy of 25.5 months after WW (HE x40). cCR, clinical complete response; HE, hematoxylin-eosin; MR, Magnetic resonance; nIT, neoadjuvant immunotherapy.

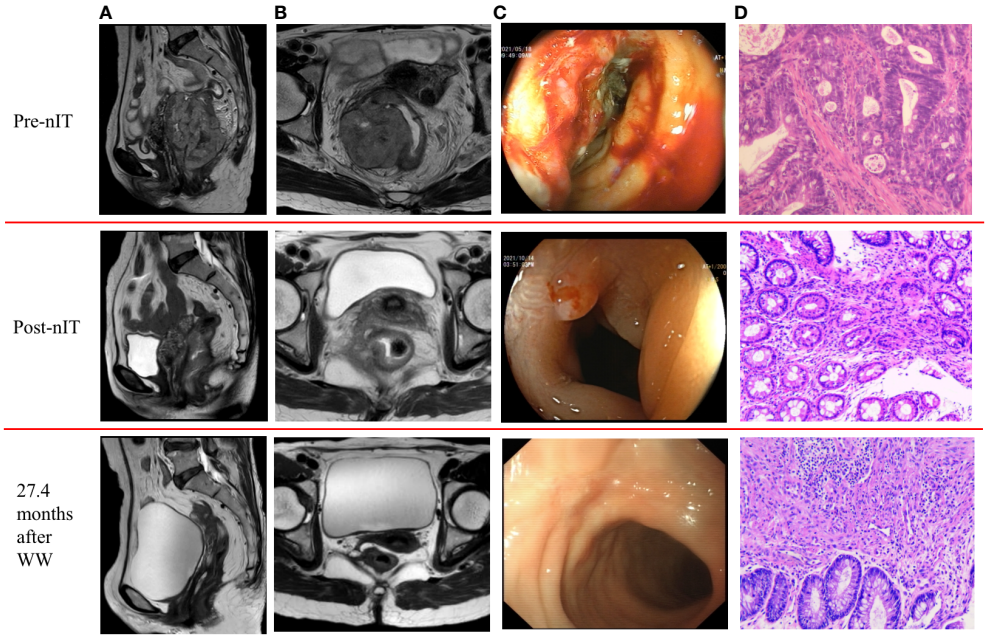

FIGURE 3
Representative radiologic, colonoscopic and pathological response to nIT in one patient with near-cCR (patient VI in Table 3). **(A)** Sagittal plane MR views of the pelvis: pre-nIT VS post-nIT VS 27.4 months after WW; **(B)** Axial plane MR views of the pelvis: pre-nIT VS post-nIT VS 27.4 months after WW; **(C)** Colonoscopy: pre-nIT VS post-nIT VS 27.4 months after WW; **(D)** Pathology: tumor biospy of pre-nIT (HE x40) VS re-biospy of post-nIT (HE x40) VS re-biospy of 27.4 months after WW (HE x40). HE, hematoxylin-eosin; MR, magnetic resonance; nIT, neoadjuvant immunotherapy;near-cCR, near clinical complete response.

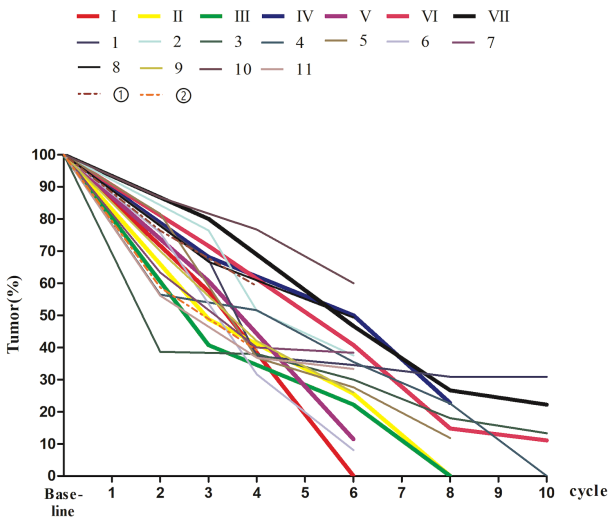

FIGURE 4
The percentage of tumor size on MRI at baseline and during nIT in 20 dMMR/MSI-H LARC patients. I-VII, the patients in the WW group; 1-11, the patients in the pCR group; ①-②, the patients who did not achieved pCR. dMMR, mismatch repair-deficient; LARC, locally advanced rectal cancer; MRI, magnetic resonance imaging; MSI-H, microsatellite instability-high; nIT, neoadjuvant immunotherapy; pCR, pathological complete response; WW, watch-and-wait.

patients with near-cCR or high-risk factors for LR and DM (EMVI +, MRF+, or T4 stage), led to a 2-year LR rate and DM rate of 0%. This remarkable efficacy may be because the nIT can convert the high level of tumor antigens produced by the primary tumor with dMMR/MSI-H into "autologous vaccines", which activate and recruit more tumor-specific T cells and promote the formation of long-term immune memory, rather than simply killing tumor cells. This kind of systemic and persistent immunity against tumors enables greater clearance of micrometastases that cannot be eliminated by surgery or radiotherapy and reduces the rate of LR and DM (35–37).

The WW strategy described herein is indeed promising, but accurate assessment of cCR and near-cCR remains a difficult problem. Due to the lack of more sensitive assessment methods, we used the same diagnostic criteria for cCR and near-cCR as used in patients after traditional nCRT. However, the mechanism of action and response of immunotherapy are markedly different from those of conventional therapy with cytotoxic drugs and radiation (38). These could lead to inconsistent clinical and pathological evaluations, as indicated by an underestimated efficacy of immunotherapy based on imaging. In this study, although the imaging results demonstrated that the 3 patients with near-cCR

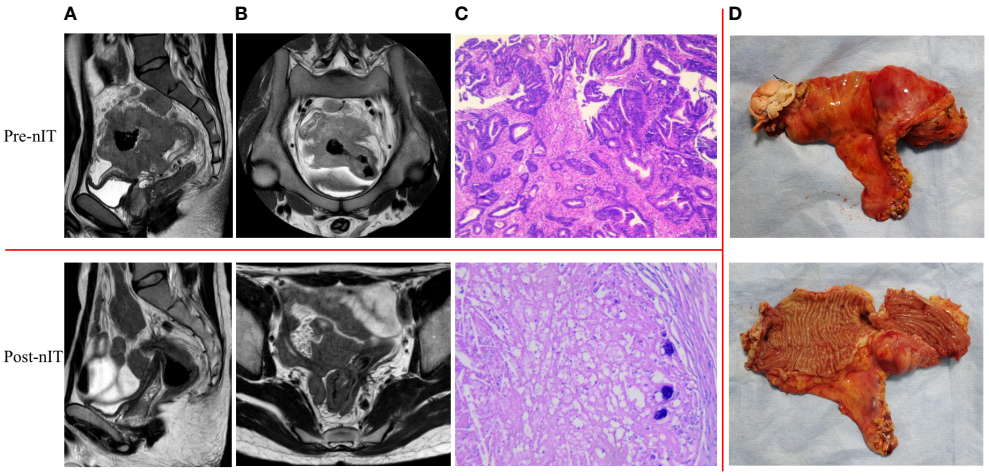

FIGURE 5
Representative radiologic, resection specimen and pathological response to nIT in one patient with pCR (patient 1 in Table 2). **(A)** Sagittal plane MR views of the pelvis: pre- VS post- nIT; **(B)** Axial plane MR views of the pelvis: pre- VS post- nIT; **(C)** Pathology: tumor biospy of pre-nIT (HE x40) VS postoperative specimen of post-nIT (HE x40); **(D)** Specimen: Resection specimen of post-nIT. HE, hematoxylin-eosin; MR, magnetic resonance; nIT, neoadjuvant immunotherapy; pCR, pathological complete response.

TABLE 4 Pathological outcomes of dMMR/MSI-H LARC patients treated with nIT and surgery.

Outcomes	nIT and surgery group (n=13)
ORR	13/13 (100%)
Pathological response rate	13/13 (100%)
MPR rate	13/13 (100%)
pCR rate	11/13(84.6%)
TRG	
0	11/13(84.6%)
1	2/13(15.4%)
2	0
3	0
Pathological T stage	
ypT0	11/13(84.6%)
ypT1	2/13(15.4%)
ypT2	0
ypT3	0
Pathological N stage	
ypN0	13/13 (100%)
ypN1	0
Pathological TNM stage	
ypT0N0M0	11/13(84.6%)
ypT1N0M0-I	2/13(15.4%)
ypT2N0M0-I	0
ypT3N0M0-IIA	0

dMMR, mismatch repair-deficient; LARC, locally advanced rectal cancer; MPR, major pathological response; MSI-H, microsatellite instability-high; nIT, neoadjuvant immunotherapy; ORR, objective response rate; pCR, pathological complete response; TNM, tumor Node Metastasis; TRG, tumor regression grade.

and the 7 patients with PR in the pCR group still had residual mass, the pathology results revealed that none of their surgical resection specimens had residual tumor cells, but instead consisted of massive inflammatory cells or mucus lakes (Table 2). The recent PICC study found that 28 of 35 patients who were evaluated as PR preoperatively had pCR based on postoperative pathology (23). This inconsistency also occurred in studies of nIT for other solid malignancies (39, 40). A possible explanation is that radiology cannot easily distinguish masses consisting of inflammatory cells, necrotic tissue, and/or fibrous tissues from masses consisting of tumor cells. This issue appears to challenge the routine use of established morphological-based response evaluation criteria.

Fortunately, tests other than conventional imaging examinations have gradually been used for efficacy evaluation in patients with malignancy. For example, ^{18}F-fluorodeoxyglucose-positron emission computed tomography (^{18}F-FDG-PET/CT), a valuable tool that combines anatomic morphologic imaging with functional metabolic imaging, can help to distinguish malignant and non-malignant masses. Goldfarb et al. first proposed the immune PET response criteria in solid tumors (iPERCIST) in 2019. They reported that this criterion could compensate for about 39% of the response underestimated by the RECIST 1.1 criteria in non-small cell lung cancer patients who received ICIs (41). In the 2022 study of Cercek et al., 12 rectal cancer patients with dMMR/MSI-H who were evaluated as cCR by traditional anatomical imaging combined with ^{18}F-FDG-PET/CT after 6 months of neoadjuvant dostarlimab treatment and adopted a WW strategy did not develop recurrence during the 6 to 25-month follow-up period (21). In addition, other studies found that changes in the level of circulating tumor DNA (ctDNA) could be used to predict response to immunotherapy (42, 43). Bratman et al. reported a 100% OS rate of patients with solid tumors who had ctDNA elimination after pembrolizumab treatment during a median follow-up time of 25.4 months (43). Hence, a regimen that combines radiological, metabolic, and hematological parameters might improve the accuracy of the efficacy evaluations of immunotherapy, and this could facilitate early identification of patients who would benefit most from a WW strategy and prevent over-treatment.

Furthermore, an underestimation of the efficacy of immunotherapy from imaging suggests that rectal cancer patients with dMMR/MSI-H who were treated with ICIs may have achieved pCR before being evaluated as near-cCR, cCR, or even PR. Another consideration is that patients who receive immunotherapy have unique remission patterns, such as delayed response, pseudo-progression (38), and long-lasting efficacy. We therefore suggest that LARC patients who are considering a WW strategy after nIT — even if imaging does not yet indicate cCR — should be offered the option of more time for observations or more cycles of ICIs followed by re-evaluation, rather than early surgical resection. Transanal local tumor resection, another organ-sparing option, may be preferred to proctectomy for rectal cancer patients who have a persistent clinical stage of ycT1N0M0 after nIT.

In terms of optimal efficacy, our results demonstrated a 90% CR rate (55% pCR, 15% cCR, and 20% near-cCR) was achieved after 6 cycles (range 4–10) of a neoadjuvant PD-1 inhibitor. This is better than reported in the NICHE study (17), the NICHE-2 study (18), and the PICC study (23), but worse than in the study of Cercek et al. (21). We believe that these differences in efficacy can be partly explained by differences in the dose and duration of the ICIs. In particular, the NICHE study and NICHE-2 study reported pCR rates of dMMR/MSI-H colon cancer patients were 69% and 67% after one dose of ipilimumab (1 mg/kg on day 1) and two doses of nivolumab (3 mg/kg on days 1 and 15). The PICC study reported the pCR rate in LARC patients with dMMR/MSI-H after 6 cycles of toripalimab (3 mg/kg) was 88% with celecoxib and 65% without celecoxib. However, the Cercek et al. study of LARC patients with dMMR/MSI-H reported the cCR rate was 100% after neoadjuvant treatment with 9 cycles of dostarlimab (500 mg every 3 weeks for 6 months).

Another consideration is that these previous studies examined tumors at different sites. The Cercek et al. (21). study and our study examined LARC patients and achieved CR rates of 90% or more; this is higher than in the NICHE study (17) and the NICHE-2 study (18), which examined patients with colon cancer. The PICC study reported a slightly higher pCR rate in rectal cancer patients

10.3389/fimmu.2023.1182299

TABLE 5 Immune-related adverse events (irAEs) of patients with dMMR/MSI-H LARC.

Adverse events	Total (n=20)			pCR group (n=11)			WW group (n=7)		
	Grade 1	Grade 2	Grade≧3	Grade 1	Grade 2	Grade≧3	Grade 1	Grade 2	Grade≧3
irAEs									
Pneumonia	1	0	0	0	1	0	0	0	0
Hypothyroidism	0	1	0	0	0	0	0	1	0
Nausea	1	0	0	1	0	0	0	0	0
Fatigue	1	0	0	0	0	0	0	0	0
Neutropenia	1	0	0	1	0	0	0	0	0
Pruritus or rash	1	0	0	1	0	0	0	0	0
Decreased appetite	1	0	0	0	0	0	1	0	0
Bowel obstruction	0	1	0	0	1	0	0	0	0
Total	6/20 (30.0%)	2/20 (10.0%)	0	3/11 (27.3%)	2/11 (18.2%)	0	1/7 (14.3%)	1/7 (14.3%)	0
	8/20(40.0%)			4/11(45.5%)			2/7 (28.6%)		
P-value				P=0.627					

dMMR, mismatch repair-deficient; irAEs; immune-related adverse events; LARC, locally advanced rectal cancer; MSI-H, microsatellite instability-high; pCR, pathological complete response; WW, watch-and-wait.

(83.33%) than in colon cancer patients (78.57%) (23), and Liu et al. reported similar results (pCR rate, rectal cancer: 100%, colon cancer: 50%) (44). These differences in efficacy suggest that rectal cancer patients with dMMR/MSI-H appear to benefit more from nIT than colon cancer patients with dMMR/MSI-H. There is also evidence of differences in the distribution of gut microbiota in different parts of the colorectum. In particular, rectal cancer patients have significantly more diverse gut microbiota than colon cancer patients (45, 46). Furthermore, several gut microbes can affect the efficacy of ICIs (39, 47), such as *Fusobacterium nucleatum*, which induces various immune responses in CRCs with distinct microsatellite states, and can enhance the efficacy of ICIs (48, 49).

However, LARC patients with dMMR/MSI-H achieved a 75% CR rate (lower than our study) after a median of 8 cycles of nIT with sintilimab (higher than our study), and a case of primary resistance to ICIs was reported in a recent study (50). It indicates that factors other than those mentioned above influence patient efficacy, among which tumor mutation burden (TMB), gene status and immune microenvironment are several research hotspots. For instance, dMMR/MSI-H CRC patients with low TMB, immunosuppressive tumor microenvironment, or mutation in the PTEN gene or PIK3CA gene are resistant to ICIs (51, 52), while pMMR/MSS CRC patients with a mutation in POLE or POLD1 gene are sensitive to ICIs (53). Therefore, despite nIT being highly effective for CRC patients with

TABLE 6 Surgical-related adverse events (srAEs) and enterostomy of patients with dMMR/MSI-H LARC ungerwent surgery.

Adverse events	Total (n=13)			pCR group (n=11)		
	Grade 1	Grade 2	Grade≧3	Grade 1	Grade 2	Grade≧3
srAEs						
Incision infection	1	0	0	1	0	0
Postoperative bleeding	1	0	0	0	0	0
Anastomotic leakage	0	1	0	0	1	0
Total	2/13 (15.4%)	1/13 (7.7%)	0	1/11 (9.1%)	1/11 (9.1%)	0
	3/13 (23.1%)			2/11 (18.2%)		
Enterostomy						
Temporary ileostomy	3/13 (23.1%)			3/11 (27.3%)		
Permanent colostomy	2/13 (15.4%)			2/11 (18.2%)		

dMMR, mismatch repair-deficient; LARC, locally advanced rectal cancer; MSI-H, microsatellite instability-high; pCR, pathological complete response; srAEs, surgical-related adverse events.

TABLE 7 Recurrence and survival in dMMR/MSI-H LARC patients with nIT.

Recurrence or survival	Total (n=20)	pCR group (n=11)	WW group (n=7)	P-Value
LR	0	0	0	>0.999
DM	0	0	0	>0.999
2-year DFS	20/20(100%)	11/11(100%)	7/7(100%)	>0.999
2-year OS	20/20(100%)	11/11(100%)	7/7(100%)	>0.999
Median Follow-up (months)	24.35 (16.4-29.9)	24.50 (16.4-29.9)	25.00 (20.5-29.0)	0.633

DFS, disease-free survival; DM, distant metastasis; dMMR, mismatch repair-deficient; LARC, locally advanced rectal cancer; LR, local recurrence; MSI-H, microsatellite instability-high; nIT, neoadjuvant immunotherapy; OS, overall survival; pCR, pathological complete response; WW, watch-and-wait.

dMMR/MSI-H, the inclusion of the analysis of the molecular profile as well as the immune contexture remains imperative.

It is currently uncertain whether continuous ICI treatment is required for CRC patients who achieve a cCR or pCR after nIT. In the NICHE study (17) and the NICHE-2 study (18), aIT was not offered to 69% (22/32) and 67% (72/107) of dMMR colon cancer patients who achieved pCR. The 12 LARC patients with dMMR/MSI-H in the study of Cercek et al. (21). who achieved a cCR also did not continue ICI treatment after adopting a WW strategy. Notably, patients in all three previous studies who attained pCR or cCR did not develop LR or DM during the follow-up period (median: 25 months for NICHE, 13 months for NICHE-2, and 12 months for Cercek et al.). However, the PICC study recommended adjuvant use of toripalimab with or without celecoxib for all patients, regardless of whether they attained pCR, until completion of 6 months of perioperative anti-PD-1 therapy (23). In our study, the median time from treatment initiation to CR was 5.25 months (range 4.5–7.5), the median time of the entire perioperative period was 6 months (range 4.5–9.0), and we observed no recurrence or metastasis during the 2-year follow-up. The value of aIT is currently unknown, indicating the need for large prospective studies.

Several studies reported that ctDNA is associated with an increased risk of recurrence (54, 55). This ctDNA reflects minimal residual disease (MRD), which is responsible for the most postoperative recurrences (56). Henriksen et al. studied patients with stage III colon cancer and compared ctDNA-negative and ctDNA-positive patients after surgery and adjuvant chemotherapy. They found a 7-fold increased risk of recurrence for patients who were ctDNA-positive after surgery and a 50-fold increased risk of recurrence for patients who were ctDNA-positive after adjuvant therapy, while patients with continuous

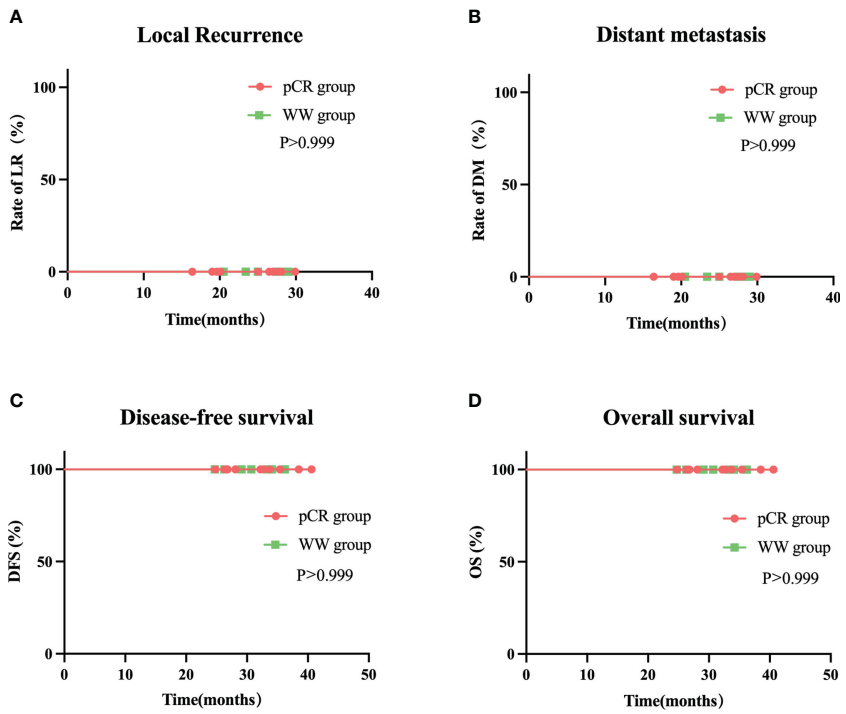

FIGURE 6
Rate of local recurrence **(A)** distant metastasis **(B)** disease-free survival **(C)** and overall survival **(D)** in WW group and pCR group during follow-up.

negative ctDNA during and after adjuvant therapy had no recurrence (57). Therefore, a ctDNA-based MRD assay may help to identify patients with high risk of relapse, and provide more personalized suggestions for adjuvant treatment and surveillance (54, 57). Three ongoing prospective clinical studies (NCT04761783; NCT05198154; NCT04636047) are examining the use of ctDNA-based MRD assays for guiding immunotherapy.

Finally, nIT for LARC is still in its infancy, and there is no unified standard regarding the therapeutic dose, course, efficacy evaluation criteria, or the need for aIT. Although outcomes appear promising, this study was limited by its retrospective design, small sample size, and short follow-up time. Firstly, a WW strategy after obtaining cCR or near-cCR following nIT is not currently a standard therapy, and the decision to circumvent proctectomy was mostly driven by an individual patient's strong desire for preservation of organ function and avoidance of enterostomy. This is why there were only 7 cases in our WW group. Secondly, the median follow-up time of our study was only 24.35 months. However, this was the longest follow-up time of any study that examined the WW strategy after nIT. In addition, due to economic and other reasons, only two patients in our study had a detection of germline genes and confirmed a diagnosis of Lynch syndrome. Given the familial heritability of Lynch syndrome and the potential for multiple primary malignancies, we will continue to encourage subjects who are young or suspected of Lynch syndrome to perform germline genetic testing for better long-term management and follow-up.

Conclusions

In conclusion, our study verified the feasibility and safety of a WW strategy for LARC patients with dMMR/MSI-H who achieved cCR or near-cCR after nIT. Our results suggest that a WW strategy for these patients could help to preserve sphincter function and improve long-term survival. Longer follow-up studies and prospective trials are needed to evaluate this promising treatment option.

Data availability statement

All datasets supporting the conclusions of this article are included within the article and its Supplementary files.The datasets used during the current study are available from the corresponding author on reasonable request.

Ethics statement

This retrospective study was conducted according to the Declaration of Helsinki, and approved to waive informed patient consent by the ethics review boards of the Yunnan Cancer Hospital (Third Affiliated Hospital of Kunming Medical University) (approval number KYLX2022053) because it was an observational and non-interventional study.

Author contributions

Drafting the work and/or revising it critically: RY, TW and JY. Final approval of the version to be published: PD, XZ, YL, and RY. All authors contributed to the article and approved the submitted version.

Funding

This study was supported by the Scientific Research Fund of Yunnan Provincial Education Department (2022J0227 to XZ), and the Joint Special Funds for the Department of Science and Technology of Yunnan Province-Kunming Medical University (202201AY070001-149 to XZ).

Acknowledgments

We thank the patients and families who made this study possible, clinical study teams, and Medjaden Inc. All authors made efforts and contributions to this article. Writing and editorial assistance were provided by Medjaden Inc.

Conflict of interest

The remaining authors declare that the research was conducted in the absence of any commercial or financial relationships that could be construed as a potential conflict of interest.

The reviewer WX declared a shared affiliation with the authors JY and PD to the handling editor at the time of review.

Publisher's note

Supplementary material

The Supplementary Material for this article can be found online at: https://www.frontiersin.org/articles/10.3389/fimmu.2023.1182299/full#supplementary-material

References

1. Sung H, Ferlay J, Siegel RL, Laversanne M, Soerjomataram I, Jemal A, et al. Global cancer statistics 2020: GLOBOCAN estimates of incidence and mortality worldwide for 36 cancers in 185 countries. *CA Cancer J Clin* (2021) 71(3):209–49. doi: 10.3322/caac.21660

2. Shi JF, Wang L, Ran JC, Wang H, Liu CC, Zhang HZ, et al. Clinical characteristics, medical service utilization, and expenditure for colorectal cancer in China, 2005 to 2014: overall design and results from a multicenter retrospective epidemiologic survey. *Cancer* (2021) 127(11):1880–93. doi: 10.1002/cncr.33445

3. Benson AB, Venook AP, Al-Hawary MM, Azad N, Chen YJ, Ciombor KK, et al. Rectal cancer, version 2.2022, NCCN clinical practice guidelines in oncology. *J Natl Compr Canc Netw* (2022) 20(10):1139–67. doi: 10.6004/jnccn.2022.0051

4. Glynne-Jones R, Wyrwicz L, Tiret E, Brown G, Rödel C , Cervantes A, et al. Rectal cancer: ESMO clinical practice guidelines for diagnosis, treatment and follow-up. *Ann Oncol* (2018) 29(Suppl 4):iv263. doi: 10.1093/annonc/mdy161

5. Chua YJ, Barbachano Y, Cunningham D, Oates JR, Brown G, Wotherspoon A, et al. Neoadjuvant capecitabine and oxaliplatin before chemoradiotherapy and total mesorectal excision in MRI-defined poor-risk rectal cancer: a phase 2 trial. *Lancet Oncol* (2010) 11(3):241–8. doi: 10.1016/S1470-2045(09)70381-X

6. Wilkins S, Haydon A, Porter I, Oliva K, Staples M, Carne P, et al. Complete pathological response after neoadjuvant long-course chemoradiotherapy for rectal cancer and its relationship to the degree of T3 mesorectal invasion. *Dis Colon Rectum* (2016) 59(5):361–8. doi: 10.1097/DCR.0000000000000564

7. Wallner C, Lange MM, Bonsing BA, Maas CP, Wallace CN, Dabhoiwala NF, et al. Causes of fecal and urinary incontinence after total mesorectal excision for rectal cancer based on cadaveric surgery: a study from the cooperative clinical investigators of the Dutch total mesorectal excision trial. *J Clin Oncol* (2008) 26(27):4466–72. doi: 10.1200/JCO.2008.17.3062

8. Hendren SK, O'Connor BI, Liu M, Asano T, Cohen Z, Swallow CJ, et al. Prevalence of male and female sexual dysfunction is high following surgery for rectal cancer. *Ann Surg* (2005) 242(2):212–23. doi: 10.1097/01.sla.0000171299.43954.ce

9. Smith JJ, Strombom P, Chow OS, Roxburgh CS, Lynn P, Eaton A, et al. Assessment of a watch-and-Wait strategy for rectal cancer in patients with a complete response after neoadjuvant therapy. *JAMA Oncol* (2019) 5(4):e185896. doi: 10.1001/jamaoncol.2018.5896

10. Maas M, Beets-Tan RG, Lambregts DM, Lammering G, Nelemans PJ, Engelen SM, et al. Wait-and-see policy for clinical complete responders after chemoradiation for rectal cancer. *J Clin Oncol* (2011) 29(35):4633–40. doi: 10.1200/JCO.2011.37.7176

11. Myint AS, Thamphya B, Gerard J-P. Does non-TME surgery of rectal cancer compromise the chance of cure? preliminary surgical salvage data from OPERA phase III randomized trial. *J Clin Oncol* (2021) 39(3_suppl):12–. doi: 10.1200/JCO.2021.39.3_suppl.12

12. Sargent DJ, Marsoni S, Monges G, Thibodeau SN, Labianca R, Hamilton SR, et al. Defective mismatch repair as a predictive marker for lack of efficacy of fluorouracil-based adjuvant therapy in colon cancer. *J Clin Oncol* (2010) 28(20):3219–26. doi: 10.1200/JCO.2009.27.1825

13. Seligmann JF, Group FC. FOxTROT: neoadjuvant FOLFOX chemotherapy with or without panitumumab (Pan) for patients (pts) with locally advanced colon cancer (CC). *J Clin Oncol* (2020) 38(15_suppl):4013–. doi: 10.1200/JCO.2020.38.15_suppl.4013

14. Le DT, Uram JN, Wang H, Bartlett BR, Kemberling H, Eyring AD, et al. PD-1 blockade in tumors with mismatch-repair deficiency. *N Engl J Med* (2015) 372(26):2509–20. doi: 10.1056/NEJMoa1500596

15. Maio M, Ascierto PA, Manzyuk L, Motola-Kuba D, Penel N, Cassier PA, et al. Pembrolizumab in microsatellite instability high or mismatch repair deficient cancers: updated analysis from the phase II KEYNOTE-158 study. *Ann Oncol* (2022) 33(9):929–38. doi: 10.1016/j.annonc.2022.05.519

16. Diaz LAJr., Shiu KK, Kim TW, Jensen BV, Jensen LH, Punt C, et al. Pembrolizumab versus chemotherapy for microsatellite instability-high or mismatch repair-deficient metastatic colorectal cancer (KEYNOTE-177): final analysis of a randomised, open-label, phase 3 study. *Lancet Oncol* (2022) 23(5):659–70. doi: 10.1016/S1470-2045(22)00197-8

17. Verschoor YL, Jvd B, Beets G, Sikorska K, Aalbers A, Av L, et al. Neoadjuvant. nivolumab, ipilimumab, and celecoxib in MMR-proficient and MMR-deficient colon cancers: final clinical analysis of the NICHE study. *J Clin Oncol* (2022) 40(16_suppl):3511–. doi: 10.1200/JCO.2022.40.16_suppl.3511

18. Chalabi M, Verschoor YL, van den Berg J, Sikorska K. Neoadjuvant immune checkpoint. inhibition in locally advanced MMR-deficient colon cancer: the NICHE-2 study [abstract]. *Ann Oncol* (2022) 33(suppl_7):Abstract LBA7. doi: 10.1016/j.annonc.2022.08.016

19. Papke DJJr., Yurgelun MB, Noffsinger AE, Turner KO, Genta RM, Redston M. Prevalence of mismatch-repair deficiency in rectal adenocarcinomas. *N Engl J Med* (2022) 387(18):1714–6. doi: 10.1056/NEJMc2210175

20. Ye SB, Cheng YK, Zhang L, Zou YF, Chen P, Deng YH, et al. Association of mismatch. repair status with survival and response to neoadjuvant chemo(radio)therapy in rectal cancer. *NPJ Precis Oncol* (2020) 4:26. doi: 10.1038/s41698-020-00132-5

21. Cercek A, Lumish M, Sinopoli J, Weiss J, Shia J, Lamendola-Essel M, et al. PD-1. blockade in mismatch repair-deficient, locally advanced rectal cancer. *N Engl J Med* (2022) 386(25):2363–76. doi: 10.1056/NEJMoa2201445

22. Zhang X, Yang R, Wu T, Cai X, Li G, Yu K, et al. Efficacy and safety of neoadjuvant monoimmunotherapy with PD-1 inhibitor for dMMR/MSI-H locally advanced colorectal cancer: a single-center real-world study. *Front Immunol* (2022) 13:913483. doi: 10.3389/fimmu.2022.913483

23. Hu H, Kang L, Zhang J, Wu Z, Wang H, Huang M, et al. Neoadjuvant PD-1 blockade with toripalimab, with or without celecoxib, in mismatch repair-deficient or microsatellite instability-high, locally advanced, colorectal cancer (PICC): a single-centre, parallel-group, non-comparative, randomised, phase 2 trial. *Lancet Gastroenterol Hepatol* (2022) 7(1):38–48. doi: 10.1016/S2468-1253(21)00348-4

24. Amin MB, Greene FL, Edge SB, Compton CC, Gershenwald JE, Brookland RK, et al. The eighth edition AJCC cancer staging manual: continuing to build a bridge from a population-based to a more "personalized" approach to cancer staging. *CA Cancer J Clin* (2017) 67(2):93–9. doi: 10.3322/caac.21388

25. Luchini C, Bibeau F, Ligtenberg MJL, Singh N, Nottegar A, Bosse T, et al. ESMO recommendations on microsatellite instability testing for immunotherapy in cancer, and its relationship with PD-1/PD-L1 expression and tumour mutational burden: a systematic review-based approach. *Ann Oncol* (2019) 30(8):1232–43. doi: 10.1093/annonc/mdz116

26. Saeed OAM, Mann SA, Luchini C, Huang K, Zhang S, Sen JD, et al. Evaluating mismatch repair deficiency for solid tumor immunotherapy eligibility: immunohistochemistry versus microsatellite molecular testing. *Hum Pathol* (2021) 115:10–8. doi: 10.1016/j.humpath.2021.05.009

27. Zito Marino F, Amato M, Ronchi A, Panarese I, Ferraraccio F, De Vita F, et al. Microsatellite status detection in gastrointestinal cancers: PCR/NGS is mandatory in Negative/Patchy MMR immunohistochemistry. *Cancers (Basel)* (2022) 14(9):2204. doi: 10.3390/cancers14092204

28. Zhu L, Huang Y, Fang X, Liu C, Deng W, Zhong C, et al. A novel and reliable method to detect microsatellite instability in colorectal cancer by next-generation sequencing. *J Mol Diagn* (2018) 20(2):225–31. doi: 10.1016/j.jmoldx.2017.11.007

29. Eisenhauer EA, Therasse P, Bogaerts J, Schwartz LH, Sargent D, Ford R, et al. New response evaluation criteria in solid tumours: revised RECIST guideline (version 1. *1). Eur J Cancer* (2009) 45(2):228–47. doi: 10.1016/j.ejca.2008.10.026

30. Habr-Gama A, Sabbaga J, Gama-Rodrigues J, São Julião GP, Proscurshim I, Bailão Aguilar P, et al. Watch and wait approach following extended neoadjuvant chemoradiation for distal rectal cancer: are we getting closer to anal cancer management? *Dis Colon Rectum* (2013) 56(10):1109–17. doi: 10.1097/DCR.0b013e3182a25c4e

31. Smith JJ, Chow OS, Gollub MJ, Nash GM, Temple LK, Weiser MR, et al. Organ preservation in rectal adenocarcinoma: a phase II randomized controlled trial evaluating 3-year disease-free survival in patients with locally advanced rectal cancer treated with chemoradiation plus induction or consolidation chemotherapy, and total mesorectal excision or nonoperative management. *BMC Cancer* (2015) 15:767. doi: 10.1186/s12885-015-1632-z

32. Freites-Martinez A, Santana N, Arias-Santiago S, Viera A. Using the common. terminology criteria for adverse events (CTCAE - version 5.0) to evaluate the severity of adverse events of anticancer therapies. *Actas Dermosifiliogr (Engl Ed)* (2021) 112(1):90–2. doi: 10.1016/j.ad.2019.05.009

33. Dindo D, Demartines N, Clavien PA. Classification of surgical complications: a new proposal with evaluation in a cohort of 6336 patients and results of a survey. *Ann Surg* (2004) 240(2):205–13. doi: 10.1097/01.sla.0000133083.54934.ae

34. van der Valk MJM, Hilling DE, Bastiaannet E, Meershoek-Klein Kranenbarg E, Beets GL, Figueiredo NL, et al. Long-term outcomes of clinical complete responders after neoadjuvant treatment for rectal cancer in the international watch & wait database (IWWD): an international multicentre registry study. *Lancet* (2018) 391(10139):2537–45. doi: 10.1016/S0140-6736(18)31078-X

35. Ganesh K, Stadler ZK, Cercek A, Mendelsohn RB, Shia J, Segal NH, et al. Immunotherapy in colorectal cancer: rationale, challenges and potential. *Nat Rev Gastroenterol Hepatol* (2019) 16(6):361–75. doi: 10.1038/s41575-019-0126-x

36. O'Donnell JS, Hoefsmit EP, Smyth MJ, Blank CU, Teng MWL. The promise of neoadjuvant immunotherapy and surgery for cancer treatment. *Clin Cancer Res* (2019) 25(19):5743–51. doi: 10.1158/1078-0432.CCR-18-2641

37. Liu J, Blake SJ, Yong MC, Harjunpää H, Ngiow SF, Takeda K, et al. Improved efficacy of neoadjuvant compared to adjuvant immunotherapy to eradicate metastatic disease. *Cancer Discov* (2016) 6(12):1382–99. doi: 10.1158/2159-8290.CD-16-0577

38. Borcoman E, Kanjanapan Y, Champiat S, Kato S, Servois V, Kurzrock R, et al. Novel patterns of response under immunotherapy. *Ann Oncol* (2019) 30(3):385–96. doi: 10.1093/annonc/mdz003

39. Cascone T, William WNJr., Weissferdt A, Leung CH, Lin HY, Pataer A, et al. Neoadjuvant nivolumab or nivolumab plus ipilimumab in operable non-small cell lung cancer: the phase 2 randomized NEOSTAR trial. *Nat Med* (2021) 27(3):504–14. doi: 10.1038/s41591-020-01224-2

40. Blank CU, Rozeman EA, Fanchi LF, Sikorska K, van de Wiel B, Kvistborg P, et al. Neoadjuvant versus adjuvant ipilimumab plus nivolumab in macroscopic stage III melanoma. *Nat Med* (2018) 24(11):1655–61. doi: 10.1038/s41591-018-0198-0

41. Goldfarb L, Duchemann B, Chouahnia K, Zelek L, Soussan M. Monitoring anti-PD-1-based immunotherapy in non-small cell lung cancer with FDG PET: introduction of iPERCIST. *EJNMMI Res* (2019) 9(1):8. doi: 10.1186/s13550-019-0473-1

42. Cabel L, Riva F, Servois V, Livartowski A, Daniel C, Rampanou A, et al. Circulating tumor DNA changes for early monitoring of anti-PD1 immunotherapy: a proof-of-concept study. *Ann Oncol* (2017) 28(8):1996–2001. doi: 10.1093/annonc/mdx212

43. Bratman SV, Yang SYC, Iafolla MAJ, Liu Z, Hansen AR, Bedard PL, et al. Personalized circulating tumor DNA analysis as a predictive biomarker in solid tumor patients treated with pembrolizumab. *Nat Cancer* (2020) 1(9):873–81. doi: 10.1038/s43018-020-0096-5

44. Liu DX, Li DD, He W, Ke CF, Jiang W, Tang JH, et al. PD-1 blockade in neoadjuvant setting of DNA mismatch repair-deficient/microsatellite instability-high colorectal cancer. *Oncoimmunology* (2020) 9(1):1711650. doi: 10.1080/2162402X.2020.1711650

45. Dejea CM, Wick EC, Hechenbleikner EM, White JR, Mark Welch JL, Rossetti BJ, et al. Microbiota organization is a distinct feature of proximal colorectal cancers. *Proc Natl Acad Sci USA* (2014) 111(51):18321–6. doi: 10.1073/pnas.1406199111

46. Flemer B, Lynch DB, Brown JM, Jeffery IB, Ryan FJ, Claesson MJ, et al. Tumour-associated and non-tumour-associated microbiota in colorectal cancer. *Gut* (2017) 66(4):633–43. doi: 10.1136/gutjnl-2015-309595

47. Gopalakrishnan V, Spencer CN, Nezi L, Reuben A, Andrews MC, Karpinets TV, et al. Gut microbiome modulates response to anti-PD-1 immunotherapy in melanoma patients. *Science* (2018) 359(6371):97–103. doi: 10.1126/science.aan4236

48. Hamada T, Zhang X, Mima K, Bullman S, Sukawa Y, Nowak JA, et al. Fusobacterium nucleatum in colorectal cancer relates to immune response differentially by tumor microsatellite instability status. *Cancer Immunol Res* (2018) 6(11):1327–36. doi: 10.1158/2326-6066.CIR-18-0174

49. Gao Y, Bi D, Xie R, Li M, Guo J, Liu H, et al. Fusobacterium nucleatum enhances the efficacy of PD-L1 blockade in colorectal cancer. *Signal Transduct Target Ther* (2021) 6(1):398. doi: 10.1038/s41392-021-00795-x

50. Chen G, Jin Y, Guan WL, Zhang RX, Xiao WW, Cai PQ, et al. Neoadjuvant PD-1 blockade with sintilimab in mismatch-repair deficient, locally advanced rectal cancer: an open-label, single-centre phase 2 study. *Lancet Gastroenterol Hepatol* (2023) 8(5):422–31. doi: 10.1016/S2468-1253(22)00439-3

51. Chida K, Kawazoe A, Kawazu M, Suzuki T, Nakamura Y, Nakatsura T, et al. A low. tumor mutational burden and PTEN mutations are predictors of a negative response to PD-1 blockade in MSI-H/dMMR gastrointestinal tumors. *Clin Cancer Res* (2021) 27(13):3714–24. doi: 10.1158/1078-0432.CCR-21-0401

52. Conciatori F, Bazzichetto C, Falcone I, Ciuffreda L, Ferretti G, Vari S, et al. PTEN function at the interface between cancer and tumor microenvironment: implications for response to immunotherapy. *Int J Mol Sci* (2020) 21(15):5337. doi: 10.3390/ijms21155337

53. Wang F, Zhao Q, Wang YN, Jin Y, He MM, Liu ZX, et al. Evaluation of POLE and POLD1 mutations as biomarkers for immunotherapy outcomes across multiple cancer types. *JAMA Oncol* (2019) 5(10):1504–6. doi: 10.1001/jamaoncol.2019.2963

54. Tie J, Cohen JD, Wang Y, Christie M, Simons K, Lee M, et al. Circulating tumor DNA analyses as markers of recurrence risk and benefit of adjuvant therapy for stage III colon cancer. *JAMA Oncol* (2019) 5(12):1710–7. doi: 10.1001/jamaoncol.2019.3616

55. Chen G, Peng J, Xiao Q, Wu HX, Wu X, Wang F, et al. Postoperative circulating tumor DNA as markers of recurrence risk in stages II to III colorectal cancer. *J Hematol Oncol* (2021) 14(1):80. doi: 10.1186/s13045-021-01089-z

56. Tarazona N, Gimeno-Valiente F, Gambardella V, Zuñiga S, Rentero-Garrido P, Huerta M, et al. Targeted next-generation sequencing of circulating-tumor DNA for tracking minimal residual disease in localized colon cancer. *Ann Oncol* (2019) 30(11):1804–12. doi: 10.1093/annonc/mdz390

57. Henriksen TV, Tarazona N, Frydendahl A, Reinert T, Gimeno-Valiente F, Carbonell-Asins JA, et al. Circulating tumor DNA in stage III colorectal cancer, beyond minimal residual disease detection, toward assessment of adjuvant therapy efficacy and clinical behavior of recurrences. *Clin Cancer Res* (2022) 28(3):507–17. doi: 10.1158/1078-0432.CCR-21-2404

frontiers | Frontiers in Immunology

TYPE Original Research
PUBLISHED 20 July 2023
DOI 10.3389/fimmu.2023.1212606

OPEN ACCESS

EDITED BY
Chi Chun Wong,
The Chinese University of Hong Kong, China

REVIEWED BY
Vanaja Konduri,
Baylor College of Medicine, United States
Valeria Lucarini,
Sapienza University of Rome, Italy

*CORRESPONDENCE
Katarzyna Węgierek-Ciura
katarzyna.wegierek@hirszfeld.pl

RECEIVED 26 April 2023
ACCEPTED 04 July 2023
PUBLISHED 20 July 2023

CITATION
Węgierek-Ciura K, Mierzejewska J, Szczygieł A, Rossowska J, Wróblewska A, Świtalska M, Goszczyński TM, Szermer-Olearnik B and Pajtasz-Piasecka E (2023) Inhibition of MC38 colon cancer growth by multicomponent chemoimmunotherapy with anti-IL-10R antibodies, HES-MTX nanoconjugate, depends on application of IL-12, IL-15 or IL-18 secreting dendritic cell vaccines. *Front. Immunol.* 14:1212606. doi: 10.3389/fimmu.2023.1212606

Inhibition of MC38 colon cancer growth by multicomponent chemoimmunotherapy with anti-IL-10R antibodies, HES-MTX nanoconjugate, depends on application of IL-12, IL-15 or IL-18 secreting dendritic cell vaccines

Katarzyna Węgierek-Ciura*, Jagoda Mierzejewska, Agnieszka Szczygieł, Joanna Rossowska, Anna Wróblewska, Marta Świtalska, Tomasz M. Goszczyński, Bożena Szermer-Olearnik and Elżbieta Pajtasz-Piasecka

Hirszfeld Institute of Immunology and Experimental Therapy, Polish Academy of Sciences, Wrocław, Poland

Background: The tumor microenvironment (TME) provides a conducive environment for the growth and survival of tumors. Negative factors present in TME, such as IL-10, may limit the effectiveness of cellular vaccines based on dendritic cells, therefore, it is important to control its effect. The influence of IL-10 on immune cells can be abolished e.g., by using antibodies against the receptor for this cytokine - anti-IL-10R. Furthermore, the anticancer activity of cellular vaccines can be enhanced by modifying them to produce proinflammatory cytokines, such as IL-12, IL-15 or IL-18. Additionally, an immunomodulatory dose of methotrexate and hydroxyethyl starch (HES-MTX) nanoconjugate may stimulate effector immune cells and eliminate regulatory T cells, which should enhance the antitumor action of immunotherapy based on DC vaccines. The main aim of our study was to determine whether the HES-MTX administered before immunotherapy with anti-IL-10R antibodies would change the effect of vaccines based on dendritic cells overproducing IL-12, IL-15, or IL-18.

Methods: The activity of modified DCs was checked in two therapeutic protocols - immunotherapy with the addition of anti-IL10R antibodies and chemoimmunotherapy with HES-MTX and anti-IL10R antibodies. The inhibition of tumor growth and the effectiveness of the therapy in inducing a specific antitumor response were determined by analyzing lymphoid and myeloid cell populations in tumor nodules, and the activity of restimulated splenocytes.

Results and conclusions: Using the HES-MTX nanoconjugate before immunotherapy based on multiple administrations of anti-IL-10R antibodies and cellular vaccines capable of overproducing proinflammatory cytokines IL-

12, IL-15 or IL-18 created optimal conditions for the effective action of these vaccines in murine colon carcinoma MC38 model. The applied chemoimmunotherapy caused the highest inhibition of tumor growth in the group receiving DC/IL-15/IL-15Rα/TAg + DC/IL-18/TAg at the level of 72.4%. The use of cellular vaccines resulted in cytotoxic activity increase in both immuno- or chemoimmunotherapy. However, the greatest potential was observed both in tumor tissue and splenocytes obtained from mice receiving two- or three-component vaccines in the course of combined application. Thus, the designed treatment schedule may be promising in anticancer therapy.

KEYWORDS

dendritic cells, interleukin 12, interleukin 15, interleukin 18, anti-IL-10R antibodies, nanoconjugate, methotrexate, colon carcinoma

1 Introduction

According to the World Health Organization, colon cancer was the second leading cause of cancer-related deaths worldwide in 2020 (1). Growing evidence has demonstrated that the fate of tumor progression is highly correlated with the presence of a specific tumor microenvironment (TME) created by tumor cells, extracellular matrix, stromal cells, as well as various types of infiltrating immune cells (2), which activity is modified by TME. For example, macrophages originating from circulating monocytes, under the influence of tumor-derived factors, can become tumor-associated macrophages (TAMs) regarded as the leading producers of immunosuppressive cytokines such as IL-10 and TGF-β (3). TAMs are able to present antigens in the MHC II-associated pathway, nevertheless, in hypoxia or under the influence of IL-10, the MHC II surface expression decreases, causing tumor progression (4–6). Myeloid-derived suppressor cells (MDSCs), other populations of myeloid cells which produce IL-10, under hypoxia conditions are able to transform into TAMs increasing the size of this population (7). TME contributes to a change in the infiltration of both T and natural killer (NK) cells. However, depending on the type of environmental factors or interaction with MDSCs, part of effector $CD4^+$ cells can convert into regulatory T cells (Tregs), which are involved in the suppression of arising antitumor activity by secretion of both TGF-β and IL-10, and their increased frequency is associated with poorer cancer patients' prognoses (8, 9).

The use of conventional treatment with various chemotherapeutics aimed at the elimination of cancer cells is still unsatisfactory, especially in the context of severe systemic side effects. Hence there is a requirement for new, safe and effective anticancer therapies based on cytostatics, for example, using novel drug delivery systems. Such an approach is the use of nanoconjugate of methotrexate and hydroxyethyl starch (HES-MTX), which was obtained by covalent coupling of two well-known therapeutic compounds – methotrexate (MTX) and hydroxyethyl starch (HES) (10). MTX represents one of the oldest antifolate chemotherapeutics, commonly used in autoimmune diseases and in anticancer therapy of solid tumors and hematologic malignancies (11), whereas HES as an amylopectin-based modified polymer is applied in medicine as colloidal plasma volume expander. The HES-MTX nanoconjugate provides a prolonged half-time in plasma compared to the free form of MTX, which further improves the distribution of the nanoconjugate in the body and effective drug release in the target tissue (10). The effect of conjugation of a low-molecular-weight drug with a high-molecular-weight carrier provides an optimal hydrodynamic diameter of the obtained HES-MTX nanoconjugate. This enables more efficient accumulation in tumor tissue, mainly through enhanced vascular permeability and retention effect (EPR), which was discussed in more detail in our previous publication (12). Moreover, the anticancer activity of HES-MTX has been confirmed in murine and human leukemia models (10), as well in the murine colon carcinoma MC38 model (12, 13).

Secreted by many leukocyte populations, IL-10 is one of the factors present in TME, contributing to the suppression of immune response (14, 15). This cytokine is involved in inhibiting antigen presentation, affects the differentiation and maturation of DCs and impairs their migration to secondary lymphoid organs. Moreover, IL-10 reduces the local antigen-specific response of $CD8^+$ cells and suppresses IL-12 secretion by DCs (16, 17). Therefore, the manipulation of IL-10 levels is a key step in controlling tumors, especially in the advanced stages of the disease (18). This can be achieved by local or systemic blockade of IL-10 activity, e.g. by administration of shRNA against IL-10 and antibodies neutralizing IL-10 or IL-10 receptor (19–24). The temporary blockade of the IL-10-specific receptor (IL-10R) with anti-IL-10R antibodies reduces the sensitivity of immune cells to IL-10, which prevents the transformation of effector cells into suppressor cells and prepares optimal conditions for triggering an efficient anticancer response.

The immune cells' responsiveness can be also restored using dendritic cell-based vaccines. Effective therapeutic vaccines should be able to prime naïve T cells, but most importantly, induce the transition of existing memory T cells to effector $CD8^+$ cells. To effectively stimulate T lymphocytes, dendritic cells must present tumor antigens *via* MHC class I and II molecules, express costimulatory ligands, and inflammatory mediators such as IL-12 or type I interferons (IFNs) (25). Accumulating evidence indicates the

possibility of using such vaccines to support conventional therapies. After using combined therapy, it is possible to obtain a synergistic effect, especially when DCs have not only been subjected to antigenic activation but also genetic modifications. The efficacy of the combined therapy may therefore rely on the use of genetically modified DCs secreting cytokines (e.g. IL-12, IL-15) enhancing the efficacy of the activated DCs to induce an antitumor response (26). Proinflammatory cytokines such as IL-12, IL-15 or IL-18 can additionally stimulate the proliferation and activity of the immune system cells.

Interleukin 12 regulates inflammation by harnessing effector mechanisms of both innate and acquired immunity (27). Most IL-12-induced effects are mediated by the IFN-γ secretion and promotion of the Th1 T helper cell differentiation (28). The effect of IL-12 on the antitumor response has been observed in preclinical models, but it has not been implemented in clinical practice due to substantial side effects after systemic administration. Thus, the delivery of IL-12 for therapeutic purposes focuses on its direct application to the tumor site (29). In turn, IL-15 stimulates the activation, proliferation, survival, and cytotoxicity of $CD8^+$ cells and memory phenotype $CD8^+$ cells. Like IL-2, IL-15 could be used to proliferate and maintain NK cells and is critical for the functional maturation of both macrophages and DCs. However, unlike IL-2, IL-15 does not lead to activation-induced T cell death, proliferation enhancement, or differentiation of immunosuppressive $CD4^+$ Treg cells (30, 31). Multiple murine immunotherapy trials in different models have revealed that IL-15 might be more effective than IL-2 in anticancer therapy (32). Still, when administered as monotherapy it has appeared to be ineffective, needing the combinate of application with other anticancer agents (31). Interleukin 18 was known as an IFN-γ inducing factor due to its function in IFN-γ enhancement. This leads to the polarization of $CD4^+$ cells towards the helper T cell type 1 (Th1) phenotype when costimulated with IL-12 or IL-15. Importantly, without IL-12 or IL-15, IL-18 does not induce IFN-γ production but plays an important role in differentiating naive T cells into Th2 cells producing IL-13 and IL-4. Using IL-18 as an adjuvant combination with other cytokines, such as IFN-α, IL-15, IL-12, and IL-2, it can also promote interaction between DCs and T cells, and the activation and proliferation of T cells in colorectal cancer patients (33, 34).

The main purpose of our study was to determine the effect of immunotherapy alone based on multiple administrations of cellular vaccines and anti-IL-10R antibodies and evaluate the efficacy of the therapy, which was preceded by a single administration of the HES-MTX nanoconjugate in an immunomodulatory dose. Based on tumor growth inhibition and changes in local and systemic immune responses, we have shown that using the HES-MTX nanoconjugate creates a suitable environment for the effective action of cell-based vaccines. This was especially evident in the groups receiving DC vaccines based on mixtures of two or three transductants, although the concentration of a single cytokine released was lower than when a single transductant was used. Such therapy resulted in a clear inhibition of tumor growth and a decrease in the population of TAM and Treg cells with a suppressor effect. There was also observed an increase in the infiltration of $CD4^+$, $CD8^+$ cells and NK cells into tumor tissue, especially after chemoimmunotherapy harnessing anti-IL-10R antibodies and mixtures of dendritic cells.

2 Materials and methods

2.1 Cell lines

The *in vivo* growing MC38 murine colon carcinoma from the Tumor Bank of the Radiobiological Institute TNO (Rijswijk, The Netherlands) was adapted to *in vitro* conditions as described by Pajtasz–Piasecka et al. (35). The culture of MC38/0 (named here MC38) cells was maintained in RPMI–1640 (Gibco) supplemented with 100 U/ml penicillin, 100 mg/ml streptomycin, 0.5% sodium pyruvate, 0.05 mM 2–mercaptoethanol (named here RPMI) and 5% fetal bovine serum (FBS; all reagents from Sigma–Aldrich). Lenti-X 293T cell line (Clontech) was maintained in high-glucose Dulbecco's Modified Eagle Medium (Gibco) supplemented with 100 U/ml penicillin, 100 mg/ml streptomycin, 1 mM sodium pyruvate and 10% FBS. Cultures were carried out under standard conditions (5% CO_2, 37°C).

2.2 Tumor cell lysate preparation

The MC38 colon cancer cells were harvested and resuspended at a density of 5×10^6 cells/mL in RPMI-1640 (Gibco) supplemented with 10% FBS (Sigma-Aldrich). All cells were subjected to 5 cycles of freezing in liquid nitrogen and quick thawing at 37°C. The cell suspension was then sonicated for 90 min. Tumor antigens (TAg) were used to stimulate dendritic cells.

2.3 Production of lentiviral vectors

Lentiviral vectors (LVs) were produced using a third-generation lentiviral system, which consisted of auxiliary vectors: pMDLg/pRRE, pRSV Rev, pMD2.G [the plasmids were a gift from Didier Trono (Addgene plasmids #12251, 12253, 12259)] and expression vector. The expression plasmids encoded the cytokine genes: *il12*, *il15/il15ra* or *il18*. In the vector carrying the *il15* gene, the gene sequence of this cytokine was preceded by a signal sequence facilitating the release of the protein from the cell. In addition, after the gene encoding the cytokine and the linker, there was a gene sequence encoding the alpha subunit of the IL-15 receptor, in order to delay the process of intracellular degradation of this protein. A control vector was also created to check the effect of lentiviral transduction on dendritic cells. All expression vectors were purchased from VectorBuilder. Lentiviral vectors were produced by Lenti-X 293T cells (ClonTech) co-transfected with the above-mentioned plasmids and cultured for 48 hours. The supernatant containing lentiviral vectors was collected and concentrated by precipitation using PEG 6000 (Sigma-Aldrich). The pellet containing the lentiviral vectors was suspended in PBS and stored at -80°C. The procedure of lentiviral vectors production was described in our previous article (36). The titer of the lentiviral vector was determined by serial dilution method using MC38 cells and flow cytometry analysis.

2.4 Animals

Female C57BL/6 mice were obtained from the Center for Experimental Medicine of the Medical University of Białystok, Poland. All experiments were performed in accordance with Directive 2010/63/EU of the European Parliament and of the Council on the protection of animals used for scientific purposes and were approved by the Local Ethic Committee for Experiments with the Use of Laboratory Animals, Wrocław, Poland (authorization number 077/2019). After the experiments, mice were sacrificed by cervical dislocation.

2.5 Generation of cellular vaccines based on transduced dendritic cells

Dendritic cells were generated from bone marrow isolated from femurs and tibias of healthy female C57BL/6 mice according to the protocol described in our previous publication (37). Cells (named here DCs) were cultured in RPMI-1640 (Gibco) supplemented with 10% FBS (Sigma-Aldrich) in the presence of recombinant murine (rm)GM–CSF (ImmunoTools, 40 ng/ml) and rmIL–4 (ImmunoTools, 10 ng/ml). After 7 days of culture, loosely attached immature DCs were transduced with LVs (with the assumption: 4 viral infectious particles per 1 dendritic cell) in the presence of 8 μg/ml polybrene (Sigma–Aldrich). After 4 hours DCs, were stimulated with tumor antigen lysates (TAg, 10% v/v). Mature dendritic cells obtained on day 8 of DC culture were collected and applied to *in vitro* DC characteristics or used as cellular vaccines in *in vivo* experiments.

2.6 Phenotype characteristic of transduced DCs

In order to estimate the influence of LV transduction on the differentiation level of DCs, the phenotype characteristic was performed on 8 and 10 days of DC culture by flow cytometry. Cells were labeled with a cocktail of monoclonal antibodies conjugated with fluorochromes: anti-CD11c Brilliant Violet 650 (clone N418), CD80 PerCP-Cy5.5 (clone 16-10A1), CD86 PE-Cy7 (clone GL-1), MHC II APC-Fire 750 (clone M5/114.15.2) (all from BioLegend) and CD40 Brilliant Violet 605 (clone 3/23) (from BD Biosciences). In order to exclude dead cells, DAPI dye (Invitrogen) was added prior to analysis, which was performed using the LSRFortessa flow cytometer with Diva software (BD Biosciences).

2.7 Primary stimulation of splenic cells by transduced DCs

The ability of the modified DCs to activate primary antigen-specific immune response was evaluated in a 5-day co-culture of mature DCs (0.18×10^6 cells) and naive spleen cells (1.8×10^6 cells) in the presence of recombinant human (rh)IL–2 (200 U/ml, Immunotools). In order to determine the percentage of $CD107a^+$ cells, the degranulation assay was performed. Primarily stimulated spleen cells were incubated for 2 hours with MC38 cells in the presence of monoclonal anti–CD107a antibodies conjugated with APC (clone 1D4B, BioLegend) together with ionomycin (1 μg/ml, Sigma-Aldrich), phorbol-12-myristate-13-acetate (50 ng/ml, Sigma-Aldrich) and rhIL-2 (200 U/ml). Afterwards, cells were harvested and stained with anti–CD45 Brilliant Violet 605 (clone 30-F11), anti–CD4 FITC (clone RM4-5), anti–CD8a APC-Fire (clone 53-6.7) and anti–NK1.1 PE-Dazzle 594 (clone PK136) (all from BioLegend). For the elimination of the dead cells, DAPI dye was used. The flow cytometry analysis was performed using the LSRFortessa flow cytometer with Diva software (BD Biosciences).

2.8 Therapeutic treatment schedule

Eight-to-ten-week-old female C57BL/6 mice were subcutaneously (s.c.) inoculated in the right flank with MC38 cells (1.1×10^6 cells/0.2 ml NaCl 0.9%/mouse). When tumor nodules were palpable, mice were randomly divided on the basis of tumor volume into ten or eleven experimental groups in immuno- and chemoimmunotherapeutic schedule, respectively. In both experiments, cellular vaccines were inoculated peritumorally (p.t.) on the 17^{th}, 24^{th} and 31^{st} days of the experiment (2×10^6 cells/0.2 ml NaCl 0.9%/mouse/injection). The anti-IL-10R antibodies (BioXCell) at a dose of 250 μg/0.2 ml/mouse/injection were administered intraperitoneally (i.p.) the day before injection of the cellular vaccines (16^{th}, 23^{rd} and 30^{th} day of the experiment). The therapeutic schedule of chemoimmunotherapy was started on the 14^{th} day of the experiment with intravenously (i.v.) HES-MTX nanoconjugate injection in the tail vein (at a dose 20 mg/kg body weight). The HES-MTX preparation was described in detail in our previous papers (10, 12). In both experiments, three types of cellular vaccines were used – non-transduced DC/TAg, DC transduced with a control vector (DC/Vctrl/TAg) and DCs modified to overproduce cytokines. Mice received 2×10^6 modified dendritic cells per 1 injection, regardless of whether the mice received cells overproducing only one cytokine or a mixture of cells producing two or three cytokines. Cellular vaccines named DC/IL-12/TAg, DC/IL-15/IL-15Rα/TAg and DC/IL-18/TAg consisted of 2×10^6 cells of appropriate transductants, DC/IL-12/TAg + DC/IL-15/IL-15Rα/TAg, DC/IL-12/TAg + DC/IL-18/TAg and DC/IL-15/IL-15Rα/TAg + DC/IL-18/TAg consisted of 1×10^6 cells of each listed transductants, while DC/IL-12/TAg + DC/IL-15/IL-15Rα/TAg + DC/IL-18/TAg was a mixture of three different transductants in the number of 0.667×10^6 cells each.

2.9 Tumor volume of tumor-bearing mice

During the experiment, two or three times a week, tumors were measured by using an electronic caliper and tumor volume was calculated according to the formula: $a/2 \times b^2$, where represents the largest and represents the smallest tumor diameter (38). MC38 tumor growth is shown as relative tumor volume. Relative tumor volume was defined as the ratio of tumor volume on the day of measurement to that tumor volume on the day of randomization (day 13). Tumor growth kinetics are presented as a non-linear least

squares regression fits of the Gompertz function. The therapeutic efficacy was determined on the basis of the tumor growth inhibition (TGI) value calculated as follows: $TGI\ (\%) = 100 - (TV_t/TV_{nt} \times 100)$, where TV_t refers to a median tumor volume in the treated group and TV_{nt} – median tumor volume in the non-treated (nt) group (37). Seven days after the last DC-based vaccine injection, spleen and tumor nodules were dissected from MC38-tumor bearing mice, homogenized, and stored in liquid nitrogen for further *ex vivo* analyses.

2.10 Analysis of myeloid and lymphoid cell populations in MC38 tumors after applied therapy

Single-cell suspensions of tumor tissue were thawed and stained for identification of myeloid and lymphoid cell subpopulations. Tumor suspensions were stained with the LIVE/DEAD Fixable Violet Dead Staining Kit (Thermo Fisher Scientific, Inc.) and then labeled with cocktails of fluorochrome–conjugated monoclonal antibodies: anti–CD3 PE–CF594 (clone 145-2C11), anti–CD19 PE–CF594 (clone 1D3), anti–NK1.1 PE–Dazzle 594 (clone PK136) (all from BD Biosciences), anti–CD45 Brilliant Violet 605 (clone 30-F11), anti–CD11b PerCP–Cy5.5 (clone M1/70), anti –CD11c Brilliant Violet 650 (clone N418), anti–F4/80 Alexa Fluor 700 (clone BM8), anti–Ly6C PE (clone HK1.4), anti–Ly6G APC–Cy7 (clone 1A8), anti–MHC II FITC (clone M5/114.15.2), (all from BioLegend) for myeloid cell identification, and anti–CD45 Brilliant Violet 605 (clone 30-F11), anti–CD3 Brilliant Violet 650 (clone 17A2), anti–CD4 FITC (clone RM4-5), anti–CD8 APC/Fire 750 (clone 53-6.7), anti-CD19 Alexa Fluor 700 (clone 6D5), anti –CD25 PE (clone PC61) (all from BioLegend) for lymphocyte identification. Then, cells were fixed using the Foxp3/ Transcription Factor Staining Buffer Set (eBioscience). Cells stained with myeloid, or lymphocyte cocktail were additionally incubated with anti–CD206 APC (clone C068C2) (BioLegend) or anti–FoxP3 APC (clone FJK-16s) (eBioscience) monoclonal antibodies, respectively. The flow cytometry analysis was performed using the LSRFortessa flow cytometer with Diva software (BD Biosciences).

2.11 Analysis of the systemic antitumor immune response of spleen cells after therapy

Spleen single-cell suspensions (2×10^6 cells) were thawed and cocultured with mitomycin C-treated MC38 cells (0.1×10^6 cells) in the presence of rhIL–2 (200 U/ml). After 5 days of restimulation, cells were harvested and the cytotoxic activity of effector splenocytes against target (MC38) cells stained with DiO lipophilic dye (Molecular Probes) was analyzed according to the previously described procedure (38). Two E:T (effector to target) ratios were investigated: 10:1 and 30:1. The dead target cells were distinguished with propidium iodide (PI, Life Technologies) solution and the percentage of DiO^+PI^+ MC38 cells was determined. The degranulation assay was used as described earlier (section: *Primary stimulation of splenic cells by transduced dendritic cells*). Supernatants were collected and stored at 4°C until ELISA was performed.

2.12 Measurement of cytokine production

Production of cytokines was evaluated using commercially available ELISA kits (IL–10, IL–4; BD Biosciences and IL-12, IL-15/IL-15Rα, IL-18, IFN–γ; eBioscience) according to the manufacturer's instructions.

2.13 Statistical analyses

All data were analyzed using GraphPad Prism 9 software (GraphPad Software, Inc.). The normality of the residuals was confirmed by the D'Agostino–Pearson omnibus test. When data were consistent with a Gaussian distribution and had equal SD values, the statistical significance was calculated using the parametric one–way ANOVA followed by Tukey's multiple comparison *post–hoc* test. When data were consistent with a Gaussian distribution, but SD values were not equal, the Brown –Forsythe and Welch ANOVA test followed by Dunnett's T3 multiple comparisons *post–hoc* test was performed. Data inconsistent with a Gaussian distribution were analyzed using the nonparametric Kruskal–Wallis test followed by Dunn's multiple comparison *post–hoc* test. The statistical significance of tumor growth kinetics was calculated using the two–way ANOVA followed by Tukey's multiple comparisons *post–hoc* test. The type of statistical analysis used is described in the captions under the figures. All statistically significant differences are presented in the graphs in the form of symbols described in Table 1.

3 Results

3.1 Characteristics of genetically modified DC-based vaccines

In the first stage of our research, we obtained mature bone marrow-derived dendritic cells (DCs) capable of increased production of interleukin: IL-12, IL-15 or IL-18 (DC/IL-12/TAg, DC/IL-15/IL-15Rα/TAg; DC/IL-18/TAg). The appropriate gene for each cytokine was introduced by transduction with lentiviral vectors. Dendritic cells were stimulated with a tumor lysate (tumor antigens, TAg) and harvested on the 8^{th} day of culture to determine their phenotypic and functional characteristics. DCs transduced with the control vector (DC/Vctrl/TAg) or non-transduced DCs (DC/TAg) stimulated with TAg were used as a control (Figure 1A). We observed a decrease in the percentage of $CD11c^+DAPI^-$ cells after transduction with vectors carrying genes of the particular cytokines in relation to the DC/TAg group (Figure 1B).

Phenotype analysis showed that the type of introduced gene considerably affected the maturation of DCs. The expression of

TABLE 1 Statistical significance markings on graphs.

p value	wording	determination of statistical significance in relation to the group:			other
		non-treated control (nt)	HES-MTX 20 mg/kg bw (H-M)	DC/Vctrl/TAg	
< 0.0001	extremely significant	****	####	xxxx	**** above the line
0.0001 to 0.001	extremely significant	***	###	xxx	*** above the line
0.001 to 0.01	very significant	**	##	xx	** above the line
0.01 to 0.05	significant	*	#	x	* above the line
≥ 0.05	not significant	no check mark	no check mark	no check mark	no check mark

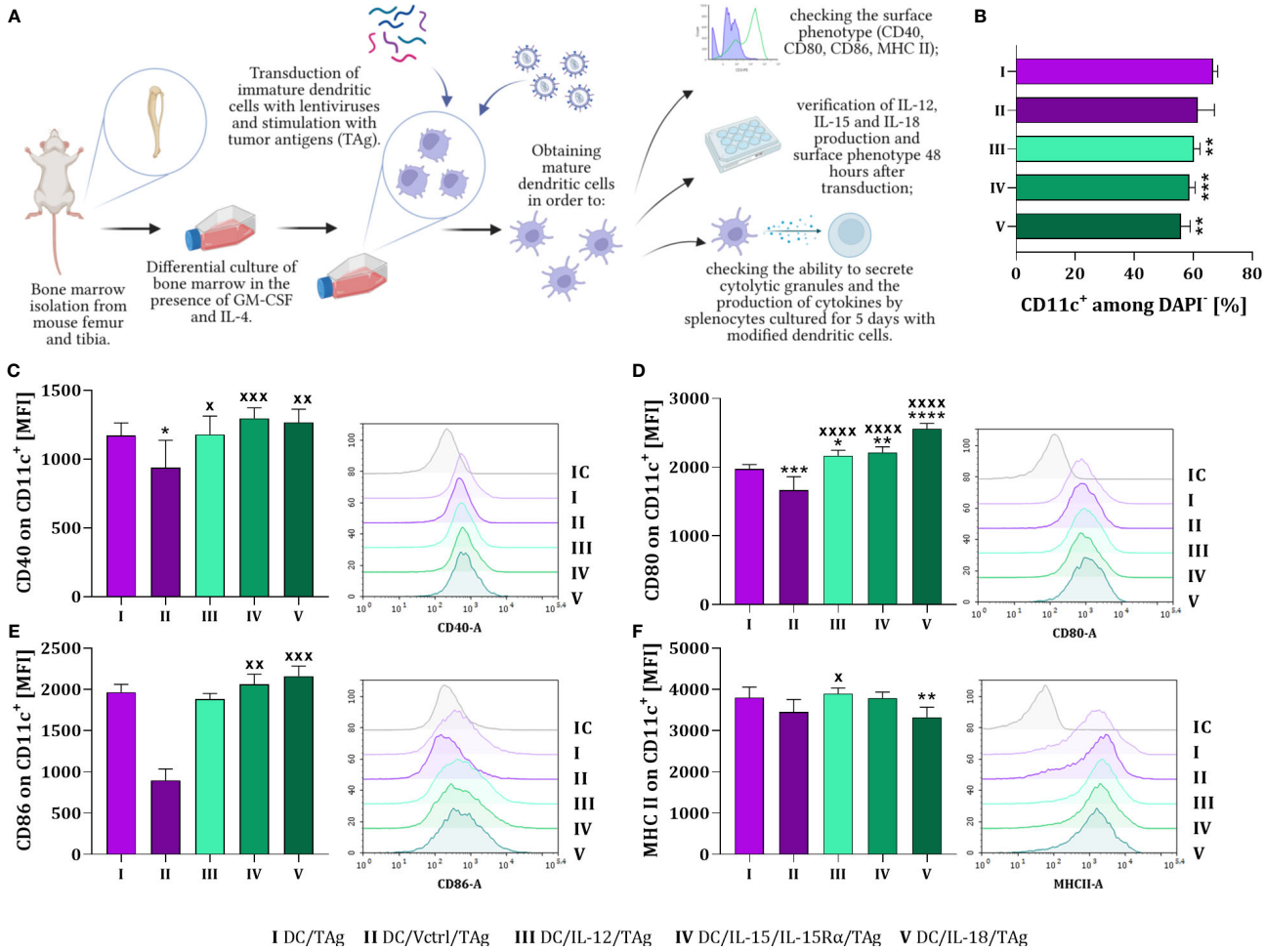

FIGURE 1
The influence of lentiviral transduction with *il12*, *il15* and *il15Rα* or *il18* genes on the phenotype of bone marrow-derived dendritic cells (DCs). **(A)** Preparation schedule of genetically modified DCs. Cells were isolated from the long bones of mice and cultured for 6 days in the presence of GM-CSF and IL-4. On day 7th, immature dendritic cells were transduced with cytokine genes and then stimulated with tumor antigens. On the 8th day of culture, the level of differentiation of the developed vaccine cells was determined. Preparation schedule created with BioRender.com. **(B)** Percentage of CD11c$^+$ cells on the 8th day of DC cultures. Expression of costimulatory molecules **(C)** CD40, **(D)** CD80, **(E)** CD86 and **(F)** MHC II on the surface of CD11c$^+$ cells. Results are presented as mean+SD calculated for 5-6 samples per group. Differences between groups were estimated using the non-parametric Kruskal-Wallis test followed by Dunn's multiple comparisons *post-hoc* test **(E)**, the parametric one-way ANOVA followed by Tukey's multiple comparisons *post-hoc* test **(C, D, F)** or the parametric Brown-Forsythe and Welch ANOVA test followed by Dunnett's T3 multiple comparisons *post-hoc* test **(B)**. The asterisks (*) presented in the graphs indicate statistically significant differences between the given groups and the DC/TAg control cells; crosses (X) indicate a statistically significant difference between the given group and the DC/Vctrl/TAg control cells – (*/^{x}p<0.05; **/^{xx}p<0.01; ***/^{xxx}p<0.001; ****/^{xxxx}p<0.0001). IC – *isotype control*.

CD40, CD80, CD86 costimulatory and MHC II molecules was determined on the surface of these cells (Figures 1C–F). DCs modified to cytokine production showed increased expression of CD40 and CD80 molecules compared to cells transduced with the control vector (DC/Vctrl/TAg) (Figures 1C, D). Compare to that control, a significantly increased expression of CD86 molecules was noticed after DC transduction with *il15* and *il18* genes (Figure 1E). Whereas only slight differences in the expression of MHC II molecules on the surface of these cells were observed (Figure 1F). The highest expression of MHC II was found on the surface of DC/IL-12/TAg and the lowest on DC/IL-18/TAg.

To assess the mutual influence of each overproduced cytokine on the level of DCs differentiation and activation of the antitumor response, all DC types were cultured for 48 hours in different configurations. We tested the simultaneous effect of two (DC/IL-12/TAg + DC/IL-15/IL-15Rα/TAg; DC/IL-12/TAg + IL-18/TAg and DC/IL-15/IL-15Rα/TAg + DC/IL-18/TAg) or three (DC/IL-12/TAg + DC/IL-15/IL-15Rα/TAg + DC/IL-18/TAg) cytokines on the DC phenotype and induction of a specific cellular response (Figure 2). Based on our former experience with using DCs as anticancer vaccines, we have known that one of the essential parameters affecting the effectiveness of the therapy is the number of injected cells. Therefore, to determine the effect of DC modifications on their antitumor activity we decided to apply the same number of cells to every single injection regardless of the composition of the vaccines. Thus, we tested control vaccines (DC/TAg and DC/Vctrl/TAg) and vaccines consisting of DCs producing one cytokine – one-component vaccine (DC/IL-12/TAg, DC/IL-15/IL-15Rα/TAg, DC/IL-18/TAg), a 1:1 mixture of two types of DCs – two-component vaccine (DC/IL-12/TAg + DC/IL-15/IL-15Rα/TAg; DC/IL-12/TAg + IL-18/TAg and DC/IL-15/IL-15Rα/TAg + DC/IL-18/TAg), or a 1:1:1 mixture of three types of DCs – three-component vaccine (DC/IL-12/TAg + DC/IL-15/IL-15Rα/TAg + DC/IL-18/TAg).

The highest concentration of introduced cytokines was noted in cultures with DCs producing one cytokine (groups III, IV and V) (Figures 2A–C). In two-component or three-component vaccines, a reduced concentration of interleukins was observed, which was related to the number of individual cytokine-producing cells in the mixture. Despite this, in mixed cultures (groups VI-IX), a greater influence of cytokines on changes in the phenotype of DCs than in monocultures was observed. The highest expression of the CD40 molecule was demonstrated on the surface of DC/IL-18/TAg cells and in a mixed culture of these cells with DC/IL-15/IL-15Rα/TAg and DC/IL-12/TAg + DC/IL-15/IL-15Rα/TAg (Figure 2D). No effect of cytokines on changes in the expression of the CD80 on the surface of vaccine cells was observed (Figure 2E). However, a slight increase in the expression of this molecule was shown in the culture of transduced DCs compared to DC/TAg. This may suggest that the presence of CD80 on the surface of transduced DCs is related to viral rather than cytokine stimulation. The expression of CD86 molecules was increased in the DCs mixed cultures, especially in relation to cells transduced with the control vector (Figure 2F). However, such an effect was not observed on the surface of one-component vaccines. An increase in the level of MHC II expression on transduced DCs in mixed cultures compared to the monoculture was determined (Figure 2G).

The DC ability to primary stimulate naïve T cells and induce a specific antitumor response was assessed in a 5-day co-culture of splenocytes with all types of vaccine cells. Changes in the percentage of $CD8^+$, $CD4^+$ and NK cells, as well as their ability for degranulation assessed by the expression of the CD107a molecule on their surface, were determined. Moreover, we investigated the ability of stimulated splenocytes to produce IFN-γ and IL-10.

The largest population of splenocytes in co-cultures were $CD8^+$ cells, which accounted for approx. 50% of all spleen cells stimulated with DCs. An increase in the percentage of these cells was observed when splenocytes were cultured with the three-component vaccine in relation to co-culture with one-component vaccines and cells modified with the control vector (Figure 2H). A decisive effect of DC/IL-12/TAg or their mixture with other transductants was found to increase the percentage of $CD4^+$ cells in the co-culture (Figure 2I), and oppositely – a decrease in NK cell percentage was revealed (Figure 2J). Among the $CD8^+$ cell populations, the highest expression of the CD107a molecule was observed after splenocytes contact with DCs overproducing IL-12, regardless of whether it was produced alone or in combination with other cytokines (Figure 2K). No significant differences in the size of the CD107a cell population were observed among $CD4^+$ cells (Figure 2L), while among NK cells (Figure 2M) a statistically significant increase was observed when splenocytes were co-cultured with DCs overproducing IL-12 (groups III, VI, VII and IX). Although increased production of IFN-γ (Figure 2N) and IL-10 (Figure 2O) was detected in all groups with DC/IL-12/TAg, the highest concentration of these cytokines was observed after splenocyte stimulation with DC/IL-12/TAg and DCs overproducing IL-15 or IL-18 (groups VI and VII).

The tested cellular vaccines were capable of secreting cytokines whose genes have been introduced using a third-generation lentiviral system. Although cellular vaccines consisting of dendritic cell mixtures produced correspondingly smaller amounts of particular cytokines, the effect of these combinations revealed stronger stimulation of DCs. Thus, a preliminary assessment of the effectiveness of DCs transduced with cytokine genes and stimulated with TAg showed their significant effect on inducing a specific cellular response in *ex vivo* conditions. Dendritic cells overproducing IL-12 alone or in combination with other cytokines could activate $CD4^+$, $CD8^+$, and NK cells, and consequently, increase their ability to produce IFN-γ and IL-10. This indicates that this way prepared vaccines can be potent inducers of the anticancer immune response.

3.2 The influence of DC-based vaccines on tumor growth inhibition

In the next research stage, we determined whether, similarly to *in vitro* conditions, the combination of transductants will cause a better therapeutic effect manifesting the inhibition of tumor growth than one-component vaccines administered in the same final number of cells. In immunotherapeutic protocol, we decided to precede the administration of cell-based vaccines with an intraperitoneal injection of anti-IL-10R antibodies to make the immune system cells insensitive to the adverse effects of IL-10

10.3389/fimmu.2023.1212606

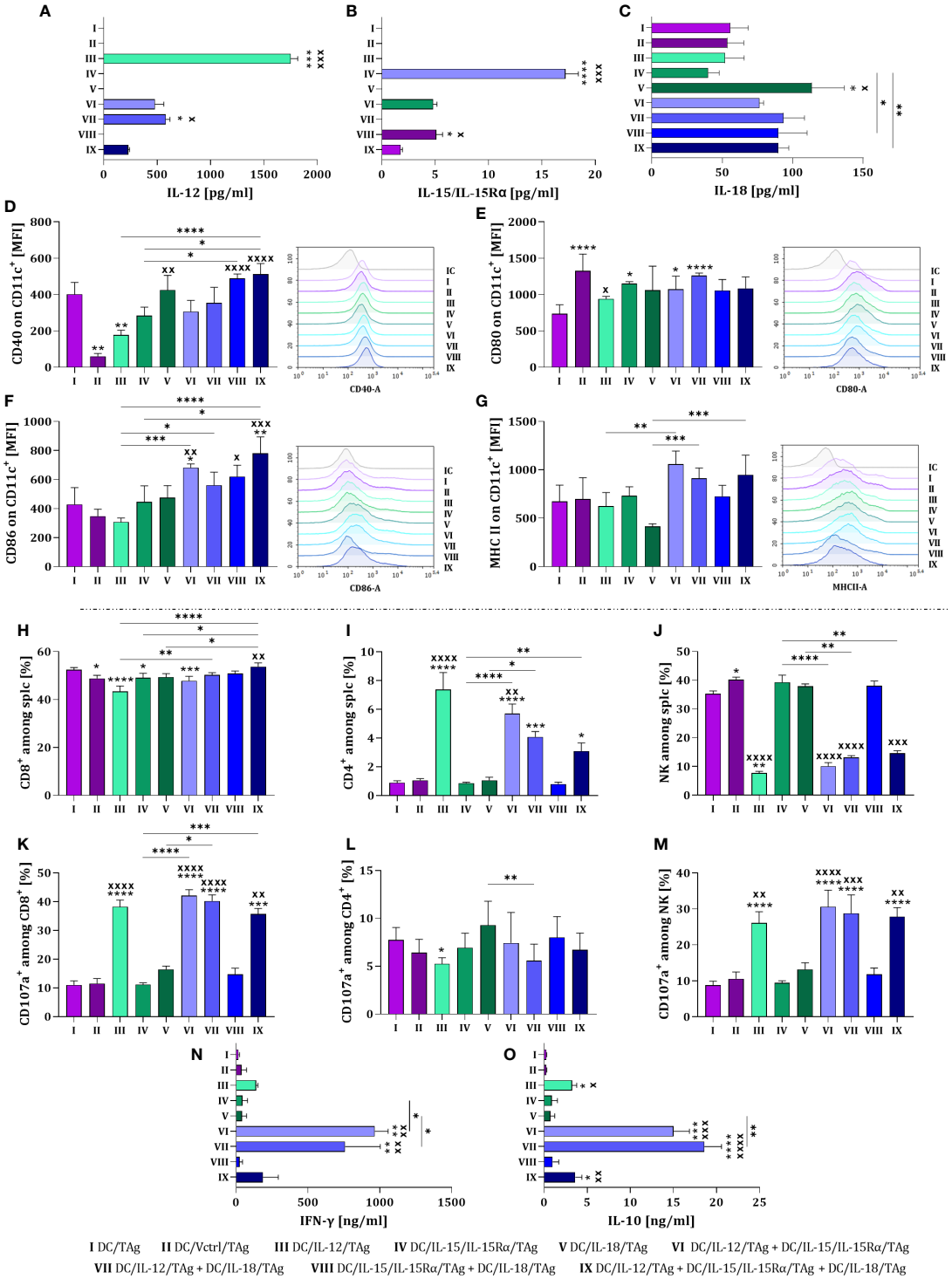

FIGURE 2
Estimation of the transduction efficiency of dendritic cells with lentiviral vectors carrying sequences of *il12*, *il15* and *il15rα* or *il18* genes. Concentration of **(A)** IL-12, **(B)** IL-15/IL-15Rα and **(C)** IL-18 in supernatants collected on the 10th day of DC culture was measured using ELISA. Expression of costimulatory molecules **(D)** CD40, **(E)** CD80, **(F)** CD86 and **(G)** MHC II on the surface of CD11c^{+} cells on the 10th day of DC culture measured by flow cytometry. On the 8th day of the culture, dendritic cells and splenocytes were co-cultured for 5 days. After this time, splenocyte activity after primary stimulation with genetically modified DCs was determined. Percentage of **(H)** CD8^{+}, **(I)** CD4^{+}, and **(J)** NK cells among activated splenocytes. Percentage of CD107a^{+} cells among **(K)** CD8^{+}, **(L)** CD4^{+} and **(M)** NK cells. Concentration of **(N)** IFN-γ and **(O)** IL-10 in supernatants after co-cultured activated spleen cells with modified DCs, measured using ELISA assay. Results are presented as mean+SD calculated for 6-12 samples per group. Differences between groups were estimated using the non-parametric Kruskal-Wallis test followed by Dunn's multiple comparisons *post-hoc* test **(A–O)**. The asterisks (*) presented in the graphs indicate statistically significant differences between the given groups and the DC/TAg control cells; crosses (X) indicate a statistically significant difference between the given group and the DC/Vctrl/TAg control cells; asterisks (*) under the line indicate statistically significant differences between the given groups – (*/^{x}p<0.05; **/^{xx}p<0.01; ***/^{xxx}p<0.001; ****/^{xxxx}p<0.0001). IC, *isotype control*.

produced in TME. This decision was based on our previous *in vitro* observations that vaccine dendritic cells are able to activate the splenocytes to produce the high IFN-γ amount accompanied by IL-10 secretion. Furthermore, after completing immunotherapy with cellular vaccines supported with anti-IL-10R antibodies, we conducted another chemoimmunotherapy experiment – in which the previous immunotherapy was supplemented with the administration of the HES-MTX nanoconjugate.

On the 16th, 23rd, and 30th day, mice were inoculated intraperitoneally with anti-IL-10R antibodies (250 μg/mouse). Day after (17th, 24th, and 31st day), cellular vaccines were administered peritumorally (p.t.) (2×10^6 cells/mice). As control cells, DC/TAg, and DC/Vctrl/TAg were used. On the 38th day, the therapeutic effect of the treatment was determined (Figure 3A). In the chemoimmunotherapy experiment, the protocol was supplemented with an intravenous injection of HES-MTX (20 mg/kg b.w.) on the 14th day of the experiment (Figure 3E).

Based on tumor volume measurements carried out during the therapeutic experiments, tumor growth curves (Figures 3B, F), and violin plots (Figures 3C, G) were prepared to determine the kinetics of tumor growth. The efficacy of both therapies was estimated based on relative tumor volume - the ratio of tumor volume on the day of measurement to tumor volume on the day of randomization (day 13). This method of presentation depicted the tumor growth rate relative to their initial volume and unified the differences between individual therapeutic groups. Hence, on the 38th day of the experiment, the degree of tumor growth inhibition (TGI) in the therapeutic groups compared to the non-treated group was calculated (Figures 3D, H).

The use of anti-IL10R antibodies in therapy inhibited the tumor growth rate in relation to the group of non-treated mice (TGI 30.2%). Moreover, the application of anti-IL10R antibodies and DC-based vaccines influenced the changes in tumor growth rate and this effect depended on the type of applied vaccine. It should be underlined that immunotherapy with one-component vaccines resulted in the greatest inhibition of tumor growth rate compared to the non-treated (nt) group (Figure 3D). The MC38 tumors growth inhibition in these groups ranged from 49.5% (for DC/IL-12/TAg) to 66% (for DC/IL-15/IL-15Rα/TAg). The effect of the two-component vaccines on TGI was weaker and an after the application of anti-IL-10R antibodies and the three-component vaccine, an ineffective treatment was shown.

In our previous studies, we found that using 20 mg/kg b.w. of the HES-MTX nanoconjugate leads to beneficial immunomodulation of the antitumor response (12). Therefore, this chemotherapeutic agent was administered to enhance the therapeutic effect of the herein used immunotherapy. The extension of the therapeutic scheme with the use of the HES-MTX prior to immunotherapy resulted in a strong increase in the value of TGI. The combined therapy resulted in the greatest inhibition of tumor growth when the vaccine containing DC/IL-15/IL-15Rα/TAg and DC/IL-18/TAg cells (72.4%, group VIII) was applied, whereas the use of the one-component vaccine (DC/IL-15/IL-15Rα/TAg or DC/IL-18/TAg, group IV and V, respectively) induced tumor growth inhibition on the level of 54.9% and 70.5% respectively (Figure 3H). Nevertheless, the most surprising result of combined chemoimmunotherapy was obtained after the administration of the three-component vaccine - supplementing the treatment schedule with the HES-MTX nanoconjugate administration resulted in an increase of TGI value to 69.9% in contrast to 24.0%, which was observed in this group but in the immunotherapeutic scheme of treatment.

Thus, our observations can suggest that the effect of the applied immunotherapy depends not only on the amount of delivered cytokines but also on their combination. Nonetheless, the administration of the HES-MTX nanoconjugate facilitated the enhancement of vaccine efficacy, even when the amount of produced cytokines turned out too weak to contribute to the therapeutic effect in the course of immunotherapy.

3.3 Leukocyte infiltration of tumor nodules in applied therapies

Interested in the changes in the tumor growth rate between the applied therapies, we decided to check their influence on leukocyte infiltration into tumors. For this purpose, MC38 tumor nodules were harvested on the 38th day of therapy and multiparameter cytometric analyses were performed to identify myeloid and lymphoid cell influxes (Figure 4A). Briefly, among alive leukocytes ($CD45^+DAPI^-$), we determined the effect of the applied therapies on changes in the percentage of lymphoid cells among leukocytes such as lymphocytes T CD8 ($CD3^+CD8^+$), T CD4 ($CD3^+CD4^+$), Treg ($CD3^+CD4^+CD25^+FoxP3^+$), NK ($CD3^-NK1.1^+$), NKT ($CD3^+NK1.1^+$) and B lymphocytes ($CD19^+$). There were also distinguished populations of the myeloid cells ($CD11b^+$) including DCs ($CD11c^+F4/80^{int}MHC\ II^+$), TAMs ($CD11c^+F4/80^+$), MDSCs ($CD11c^-Ly6C^+$), M1 ($CD206^-$) and M2 ($CD206^+$) macrophages. Despite extensive cytometric analysis of cells infiltrating tumor tissue, we did not observe significant differences in all populations. Therefore we decided to discuss only some of them in more detail.

After the application of immunotherapy, we observed a slight increase in the percentage of leukocytes in tumor tissue obtained from mice treated with DC-based vaccines, which was the highest when DC/IL-12/TAg was used. (Figure 4B). However, based on summary graphs presenting normalized data, we also visualized the differences in individual subpopulations of leukocytes infiltrating tumor tissue (Figure 4C).

The percentage of $CD8^+$ cells infiltrating tumor tissue increased after the administration of cellular vaccines and anti-IL10R antibodies. However, a statistically significant increase was observed only after the use of DC/IL-12/TAg + DC/IL-18/TAg (Figure 4D). Application of DC-based vaccines generated an increase in the percentage of $CD4^+$ cells relative to the non-treated (nt) and antibodies-treated (Ab) groups. A statistically significant increase in the percentage of $CD4^+$ cells was observed after the use of DC/IL-12/TAg and DC/IL-15/IL-15Rα/TAg and two-component vaccines (Figure 4E). At the same time, there was a substantial reduction in the population size of regulatory T cells among $CD4^+$ cells in tumor tissue. This decrease in the percentage of Tregs was rather related to the use of DC-based vaccines,

10.3389/fimmu.2023.1212606

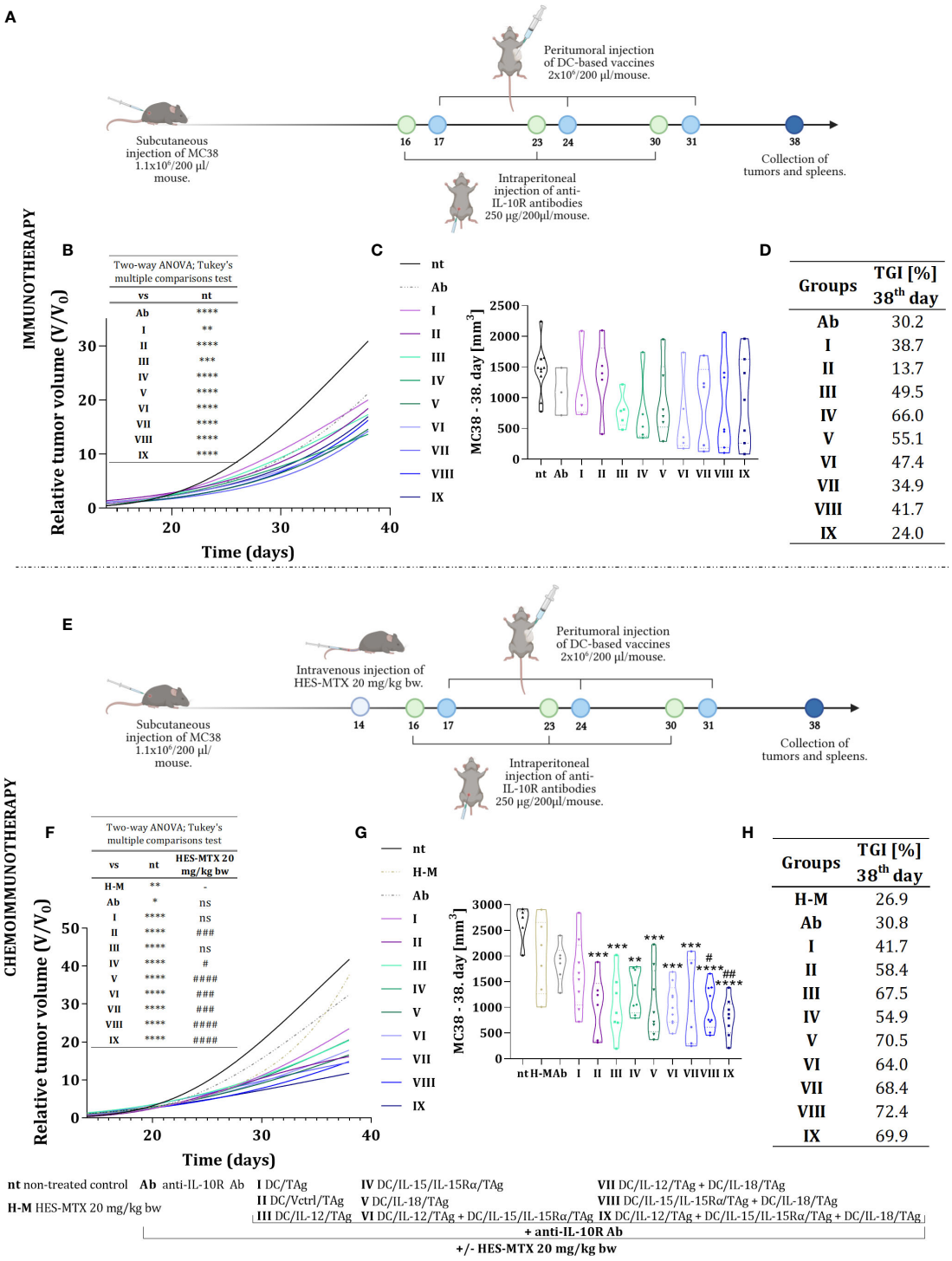

FIGURE 3
Growth of MC38 tumors in mice treated with immunotherapy or chemoimmunotherapy with nanoconjugate HES-MTX followed by multiple injections of anti-IL-10R antibodies and DC-based vaccines. Treatment schedule of immunotherapy **(A)** and chemoimmunotherapy **(E)** created with BioRender.com. **(B, F)** Graph presenting the growth kinetics of MC38 tumor (shown as relative tumor volume) in mice after immunotherapy or chemoimmunotherapy (data was normalized). **(C, G)** Truncated violin plot presenting individual tumors volume and designated median tumor volume for each group, calculated on the 38th day of the immunotherapy or chemoimmunotherapy experiment. Results are presented as median for 3-10 mice per group. **(D, H)** Table presenting MC38 tumor growth inhibition (TGI) calculated on the 38th day of the experiment in relation to the non-treated group (nt). Differences between groups were estimated using the two–way ANOVA followed by Tukey's multiple comparisons *post–hoc* test **(B, E)** or nonparametric Kruskal–Wallis test followed by Dunn's multiple comparisons test **(C, G)**. The asterisks (*) presented in the graphs indicate statistically significant differences between the given groups and the non-treated control group (nt); hashtags (#) above a bar indicate a statistically significant difference between the given group and the HES-MTX treated group (H-M) – (*/$^{\#}$p<0.05; **/$^{\#\#}$p<0.01; ***/$^{\#\#\#}$p<0.001; ****/$^{\#\#\#\#}$p<0.0001).

10.3389/fimmu.2023.1212606

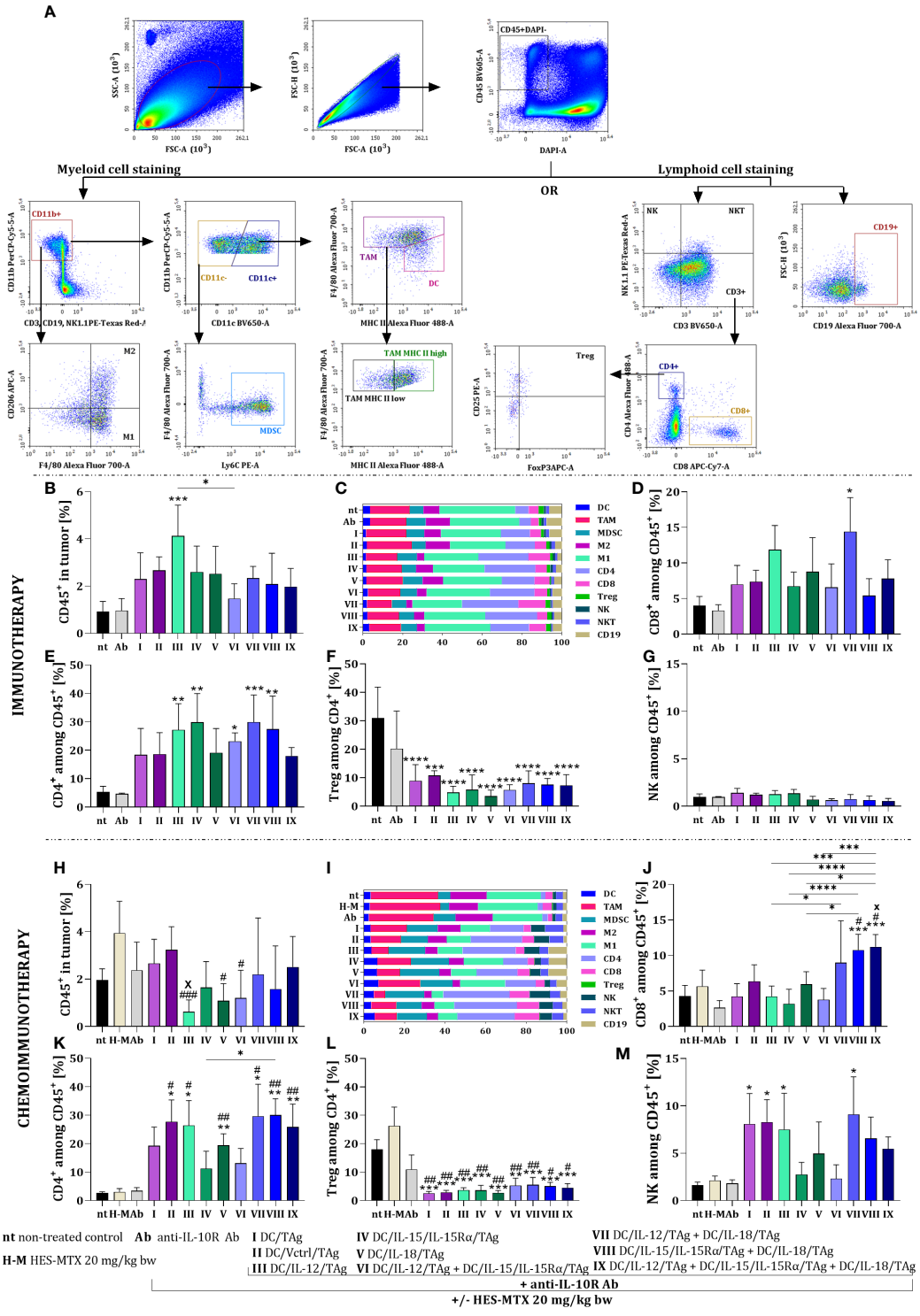

FIGURE 4
Influence of applied immunotherapy or chemoimmunotherapy on MC38 tumor nodules infiltration with leukocytes. **(A)** Scheme of the multiparameter flow cytometric analysis of lymphoid and myeloid cells in tumor tissue. **(B, H)** Percentage of live CD45$^+$ cells in tumor tissue. Percentage of **(C, I)** each leukocyte population, **(D, J)** CD8$^+$, **(E, K)** CD4$^+$, **(G, M)** NK cells among CD45$^+$ cells in tumor. **(F, L)** Percentage of T regulatory lymphocytes among CD4$^+$ cells in tumor tissue. Results are presented as mean+SD calculated for 3-7 mice per group. Differences between groups were estimated using the non-parametric Kruskal-Wallis test followed by Dunn's multiple comparisons *post-hoc* test **(J, M)**, the parametric one-way ANOVA followed by Tukey's multiple comparisons *post-hoc* test **(B, D, H, K, L)** or the parametric Brown-Forsythe and Welch ANOVA test followed by Dunnett's T3 multiple comparisons *post-hoc* test **(E, F)**. The asterisks (*) presented in the graphs indicate statistically significant differences between the given groups and the non-treated control group (nt); hashtags (#) above a bar indicate a statistically significant difference between the given group and the HES-MTX treated group (H-M); crosses (X) indicate a statistically significant difference between the given group and DC/Vctrl/TAg treated group; asterisks (*) under the line indicate statistically significant differences between the given groups – (*/$^{\#}$/^{X}p<0.05; **/$^{\#\#}$p<0.01; ***/$^{\#\#\#}$p<0.001; ****p<0.0001).

regardless of the ability of DCs to overproduce cytokines (Figure 4F). We also observed a slight reduction in the percentage of NK cells after the administration of DC-based vaccines consisted of more than one type of produced cytokines (groups VI-IX) (Figure 4G).

After chemoimmunotherapy, a slight reduction in the leukocyte population size was noted in all therapeutic groups (Figure 4H). The lowest percentage of CD45$^+$ cells was found after using DC/IL-12/TAg (group III). In addition, there were substantial differences between the effects of different types of vaccines on TAM, M1, M2, CD4+, CD8+, and NK cell population sizes (Figure 4I).

A statistically significant increase in the percentage of CD8$^+$ cells was observed as a result of chemoimmunotherapy containing a mixture of DCs overproducing IL-15 and IL-18 (group VIII) or all three tested cytokines (group IX) in relation to control groups (groups nt, H-M) and one-component DC-based vaccines. Furthermore, a slight increase in the size of the CD8$^+$ cell population was observed after the administration of DC/IL-12/TAg + DC/IL-18/TAg (group VII) (Figure 4J). The high percentage of CD4$^+$ cells in tumor tissue was always observed when DC-based vaccines were applied (Figure 4K). In both T lymphocyte subpopulations, using the nanoconjugate prior to immunotherapy was the most conducive to the effect of two or three-component vaccines. The administration of the chemotherapeutic agent did not enhance the effect of the immunotherapy on changes in the size of Treg cell population (Figure 4L). Meanwhile, an increase in the percentage of NK cell population was visible, especially in groups I, II, III and VII (Figure 4M).

In the case of the immunotherapeutic treatment schedule, the applied DC-based vaccines did not cause significant changes in the percentage of myeloid cells in tumor tissue. Although there was no effect of this therapy on changes in the size of the TAM population (Figure 5A), we observed differences in their activation level. Based on the ratio of TAM MHC II^{high} to TAM MHC II^{low}, we found that in the groups receiving cellular vaccines, TAMs with high expression of MHC II were slightly dominated and the highest value of this ratio was observed after the administration of a two-component DC vaccine containing DC/IL-12/TAg and DC/IL-18/TAg (Figure 5B). Besides, analyzing the effect of therapy influences on macrophage influx, we observed an increased M1 to M2 macrophage ratio in the groups receiving two-component and three-component DC vaccines (Figure 5C).

The combined therapy with the use of the HES-MTX nanoconjugate induced statistically significant changes in the

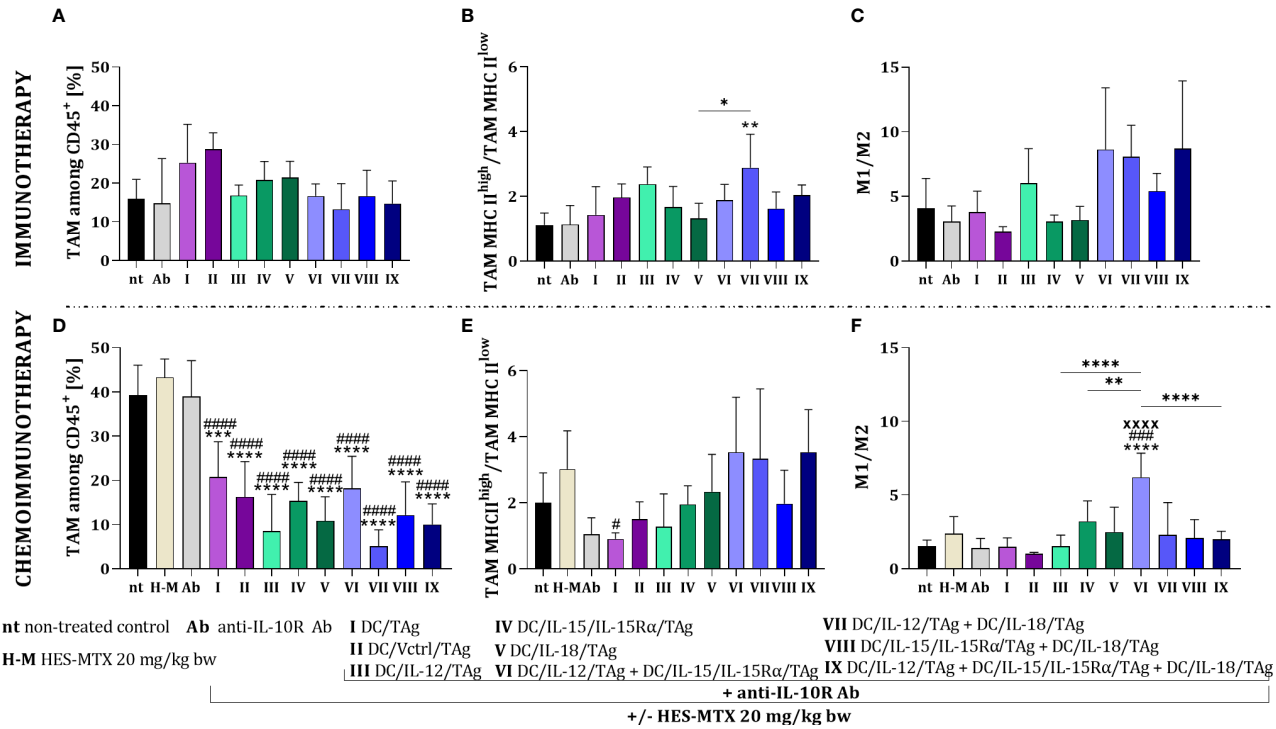

FIGURE 5
Evaluation of macrophage polarization in MC38 tumor tissue after immunotherapy or chemoimmunotherapy. Scheme of the multiparameter flow cytometric analysis of macrophage subpopulation in MC38 tumor nodules obtained from mice after immunotherapy or chemoimmunotherapy is shown in Figure 4A. **(A, D)** Percentage of TAM among CD45$^+$ cells in tumors. **(B, E)** TAM MHC II^{high}/TAM MHC II^{low} and **(C, F)** M1/M2 ratios showing the polarization of TAMs in MC38 tumor tissue. Results are presented as mean+SD calculated for 3-7 mice per group. Differences between groups were estimated using the non-parametric Kruskal-Wallis test followed by Dunn's multiple comparisons *post-hoc* test **(E)** or the parametric one-way ANOVA followed by Tukey's multiple comparisons *post-hoc* test **(B, D, F)**. The asterisks (*) presented in the graphs indicate statistically significant differences between the given groups and the non-treated control group (nt); hashtags (#) above a bar indicate a statistically significant difference between the given group and the HES-MTX treated group (H-M); crosses (X) indicate a statistically significant difference between the given group and the DC/Vctrl/TAg treated group; asterisks (*) under the line indicate statistically significant differences between the given groups – (*/$^{\#}$p<0.05; **p<0.01; ***/$^{\#\#\#}$p<0.001; ****/$^{\#\#\#\#}$/^{XXXX}p<0.0001).

TAM percentage relative to the non-treated or the chemotherapeutic treated groups (Figure 5D). The highest value of the TAM MHC II^{high}/TAM MHC II^{low} ratio was shown after the administration of chemoimmunotherapy containing two or three-component vaccines comprising DC/IL-12/TAg (Figure 5E). On the other hand, the highest value of the M1/M2 ratio was demonstrated after therapy with HES-MTX, anti-IL-10R and DC/IL-12/TAg + DC/IL-15/IL-15Rα/TAg (Figure 5F).

The use of the HES-MTX nanoconjugate before immunotherapy created optimal conditions for the effective action of cell-based vaccines. The most favorable effect was observed in the groups receiving dendritic cell mixtures, especially the three-component vaccine.

3.4 Influence of multicomponent treatment on systemic antitumor response

To confirm the assumption that the enhancement of the effect of both multicomponent immunotherapy and chemoimmunotherapy depends mainly on the use of DCs mixtures, we assessed their effect on the activity of systemic antitumor response. For this purpose, on the 38th day of both therapies' spleens from treated tumor-bearing mice were harvested and restimulated with MC38 cells in a 5-day mixed culture. Next, multiparameter cytometric analyses were performed among alive splenocytes (CD45$^+$DAPI$^-$), to identify changes in the percentage of CD8$^+$, CD4$^+$ and NK cells as well as their ability to secrete cytolytic granules based on the expression of the CD107a molecule (Figure 6A).

There was no significant change in the size of the CD8$^+$ cell population among restimulated splenocytes obtained from mice after immunotherapy with cytokine-secreting DC-based vaccines (Figure 6B). Solely after the application of anti-IL-10R and DC/TAg (group I) the percentage of these cells was significantly lower than in the untreated group. An increase in the percentage of CD4$^+$ cells was seen after treatment with cellular vaccines, especially after administration of DC/IL-12/TAg + DC/IL-15/IL-15Rα/TAg and DC/IL-12/TAg + DC/IL-18/TAg (Figure 6C). However, after the application of all cell-based vaccines, there was a reduction in the percentage of NK cell population (Figure 6D). The applied therapy did not significantly change the percentage of CD107a$^+$ cells among CD8$^+$ cells (Figure 6E) and NK cells (Figure 6G) in comparison to their controls. Meanwhile, the ability to release cytolytic granules increased among CD4$^+$ cell populations, turn to be related to the anti-IL-10R antibodies administration (Figure 6F).

The supplementation of treatment with the HES-MTX nanoconjugate caused a reduction in the percentage of CD8$^+$ cells, especially after DC/Vctrl/TAg (group II), DC/IL-12/TAg (group III), and DC/IL-15/IL-15Rα/TAg (group IV). However, the visible increase in the percentage of this population in relation to DC/Vctrl/TAg occurred after the administration of DC/IL-12/TAg + DC/IL-18/TAg (group VII) vaccines (Figure 6H). The administration of combined therapy with cytostatic caused an increase in the percentage of CD4$^+$ cells, like immunotherapy, but the changes concerned other therapeutic groups. This cell population's size increased after the DC/Vctrl/TAg (group II) and DC/IL-12/TAg (group III) vaccines. An enhanced effect of DC/IL-15/IL-15Rα/TAg and the three-component vaccine on the population of restimulated splenic CD4$^+$ cells (Figure 6I) was also observed. The administration of the chemotherapeutic agent and DC-based vaccines supported with anti-IL-10R antibodies deepened the reduction in the percentage of NK cells in relation to immunotherapy alone (Figure 6J). The effect of the applied chemoimmunotherapy on the size of the cell subpopulations able to release cytolytic granules was also revealed. The lowest ability to secrete cytolytic granules was found in CD8$^+$ cells obtained from mice treated with HES-MTX + anti-IL-10R + DC/Vctrl/TAg (Figure 6K). In contrast, among CD4$^+$ cells, the highest cytolytic activity was observed in the group of mice receiving dendritic cells modified to overproduce IL-15/IL-15Rα (Figure 6L). The size of NK CD107a$^+$ population increased in all groups receiving DC-based vaccines in relation to control groups (groups: nt, H-M and Ab) (Figure 6M).

Comparison of both therapies harnessing schedules, including treatment with antibodies, and/or additional supplementation with HES-MTX, resulted in marked differences compared to the non-treated group. The use of cytostatic agent deepened variations among particular groups and enhanced the mixture effect of the DC-based vaccines, especially these three-component. Consequently, such a multicomponent combination enhanced the systemic activity of main populations of immune cells.

As confirmation of the potential for antitumor activity, the ability of restimulated splenocytes to produce cytokines and their cytotoxic activity against MC38 cells was examined. In the case of immunotherapy, splenocytes obtained from mice treated with DC/IL-12/TAg were able to produce the highest amount of IFN-γ (Figure 7A). The highest production of IL-4 was noted after the application of the therapy consisted of DC/IL-15/IL-15Rα/TAg (group IV) and DC/IL-12/TAg + DC/IL-15/IL-15Rα/TAg (group VI) (Figure 7B). In contrast, increased production of IL-10 by splenocytes was shown in the groups of mice treated with DC-based vaccines, as well as anti-IL-10R antibodies alone (Figure 7C). The highest cytotoxic activity of splenocytes against MC38 cells (Figure 7D) was observed in all groups treated with DC-based vaccines, especially after the application of DC/TAg (group I), DC/IL-15/IL-15/Rα/TAg (group IV) and the three-component vaccine (group IX).

The use of the HES-MTX nanoconjugate prior to immunotherapy strongly changed the type and level of cytokine production by splenocytes causing an increase in their ability to produce IFN-γ (Figure 7E). Thus, while the production level of this cytokine did not change markedly after the administration of DC/IL-12/TAg alone, the splenocyte's ability to produce IFN-γ increased after the use of DCs mixed cultures, especially in DC/IL-12/TAg + DC/IL-18/TAg group (group VII). The HES-MTX nanoconjugate also influenced changes in the production of IL-4 by spleen cells obtained from mice after therapy. The highest ability to produce IL-4 was characterized by splenocytes obtained from mice treated with combination therapy with DC/IL-15/IL-15Rα/TAg (group IV), DC/IL-15/IL-15Rα/TAg + DC/IL-18/TAg (group VIII) and three-component vaccine (group IX) (Figure 7F).

10.3389/fimmu.2023.1212606

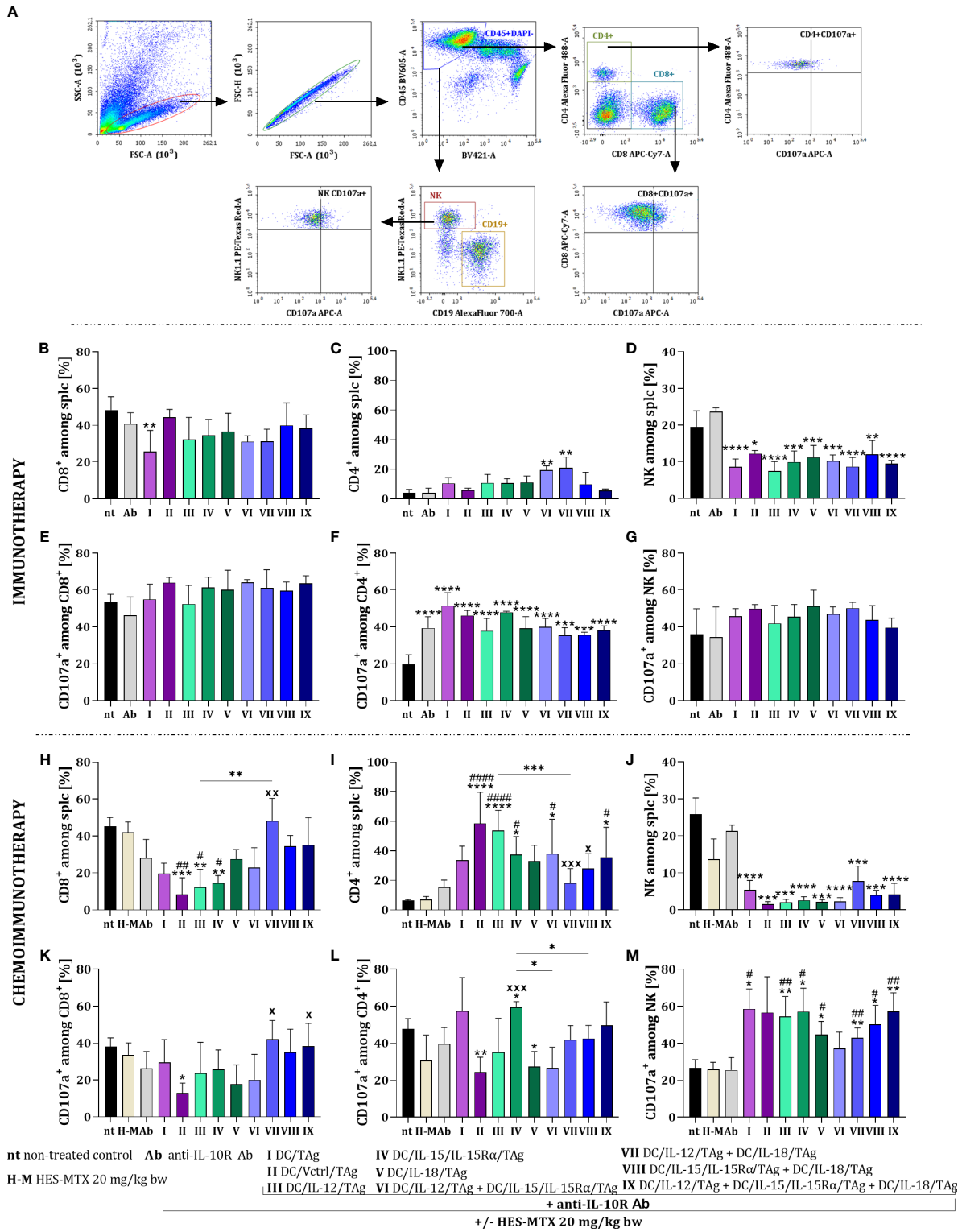

FIGURE 6
Effect of applied immunotherapy and chemoimmunotherapy on activation of the restimulated splenocytes. **(A)** Scheme of the multiparameter flow cytometric analysis of activated $CD8^+$, $CD4^+$, and NK cells among restimulated splenocytes measured by CD107a degranulation assay. Percentage of **(B, H)** $CD8^+$, **(C, I)** $CD4^+$, and **(D, J)** NK cells among restimulated splenocytes. Percentage of $CD107a^+$ cells among **(E, K)** $CD8^+$, **(F, L)** $CD4^+$ and **(G, M)** NK cells. Results are presented as mean+SD calculated for 3-7 mice per group. Differences between groups were estimated using the non-parametric Kruskal-Wallis test followed by Dunn's multiple comparisons *post-hoc* test **(C)**, the parametric one-way ANOVA followed by Tukey's multiple comparisons *post-hoc* test **(B, D, F, H–M)**. The asterisks (*) presented in the graphs indicate statistically significant differences between the given groups and the non-treated control group (nt); hashtags (#) above a bar indicate a statistically significant difference between the given group and the HES-MTX treated group (H-M); crosses (X) indicate a statistically significant difference between the given group and the DC/Vctrl/TAg treated group; asterisks (*) under the line indicate statistically significant differences between the given groups – (*/#/^{x}p<0.05; **/##/^{xx}p<0.01; ***/^{xxx}p<0.001; ****/$^{####}$p<0.0001).

10.3389/fimmu.2023.1212606

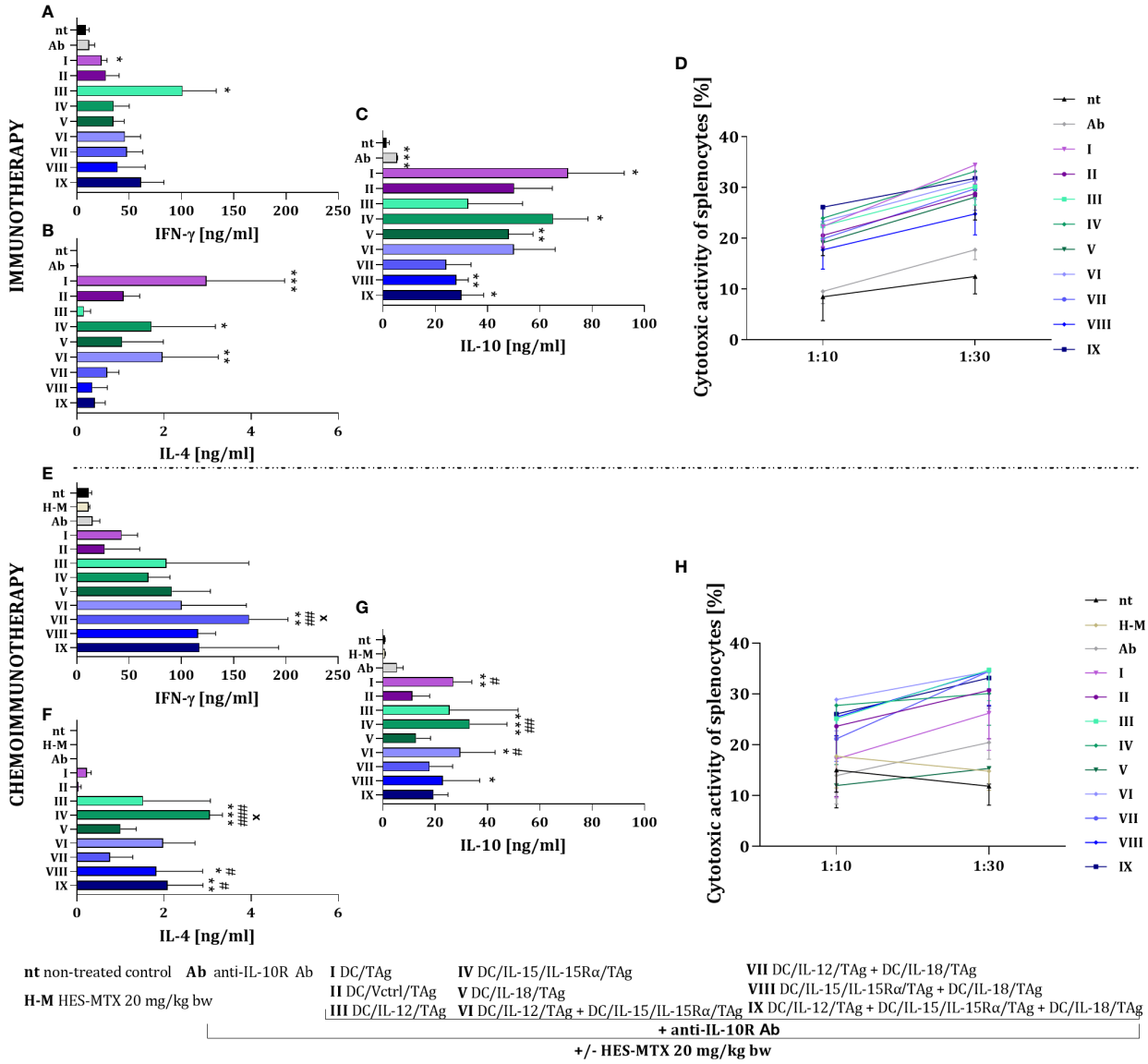

FIGURE 7
Impact of conducted immunotherapy and chemoimmunotherapy on activation of the systemic antitumor response. Concentration of **(A, E)** IFN-γ, **(B, F)** IL-4 and **(C, G)** IL-10 in supernatants after restimulation of spleen cells with MC38 cells, measured using ELISA assay. **(D, H)** Cytotoxic activity of splenocytes (effector cells, E) against DiO^{+} MC38 cells (target cells, T) after 4-hour incubation in 10:1 and 30:1 E:T ratios, measured using flow cytometry. Results are presented as mean+SD calculated for 3-7 mice per group. Differences between groups were estimated using the non-parametric Kruskal-Wallis test followed by Dunn's multiple comparisons *post-hoc* test **(B, C, E–G)** or the parametric Brown-Forsythe and Welch ANOVA test followed by Dunnett's T3 multiple comparisons *post-hoc* test **(A)**. The asterisks (*) presented in the graphs indicate statistically significant differences between the given groups and the non-treated control group (nt); hashtags (#) above a bar indicate a statistically significant difference between the given group and the HES-MTX treated group (H-M); crosses (X) indicate a statistically significant difference between the given group and the DC/Vctrl/TAg treated group – (*/$^{\#}$/^{x}p<0.05; **/$^{\#\#}$p<0.01; ***/$^{\#\#\#}$p<0.001).

Splenocytes obtained from mice which were treated with vaccines containing DCs showed a decrease in IL-10 production which suggest the influence of the HES-MTX nanoconjugate on the prolongation of the decrease of suppressor cell activity (Figure 7G). The addition of the nanoconjugate involved a slight increase in the splenocytes' cytotoxic activity compared to immunotherapy. However, it depended on the type of vaccine and did not reveal which modified dendritic cell mixtures should be considered the most powerful (Figure 7H).

The observed changes in the systemic anticancer response confirm that the use of the HES-MTX chemotherapeutic agent has the most beneficial action on the cellular vaccines that are a mixture of two or three transductants. In these groups, an increase in IFN-γ and a decrease in IL-10 production, as well as an enhancement in the cytotoxic activity of restimulated splenocytes are particularly visible.

The use of the developed vaccines in anticancer therapy in combination with anti-IL-10R antibodies and/or a chemotherapeutic

agent influenced both the changes in the tumor microenvironment and the activation of the systemic immune response. Both the antibodies and the chemotherapeutic administered prior to DC-based vaccines created a favorable microenvironment in which the vaccines were characterized by different mechanisms of action (Figure 8 and Supplementary Tables 1–4) mainly representing the effect of overproduced cytokines. By virtue of the use of each of the developed vaccines, the percentage of Treg lymphocytes in both immuno- and chemoimmunotherapy decreased. The supplement of the cellular vaccines treatment with the HES-MTX nanoconjugate affected the enhanced tumor growth inhibition, with the exception of the DC/IL-15/IL-15Rα/TAg.

In the immunotherapy, the DC/IL-12/TAg mainly increased the influx of $CD8^+$, $CD4^+$ and NK cells to tumor nodules, which was accompanied by a decrease in the population of Treg and TAMs and an increase in IFN-γ production and cytotoxic activity of splenocytes. The addition of HES-MTX agent had a positive effect primarily on the systemic immune response. The use of DC/IL-15/IL-15Rα/TAg increased the influx of $CD4^+$ and NK cells into tumors. The potential of splenocytes to release cytolytic granules by $CD8^+$ and $CD4^+$ cells, IL-10 production and cytotoxic activity also increased. Meanwhile, supplementation of the immunotherapy schedule with nanoconjugate did not favorably affect the effect of this vaccine in tumor tissue, resulting in a reduction of $CD4^+$ and NK cell percentage. In addition, a decrease in the percentage of $CD8^+$ cells and no change in the cytotoxic activity of this cell subpopulation among the restimulated splenocytes was observed. However, this treatment resulted in an increase in the percentage of

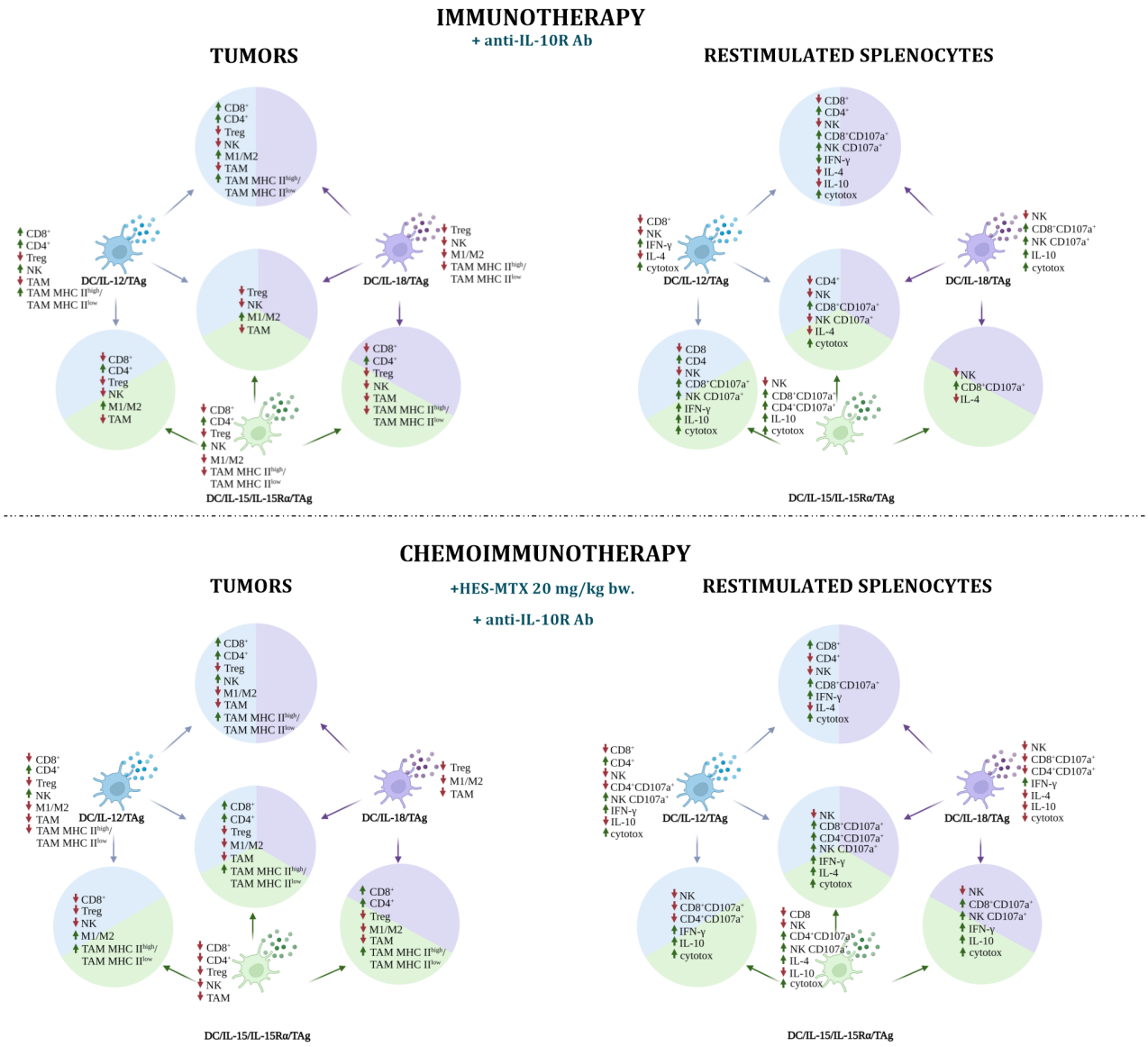

FIGURE 8
Impact of immunotherapy and chemoimmunotherapy based on DC-based vaccines on individual populations of immune cells in tumors and restimulated splenocytes. The diagrams show the effect of cellular vaccines on the increase (up arrow ↑) and decrease (down arrow ↓) of $CD8^+$, $CD4^+$, Treg, NK, TAM cell populations and M1/M2 and TAM MHC II^{high}/TAM MHC II^{low} ratios in tumors and of $CD8^+$, $CD4^+$, NK, $CD107a^+$ cell populations, IFN-γ, IL-10 production and cytotoxic activity among restimulated splenocytes. The figure was created with BioRender.com.

$CD4^+CD107a^+$, NK $CD107a^+$ cells, IL-4 production and cytotoxic activity. Dendritic cells overproducing IL-18 mainly affected the percentage reduction of Treg lymphocytes, NK cells, M1/M2 and TAM MHC II^{high}/TAM MHC II^{low} ratios in tumors, while the population of $CD8^+CD107a^+$ and NK $CD107a^+$ cells and cytotoxic activity of splenocytes increased. The therapy combined with nanoconjugate caused the reduction of TAM percentage. Although among the restimulated splenocytes the percentage of cells capable of releasing cytolytic granules and production of IL-10 decreased, the production of IFN-γ increased.

In immunotherapy, all two-component vaccines caused a reduction of TAMs and NK cell populations in tumors, but a higher percentage of $CD8^+CD107a^+$ cells was observed among restimulated splenocytes. During immunotherapy, the DC/IL-12/TAg + DC/IL-15/IL-15Rα/TAg vaccine increased the percentage of $CD4^+$ cells and the M1/M2 macrophages ratio in tumors, while the percentage of $CD8^+$ cells, Treg, NK and TAMs decreased. Among the splenocytes, a higher percentage of $CD4^+$, $CD8^+CD107a^+$ and NK $CD107a^+$ cells, production of IFN-γ and IL-10 and cytotoxic activity were observed. During chemoimmunotherapy, only the M1/M2 ratio remained at an increased level and a high TAM MHC II^{high}/TAM MHC II^{low} ratio was observed. Among splenocytes, in addition to a decrease in the population of NK, $CD8^+CD107a^+$, $CD4^+CD107a^+$cells, an increase in the production of IFN-γ, IL-10 and cytotoxic activity was revealed. Administration of DC/IL-12/TAg + DC/IL-18/TAg resulted in an augmented influx of $CD4^+$ and $CD8^+$ cells into the tumors and growth of M1/M2 and TAM MHC II^{high}/TAM MHC II^{low} ratios. Among the splenocytes, an increase in the percentage of $CD4^+$ cells and cytolytic activity of $CD8^+$ and NK cells was observed, as well as higher production of IFN-γ and a decrease in the production of both IL-4 and IL-10, which could have enhanced the cytotoxic activity of splenocytes. The addition of the chemotherapeutic intensified the influx of NK cells, but the M1/M2 ratio decreased. In the spleens, an increase in the percentage of $CD8^+$ cells was observed, with a simultaneous reduction of $CD4^+$ cell percentage. During immunotherapy, a vaccine combining DC/IL-15/IL-15Rα/TAg and DC/IL-18/TAg induced tumor growth inhibition of 41.7%, which may be the result of the influx of $CD4^+$ cells with a simultaneous reduction in the percentage of tumor suppressor Tregs and TAMs. However, this vaccine induced a decrease in the percentage of $CD8^+$ and NK cells. Among the splenocytes, a decrease in the percentage of NK cells and a higher percentage of $CD8^+CD107a^+$ cells were observed. The addition of the chemotherapeutic agent resulted in this vaccine eliciting the highest tumor growth inhibition (72.4%), which may have been due to the additional influx of CD8 lymphocytes and the increase in the TAM MHC II^{high} to TAM MHC II^{low} ratio, while the overall TAM cell population, Treg, M1/M2 ratio decreased. In restimulated splenocytes, an increased percentage of $CD8^+$ and NK cells capable of releasing cytolytic granules was observed, and in addition, these cells were capable of high IFN-γ and IL-10 production and were characterized by high cytotoxic activity.

The three-component vaccine DC/IL-12/TAg + DC/IL-15/IL-15Rα/TAg + DC/IL-18/TAg during immunotherapy showed a negligible therapeutic effect. Inhibition of tumor growth was only 24%, and we did not observe an increased influx of $CD4^+$ and $CD8^+$ cells in tumors, but a higher M1/M2 macrophage ratio and a decrease in the percentage of Treg, NK cells and TAMs. In the spleens, a reduction of $CD4^+$, NK, NK $CD107a^+$ cell percentage and IL-4 production was revealed, while an increase in the percentage of $CD8^+CD107a^+$ cells and cytotoxic activity was observed. However, the addition of the HES-MTX nanoconjugate to the therapy resulted in enhanced tumor inhibition (69.9%), an augmented influx of $CD8^+$, $CD4^+$ cells, and a higher TAM MHC II^{high}/TAM MHC II^{low} ratio in a tumor, at the same time reducing the percentage of Treg, M1/M2 ratio and TAMs. On the other hand, in the spleens, we observed an increase in the cytolytic activity of $CD4^+$, $CD8^+$ and NK cells, an increase in the production of IFN-γ and IL-4 and cytotoxic activity.

4 Discussion

The main aim of our study was to determine whether the administration of HES-MTX before immunotherapy would change the antitumor effect of dendritic cells modified for overproduction of IL-12, IL-15, or IL-18. As numerous literature reports showed a beneficial effect resulting from the combination of different cytokines we decided to apply a combination of modified cells (39–41). Furthermore, DC-based therapy was enriched with components able to reduce the hostile impact of TME on applied vaccines. For this purpose, we used antibodies directed against the IL-10R receptor, which should partially block the negative effect of IL-10 on the cells of the immune system (23, 42) and HES-MTX as an immunomodulatory chemotherapeutic agent.

We started our research by characterizing the obtained dendritic cell transductants. Modification of DCs with a lentiviral control vector (DC/Vctrl/TAg) caused a short-term reduction in the expression of costimulatory molecules CD40, CD80, CD86, and MHC II, which is consistent with the research of French scientists (43). However, cytokines' action abolished the transduction's negative effect. Compared to monocultures, the increased expression of costimulatory molecules and MHC II was observed on the two-component cellular vaccines. Nevertheless, three-component vaccines revealed the highest maturity despite the lowest production of single cytokines. It showed that the cooperation of these cytokines might potentiate DC activity, which confirmed reports, that the presence of proinflammatory cytokines in the environment of DCs allows for achieving a higher degree of cell maturity than after activation with TAg alone (37). Many works showed the influence of IL-12, IL-15, or IL-18 on changes in the surface phenotype of dendritic cells (44–47). However, none of them tested the effect of these three cytokines simultaneously.

As part of the functional characterization of the vaccine cells, the ability of transduced TAg-stimulated DCs to activate splenocytes was assessed. Among the splenocytes from co-culture, changes in the percentage of $CD4^+$, $CD8^+$, NK, and $CD107a^+$ cells were determined, as well as the production of IFN-γ and IL-10. The $CD8^+$ and NK cells cultured in the presence of DCs modified to overproduce IL-12 were characterized by the greatest ability to secrete cytolytic granules, regardless of whether DCs were used as a

monoculture or in combination with other cytokines. Notably, the activation level of $CD8^+$ and NK cells was similar in each of these mixtures. However, splenocytes cultured with DC/IL-12/TAg + DC/IL-15/IL-15Rα/TAg or DC/IL-12/TAg + DC/IL-18/TAg had the highest potential for IFN-γ secretion. This observation is consistent with numerous studies showing the synergistic effect of IL-12 and IL-18 or IL-15 on IFN-γ production (48–50). Moreover, Martinović et al. showed that simultaneous stimulation by IL-12 and IL-18 induced an increase in the cytotoxic activity of NK cells and expression of CD107a on their surface, as well as IFN-γ production, than independent stimulation (51).

We used the tested cellular vaccines in two experiments - immunotherapeutic and chemoimmunotherapeutic. In the immunotherapeutic part, antibodies blocking the IL-10 receptor were administered to mice prior to the application of cellular vaccines. This was conducted due to reports that in cancer patients elevated IL-10 levels are associated with a poorer prognostic (52, 53). Moreover, Llopiz et al. observed that IL-10 induced in DCs less mature phenotype and decreased T-cell activation capacity (54). Therefore, it seems justified to use antibodies blocking the IL-10 receptor to abolish the negative impact of this cytokine on all immune cells.

The applied therapies based on dendritic cells caused an increase in the percentage of $CD4^+$ and $CD8^+$ cells among cells infiltrating tumor tissue and a simultaneous decrease in the percentage of Treg cells among $CD4^+$ lymphocytes. Although literature data indicate the influence of IL-12, IL-15 and IL-18 on the increase in the percentage of NK cells (55), we did not observe such changes in our studies. It should be emphasized that in the data presented by Oka et al. study recombinant cytokines were used in high doses. In our research, dendritic cells were used as producers of these cytokines, which released them over a long period, but in lower concentrations.

The use of the HES-MTX nanoconjugate before administration of the immunotherapy enhanced the therapeutic efficacy of the vaccines, especially those three-component. In the case of immunotherapy alone, the use of a three-component vaccine did not significantly inhibit tumor growth (24.0% TGI), while the addition of cytostatic affected its effectiveness (69.9% TGI). It should be highlighted that the three-component vaccine showed the highest anti-cancer potential in *in vitro* studies. This may indicate that ability of these types of DC-based vaccines to trigger effective anti-tumor immune response has been diminished by a hostile tumor microenvironment. HES-MTX alone resulted in a 26.9% inhibition of tumor growth. As literature has shown, other methotrexate-based chemotherapeutics, such as glucose-methotrexate conjugate (GLU-MTX) and hydroxyethyl cellulose-methotrexate (HEC-MTX) also caused significant tumor growth delay *in vivo* in breast cancer-bearing mice (56, 57).

The inclusion in the therapy of a chemotherapeutic agent further reduced the percentage of TAMs in the groups receiving anti-IL-10R antibodies and cellular vaccines, especially those capable of releasing cytokines. The reduction of TAMs is a good prognostic marker because these cells can promote tumor progression by producing factors and cytokines that support tumor cell proliferation (58). The decrease in the TAM percentage observed after chemoimmunotherapeutic treatment should be related to the immunomodulatory potential of the HES-MTX, which we have already confirmed in our previous work (12). We had shown, that on the third day after the HES-MTX administration, the percentages of cells with suppressor activity (such as TAMs, Tregs) had decreased while the infiltration of $CD8^+$ and NK cells into MC38 tumor tissue had increased. Thus, we postulate, that application of the HES-MTX created the optimal tumor milieu for DCs applied p.t., which were capable of generating an efficient antitumor immune response in such an environment. In turn, this contributed to the further decrease in the TAM percentage and an increased influx of effector lymphocytes ($CD8^+$, NK cells) into MC38 tumor tissue. In addition, the level of MHC II expression may indicate changes in tumor progression. The population of TAM MHC II^{high} is associated with the early phase of tumor development and tumor suppression, whereas TAM MHC class II^{low} dominates as the tumor progresses (5). Our research showed an increase in the TAM MHC II^{high}/TAM MHC II^{low} ratio caused primarily by the effect of cell-based vaccines, especially two- or three-component vaccines.

In particular, it should be emphasized that the supplementation of immunotherapy with the administration of the HES-MTX significantly influenced the activation of the systemic anticancer response. The use of the chemotherapeutic or anti-IL-10R antibodies alone did not affect the degree of activation of restimulated splenocytes. However, the use of two- or three-component vaccines secreting, among others, IL-12, increased the percentage of cells capable of releasing cytolytic granules, compared to the vaccine based on dendritic cells modified with the control vector. The highest cytotoxic activity was found in restimulated splenocytes obtained from mice that received immuno- and chemoimmunotherapy based on two- and three-component vaccines, however, chemoimmunotherapy induced increased production of IFN-γ.

To sum up, the use of the HES-MTX nanoconjugate prior to immunotherapy involving multiple administrations of anti-IL-10R antibodies and DC-based vaccines capable of overproducing proinflammatory cytokines IL-12, IL-15 or IL-18 created optimal conditions for the effective action of these vaccines in mouse colorectal cancer. Of these, two- or three-component vaccines revealed the greatest potential for use in anticancer therapy characterized by the highest level of expression of costimulatory molecules and MHC II. The applied chemoimmunotherapy caused the highest inhibition of tumor growth in the group receiving DC/IL-15/IL-15Rα/TAg + DC/IL-18/TAg at the level of 72.4%. But HES-MTX also enhanced the activity of the three-component vaccine leading to 69.9% inhibition of tumor growth in course of chemoimmunotherapy, compared to 24.0% in immunotherapy alone. A decrease in the percentage of Treg cells was observed in both applied therapeutic schedules. Apart from this, chemoimmunotherapy using DC-based vaccines induced an increase in NK cell infiltration into the tumor and a decrease in the percentage of TAM. Nevertheless, the highest ratio of TAM MHC II^{high} to TAM MHC II^{low} was noticed when mice received

two- or three-component vaccines. The use of dendritic cells as vaccines increased cytotoxic activity in both experiments, but the highest ability to both kill tumor cells and produce IFN-γ was found in splenocytes obtained from mice receiving two- or three-component vaccines in chemoimmunotherapy.

5 Conclusions

In chemoimmunotherapy, two- or three-component vaccines had the greatest potential, even though individual cytokines were produced in smaller amounts than in a single-component vaccine. Their use resulted in the greatest inhibition of tumor growth and effective response of immune cells. The obtained results suggest that the developed chemoimmunotherapy may have a promising application in anticancer therapy.

Data availability statement

The raw data supporting the conclusions of this article will be made available by the authors, without undue reservation.

Ethics statement

The animal study was reviewed and approved by Local Ethic Committee for Experiments with the Use of Laboratory Animals, Wrocław, Poland (authorization number 077/2019).

Author contributions

Conceptualization, KW-C and EP-P; Methodology, EP-P, JR, TG.; Formal Analysis, KW-C, JM, AS and EP-P; Investigation, KW-C, JM, AS, JR, AW, MŚ, BS-O and EP-P; Resources, EP-P; Supervision, EP-P; Writing – Original Draft Preparation, KW-C and EP-P; Writing – Review and Editing, KW-C, EP-P, JM, AS, AW, JR, BS-O, TG, MŚ; Project Administration, KW-C and EP-P; Funding Acquisition, EPP. All authors have read and agreed to the published version of the manuscript.

Funding

This research was funded by National Science Centre, Poland (grant no. 2017/27/B/NZ6/02702).

Acknowledgments

We would like to thank Didier Trono Lab Materials at Addgene for kindly providing the plasmids necessary for lentiviral transduction.

Conflict of interest

The authors declare that the research was conducted in the absence of any commercial or financial relationships that could be construed as a potential conflict of interest.

Publisher's note

Supplementary material

The Supplementary Material for this article can be found online at: https://www.frontiersin.org/articles/10.3389/fimmu.2023.1212606/full#supplementary-material

References

1. Xi Y, Xu P. Global colorectal cancer burden in 2020 and projections to 2040. *Transl Oncol* (2021) 14(10):101174. doi: 10.1016/j.tranon.2021.101174

2. Cheng B, Yu Q, Wang W. Intimate communications within the tumor microenvironment: stromal factors function as an orchestra. *J BioMed Sci* (2023) 30 (1):1. doi: 10.1186/s12929-022-00894-z

3. Petty AJ, Yang Y. Tumor-associated macrophages: implications in cancer immunotherapy. *Immunotherapy.* (2017) 9(3):289–302. doi: 10.2217/imt-2016-0135

4. Movahedi K, Laoui D, Gysemans C, Baeten M, Stangé G, Van den Bossche J, et al. Different tumor microenvironments contain functionally distinct subsets of macrophages derived from Ly6C(high) monocytes. *Cancer Res* (2010) 70(14):5728–39. doi: 10.1158/0008-5472.CAN-09-4672

5. Wang B, Li Q, Qin L, Zhao S, Wang J, Chen X. Transition of tumor-associated macrophages from MHC class IIhi to MHC class IIlow mediates tumor progression in mice. *BMC Immunol* (2011) 12:43. doi: 10.1186/1471-2172-12-43

6. Laoui D, Van Overmeire E, Di Conza G, Aldeni C, Keirsse J, Morias Y, et al. Tumor hypoxia does not drive differentiation of tumor-associated macrophages but rather fine-tunes the M2-like macrophage population. *Cancer Res* (2014) 74(1):24–30. doi: 10.1158/0008-5472.CAN-13-1196

7. Kumar V, Patel S, Tcyganov E, Gabrilovich DI. The nature of myeloid-derived suppressor cells in the tumor microenvironment. *Trends Immunol* (2016) 37(3):208–20. doi: 10.1016/j.it.2016.01.004

8. Ha TY. The role of regulatory T cells in cancer. *Immune Netw* (2009) 9(6):209–35. doi: 10.4110/in.2009.9.6.209

9. Huppert LA, Green MD, Kim L, Chow C, Leyfman Y, Daud AI, et al. Tissue-specific tregs in cancer metastasis: opportunities for precision immunotherapy. *Cell Mol Immunol* (2022) 19(1):33–45. doi: 10.1038/s41423-021-00742-4

10. Goszczyński TM, Filip-Psurska B, Kempińska K, Wietrzyk J, Boratyński J. Hydroxyethyl starch as an effective methotrexate carrier in anticancer therapy. *Pharmacol Res Perspect* (2014) 2(3):e00047. doi: 10.1002/prp2.47

11. Koźmiński P, Halik PK, Chesori R, Gniazdowska E. Overview of dual-acting drug methotrexate in different neurological diseases, autoimmune pathologies and cancers. *Int J Mol Sci* (2020) 21(10):3483. doi: 10.3390/ijms21103483

12. Szczygieł A, Anger-Góra N, Węgierek-Ciura K, Mierzejewska J, Rossowska J, Goszczyński TM, et al. Immunomodulatory potential of anticancer therapy composed of methotrexate nanoconjugate and dendritic cell-based vaccines in murine colon carcinoma. *Oncol Rep* (2021) 45(3):945–62. doi: 10.3892/or.2021.7930

13. Szczygieł A, Węgierek-Ciura K, Wróblewska A, Mierzejewska J, Rossowska J, Szermer-Olearnik B, et al. Combined therapy with methotrexate nanoconjugate and dendritic cells with downregulated IL-10R expression modulates the tumor microenvironment and enhances the systemic anti-tumor immune response in MC38 murine colon carcinoma. *Front Immunol* (2023) 14. doi: 10.3389/fimmu.2023.1155377

14. Peña-Romero AC, Orenes-Piñero E. Dual effect of immune cells within tumour microenvironment: pro- and anti-tumour effects and their triggers. *Cancers.* (2022) 14 (7):1681. doi: 10.3390/cancers14071681

15. Kicielińska J, Pajtasz-Piasecka E. The role of IL-10 in the modulation of the immune response in normal conditions and the tumor environment. *Postepy Hig Med Doswiadczalnej Online.* (2014) 68:879–92. doi: 10.5604/17322693.1111123

16. Perona-Wright G, Anderton SM, Howie SEM, Gray D. IL-10 permits transient activation of dendritic cells to tolerize T cells and protect from central nervous system autoimmune disease. *Int Immunol* (2007) 19(9):1123–34. doi: 10.1093/intimm/dxm084

17. Wu Y, Yi M, Niu M, Mei Q, Wu K. Myeloid-derived suppressor cells: an emerging target for anticancer immunotherapy. *Mol Cancer.* (2022) 21:184. doi: 10.1186/s12943-022-01657-y

18. Silva JR, Sales NS, Silva MO, Aps LRMM, Moreno ACR, Rodrigues EG, et al. Expression of a soluble IL-10 receptor enhances the therapeutic effects of a papillomavirus-associated antitumor vaccine in a murine model. *Cancer Immunol Immunother CII.* (2019) 68(5):753–63. doi: 10.1007/s00262-018-02297-2

19. Rossowska J, Anger N, Szczygieł A, Mierzejewska J, Pajtasz-Piasecka E. Reprogramming the murine colon cancer microenvironment using lentivectors encoding shRNA against IL-10 as a component of a potent DC-based chemoimmunotherapy. *J Exp Clin Cancer Res CR.* (2018) 37:126. doi: 10.1186/s13046-018-0799-y

20. Rossowska J, Anger N, Kicielińska J, Pajtasz-Piasecka E, Bielawska-Pohl A, Wojas-Turek J, et al. Temporary elimination of IL-10 enhanced the effectiveness of cyclophosphamide and BMDC-based therapy by decrease of the suppressor activity of MDSCs and activation of antitumour immune response. *Immunobiology.* (2015) 220 (3):389–98. doi: 10.1016/j.imbio.2014.10.009

21. Gordy JT, Luo K, Francica B, Drake C, Markham RB. Anti-IL-10 mediated enhancement of anti-tumor efficacy of a dendritic-cell targeting MIP3α-gp100 vaccine in the B16F10 mouse melanoma model is dependent on type I interferons. *J Immunother* (2018) 41(4):181–9. doi: 10.1097/CJI.0000000000000212

22. Chen S, Wang X, Wu X, Wei MQ, Zhang B, Liu X, et al. IL-10 signalling blockade at the time of immunization inhibits human papillomavirus 16 E7 transformed TC-1 tumour cells growth in mice. *Cell Immunol* (2014) 290(1):145–51. doi: 10.1016/j.cellimm.2014.06.002

23. Vicari AP, Chiodoni C, Vaure C, Aït-Yahia S, Dercamp C, Matsos F, et al. Reversal of tumor-induced dendritic cell paralysis by CpG immunostimulatory oligonucleotide and anti-interleukin 10 receptor antibody. *J Exp Med* (2002) 196 (4):541–9. doi: 10.1084/jem.20020732

24. Anger-Góra N, Węgierek-Ciura K, Szczygieł A, Mierzejewska J, Pajtasz-Piasecka E, Rossowska J. Treatment with lentiviral vectors encoding shRNA against interleukin 10 modulates the immunosuppressive activity of murine colon carcinoma-associated myeloid-derived suppressor cells. *Oncol Lett* (2021) 22(2):582. doi: 10.3892/ol.2021.12843

25. Mac Keon S, Ruiz MS, Gazzaniga S, Wainstok R. Dendritic cell-based vaccination in cancer: therapeutic implications emerging from murine models. *Front Immunol* (2015) 6. doi: 10.3389/fimmu.2015.00243

26. Szczygieł A, Pajtasz-Piasecka E. Between biology and medicine: perspectives on the use of dendritic cells in anticancer therapy. *Postepy Hig Med Doswiadczalnej Online.* (2017) 71(0):921–41. doi: 10.5604/01.3001.0010.5808

27. Sun L, He C, Nair L, Yeung J, Egwuagu CE. Interleukin 12 (IL-12) family cytokines: role in immune pathogenesis and treatment of CNS autoimmune disease. *Cytokine.* (2015) 75(2):249–55. doi: 10.1016/j.cyto.2015.01.030

28. Hamza T, Barnett JB, Li B. Interleukin 12 a key immunoregulatory cytokine in infection applications. *Int J Mol Sci* (2010) 11(3):789–806. doi: 10.3390/ijms11030789

29. Nguyen KG, Vrabel MR, Mantooth SM, Hopkins JJ, Wagner ES, Gabaldon TA, et al. Localized interleukin-12 for cancer immunotherapy. *Front Immunol* (2020) 11:575597. doi: 10.3389/fimmu.2020.575597

30. Wegierek-Ciura K, Pajtasz-Piasecka E. Perspectives for the application of interleukin 15 in anti-cancer therapy. *Postępy Hig Med Dośw.* (2019) 73:850–64. doi: 10.5604/01.3001.0013.7194

31. Waldmann TA, Dubois S, Miljkovic MD, Conlon KC. IL-15 in the combination immunotherapy of cancer. *Front Immunol* (2020) 11. doi: 10.3389/fimmu.2020.00868

32. Zhou Y, Husman T, Cen X, Tsao T, Brown J, Bajpai A, et al. Interleukin 15 in cell-based cancer immunotherapy. *Int J Mol Sci* (2022) 23(13):7311. doi: 10.3390/ijms23137311

33. Saetang J, Chonpathompikunlert P, Sretrirutchai S, Roongsawang N, Kayasut K, Voravuthikunchai SP, et al. Anti-cancer effect of engineered recombinant interleukin 18. *Adv Clin Exp Med Off Organ Wroclaw Med Univ* (2020) 29(10):1135–43. doi: 10.17219/acem/126298

34. Dinarello C, Novick D, Kim S, Kaplanski G. Interleukin-18 and IL-18 binding protein. *Front Immunol* (2013) 4. doi: 10.3389/fimmu.2013.00289

35. Pajtasz-Piasecka E, Szyda A, Rossowska J, Krawczenko A, Indrová M, Grabarczyk P, et al. Loss of tumorigenicity of murine colon carcinoma MC38/0 cell line after transduction with a retroviral vector carrying murine IL-12 genes. *Folia Biol (Praha).* (2004) 50(1):7–14.

36. Rossowska J, Anger N, Szczygieł A, Mierzejewska J, Pajtasz-Piasecka E. Intratumoral lentivector-mediated TGF-β1 gene downregulation as a potent strategy for enhancing the antitumor effect of therapy composed of cyclophosphamide and dendritic cells. *Front Immunol* (2017) 8:713. doi: 10.3389/fimmu.2017.00713

37. Rossowska J, Pajtasz-Piasecka E, Szyda A, Krawczenko A, Zietara N, Dus D. Tumour antigen-loaded mouse dendritic cells maturing in the presence of inflammatory cytokines are potent activators of immune response *in vitro* but not *in vivo*. *Oncol Rep* (2009) 21(6):1539–49. doi: 10.3892/or_00000386

38. Pajtasz-Piasecka E, Rossowska J, Szyda A, Krawczenko A, Dus D. Generation of anti-tumor response by JAWS II mouse dendritic cells transduced with murine interleukin 12 genes. *Oncol Rep* (2007) 17(5):1249–57. doi: 10.3892/or.17.5.1249

39. Mierzejewska J, Węgierek-Ciura K, Rossowska J, Szczygieł A, Anger-Góra N, Szermer-Olearnik B, et al. The beneficial effect of IL-12 and IL-18 transduced dendritic cells stimulated with tumor antigens on generation of an antitumor response in a mouse colon carcinoma model. *J Immunol Res* (2022) 2022:7508928. doi: 10.1155/2022/7508928

40. Poznanski SM, Lee AJ, Nham T, Lusty E, Larché MJ, Lee DA, et al. Combined stimulation with interleukin-18 and interleukin-12 potently induces interleukin-8 production by natural killer cells. *J Innate Immun* (2017) 9(5):511–25. doi: 10.1159/000477172

41. Lusty E, Poznanski SM, Kwofie K, Mandur TS, Lee DA, Richards CD, et al. IL-18/IL-15/IL-12 synergy induces elevated and prolonged IFN-γ production by *ex vivo* expanded NK cells which is not due to enhanced STAT4 activation. *Mol Immunol* (2017) 88:138–47. doi: 10.1016/j.molimm.2017.06.025

42. Ruffell B, Chang-Strachan D, Chan V, Rosenbusch A, Ho CMT, Pryer N, et al. Macrophage IL-10 blocks CD8+ T cell-dependent responses to chemotherapy by suppressing IL-12 expression in intratumoral dendritic cells. *Cancer Cell* (2014) 26 (5):623–37. doi: 10.1016/j.ccell.2014.09.006

43. Anna F, Lopez J, Moncoq F, Blanc C, Authié P, Noirat A, et al. A lentiviral vector expressing a dendritic cell-targeting multimer induces mucosal anti-mycobacterial CD4+ T-cell immunity. *Mucosal Immunol* (2022) 15(6):1389–404. doi: 10.1038/s41385-022-00566-z

44. Saikh KU, Khan AS, Kissner T, Ulrich RG. IL-15-induced conversion of monocytes to mature dendritic cells. *Clin Exp Immunol* (2001) 126(3):447–55. doi: 10.1046/j.1365-2249.2001.01672.x

45. Li J, Lamine Mbow M, Sun L, Li L, Yang G, Griswold DE, et al. Induction of dendritic cell maturation by IL-18. *Cell Immunol* (2004) 227(2):103–8. doi: 10.1016/j.cellimm.2004.02.002

46. Tatsumi T, Huang J, Gooding WE, Gambotto A, Robbins PD, Vujanovic NL, et al. Intratumoral delivery of dendritic cells engineered to secrete both interleukin (IL)-12 and IL-18 effectively treats local and distant disease in association with broadly reactive Tc1-type immunity. *Cancer Res* (2003) 63(19):6378–86.

47. Stober D, Schirmbeck R, Reimann J. IL-12/IL-18-Dependent IFN-γ release by murine dendritic Cells1. *J Immunol* (2001) 167(2):957–65. doi: 10.4049/jimmunol.167.2.957

48. Otani T, Nakamura S, Toki M, Motoda R, Kurimoto M, Orita K. Identification of IFN-gamma-producing cells in IL-12/IL-18-treated mice. *Cell Immunol* (1999) 198 (2):111–9. doi: 10.1006/cimm.1999.1589

49. Tominaga K, Yoshimoto T, Torigoe K, Kurimoto M, Matsui K, Hada T, et al. IL-12 synergizes with IL-18 or IL-1β for IFN-γ production from human T cells. *Int Immunol* (2000) 12(2):151–60. doi: 10.1093/intimm/12.2.151

50. Fehniger TA, Shah MH, Turner MJ, VanDeusen JB, Whitman SP, Cooper MA, et al. Differential cytokine and chemokine gene expression by human NK cells following activation with IL-18 or IL-15 in combination with IL-12: implications for the innate immune Response1. *J Immunol* (1999) 162(8):4511–20. doi: 10.4049/jimmunol.162.8.4511

51. Mirjačić Martinović K, Babović N, Džodić R, Jurišić V, Matković S, Konjević G. Favorable *in vitro* effects of combined IL-12 and IL-18 treatment on NK cell cytotoxicity and CD25 receptor expression in metastatic melanoma patients. *J Transl Med* (2015) 13(1):120. doi: 10.1186/s12967-015-0479-z

52. Fujieda S, Lee K, Sunaga H, Tsuzuki H, Ikawa H, Fan GK, et al. Staining of interleukin-10 predicts clinical outcome in patients with nasopharyngeal carcinoma. *Cancer.* (1999) 85(7):1439–45. doi: 10.1002/(SICI)1097-0142(19990401)85:7<1439::AID-CNCR3>3.0.CO;2-6

53. Chau GY, Wu CW, Lui WY, Chang TJ, Kao HL, Wu LH, et al. Serum interleukin-10 but not interleukin-6 is related to clinical outcome in patients with

resectable hepatocellular carcinoma. *Ann Surg* (2000) 231(4):552–8. doi: 10.1097/00000658-200004000-00015

54. Llopiz D, Ruiz M, Infante S, Villanueva L, Silva L, Hervas-Stubbs S, et al. IL-10 expression defines an immunosuppressive dendritic cell population induced by antitumor therapeutic vaccination. *Oncotarget.* (2016) 8(2):2659–71. doi: 10.18632/oncotarget.13736

55. Oka N, Markova T, Tsuzuki K, Li W, El-Darawish Y, Pencheva-Demireva M, et al. IL-12 regulates the expansion, phenotype, and function of murine NK cells activated by IL-15 and IL-18. *Cancer Immunol Immunother.* (2020) 69(9):1699–712. doi: 10.1007/s00262-020-02553-4

56. Woźniak M, Pastuch-Gawołek G, Makuch S, Wiśniewski J, Krenács T, Hamar P, et al. *In vitro* and *In vivo* efficacy of a novel glucose–methotrexate conjugate in targeted cancer treatment. *Int J Mol Sci* (2021) 22(4):1748. doi: 10.3390/ijms22041748

57. Ciekot J, Psurski M, Jurec K, Boratyński J. Hydroxyethylcellulose as a methotrexate carrier in anticancer therapy. *Invest New Drugs* (2021) 39(1):15–23. doi: 10.1007/s10637-020-00972-9

58. Xiang X, Wang J, Lu D, Xu X. Targeting tumor-associated macrophages to synergize tumor immunotherapy. *Signal Transduct Target Ther* (2021) 6(1):1–12. doi: 10.1038/s41392-021-00484-9

frontiers | Frontiers in Immunology

TYPE Systematic Review
PUBLISHED 21 July 2023
DOI 10.3389/fimmu.2023.1219929

OPEN ACCESS

EDITED BY
Qun Zhao,
Fourth Hospital of Hebei Medical University, China

REVIEWED BY
Ye Miao,
First Affiliated Hospital of Jinzhou Medical University, China
Kangyu Jin,
Zhejiang University, China
Xiaochen Qi,
Dalian Medical University, China
Yunfei Liu,
Ludwig Maximilian University of Munich, Germany

*CORRESPONDENCE
Baohong Hu
479723599@qq.com
Weixing Wang
sate.llite@163.com

†These authors have contributed equally to this work

RECEIVED 09 May 2023
ACCEPTED 19 June 2023
PUBLISHED 21 July 2023

CITATION
Zhang L, Ma W, Qiu Z, Kuang T, Wang K, Hu B and Wang W (2023) Prognostic nutritional index as a prognostic biomarker for gastrointestinal cancer patients treated with immune checkpoint inhibitors. *Front. Immunol.* 14:1219929. doi: 10.3389/fimmu.2023.1219929

Prognostic nutritional index as a prognostic biomarker for gastrointestinal cancer patients treated with immune checkpoint inhibitors

Lilong Zhang[1,2†], Wangbin Ma[1,2†], Zhendong Qiu[1,2†], Tianrui Kuang[1,2], Kunpeng Wang[1,2], Baohong Hu[1,2*] and Weixing Wang[1,2*]

[1]Department of General Surgery, Renmin Hospital of Wuhan University, Wuhan, China, [2]Key Laboratory of Hubei Province for Digestive System Disease, Wuhan, China

Objective: Our study represents the first meta-analysis conducted to evaluate the prognostic utility of the baseline prognostic nutritional index (PNI) in patients with gastrointestinal cancer (GIC) who received immune checkpoint inhibitor (ICI) therapy.

Methods: We searched PubMed, the Cochrane Library, EMBASE, and Google Scholar until April 23, 2023, to obtain relevant articles for this study. Our analysis examined several clinical outcomes, including overall survival (OS), progression-free survival (PFS), objective response rate (ORR), and disease control rate (DCR).

Results: In this analysis, a total of 17 articles with 2883 patients were included. Our pooled results indicated that patients with high PNI levels had longer OS (HR: 0.530, 95% CI: 0.456-0.616, $p < 0.001$) and PFS (HR: 0.740, 95% CI: 0.649-0.844, $p < 0.001$), as well as higher ORR (OR: 1.622, 95% CI: 1.251-2.103, $p < 0.004$) and DCR (OR: 1.846, 95% CI: 1.428-2.388, $p < 0.001$). Subgroup analysis showed that PNI cutoff values of 40 to 45 showed greater predictive potential. Subgroup analysis also confirmed that the above findings still hold true in patients with esophageal cancer, gastric cancer, and hepatocellular carcinomas.

Conclusion: The PNI were reliable predictors of outcomes in GIC patients treated with ICIs.

KEYWORDS

prognostic nutrition index, immune checkpoint inhibitors, gastrointestinal cancers, esophageal cancer, gastric cancer, hepatocellular carcinoma

1 Introduction

Approximately one-fourth of all cancer cases and one-third of all cancer-related deaths worldwide can be attributed to gastrointestinal cancers (GIC) (1). Systemic therapy remains the cornerstone of treatment for patients with locally advanced or metastatic GIC (2). However, there is a critical need for strategies to reduce metastasis and improve survival. The introduction of immune checkpoint inhibitors (ICIs) over the past five years has resulted in significant advances in the treatment of advanced GIC patients, achieving durable antitumor immune responses and improvements in overall survival (OS) (3–5). But because of the low response rate, scientists are looking for new potential biomarkers that can predict treatment outcomes (3, 6). The identification of well-characterized and predictive biomarkers would facilitate personalized treatment selection based on the anticipated efficacy of therapy and avoid the cost of ineffective treatment.

Numerous studies have demonstrated the relationship between nutritional status and cancer prognosis (7–11). Patients with GIC are particularly affected by nutritional status due to their anatomical features (12). The prognostic nutrition index (PNI) is an index that utilizes the levels of serum albumin and peripheral blood lymphocyte count, initially created to forecast the probability of postoperative complications in surgical patients by evaluating their nutritional status before the operation (13). Recent studies have demonstrated the high accuracy of PNI in predicting treatment outcomes for various cancers, especially GIC (14, 15). Immune system function plays a critical role in the efficacy of ICIs, and the levels of serum albumin and lymphocytes are significant indicators of immune system function.

Notably, the association between PNI levels and the prognosis of GIC patients treated with ICIs remains controversial, and no meta-analysis has been conducted to date. Hence, the aim of this study was to systematically evaluate the predictive value of PNI in ICI-treated GIC patients. The findings of this study can aid in developing effective treatment strategies that facilitate the administration of precise, cost-effective treatments with minimal adverse effects.

2 Methods

2.1 Literature search strategies

The analysis performed in this study was conducted following the guidelines of the PRISMA statement (16). On April 23, 2023, a comprehensive literature search was carried out using PubMed, EMBASE, and the Cochrane Library. Various search terms, including MeSH terms and keywords, were used to retrieve relevant studies, such as "Immune Checkpoint Inhibitors [MeSH]", "PD-1 Inhibitors", "PD-L1 Inhibitors", "CTLA-4 Inhibitors", "Pembrolizumab", "Nivolumab", "Atezolizumab", "Ipilimumab", "Avelumab", "Tremelimumab", "Durvalumab", "Cemiplimab", "Prognostic Nutritional Index", "PNI". Search restricted to English literature. A detailed description of the search strategies is provided in Table S1. Additionally, gray literature was searched using Google Scholar, and the reference lists of eligible studies were screened manually.

2.2 Inclusion and exclusion criteria

In our study, we strictly included research articles that met the following criteria: patients who were diagnosed with GIC underwent treatment with ICIs, and the prognostic value of PNI was evaluated. Furthermore, these articles reported on at least one of the following outcomes: overall survival (OS), progression-free survival (PFS), objective response rate (ORR), and disease control rate (DCR). We excluded conference abstracts, comments, and case reports from our analysis. In situations where studies had overlapping patients, we prioritized those with the most comprehensive data and robust methodology (3).

2.3 Data extraction and quality assessment

In this study, we gathered diverse information from the chosen articles, including the names of the authors, year of publication, duration and location of the study, drugs used for treatment, cancer type, sample size, patient age and gender, and relevant cut-off values and outcomes. We placed greater emphasis on obtaining data from multivariate analyses of hazard ratios (HR) compared to univariate analyses. We also employed the Newcastle-Ottawa Scale (NOS) to appraise the quality of observational studies and classified those with a NOS score of 6 or above as high-quality literature (17). All of the above steps were completed and cross-checked independently by two authors, with decisions sought from the corresponding author on points of dispute.

2.4 Statistical methods

Statistical analyses were performed using Stata 15.0 software. To assess heterogeneity, we utilized the chi-squared test. We employed a random effects model when the p-value < 0.1 or the I^2 statistic was > 50%, and a fixed effects model otherwise. We estimated publication bias using both Egger's and Begg's tests, and if bias was detected, we utilized the "trim and fill" method to evaluate the influence of the bias on the pooled results. Furthermore, we conducted a sensitivity analysis by excluding each study independently to assess the robustness of the results. $p < 0.05$ was considered statistically significant.

3 Results

3.1 Characteristics of studies

After excluding duplicates and screening titles and abstracts, we identified 25 articles for full-text evaluation, among which 17 met

the eligibility criteria, resulting in a total of 2883 patients (18–34). The PRISMA flowchart in Figure 1 depicts the study selection process. Table 1 provides a comprehensive overview of the characteristics of the eligible studies. We assessed the risk of bias using the Newcastle-Ottawa Scale (NOS), with scores ranging from 6 to 8, indicating a low risk of bias in all included studies. Of the 17 studies, 16 were retrospective, and one was prospective. Four studies were in esophageal squamous cell carcinoma (ESCC) patients; five studies were in gastric cancer (GC) patients; and four studies were in hepatocellular carcinoma (HCC) patients. In addition, there is one study on esophageal cancer (EC) patients, one study on intrahepatic cholangiocarcinoma (ICC) patients, one study on upper gastrointestinal cancer (UGIC) patients and one study on biliary tract cancers (BTC) patients.

3.2 Baseline PNI levels and OS

Through the analysis of data from 14 studies with 2293 patients, we aimed to explore the correlation between PNI levels and OS in ICI-treated GIC patients. Considering no significant heterogeneity across the studies (I^2 = 33.2%, p = 0.109), we employed a fixed-effects model to estimate the pooled HR. The results revealed that high PNI levels were significantly related to longer OS (HR: 0.530, 95% CI: 0.456-0.616, p < 0.001), as depicted in Figure 2.

We performed a subgroup analysis based on cancer type, cut-off values, and the Cox model. We found that a high PNI was associated with a better prognosis in patients with EC, GC, HCC, or BTC (Figure 3). Differences in PNI cutoff values do not affect the correlation between PNI and OS in ICI-treated GIC patients (Figure 4). Both univariate and multivariate analyses confirmed the above findings (Figure S1).

3.3 Baseline PNI levels and PFS

We also investigate the correlation between PNI and PFS in GIC patients treated with ICIs using data from 12 studies with 1733 patients. We demonstrated that patients with high PNI levels had a lower risk of progression (HR: 0.740, 95% CI: 0.649-0.844, p < 0.001, Figure 5). No significant heterogeneity was observed (I^2 = 22.1%, p = 0.226); we used a fixed-effects model for our analysis.

The results of the subgroup analysis showed that the relationship between high PNI levels and longer PFS was consistent in GIC patients with EC, GC, and HCC (Figure 6). Notably, PNI predicted PFS in patients with GIC only when the cut-off value was between 40 and 45 (Figure 7).

The findings of the multivariate analysis also support these findings; although the univariate analysis revealed that PNI was not associated with patient PFS, we consider the conclusions drawn from the former to be more reliable due to its more methodologically rigorous nature and larger number of inclusions (Figure S2).

3.4 Baseline PNI levels and ORR and DCR

Subsequently, we conducted an analysis to investigate the correlation between PNI levels and response to ICI therapy in GIC

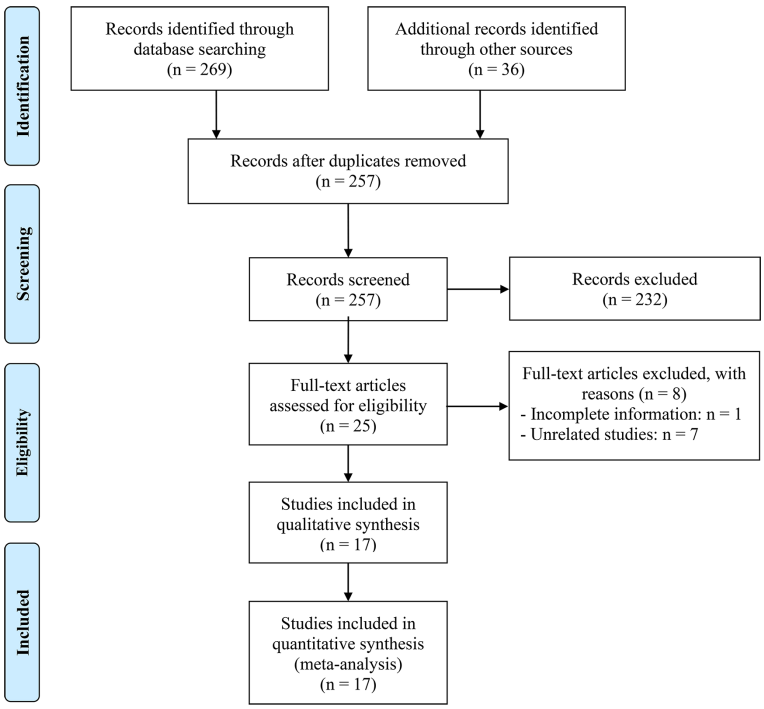

FIGURE 1
The flow diagram for identifying eligible studies.

patients. The presence of notable heterogeneity was not observed in the results presented in Figures 8A, B, and hence a fixed-effect model was implemented. Our findings revealed that GIC patients with high PNI levels had a higher ORR (5 studies with 1430 patients, OR: 1.622, 95% CI: 1.251-2.103, $p < 0.004$, Figure 8A) and DCR (7 studies with 1551 patients, OR: 1.846, 95% CI: 1.428-2.388, $p < 0.001$, Figure 8B).

3.5 Sensitivity analysis

To assess the robustness of the findings, a sensitivity analysis was conducted by iteratively excluding each study and examining the impact on the overall results. Our analysis indicated that the exclusion of any individual study did not significantly affect the pooled HR for OS. Specifically, the HR estimates for OS ranged from 0.474 (95% CI: 0.398-0.566) when excluding Muhammed et al., 2021 (25) to 0.547 (95% CI: 0.469-0.637) when excluding Yang et al., 2022 (34), as depicted in Figure 9A. Furthermore, the sensitivity analysis demonstrated that the removal of any individual study did not significantly impact the overall results for PFS. The range of HR values varied from 0.662 (95% CI: 0.547-0.800) after excluding Persano et al., 2023 (27) to 0.754 (95% CI: 0.659-0.862) after excluding Yang et al., 2022 (33) (Figure 9B). Similarly, sensitivity analysis showed that removing any of the studies did not affect the ORR and DCR results (Figures 10A, B).

TABLE 1 Main characteristics of the studies included.

Study	Study design	Study period	Study region	ICI treatment	Cancer Type	Sample size	Age	Gender (male/female)	Cut-off	Outcome
Chen et al., 2023 (19)	R	08/2019-08/2021	China	Pembrolizumab, Camrelizumab, Sintilimab, Tislelizumab	ESCC	54	67 (43-78)[a]	43/11	45.2	PFS
Ikoma et al., 2023 (20)	R	01/2017-06/2021	Japan	Nivolumab	ESCC	93	70 (38-80)[a]	72/21	48.4	OS
Persano et al., 2023 (27)	R	10/2018-04/2022	Italy, Germany, Portugal, Japan, Korea	Atezolizumab plus Bevacizumab	HCC	773	72 (27-94)[a]	662/111	41.0	OS, PFS
Qi et al., 2023 (28)	P	03/2019-03/2022	China	Pembrolizumab	ESCC	51	62 (39-75)[a]	44/7	52.4	PFS
Tada et al., 2023 (30)	R	09/2020-05/2022	Japan	Atezolizumab plus Bevacizumab	HCC	485	74 (68-80)[a]	389/96	47.0	OS, PFS, ORR, DCR
Wu et al., 2023 (32)	R	09/2018-05/2022	China	Camrelizumab, Pembrolizumab, Nivolumab, Sintilimab, Tislelizumab, Toripalimab	EC	78	58 (46–87)[a]	65/13	40.6	OS, PFS
Yang et al., 2023 (33)	R	03/2017-04/2022	China	Camrelizumab, Sintilimab, Nivolumab, Pembrolizumab	BTC	31	61.0 ± 11.8[c]	19/12	44.3	OS, PFS, ORR, DCR
Book et al., 2022 (18)	R	10/2017-12/2021	Japan	Nivolumab, Pembrolizumab	UGIC	61	71 (46-86)[a]	49/12	-[d]	OS, PFS, DCR
Kim et al., 2022 (21)	R	2015-2019	Korea	Nivolumab, Pembrolizumab	ESCC	60	68 (52–76)[a]	56/4	35.9	OS, PFS, DCR
Lee et al., 2022 (22)	R	10/2017-02/2021	Korea	Nivolumab	GC	35	55 (25-71)[a]	19/16	40.0	OS, PFS
Morelli et al., 2022 (24)	R	06/2014-12/2018	United Kingdom	Pembrolizumab, Nivolumab, Avelumab	GC	57	61 (29-85)[a]	43/14	33.0	OS
Sun et al., 2022 (29)	R	08/2016-12/2020	China	ICIs	GC	89	-	-	44.6	OS, PFS

(Continued)

TABLE 1 Continued

Study	Study design	Study period	Study region	ICI treatment	Cancer Type	Sample size	Age	Gender (male/female)	Cut-off	Outcome
Yang et al., 2022 (34)	R	02/2019-02/2021	China	Nivolumab, Pembrolizumab, Toripalimab, Camrelizumab, Sintilimab	ICC	73	57 (31-75)[a]	49/24	49.0	OS
Mei et al., 2021 (23)	R	07/2018-12/2019	China	Nivolumab, Pembrolizumab, Toripalimab, Sintilimab, Camrelizumab	HCC	442	52 (21-75)[a]	382/60	48.0	OS, ORR, DCR
Muhammed et al., 2021 (25)	R	2015-2018	Europe, North, America, Asia	ICIs	HCC	362	65 (15-87)[a]	284/78	45.0	OS, PFS, ORR, DCR
Watanabe et al., 2021 (31)	R	10/2015-12/2019	Japan	Nivolumab	GC	110	71/39[b]	79/31	40.0	OS, PFS, ORR, DCR
Namikawa et al., 2020 (26)	R	10/2017-12/2019	Japan	Nivolumab	GC	29	71 (49–86)[a]	19/10	31.1	OS, PFS

[a]medians (ranges); [b]≥ 65 vs. < 65; [c]mean ± standard deviation; [d]ESCC patients with cut-off = 42.8 and GC patients with cut-off = 37.2; R, retrospective study; P, prospective study; OS, overall survival; PFS, progression-free survival; ORR, objective response rate; DCR, disease control rate; ESCC, esophageal squamous cell carcinoma; EC, esophageal cancer; GC, gastric cancer; HCC, hepatocellular carcinoma; BTC, biliary tract cancers; ICC, intrahepatic cholangiocarcinoma; UGIC, upper gastrointestinal cancer; ICIs, immune checkpoint inhibitors.

3.6 Publication bias

We performed Begg's and Egger's tests to evaluate the potential publication bias in our meta-analysis. The findings indicated no considerable publication bias for ORR (Egger's test: $p = 0.241$, Begg's test: $p = 0.230$) and DCR (Egger's test: $p = 0.086$, Begg's test: $p = 0.081$). Nevertheless, we detected publication bias in OS (Egger's test: $p = 0.003$, Begg's test: $p = 0.021$) and PFS (Egger's test: $p = 0.027$, Begg's test: $p = 0.064$) based on Egger's test. To address this issue, we utilized the trim and fill method to estimate the number of potential missing studies in OS. The results showed no change in pooled HR without the missing study being incorporated (Figure 11).

4 Discussion

Our investigation aimed to explore the prognostic significance of PNI in GIC patients receiving ICI therapy. Through a meta-analysis of relevant studies, we established a strong association between elevated PNI levels and favorable OS and PFS and higher ORR and DCR. Furthermore, subgroup analysis showed that PNI cutoff values of 40 to 45 showed greater predictive potential.

While ICIs have emerged as a promising treatment for GIC patients, the factors affecting their efficacy remain unclear. Multiple biomarkers have been proposed for predicting response to ICIs, including tumor mutation burden, microsatellite instability/

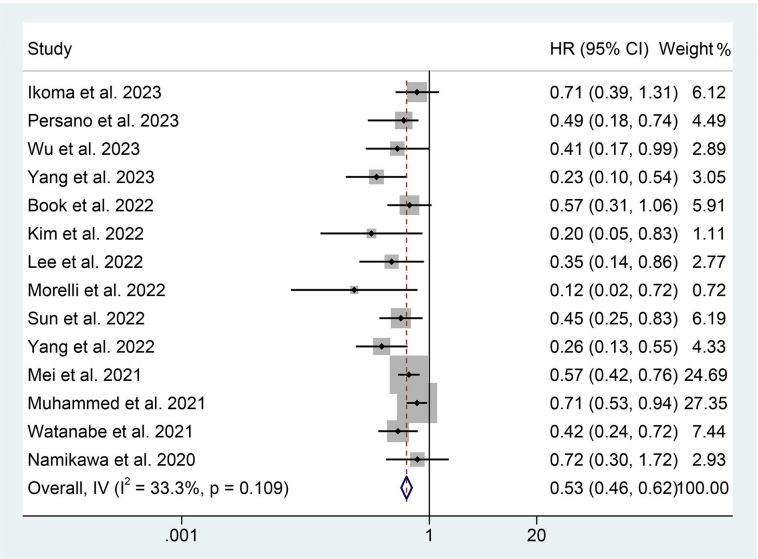

FIGURE 2
Forest plots of the relationship between prognostic nutritional index and overall survival. HR, hazard ratio; CL, confidence interval.

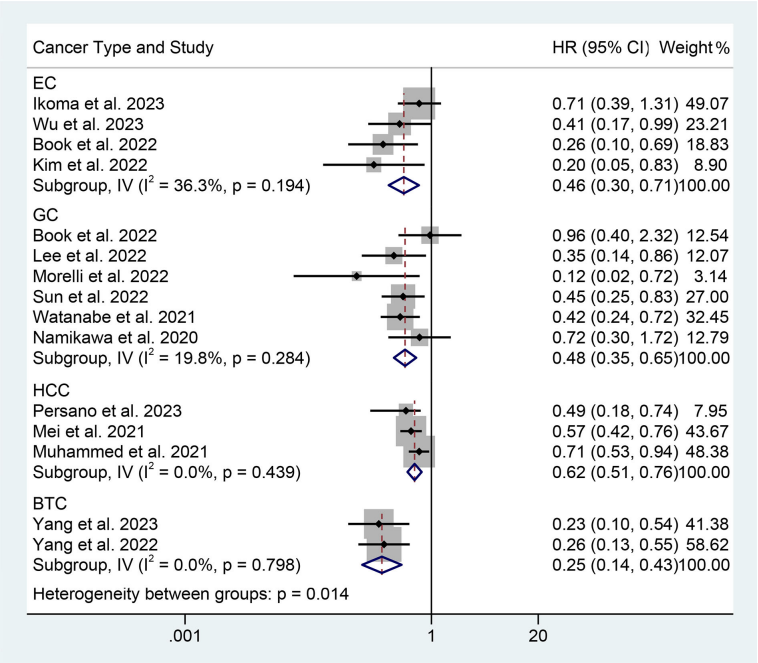

FIGURE 3
Subgroup analysis of the relationship between prognostic nutritional index and overall survival based on the cancer type. HR, hazard ratio; CL, confidence interval.

mismatch repair deficiency, tertiary lymphoid structures, and tumor-infiltrating lymphocytes (35). However, the application of these biomarkers in clinical practice is limited by challenges such as immature detection technology, difficulty obtaining specimens, and high costs.

PNI is calculated as 5 × peripheral lymphocyte count (10^9/L) +serum albumin (g/L), which includes albumin and lymphocyte count, reflecting nutritional and immune status, respectively. In upper gastrointestinal cancer patients, nutritional problems are prevalent in up to 90% of cases, mainly due to reduced food intake and increased nutrition consumption by tumors (36). Long-standing research has linked malnutrition to a worse tumor prognosis (37, 38). While low albumin levels are indicative of malnutrition, they can also serve as a biomarker for systemic

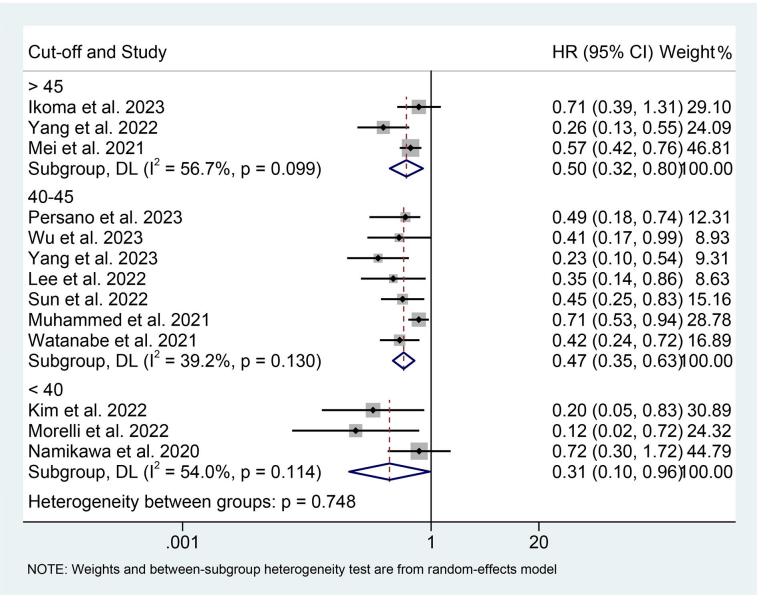

FIGURE 4
Subgroup analysis of the relationship between prognostic nutritional index and overall survival based on the cut-off. HR, hazard ratio; CL, confidence interval.

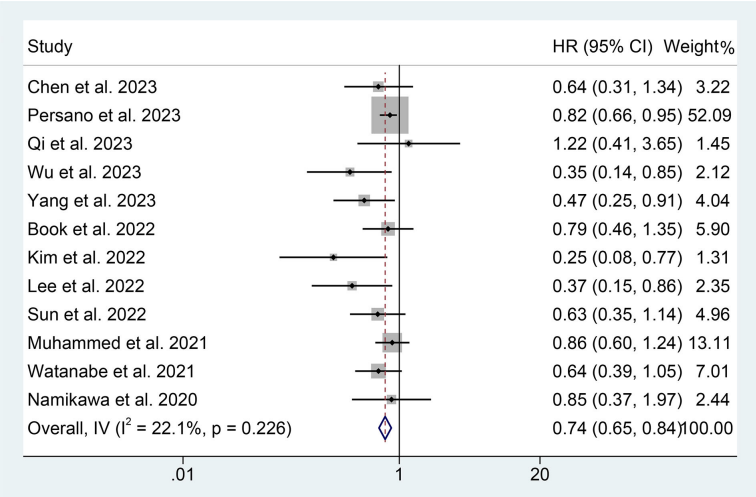

FIGURE 5
Forest plots of the relationship between prognostic nutritional index and progression-free survival. HR, hazard ratio; CL, confidence interval.

inflammation (39). Inflammatory factors have been shown to inhibit albumin synthesis, while oxidative stress can result in albumin denaturation, contributing to a rapid decrease in serum albumin levels in patients with an inflammatory state (40, 41). Another crucial element in the development of tumors is the tumor microenvironment. Through the attraction of T lymphocytes, tumor-associated macrophages, and circulating cytokines, inflammatory factors can significantly impact tumor cell proliferation, angiogenesis, and tumor invasion/metastasis (42, 43). A crucial component of adaptive immunity is the lymphocyte. The immune system's capacity to prevent tumor cell growth and metastasis may decline when lymphocyte numbers drop, hastening the development of tumors (44, 45). Therefore, the combination of albumin and lymphocyte counts in the PNI can provide a more comprehensive reflection of the host condition.

Initially used to evaluate the immunotrophic status and surgical risks of gastrointestinal surgery patients, PNI has since been applied to other cancer types, including EC (46), GC (26), HCC (47), and pancreatic cancer (48). The success of ICIs in combating tumors is attributed to their ability to alleviate the suppression of tumor cells by the immune system. Hence, the nutritional and immune statuses of patients are critical determinants of the efficacy of ICIs (49). In

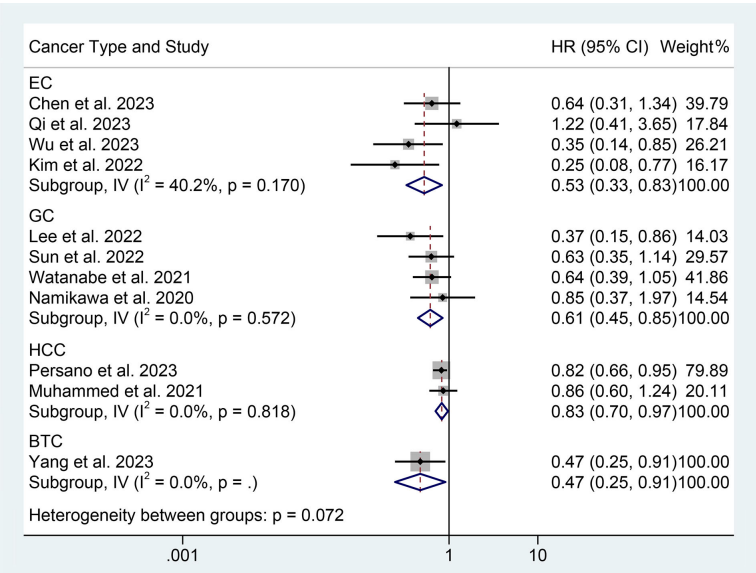

FIGURE 6
Subgroup analysis of the relationship between prognostic nutritional index and progression-free survival based on the cancer type. HR, hazard ratio; CL, confidence interval.

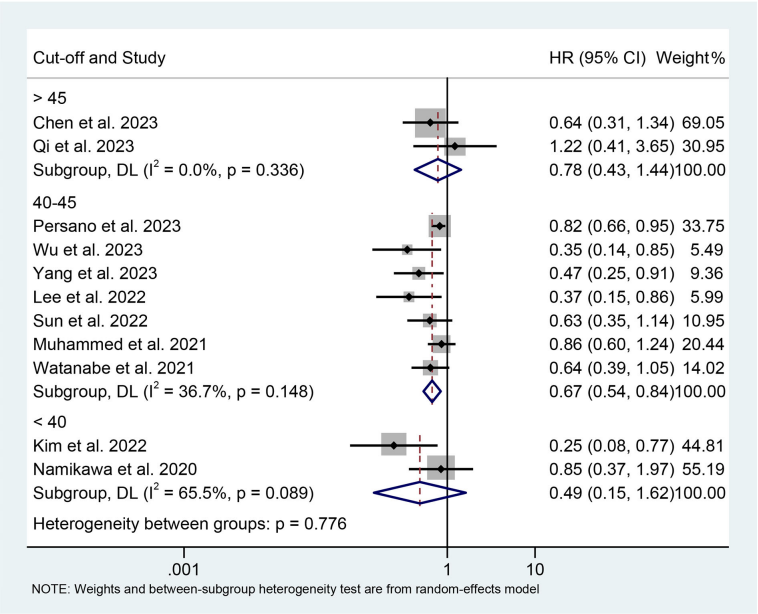

FIGURE 7
Subgroup analysis of the relationship between prognostic nutritional index and progression-free survival based on the cut-off. HR, hazard ratio; CL, confidence interval.

this study, we performed the first meta-analysis to confirm that PNI predicted the response of GIC patients to ICI therapy. PNI possesses several benefits that make it convenient for daily clinical practice. It is readily available, easily quantifiable, repeatable, and relatively cost-effective to assess (50). As a result, due to its well-established impact on the host's nutritional and immune status as well as cancer, the PNI could serve as a useful tool in predicting the therapeutic outcomes of ICIs in GIC patients. Individualized and timely nutritional and immunological interventions may improve the prognosis of patients with low baseline PNI.

It is noteworthy that the majority of studies included in this analysis were retrospective cohort studies, which may limit their

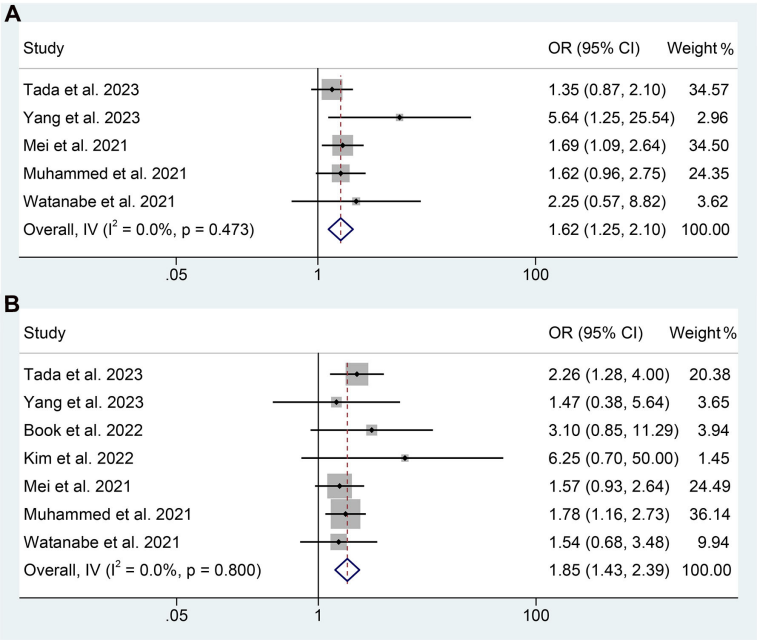

FIGURE 8
Forest plots of the relationship between prognostic nutritional index and objective response rate **(A)** and disease control rate **(B)**. OR, odds ratio; CL, confidence interval.

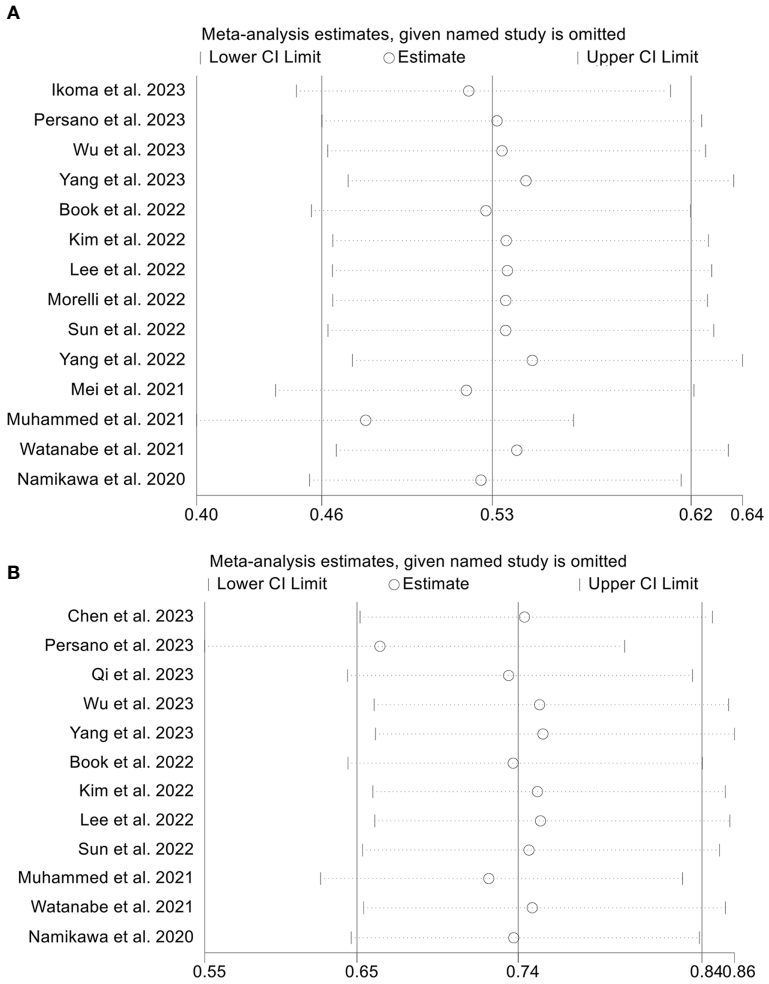

FIGURE 9
Sensitivity analysis of the association between prognostic nutritional index and overall survival **(A)** and progression-free survival **(B)**. CL, confidence interval.

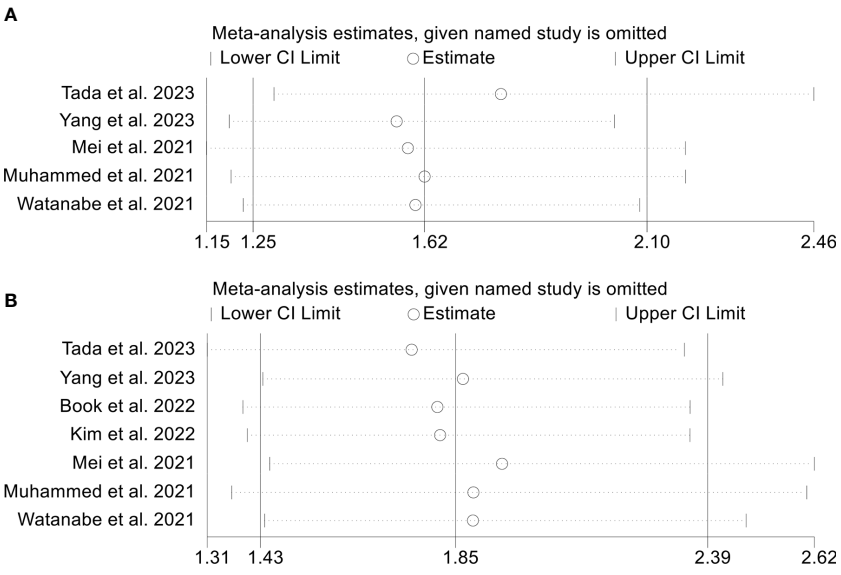

FIGURE 10
Sensitivity analysis of the association between prognostic nutritional index and objective response rate **(A)** and disease control rate **(B)**. CL, confidence interval.

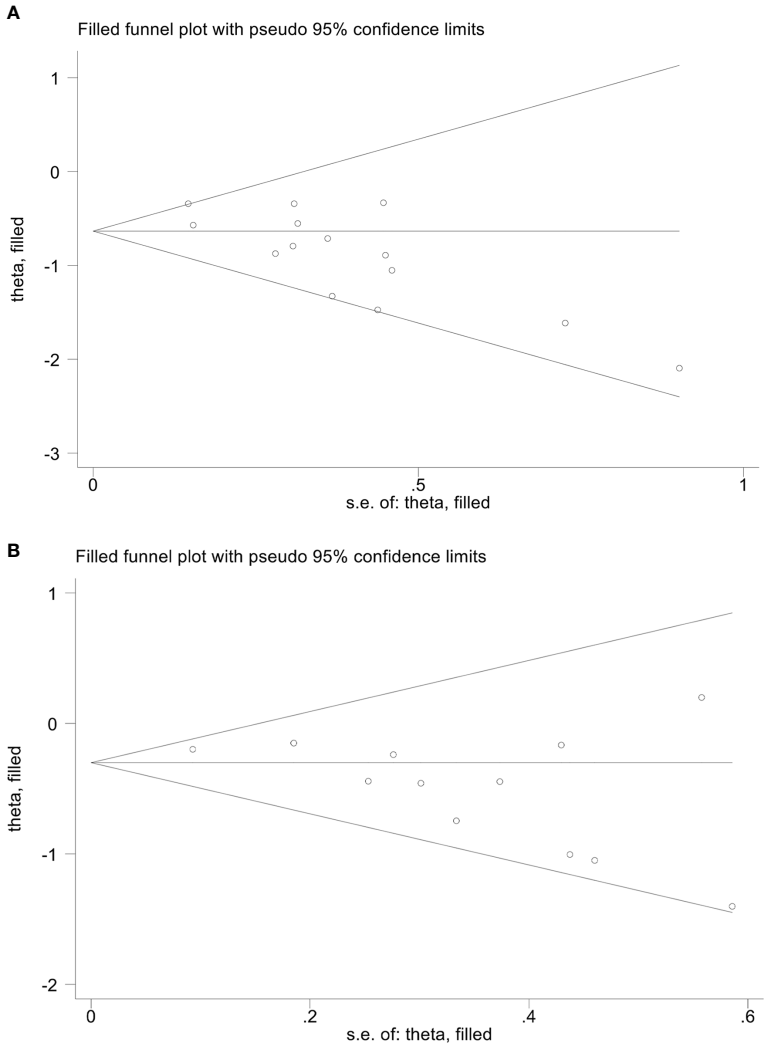

FIGURE 11
The picture of the trim-and-fill method terms of overall survival **(A)** and progression-free survival **(B)**. Theta, the effect estimate; S.e. of: theta, the corresponding standard error.

statistical validity. In addition, the types of ICIs used in each study are not entirely consistent. Therefore, it is imperative to perform additional high-quality investigations with larger sample sizes, particularly multicenter prospective studies, to corroborate and refine our findings.

Data availability statement

The original contributions presented in the study are included in the article/Supplementary Material. Further inquiries can be directed to the corresponding authors.

Author contributions

LZ, WM, BH, and WW conceived and designed the study. LZ, WM, ZQ, TK, and KW were responsible for the collection and assembly of data, data analysis, and interpretation. LZ, ZQ, and WM were involved in writing the manuscript. LZ, QZ, WM, BH, and WW revised the manuscript. All authors contributed to the article and approved the submitted version.

Conflict of interest

The authors declare that the research was conducted in the absence of any commercial or financial relationships that could be construed as a potential conflict of interest.

Publisher's note

All claims expressed in this article are solely those of the authors and do not necessarily represent those of their affiliated organizations, or those of the publisher, the editors and the reviewers. Any product that may be evaluated in this article, or claim that may be made by its manufacturer, is not guaranteed or endorsed by the publisher.

Supplementary material

The Supplementary Material for this article can be found online at: https://www.frontiersin.org/articles/10.3389/fimmu.2023.1219929/full#supplementary-material

SUPPLEMENTARY TABLE 1
The detailed search strategies for Pubmed.

SUPPLEMENTARY FIGURE 1
Subgroup analysis of the relationship between prognostic nutritional index and overall survival based on the Cox model. HR, hazard ratio; CL, confidence interval.

SUPPLEMENTARY FIGURE 2
Subgroup analysis of the relationship between prognostic nutritional index and progression-free survival based on the Cox model. HR, hazard ratio; CL, confidence interval.

References

1. Arnold M, Abnet CC, Neale RE, Vignat J, Giovannucci EL, McGlynn KA, et al. Global burden of 5 major types of gastrointestinal cancer. *Gastroenterology* (2020) 159 (1):335–349.e315. doi: 10.1053/j.gastro.2020.02.068

2. Wang Y, Zou J, Li Y, Jiao X, Wang Y, Zhuo N, et al. Serological biomarkers predict immune-related adverse events and clinical benefit in patients with advanced gastrointestinal cancers. *Front Immunol* (2022) 13:987568. doi: 10.3389/fimmu.2022.987568

3. Zhang L, Chen C, Chai D, Li C, Guan Y, Liu L, et al. The association between antibiotic use and outcomes of HCC patients treated with immune checkpoint inhibitors. *Front Immunol* (2022) 13:956533. doi: 10.3389/fimmu.2022.956533

4. Boku N, Ryu MH, Kato K, Chung HC, Minashi K, Lee KW, et al. Safety and efficacy of nivolumab in combination with s-1/capecitabine plus oxaliplatin in patients with previously untreated, unresectable, advanced, or recurrent gastric/gastroesophageal junction cancer: interim results of a randomized, phase II trial (ATTRACTION-4). *Ann Oncol* (2019) 30(2):250–8. doi: 10.1093/annonc/mdy540

5. Santini D, Zeppola T, Russano M, Citarella F, Anesi C, Buti S, et al. PD-1/PD-L1 checkpoint inhibitors during late stages of life: an ad-hoc analysis from a large multicenter cohort. *J Transl Med* (2021) 19(1):270. doi: 10.1186/s12967-021-02937-9

6. Zhang L, Jin Q, Chai D, Kuang T, Li C, Guan Y, et al. The correlation between probiotic use and outcomes of cancer patients treated with immune checkpoint inhibitors. *Front Pharmacol* (2022) 13:937874. doi: 10.3389/fphar.2022.937874

7. Ding P, Lv J, Sun C, Chen S, Yang P, Tian Y, et al. Combined systemic inflammatory immunity index and prognostic nutritional index scores as a screening marker for sarcopenia in patients with locally advanced gastric cancer. *Front Nutr* (2022) 9:981533. doi: 10.3389/fnut.2022.981533

8. Ding P, Guo H, He X, Sun C, Lowe S, Bentley R, et al. Effect of skeletal muscle loss during neoadjuvant imatinib therapy on clinical outcomes in patients with locally advanced GIST. *BMC Gastroenterol* (2022) 22(1):399. doi: 10.1186/s12876-022-02479-4

9. Ding P, Guo H, Sun C, Yang P, Kim NH, Tian Y, et al. Combined systemic immune-inflammatory index (SII) and prognostic nutritional index (PNI) predicts chemotherapy response and prognosis in locally advanced gastric cancer patients receiving neoadjuvant chemotherapy with PD-1 antibody sintilimab and XELOX: a prospective study. *BMC Gastroenterol* (2022) 22(1):121. doi: 10.1186/s12876-022-02199-9

10. Kim JH, Bae YJ, Jun KH, Chin HM. Long-term trends in hematological and nutritional status after gastrectomy for gastric cancer. *J Gastrointest Surg* (2017) 21 (8):1212–9. doi: 10.1007/s11605-017-3445-7

11. Kim YN, Choi YY, An JY, Choi MG, Lee JH, Sohn TS, et al. Comparison of postoperative nutritional status after distal gastrectomy for gastric cancer using three reconstructive methods: a multicenter study of over 1300 patients. *J Gastrointest Surg* (2020) 24(7):1482–8. doi: 10.1007/s11605-019-04301-1

12. Yu J, Huang C, Sun Y, Su X, Cao H, Hu J, et al. Effect of laparoscopic vs open distal gastrectomy on 3-year disease-free survival in patients with locally advanced gastric cancer: the CLASS-01 randomized clinical trial. *JAMA* (2019) 321(20):1983–92. doi: 10.1001/jama.2019.5359

13. Mohri Y, Inoue Y, Tanaka K, Hiro J, Uchida K, Kusunoki M. Prognostic nutritional index predicts postoperative outcome in colorectal cancer. *World J Surg* (2013) 37(11):2688–92. doi: 10.1007/s00268-013-2156-9

14. Park SH, Lee S, Song JH, Choi S, Cho M, Kwon IG, et al. Prognostic significance of body mass index and prognostic nutritional index in stage II/III gastric cancer. *Eur J Surg Oncol* (2020) 46(4 Pt A):620–5. doi: 10.1016/j.ejso.2019.10.024

15. Liu JY, Dong HM, Wang WL, Wang G, Pan H, Chen WW, et al. The effect of the prognostic nutritional index on the toxic side effects of radiochemotherapy and prognosis after radical surgery for gastric cancer. *Cancer Manag Res* (2021) 13:3385–92. doi: 10.2147/CMAR.S301140

16. Liberati A, Altman DG, Tetzlaff J, Mulrow C, Gøtzsche PC, Ioannidis JP, et al. The PRISMA statement for reporting systematic reviews and meta-analyses of studies that evaluate health care interventions: explanation and elaboration. *PloS Med* (2009) 6 (7):e1000100. doi: 10.1371/journal.pmed.1000100

17. Zhang L, Feng J, Kuang T, Chai D, Qiu Z, Deng W, et al. Blood biomarkers predict outcomes in patients with hepatocellular carcinoma treated with immune checkpoint inhibitors: a pooled analysis of 44 retrospective sudies. *Int Immunopharmacol* (2023) 118:110019. doi: 10.1016/j.intimp.2023.110019

18. Booka E, Kikuchi H, Haneda R, Soneda W, Kawata S, Murakami T, et al. Neutrophil-to-Lymphocyte ratio to predict the efficacy of immune checkpoint inhibitor in upper gastrointestinal cancer. *Anticancer Res* (2022) 42(6):2977–87. doi: 10.21873/anticanres.15781

19. Chen W, Li D, Bian X, Wu Y, Xu M, Wu M, et al. Peripheral blood markers predictive of progression-free survival in advanced esophageal squamous cell carcinoma patients treated with PD-1 inhibitors plus chemotherapy as first-line therapy. *Nutr Cancer* (2023) 75(1):207–18. doi: 10.1080/01635581.2022.2123533

20. Ikoma T, Shimokawa M, Matsumoto T, Boku S, Yasuda T, Shibata N, et al. Inflammatory prognostic factors in advanced or recurrent esophageal squamous cell carcinoma treated with nivolumab. *Cancer Immunol Immunother* (2023) 72(2):427–35. doi: 10.1007/s00262-022-03265-7

21. Kim JH, Ahn B, Hong SM, Jung HY, Kim DH, Choi KD, et al. Real-world efficacy data and predictive clinical parameters for treatment outcomes in advanced esophageal squamous cell carcinoma treated with immune checkpoint inhibitors. *Cancer Res Treat* (2022) 54(2):505–16. doi: 10.4143/crt.2020.1198

22. Lee J, Choi SH, Baek JH, Baek DW, Kim JG, Kang BW. Clinical impact of prognostic nutrition index for advanced gastric cancer patients with peritoneal metastases treated nivolumab monotherapy. *Chonnam Med J* (2022) 58(1):24–8. doi: 10.4068/cmj.2022.58.1.24

23. Mei J, Sun XQ, Lin WP, Li SH, Lu LH, Zou JW, et al. Comparison of the prognostic value of inflammation-based scores in patients with hepatocellular carcinoma after anti-pd-1 therapy. *J Inflamm Res* (2021) 14:3879–90. doi: 10.2147/JIR.S325600

24. Morelli C, Formica V, Patrikidou A, Rofei M, Shiu KK, Riondino S, et al. Nutritional index for immune-checkpoint inhibitor in patients with metastatic gastro-esophageal junction/gastric cancer. *J Gastrointest Oncol* (2022) 13(5):2072–81. doi: 10.21037/jgo-22-217

25. Muhammed A, Fulgenzi CAM, Dharmapuri S, Pinter M, Balcar L, Scheiner B, et al. The systemic inflammatory response identifies patients with adverse clinical outcome from immunotherapy in hepatocellular carcinoma. *Cancers (Basel)* (2021) 14 (1):186. doi: 10.3390/cancers14010186

26. Namikawa T, Yokota K, Tanioka N, Fukudome I, Iwabu J, Munekage M, et al. Systemic inflammatory response and nutritional biomarkers as predictors of nivolumab efficacy for gastric cancer. *Surg Today* (2020) 50(11):1486–95. doi: 10.1007/s00595-020-02048-w

27. Persano M, Rimini M, Tada T, Suda G, Shimose S, Kudo M, et al. Role of the prognostic nutritional index in predicting survival in advanced hepatocellular carcinoma treated with atezolizumab plus bevacizumab. *Oncology* (2023) 101 (5):283–91. doi: 10.1016/j.iotech.2022.100212

28. Qi WX, Wang X, Li C, Li S, Li H, Xu F, et al. Pretreatment absolute lymphocyte count is an independent predictor for survival outcomes for esophageal squamous cell carcinoma patients treated with neoadjuvant chemoradiotherapy and pembrolizumab: an analysis from a prospective cohort. *Thorac Cancer* (2023) 14(17):1556–66. doi: 10.1111/1759-7714.14898

29. Sun H, Chen L, Huang R, Pan H, Zuo Y, Zhao R, et al. Prognostic nutritional index for predicting the clinical outcomes of patients with gastric cancer who received immune checkpoint inhibitors. *Front Nutr* (2022) 9:1038118. doi: 10.3389/fnut.2022.1038118

30. Tada T, Kumada T, Hiraoka A, Kariyama K, Tani J, Hirooka M, et al. Nutritional status is associated with prognosis in patients with advanced unresectable hepatocellular carcinoma treated with atezolizumab plus bevacizumab. *Oncology* (2023) 101(4):270–82. doi: 10.1159/000527676

31. Watanabe H, Yamada T, Komori K, Hara K, Kano K, Takahashi K, et al. Effect of prognostic nutrition index in gastric or gastro-oesophageal junction cancer patients undergoing nivolumab monotherapy. *In Vivo* (2021) 35(1):563–9. doi: 10.21873/invivo.12292

32. Wu M, Zhu Y, Chen X, Wang X, Lin X, Yan X, et al. Prognostic nutritional index predicts the prognosis of patients with advanced esophageal cancer treated with immune checkpoint inhibitors: a retrospective cohort study. *J Gastrointest Oncol* (2023) 14(1):54–63. doi: 10.21037/jgo-23-48

33. Yang L, Zhong J, Wang W, Zhou F. Prognostic nutritional index associates with immunotherapy response in patients with metastatic biliary tract cancer. *Nutr Cancer* (2023) 75(2):696–706. doi: 10.1080/01635581.2022.2153880

34. Yang Z, Zhang D, Zeng H, Fu Y, Hu Z, Pan Y, et al. Inflammation-based scores predict responses to PD-1 inhibitor treatment in intrahepatic cholangiocarcinoma. *J Inflamm Res* (2022) 15:5721–31. doi: 10.2147/JIR.S385921

35. Grecea M, Soritau O, Dulf D, Ciuleanu TE, Zdrenghea M. Potential biomarkers for the efficacy of PD-1-PD-L blockade in cancer. *Onco Targets Ther* (2021) 14:5275–91. doi: 10.2147/OTT.S283892

36. Furness K, Silvers MA, Savva J, Huggins CE, Truby H, Haines T. Long-term follow-up of the potential benefits of early nutritional intervention in adults with upper gastrointestinal cancer: a pilot randomised trial. *Support Care Cancer* (2017) 25 (11):3587–93. doi: 10.1007/s00520-017-3789-2

37. Fearon K, Strasser F, Anker SD, Bosaeus I, Bruera E, Fainsinger RL, et al. Definition and classification of cancer cachexia: an international consensus. *Lancet Oncol* (2011) 12(5):489–95. doi: 10.1016/S1470-2045(10)70218-7

38. Yuan Q, Zhang W, Shang W. Identification and validation of a prognostic risk-scoring model based on sphingolipid metabolism-associated cluster in colon adenocarcinoma. *Front Endocrinol (Lausanne)* (2022) 13:1045167. doi: 10.3389/fendo.2022.1045167

39. Evans DC, Corkins MR, Malone A, Miller S, Mogensen KM, Guenter P, et al. The use of visceral proteins as nutrition markers: an ASPEN position paper. *Nutr Clin Pract* (2021) 36(1):22–8. doi: 10.1002/ncp.10588

40. Coffelt SB, de Visser KE. Cancer: inflammation lights the way to metastasis. *Nature* (2014) 507(7490):48–9. doi: 10.1038/nature13062

41. Bito R, Hino S, Baba A, Tanaka M, Watabe H, Kawabata H. Degradation of oxidative stress-induced denatured albumin in rat liver endothelial cells. *Am J Physiol Cell Physiol* (2005) 289(3):C531–542. doi: 10.1152/ajpcell.00431.2004

42. Condeelis J, Pollard JW. Macrophages: obligate partners for tumor cell migration, invasion, and metastasis. *Cell* (2006) 124(2):263–6. doi: 10.1016/j.cell.2006.01.007

43. Yuan Q, Deng D, Pan C, Ren J, Wei T, Wu Z, et al. Integration of transcriptomics, proteomics, and metabolomics data to reveal HER2-associated metabolic heterogeneity in gastric cancer with response to immunotherapy and neoadjuvant chemotherapy. *Front Immunol* (2022) 13:951137. doi: 10.3389/fimmu.2022.951137

44. Dunn GP, Old LJ, Schreiber RD. The immunobiology of cancer immunosurveillance and immunoediting. *Immunity* (2004) 21(2):137–48. doi: 10.1016/j.immuni.2004.07.017

45. Kitayama J, Yasuda K, Kawai K, Sunami E, Nagawa H. Circulating lymphocyte number has a positive association with tumor response in neoadjuvant chemoradiotherapy for advanced rectal cancer. *Radiat Oncol* (2010) 5:47. doi: 10.1186/1748-717X-5-47

46. Nakatani M, Migita K, Matsumoto S, Wakatsuki K, Ito M, Nakade H, et al. Prognostic significance of the prognostic nutritional index in esophageal cancer patients undergoing neoadjuvant chemotherapy. *Dis Esophagus* (2017) 30(8):1–7. doi: 10.1093/dote/dox020

47. Wang D, Hu X, Xiao L, Long G, Yao L, Wang Z, et al. Prognostic nutritional index and systemic immune-inflammation index predict the prognosis of patients with HCC. *J Gastrointest Surg* (2021) 25(2):421–7. doi: 10.1007/s11605-019-04492-7

48. Fu M, Yu L, Yang L, Chen Y, Chen X, Hu Q, et al. Predictive value of the preoperative prognostic nutritional index for postoperative progression in patients with pancreatic neuroendocrine neoplasms. *Front Nutr* (2022) 9:945833. doi: 10.3389/fnut.2022.945833

49. Yang Y. Cancer immunotherapy: harnessing the immune system to battle cancer. *J Clin Invest* (2015) 125(9):3335–7. doi: 10.1172/JCI83871

50. Kang BW, Chau I. Current status and future potential of predictive biomarkers for immune checkpoint inhibitors in gastric cancer. *ESMO Open* (2020) 5(4):e000791. doi: 10.1136/esmoopen-2020-000791

frontiers | Frontiers in Immunology

TYPE Original Research
PUBLISHED 23 August 2023
DOI 10.3389/fimmu.2023.1204338

OPEN ACCESS

EDITED BY
Chi Chun Wong,
The Chinese University
of Hong Kong, China

REVIEWED BY
Hualin Chen,
Peking Union Medical College Hospital
(CAMS), China
Zhirui Zeng,
Guizhou Medical University, China

*CORRESPONDENCE
Wenxiang Huang
wenxianghuang2018@163.com

RECEIVED 12 April 2023
ACCEPTED 04 August 2023
PUBLISHED 23 August 2023

CITATION
Wang Z, Chen X, Zhang J, Chen X, Peng J and Huang W (2023) Based on disulfidptosis-related glycolytic genes to construct a signature for predicting prognosis and immune infiltration analysis of hepatocellular carcinoma.
Front. Immunol. 14:1204338.
doi: 10.3389/fimmu.2023.1204338

Based on disulfidptosis-related glycolytic genes to construct a signature for predicting prognosis and immune infiltration analysis of hepatocellular carcinoma

Zhijian Wang[1], Xuenuo Chen[2], Jia Zhang[3], Xuanxin Chen[2], Jiayi Peng[3] and Wenxiang Huang[3]*

[1]Department of General Practice, The First Affiliated Hospital of Chongqing Medical University, Chongqing, China, [2]Department of Infectious Disease, The First Affiliated Hospital of Chongqing Medical University, Chongqing, China, [3]Department of Geriatrics, The First Affiliated Hospital of Chongqing Medical University, Chongqing, China

Background: Hepatocellular carcinoma (HCC) comprises several distinct molecular subtypes with varying prognostic implications. However, a comprehensive analysis of a prognostic signature for HCC based on molecular subtypes related to disulfidptosis and glycolysis, as well as associated metabolomics and the immune microenvironment, is yet to be fully explored.

Methods: Based on the differences in the expression of disulfide-related glycolytic genes (DRGGs), patients with HCC were divided into different subtypes by consensus clustering. Establish and verify a risk prognosis signature. Finally, the expression level of the key gene SLCO1B1 in the signature was evaluated using immunohistochemistry (IHC) and quantitative real-time PCR (qRT-PCR) in HCC. The association between this gene and immune cells was explored using multiplex immunofluorescence. The biological functions of the cell counting kit-8, wound healing, and colony formation assays were studied.

Results: Different subtypes of patients have specific clinicopathological features, prognosis and immune microenvironment. We identified seven valuable genes and constructed a risk-prognosis signature. Analysis of the risk score revealed that compared to the high-risk group, the low-risk group had a better prognosis, higher immune scores, and more abundant immune-related pathways, consistent with the tumor subtypes. Furthermore, IHC and qRT-PCR analyses showed decreased expression of SLCO1B1 in HCC tissues. Functional experiments revealed that SLCO1B1 overexpression inhibited the proliferation, migration, and invasion of HCC cells.

Conclusion: We developed a prognostic signature that can assist clinicians in predicting the overall survival of patients with HCC and provides a reference value for targeted therapy.

KEYWORDS

hepatocellular carcinoma (HCC), disulfidptosis, glycolysis, subtype, prognostic signature, tumor microenvironment, SLCO1B1

1 Introduction

Primary liver cancer is a prevalent malignancy worldwide and the fourth leading cause of cancer-related deaths. The highest incidences were observed in East Asia, Southeast Asia, and North Africa (1). Hepatocellular carcinoma (HCC) accounts for approximately 80% of all primary HCCs (2). HCC typically arises from the progression of metabolic liver disease or viral hepatitis B and C infections (2). Numerous genetic mutations build up during the development of HCC, including TP53 mutations in hepatitis B-associated HCC and CTNNB1 and TERT mutations in HCC associated with alcoholic liver disease (3). Owing to its insidious onset, HCC is usually diagnosed at an advanced stage when surgical intervention is not feasible. Current treatment options for patients with advanced HCC include radiotherapy, immunotherapy, and targeted therapy. However, their efficacy is often limited by drug resistance (4, 5). Therefore, identifying new tumor markers is crucial for improving HCC-targeted therapies.

Recent studies have revealed that the accumulation of intracellular disulfide induces a stress response leading to disulfidptosis, a novel form of programmed cell death (6). Cancer cells typically rely on the amino acid transporter protein SLC7A11 to transport cystine intracellularly and regulate tumor growth. However, cystine is a disulfide that may have cytotoxic effects. To balance this, cells rapidly convert toxic disulfide to other non-toxic molecules using nicotinamide adenine dinucleotide phosphate (NADPH) (7). NADPH is mainly produced by glucose metabolism, and in cases where tumor cells are deficient in glucose, it can trigger disulfidptosis in tumor cells, which in turn inhibits tumor growth. However, this process does not cause cytotoxic to normal tissues (8). Since the introduction of the concept of disulfidptosis, it has attracted considerable attention from the medical community, particularly in the field of tumor treatment (9). Therefore, understanding the state of disulfidptosis in different patients with HCC is valuable for exploring targeted therapies for HCC.

Glycolysis is a method of metabolic reprogramming in tumor cells and was initially identified during the study of HCC. The hallmark feature is that tumor cells use glycolysis as the main energy source, even when mitochondria function normally and oxygen is available, leading to a significant increase in the cellular uptake of glucose and lactic acid production (10, 11). In addition to playing a crucial role in tumor proliferation, metastasis, and invasion, glycolysis partly explains the development of resistance to sorafenib in HCC (12, 13). Targeting glycolysis holds promise for improving drug resistance and is a potential therapeutic target for HCC.

As two important biological processes in tumors, the relationship between disulfidptosis and glycolysis has received considerable attention. Although the concept of disulfidptosis is relatively new, studies on sulfur metabolism in tumors have been reported. Researchers have proposed that sulfur-containing compounds from garlic inhibit the proliferation of HCC cell lines, a process closely associated with the highly reactive sulfane sulfur (14, 15). In humans, sulfur-containing amino acids, such as cysteine, and sulfur-containing proteins, such as glutathione, are metabolized to produce sulfane sulfur, which has both anti-cancer and pro-cancer effects. However, the mechanism of action is unclear, and we speculate that there may be a link between disulfidopathy and the therapeutic outcomes of sulfur-containing compounds (14, 16–18). Additionally, sulfur-containing amino acids and disulfide proteomics have great potential for regulating glycolysis (19, 20). These studies inspired us to further explore the association between disulfidroptosis and glycolysis in patients with HCC and healthy individuals to guide targeted therapy and prognosis of HCC. In this study, we developed a prognostic signature by combining disulfide-related genes (DRGs) and glycolysis-related genes (GRGs) to predict the prognosis of HCC patients. The flowchart in Figure 1 illustrates how this study was conducted.

2 Materials and methods

2.1 Collation and collection of data

First, we downloaded clinicopathological information, gene expression matrix data, and somatic mutation data of patients with HCC from The Cancer Genome Atlas (TCGA) database. Another set of data containing the survival information of patients with HCC was downloaded from the Gene Expression Omnibus (GEO) database, and joint analysis of data from multiple databases helped reduce the heterogeneity of individual datasets. The GSE76427 and TCGA-LIHC data downloaded from the GEO

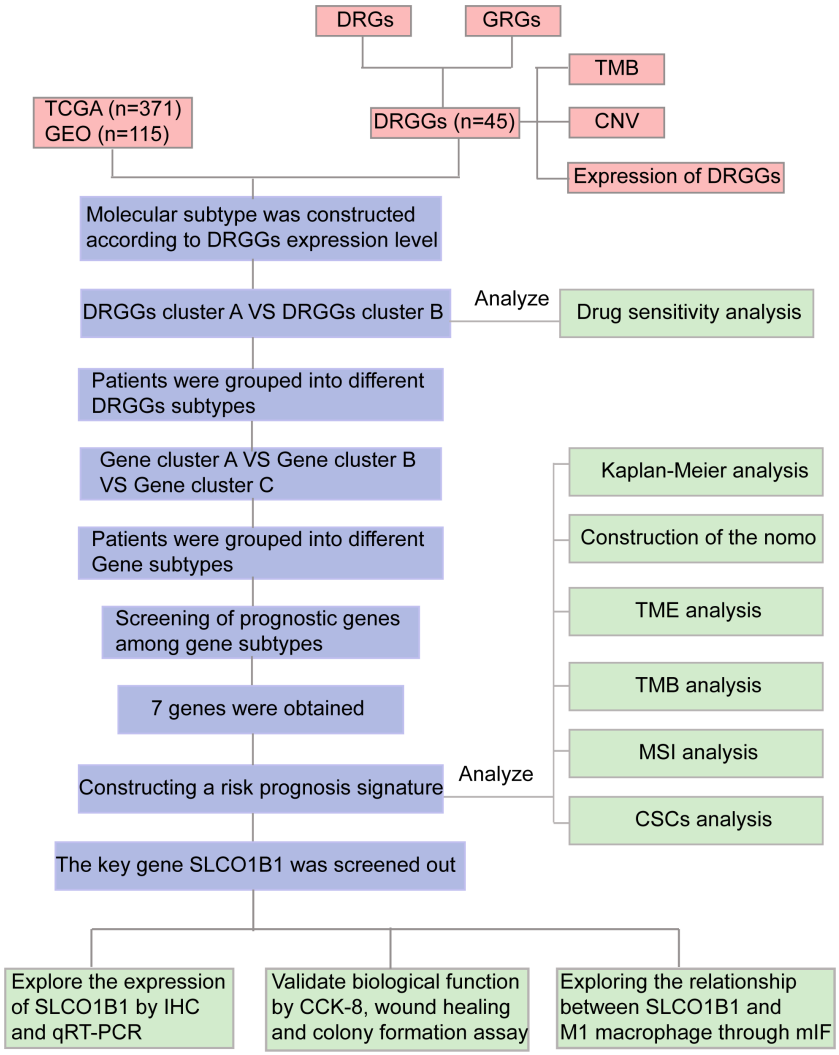

FIGURE 1
Flow chart of our study. DRGs, disulfidptosis related genes; GRGs, glycolysis related genes; DRGGs, disulfidptosis related glycolytic genes; TCGA, The Cancer Genome Atlas; GEO, Gene Expression Omnibus; TMB, tumor mutational burden; CNV, copy number variation; GSEA, Gene Set Enrichment Analyses; TME, tumor microenvironment; MSI, microsatellite instability; CSCs, cancer stem cells; IHC, immunohistochemical; DEGs, differentially expressed genes; CCK-8, Cell counting kit-8; mIF, multiplex immunofluorescence.

database were combined using the "merge" package (21). The "sva" package in R language was used to correct for differences and normalize for different sequencing batches (22), excluding patients with missing survival information. We finally obtained 371 patients with HCC from TCGA database and 115 patients from the GEO database, which were used for the subsequent analysis.

2.2 Clinical sample collection

We randomly collected 14 pairs of fresh HCC and adjacent normal tissue samples from the First Affiliated Hospital of Chongqing Medical University (Chongqing, China) between February and March 2023. In addition, 26 pairs of paraffin-embedded sections of HCC and para-cancerous tissues between June 2022 and December 2022 from the Pathological Diagnosis Center of Chongqing Medical University (Chongqing, China). None of the patients participating in our study underwent radiotherapy, chemotherapy, and immunotherapy before surgery. This study was approved by the Ethics Committee of the First Affiliated Hospital of Chongqing Medical University.

2.3 Cell culture and transfection

Human HepG2 and Huh7 HCC cells were purchased from the Cell Collection Center of the Chinese Academy of Sciences (Shanghai, China). All cells were maintained in Dulbecco's Modified Eagle's Medium (DMEM; Gibco, USA) containing 10% Fetal Bovine Serum (Wisent, Canada) and cultured at 37°C in a cell incubator with 5% CO2.

Lentiviruses targeting SLCO1B1 (forward, 5'-GGGGTAC CATCATGGACCAAAATCAAC-3', and reverse 5'-CTCGAGT GGAAACACAGAAGCAGAAG-3') were purchased from

GeneChem (Shanghai, China). Huh7 and HepG2 cells were transfected according to the manufacturer's instructions. Stable strains were screened using 2 μg/ml puromycin. Three days after transfection, gene expression of the SLCO1B1 marker was observed under a fluorescence microscope, and cells with a transfection efficiency of >80% were selected for subsequent analysis.

2.4 Quantitative real time PCR

Total RNA was extracted from 14 pairs of fresh HCC and paraneoplastic tissues using the TRIZOL reagent (Takara Biotechnology Co., Ltd., Dalian, China) according to the manufacturer's instructions. Total RNA was reverse transcribed into cDNA using the PrimeScrip™ RT kit (Takara Biotechnology Co., Ltd.). The polymerase chain reaction (PCR) was performed according to the manufacturer's instructions. The amplification product was designed by Takara Biotechnology Co., Ltd. with the following sequence: SLCO1B1: forward, 5'-GAATGCCCA AGATGATGCTT-3', and reverse, 5'-AATCCAGTGCAAGT GATTTCAAT-3'; β-actin: forward, 5'-AGAAAATCTGGCAC CACACCT-3', and reverse, 5'-GATAGCACAGCCTGGA TAGCA-3'. Expression was normalized to that of β-actin and relative expression was calculated using the $2^{-\Delta\Delta Ct}$ method (23).

2.5 Immunohistochemistry stain

IHC was performed on 18 pairs of paraffin-embedded HCC and normal paracancerous tissue samples. The specific experiments were performed as previously described (24). Anti-human SLCO1B1 antibody (1:500, DF4534, Affinity Biosciences, China) was used to incubate the tissues overnight at 4°C. After application of the appropriate secondary antibody, the labeled antigen was visualized using a standard 3, 3'-diaminobenzidine (DAB) protocol. The slides were stained with hematoxylin. Two pathologists evaluated the staining results in a double-blind manner. The intensity of IHC staining was calculated from the intensity and number of stained cellular sections. The evaluation criteria for staining intensity were as follows: 0, 1, 2, and 3 represented negative, weak, moderate, and strong staining, respectively. The evaluation criteria for the number of stained cells were 0, 1, 2, 3, and 4, representing the percentages of stained cells as <10%, 10–25%, 25–50%, 50–75%, and >75%, respectively. IHC score = staining intensity × staining number. A score ≥6 is a high expression; otherwise, it is a low expression (25).

2.6 Multiplex immunofluorescence analysis

MIF detection of SLCO1B1 and CD86 was performed in pathological sections of HCC and adjacent normal tissues. First, the sections were deparaffinized and rehydrated, and antigen retrieval was performed using EDTA antigen retrieval buffer. Subsequently, the sections were incubated with 3% hydrogen peroxide at room temperature for 25 min in the dark to block endogenous peroxidase, and 3% Bovine Serum Albumin was used to block the sections for 30 min. Cyclic staining for both antigens in each section was then performed, including incubation with primary and secondary antibodies, fluorescence signal enhancement by Cyanine 3 Tyramide, and removal of Tyramide Signal Amplification (TSA) -antibody complexes using EDTA buffer. Subsequently, the cell nuclei were counterstained with DAPI for 10 min, and an autofluorescence quencher was added, reacted for 5 min, and rinsed with distilled water. Subsequently, sections were mounted in an anti-fluorescence quenching mounting medium. Finally, observed and collected images were obtained using a fluorescence microscope (Nikon ECLIPSE C1, Nikon DS-U3).

The scanned images were analyzed using the InForm software, and the results were independently analyzed by two experienced pathologists. The numbers 1, 2, and 3 represented low, medium, and high fluorescence intensities, respectively. The histochemical scoring formula was as follows: (high fluorescence intensity) × 3 + (median fluorescence intensity) × 2 + (low fluorescence intensity) × 1 (26).

We used SLCO1B1 and CD86 (Proteintech, 13395-1-ap) as primary antibodies, of which, SLCO1B1 was the key gene in our signature, and CD86 was the surface marker of M1 macrophages (27, 28). Goat Anti-Mouse IgG (H+L)-Alexa Fluor 488 was used as the secondary antibody (AIFang biological, SA002).

2.7 Colony formation assay

Cells (1×10^3 cells per well in a six-well plate, and 5 ml of complete medium) was added to each well, shaken, mixed, and cultured in a cell incubator for approximately 14 days. The cells were fixed with 4% paraformaldehyde, stained with 1 ml of 0.5% crystal violet, rinsed with tap water, dried, and photographed.

2.8 Cell counting kit-8

First, we inoculated the well-growing cells into a 96-well plate, adjusted the cell concentration to 1.5×10^4/ml, added 200 μl of cell suspension to each well, repeated three times for each group of cells, and place them in an incubator for culture. Then, after the cells adhered to the wall, 100 μl of CCK-8 working solution was added to each well, which was recorded as 0 h of the measurement, and the cells were placed in the incubator for 2.5 h. Finally, at specified time points (0, 24, 48, and 72 h), the absorbance value was measured at a wavelength of 450 nm by a microplate reader (Varioskan Flash, version: 4.00.53), and the cell viability curve was drawn according to the absorbance value.

2.9 Wound healing

First, we adjusted the cell concentration to 3×10^5/ml, inoculated them into a 6-well plate, cultured in an incubator,

observed that the cell confluence reached 100%, took a 200 μl sterile pipette tip and drew three vertical lines, and washed the exfoliated cells using the sterile phosphate buffered saline, and then, 2 ml DMEM was added to each well. Finally, the scratches were observed under a microscope and photographed at 0, 12, and 24 h.

2.10 Differential analysis, genomic characteristics of DRGGs and drug sensitivity analysis of DRGGs subtypes

We retrieved 14 DRGs from the relevant literature (Supplementary Table 1), 326 GRGs were extracted from the MSigDB website (https://www.gsea-msigdb.org/gsea/msigdb/) (Supplementary Table 2). Then, we normalized the data from TCGA and GEO databases using the "limma" and "survival" package of R language, and obtained 45 disulfidptosis-related glycolytic genes (DRGGs) with the screening condition of |cor|>0.65 (29). Then, the frequency and type of mutations of 45 DRGGs in patients with HCC were analyzed by the "maftools" package, and the results were presented as "waterfall plots" (30). In addition, the somatic copy number variation (CNV) frequencies of the above genes were shown by "bubble plots", and the sites where the mutations occurred were shown by "circle plots". Next, in order to clarify the sensitivity of patients with DRGGs molecular subtypes of HCC to chemotherapy drugs, we calculated the drug concentration values when half of the cells were induced to undergo apoptosis by drugs for the treatment of HCC (IC50) using the "pRRophetic" package (31).

2.11 Consensus clustering analysis of DRGGs

Consensus clustering analysis was performed using the "ConsensusClusterPlus" R language package to classify the enrolled patients with HCC were divided into different molecular subtypes according to the differential expression of DRGGs (32). Intragroup associations were enhanced and intergroup associations were reduced after clustering. Subsequently, heterogeneity between the two groups was described by principal components analysis (PCA) and cumulative density functional (CDF) curves. To assess the value of consistent clustering analysis in the treatment of patients with HCC, we compared the between-group differences in clinicopathological characteristics of patients with different subtypes by heat map. Kaplan-Meier (K-M) curves were used to determine survival differences between the two subtypes by the "survival" and "survminer" package in R Studio. To clarify the functional differences between the two subtypes, gene set variation analysis (GSVA) was performed by the Kyoto Encyclopedia of Genes and Genomes (KEGG). In addition, differences in immune cell infiltration were analyzed using single-sample gene set enrichment analysis (ssGSEA) to understand the differences in the immune microenvironment between the groups.

2.12 Screening, functional analysis and prognostic analysis of differential genes between molecular subtypes of DRGGs

Differentially expressed genes (DEGs) between molecular subtypes of DRGGs were screened using the "limma" package in R language with FDR<0.05 and |log2fold change (FC)|≥0.585 as criteria. Functional enrichment analysis was conducted using Gene Ontology (GO) and KEGG to further explore the potential gene functions and enrichment pathways of DRGGs.

Next, differential genes with prognostic value between the two subtypes were screened by univariate Cox regression analysis, and patients were classified into different genetic subtypes based on these genes. Survival analysis was performed using K-M to verify the prognostic differences between different gene subtypes. In addition, differences in clinicopathological characteristics between patients with different subtypes were assessed to guide the direction for targeted therapy.

2.13 Construction of a prognostic signature

First, genes with prognostic value were screened using univariate Cox regression analysis, and the accuracy of the signature was improved using LASSO regression analysis. Independent prognostic factors associated with HCC were screened based on multivariate Cox regression analysis, and the risk score was calculated using the multivariate Cox regression coefficients and the expression of DRGGs in patients with HCC. Then, the prognostic signature was constructed. The scoring formula was as follows:

$$risk\ \ score\ \ = \sum(\text{Expi}\ \ *\ \ \text{coefi})$$

where Expi and coefi represent the expression of genes and regression coefficients, respectively. Subsequently, all patients with HCC were randomly divided into a training group and test group at a 1:1 ratio. Then, the patients were further classified into high-risk and low-risk groups based on their median of the prognostic scores.

2.14 Analysis and validation of clinical relevance of the prognostic signature

First, we calculated the differences in risk scores across the DRGGs molecular subtypes and gene clusters to assess whether the risk score retained its predictive power across subgroups. Differential expression maps of DRGGs between the high- and low-risk groups were constructed using the "ggplot2" package. The prognostic value of clinicopathological elements and risk scores was assessed by Cox regression analysis. Next, survival differences between patients in various risk groups were identified using the K-M survival analysis, plotting receiver operating characteristic (ROC) curves to assess the diagnostic value of the scoring system. Then, the accuracy of the results was further validated in the test group.

2.15 Creation and verification of nomogram

To evaluate the prognostic characteristics of patients at 1-, 3- and 5-year, the "rms" and the "regplot" packages of R language were used to construct the nomogram by combining clinical features such as age, gender, risk scores and tumor stage of patients. Each patient's clinical information corresponded to a score and the total score was the sum of each index used for the scoring system of the nomogram. Finally, the scores were used to assess the probability of survival at 1-,3-,5-year intervals.

2.16 Exploration of tumor immune microenvironment

The main characteristics of the TIME include the extent of immune cells infiltrate, expression profile of immune checkpoints, and activity of anti-cancer immune responses. First, we assessed the relation between risk scores and the proportion of immune cells infiltration in patients with HCC using Spearman's correlation analysis. We also used the "CIBERSORT" package in R language to quantify the enrichment of different immune cells in each tumor sample and analyzed the relationship between genes and immune cells in the signature. To further understand the differences in the TIME between different risk groups and their relevance to immunotherapy, we evaluated the differences in immune checkpoint expression between the high- and low-risk groups. In addition, the ESTIMATE algorithm was applied to calculate the stromal, immune and estimated scores in the two risk groups, reflecting the degree of stromal and immune cell infiltration and tumor purity for each risk group, respectively, and a violin plot was used to visualize the differences between groups. Besides, we evaluated the enrichment of immune-related pathways in the different groups using gene set enrichment analysis (GSEA) and the activity of the seven steps of the anticancer immune response using ssGSEA to understand the role of risk scores in the TIME and thus assess tumor prognosis (33, 34).

2.17 Exploration of genomic features in prognostic signature

We applied mutation data downloaded from TCGA-LIHC to analyze the tumor mutation burden (TMB) and major mutation types in the different risk groups. TMB has emerged as a biomarker to forecast the efficacy of immunotherapy (35). In addition, it has been shown that microsatellite instability (MSI) is associated with tumorigenesis, generally caused by DNA replication defects (36). We used MSI analysis between different risk groups as a reference for prognostic assessment. The poor prognostic of HCC is intimately associated with the emergence of drug resistance, and researches on cancer stem cells (CSCs) indicate that tumor development was driven by a fraction of stem cells; therefore, it is crucial to explore the stemness of CSCs (37). We assessed the degree of resemblance between stem cells and tumor cells by calculating mRNAsi to quantify the association between CSCs and risk scores.

2.18 Statistical analysis

We analyzed the data using the R language software (version 4.2.2), performed t-tests for normally distributed data, and applied Spearman's test for correlation analysis. GraphPad Prism software (version 8.0.1) was used for plotting the images, with $P<0.05$ as the threshold of significance for all statistical analyses.

3 Results

3.1 Characterization and expression of DRGGs mutations in HCC

First, we demonstrated the interactions between DRGs and GRGs using a Sankey diagram (Figure 2A). TMB analysis of DRGGs showed that 89 (23.99%) of the 371 patients had mutations. Among these, the COL5A1 mutation frequency was the highest (4%), followed by RANBP2 (Figure 2B). Next, the somatic CNV frequency of DRGGs in HCC was further evaluated and copy number alterations were found in all gene numbers. Among them, most genes, such as TPR, NUP153, HK3, FLNA and PAXIP1, had increased CNV frequencies, whereas ENO1, FLNB, AGRN, CAPZB and ZBTB7A had decreased CNV (Figure 2C). In addition, we showed the location of CNV of DRGGs occurring on chromatin by a ring plot (Figure 2D) and found that most DRGGs were located on chromosomes 1, 2, 3, and 7. Besides, we compared the expression of DRGGs between HCC tissues and normal samples and found that most genes, such as AGRN, B3GNT3 and FLNA, were highly expressed in tumor tissues (Figure 2E), resulting in a worse patient prognosis (Figures S1A–P, Figures S2A–P, Figures S3A–E). Figure 2F shows that DRGGs are positively correlated and play a promoting role in HCC progression. In addition, most genes were positive associated with CNV changes, indicating that CNV may be one of the factors affecting gene expression levels (Figures 2E, F). Thus, the analysis of mutations and expression of DRGGs showed significant differences between HCC and normal tissues, indicating that this gene cluster may play a key role in HCC progression.

3.2 Construction and prognostic analysis of molecular subtypes of DRGGs in patients with HCC

We evaluated the HCC subtypes based on differences in the expression of DRGGs and performed a cluster analysis of patients with HCC using TCGA-LIHC and GEO (GSE76427) databases. During the cluster analysis of the 486 samples, k=2 was considered the best clustering method to minimize the differences between groups, and the patients with HCC were divided into two subtypes: DRGGs cluster A and DRGGs cluster B (Figure 3A). Besides, the results were verified by PCA (Figure 3B) and CDF curves (Figure S3F). In addition, the tracking plot showed that the sample was the most stable when k = 2 (Figure S3G). In the K-M survival analysis of

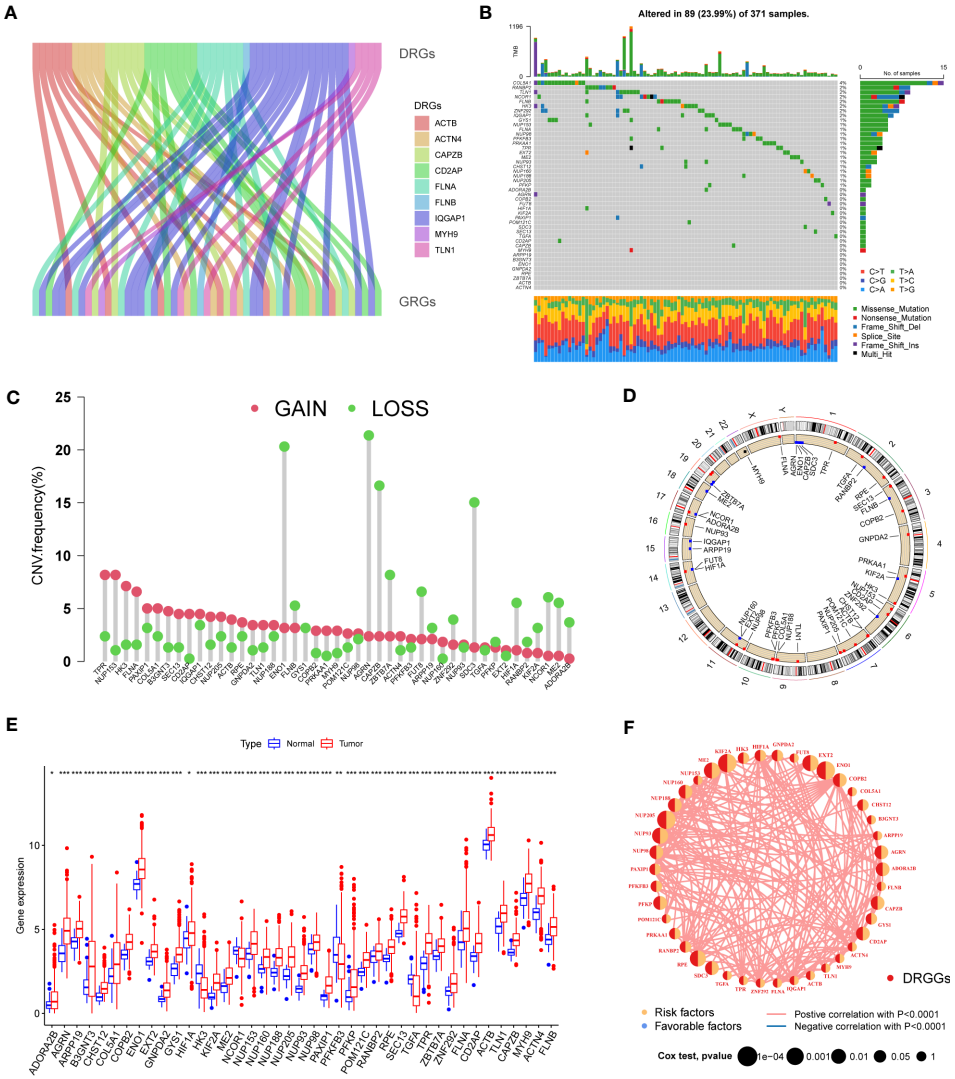

FIGURE 2
(A) The Sankey diagram showing the correlation between DRGs and GRGs. **(B)** Mutation frequencies and mutation types of 45 DRGGs in 371 patients with HCC from the TCGA database. **(C)** Frequency of increased and decreased CNV in DRGGs. **(D)** Location of CNV of DRGGs on 24 chromosomes. Red dots indicate increased copy number and blue dots indicate decreased copy number. **(E)** Expression of 45 DRGGs between normal and HCC tissues. * represents P<0.05, ** represents P<0.01, *** represents P<0.001. **(F)** Interaction relationship between DRGGs in HCC. The thickness of the connecting line indicates the strength of the correlation effect between genes, and the pink color represents positive correlation.

patients with both subtypes, it was found that the DRGGs cluster A had a better survival outcome (Figure 3C).

3.3 Gene set variation analysis and TIME analysis of molecular subtypes of DRGGs

First, we plotted a heat map using clinicopathological information, which showed the relationship between sex, age, T and N stages, and DRGGs cluster, where DRGGs were highly expressed in DRGGs cluster B and almost all of them were oncogenes (Figure 3D), explaining the adverse prognosis of DRGGs cluster B patients. Then, GSVA analysis of the two subtypes was performed using KEGG to compare the variation in the enrichment pathways, it was found that DRGGs cluster A was highly enriched in the drug metabolism cytochrome P450, steroid hormone biosynthesis, tyrosine metabolism, PPAR signaling pathway, whereas the remaining pathways, such as cancer pathway, pathogenic E. coli infection and actin cytoskeleton regulation were highly enriched in DRGGs cluster B. (Figure 3E). Besides, we explored the variation in the degree of the immune cell infiltration for both subtypes by ssGSEA. Most of the 23 immune cells were highly infiltrated in DRGGs cluster B (Figure 3F). However, patients with cluster B had a significantly lower CD8 T cell/T cell regulatory (Treg) ratio than patients with subtype A, resulting in a poorer prognosis (Figure S3H).

10.3389/fimmu.2023.1204338

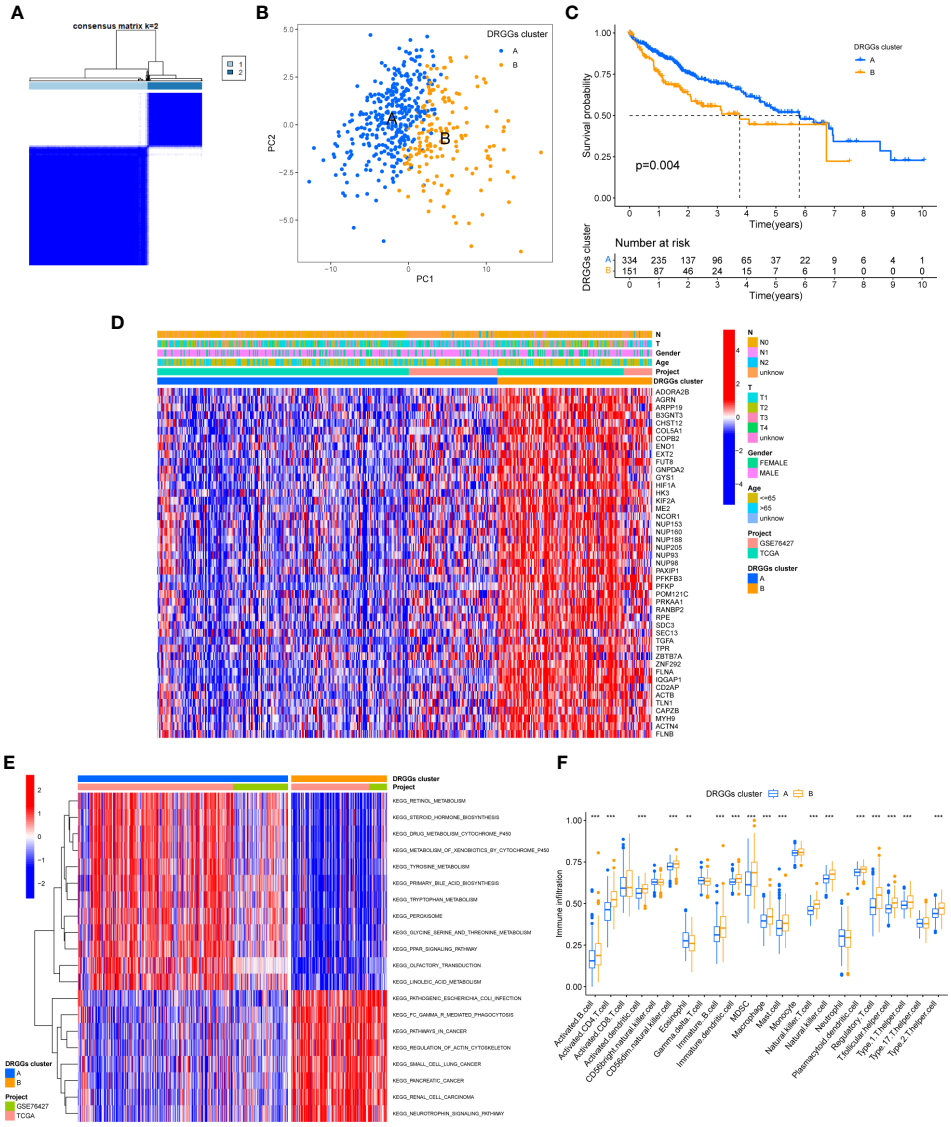

FIGURE 3
(A) Diagram of the consensus matrix defining the correlated regions of the two subtypes. **(B)** PCA analysis showing significant differences between the two subtypes. **(C)** K-M analysis showing the prognostic characteristics of patients in both subtypes. **(D)** Differences in clinicopathological features and expression levels of DRGGs between the two different subtypes. **(E)** GSVA of biological pathways between the two different subtypes, red and blue represent activating and inhibiting pathways, respectively. **(F)** The extent of infiltration of 23 immune cells in HCC subtypes. PCA, principal component analysis; GSVA, gene set variation analysis; K-M, Kaplan-Meier. ** represents P<0.01, *** represents P<0.001.

3.4 Drug sensitivity analysis

We explored the sensitivity of patients with HCC with the two DRGGs molecular subtypes to the chemotherapy drugs commonly used to treat HCC, and found that patients with DRGGs cluster A were sensitive to AICAR, BIX02189, CABOZANTINIB, NG-25, PFI-3, RTRAIL, TASELISIB, and Y-39983 drugs. However, patients in DRGGs cluster B were more sensitive to AXITINIB, AZD8055, DIHYDROROTENONE, FH535, OLAPARIB, PAZOPANIB, PONATINIB, and SB−590885 (Figure 4). There were significant differences in drug sensitivity among different subtypes of HCC, which could provide direction for personalized treatment of HCC.

3.5 Construction of gene subtypes based on differential genes between molecular subtypes of DRGGs and validation

First, to detect the possible biological behavior of tumor cells, we screened a total of 3451 differential genes between DRGGs cluster A and cluster B by “BiocManager” and “limma” packages in R Studio. Next, using GO functional enrichment analysis, we found that the differential genes were mainly enriched in biological processes (BP) functional set, such as cytoplasmic translation and xenobiotic metabolic processes, and associated with cellular component (CC), such as cell-substrate junction and focal adhesion. As for molecular function (MF), extracellular matrix

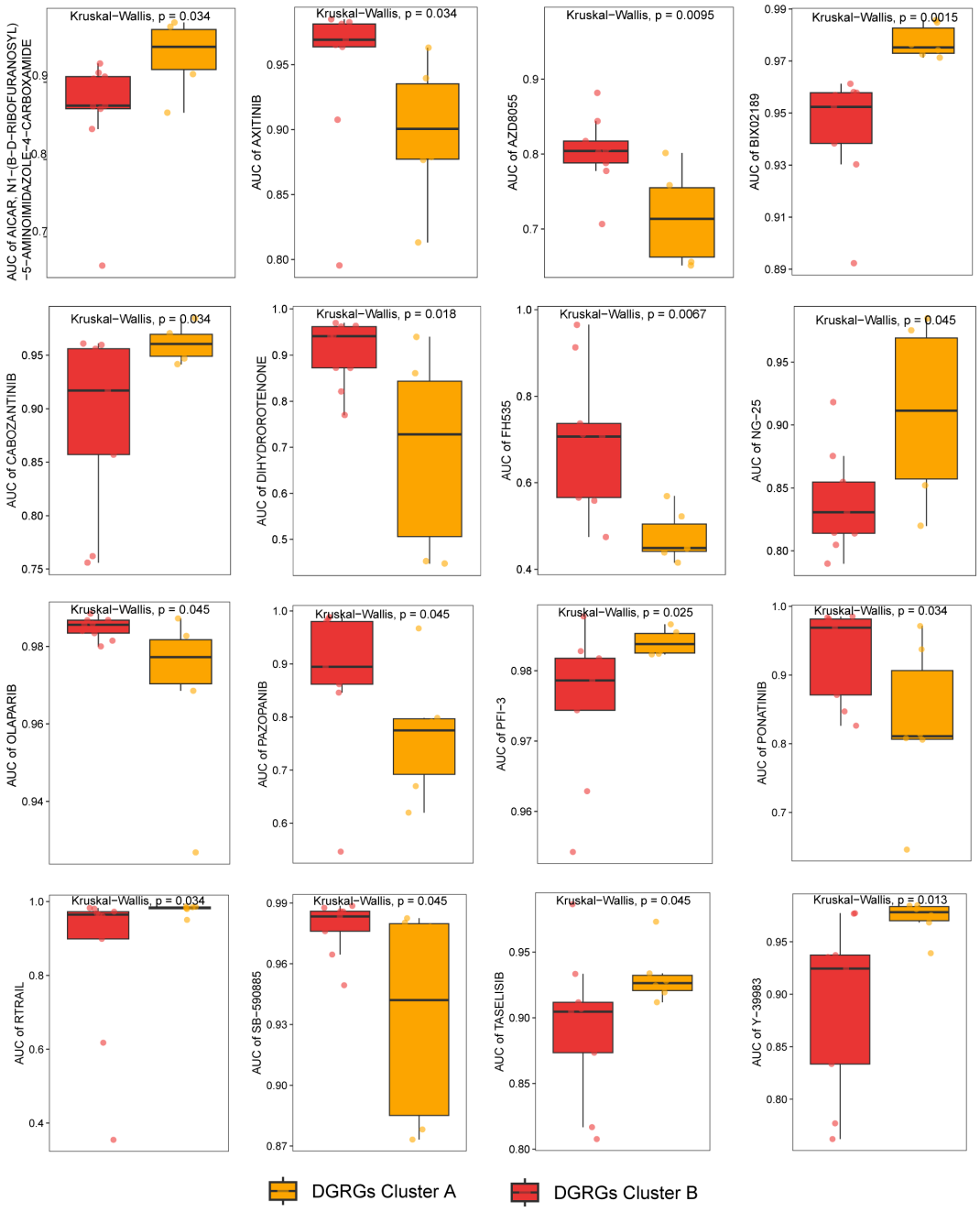

FIGURE 4
The relationship between patients with different DRGGs subtypes and chemotherapy sensitivity.

structural constituent and actin binding played an essential part in neoplasm proliferation (Figure 5A) (Supplementary Table 3). Next, The KEGG enrichment analysis was conducted on the different genes, and the findings showed that the main pathways were focused on metabolism, membrane transport, signal transduction, genetic information processing, and other related pathways (Figure 5B) (Supplementary Table 4). Therefore, DRGGs play an essential role in HCC progression.

We then acquired 1,167 genes with prognostic value using univariate Cox regression analysis. To further validate this regulatory mechanism, the samples were typed again according to the 1167 prognostic genes, and the clustering diagram was obtained using the "ConsensusClusterPlus" algorithm in R language. K=3 was the best clustering method for the samples (Figure 5C), and three genetic subtypes were obtained, namely gene clusters A, B and C. The CDF curves verified the clustering accuracy (Figure S3I). K-M analysis suggested that patients with gene cluster C had the worst prognosis, whereas those with gene cluster B had a higher survival rate ($p < 0.001$) (Figure 5D). A heat map of the clinicopathological features showed that gene cluster C mainly corresponded to DRGGs

10.3389/fimmu.2023.1204338

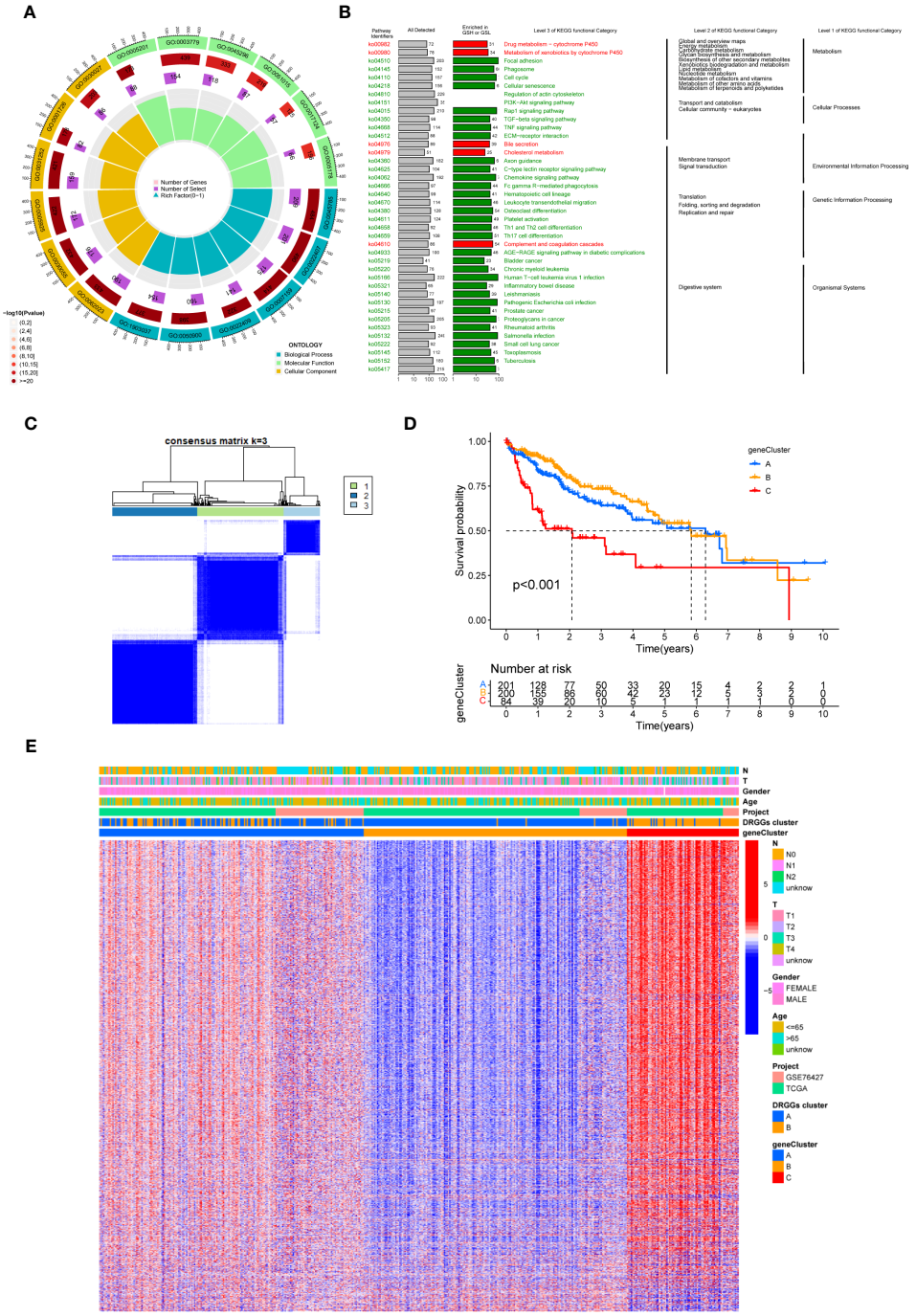

FIGURE 5
(A) GO enrichment analysis of DEGs between two DRGGs subtypes. The red part of the graph represents the number of enriched genes and the redder the color, the more significant gene enrichment; the purple part represents the number of enriched differential genes. The bar graph represents the proportion of genes. **(B)** KEGG enrichment analysis of DEGs between two DRGGs subtypes. **(C)** Diagram of the consensus matrix defining the correlated regions of three cluster-related regions. **(D)** K-M curves for the three gene subtypes. **(E)** Relationship between the three gene subtypes and clinicopathological features.

cluster B, and that patients with both subtypes had the worst prognosis (Figure 5E). Additionally, analysis of the expression of DRGGs in patients with the three gene subtypes revealed that the expression of DRGGs decreased sequentially in gene cluster C, gene cluster A, and gene cluster B, with statistically significant differences (P<0.001) (Figure 6A).

3.6 Construction and validation of risk prognostic signature

First, we constructed a prognostic signature for DRGGs from the differential genes among the three gene subtypes based on significant gene data obtained from multifactorial Cox regression

10.3389/fimmu.2023.1204338

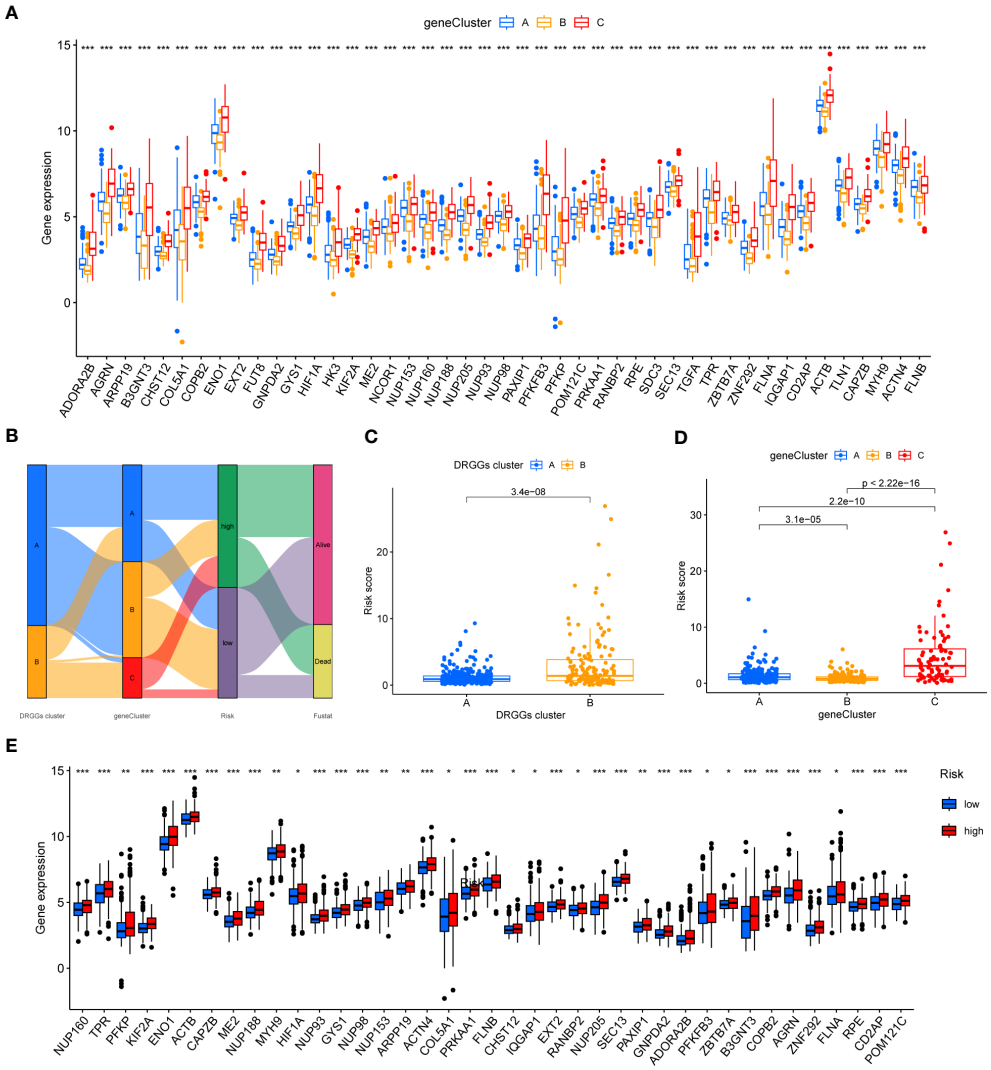

FIGURE 6
(A) Differential expression of 45 DRGGs in the three gene subtypes. **(B)** Sankey diagram of different HCC subtypes and survival outcomes. **(C)** Differences in risk score among DRGGs subtypes. **(D)** Risk score differences among different gene subtypes. **(E)** Expression differences of 45 DRGGs in high-risk and low-risk groups. * represents P<0.05, ** represents P<0.01, *** represents P<0.001.

analysis using LASSO regression analysis to avoid overfitting (Figures S3J, K). Seven genes included were ETV5, FZD7, CD5, SLCO1B1, CD79A, SNX7, and SLC1A7, and the risk score equation was: Risk score = (0.3039 * expression of ETV5) + (0.3091 * expression of FZD7) + (-0.2449 * expression of CD5) + (-0.1656 * expression of SLCO1B1) + (-0.3676 * expression of CD79A) + (0.2673 * expression of SNX7) + (0.1420 * expression of SLC1A7). Besides, Sankey plots indicated a consistent relationship among the two molecular subtypes of DRGGs, the three genetic subtypes, the different risk groups for prognostic features, and the prognosis of patients (Figure 6B). Next, we assessed the association between the three gene subtypes and risk scores and observed that gene cluster B had the lowest risk score, whereas cluster C had the highest risk score. More importantly, DRGGs cluster B exhibited a higher risk score compared to DRGGs cluster A, consistent with data from previous survival analyses (Figures 6C, D). In addition, DRGGs were high expression in the high-risk group, further confirming the accuracy of the differences between HCC and normal adjacent tissues (Figure 6E).

Next, we further validated the value of the prognostic signature. The results of survival analysis revealed remarkably shorter survival times in the high-risk group, both in the overall study cohort and in the train and test groups (P<0.01) (Figures 7A, B, Figure S3L). ROC analysis of all patients with HCC according to the prognostic signature showed that the areas under the curve (AUC) were 0.753, 0.708 and 0.666 at 1-, 3- and 5- years, respectively (Figure S3M). In the train group, the 1-, 3-, and 5-year AUCs were 0.814, 0.757, and 0.804, respectively (Figure 7C), whereas those in the test group were 0.692, 0.661, and 0.575, respectively, strongly confirming the diagnostic power of the signature (Figure 7D). Subsequently, we found the prognostic value of the tumor stage and risk score in the train group using univariate Cox regression

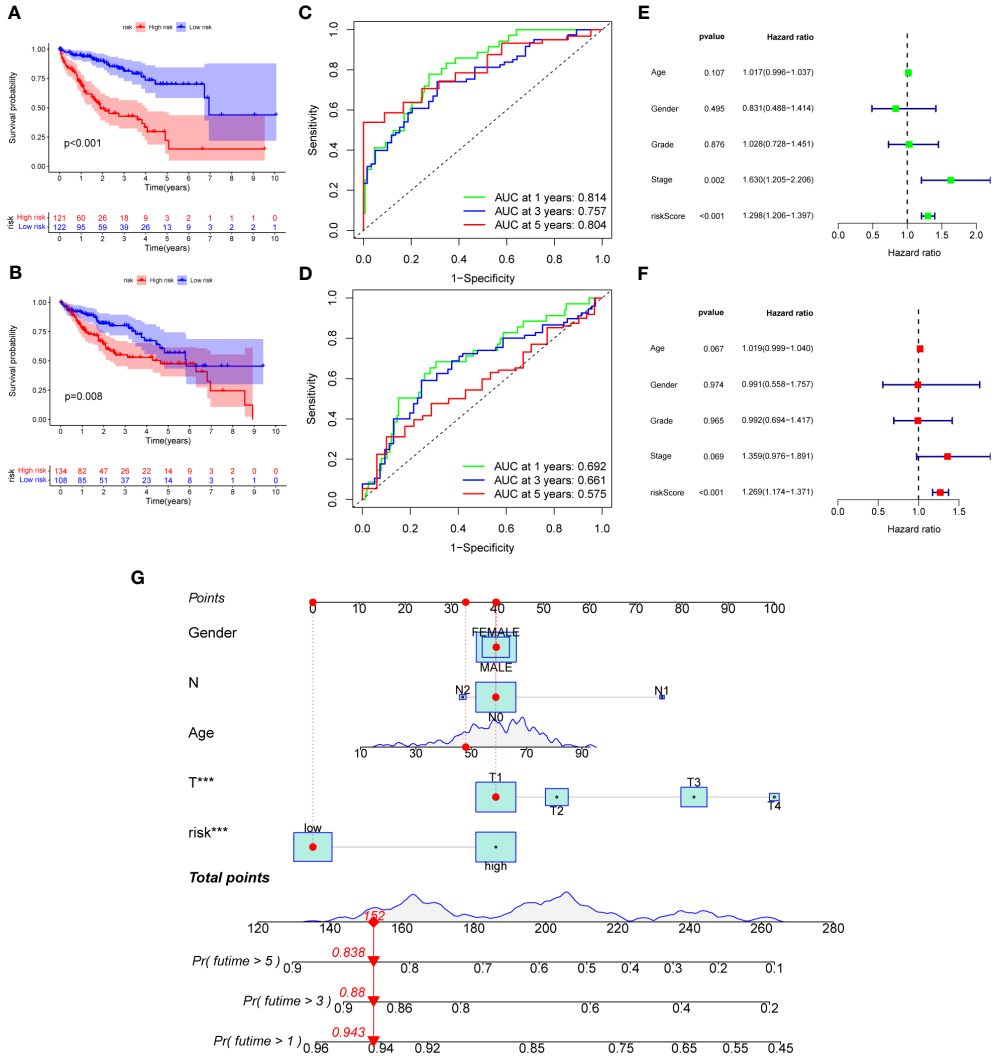

FIGURE 7
(A) K-M analysis of the Recurrence free survival (RFS) of high-risk and low-risk patients in the train group. **(B)** K-M analysis of the RFS of high-risk and low-risk patients in the train group. **(C)** ROC curves for predicting the 1-, 3-, and 5-year survival rates of patients in the train group. **(D)** ROC curves for predicting the 1-, 3-, and 5-year survival rates of patients in the test group. **(E)** The univariate Cox regression analysis of clinical characteristics and risk score in the train group. **(F)** The multivariate Cox regression analysis of clinical characteristics and risk score in the train group. **(G)** Construction of a nomogram based on clinical characteristics and risk score for prognostic signature. RFS, recurrence free survival; ROC, receiver operating characteristic.

analysis. Multivariate Cox regression analysis suggested that the risk score was an independent prognostic factor in all groups (Figures 7E, F).

3.7 Creation of nomogram

Owing to the limitations of the scoring system alone in clinical application, we integrated risk scores with the clinical information of patients to create a nomogram to predict patients' survival time at 1-, 3- and 5- years. Both T-stage and risk scores were independent prognostic factors (Figure 7G). A calibration chart further confirmed the accuracy of the signature (Figure S3N).

3.8 Assessment of TIME and biological characteristics between the risk groups

First, correlation between the risk scores and immune cells was visualized using scatter plot. The results showed that naive B cells, CD8+ T cells and plasma cells negatively related to risk scores, whereas M2 macrophages and neutrophils positively associated with risk scores (Figures 8A–E). In addition, the TME scores indicated that the low-risk group had higher tumor purity, stromal and immune scores (Figure 8F). Second, the differences in immune checkpoint expression suggested that most immune checkpoint molecules such as CD40LG, CD48, IDO1, CD27, PDCD1 were strongly expressed in the low-risk population.

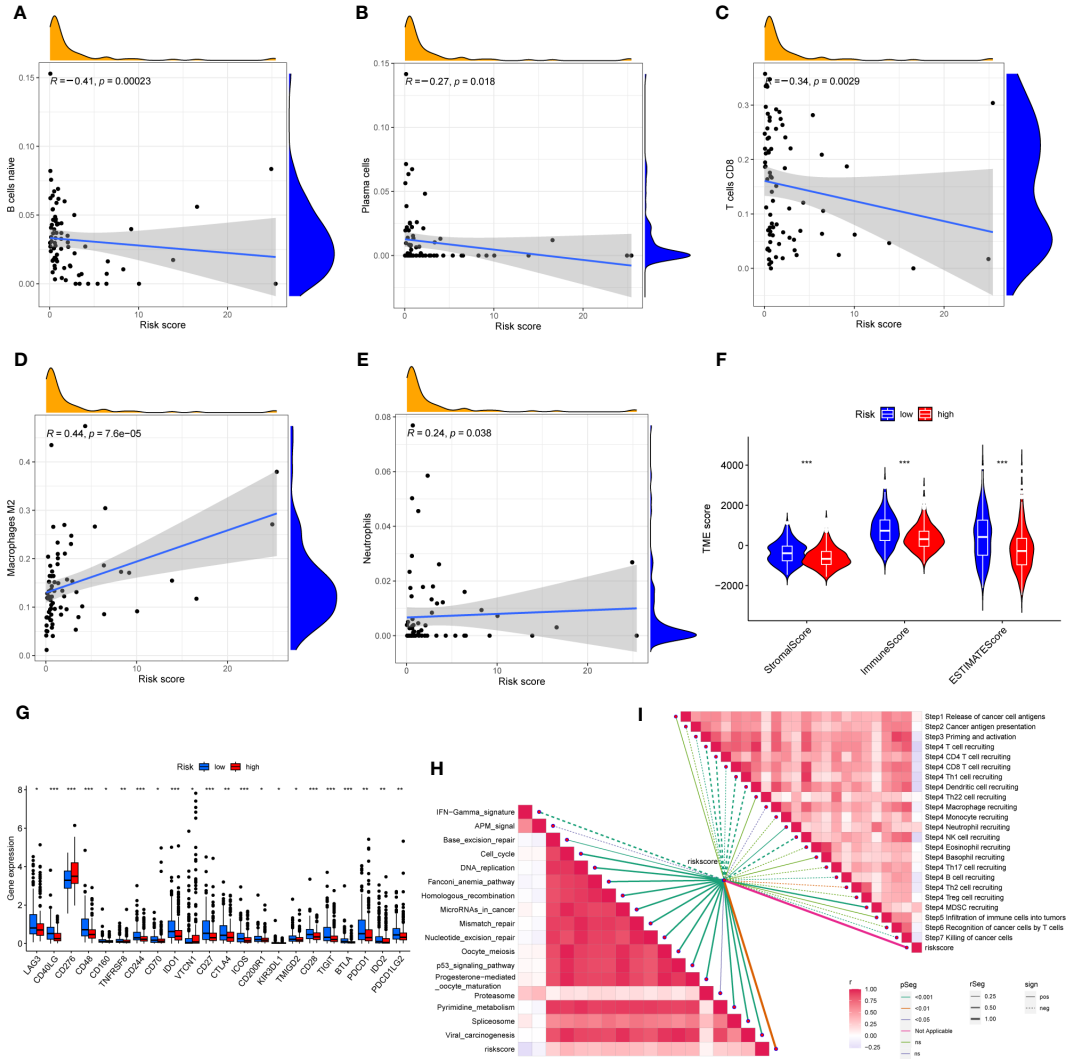

FIGURE 8
(A–E) Correlation of risk score with immune cells. **(F)** Correlation of risk score with immune score, stromal score and tumor purity. **(G)** Differences in the expression of immune checkpoints in the high-risk and low-risk groups. **(H)** The correlation between risk score and the enrichment of the relevant pathways for immunotherapy. **(I)** The correlation between risk score and the steps of the cancer immunity cycle. * represents P<0.05, ** represents P<0.01, *** represents P<0.001.

However, CD276 was expressed highly in the high-risk population (Figure 8G), suggesting that immune checkpoints were involved in tumor progression and are promising applications in the low-risk population to help guide immunotherapy. Finally, based on the study by Jiao Hu et al., we obtained the steps of the cancer immunity cycle and the enrichment scores of the immunotherapy-predicted pathways dataset (38). The "ggcor" package was used to construct the correlation of the risk scores with the dataset. The results showed that the IFN-γ signaling pathway was mainly concentrated in the low-risk group, and p53 signaling pathway, cell cycle, DNA replication, and microRNAs in cancer were more significantly enriched in the high-risk group (Figure 8H) (Supplementary Table 5). In addition, the risk score was mostly negatively correlated with the steps of the cancer immunity cycle, including the recruitment process of T cell, CD4+ T cell, Th1 cell, dendritic cell, and NK cell, whereas the recruitment of neutrophil was more active in the high-risk group (Figure 8I) (Supplementary Table 6).

3.9 Relationship between risk scores and TMB, MSI, and CSCs

HCC development is influenced by multiple complex factors, including TMB, MSI, and CSCs. Therefore, it is crucial to explore the relationships between the prognostic signature and these factors. It has been suggested that patients with higher TMB may have stronger immunogenicity and thus higher sensitivity to immunotherapy (39). Therefore, we included 361 HCC patients with complete mutation information from the TCGA database, counted the number of variants and mutation types in each sample. The top 20 genes in terms of mutation frequencies were selected

10.3389/fimmu.2023.1204338

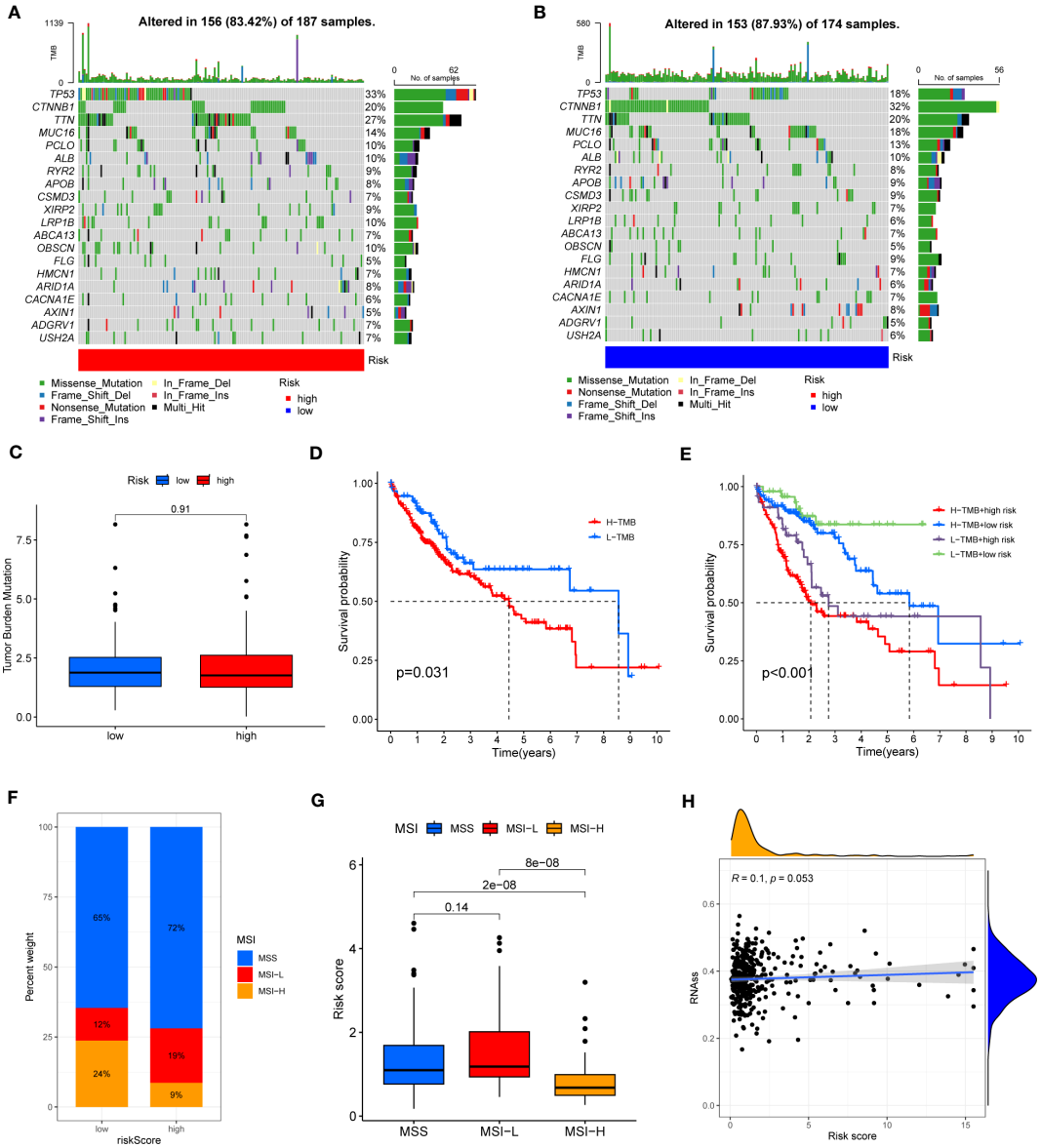

FIGURE 9
(A, B) Waterfall plots of somatic mutation frequency and mutation type between different risk groups. Each column represents an individual patient. The bar above each column shows the TMB, numbers on the right side indicates the mutation frequency of each gene, and the bars on the right show the proportion of each mutation type. **(C)** TMB differences in different risk groups. **(D)** Differences in survival between the high TMB and low TMB groups. **(E)** Survival differences between patients assessed by TMB and risk score combined. **(F, G)** Relationship between risk score, MSS and MSI. **(H)** Relationship between risk score and CSCs.

using waterfall plots. Comparative analysis of different risk groups showed that TMB occurred in 87.93% of patients in low-risk group, with the most significant mutation in CTNNB1 (32%). However, TMB occurred in 83.42% of the patients with HCC in the high-risk group, with the most significant mutation in TP53 (33%). Besides, the difference in TMB between the two risk groups was not statistically significant (P=0.91) (Figures 9A–C). However, it is worth mentioning that survival analysis suggested a better prognosis in the low TMB group (P<0.05) (Figure 9D). In addition, by combining the risk score and the TMB from the prognostic signature, survival analysis showed statistically significant survival among the four groups (p<0.001) (Figure 9E). In conclusion, there was no significant difference in TMB between the high-risk and low-risk groups, but TMB combined with risk score was a better predictor of overall survival time.

In addition, it has been shown that for oncology patients, the higher the MSI, the higher the potential for selecting immunotherapy (40). It has been suggested that MSI is a biomarker for determining response to immune checkpoint therapy (41). Our analysis of patients with HCC showed that the MSI-H group had a lower risk score than the MSS and MSI-L groups (P<0.001) (Figures 9F, G).

Besides, we assessed the association between CSCs and the signature risk score. The results showed no statistically significant relationship (r = 0.1, p = 0.053). These suggested that the differential

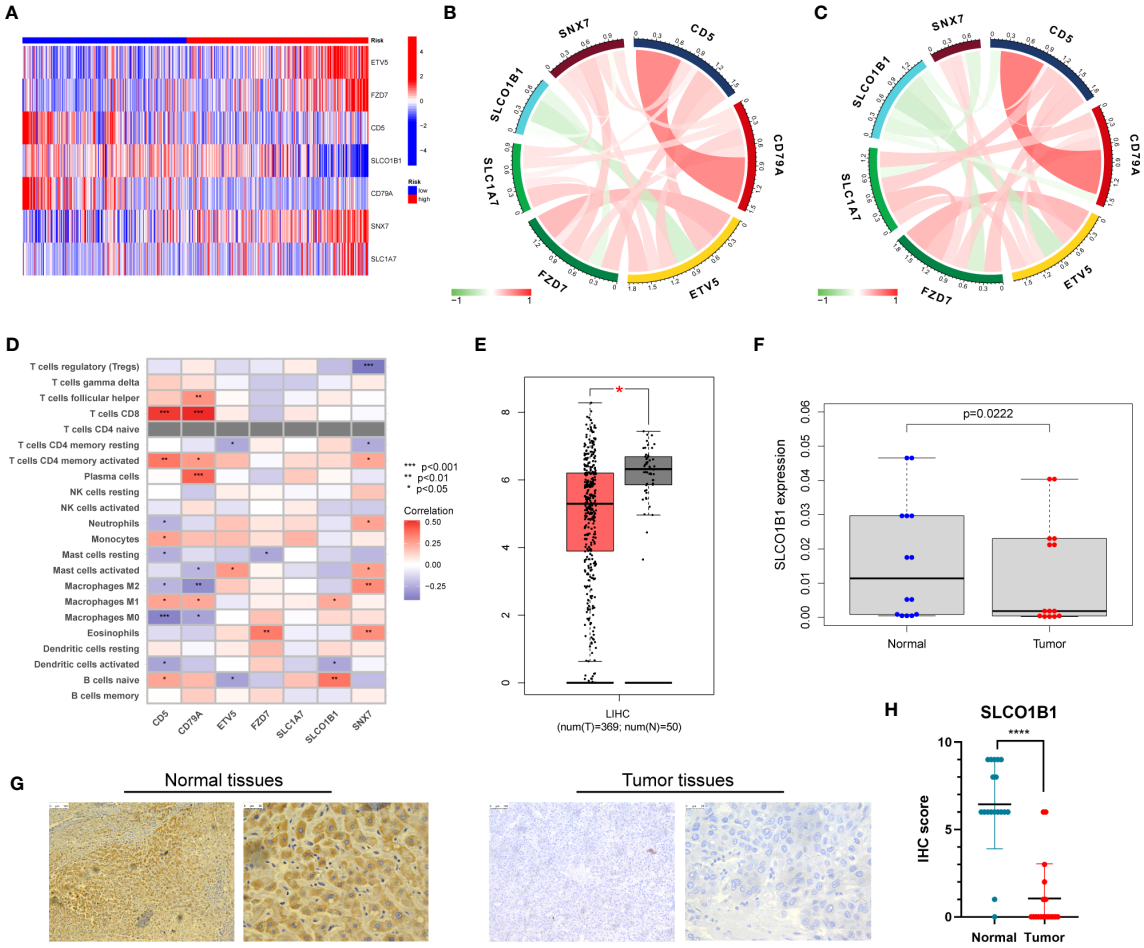

FIGURE 10
(A) Expression of the seven genes in the risk signature in the high-risk and low-risk groups. **(B)** Correlation of the seven genes in the train group. **(C)** Correlation of the seven genes in the test group. **(D)** Correlation between the level of immune cell infiltration and the seven genes in the risk model. **(E)** Differential expression of SLCO1B1 in HCC tissues and normal tissues. The red part represents HCC patient samples, and the gray part represents normal patient tissue samples. **(F)** The result of qRT-PCR. **(G)** Normal and cancer images of SLCO1B1 expression in liver tissues (100× and 400×) detected by IHC staining. **(H)** IHC score for all samples. **** represents P<0.0001.

tumor stemness of patients between the two risk groups was not significant and that the prognosis of patients with HCC was mainly influenced by a combination of other factors (Figure 9H).

3.10 Expression and immune infiltration characteristics of 7 genes in the signature

First, we evaluated the differential expression of the seven genes in different risk groups, and the results are shown in Figure 10A. We then explored the association of the seven genes in the training group and discovered that SLCO1B1 was negatively correlated with the other six genes and positively correlated with the remaining six genes (Figure 10B), in accordance with the validation results of the test group (Figure 10C). In addition, we evaluated the relationship between seven genes in the signature and immune cells and found that CD5, CD79A, SNX7, and SLCO1B1 were relatively strongly correlated with immune cells, especially CD5, CD79A, and SNX7 (Figure 10D).

Next, we explored the expression of these seven genes in HCC samples and paracancerous tissues using the data and found that SLCO1B1 was expressed at low levels in HCC samples (P<0.05) (Figure 10E), and the differential expression of the remaining genes was not statistically significant. Therefore, we verified the expression levels of SLCO1B1 based on qRT-PCR and IHC, which showed low expression in HCC samples (Figures 10F–H) (Supplementary Table 7), and the results were in accordance with the data from TCGA. In addition, through pan-cancer analysis, we further demonstrated that SLCO1B1 has a high immune infiltration status in most tumors, especially in B cells, dendritic cells, CD8+ T cells, macrophages, Tregs, and T-cell follicular helper cells. In addition, M1 macrophages, NK cells, and CD8+ T cells showed significant infiltration into the HCC (Figure 11). The above results indicate that SLCO1B1 is strongly correlated with M1 macrophages, and inducing the polarization of the TIME to the tumor-suppressive M1 phenotype is the key to improving the effect of immunotherapy (42, 43). Therefore, we selected the surface marker CD86 of M1 macrophages and evaluated the localization and expression of CD86

10.3389/fimmu.2023.1204338

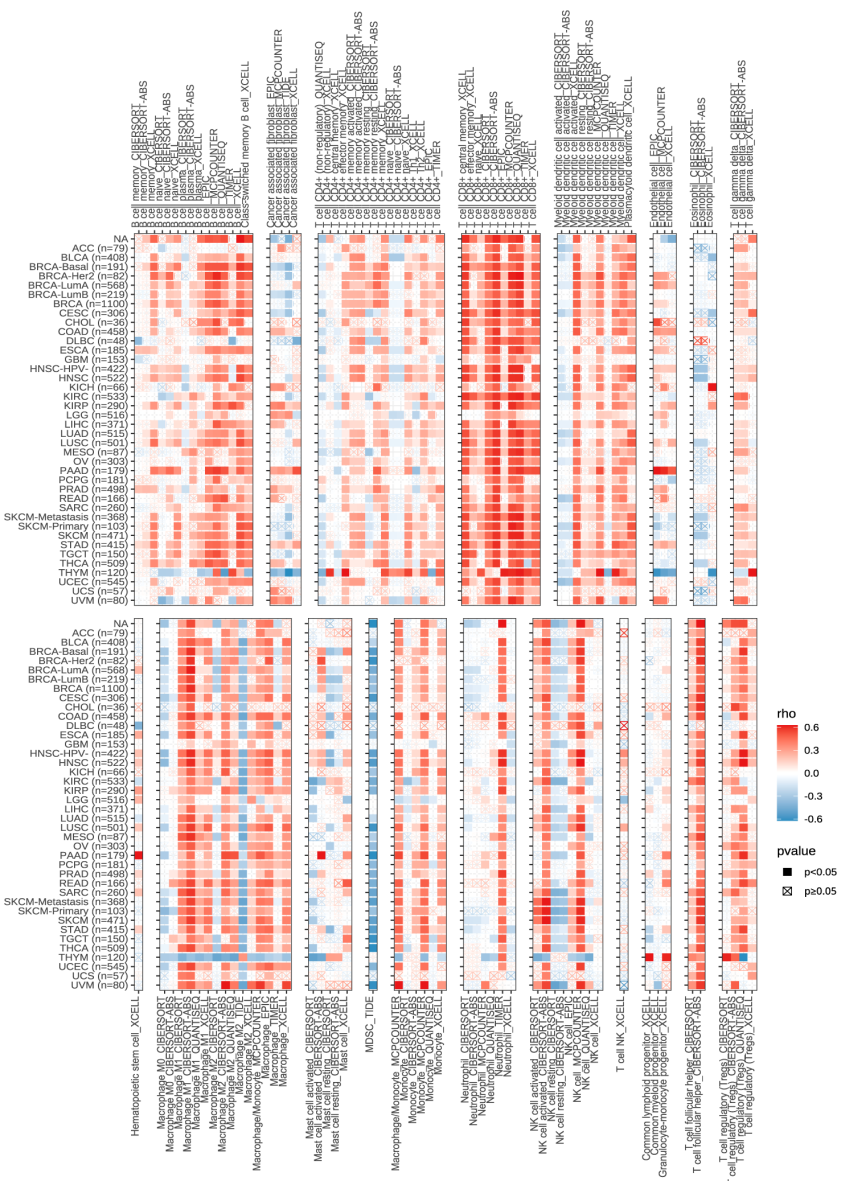

FIGURE 11
Correlation of SLCO1B1 expression with the level of infiltration of various immune cells in cancers.

and SLCO1B1 in the liver tissue by mIF. The results showed that the expression levels of CD86 and SLCO1B1 in HCC tissues were downregulated and were positively correlated (Figure 12A).

3.11 SLCO1B1 inhibits the proliferation, migration and invasion of HCC cells *in vitro*

We confirmed low expression of SLCO1B1 in HCC tissues. To further explore the biological function of SLCO1B1, we first constructed HCC cell lines overexpressing SLCO1B1 and then conducted a series of experiments to explore whether SLCO1B1 could regulate tumor cell proliferation and migration. The results of the colony formation experiments showed that overexpression of SLCO1B1 inhibited colony formation in HepG2 and Huh7 cells compared to the control group (Figure 12B). In addition, the CCK-8 assay showed that the overexpression of SLCO1B1 inhibited the proliferation of HepG2 and Huh7 cells (Figure 12C). In addition, the results of the migration experiments showed that overexpression of SLCO1B1 inhibited the migration ability of HCC cells (Figure 12D). Collectively, these results suggested that SLCO1B1 inhibited the proliferation, migration, and invasion of HCC cells.

4 Discussion

HCC is a highly heterogeneous tumor, with considerable variation in genomics, transcriptomics, proteomics, and metabolomics (44). Disulfidptosis is a recently identified pattern of programmed cell death in which excessive accumulation of

10.3389/fimmu.2023.1204338

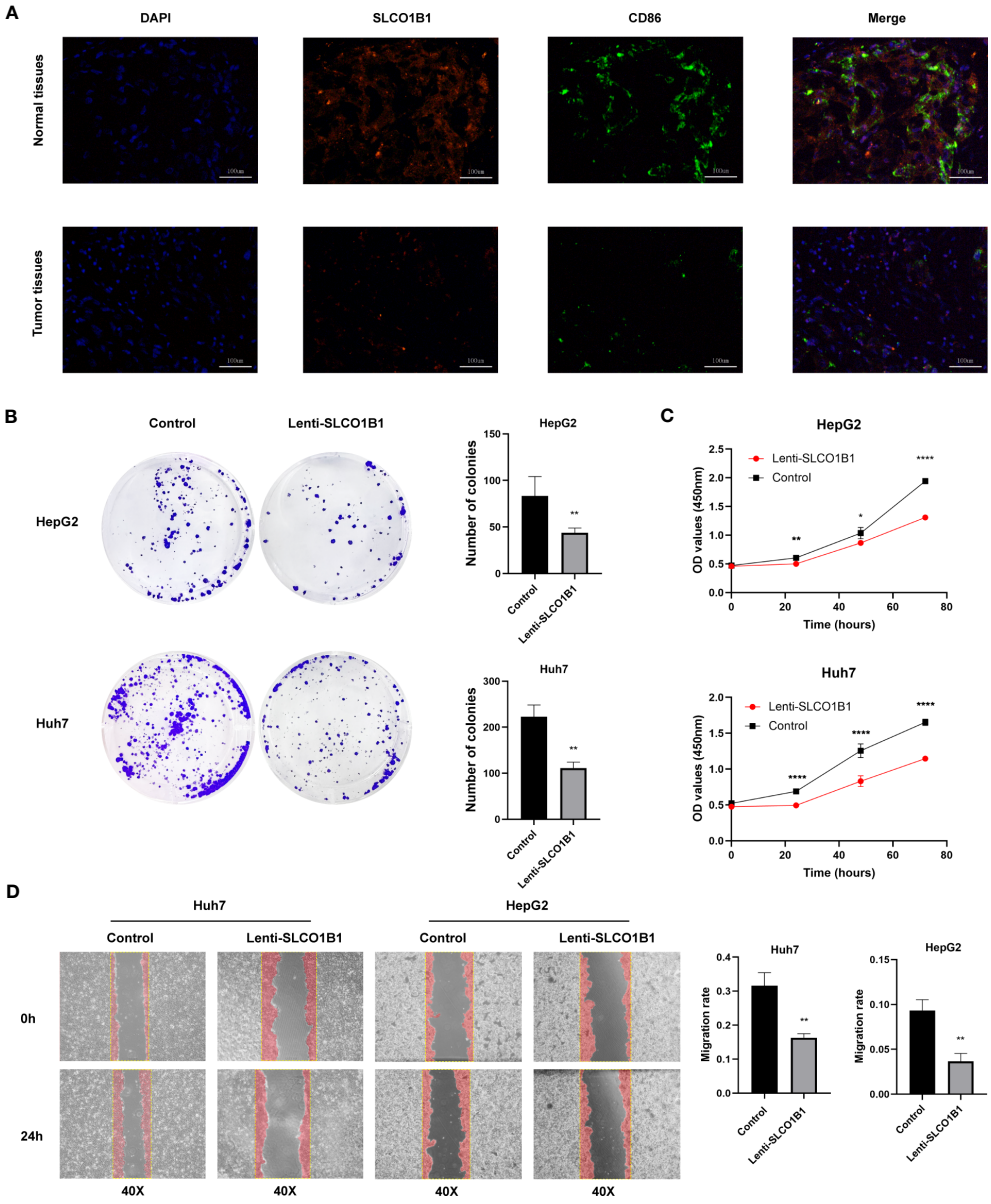

FIGURE 12
(A) Representative immunofluorescence images (magnification: ×200) of the SLCO1B1 and CD86 expressions in HCC and normal adjacent tissues. DAPI, 4′,6-diamidino-2-phenylindole. **(B)** Colony formation of control group and Lenti-SLCO1B1 group. **(C)** The viability of HCC cells at 0 h, 24 h, 48 h, 72 h was detected by Cell counting kit-8. (*p < 0.5, **p < 0.01, ****P < 0.0001). **(D)** Wound Healing of control group and Lenti-SLCO1B1 group.

intracellular cystine leads to disulfidptosis. Tumor cells expedite the reduction of ingested cystine to cysteine to avoid disulfidptosis (45). Several studies have demonstrated the potential of targeting disulfidptosis in tumor therapy (6, 8). Additionally, the immunomodulatory drug dimethyl fumarate (DMF) targets glycolysis by catalyzing cysteine, which acts as an anti-inflammatory agent (46). The glycolytic enzyme GAPDH is also involved in regulating the glycolytic process by catalyzing cysteine production during the tricarboxylic acid cycle, and many GRGs have been identified as effective prognostic markers of HCC (47, 48). However, the roles of genes related to disulfidptosis and glycolysis in HCC has not been well-studied.

In this study, we explored the correlation between DRGGs and HCC. Surprisingly, these genes were not significantly mutated in HCC. However, their differential expression between HCC and normal tissues is equally important. Subsequently, HCC patients were divided into two distinct molecular subtypes based on DRGG expression. The pathological staging and overall survival time of patients with DRGG cluster B were not satisfactory compared to those of patients with cluster A. In addition, there were significant differences in gene expression, pathway enrichment, and immune cell infiltration between the two subtypes. In particular, patients with cluster B had lower CD8+ T cell/Treg ratios, leading to a poorer prognosis, as demonstrated in a previous HCC study (49). In

addition, by constructing a risk-prognosis signature we found that patients in the high- and low-risk groups had significant differences in clinicopathological characteristics and prognosis by constructing a risk prognosis signature, which would help clinicians evaluate the prognostic characteristics of patients and formulate targeted treatment plans.

Several factors influence the expression of prognosis-related genes in HCC. Among the seven genes used to construct the signature, SLCO1B1 was expressed at low levels in HCC tissues, whereas the expression of the remaining genes did not differ significantly between HCC and normal tissues. However, from a prognostic perspective, CD5, SLCO1B1, and CD79A have been demonstrated to have protective value in various tumors, whereas ETV5, FZD7, SNX7, and SLC1A7 are involved in tumor progression. The key gene, SLCO1B1, encodes a transporter protein located on the cell membrane, which is downregulated in HCC and acts as a mediator of chemotherapeutic drugs, facilitating drug entry into cells (50, 51). In our study, we observed that the expression of SLCO1B1 decreased at the mRNA and protein levels in HCC tissues and was positively correlated with the infiltration of M1 macrophages. Furthermore, we found that SLCO1B1 overexpression inhibited the proliferation, migration, and invasion of HCC cells.

The liver is a vital immune organ containing a wide variety of immune cells. These immune cells play crucial roles in promoting tumor growth and inhibiting cancer progression. Therefore, immunotherapy has become a popular topic in tumor treatment. In this study, we combined the risk score with Spearman's correlation analysis of immune cells and an activity analysis of the anti-cancer response process. We found that M2 macrophages and neutrophils were highly infiltrated in the high-risk group, whereas CD8+ T cells, plasma cells, and naïve B cells showed low infiltration and a more active recruitment of neutrophils. In contrast, T-, Th1, NK killer, and dendritic cells are more actively recruited in low-risk populations.

Studies have demonstrated that the induction of interleukin 4 and interleukin 13 speeds up the proliferation and metastasis of HCC cells in M2 macrophages (52, 53). Additionally, neutrophils play an essential immunosuppressive role in the tumor microenvironment, promote tumor progression, and serve as prospective treatment targets for HCC (54). However, CD8+ T cells mainly mediate tumor cell killing and infiltrate at lower levels into the tumor microenvironment of HCC (55). Furthermore, naïve B cells, which are the main immune cells involved in adaptive immunity and assist other immune cells in their anti-cancer role, have a reduced relative proportion in HCC (56). Patients in the low-risk group had higher immune scores and significantly more expressed immune checkpoint-related genes than those in the high-risk group, indicating that they may be more sensitive to immunotherapy. Moreover, we found that IFN-γ signaling was significantly enriched in low-risk populations. IFN-γ acts as an anti-tumor factor and plays an immunosuppressive role in tumors such as melanoma and lung cancer by enhancing the immune response of T lymphocytes (57). However, the p53 signaling pathway, cell cycle, microRNAs in cancer, and DNA replication were significantly enriched in the high-risk populations. In our constructed signature, the risk score was consistent with the expression levels of tumor-infiltrating immune cells and their immune checkpoints, indicating that the high-risk group had a stronger immunosuppressive microenvironment that promoted tumorigenesis and metastasis, leading to a worse prognosis. Future studies on immune checkpoints may benefit low-risk groups expected to have a better prognosis.

Our study provides a new direction for personalized targeted therapy in patients with HCC. However, this study has several limitations. First, all patient information was obtained from public databases and previous surgical patients at our hospital, which lacked representative prospective data. Secondly, the clinical information of the samples was limited, and some essential factors for determining patient prognosis, such as alpha-fetoprotein, ascites, portal hypertension, and postoperative complications, were missing. in the future, we plan to recruit more patients who meet our criteria at our hospital for prospective research and improve mechanistic research to gain an in-depth understanding of the clinical application value of this signature.

5 Conclusions

Recently, bioinformatics has become increasingly popular in the medical field. Benefiting from progress in this technology, we developed a prognostic signature for HCC based on disulfidptosis and GRGs. The signature showed a strong performance in predicting patient prognosis and response to immunotherapy, among other factors. In the future, it will have broad application prospects in the treatment of HCC. It can identify high-risk patients early and screen potential patients for immunotherapy to improve their survival. In addition, we found that SLCO1B1 is an important component of this signature; the gene is under-expressed in HCC and suppresses the proliferation, migration, and invasion of HCC cells. To some extent, these findings guide the development of targeted therapies for HCC.

Data availability statement

The datasets presented in this study can be found in online repositories. The names of the repository/repositories and accession number(s) can be found in the article/Supplementary Material.

Ethics statement

The studies involving humans were approved by The Ethics Committee of the First Affiliated Hospital of Chongqing Medical University. The studies were conducted in accordance with the local legislation and institutional requirements. The participants provided their written informed consent to participate in this study.

Author contributions

ZW designed the study. ZW and XNC analyzed the data, conducted the experiments, and drafted the manuscript. JZ, XXC,

JP and WH revised the manuscript. All authors contributed to the article and approved the submitted version.

Acknowledgments

Thanks to all those involved in the creation of the paper, and to the reviewers for their contributions to the revision of my paper.

Conflict of interest

The authors declare that the research was conducted in the absence of any commercial or financial relationships that could be construed as a potential conflict of interest.

Publisher's note

Supplementary material

The Supplementary Material for this article can be found online at: https://www.frontiersin.org/articles/10.3389/fimmu.2023.1204338/full#supplementary-material

References

1. Bray F, Ferlay J, Soerjomataram I, Siegel RL, Torre LA, Jemal A. Global cancer statistics 2018: GLOBOCAN estimates of incidence and mortality worldwide for 36 cancers in 185 countries. *CA Cancer J Clin* (2018) 68:394–424. doi: 10.3322/caac.21492

2. Yang JD, Hainaut P, Gores GJ, Amadou A, Plymoth A, Roberts LR. A global view of hepatocellular carcinoma: trends, risk, prevention and management. *Nat Rev Gastroenterol Hepatol* (2019) 16:589–604. doi: 10.1038/s41575-019-0186-y

3. Peneau C, Imbeaud S, La Bella T, Hirsch TZ, Caruso S, Calderaro J, et al. Hepatitis B virus integrations promote local and distant oncogenic driver alterations in hepatocellular carcinoma. *Gut* (2022) 71:616–26. doi: 10.1136/gutjnl-2020-323153

4. Kuczynski EA, Lee CR, Man S, Chen E, Kerbel RS. Effects of sorafenib dose on acquired reversible resistance and toxicity in hepatocellular carcinoma. *Cancer Res* (2015) 75:2510–9. doi: 10.1158/0008-5472.CAN-14-3687

5. Llovet JM, Zucman-Rossi J, Pikarsky E, Sangro B, Schwartz M, Sherman M, et al. Hepatocellular carcinoma. *Nat Rev Dis Primers* (2016) 2:16018. doi: 10.1038/nrdp.2016.18

6. Liu X, Olszewski K, Zhang Y, Lim EW, Shi J, Zhang X, et al. Cystine transporter regulation of pentose phosphate pathway dependency and disulfide stress exposes a targetable metabolic vulnerability in cancer. *Nat Cell Biol* (2020) 22:476–86. doi: 10.1038/s41556-020-0496-x

7. Koppula P, Zhuang L, Gan B. Cystine transporter SLC7A11/xCT in cancer: ferroptosis, nutrient dependency, and cancer therapy. *Protein Cell* (2021) 12:599–620. doi: 10.1007/s13238-020-00789-5

8. Liu X, Nie L, Zhang Y, Yan Y, Wang C, Colic M, et al. Actin cytoskeleton vulnerability to disulfide stress mediates disulfidptosis. *Nat Cell Biol* (2023) 25:404–14. doi: 10.1038/s41556-023-01091-2

9. Chen H, Yang W, Li Y, Ma L, Ji Z. Leveraging a disulfidptosis-based signature to improve the survival and drug sensitivity of bladder cancer patients. *Front Immunol* (2023) 14:1198878. doi: 10.3389/fimmu.2023.1198878

10. Li S, Li J, Dai W, Zhang Q, Feng J, Wu L, et al. Genistein suppresses aerobic glycolysis and induces hepatocellular carcinoma cell death. *Br J Cancer* (2017) 117:1518–28. doi: 10.1038/bjc.2017.323

11. Feng J, Li J, Wu L, Yu Q, Ji J, Wu J, et al. Emerging roles and the regulation of aerobic glycolysis in hepatocellular carcinoma. *J Exp Clin Cancer Res* (2020) 39:126. doi: 10.1186/s13046-020-01629-4

12. Bhattacharya B, Mohd Omar MF, Soong R. The Warburg effect and drug resistance. *Br J Pharmacol* (2016) 173:970–9. doi: 10.1111/bph.13422

13. Zhang Z, Tan X, Luo J, Yao H, Si Z, Tong JS. The miR-30a-5p/CLCF1 axis regulates sorafenib resistance and aerobic glycolysis in hepatocellular carcinoma. *Cell Death Dis* (2020) 11:902. doi: 10.1038/s41419-020-03123-3

14. Iciek MB, Rokita HB, Wlodek LB. Effects of diallyl disulfide and other donors of sulfane sulfur on the proliferation of human hepatoma cell line (HepG2). *Neoplasma* (2001) 48:307–12.

15. Iciek M, Kwiecien I, Chwatko G, Sokolowska-Jezewicz M, Kowalczyk-Pachel D, Rokita H. The effects of garlic-derived sulfur compounds on cell proliferation, caspase 3 activity, thiol levels and anaerobic sulfur metabolism in human hepatoblastoma HepG2 cells. *Cell Biochem Funct* (2012) 30:198–204. doi: 10.1002/cbf.1835

16. Jackson MR, Melideo SL, Jorns MS. Human sulfide:quinone oxidoreductase catalyzes the first step in hydrogen sulfide metabolism and produces a sulfane sulfur metabolite. *Biochemistry* (2012) 51:6804–15. doi: 10.1021/bi300778t

17. Gao X, Sanderson SM, Dai Z, Reid MA, Cooper DE, Lu M, et al. Dietary methionine influences therapy in mouse cancer models and alters human metabolism. *Nature* (2019) 572:397–401. doi: 10.1038/s41586-019-1437-3

18. Zhen Y, Wu Q, Ding Y, Zhang W, Zhai Y, Lin X, et al. Exogenous hydrogen sulfide promotes hepatocellular carcinoma cell growth by activating the STAT3-COX-2 signaling pathway. *Oncol Lett* (2018) 15:6562–70. doi: 10.3892/ol.2018.8154

19. Zhang X, Chen M, Ni X, Wang Y, Zheng X, Zhang H, et al. Metabolic reprogramming of sulfur in hepatocellular carcinoma and sulfane sulfur-triggered anti-cancer strategy. *Front Pharmacol* (2020) 11:571143. doi: 10.3389/fphar.2020.571143

20. Lindahl M, Mata-Cabana A, Kieselbach T. The disulfide proteome and other reactive cysteine proteomes: analysis and functional significance. *Antioxid Redox Signal* (2011) 14:2581–642. doi: 10.1089/ars.2010.3551

21. Attimonelli M, Lanave C, Liuni S, Pesole G. MERGE: a software package for generating a single data-base starting from EMBL and GenBank collections. *Nucleic Acids Res* (1988) 16:1681–2. doi: 10.1093/nar/16.5.1681

22. Leek JT, Johnson WE, Parker HS, Jaffe AE, Storey JD. The sva package for removing batch effects and other unwanted variation in high-throughput experiments. *Bioinformatics* (2012) 28:882–3. doi: 10.1093/bioinformatics/bts034

23. Livak KJ, Schmittgen TD. Analysis of relative gene expression data using real-time quantitative PCR and the 2(-Delta Delta C(T)) Method. *Methods* (2001) 25:402–8. doi: 10.1006/meth.2001.1262

24. Chen X, Jiang Z, Pu Y, Jiang X, Xiang L, Jiang Z. Zinc finger and BTB domain-containing 7C (ZBTB7C) expression as an independent prognostic factor for colorectal cancer and its relevant molecular mechanisms. *Am J Transl Res* (2020) 12:4141–59.

25. Chen Y, Tang L, Huang W, Abisola FH, Zhang Y, Zhang G, et al. Identification of a prognostic cuproptosis-related signature in hepatocellular carcinoma. *Biol Direct* (2023) 18:4. doi: 10.1186/s13062-023-00358-w

26. Peng H, Wu X, Zhong R, Yu T, Cai X, Liu J, et al. Profiling tumor immune microenvironment of non-small cell lung cancer using multiplex immunofluorescence. *Front Immunol* (2021) 12:750046. doi: 10.3389/fimmu.2021.750046

27. Chu W, Li YL, Li JJ, Lin J, Li M, Wang J, et al. Guiqi Baizhu prescription ameliorates cytarabine-induced intestinal mucositis by targeting JAK2 to inhibit M1 macrophage polarization. *BioMed Pharmacother* (2023) 164:114902. doi: 10.1016/j.biopha.2023.114902

28. Wang L, He T, Liu J, Tai J, Wang B, Chen Z, et al. Pan-cancer analysis reveals tumor-associated macrophage communication in the tumor microenvironment. *Exp Hematol Oncol* (2021) 10:31. doi: 10.1186/s40164-021-00226-1

29. Ritchie ME, Phipson B, Wu D, Hu Y, Law CW, Shi W, et al. limma powers differential expression analyses for RNA-sequencing and microarray studies. *Nucleic Acids Res* (2015) 43:e47. doi: 10.1093/nar/gkv007

30. Mayakonda A, Lin DC, Assenov Y, Plass C, Koeffler HP. Maftools: efficient and comprehensive analysis of somatic variants in cancer. *Genome Res* (2018) 28:1747–56. doi: 10.1101/gr.239244.118

31. Geeleher P, Cox N, Huang RS. pRRophetic: an R package for prediction of clinical chemotherapeutic response from tumor gene expression levels. *PLoS One* (2014) 9:e107468. doi: 10.1371/journal.pone.0107468

32. Chen H, Yang W, Ji Z. Machine learning-based identification of tumor-infiltrating immune cell-associated model with appealing implications in improving

prognosis and immunotherapy response in bladder cancer patients. *Front Immunol* (2023) 14:1171420. doi: 10.3389/fimmu.2023.1171420

33. Chen DS, Mellman I. Oncology meets immunology: the cancer-immunity cycle. *Immunity* (2013) 39:1–10. doi: 10.1016/j.immuni.2013.07.012

34. Xu L, Deng C, Pang B, Zhang X, Liu W, Liao G, et al. TIP: A web server for resolving tumor immunophenotype profiling. *Cancer Res* (2018) 78:6575–80. doi: 10.1158/0008-5472.CAN-18-0689

35. Zhu ZY, Tang N, Wang MF, Zhou JC, Wang JL, Ren HZ, et al. Comprehensive pan-cancer genomic analysis reveals PHF19 as a carcinogenic indicator related to immune infiltration and prognosis of hepatocellular carcinoma. *Front Immunol* (2021) 12:781087. doi: 10.3389/fimmu.2021.781087

36. Nozaki I, Ohashi R, Matsubara N, Hirai R, Andou A, Miyazaki M, et al. Microsatellite instability correlates with normal expression of cyclin E in hepatocellular carcinomas. *Int J Oncol* (2001) 18:1265–9. doi: 10.3892/ijo.18.6.1265

37. Lee TK, Guan XY, Ma S. Cancer stem cells in hepatocellular carcinoma - from origin to clinical implications. *Nat Rev Gastroenterol Hepatol* (2022) 19:26–44. doi: 10.1038/s41575-021-00508-3

38. Hu J, Yu A, Othmane B, Qiu D, Li H, Li C, et al. Siglec15 shapes a non-inflamed tumor microenvironment and predicts the molecular subtype in bladder cancer. *Theranostics* (2021) 11:3089–108. doi: 10.7150/thno.53649

39. Wu X, Gu Z, Chen Y, Chen B, Chen W, Weng L, et al. Application of PD-1 blockade in cancer immunotherapy. *Comput Struct Biotechnol J* (2019) 17:661–74. doi: 10.1016/j.csbj.2019.03.006

40. Ganesh K, Stadler ZK, Cercek A, Mendelsohn RB, Shia J, Segal NH, et al. Immunotherapy in colorectal cancer: rationale, challenges and potential. *Nat Rev Gastroenterol Hepatol* (2019) 16:361–75. doi: 10.1038/s41575-019-0126-x

41. Lemery S, Keegan P, Pazdur R. First FDA approval agnostic of cancer site - when a biomarker defines the indication. *N Engl J Med* (2017) 377:1409–12. doi: 10.1056/NEJMp1709968

42. Wang L, Yi X, Xiao X, Zheng Q, Ma L, Li B. Exosomal miR-628-5p from M1 polarized macrophages hinders m6A modification of circFUT8 to suppress hepatocellular carcinoma progression. *Cell Mol Biol Lett* (2022) 27:106. doi: 10.1186/s11658-022-00406-9

43. Yu Z, Li Y, Li Y, Zhang J, Li M, Ji L, et al. Bufalin stimulates antitumor immune response by driving tumor-infiltrating macrophage toward M1 phenotype in hepatocellular carcinoma. *J Immunother Cancer* (2022) 10. doi: 10.1136/jitc-2021-004297

44. Zhang Q, Lou Y, Yang J, Wang J, Feng J, Zhao Y, et al. Integrated multiomic analysis reveals comprehensive tumour heterogeneity and novel immunophenotypic classification in hepatocellular carcinomas. *Gut* (2019) 68:2019–31. doi: 10.1136/gutjnl-2019-318912

45. Machesky LM. Deadly actin collapse by disulfidptosis. *Nat Cell Biol* (2023) 25:375–6. doi: 10.1038/s41556-023-01100-4

46. Kornberg MD, Bhargava P, Kim PM, Putluri V, Snowman AM, Putluri N, et al. Dimethyl fumarate targets GAPDH and aerobic glycolysis to modulate immunity. *Science* (2018) 360:449–53. doi: 10.1126/science.aan4665

47. Kong J, Yu G, Si W, Li G, Chai J, Liu Y, et al. Identification of a glycolysis-related gene signature for predicting prognosis in patients with hepatocellular carcinoma. *BMC Cancer* (2022) 22:142. doi: 10.1186/s12885-022-09209-9

48. Du D, Liu C, Qin M, Zhang X, Xi T, Yuan S, et al. Metabolic dysregulation and emerging therapeutical targets for hepatocellular carcinoma. *Acta Pharm Sin B* (2022) 12:558–80. doi: 10.1016/j.apsb.2021.09.019

49. Gao Q, Qiu SJ, Fan J, Zhou J, Wang XY, Xiao YS, et al. Intratumoral balance of regulatory and cytotoxic T cells is associated with prognosis of hepatocellular carcinoma after resection. *J Clin Oncol* (2007) 25:2586–93. doi: 10.1200/JCO.2006.09.4565

50. Hu DG, Marri S, McKinnon RA, Mackenzie PI, Meech R. Deregulation of the genes that are involved in drug absorption, distribution, metabolism, and excretion in hepatocellular carcinoma. *J Pharmacol Exp Ther* (2019) 368:363–81. doi: 10.1124/jpet.118.255018

51. Sharma P, Singh N, Sharma S. Polymorphisms in solute carrier genes (SLC19A1, SLCO1B1, and SLCO1B3) predicts survival and toxicity in North Indian lung cancer patients undergoing platinum-based doublet chemotherapy. *J Clin Pharm Ther* (2022) 47:2049–67. doi: 10.1111/jcpt.13748

52. Xu Y, Luan G, Liu F, Zhang Y, Li Z, Liu Z, et al. Exosomal miR-200b-3p induce macrophage polarization by regulating transcriptional repressor ZEB1 in hepatocellular carcinoma. *Hepatol Int* (2023). doi: 10.1007/s12072-023-10507-y

53. Zhang M, Liu K, Zhang Q, Xu J, Liu J, Lin H, et al. Alpha fetoprotein promotes polarization of macrophages towards M2-like phenotype and inhibits macrophages to phagocytize hepatoma cells. *Front Immunol* (2023) 14:1081572. doi: 10.3389/fimmu.2023.1081572

54. Geh D, Leslie J, Rumney R, Reeves HL, Bird TG, Mann DA. Neutrophils as potential therapeutic targets in hepatocellular carcinoma. *Nat Rev Gastroenterol Hepatol* (2022) 19:257–73. doi: 10.1038/s41575-021-00568-5

55. Zheng C, Zheng L, Yoo JK, Guo H, Zhang Y, Guo X, et al. Landscape of infiltrating T cells in liver cancer revealed by single-cell sequencing. *Cell* (2017) 169:1342–1356.e16. doi: 10.1016/j.cell.2017.05.035

56. Zou J, Luo C, Xin H, Xue T, Xie X, Chen R, et al. The role of tumor-infiltrating B cells in the tumor microenvironment of hepatocellular carcinoma and its prognostic value: a bioinformatics analysis. *J Gastrointest Oncol* (2022) 13:1959–66. doi: 10.21037/jgo-22-717

57. Dong S, Guo X, Han F, He Z, Wang Y. Emerging role of natural products in cancer immunotherapy. *Acta Pharm Sin B* (2022) 12:1163–85. doi: 10.1016/j.apsb.2021.08.020

frontiers | Frontiers in Immunology

TYPE Original Research
PUBLISHED 20 September 2023
DOI 10.3389/fimmu.2023.1235575

OPEN ACCESS

EDITED BY
Qun Zhao,
Fourth Hospital of Hebei Medical University, China

REVIEWED BY
Wei Yuan,
Chinese Academy of Medical Sciences and Peking Union Medical College, China
Yuedan Wang,
Peking University, China

*CORRESPONDENCE
Zhenpeng Yang
yangzhenpeng926@ccmu.edu.cn
Penghui Yang
yangpenghui@301hospital.com.cn
Benqiang Rao
raobenqiang@bjsjth.cn

†These authors have contributed equally to this work

RECEIVED 06 June 2023
ACCEPTED 31 August 2023
PUBLISHED 20 September 2023

CITATION
Lu S, Sun X, Zhou Z, Tang H, Xiao R, Lv Q, Wang B, Qu J, Yu J, Sun F, Deng Z, Tian Y, Li C, Yang Z, Yang P and Rao B (2023) Mechanism of Bazhen decoction in the treatment of colorectal cancer based on network pharmacology, molecular docking, and experimental validation. *Front. Immunol.* 14:1235575. doi: 10.3389/fimmu.2023.1235575

Mechanism of Bazhen decoction in the treatment of colorectal cancer based on network pharmacology, molecular docking, and experimental validation

Shuai Lu[1†], Xibo Sun[1,2†], Zhongbao Zhou[3†], Huazhen Tang[1], Ruixue Xiao[4], Qingchen Lv[5], Bing Wang[1], Jinxiu Qu[1], Jinxuan Yu[6], Fang Sun[7], Zhuoya Deng[7], Yuying Tian[4], Cong Li[4], Zhenpeng Yang[8*], Penghui Yang[7*] and Benqiang Rao[1*]

[1]Key Laboratory of Cancer Foods for Special Medical Purpose (FSMP) for State Market Regulation, Department of Gastrointestinal Surgery/Clinical Nutrition, Beijing Shijitan Hospital, Capital Medical University, Beijing International Science and Technology Cooperation Base for Cancer Metabolism and Nutrition, Beijing, China, [2]Department of Breast Surgery, The Second Affiliated Hospital of Shandong First Medical University, Shandong, China, [3]Department of Urology, Beijing TianTan Hospital, Capital Medical University, Beijing, China, [4]Key Laboratory of Molecular Pathology, Inner Mongolia Medical University, Hohhot, China, [5]Medical Laboratory College, Hebei North University, Zhangjiakou, China, [6]First Clinical Medical College, Binzhou Medical University, Yantai, China, [7]Institute of Hepatobiliary Surgery, The First Medical Center of Chinese People's Liberation Army (PLA) General Hospital, Beijing, China, [8]Department of General Surgery, Qilu Hospital of Shandong University, Jinan, China

Objective: Bazhen Decoction (BZD) is a common adjuvant therapy drug for colorectal cancer (CRC), although its anti-tumor mechanism is unknown. This study aims to explore the core components, key targets, and potential mechanisms of BZD treatment for CRC.

Methods: The Traditional Chinese Medicine Systems Pharmacology (TCMSP) was employed to acquire the BZD's active ingredient and targets. Meanwhile, the Drugbank, Therapeutic Target Database (TTD), DisGeNET, and GeneCards databases were used to retrieve pertinent targets for CRC. The Venn plot was used to obtain intersection targets. Cytoscape software was used to construct an "herb-ingredient-target" network and identify core targets. GO and KEGG pathway enrichment analyses were conducted using R language software. Molecular docking of key ingredients and core targets of drugs was accomplished using PyMol and Autodock Vina software. Cell and animal research confirmed Bazhen Decoction efficacy and mechanism in treating colorectal cancer.

Results: BZD comprises 173 effective active ingredients. Using four databases, 761 targets related to CRC were identified. The intersection of BZD and CRC yielded 98 targets, which were utilized to construct the "herb-ingredient-target" network. The four key effector components with the most targets were quercetin, kaempferol, licochalcone A, and naringenin. Protein-protein

interaction (PPI) analysis revealed that the core targets of BZD in treating CRC were AKT1, MYC, CASP3, ESR1, EGFR, HIF-1A, VEGFR, JUN, INS, and STAT3. The findings from molecular docking suggest that the core ingredient exhibits favorable binding potential with the core target. Furthermore, the GO and KEGG enrichment analysis demonstrates that BZD can modulate multiple signaling pathways related to CRC, like the T cell receptor, PI3K-Akt, apoptosis, P53, and VEGF signaling pathway. *In vitro*, studies have shown that BZD dose-dependently inhibits colon cancer cell growth and invasion and promotes apoptosis. Animal experiments have shown that BZD treatment can reverse abnormal expression of PI3K, AKT, MYC, EGFR, HIF-1A, VEGFR, JUN, STAT3, CASP3, and TP53 genes. BZD also increases the ratio of $CD4^+$ T cells to $CD8^+$ T cells in the spleen and tumor tissues, boosting IFN-γ expression, essential for anti-tumor immunity. Furthermore, BZD has the potential to downregulate the PD-1 expression on T cell surfaces, indicating its ability to effectively restore T cell function by inhibiting immune checkpoints. The results of HE staining suggest that BZD exhibits favorable safety profiles.

Conclusion: BZD treats CRC through multiple components, targets, and metabolic pathways. BZD can reverse the abnormal expression of genes such as PI3K, AKT, MYC, EGFR, HIF-1A, VEGFR, JUN, STAT3, CASP3, and TP53, and suppresses the progression of colorectal cancer by regulating signaling pathways such as PI3K-AKT, P53, and VEGF. Furthermore, BZD can increase the number of T cells and promote T cell activation in tumor-bearing mice, enhancing the immune function against colorectal cancer. Among them, quercetin, kaempferol, licochalcone A, naringenin, and formaronetin are more highly predictive components related to the T cell activation in colorectal cancer mice. This study is of great significance for the development of novel anti-cancer drugs. It highlights the importance of network pharmacology-based approaches in studying complex traditional Chinese medicine formulations.

KEYWORDS

Bazhen detection, colored cancer, network pharmacology, molecular docking, tumor immunity

1 Introduction

CRC is the third most common malignant tumor and the second leading cause of cancer deaths worldwide. It accounts for 10% of cancer incidence and 9% of deaths (1). Despite the steady advancements in screening, diagnosis, and treatment of CRC in recent years (2–4), the CRC patients' prognosis remains bleak due to the absence of early detection, frequent metastasis, and recurrence. CRC remains a global health issue. Traditional Chinese medicine, together with surgery, chemotherapy, radiotherapy, immunotherapy, and targeted therapy, can treat colorectal cancer, according to a recent pharmacological study. It has been found to effectively impede cancer progression and enhance the quality of life of cancer patients (5–7). As a valuable and rich source for advancing modern pharmacology, traditional Chinese medicine plays a distinctive role in mitigating adverse reactions in tumor treatment, reducing the likelihood of recurrence, and enhancing patients' quality of life (8, 9). Traditional Chinese medicine has several advantages in treating tumors, like multi-ingredient, multi-target, and low drug resistance. Additionally, it has demonstrated promising outcomes in treating CRC (10). Due to its multi-ingredient and multi-target nature, traditional Chinese medicine has complex interactions across its targets, resulting in confusing molecular mechanisms and a gap between basic research and therapeutic applications. Consequently, addressing this issue has emerged as a pressing imperative for advancing traditional Chinese medicine.

Network pharmacology integrates bioinformatics, systems biology, and pharmacology to reveal the complex relationship between traditional Chinese medicine and disorders. It also follows the holistic and comprehensive concepts of Traditional Chinese Medicine (11, 12). Network pharmacology has updated the "one target, one drug" model to the "multi-component, multi-target" model, elucidating complex interactions between drugs and disease-related targets from a network perspective, providing a possibility for

us to systematically study the relationship between traditional Chinese medicine and diseases (13, 14). Molecular docking simulates atomic-level interactions between small molecule compounds and protein targets, predicts ligand and receptor conformations, and calculates affinity to evaluate the combination. This technology is both low-cost and accurate and is primarily employed for drug design and elucidation of biochemical pathways (15). In recent years, network pharmacology and molecular docking technology have been extensively researched to identify active compounds and mechanisms of action in Chinese medicine (16, 17).

Traditional Chinese medicine considers the "spleen" an essential organ that digests and absorbs food. According to modern medicine, the stomach, small intestine, large intestine, and pancreas depend on the spleen. Traditional Chinese medicine theory also posits that each internal organ possesses its unique "qi," with the spleen serving as the primary "qi" generation source. Qi is a fundamental substance that sustains the vital functions of the human body, augmenting immune defense and physiological processes. Spleen weakness reduces qi production, which impairs digestion and gastrointestinal tract immunity. Unhealthy dietary practices can generate "dampness toxins" that impair the spleen, resulting in reduced gas production, compromised intestinal immune function, and eventual cancer development (18). Hence, CRC pathogenesis is primarily attributed to spleen deficiency and qi deficiency. BZD, derived from the "Experience Formula of Rui Zhu Decoction," is a classic formula with more than 700 years of history. It includes ginseng, Atractylodes macrocephala, Poria cocos, Angelica sinensis, Chuanxiong, Paeonia lactiflora, Rehmannia glutinosa, and licorice, and is known for its ability to nourish qi and blood. Qi and blood deficit caused by a post-disease imbalance or excessive blood loss are treated with it. According to a study, BZD improves immune function and bone marrow hematopoietic function 0 (19, 20). Recently, it has been extensively employed in immunizing diverse malignant tumors and as adjuvant therapy for radiotherapy and chemotherapy, resulting in favorable clinical outcomes. BZD has the potential to augment the immune function of cancer patients (21–23), mitigate the toxic side effects of chemotherapy drugs (24, 25), and enhance patient prognosis (26, 27). BZD treats several cancers, including CRC, gastric lung, breast, cervical cancer, and acute lymphoblastic leukemia (27–32). Xu et al.'s clinical investigations have demonstrated that the combination of BZD and capecitabine, as opposed to capecitabine monotherapy, can decrease the likelihood of disease progression in elderly patients with advanced CRC, provide superior survival advantages, and reduce the incidence of chemotherapy-related adverse reactions, thereby significantly facilitating patients' fatigue and gastrointestinal symptoms (33). Zhou et al. also revealed that combining BZD and chemotherapy can improve advanced colon cancer treatment and survival outcomes (34). BZD's mechanism in treating CRC is unknown. A better understanding of the regulatory role of herbs in cancer will provide new avenues for cancer treatment.

This study employed network pharmacology study examined BZD's active components, targets, and mechanism of action in CRC treatment. The predictions were subsequently validated through molecular docking and *in vitro* and *in vivo* experimental studies. Additionally, a target network was established to elucidate the interaction between drug ingredients and diseases, thereby providing a foundation for comprehending the mechanism of action of BZD in treating CRC. The study's methodology is depicted in Figure 1.

2 Materials and methods

2.1 Collection of effective ingredients and targets of BZD

The TCMSP database (https://tcmspw.com/tcmsp.php) was used to find the chemical components of various drugs in BZD. This study selected the criteria of oral bioavailability (OB) ≥ 20% and drug-likeness (DL) ≥ 0.1 as effective ingredient screening conditions (35). The active drugs' target proteins were matched with TCMID and DrugBank databases, and then these target proteins were standardized to human species genes through the UniProt database.

2.2 Collection of CRC targets

The targets for colorectal cancer (CRC) were obtained from four databases, namely Drugbank (https://go.drugbank.com/) (36), GeneCards (https://genecards.weizmann.ac.il/v3/) (37), TTD (https://db.idrblab.net/ttd/) (38), and Dis-GeNET (https://www.disgenet.org/) (39). The search results from these databases were integrated, and any duplicate targets were eliminated.

2.3 Intersection target and construction of "herb-ingredient-target" network

The BZD and CRC intersection target was obtained using R language version 4.2.1. Integrate herbs, active ingredients, and intersection targets into Cytoscape 3.8.0 to construct a "herb-ingredient-target" network (40).

2.4 Analysis of protein-protein interaction

Intersection target of BZD and CRC input to STRING database (https://string-db.org/), select protein interaction data with a confidence level (score>0.4), and save it in a TSV format file. The information of node1, node2, and combination scores was imported from the file into Cytoscape software to construct a PPI network and screened hub genes through the cytohub plugin. The R language version 4.2.1 be used to draw Sangi diagrams of drugs, core components, and central genes.

2.5 GO and KEGG enrichment analysis

The "ClusterProfiler" package was employed to conduct GO and KEGG enrichment analysis on intersecting targets. The

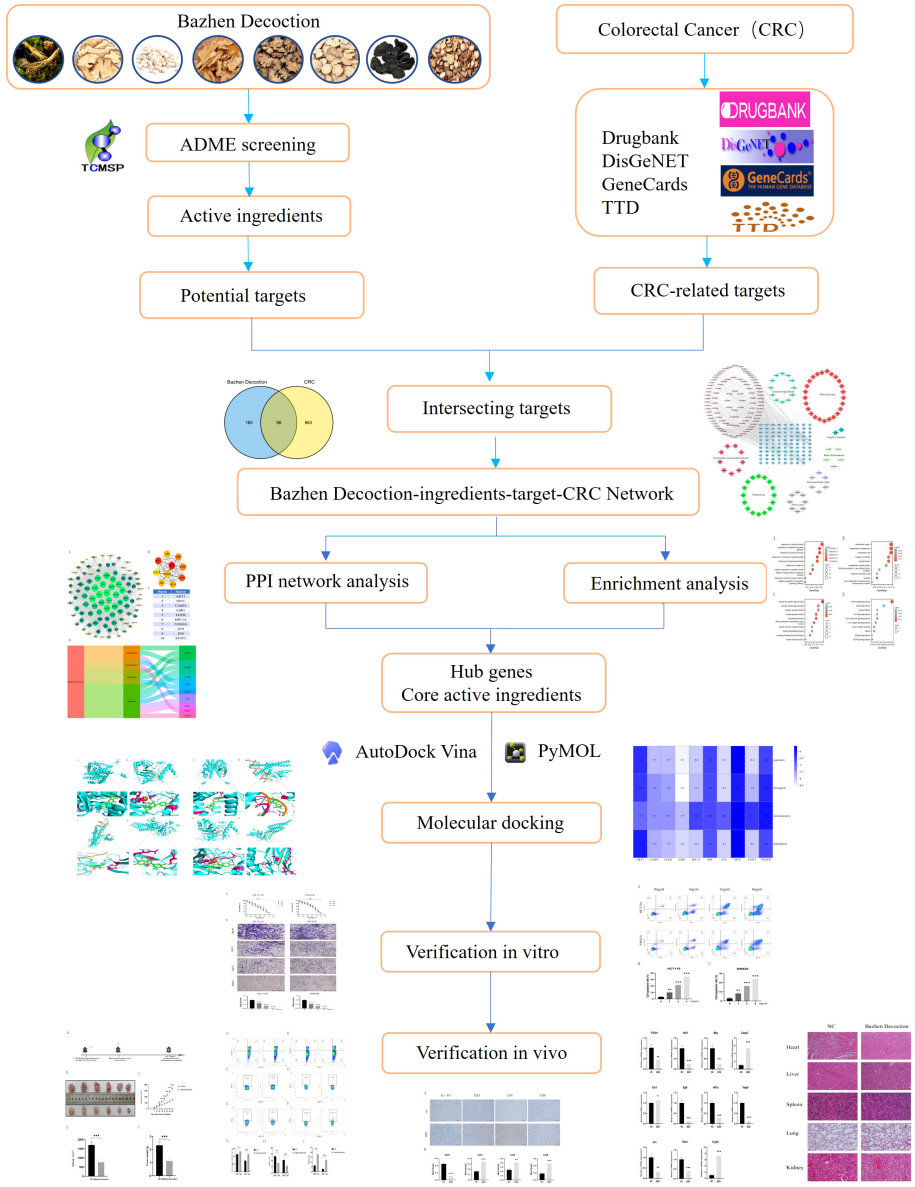

FIGURE 1
The flowchart of this study.

visualization of the enrichment analysis outcomes was accomplished by the "ggplot2" package, while the R language version 4.2.1 was utilized to generate the bubble chart.

2.6 Molecular docking

The key ingredient's 3D structural files in SDF format were obtained from the PubChem database and converted to PDB format using Open Babel. The 3D crystal structure of the hub gene was also obtained from the PDB database (https://www.pdbus.org/) and processed by removing ions and water molecules through PyMol 2.4.0 (41), resulting in PDB files. The essential ingredients and core targets were translated to PDBQT format to find the active pocket. Finally, molecular docking simulation was conducted using Autodock Vina software and visualized using PyMol 2.4.0.

2.7 Preparation of BZD freeze-dried powder

BZD comprises ginseng, atractylodes macrocephala, poria cocos, licorice, chuanxiong, paeonia lactiflora, rehmannia glutinosa, and angelica sinensis (Tongren Tang Pharmacy, Beijing, China) at a dose ratio of 1:1:1:1:1:1:1:1 as per the Orthodox Tradition of Medicine. Production method: We placed the above medicinal herbs in pure water, covered the top of the herbs with pure water, soaked them for 1 h, boiled them for 40 min,

and then poured out the liquid. Then we added pure water, which still needed to cover the top of the herb, and boiled directly. After 30 min boiling, we poured out the liquid. Then two types of water extracts were mixed and filtered with gauze. The supernatant was concentrated to 300 mL by a rotary evaporator. Freeze the supernatant overnight at -80°C. The freeze-dried product was freeze-dried to produce 51g of powder. In *in vitro* experiments, we dissolved BZD powder in the required concentration of culture medium. The negative control used a culture medium without BZD. In animal experiments, BZD was administered orally to mice.

2.8 Cell culture

The CRC cell lines, namely HCT116, SW620, and MC38, were procured from Procell Life Science&Technology Co., Ltd. (Procell, Wuhan, China). The SW620 and MC38 cell lines were cultured in DMEM medium (Gibco, USA) enhanced with 10% fetal bovine serum (FBS) and 1% antibiotics (100 U/mL penicillin and 100 μG/mL streptomycin). HCT116 was maintained in RPMI-1640 medium supplemented with 10% FBS (Gibco, USA) and 1% penicillin/streptomycin (Gibco).

2.9 Cell proliferation detection

The BZD's inhibitory effect on human CRC cells was assessed using CCK-8 (Dojindo, Kumamoto, Japan) reagent. 5000 HCT116 and SW620 cells were seeded per well in a 96-well plate. The cells are treated with BZD or cell culture medium without BZD for 12, 24, or 48 hours after adhering to the wall. Following treatment, the tumor cells were washed twice with PBS and incubated with a 1:10 diluted CCK-8 reagent in a serum-free medium. After a 2-h incubation at 37 °C, 100 uL of the diluted CCK-8 reagent was added to each well of the cell culture plate. The absorbance of the cells at 450 nm was observed at three experimental nodes.

2.10 Cell invasion detection

Cell invasion experiments were performed utilizing a 24-well Transwell plate (Corning, USA). HCT116 and SW620 cells were added to the Transwell chamber with a pore size of 0.8 μm (BioCoat, 354480), and the invasiveness of the cells was assessed. Briefly, 600 μL of complete culture media with 10% FBS was applied to each lower chamber well of the 24-well plate. Subsequently, 2×10^5 cells were treated with 100 μL of resuspended serum-free culture medium containing varying BZD concentrations (0, 1, 2, and 4 mg/mL). They were then inoculated in the upper chamber and cultured in a cell incubator. After 24 h of cultivation, gently wipe the non-metastatic cells in the upper compartment with a damp cotton swab. Fixed the cells invading the lower lumen with a 4% paraformaldehyde solution for 30 min and then stained with a 0.1% crystal violet solution for 20 min. Subsequently, photos were taken using a microscope and statistically analyzed.

2.11 Cell apoptosis detection

BZD's effect on colorectal cancer cell apoptosis was examined using flow cytometry. Logarithmic growth stage HCT116 and SW620 cells were seeded in a 6-well plate at a density of 2×10^5 cells per well. Following cell adhesion, varying concentrations of Bazhen decoction (0, 1, 2, and 4 mg/mL) were administered for intervention. After 24 h, cells were harvested following the instructions of the membrane-associated protein V-APC/7-AAD cell apoptosis kit (Elabscience, E-CK-A218) and analyzed by flow cytometry within 30 min.

2.12 Animal experiments

Female C57BL/6 mice aged 4–6 weeks were obtained from SPF (Beijing) Biotechnology Co., Ltd. and maintained in an SPF environment. Following a week of adaptive feeding, subcutaneously injected 100 μL of MC38 cell suspension with 1×10^6 cells into the right side of each mouse. The experiment commenced on the 7th day after tumor inoculation, when the tumor volume reached approximately 100 mm^3. The mice were randomly allocated into two groups: the control group received daily gavage of sterile water (200 μL), and the BZD group received daily BZD (200 μL, 6.63 g/kg) for three weeks. The daily dose of BZD was determined based on the average adult body weight of 70 kg and a conversion coefficient 9.1 between humans and mice (42, 43). If the clinical drug dose for a 70 kg adult is X mg/kg, then the dosage for a 20 g mouse would be X mg/kg × 70 kg/0.02 kg × 0.0026. Since the clinical use of BZD for adults is 1 pair/day (51 g freeze-dried powder), the drug dose for a 70 kg adult would be about 728.6 mg/kg. By the above formula, the daily dosage for mice can be calculated as 6.63 g/kg, and the dosage of BZD for a 20 g mouse is 132.6 mg per day, with a gavage volume of 0.2 mL. Therefore, 663 mg/mL of sterile water was prepared to administer BZD. The tumor size was measured every two days using a digital caliper, and the tumor volume was calculated using the formula: tumor volume (mm^3) = length × width × width × width × 0.52. Kaplan Meier survival curves were plotted after three weeks. The mice were euthanized, and their heart, liver, spleen, lungs, kidneys, and tumor tissues were collected for study. All experimental procedures were authorized by the Animal Ethics Committee of Beijing Shijitan Hospital, Affiliated with Capital Medical University (The ethical approval permit numbers are SJTKY11-1X-2021(59)).

2.13 Quantitative real-time polymerase chain reaction

The total RNA was extracted from the mice tumor tissues in the control and the Ba Zhen Decoction group using TRIzol reagent. The

RNA was then converted into cDNA using TransScript first-strand cDNA synthesis SuperMix (TransGen Biotech, AT301). Then, qRT-PCR was performed using SYBR Green Master Mix (Applied Biosystems, USA). All primers employed for PCR amplification were designed using the NCBI Primer-BLAST and bought from Beijing Liuhe Huada Gene Technology Co., Ltd. The primer sequences are shown in Table 1. The GAPDH gene expression was determined simultaneously as an internal control. The relative gene expression was determined using the 2-ΔΔCT method. All samples were run in triplicate. Each primer pair's specificity was validated by computer analysis (NCBI primer BLAST) and melt curve analysis after qPCR amplification.

2.14 T lymphocyte activation

To analyze T cell activation and immune cell phenotype, the spleen of MC38 tumor-bearing mice was taken, minced, and ground in a 40-μm cell strainer. Then, the single-cell suspension was collected by filling it with staining buffer (PBS containing 3% FBS). Cell surface staining was performed by staining the single-cell suspension with APC-Cy7 anti-mouse CD45, FITC anti-mouse CD3, PerCP-Cy5.5 anti-mouse CD4, PE-Cy7 anti-mouse CD8, and BV421 anti-mouse PD-1 antibodies at room temperature for 30 minutes, followed by detection using a flow cytometer. For intracellular staining of the T cell cytokine IFN-γ, the filtered cell suspension was stimulated with Cell Activation Cocktail (BioLegend, 423303) for 6 h. Then the cells were collected and stained for surface markers (44–48). Fixation Buffer (BioLegend, 420801) fixed the cells at room temperature for 20–30 min. After two washes with 1X Permeabilization Buffer (BioLegend, 421002), the cells were stained with APC anti-mouse IFN- γ for 20 min. After washing the samples with a staining buffer, they were detected using a flow cytometer. The data were analyzed and visualized using FlowJo software.

2.15 Pathological and immunohistochemical testing

To assess the BZD's safety, tissue samples from mice's heart, liver, spleen, lungs, and kidneys were procured, embedded in paraffin, sectioned, and subjected to hematoxylin and eosin (H&E) staining. Additionally, tumor samples from each mice group were obtained, embedded in paraffin, sectioned, and subjected to immunohistochemical testing by CD3, CD4, CD8, and Ki67 antibodies. Image-Pro was used to calculate each picture's integrated optical density (IOD) and area. Mean density (IOD/area) was used to analyze protein expression.

2.16 Statistical analysis

The statistical analysis of the data was performed using GraphPad Prism software V9.0. The t-tests were utilized to measure the differences between the two groups, while the one-way analysis of variance (ANOVA) was employed to evaluate the comparisons between the groups. The experimental data was presented as mean ± standard deviation, with a statistical significance level of $p<0.05$. The differences were denoted as ns, $P > 0.05$,* $p \leq 0.05$, ** $p \leq 0.01$, and *** $p \leq 0.001$.

3 Results

3.1 Active ingredients screening

The TCMSP database provided the drug's active components using ADME screening conditions. The database yielded 69 ginseng, 19 *atractylodes macrocephala*, 19 *poria cocos*, 11 *angelica sinensis*, 35 *ligusticum chuanxiong*, 28 *paeonia lactiflora*, 24

TABLE 1 Sequences of PCR primers.

Gene symbol	Accession number	Forward primer (5′–3′)	Reverse primer (5′–3′)	Amplicon size
Gapdh	NM_001289726.2	AGGTCGGTGTGAACGGATTTG	TGTAGACCATGTAGTTGAGGTCA	147
Pik3r1	NM_001024955.2	TGGACTATGGAAGACCTGGACTTAGAG	TTGTTGTTCATGCTGTTGTTGGCTAC	149
Akt1	NM_001165894.2	ATGAACGACGTAGCCATTGTG	TTGTAGCCAATAAAGGTGCCAT	116
Myc	NM_001177352.1	CCCTATTTCATCTGCGACGAG	GAGAAGGACGTAGCGACCG	185
Casp3	NM_001284409.1	ATGGAGAACAACAAAACCTCAGT	TTGCTCCCATGTATGGTCTTTAC	74
Esr1	NM_001302531.1	CCCGCCTTCTACAGGTCTAAT	CTTTCTCGTTACTGCTGGACAG	76
Egfr	NM_007912.4	GCCATCTGGGCCAAAGATACC	GTCTTCGCATGAATAGGCCAAT	101
Hif1a	NM_001313919.2	CCACAACTGCCACCACTGATGAA	TGCCACTGTATGCTGATGCCTTAG	138
Vegfa	NM_001025250.3	GCACATAGAGAGAATGAGCTTCC	CTCCGCTCTGAACAAGGCT	105
Jun	NM_010591.2	TTCCTCCAGTCCGAGAGCG	TGAGAAGGTCCGAGTTCTTGG	133
Stat3	NM_011486.5	GCTTGGGCATCAATCCTGTGGTAT	GCTTGGTGGTGGACGAGAACTG	136
Trp53	NM_001127233.1	CACAGCACATGACGGAGGTC	TCCTTCCACCCGGATAAGATG	101

rehmannia glutinosa, and 126 *glycyrrhiza uralensis* ingredients. The database also provided 258 ingredient target genes.

3.2 CRC targets acquisition

Briefly, 104, 77, 390, and 353 targets were obtained from TTD, Drugbank, GeneCards, and DisGeNET databases, respectively. After merging and removing duplicates of disease targets from the four databases, 761 colorectal cancer-related targets were retained (Figure 2A).

3.3 "Herb-ingredient-target" network construction

The BZD's component action targets were intersected with targets correlated to colorectal cancer, identifying 98 intersecting targets (Figure 2B). Subsequently, 173 effective ingredients, 98 cross targets, and individual drug names that BZD can act on colorectal cancer targets were imported into Cytoscape 3.8.0 to construct a "herbal- ingredient -target" network (Figure 3).

Nodes with greater degree values may be essential in a network. Quercetin displays the highest number of targets, encompassing 73 potential targets, followed by kaempferol, licorice ketone, and naringin, with 22, 16, and 15 targets, respectively. BZD's key ingredients may be these active compounds with more targets. Table 2 presents the top 10 active ingredients in the degree ranking.

3.4 Protein-protein interaction analysis of intersection targets

Ninety-eight intersection targets of BZD and CRC were imported into the STRING 11.0 database (https://www.string-db.org/) for analysis, acquiring a PPI network of intersection targets between BZD and CRC. The network comprises 98 nodes and 1835 edges. Nodes indicate intersecting targets, while edges express associations between them. Cytoscape 3.8.0 was employed to present the PPI network diagram (Figure 4A), while the Cytohubba plugin was utilized to compute the target set for further refinement of the core targets. The top 10 hub genes in degree ranking, AKT1, MYC, CASP3, ESR1, EGFR, HIF1A, VEGFA, JUN, INS, and STAT3, were identified (Figures 4B, C). The Sankey diagram also showed the link between BZD, the four basic components, and the ten core genes (Figure 4D).

3.5 GO and KEGG enrichment analysis of intersecting targets

The key biological functions of BZD in treating CRC were determined by utilizing GO and KEGG enrichment analysis. The bubble plots of the top 10 biological processes (BP), cellular composition (CC), and molecular function (MF) in GO analysis are presented in Figures 5A-C. The biological processes focus on cell death signals and oxidative stress responses. In contrast, the cellular composition changes are mostly related to membrane rafts, membrane microregions, and cyclin-dependent protein kinase holoenzyme complexes. The MF modifications primarily focused on binding with ubiquitin-like protein ligase, RNA polymerase II transcription factor, ubiquitin protein connexin, and protein phosphatase. Through KEGG pathway enrichment analysis, 165 signal pathways were identified. The KEGG enrichment analysis indicates that the PI3K-AKT, T cell receptor, P53, and VEGF signaling pathways could potentially serve as crucial pathways for treating colorectal cancer with BZD, as illustrated in Figure 5D.

3.6 Molecular docking

Molecular docking was performed on four core ingredients (quercetin, naringenin, licochalcone A, kaempferol) and 10 hub genes (AKT1, CASP3, EGFR, ESR1, HIF1A, INS, JUN, MYC, STAT3, and VEGFR) to assess the protein-ligand binding potential. Affinity refers to the capacity of a ligand to bind with receptors, and a higher absolute affinity value indicates a stronger binding ability (with a negative value). Figure 6 illustrates the binding energy of the core

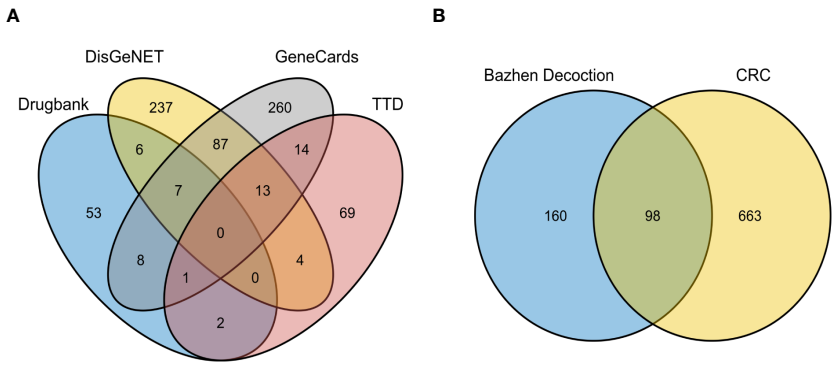

FIGURE 2
Intersection Target of CRC and Ingredient Action Target of BZD with CRC. **(A)** Venn diagram displaying CRC-related targets among the four databases. **(B)** Venn diagram of the intersection target of BZD and CRC.

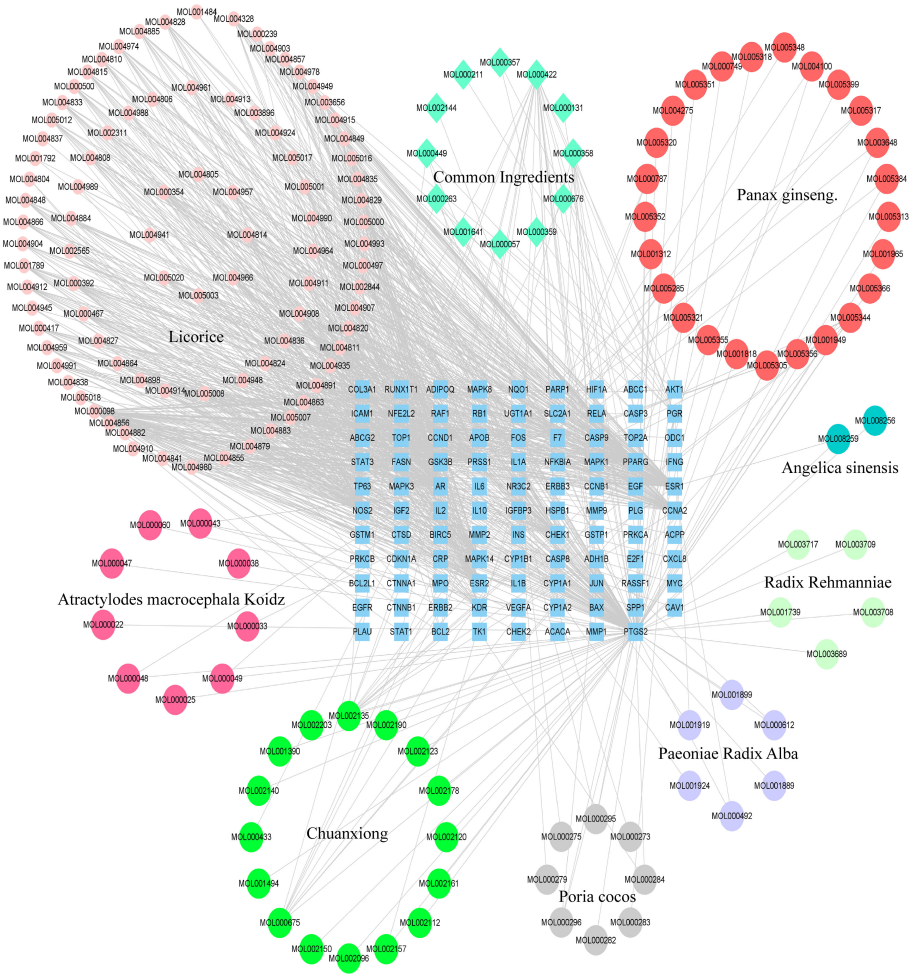

FIGURE 3
The "herbal-ingredient-target" network of BZD in treating CRC.

ingredients docked with the hub genes. The findings indicate that quercetin exhibits favorable docking effects with ESR1, HIF-1A, JUN, and STAT3, with respective binding energies of -8.5, -8.0, -8.2, and -8.2 kcal/mol. Naringenin's binding energies of -8.8 and -8.2 kcal/mol with ESR1 and JUN are favorable.

Similarly, Kaempferol demonstrates a favorable docking effect with HIF-1A, STAT3, ESR1, and JUN, with corresponding binding energies of -8.0 kcal/mol, -8.0 kcal/mol, -8.2 kcal/mol, and -8.1 kcal/mol, respectively. The molecular docking models are depicted in a 3D diagram using PyMol 2.4.0. Figure 7 illustrates the interactions between quercetin and ESR1, HIF-1A, JUN, and STAT3. Figure 8 showcases the interactions between naringin and ESR1, JUN, and the interaction between kaempferol and HIF-1A and STAT3.

TABLE 2 The top ten ingredients in the herbal ingredient CRC target network.

Mol ID	Degree	Molecule name
MOL000098	73	quercetin
MOL000422	22	kaempferol
MOL000497	16	licochalcone A
MOL004328	15	naringenin
MOL000354	13	isorhamnetin
MOL004966	13	3'-Hydroxy-4'-O-Methylglabridin
MOL002135	12	Myricanone
MOL001789	12	isoliquiritigenin
MOL000392	12	formononetin
MOL004828	12	Glepidotin A

3.7 In a time- and dose-dependent manner, BZD suppresses the proliferation and invasion of CRC cells while facilitating their apoptosis

CCK-8 assays measured the proliferation of CRC cell lines HCT116 and SW620 treated with different BZD doses. Ten concentration gradients were used, which are 0, 0.125, 0.25, 0.5, 1, 2, 4, 8, 16, and 32 mg/mL. The findings indicate that BZD effectively suppressed the

10.3389/fimmu.2023.1235575

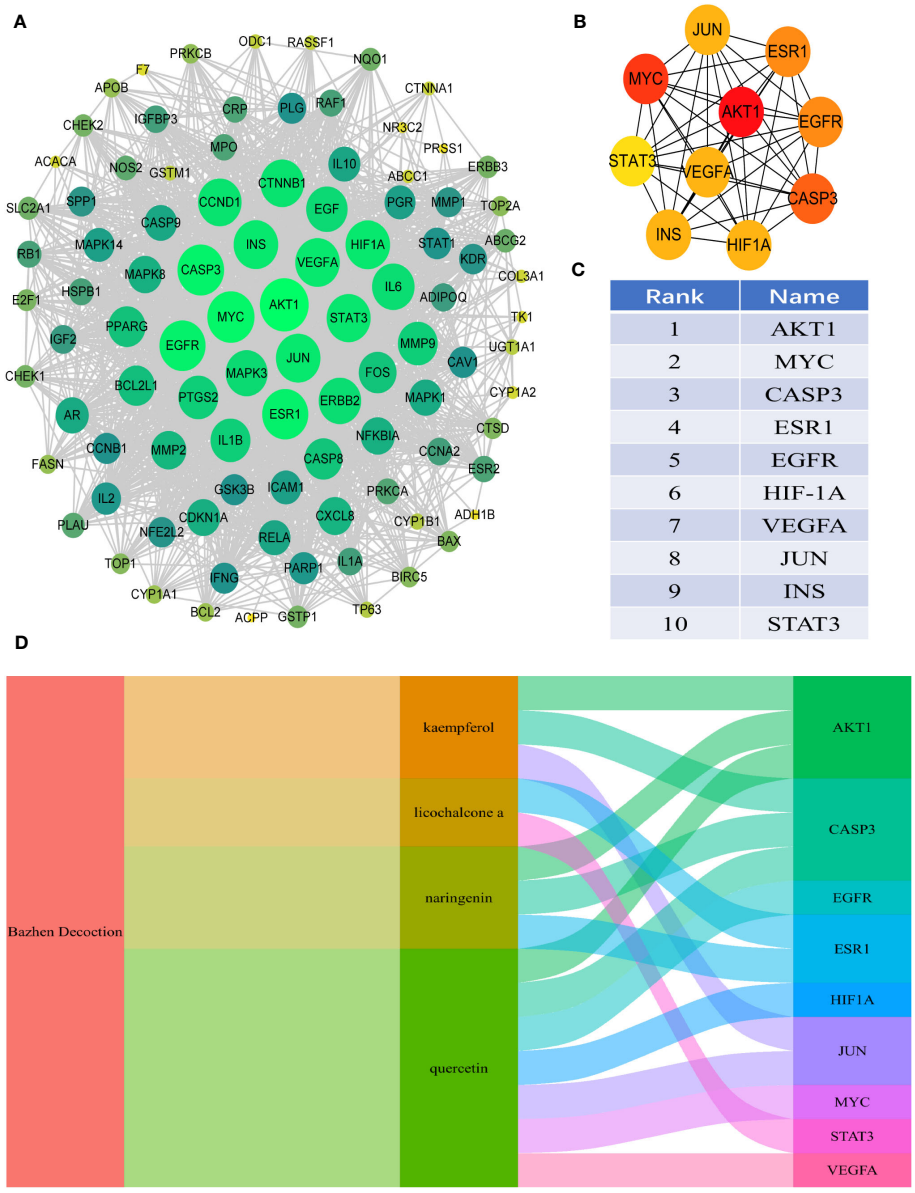

FIGURE 4
PPI analysis of the intersection target between BZD and CRC. **(A)** PPI interaction network between BZD and the intersection target of CRC. **(B, C)** The top 10 core genes were obtained from PPI network analysis. **(D)** The Sankey diagram reveals the relationship between BZD, core ingredients, and central genes.

CRC cells' activity in a dose- and time-dependent manner, as illustrated in Figure 9A.

Furthermore, the impact of varying concentrations (0, 1, 2, 4 mg/mL) of BZD on the invasion capacity and apoptotic rate of the two CRC cell lines was assessed. The findings indicated that BZD exhibited a dose-dependent suppression of CRC cell invasion (Figure 9B) and promoted apoptosis of CRC cells (Figure 10).

3.8 BZD inhibits tumor progression in mice

An MC38 tumor-bearing mouse model was created to test BZD's CRC treatment efficacy. Figure 11A shows the mice's experimental protocol. Following three weeks of consistent oral administration of BZD, a noteworthy reduction in subcutaneous tumor volume was observed in the BZD group compared to the sterile water group ($p \leq 0.001$; Figure 11B), as illustrated by the tumor volume curve in Figure 11C. After 21 days, the control group had a mean tumor size of 1703.15 mm^3, while the BZD group had 760.94 mm^3 (Figure 11D). On day 28, the mice were humanely euthanized to obtain the tumor. The average tumor weights for the control and BZD groups were 2.32 and 1.13 g, respectively (Figure 11E). H&E staining of the heart, liver, spleen, lungs, and kidneys showed no significant differences between experimental groups (Figure 12), demonstrating that BZD is non-toxic and does not damage tissue. Consequently, the BZD intragastric

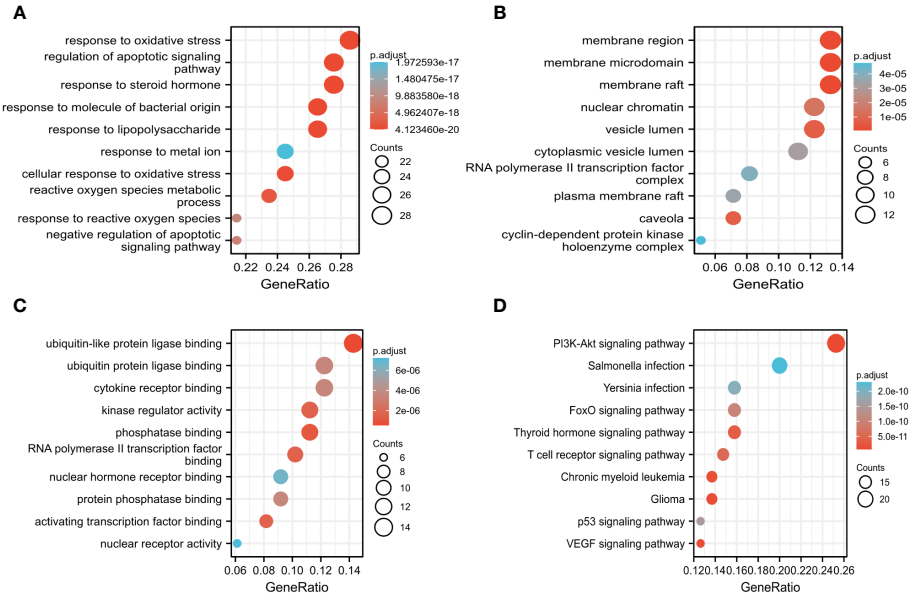

FIGURE 5
GO, and KEGG analysis determine the key biological processes of BZD in treating CRC. **(A–C)** GO enrichment analysis results in biological processes (BP), cellular ingredients (CC), and molecular functions (MF). **(D)** KEGG enrichment analysis results.

administration effectively suppressed the development of subcutaneous tumors in MC38 mice.

3.9 The effect of BZD on key genes and KEGG pathway-related genes

To test whether BZD can prevent colorectal cancer growth by altering the core genes in the network pharmacology analysis results and the KEGG enrichment pathway-related genes, RT-qPCR was used to measure target protein mRNA expression levels in tumor tissues of NC and BZD group mice. The BZD group had significantly lower Pik3r1, Akt1, Myc, Esr1, Egfr, Hif1a, Vegfa, Jun, and Stat3 mRNA expression levels than the NC group, according to PCR data. Compared to the NC group, the expression levels of Casp3 and Trp53 in the BZD group were significantly increased. There was no difference in the mRNA expression levels of Esr1 between the NC and BZT groups' tumor tissues (Figure 13). Network pharmacology analysis results show that BZD can prevent colorectal cancer progression by acting on critical core genes and KEGG enrichment pathways. Moreover, these core genes (Pik3r1, Akt1, Myc, Egfr, Hif1a, Vegfr, Jun, and Stat3) are closely related to the tumor immune microenvironment, exclusively T cell immune function.

3.10 BZD induces T cell activation in tumor-bearing mice

BZD, a traditional formula in the "Fuzheng Guben" treatment principle, can supplement qi, nourish the blood, and enhance the

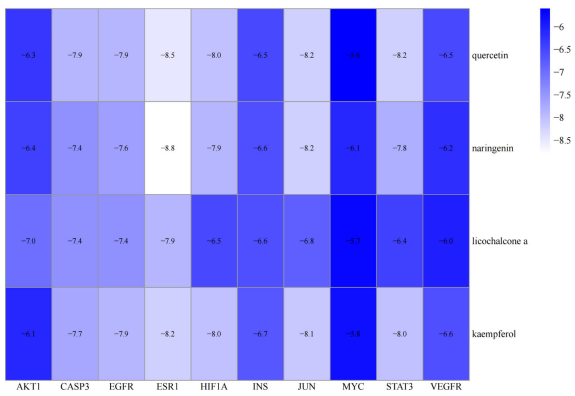

FIGURE 6
Heatmap of the binding energy of molecular docking between 4 core ingredients and 10 core targets.

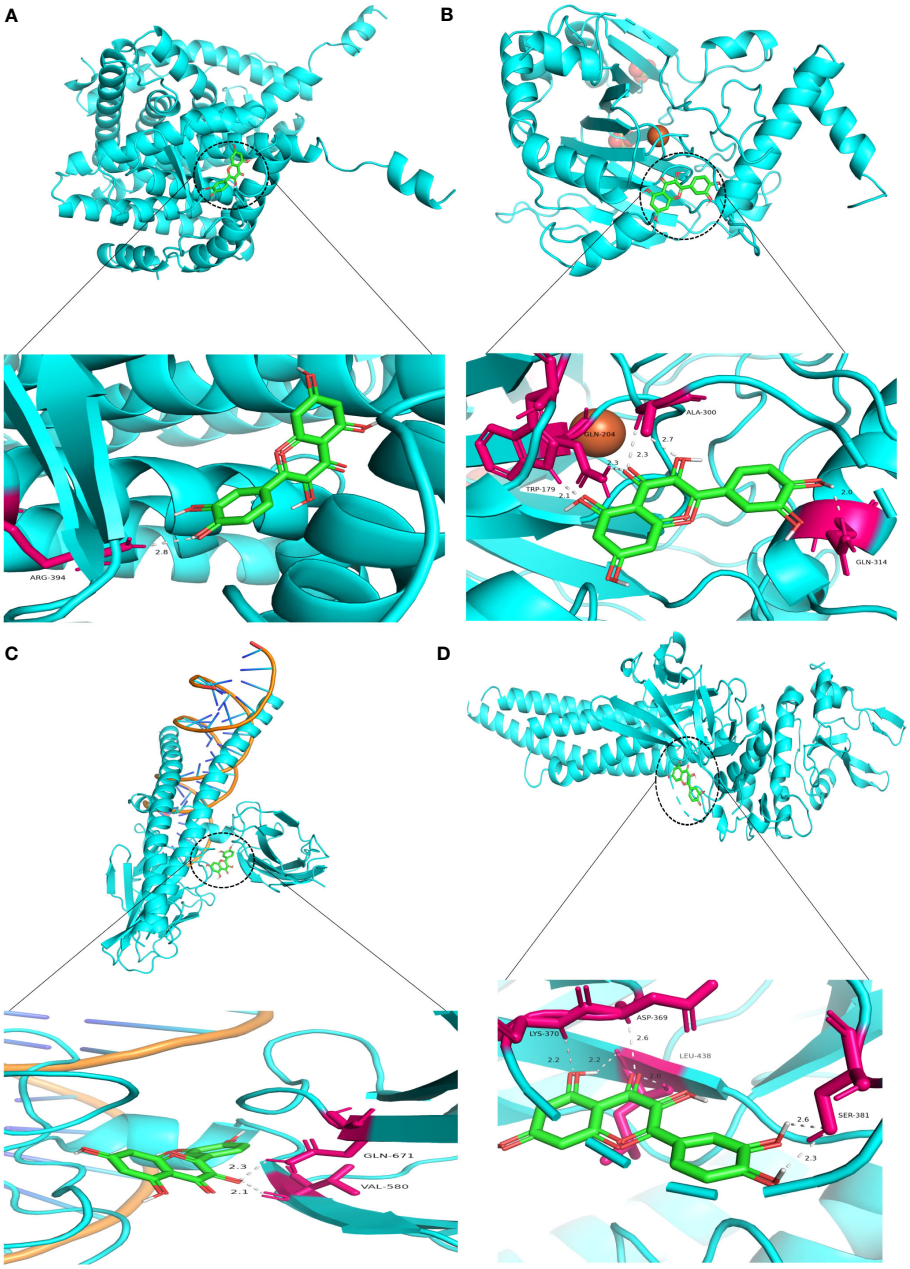

FIGURE 7
Molecular docking model 3D diagram. Quercetin binds to ESR1 **(A)**, HIF-1A **(B)**, JUN **(C)**, and STAT3 **(D)**.

immune system. To clarify the mechanism of the BZD anti-tumor effect, we conducted a flow cytometric analysis of spleen tissues from two groups of mice. The results showed that compared to the control group, BZD increased the proportion of $CD3^+CD4^+$ and $CD3^+CD8^+$ T cells in the spleen (Figures 14A, B, G) and decreased the proportion of exhausted T cells ($CD4^+PD\text{-}1^+$ and $CD8^+PD\text{-}1^+$T cells) in the spleen (Figures 14C, D, H). Furthermore, BZD promoted the activation of $CD4^+$ and $CD8^+$ T cells in the spleen and increased the level of IFN-γ in the body (Figures 14E, F, I). These data imply that BZD can reduce the number of exhausted T cells in the spleen of tumor-bearing mice and upregulate IFN-γ to elicit an anti-tumor immune response by infiltrating and activating effector T cells.

3.11 BZD promotes T-cell infiltration in tumor tissue of tumor-bearing mice

To further explore the BZD effects on the tumor microenvironment, we performed immunohistochemical staining on the tumor tissues of two groups of mice. In mice's tumor tissues, the BZD group had more $CD3^+$, $CD4^+$, and $CD8^+$ T cells than the control group. Moreover, the Ki67 staining in the control group was enhanced, indicating that BZD inhibited tumor cell proliferation (Figure 15). The results indicate that BZD can promote T cell infiltration in tumor tissues, enhance anti-tumor immune response, and suppress colorectal cancer progression.

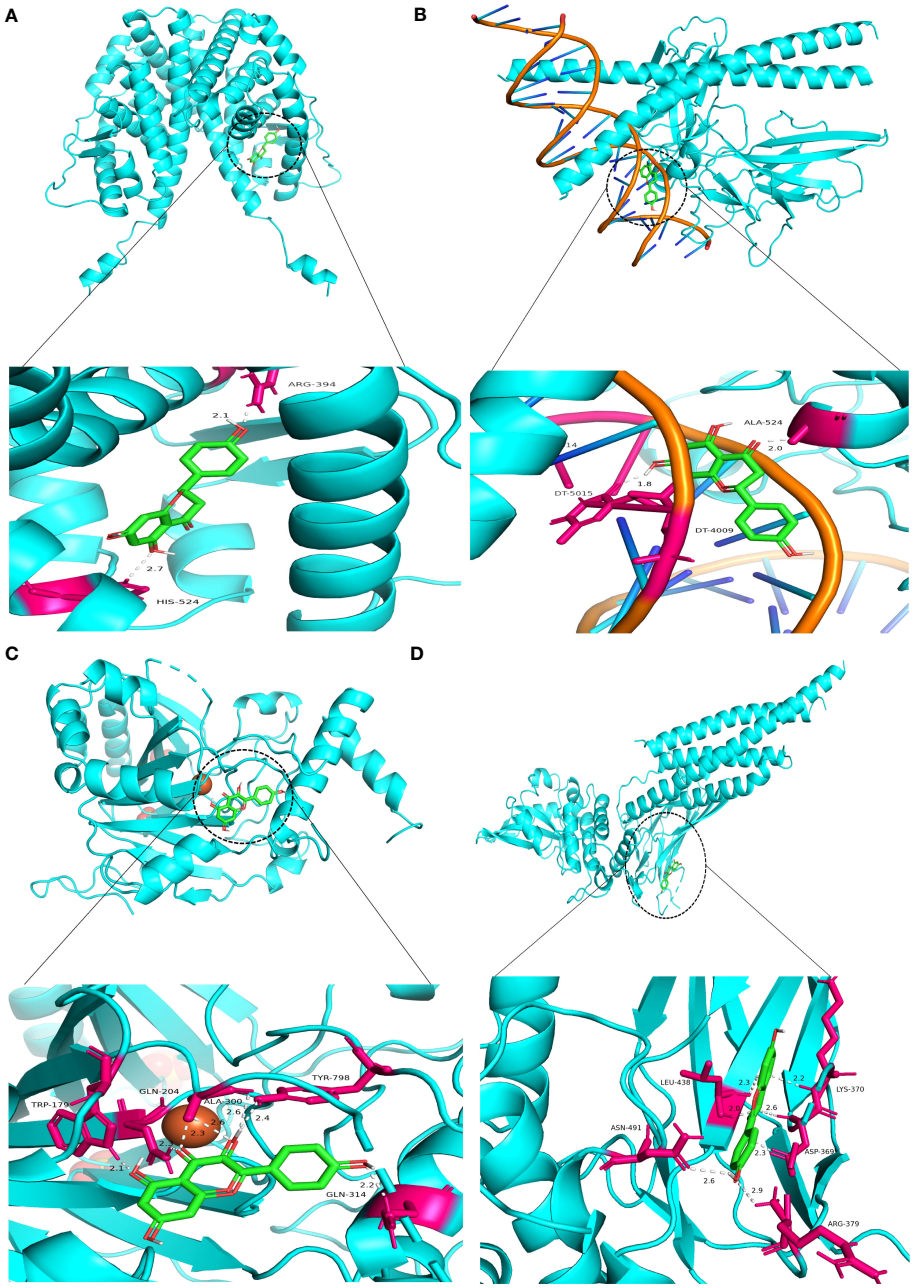

FIGURE 8
Molecular docking model 3D diagram. Naringin binds to ESR1 **(A)** and JUN **(B)**, while kaempferol binds to HIF-1A **(C)** and STAT3 **(D)**.

4 Discussion

CRC accounts for 10% of all cancer cases, ranking third in men and second in women (49, 50). In 2020, there were an estimated 1.9 million new cases and 900,000 deaths globally, rendering it the second leading cause of cancer-related deaths. CRC incidence, mortality, and healthcare services are global public health issues (51). At the time of diagnosis, approximately 20% of CRC patients have already experienced metastasis, and 50% of early-stage patients will eventually develop metastasis (52). Locally advanced rectal and metastatic colorectal cancer (CRC) patients have a poor long-term prognosis, and CRC treatment remains difficult (53). Current treatment modalities involve a multimodal approach, including surgery, radiotherapy, and chemotherapy. However, despite these interventions, recurrence, and metastasis rates remain high. Traditional Chinese medicine has a long history of effectiveness in treating complicated ailments like severe infectious diseases, cardiovascular diseases, and malignant tumors. Traditional Chinese medicine's characteristics encompass many ingredients, targets, and synergistic effects. Inducing cell apoptosis and autophagy, inhibiting tumor cell proliferation, suppressing epithelial-mesenchymal transition and angiogenesis, modulating chemotherapy resistance, tumor metabolism, and tumor immune regulation may treat colorectal cancer (54–56). In contrast to the

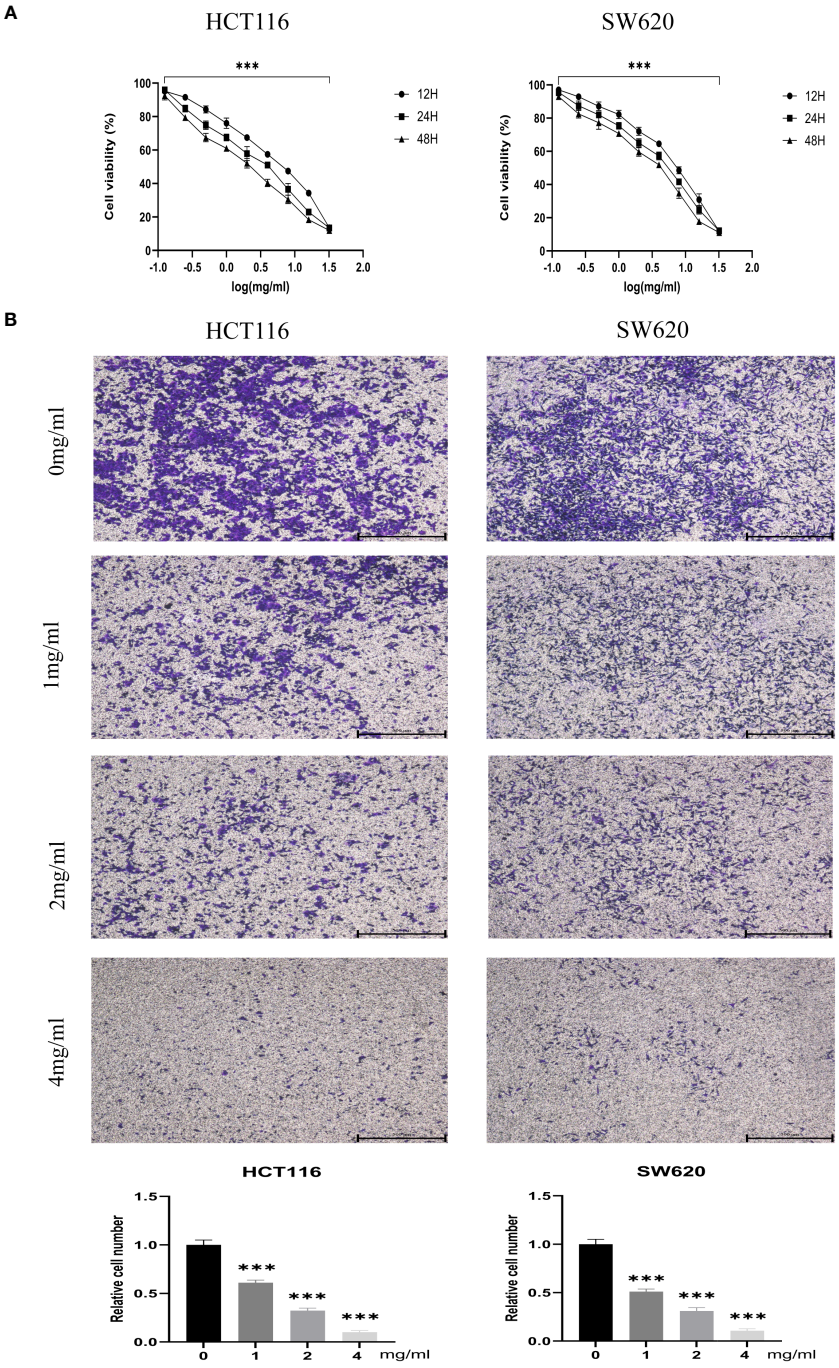

FIGURE 9
BZD inhibits the proliferation and invasion of colon cancer cells in a dose-dependent manner. **(A)** HCT116 and SW620 cells were subjected to 10 concentration gradients of BZD for 12, 24, and 48 h, and the resulting cell viability was assessed using CCK8. **(B)** The invasiveness of HCT116 and SW620 cells was measured after exposure to four BZD concentration gradients for 24 h. ***P < 0.001.

adverse effects associated with chemotherapy drugs, including bone marrow suppression, reduced blood cell count, gastrointestinal reactions, liver function impairment, and alopecia, the use of traditional Chinese medicine for treating colorectal cancer exhibits a lower incidence of side effects and drug resistance (57, 58).

BZD, a classic formula utilized in the treatment principle of "Fuzheng Guben," has been observed to possess the ability to nourish qi and blood. Clinical studies have demonstrated its efficacy in treating various solid tumors. BZD's mechanism in CRC treatment is unknown. This study is the first to employ network pharmacology and molecular docking to anticipate the core components, core targets, and likely mechanisms of BZD in colorectal cancer treatment. Subsequently, the *in vitro* anticancer effect of BZD was validated using two human colorectal cancer cell lines (HCT116 and SW620). Subsequently, we proceeded to validate

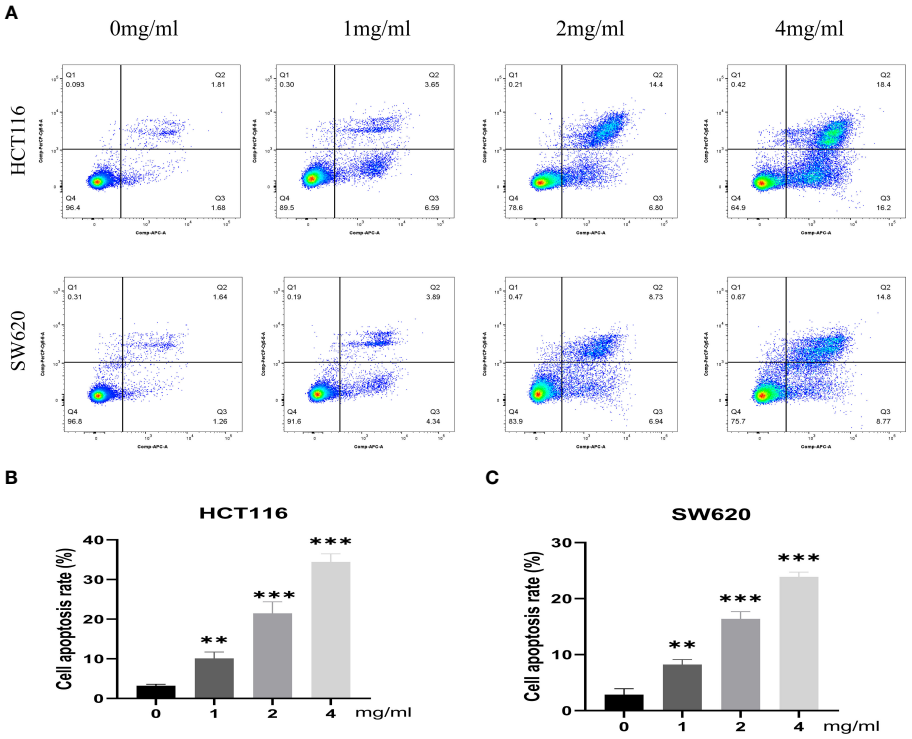

FIGURE 10
BZD promotes apoptosis of colon cancer cells in a dose-dependent manner. **(A)** Flow cytometry revealing that BZD can dose-dependently induce apoptosis in HCT116 and SW620 cells. **(B, C)** Histogram showing that BZD can induce apoptosis in HCT116 and SW620 cells in a dose-dependent manner. **P < 0.01, ***P < 0.001.

the BZD efficacy in inhibiting the progression of colorectal cancer *in vivo* using the MC38 subcutaneous tumor mouse model. We used qRT-PCR to assess gene expression changes in tumor tissues from the control and BZD groups to understand the processes. Additionally, we conducted flow cytometry analysis of the spleen and immunohistochemistry of the tumor tissue to investigate further the relevant mechanism of BZD in treating colorectal cancer. Finally, we evaluated the BZD organ toxicity through HE staining.

In this study, we screened each herb in BZD through ADME to obtain active drug components. Additionally, 258 drug targets were retrieved from databases. We obtained 761 targets correlated to colorectal cancer from the TTD, Drugbank, GeneCards, and DisGeNET databases. By intersecting the targets of drug components with those of colorectal cancer, we obtained 98 overlapping targets. In the herb-ingredient-target network, quercetin, kaempferol, licochalcone A, naringenin, isorhamnetin, 3 '- Hydroxy-4' - O-Methylgabridin, Myricanone, isoliquiritigenin, formonetin, and Glepidotin A have more therapeutic targets for colorectal cancer than other ingredients; thus, they may be the core effector components of BZD in treating colorectal cancer. Quercetin, kaempferol, licochalcone A, naringenin, isorhamnetin, myricanone, and isoliquiritigenin are flavonoid compounds, while formononetin belongs to the isoflavone class. To fight cancer, Quercetin regulates several biological processes, including cell death, autophagy, angiogenesis, metastasis, cell cycle, proliferation, and anti-tumor immune activation (59–64). Quercetin weakens the inhibitory effect of PD-L1 on T cells by inhibiting the PD-1/PD-L1 interaction, promoting the CD8, GZMB, and IFN-γ expression in mouse tumor tissues, and enhancing the anti-tumor immune response (65). Kaempferol is a major flavonoid glycoside with multiple anti-cancer mechanisms (66). It can cause G2/M phase arrest and block cell death in colorectal cancer cells, preventing their proliferation (67). Furthermore, kaempferol can enhance the anti-tumor immune response, synergistically creating a favorable tumor immune microenvironment with radiotherapy and chemotherapy (68). Kaempferol can also enhance anti-tumor immune function by targeting multiple immune-related molecules (69). Kaempferol treatment effectively prevents the decrease of $CD4^+$ T cells and $CD8^+$ T cells in mouse blood induced by cold stress (70). Kaempferol increases NKT and $CD8^+$ T cells and decreases MDSC cells, preventing mouse tumor growth (71). Furthermore, kaempferol is vital in overcoming 5-Fu resistance by inhibiting the glycolysis process in resistant colorectal cancer cells (72). Licochalcone A can inhibit the colorectal cancer cell line HCT116 proliferation by promoting G0/G1 phase arrest, cell apoptosis, and high ROS production (73). Licochalcone A reduces DNA synthesis dose-dependently, thereby inhibiting the mouse colon cancer cells' CT-26 proliferation and alleviating liver and kidney function damage caused by cisplatin treatment (74). LCA increases T cell anti-tumor efficacy by decreasing PD-L1 expression (75). Licochalcone A therapy can boost cytotoxic T lymphocyte activity and kill tumor cells (76). Other studies have shown that

10.3389/fimmu.2023.1235575

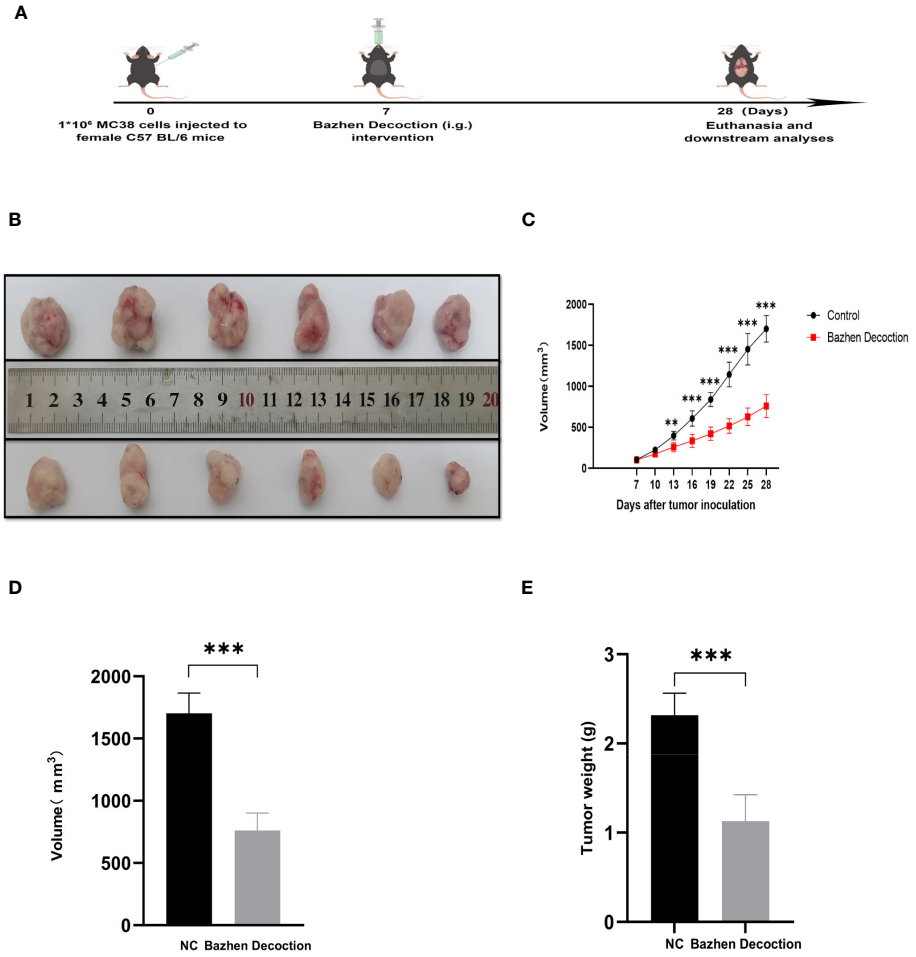

FIGURE 11
BZD inhibits tumor progression in MC38 tumor-bearing mice. **(A)** Schedule of MC38 tumor-bearing mouse model. **(B)** On the 28th day, images of tumors in both groups of mice were obtained. **(C)** Curve plots of tumor volume change in two groups of tumors bearing mice. **(D)** Histograms of tumor volume comparison between two groups of tumors bearing mice. **(E)** Histogram comparison of tumor weight between two groups of tumors bearing mice. **P < 0.01, ***P < 0.001.

licochalcone A promotes T and B cell proliferation in mice's spleen and whole blood by activating the IL-17 signaling pathway and improving cognitive ability (77). Naringenin can inhibit cancer progression through various mechanisms, like inducing apoptosis, cell cycle arrest, inhibiting angiogenesis, and modifying various signaling pathways, including Wnt/β- Catenin, PI3K/Akt, NF- κB and TGF- β Pathway (78). Naringenin can enhance CD169 macrophages in lymph nodes of mice with oral squamous cell carcinoma (OSCC) and suppress tumor growth through T-cell-mediated anti-tumor immune activity (79). Moreover, in the mouse colon adenocarcinoma model, Naringenin induced more CD103 DC to infiltrate the tumor, promoted the $CD8^+$ T cell activation,

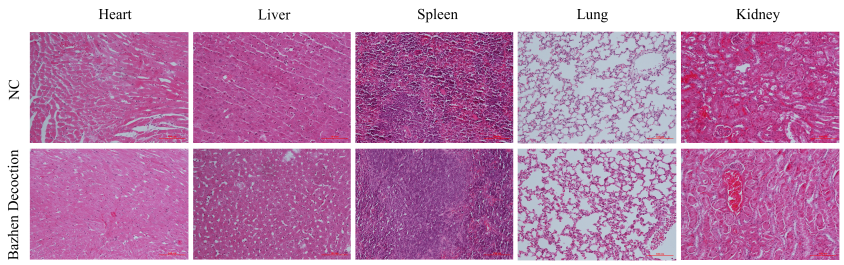

FIGURE 12
Organ toxicity of BZD. Two groups of mice were euthanized at the end of treatment, and their hearts, liver, spleen, lungs, and kidneys were removed for H&E staining to evaluate organ toxicity (scale: 100 mm).

10.3389/fimmu.2023.1235575

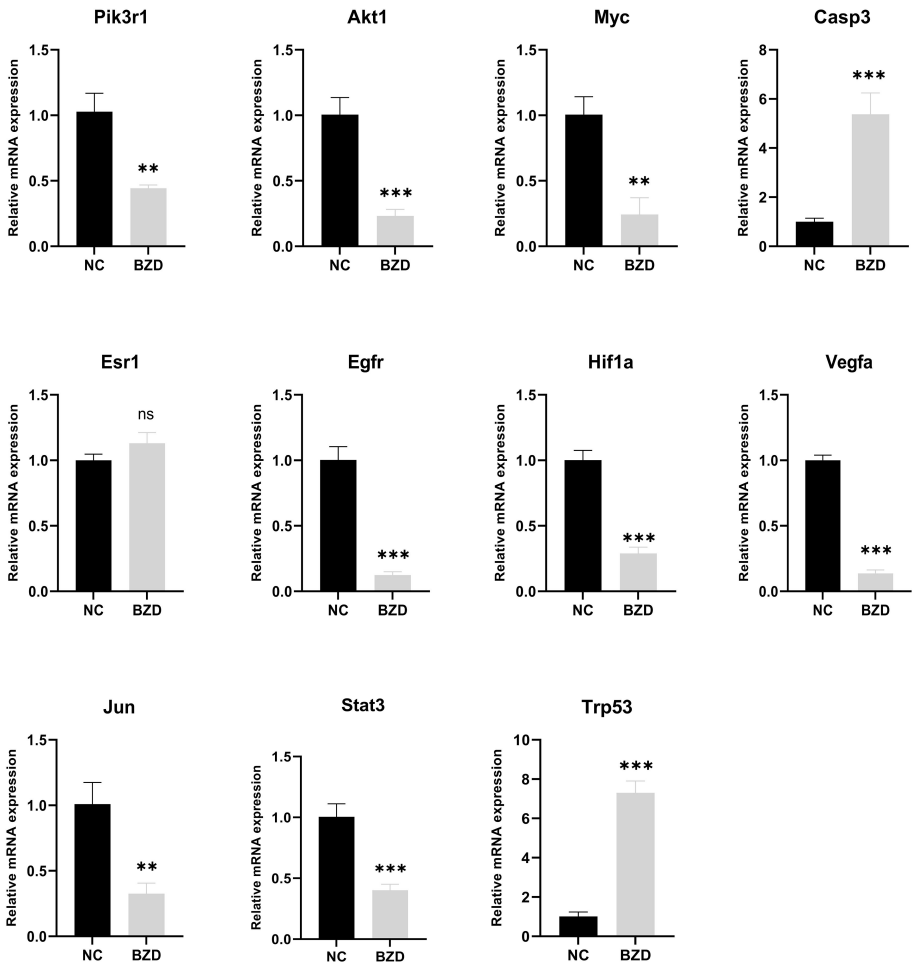

FIGURE 13
Effect of BZD on Key Genes and KEGG Pathway-Related Genes. Compared to NC group, mRNA expression levels of Pik3r1, Akt1, Myc, Esr1, Egfr, Hif1a, Vegfa, Jun, and Stat3 in BZD group were significantly reduced, while the levels of Casp3 and Trp53 were significantly increased. There was no significant difference in Esr1 expression between BZD and NC groups. ns: $P > 0.05$, **$P < 0.01$, ***$P < 0.001$.

and enhanced the performance of the E7 vaccine against TC-1 mouse cancer treatment (80). After breast cancer surgery, naringenin therapy reduces lung metastases and extends mouse life. Flow cytometry demonstrated that Naringenin-treated mice had less regulatory T cells, activated $CD8^+$ and $CD4^+$ T cells, and IFN-γ. The secretion level of IL-2 has significantly increased (81). Isorhamnetin can block the cell cycle, inhibit proliferation and induce apoptosis by down-regulation of the Bcl-2 gene, upregulation of the Bax gene, inhibition of telomere activity, and reduction of related protein expression (82). Myristone induces apoptosis in two types of cancer cells (HeLa and PC3) by activating caspase and downregulating NF-KB and STAT3 signaling cascade inhibits tumor cell proliferation (83). Myristone has a significant dose-dependent sexual inhibition effect on human lung cancer cell A549 and can promote the apoptosis of lung cancer cells (84). Myristone causes HepG2 apoptosis through ROS generation, mitochondrial membrane depolarization, early cytochrome c release, HSP70 downregulation, and caspase cascade activation (85). Isoliquiritigenin is a natural pigment with a simple Chalcone structure, which can be separated from the root of licorice and is considered a potential Natural product. It is reported that isoliquiritigenin has therapeutic potential for many cancer cell lines, including leukemia, gastrointestinal, breast, colon, ovarian, lung, and melanoma (86). Isoliquiritigenin mediates HIF-1 α stability and inhibits the glycolysis of colorectal cancer cells, thereby inhibiting the proliferation of colon cancer cells (87). Isoliquiritigenin affects the metabolic pathways of tumor cells and inhibits colorectal cancer growth by triggering cell cycle arrest, apoptosis, and autophagy and altering tumor cell metabolism (86, 88). Formononetin is a common component in legumes, particularly rich in *Trifolium pratense L.* and *Astragalus membranaceus*. Formononetin can inhibit tumor cell proliferation by inducing cell cycle arrest and induce cell apoptosis by regulating Bax, Bcl-2, and caspase-3 proteins. Moreover, formononetin inhibits cell invasion by regulating Vascular endothelial growth factor (VEGF) and Fibroblast growth factor 2 (FGF2). Anthocyanin's anticancer properties can be enhanced by synergistic effects with other chemotherapy drugs (89). Other studies have shown that formononetin enhances T cells' activity and killing ability by inhibiting the PD-L1 expression on the cell

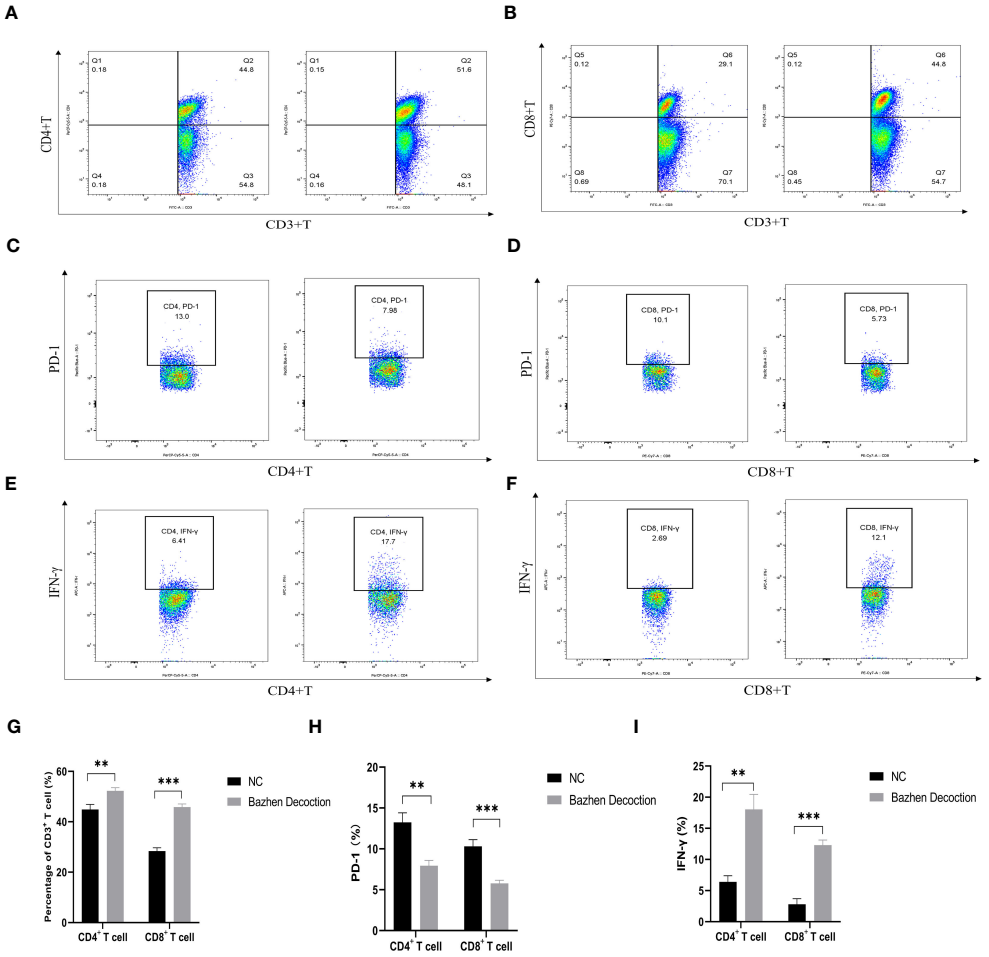

FIGURE 14
BZD plays an anti-tumor role by significantly increasing the number of tumors infiltrating lymphocytes (TIL) in the body and promoting the activation of T cells. **(A, B, G)** BZD increased the number of $CD3^+CD4^+$ T cells and $CD3^+CD8^+$ T cells in the spleen. **(C, D, H)** BZD reduced the number of $CD4^+PD\text{-}1^+$ T cells and $CD8^+PD\text{-}1^+$ T cells in the spleen. **(E, F, I)** BZD facilitates the activation of CD4+ and CD8+ T cells within the spleen and increases the levels of IFN-γ within the body. $^{**}P < 0.01$, $^{***}P < 0.001$.

surface, thereby inhibiting tumor proliferation, angiogenesis, migration, and invasion (90). However, there are no reports on treating cancer with the two active ingredients, 3 '- Hydroxy-4' - O-Methylgabridin and Glepidotin A, which need to be explored in future research. Besides inhibiting the proliferation and invasion of colorectal cancer cells and promoting colorectal cancer cells apoptosis, the five core effector components (quercetin, kaempferol, licochalcone A, naringenin, and formaronetin) of BZD can also enhance the immune function against colorectal cancer by promoting the T cells activation and killing ability.

In the PPI network, we identified 10 key genes, namely AKT1, MYC, CASP3, ESR1, EGFR, HIF-1A, VEGFA, JUN, INS, and STAT3, which may be the core targets of BZD therapy for CRC. AKT1, a proto-oncogene in the serine/threonine kinase family, regulates tumor cell proliferation, survival, and metabolism through inflammation and metabolism-related signaling pathways (91). About 70% of colorectal cancers exhibit highly activated AKT, closely associated with cancer development. Abu-Eid found that after using AKT inhibitors, tregs were more susceptible to inhibition, increasing the number of $CD8^+$ T cells in tumor tissue and improving control of tumor lesions (92). Modified-Bu-zhong-yi-qi decoction (mBYD) directly enhances T lymphocyte proliferation and activation by blocking the PI3K/AKT signaling pathway and suppressing cancer cell PD-L1 expression, ultimately preventing gastric cancer growth (93). The MYC oncogene is part of the gene superfamily, and its product is commonly activated in human cancers (94, 95). The mechanisms by which MYC activation promotes tumor progression mainly involve cell proliferation, cell invasion, metabolic reprogramming, genomic instability, angiogenesis, and immune evasion (96, 97). MYC can reshape the tumor microenvironment, evading host immune responses (98). Myc inhibitors decrease the stable state of regulatory T (Treg) cells in tumors and the differentiation of resting treg (rTreg) to activated Treg (aTreg), which activates $CD8^+$T cells and induces anti-tumor immune response (99). Cysteine Aspartic protease 3 (CASP3) serves as the primary mediator of apoptosis in tumor cells when exposed to cytotoxic drugs, radiotherapy, or immunotherapy, making it a commonly employed marker for assessing the efficacy of cancer treatment. Targeting CASP3 therapeutically increases tumor cell sensitivity to chemotherapy and radiotherapy and

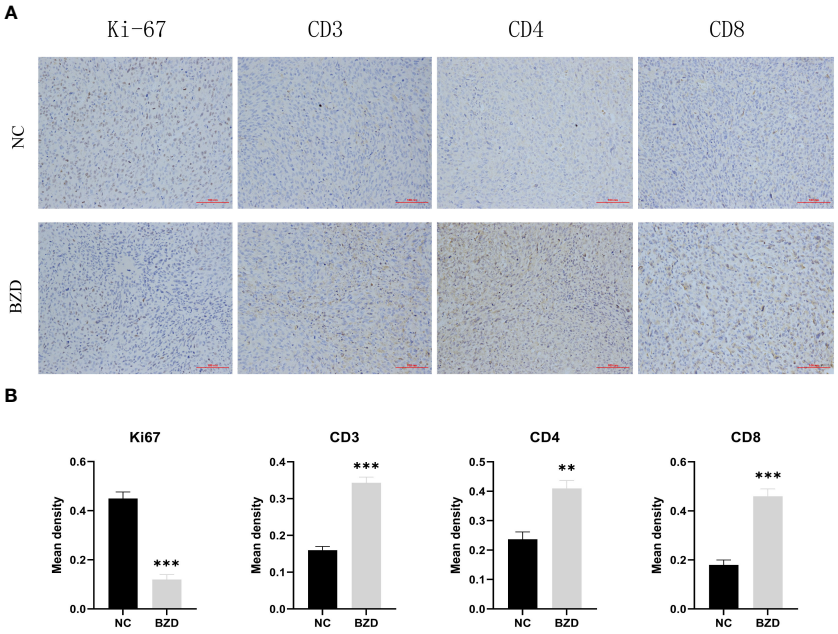

FIGURE 15
BZD significantly increased the number of Tumor-infiltrating lymphocytes (TIL) *in vivo* and inhibited the expression of Ki67. **(A)** An immunohistochemistry assay is used to detect the CD3, CD4, CD8, and Ki67 expression levels in transplanted tumors (×200). **(B)** Histogram showing the expression levels of CD3, CD4, CD8, and Ki67 in tumor tissues of the control group and BZD group. **P < 0.01, ***P < 0.001.

inhibits cancer cell invasion and metastasis (100). Studies have shown that ESR1 mutations can promote tumor progression and metastasis. During treating metastatic estrogen receptor (ER) positive breast cancer with Aromatase inhibitors, ESR1 mutations are a common mechanism of hormone therapy resistance (101). Epidermal growth factor receptor (EGFR) is key for cell proliferation, differentiation, and survival (102). EGFR is overexpressed in 25–77% of colorectal cancer, which is related to the poor prognosis of cancer patients (103–105). Besides directly promoting tumor cell proliferation, EGFR can also serve as a modulator for tumor immune monitoring, promoting the PD-L1 expression by activating the JAK/STAT3 signaling pathway, inducing T cell apoptosis and immune escape. EGFR Tyrosine kinase inhibitors (TKIs) can enhance the effect of MHC class I and II antigens on IFN-γ to increase $CD8^+$T cells and DC cells levels, eliminate $FOXP3^+$Tregs, inhibit Macrophage polarization to M2 phenotype, and reduce the PD-L1 expression in cancer cells (106).

HIF-1α is a transcription activator that is reliant on oxygen levels. Through various mechanisms, including angiogenesis, cellular proliferation and survival, metabolic reprogramming, invasion and metastasis, maintenance of cancer stem cells, induction of genetic instability, and resistance to therapeutic interventions, the upregulation of its downstream genes contributes to the growth of tumors. Consequently, modulating the downstream signaling molecule of HIF-1α presents an opportunity to regulate the initiation and progression of tumors (107). Hypoxia increases the PD-L1 expression and induces apoptosis of cytotoxic T lymphocytes (CTLs), thereby promoting the immune escape of tumor cells (108, 109). According to research findings, the inhibitor echinocandin of HIF-1 α has been observed to augment the immune tolerance function of the PD-1/PD-L1 checkpoint in normal tissues. Additionally, it has been found to enhance both the quantity and efficacy of Tumor-infiltrating lymphocytes, thereby leading to a safer and more efficacious approach to immunotherapy (110). VEGF-A is a highly conserved secretory signaling protein known for its role in vascular development and angiogenesis (111). Targeting VEGF is a feasible strategy for preventing tumor growth and metastasis (112). Research has indicated that VEGF-A is critical in triggering tumor immunosuppression and boosting angiogenesis. VEGF-A encourages immune-suppressive cell growth, prevents T-cell infiltration of malignancies, and encourages T-cell depletion (113). In a mouse model of colorectal cancer (CT26) targeting VEGFR therapy, it was found that targeting VEGF-a-VEGFR can reduce the co-expression of inhibitory receptors (PD-1, Tim-3, CTLA-4, and Lag-3) related to T cell failure and restore the $CD8^+$ T cells infiltration into the tumor to produce IFN- γ ability (114). In mice, Sunitinib increased the $CD4^+$ and $CD8^+$ T cells proportion in Tumor-infiltrating lymphocytes (115). C-Jun is the most widely studied protein in the activator protein-1 (AP-1) complex and participates in many cell activities, like proliferation, apoptosis, survival, tumorigenesis, and tissue Morphogenesis (116). As an early stage of human colorectal cancer development, adenomas and adenocarcinomas have significantly higher levels of c-Jun protein expression (117). JNK1 is highly expressed in HCT116 colon and PANC1 pancreatic cancer cells. Using licorice chalcone A or knocking down JNK1 expression can inhibit the proliferation and colony formation of colon cancer and pancreatic cancer cells (118). STAT3 is a tumor-promoting oncogene shown in several tumors and is intimately linked to inflammation and immunity (119). In

the adaptive immune subgroup, elevated STAT3 activity can inhibit the aggregation of effector T cells, thereby inhibiting their anti-tumor effects (120–122). Targeting STAT3 may reduce tumor cell-intrinsic proliferation, increase tumor-infiltrating immune cell anti-tumor activity, and improve TME immune suppression (123). The molecular docking results indicate that the central genes and core components possess significant binding potential, indicating that BZD could inhibit colorectal cancer progression by targeting these key genes.

GO enrichment analysis shows that BZD treats colorectal cancer by regulating biological processes like cell proliferation, apoptosis, energy metabolism, and immune response. KEGG enrichment analysis results showed that PI3K-AKT, T-cell receptor, P53, and VEGF signaling pathway may be the potential key pathway of BZD in treating colorectal cancer. Numerous cancer forms hyperactivate or modify the PI3K-AKT signaling system, which controls cellular activities like survival, proliferation, growth, metabolism, angiogenesis, metastasis, and immune response (124, 125). PI3K activity suppression can decrease PD-L1 expression and heightened IFN-γ mediated anti-tumor effects (126). A specific inhibitor (IPI-549) that targets PI3K-γ has the potential to remodel the immune milieu within the tumor microenvironment (TME) and facilitate CTL-mediated tumor regression (127). The T-cell receptor (TCR) signaling pathway is vital in promoting the development, homeostasis, proliferation, differentiation of T cells, and the production of cytokines, thereby eliciting a robust anti-tumor immune response (128). The tumor cell cycle, aging, apoptosis, metabolism, and immune response are regulated by P53, a well-studied tumor suppressor gene (129, 130). Multiple plant components can inhibit the progression of colorectal cancer cells by upregulating p53 to induce G2/M phase arrest and cell apoptosis (131–133). The VEGF-VEGFR signaling pathway is widely recognized as the most crucial pathway for inducing angiogenesis. Inhibition of this cascade reaction has proven to be effective in the treatment of tumors (134). Extensive research has demonstrated that targeting the VEGF signaling pathway increases tumor $CD8^+$T cell invasion and activation, boosting T cell cytokine output (135–137).

To explore the anticancer mechanism of BZD, we first compared the expression differences of key genes (core genes in PPI and related genes in KEGG enrichment pathway in network pharmacology analysis) in mouse tumor tissues between the control and BZD group through qRT-PCR experiments. The experimental results showed that compared with the control group, the expression of Pik3r1, Akt1, Myc, Egfr, Hif1a, Vegfr, Jun, and Stat3 genes in the tumor tissue of mice in the BZD group was significantly reduced, and the Casp3 and Trp53 genes expression was significantly increased; this is consistent with the predicted results of network pharmacology. The results show that BZD can suppress colorectal cancer growth by modulating the above essential genes. Moreover, these key genes are closely related to the tumor immune microenvironment, uniquely T cell immune function. As a classic formula utilized in the "Fuzheng Guben" treatment principle, the main effect of BZD is to supplement both qi and blood and enhance the body's immune system. Considering BZD's main efficacy, qRT-PCR, and the T-cell receptor signal pathway in KEGG enrichment analysis, we used flow cytometry to detect T lymphocyte subsets in tumor-bearing mice's spleens. The results showed that compared to the control group, BZD significantly increased the number of $CD4^+$ and $CD8^+$T cells in the spleen of tumor-bearing mice, promoted T cell activation, and increased IFN-γ level. Furthermore, BZD reduced the number of $PD\text{-}1^+CD4^+$ and $PD\text{-}1^+CD8^+$ T cells. IFN-γ is the main cytokine that enhances the host's anti-tumor immune function and is stably produced during $CD8^+$ T cell differentiation into cytotoxic T lymphocytes and memory cells in response to TCR stimulation. Therefore, IFN-γ elevated expression effectively indicates $CD8^+$T cell activation and anti-tumor immune response. The lower $PD\text{-}1^+CD4^+$T cells and $PD\text{-}1^+CD8^+$T cell populations showed a decrease in depleted T cell proportion. We performed immunohistochemistry labeling on the tumor tissues of two groups of mice to determine T-cell infiltration and cancer cell growth. The results showed that compared to the control group, the infiltration of $CD3^+$, $CD4^+$, and $CD8^+$ T cells in the tumor tissue of the BZD group increased while the Ki67 expression decreased. Therefore, BZD can enhance the anti-colorectal cancer immune function by increasing T cell infiltration in tumor tissue. These immunological results are not only consistent with the tumor volume and weight in mice, but also consistent with the potential mechanisms of tumor inhibition by previous "Fu Zheng Gu Ben" formula, Liu Jun Zi Decoction, and Bu Shen Hui Yang formula (138, 139). Additionally, pathological results showed that BZD does not cause any organ damage and is considered safe.

To our knowledge, this study is the first to explore the efficacy and mechanism of BZD in the treatment of CRC. In this study, we accomplished the following work: (1) The core components, key targets, and signaling pathways of BZD in the treatment of CRC were analyzed using network pharmacology. (2) This study validated the good binding ability of core drug components to key targets through molecular docking. (3) This study verified through *in vitro* experiments that BZD inhibits the proliferation and invasion of CRC cells in a time- and dose-dependent manner, while promoting apoptosis of CRC cells. (4) This study verified through animal experiments that BZD can significantly inhibit the progression of CRC and has no organ toxicity. (5) Our experiments demonstrated that BZD inhibit CRC by regulating the core targets and signaling pathways in the tumor microenvironment. (6) BZD promotes T cell infiltration and activation in the spleen and tumor tissue of tumor bearing mice, inhibits PD-1 expression on the surface of T cells, restores T cell killing ability, and enhances immune function against colorectal cancer. However, it is undeniable that there are still deficiencies in our experiment. Although we have confirmed the anticancer effect of BZD on CRC, its underlying substance basis is not yet clear. Furthermore, the mechanism by which BZD inhibits CRC is not thorough enough. Therefore, in future studies, we will further explore the main active components and more detailed mechanisms of BZD in inhibiting CRC.

5 Conclusion

BZD treats CRC through multiple components, targets, and metabolic pathways. Our research confirmed BZD's anti-colorectal cancer efficacy for the first time and studied its essential components, core targets, and potential mechanism using network pharmacology, molecular docking, and experiments. BZD can reverse the abnormal expression of PI3K, AKT, MYC, EGFR, HIF-1A, VEGFR, JUN, STAT3, CASP3, and TP53 genes in the tumor microenvironment and inhibit the progression of colorectal cancer by regulating the signaling pathways such as PI3K-AKT, P53, and VEGF. In addition, BZD can promote infiltration and activation of T cells in tumor-bearing mice, suppress the expression of PD-1 on T cell surface, restore T cell cytotoxicity, enhance anti-tumor immune response, and inhibit the progression of colorectal cancer. Among them, quercetin, kaempferol, licochalcone A, naringenin, and formaronetin are more highly predictive components related to the T cell activation in colorectal cancer mice. This study may offer new perspectives to the treatment of colorectal cancer and provide new ideas for exploring new anticancer drugs. However, the main active ingredients and more detailed mechanisms of BZD inhibition on CRC still need to be further explored in future studies.

Data availability statement

The original contributions presented in the study are included in the article/supplementary materials, further inquiries can be directed to the corresponding author/s.

Ethics statement

The Ethics Committee of Beijing Shijitan Hospital Affiliated to Capital Medical University reviewed and granted approval for this study (The ethical approval permit numbers are SJTKY11-1X-2021 (59)). The study was conducted in accordance with the local legislation and institutional requirements.

Author contributions

SL and BR conceived and designed this study. SL, XS, ZZ, and QL conducted network pharmacology analysis. HT, BW, and JQ conducted molecular docking. JY, FS, and YT conducted statistical analysis. ZD and CL completed the figures. SL and RX completed *in vitro* and *in vivo* experiments. SL, XS, and ZZ wrote the manuscript. BR, PY, and ZY participated in the review and revision of the manuscript. All authors contributed to the article and approved the submitted version.

Funding

This research was supported by the National Key Research and Development Plan (2022YFC2009601) and Project of Beijing Key Laboratory (2020KF01).

Conflict of interest

The authors declare that the research was conducted in the absence of any commercial or financial relationships that could be construed as a potential conflict of interest.

Publisher's note

References

1. Sung H, Ferlay J, Siegel RL, Laversanne M, Soerjomataram I, Jemal A, et al. Global cancer statistics 2020: GLOBOCAN estimates of incidence and mortality worldwide for 36 cancers in 185 countries. *CA Cancer J Clin* (2021) 71(3):209–49. doi: 10.3322/caac.21660

2. Kuipers EJ, Grady WM, Lieberman D, Seufferlein T, Sung JJ, Boelens PG, et al. Colorectal cancer. *Nat Rev Dis Primers* (2015) 1:15065. doi: 10.1038/nrdp.2015.65

3. Brown KGM, Solomon MJ. Progress and future direction in the management of advanced colorectal cancer. *Br J Surg* (2018) 105(6):615–7. doi: 10.1002/bjs.10759

4. Matsuda T, Yamashita K, Hasegawa H, Oshikiri T, Hosono M, Higashino N, et al. Recent updates in the surgical treatment of colorectal cancer. *Ann Gastroenterol Surg* (2018) 2(2):129–36. doi: 10.1002/ags3.12061

5. Ooft SN, Weeber F, Dijkstra KK, McLean CM, Kaing S, van Werkhoven E, et al. Patient-derived organoids can predict response to chemotherapy in metastatic colorectal cancer patients. *Sci Trans Med* (2019) 11(513):eaay2574. doi: 10.1126/scitranslmed.aay2574

6. Halama N, Zoernig I, Berthel A, Kahlert C, Klupp F, Suarez-Carmona M, et al. Tumoral immune cell exploitation in colorectal cancer metastases can Be targeted effectively by anti-CCR5 therapy in cancer patients. *Cancer Cell* (2016) 29(4):587–601. doi: 10.1016/j.ccell.2016.03.005

7. Dekker E, Rex DK. Advances in CRC prevention: screening and surveillance. *Gastroenterology* (2018) 154(7):1970–84. doi: 10.1053/j.gastro.2018.01.069

8. Xu HY, Zhang YQ, Liu ZM, Chen T, Lv CY, Tang SH, et al. Etcm: An encyclopaedia of traditional Chinese medicine. *Nucleic Acids Res* (2019) 47(D1): D976–82. doi: 10.1093/nar/gky987

9. Luo X-Y, Wu K-M, He X-X. Advances in drug development for hepatocellular carcinoma: clinical trials and potential therapeutic targets. *J Exp Clin Cancer research: CR* (2021) 40(1):172. doi: 10.1186/s13046-021-01968-w

10. Kong M-Y, Li L-Y, Lou Y-M, Chi H-Y, Wu J-J. Chinese herbal medicines for prevention and treatment of colorectal cancer: From molecular mechanisms to potential clinical applications. *J Integr Med* (2020) 18(5):369–84. doi: 10.1016/j.joim.2020.07.005

11. Song YJ, Bao JM, Zhou LY, Li G, Sng KS, Wang YJ, et al. An analysis of the antineuropathic effects of qi she pill based on network pharmacology. *Evidence-Based Complement Altern Med* (2020) 2020:1–15. doi: 10.1155/2020/7193832

12. Song Y, Wang H, Pan Y, Liu T. Investigating the multi-target pharmacological mechanism of Hedyotis diffusa willd acting on prostate cancer: a network pharmacology approach. *Biomolecules* (2019) 9(10):591. doi: 10.3390/biom9100591

13. Ren B, Tan L, Xiong Y, Ji W, Mu J, Pei Y, et al. Integrated analysis of the mechanisms of da-chai-hu decoction in type 2 diabetes mellitus by a network pharmacology approach. *Evidence-Based Complement Altern Med* (2020) 2020 (10027):1–21. doi: 10.1155/2020/9768414

14. Meng Z, Liu X, Wu J, Zhou W, Wang K, Jing Z, et al. Mechanisms of compound kushen injection for the treatment of lung cancer based on network pharmacology. *Evidence-Based Complement Altern Med* (2019) 2019:1–15. doi: 10.1155/2019/4637839

15. Meng XY, Zhang HX, Mezei M, Cui M. Molecular docking: a powerful approach for structure-based drug discovery. *Curr Comput Aided Drug Des* (2011) 7(2):146–57. doi: 10.2174/157340911795677602

16. Guo W, Huang J, Wang N, Tan HY, Cheung F, Chen F, et al. Integrating network pharmacology and pharmacological evaluation for deciphering the action mechanism of herbal formula zuojin pill in suppressing hepatocellular carcinoma. *Front Pharmacol* (2019) 10:1185. doi: 10.3389/fphar.2019.01185

17. Liu J, Liu J, Tong X, Peng W, Wei S, Sun T, et al. Network pharmacology prediction and molecular docking-based strategy to discover the potential pharmacological mechanism of huai hua san against ulcerative colitis. *Drug Des Devel Ther* (2021) 15:3255–76. doi: 10.2147/DDDT.S319786

18. Lahans T. Integrating Chinese and conventional medicine in colorectal cancer 13 treatment. *Integr Cancer Therapies* (2007) 6(1):89. doi: 10.1177/1534735406298991

19. Cao X, Yan X. Clinical efficacy of Bazhen Tang combined with radiotherapy and chemotherapy in the treatment of cervical cancer and its impact on patient immune function, cancer-related fatigue, and toxic side effects. *Clin Med Res Pract* (2022) 7 (12):138–41. doi: 10.19347/j.cnki. 2096-1413.20221203

20. Yang H, Guo J, Jing R. The effect of modified Bazhen Tang combined with moxibustion on tolerance, analgesic effect, and quality of life in patients with advanced cervical cancer undergoing radiotherapy and chemotherapy. *Chin J Exp Prescript* (2018) 24(9):173–8.

21. Xu AH, Gong YX, Gu WR, Wang XW. Comparison of the effect of sijunzi decoction, siwu decoction and bazhen decoction on immune function in mice. *Zhongguo Zhong yao za zhi = Zhongguo zhongyao zazhi = China J Chin mater Med* (1993) 18(4):240–2, 256.

22. Liu X, Wang X, Li Z, Chen ,Y, Chen J. *In vitro* study for detecting the effects of Bazhen decoction on proliferation and activation of T lymphocytes. *Sheng wu yi xue gong cheng xue za zhi = J Biomed Eng = Shengwu yixue gongchengxue zazhi* (2010) 27 (4):855–8.

23. Wang H-x, Li J-p. Effects of modified bazhen decoction in assistant with enteral nutrition on the growth hormone, the nutritional state, and the immune function in patients with gastric cancer after operation. *Zhongguo Zhong xi yi jie he za zhi Zhongguo Zhongxiyi jiehe zazhi = Chin J integrated traditional Western Med* (2011) 31(10):1317–21.

24. Shi T, Chen B, Liu C, Lu K. Study on huangqi bazhen decoction on relieving chemotherapy intestinal mucositis in capecitabine gavage mice. *Contrast media Mol Imaging* (2022) 2022:3826080. doi: 10.1155/2022/3826080

25. Tian Y, Xiang Y, Wan G, Wan D, Zhu H. Effects and mechanisms of Bazhen decoction, Siwu decoction, and Sijunzi decoction on 5-fluorouracil-induced anemia in mice. *J traditional Chin Med = Chung i tsa chih ying wen pan* (2016) 36(4):486–95.

26. Lu X, Zheng Y, Wen F, Huang W, Shu P. Effectiveness and Safety of Oral Chinese Patent Medicines Combined with Chemotherapy for Gastric Cancer: A Bayesian Network Meta-Analysis. Evidence-based complementary and alternative medicine. *eCAM* (2020) 2020:8016531. doi: 10.1155/2020/8016531

27. Niu ZE, Jing DX, Xu CY. Clinical effect of bazhen decoction combined with sequential treatment of chemotherapy on acute lymphoblastic leukemia patients with deficiency of qi and yin. *Zhongguo Shi Yan Xue Ye Xue Za Zhi* (2022) 30(1):119–25. doi: 10.19746/J.CNKI.ISSN.1009-2137.2022.01.19

28. Zhang J, Xu J, Jin Z. The effect of modified Bazhen decoction combined with chemotherapy on the nutritional status and immune function of postoperative colon cancer patients. *J Anhui Univ Traditional Chin Med* (2023) 42(03):9–13.

29. Jiao J, Qu X, Ding B. The therapeutic effect of modified Bazhen Tang combined with chemotherapy on postoperative patients with gastric cancer. *J Pract Clin Med* (2019) 23(15):86–9.

30. Xu N, Xiao M, Luo T, Ma H, Liu Y. Clinical efficacy of Bazhen Tang as an adjuvant chemotherapy in the treatment of advanced non-small cell lung cancer in the elderly. *Clin Med Res Pract* (2021) 6(19):128–129+139. doi: 10.19347/j.cnki.2096-1413.202119040

31. Chen B, Sun J, Wang H. Bazhen Decoction combined with neoadjuvant chemotherapy in the treatment of 70 cases of breast cancer. *Natl Med Forum* (2021) 36(02):37–8. doi: 10.13913/j.cnki.41-1110/r.2021.02.016

32. Wu Y, Chen L. Modified Bazhen Tang combined with radiotherapy for the treatment of advanced cervical cancer and its effect on the cellular immune level and nutritional status of patients. *Shaanxi Traditional Chin Med* (2022) 43(08):1052–5.

33. Xu Z, Jin Y, Tao Z, Yu X, Fang M, Tong X. Clinical observation of modified Bazhen Tang combined with capecitabine in the maintenance treatment of elderly patients with advanced colon cancer. *Chin J Traditional Chin Med Sci Technol* (2022) 29(06):1123–5.

34. Zhou Y, Lv X. Observation on the efficacy of Bazhen Tang combined with chemotherapy in the treatment of advanced colon cancer. *World J Integrated Traditional Chin Western Med* (2020) 15(08):1524–7. doi: 10.13935/j.cnki.sjzx.200833

35. Xu Z, Wang C, Luan Z, Zhang D, Dong B. Exploring the potential targets of the *Abrus cantoniensis* Hance in the treatment of hepatitis E based on network pharmacology. *Front Vet Sci* (2023) 10:1155677. doi: 10.3389/fvets.2023.1155677

36. Wishart DS, Feunang YD, Guo AC, Lo EJ, Marcu A, Grant JR, et al. DrugBank 5.0:a major update to the DrugBank database for 2018. *Nucleic Acids Res* (2018) 46(D1): D1074–82. doi: 10.1093/nar/gkx1037

37. Mok SRS, Mohan S, Grewal N, Elfant AB, Judge TA. A genetic database can be utilized to identify potential biomarkers for biphenotypic hepatocellular carcinoma-cholangiocarcinoma. *J Gastrointest Oncol* (2016) 7(4):570–9. doi: 10.21037/jgo.2016.04.01

38. Li YH, Yu CY, Li XX, Zhang P, Tang J, Yang Q, et al. Therapeutic target databaseupdate 2018: enriched resource for facilitating bench-to-clinicresearch of targeted therapeutics. *Nucleic Acids Res* (2018) 46(D1):D1121–7. doi: 10.1093/nar/gkx1076

39. Piñero J, Queralt-Rosinach N, Bravo A, Deu-Pons J, Bauer-Mehren A, Baron M, et al. DisGeNET: a discovery platform for the dynamical exploration of human diseases and their genes. *Database* (2015) 2015(0):bav028. doi: 10.1093/database/bav028

40. Franz M, Lopes CT, Huck G, Dong Y, Sumer O, Bader GD. Cytoscape.js: a graph theory library for visualisation and analysis. *Bioinformatics* (2016) 32(2):309–11. doi: 10.1093/bioinformatics/btv557

41. Wang F, Yuan C, Wu HZ, Liu B, Yang YF. Bioinformatics, molecular docking and experiments in vitro analyze the prognostic value of CXC chemokines in breast cancer. *Front Oncol* (2021) 11:665080. doi: 10.3389/fonc.2021.665080

42. Chen Y, Zhou Q, Zhang H, Xu L, Lu L, Shu B, et al. Qingdai Decoction suppresses prostate cancer growth in lethal-stage prostate cancer models. *J Ethnopharmacol* (2023) 308:116333. doi: 10.1016/j.jep.2023.116333

43. Zhang M, Wu W, Huang C, Cai T, Zhao N, Liu S, et al. Shuxie-1 decoction alleviated CUMS -induced liver injury via IL-6/JAK2/STAT3 signaling. *Front Pharmacol* (2022) 13:848355. doi: 10.3389/fphar.2022.848355

44. Triplett TA, Garrison KC, Marshall N, Donkor M, Blazeck J, Lamb C, et al. Reversal of indoleamine 2,3-dioxygenase-mediated cancer immune suppression by systemic kynurenine depletion with a therapeutic enzyme. *Nat Biotechnol* (2018) 36 (8):758–64. doi: 10.1038/nbt.4180

45. Wu Y, Hao X, Wei H, Sun R, Chen Y, Tian Z. Blockade of T-cell receptor with Ig and ITIM domains elicits potent antitumor immunity in naturally occurring HBV-related HCC in mice. *Hepatology* (2023) 77(3):965–81. doi: 10.1002/hep.32715

46. Dai X, Lu L, Deng S, Meng J, Wan C, Huang J, et al. USP7 targeting modulates anti-tumor immune response by reprogramming Tumor-associated Macrophages in Lung Cancer. *Theranostics* (2020) 10(20):9332–47. doi: 10.7150/thno.47137

47. Kan X, Zhou G, Zhang F, Ji H, Shin DS, Monsky W, et al. Enhanced efficacy of direct immunochemotherapy for hepatic cancer with image-guided intratumoral radiofrequency hyperthermia. *J Immunother Cancer* (2022) 10(11):e005619. doi: 10.1136/jitc-2022-005619

48. Wu X, Zhang H, Xing Q, Cui J, Li J, Li Y, et al. PD-1(+) CD8(+) T cells are exhausted in tumours and functional in draining lymph nodes of colorectal cancer patients. *Br J Cancer* (2014) 111(7):1391–9. doi: 10.1038/bjc.2014.416

49. Siegel RL, Miller KD, Fuchs HE, Jemal A. Cancer statistics, 2022. *CA Cancer J Clin* (2022) 72:7–33. doi: 10.3322/caac.21708

50. Siegel RL, Miller KD, Goding Sauer A, Fedewa SA, Butterly LF, Anderson JC, et al. Colorectal cancer statistics, 2020. *CA Cancer J Clin* (2020) 70:145–164. doi: 10.3322/caac.21601

51. Global Burden of Disease 2019 Cancer Collaboration, Kocarnik JM, Compton K, Dean FE, Fu W, Gaw BL, Harvey JD, et al. Cancer incidence, mortality, years of life lost, years lived with disability, and disability- adjusted life years for 29 cancer groups from 2010 to 2019: a systematic analysis for the Global Burden of Disease Study 2019. *JAMA Oncol* (2021) 8(3):420–444. doi: 10.1001/jamaoncol.2021.6987

52. Ciardiello F, Ciardiello D, Martini G, Napolitano S, Tabernero J, Cervantes A. Clinical management of metastatic colorectal cancer in the era of precision medicine. *CA Cancer J Clin* (2022) 72(4):372–401. doi: 10.3322/caac.21728

53. Shi J, Sun Z, Gao Z, Huang D, Hong H, Gu J. Radioimmunotherapy in colorectal cancer treatment: present and future. *Front Immunol* (2023) 14:1105180. doi: 10.3389/fimmu.2023.1105180

54. Lin X, Yang X, Yang Y, Zhang H, Huang X. Research progress of traditional Chinese medicine as sensitizer in reversing chemoresistance of colorectal cancer. *Front Oncol* (2023) 13:1132141. doi: 10.3389/fonc.2023.1132141

55. Chen JF, Wu SW, Shi ZM, Hu B. Traditional Chinese medicine for colorectal cancer treatment: potential targets and mechanisms of action. *Chin Med* (2023) 18 (1):14. doi: 10.1186/s13020-023-00719-7

56. Li W, Li C, Zheng H, Chen G, Hua B. Therapeutic targets of Traditional Chinese Medicine for colorectal cancer. *J Tradit Chin Med* (2016) 36(2):243–9. doi: 10.1016/s0254-6272(16)30034-6

57. Fei Z, Lijuan Y, Xi Y, Wei W, Jing Z, Miao D, et al. Gut microbiome associated with chemotherapy-induced diarrhea from the CapeOX regimen as adjuvant chemotherapy in resected stage III colorectal cancer. *Gut Pathog* (2019) 11(1):18. doi: 10.1186/s13099-019-0299-4

58. Zimmer P, Trebing S, Timmers-Trebing U, Schenk A, Paust R, Bloch W, et al. Eight-week, multimodal exercise counteracts a progress of chemotherapy-induced peripheral neuropathy and improves balance and strength in metastasized colorectal

cancer patients: a randomized controlled trial. *Support Care Cancer* (2018) 26(2):615–24. doi: 10.1007/s00520-017-3875-5

59. Homayoonfal M, Gilasi H, Asemi Z, Khaksary Mahabady M, Asemi R, Y ousefi B. Quercetin modulates signal transductions and targets non-coding RNAs against cancer development. *Cell Signal* (2023) 107:110667. doi: 10.1016/j.cellsig.2023.110667

60. Golmohammadi M, Elmaghraby DA, Ramí rez-Coronel AA, Rakhimov N, Mohammed SS, Romero-Parra RM, et al. A comprehensive view on the quercetin impact on bladder cancer: Focusing on oxidative stress, cellular, and molecular mechanisms. *Fundam Clin Pharmacol* (2023) 37(5):900–9. doi: 10.1111/fcp.12896

61. Lotfi N, Y ousefi Z, Golabi M, Khalilian P, Ghezelbash B, Montazeri M, et al. The potential anti-cancer effects of quercetin on blood, prostate and lung cancers: An update. *Front Immunol* (2023) 14:1077531. doi: 10.3389/fimmu.2023.1077531

62. Sethi G, Rath P, Chauhan A, Ranjan A, Choudhary R, Ramniwas S, et al. Apoptotic mechanisms of quercetin in liver cancer: recent trends and advancements. *Pharmaceutics* (2023) 15(2):712. doi: 10.3390/pharmaceutics15020712

63. Maugeri A, Calderaro A, Patanè GT, Navarra M, Barreca D, Cirmi S, et al. Targets involved in the anti-cancer activity of quercetin in breast, colorectal and liver neoplasms. *Int J Mol Sci* (2023) 24(3):2952. doi: 10.3390/ijms24032952

64. Zhang J, Shen L, Li X, Song W, Liu Y, Huang L. Nanoformulated codelivery of quercetin and alantolactone promotes an antitumor response through synergistic immunogenic cell death for microsatellite-stable colorectal cancer. *ACS Nano* (2019) 13(11):12511–24. doi: 10.1021/acsnano.9b02875

65. Jing L, Lin J, Yang Y, Tao L, Li Y, Liu Z, et al. Quercetin inhibiting the PD-1/PD-L1 interaction for immune-enhancing cancer chemopreventive agent. *Phytother Res* (2021) 35(11):6441–51. doi: 10.1002/ptr.7297

66. Imran M, Salehi B, Sharifi- Rad J, Aslam Gondal T, Saeed F, Imran A, et al. Kaempferol: a key emphasis to its anticancer potential. *Molecules* (2019) 24(12):2277. doi: 10.3390/molecules24122277

67. Choi JB, Kim JH, Lee H, Pak JN, Shim BS, Kim SH. Reactive Oxygen Species and p53 Mediated Activation of p38 and Caspases is Critically Involved in Kaempferol Induced Apoptosis in Colorectal Cancer Cells. *J Agric Food Chem* (2018) 66(38):9960–7. doi: 10.1021/acs.jafc.8b02656

68. Huang X, Wang Y, Yang W, Dong J, Li L. Regulation of dietary polyphenols on cancer cell pyroptosis and the tumor immune microenvironment. *Front Nutr* (2022) 9:974896. doi: 10.3389/fnut.2022.974896

69. Hofer S, Geisler S, Lisandrelli R, Nguyen Ngoc H, Ganzera M, Schennach H, et al. Pharmacological targets of kaempferol within inflammatory pathways-A hint towards the central role of tryptophan metabolism. *Antioxid (Basel).* (2020) 9(2):180. doi: 10.3390/antiox9020180

70. Jia Z, Chen A, Wang C, He M, Xu J, Fu H, et al. Amelioration effects of Kaempferol on immune response following chronic intermittent cold-stress. *Res Vet Sci* (2019) 125:390–6. doi: 10.1016/j.rvsc.2019.08.012

71. Qiang D, Ci C, Liu W, Wang J, He C, Ji B, et al. Inhibitory effect of kaempferol on mouse melanoma cell line B16 *in vivo* and *in vitro*. *Adv Dermatol Allergol* (2021) 38:498–504. doi: 10.5114/ada.2020.94257

72. Wu H, Du J, Li C, Li H, Guo H, Li Z. Kaempferol can reverse the 5-fu resistance of colorectal cancer cells by inhibiting PKM2-mediated glycolysis. *Int J Mol Sci* (2022) 23(7):3544. doi: 10.3390/ijms23073544

73. Wu P, Y u T, Wu J, Chen J. Licochalcone a induces ROS-mediated apoptosis through trxR1 inactivation in colorectal cancer cells. *BioMed Res Int* (2020) 2020:5875074. doi: 10.1155/2020/5875074

74. Lee CK, Son SH, Park KK, Park JH, Lim SS, Kim SH, et al. Licochalcone A inhibits the growth of colon carcinoma and attenuates cisplatin-induced toxicity without a loss of chemotherapeutic efficacy in mice. *Basic Clin Pharmacol Toxicol* (2008) 103(1):48–54. doi: 10.1111/j.1742-7843.2008.00238.x

75. Y uan LW, Jiang XM, Xu YL, Huang MY, Chen YC, Y u WB, et al. Licochalcone A inhibits interferon-gamma-induced programmed death-ligand 1 in lung cancer cells. *Phytomedicine* (2021) 80:153394. doi: 10.1016/j.phymed.2020.153394

76. Liu X, Xing Y, Li M, Zhang Z, Wang J, Ri M, et al. Licochalcone A inhibits proliferation and promotes apoptosis of colon cancer cell by targeting programmed cell death-ligand 1 via the NF-κB and Ras/Raf/MEK pathways. *J Ethnopharmacol* (2021) 273:113989. doi: 10.1016/j.jep.2021.113989

77. Wu Y, Zhu J, Liu H, Liu H. Licochalcone A improves the cognitive ability of mice by regulating T- and B-cell proliferation. *Aging (Albany NY).* (2021) 13(6):8895–915. doi: 10.18632/aging.202704

78. Motallebi M, Bhia M, Rajani HF, Bhia I, Tabarraei H, Mohammadkhani N, et al. Naringenin: A potential flavonoid phytochemical for cancer therapy. *Life Sci* (2022) 305:120752. doi: 10.1016/j.lfs.2022.120752

79. Kawaguchi S, Kawahara K, Fujiwara Y. Naringenin potentiates anti-tumor immunity against oral cancer by inducing lymph node CD169-positive macrophage activation and cytotoxic T cell infiltration. *Cancer Immunol Immunother* (2022) 71 (9):2127–39. doi: 10.1007/s00262-022-03149-w

80. Wang L, Zeng W, Wang L, Wang Z, Yin X, Qin Y, et al. Naringenin enhances the antitumor effect of therapeutic V accines by promoting antigen cross-presentation. *J Immunol* (2020) 204(3):622–31. doi: 10.4049/jimmunol.1900278

81. Qin L, Jin L, Lu L, Lu X, Zhang C, Zhang F, et al. Naringenin reduces lung metastasis in a breast cancer resection model. *Protein Cell* (2011) 2(6):507–16. doi: 10.1007/s13238-011-1056-8

82. Gong G, Guan YY, Zhang ZL, Rahman K, Wang SJ, Zhou S, et al. Isorhamnetin: A review of pharmacological effects. *BioMed Pharmacother* (2020) 128:110301. doi: 10.1016/j.biopha.2020.110301

83. Paul A, Das S, Das J, Samadder A, Bishayee K, Sadhukhan R, et al. Diarylheptanoid-myricanone isolated from ethanolic extract of Myrica cerifera shows anticancer effects on HeLa and PC3 cell lines: signalling pathway and drug-DNA interaction. *J Integr Med* (2013) 11(6):405–15. doi: 10.3736/jintegrmed2013057

84. Dai G, Tong Y, Chen X, Ren Z, Yang F. *In vitro* anticancer activity of myricanone in human lung adenocarcinoma A549 cells. *Chemotherapy* (2014) 60(2):81–7. doi: 10.1159/000371738

85. Paul A, Das J, Das S, Samadder A, Khuda-Bukhsh AR. Anticancer potential of myricanone, a major bioactive component of Myrica cerifera: novel signaling cascade for accomplishing apoptosis. *J Acupunct Meridian Stud* (2013) 6(4):188–98. doi: 10.1016/j.jams.2013.05.003

86. Peng F, Du Q, Peng C, Wang N, Tang H, Xie X, et al. A review: the pharmacology of isoliquiritigenin. *Phytother Res Ptr* (2015) 29:969–77. doi: 10.1002/ptr.5348

87. Wang G, Yu Y, Wang Y-Z, Yin P-H, Xu K, Zhang H. The effects and mechanisms of isoliquiritigenin loaded nanoliposomes regulated AMPK/mTOR mediated glycolysis in colorectal cancer. *Artif Cells Nanomed Biotechnol* (2020) 48:1231–49. doi: 10.1080/21691401.2020.1825092

88. Wang KL, Yu YC, Hsia SM. Perspectives on the role of isoliquiritigenin in cancer. *Cancers (Basel)* (2021) 13(1):115. doi: 10.3390/cancers13010115

89. Tay KC, Tan LT, Chan CK, Hong SL, Chan KG, Yap WH, et al. Formononetin: A review of its anticancer potentials and mechanisms. *Front Pharmacol* (2019) 10:820. doi: 10.3389/fphar.2019.00820

90. Wang JY, Jiang MW, Li MY, Zhang ZH, Xing Y, Ri M, et al. Formononetin represses cervical tumorigenesis by interfering with the activation of PD-L1 through MYC and STAT3 downregulation. *J Nutr Biochem* (2022) 100:108899. doi: 10.1016/j.jnutbio.2021.108899

91. Li D, Wang G, Jin G, Yao K, Zhao Z, Bie L, et al. Resveratrol suppresses colon cancer growth by targeting the AKT/STAT3 signaling pathway. *Int J Mol Med* (2018) 43(1):630–40. doi: 10.3892/ijmm.2018.3969

92. Abu-Eid R, Samara RN, Ozbun L, Abdalla MY, Berzofsky JA, Friedman KM, et al. Selective inhibition of regulatory T cells by targeting the PI3KAkt pathway. *CancerImmunol Res* (2014) 2(11):1080–1089. doi: 10.1158/2326-6066.CIR-14-0095

93. Xu R, Wu J, Zhang X, Zou X, Li C, Wang H, et al. Modified Bu-zhong-yi-qi decoction synergies with 5 fluorouracile to inhibits gastric cancer progress via PD-1/PD- L1-dependent T cell immunization. *Pharmacol Res* (2020) 152:104623. doi: 10.1016/j.phrs.2019.104623

94. Schaub FX, Dhankani V, Berger AC, Trivedi M, Richardson AB, Shaw R, et al. Pan- cancer alterations of the MYC oncogene and its proximal network across The Cancer Genome Atlas. *Cell Syst* (2018) 6:282–300.e2. doi: 10.1016/j.cels.2018.03.003

95. Kalkat M, De Melo J, Hickman KA, Lourenco C, Redel C, Resetca D, et al. MYC deregulation in primary human cancers. *Genes* (2017) 8:151. doi: 10.3390/genes8060151

96. Carroll PA, Freie BW, Mathsyaraja H, Eisenman RN. The MYC transcription factor network: balancing metabolism, proliferation and oncogenesis. *Front Med* (2018) 12:412–25. doi: 10.1007/s11684-018-0650-z

97. Casey SC, Baylot V, Felsher DW. The MYC oncogene is a global regulator of the immune response. *Blood* (2018) 131:2007–15. doi: 10.1182/blood-2017-11-742577

98. Casacuberta- Serra S, Soucek L. Myc and Ras, the Bonnie and Clyde of immune evasion. *Transl Cancer Res* (2018) 7(Suppl. 4):S457–9. doi: 10.21037/tcr.2018.03.09

99. Yang C, Liu Y, Hu Y, Fang L, Huang Z, Cui H, et al. Myc inhibition tips the immune balance to promote antitumor immunity. *Cell Mol Immunol* (2022) 19 (9):1030–41. doi: 10.1038/s41423-022-00898-7

100. Zhou M, Liu X, Li Z, Huang Q, Li F, Li CY. Caspase-3 regulates the migration, invasion and metastasis of colon cancer cells. *Int J Cancer* (2018) 143(4):921–30. doi: 10.1002/ijc.31374

101. Dustin D, Gu G, Fuqua SAW. ESR1 mutations in breast cancer. *Cancer* (2019) 125(21):3714–28. doi: 10.1002/cncr.32345

102. Wang F, Fu X, Chen P, Wu P, Fan X, Li N, et al. SPSB1-mediated HnRNP A1 ubiquitylation regulates alternative splicing and cell migration in EGF signaling. *Cell Res* (2017) 27(4):540–58. doi: 10.1038/cr.2017.7

103. Hsu JL, Hung MC. The role of HER2, EGFR, and other receptor tyrosine kinases in breast cancer. *Cancer Metastasis Rev* (2016) 35:575–88. doi: 10.1007/s10555-016-9649-6

104. Rotow J, Bivona TG. Understanding and targeting resistance mechanisms in NSCLC. *Nat Rev Cancer* (2017) 17:637–58. doi: 10.1038/nrc.2017.84

105. Roskoski R Jr. The ErbB/HER family of protein-tyrosine kinases and cancer. *Pharm Res* (2014) 79:34–74. doi: 10.1016/j.phrs.2013.11.002

106. Madeddu C, Donisi C, Liscia N, Lai E, Scartozzi M, Macciò A. EGFR-mutated non-small cell lung cancer and resistance to immunotherapy: role of the tumor microenvironment. *Int J Mol Sci* (2022) 23(12):6489. doi: 10.3390/ijms23126489

107. Rashid M, Zadeh LR, Baradaran B, Molavi O, Ghesmati Z, Sabzichi M, et al. Up-down regulation of HIF-1α in cancer progression. *Gene* (2021) 798:145796. doi: 10.1016/j.gene.2021.145796

108. Barsoum IB, Koti M, Siemens DR, Graham CH. Mechanisms of hypoxia-mediated immune escape in cancer. *Cancer Res* (2014) 74(24):7185–90. doi: 10.1158/0008-5472.CAN-14-2598

109. Giatromanolaki A, Koukourakis IM, Balaska K, Mitrakas AG, Harris AL, Koukourakis MI. Programmed death-1 receptor (PD-1) and PD-ligand-1 (PD-L1) expression in non-small cell lung cancer and the immune-suppressive effect of anaerobic glycolysis. *Med Oncol* (2019) 36(9):1–12. doi: 10.1007/s12032-019-1299-4

110. Bailey CM, Liu Y, Liu M, Du X, Devenport M, Zheng P, et al. Targeting HIF-1α abrogates PD-L1-mediated immune evasion in tumor microenvironment but promotes tolerance in normal tissues. *J Clin Invest* (2022) 132(9):e150846. doi: 10.1172/JCI150846

111. Wiszniak S, Schwarz Q. Exploring the intracrine functions of VEGF-A. *Biomolecules* (2021) 11(1):128. doi: 10.3390/biom11010128

112. Siveen KS, Prabhu K, Krishnankutty R, Kuttikrishnan S, Tsakou M, Alali FQ, et al. Vascular endothelial growth factor (VEGF) signaling in tumour vascularization: potential and challenges. *Curr Vasc Pharmacol* (2017) 15(4):339–51. doi: 10.2174/1570161115666170105124038

113. Lapeyre-Prost A, Terme M, Pernot S, Pointet AL, Voron T, Tartour E, et al. Immunomodulatory activity of VEGF in cancer. *Int Rev Cell Mol Biol* (2017) 330:295–342. doi: 10.1016/bs.ircmb.2016.09.007

114. Voron T, Terme M. VEGF-A modulates expression of inhibitory checkpoints on CD8+ T cells in tumors. *J Exp Med* (2015) 212(2):139–48. doi: 10.1084/jem.20140559

115. Ozao-Choy J, Chen SH. The novel role of tyrosine kinase inhibitor in the reversal of immune suppression and modulation of tumor microenvironment for immune-based cancer therapies. *Cancer Res* (2009) 69(6):2514–22. doi: 10.1158/0008-5472.CAN-08-4709

116. Meng Q, Xia Y. c-Jun, at the crossroad of the signaling network. *Protein Cell* (2011) 2(11):889–98. doi: 10.1007/s13238-011-1113-3

117. Suto R, Tominaga K, Mizuguchi H, Sasaki E, Higuchi K, Kim S, et al. Dominant-negative mutant of c-Jun gene transfer: A novel therapeutic strategy for colorectal cancer. *Gene Ther* (2004) 11(2):187–93. doi: 10.1038/sj.gt.3302158

118. Yao K, Chen H, Lee MH, Li H, Ma W, Peng C, et al. a natural inhibitor of c-Jun N-terminal kinase 1. *Cancer Prev Res (Phila)* (2014) 7(1):139–49. doi: 10.1158/1940-6207.CAPR-13-0117

119. Jiang H, Liu X, Knolhoff BL, Hegde S, Lee KB, Jiang H, et al. Development of resistance to FAK inhibition in pancreatic cancer is linked to stromal depletion. *Gut* (2020) 69(1):122–32. doi: 10.1136/gutjnl-2018-317424

120. Rebe C, Ghiringhelli F. STAT3, a master regulator of anti-tumor immune response. *Cancers (Basel)* (2019) 11(9):1280. doi: 10.3390/cancers11091280

121. Huynh J, Chand A, Gough D, Ernst M. Therapeutically exploiting STAT3 activity in cancer - using tissue repair as a road map. *Nat Rev Cancer* (2019) 19:82–96. doi: 10.1038/s41568-018-0090-8

122. Yu H, Kortylewski M, Pardoll D. Crosstalk between cancer and immune cells: role of STAT3 in the tumour microenvironment. *Nat Rev Immunol* (2007) 7:41–51. doi: 10.1038/nri1995

123. Zou S, Tong Q, Liu B, Huang W, Tian Y, Fu X. Targeting STAT3 in cancer immunotherapy. *Mol Cancer* (2020) 19(1):145. doi: 10.1186/s12943-020-01258-7

124. Ersahin T, Tuncbag N, Cetin-Atalay R. The PI3K/AKT/mTOR interactive pathway. *Mol Biosyst* (2015) 11(7):1946–54. doi: 10.1039/C5MB00101C

125. Zhao R, Song Y, Wang Y, Huang Y, Li Z, Cui Y, et al. PD-1/PD-L1 blockade rescue exhausted CD8+ T cells in gastrointestinal stromal tumours via the PI3K/Akt/mTOR signalling pathway. *Cell Proliferation* (2019) 52(3):e12571. doi: 10.1111/cpr.12571

126. Gao Y, Yang J, Cai Y, Fu S, Zhang N, Fu X, et al. IFN-γ-mediated inhibition of lung cancer correlates with PD-L1 expression and is regulated by PI3K-AKT signaling. *Int J Cancer* (2018) 143(4):931–43. doi: 10.1002/ijc.31357

127. De Henau O, Rausch M, Winkler D, Campesato LF, Liu C, Cymerman DH, et al. Overcoming resistance to checkpoint blockade therapy by targeting PI3Kgamma in myeloid cells. *Nature* (2016) 539:443–7. doi: 10.1038/nature20554

128. Srikanth S, Gwack Y. Orai1-NFAT signalling pathway triggered by T cell receptor stimulation. *Mol Cells* (2013) 35(3):182–94. doi: 10.1007/s10059-013-0073-2

129. Huang J. Current developments of targeting the p53 signaling pathway for cancer treatment. *Pharmacol Ther* (2021) 220:107720. doi: 10.1016/j.pharmthera.2020.107720

130. Liu J, Zhang C, Wang J, Hu W, Feng Z. The Regulation of Ferroptosis by Tumor Suppressor p53 and its Pathway. *Int J Mol Sci* (2020) 21(21):8387. doi: 10.3390/ijms21218387

131. Jin J, Lin G, Huang H, Xu D, Yu H, Ma X, et al. Capsaicin mediates cell cycle arrest and apoptosis in human colon cancer cells via stabilizing and activating p53. *Int J Biol Sci* (2014) 10(3):285–95. doi: 10.7150/ijbs.7730

132. Li D, Wang G, Jin G, Yao K, Zhao Z, Bie L, et al. Resveratrol suppresses colon cancer growth by targeting the AKT/STAT3 signaling pathway. *Int J Mol Med* (2019) 43(1):630–40. doi: 10.3892/ijmm.2018.3969

133. Zhang S, Wang Y, Sun Y, Zhao G, Wang J, Liu L, et al. Hinokiflavone, as a MDM2 inhibitor, activates p53 signaling pathway to induce apoptosis in human colon cancer HCT116 cells. *Biochem Biophys Res Commun* (2022) 594:93–100. doi: 10.1016/j.bbrc.2022.01.032

134. Kim HJ, Kim SK, Kim BS, Lee SH, Park YS, Park BK, et al. Apoptotic effect of quercetin on HT-29 colon cancer cells via the AMPK signaling pathway. *J Agric Food Chem* (2010) 58(15):8643–50. doi: 10.1021/jf101510z

135. Liu G, Chen T, Ding Z, Wang Y, Wei Y, Wei X. Inhibition of FGF-FGFR and VEGF-VEGFR signalling in cancer treatment. *Cell Prolif* (2021) 54(4):e13009. doi: 10.1111/cpr.13009

136. de Almeida PE, Mak J, Hernandez G, Jesudason R, Herault A, Javinal V, et al. Anti-VEGF treatment enhances $CD8^+$ T-cell antitumor activity by amplifying hypoxia. *Cancer Immunol Res* (2020) 8(6):806–18. doi: 10.1158/2326-6066.CIR-19-0360

137. Adachi Y, Kamiyama H, Ichikawa K, Fukushima S, Ozawa Y, Yamaguchi S, et al. Inhibition of FGFR reactivates IFNγ Signaling in tumor cells to enhance the combined antitumor activity of lenvatinib with anti-PD-1 antibodies. *Cancer Res* (2022) 82(2):292–306. doi: 10.1158/0008-5472.CAN-20-2426

138. Han Y, Fan X, Fan L, Wu Y, Zhou Z, Wang G, et al. Liujunzi decoction exerts potent antitumor activity in oesophageal squamous cell carcinoma by inhibiting miR-34a/STAT3/IL-6R feedback loop, and modifies antitumor immunity. *Phytomedicine* (2023) 111:154672. doi: 10.1016/j.phymed.2023.154672

139. Wang Y, Tan J, Hu P, Pei Q, Wen Y, Ma W, et al. Traditional Chinese medicine compound, Bu Sheng Hui Yang Fang, promotes the proliferation of lymphocytes in the immunosuppressed mice potentially by upregulating IL-4 signaling. *BioMed Pharmacother* (2021) 134:111107. doi: 10.1016/j.biopha.2020.111107

frontiers | Frontiers in Immunology

TYPE Review
PUBLISHED 13 November 2023
DOI 10.3389/fimmu.2023.1269341

OPEN ACCESS

EDITED BY
Ganesan Ramamoorthi,
Moffitt Cancer Center, United States

REVIEWED BY
Jianwei Zhang,
The Sixth Affiliated Hospital of Sun Yat-sen University, China
Srijayaprakash Babu Uppada,
Emory University, United States

*CORRESPONDENCE
Meng Qiu
qiumeng@hotmail.com

†These authors have contributed equally to this work

RECEIVED 29 July 2023
ACCEPTED 25 October 2023
PUBLISHED 13 November 2023

CITATION
Chen J-T, Zhou Y-W, Han T-R, Wei J-L and Qiu M (2023) Perioperative immune checkpoint inhibition for colorectal cancer: recent advances and future directions. *Front. Immunol.* 14:1269341. doi: 10.3389/fimmu.2023.1269341

Perioperative immune checkpoint inhibition for colorectal cancer: recent advances and future directions

Jiao-Ting Chen[1†], Yu-Wen Zhou[1†], Ting-Rui Han[2], Jun-Lun Wei[2] and Meng Qiu[1*]

[1]Department of Colorectal Cancer Center, West China Hospital, Sichuan University, Chengdu, China, [2]West China School of Medicine, Sichuan University, Chengdu, China

For colorectal cancer (CRC), surgical resection remains essential for achieving good prognoses. Unfortunately, numerous patients with locally advanced CRC and metastatic CRC failed to meet surgical indications or achieve pathological complete response after surgery. Perioperative therapy has been proven to effectively lower tumor staging and reduce recurrence and metastasis. Immune checkpoint inhibitors (ICIs) have shown unprecedented prolongation of survival time and satisfactory safety in patients with high microsatellite instability/deficient mismatch repair (MSI-H/dMMR), while the therapeutic effect obtained by patients with mismatch repair-proficient or microsatellite stable (pMMR/MSS) was considered minimal. However, recent studies found that certain CRC patients with dMMR/MSI-H presented intrinsic or acquired immune resistance, and pMMR/MSS CRC patients can also achieve better efficacy. Therefore, more predictors are required for screening patients with potential clinical benefits. Since the discovery of synergistic effects between immunotherapy, chemotherapy, and radiotherapy, different immunotherapy-based therapies have been applied to the perioperative therapy of CRC in an increasing number of research. This review comprehensively summarized the past and current progress of different combinations of immunotherapy in perioperative clinical trials for CRC, focusing on the efficacy and safety, and points out the direction for future development.

KEYWORDS

colorectal cancer, perioperative therapy, immune checkpoint inhibition, microsatellite instability-high, mismatch repair deficiency, mismatch repair proficiency, microsatellite stable

1 Introduction

Colorectal cancer (CRC) is the third most common cancer and the leading cause of cancer death worldwide (1–4). Due to the lack of early symptoms, 36% of patients were diagnosed with locally advanced CRC (LACRC) (stage II (cT3–4, N0)/stage III (any cT, N+)), and 22% presented with distant metastasis (5). The perioperative therapy (days before

and after surgery) is of great significance in promoting tumor downgrading and reducing the local recurrence and metastasis, including neoadjuvant (preoperative) therapy and adjuvant (postoperative) therapy (6–9). Given the compelling long-term durable remission in metastatic CRC (mCRC), immune checkpoint inhibitors (ICIs) have attracted great attention in the perioperative therapy of CRC. DNA mismatch repair (MMR) and Microsatellite instability (MSI) are considered important predictors of sensitivity for immunotherapy-based strategies (10) DNA mismatch repair (MMR) is an important pathway to maintain genomic stability (10, 11). Microsatellites are highly polymorphic repetitive DNA sequences in the human genome and MSI is defined as genomic instability in cancer cells due to a deficiency in MMR (dMMR) (10–12). MSI CRC accounts for 15% of all sporadic CRC, which can be divided into MSI-high (MSI-H) and MSI-low (MSI-L) according to the frequency of microsatellite marker instability (10, 11, 13). The remaining CRC is classified as microsatellite stable (MSS), with proficiency in MMR (pMMR) (10, 11). dMMR/MSI-H CRC is associated with a higher tumor mutation burden and neoantigen load and more lymphocyte infiltration than pMMR/MSS/MSI-L CRC (10, 11, 14).

dMMR/MSI-H CRC patients, whose sensitivity to ICIs is significantly higher than that of patients with pMMR/MSS/MSI-L, have derived notable pathological responses from neoadjuvant immunotherapy (14–17). However, 40% -60% of MSI-H CRC are inherently resistant to immunotherapy (14, 18) Therefore, the main challenge is to provide more benefits of immunotherapy for the majority of patients with pMMR, MSS, MSI-L, or insensitive MSI-H CRC (19) Fortunately, it is discovered that there is a synergistic effect between immunotherapy, chemotherapy, and radiotherapy (20, 21). An increasing number of clinical trials have explored the efficacy and safety of different immunotherapy-based therapies in the perioperative period (6, 17). Therefore, this article comprehensively reviewed previous achievements and the latest progress of different immunotherapy combination therapies in the perioperative period, which may provide new therapy strategies for CRC patients to achieve better efficacy and safety, as well as the mechanism of immunotherapy combination therapy and promising predictors to identify the patients with potential benefits.

2 Overview of immunotherapy for colorectal cancer

2.1 Current status of immunotherapy for colorectal cancer

In 2015, after a phase 2 clinical trial first proved that MSI CRC was a potential beneficiary, ICIs has been explored more extensively in CRC (22). Thereafter the impressive efficacy and safety of CheckMate-142 (23) and KEYNOTE-177 (16) in the treatment of dMMR/MSI-H mCRC promoted the Food and Drug Administration (FDA) 's approval of pembrolizumab, a programmed cell death-1 (PD-1) inhibitor, as the first-line treatment for MSI-H advanced CRC. Recently, ipilimumab combined with nivolumab, inhibitors of a cytotoxic T-lymphocyte-associated protein 4 (CTLA-4) and PD-1, has also been granted approval by the FDA for the treatment of dMMR/MSI-H mCRC (15, 24). The encouraging results motivated researchers to investigate the application of immunotherapy in the perioperative period of CRC. Recently, studies on immunotherapy combined with chemoradiotherapy and targeted drugs have been emerging. Additionally, various immunotherapy strategies have been developed to change the situation of "cold tumor" treatment, such as oncolytic virus (25, 26), cytokine therapy (27), and chimeric antigen receptor T cell therapy (28, 29).

At present, the MMR/MSI system has become the most important classification standard for CRC (30, 31). dMMR/MSI-H represents a good prognosis in early-stage CRC, while in metastatic disease it seems to confer a poor prognosis (10). Moreover, there is evidence showing that patients with dMMR/MSI-H CRC can obtain high reactivity of ICIs therapy, but for a majority of patients with pMMR or MSS, the clinical benefits from ICIs are generally minimal (12, 14, 17, 18, 32–37). However, recent studies have shown that certain CRC patients with MSI-H presented intrinsic or acquired immune resistance, while the patients with pMMR/MSS can also achieve a higher pathological complete response (pCR) rate (38, 39). Therefore, the optimal biomarkers for screening patients with potential clinical benefits are needed (40).

2.2 Potential predictive indicators for perioperative immunotherapy

Currently, an increased tumor mutation burden has been observed in MSI-H CRC patients who benefit from immunotherapy, as well as MSS CRC patients, which is considered another effective biomarker (14, 19, 32). Moreover, research has identified two distinct subtypes, MSI-H1 and MSI-H2, each with different prognostic implications (41). Notably, the MSI-H1 subgroup, enriched with M2 macrophages and characterized by high PD-L2 expression, tends to indicate a lower survival rate (41). Among dMMR CRCs, beta-2-microglobulin mutations that result in complete beta-2-microglobulin loss are associated with reduced recurrence and metastasis (19).

Assessing the extent of infiltration and co-expression of $CD8^+$ and PD-1 of T cells in tumors may be warranted to predict the overall survival rate and pCR rate of pMMR patients (38, 42). Additionally, polymerase epsilon exonuclease domain mutations (POLE EDM) (43–45), guanylate binding protein 2 expression (46), and soluble PD-L1 level may also be promising indicators to identify the pMMR patients with a favorable response to ICIs. Furthermore, CMTM6 expression in M2 macrophages (47), circulating L-arginine (48), the human gastrointestinal microbiome (49), fibroblast growth factor receptor 1-3 deficiency (50), and circulating tumor DNA (45, 51) may also play crucial roles in monitoring immunotherapy efficacy.

2.3 The mechanism of immunotherapy combination therapy

2.3.1 Immunotherapy combinations

PD-1 and CTLA-4 are key immune checkpoints for T cells, PD-1 and programmed death-ligand 1 (PD-L1) play a role by inhibiting the proximal signaling of T cell antigen receptor, while CTLA-4 weakens costimulatory signals through the co-receptor CD28, suppressing T cell activation (52, 53). Excessive activation or expression of immune checkpoints in cancer may promote malignant proliferation and metastasis (53). Therefore, PD-1-CTLA-4 inhibitors may have a synergistic effect by simultaneously inhibiting both pathways, achieving better therapeutic effects than ICIs monotherapy. However, the effective response to PD-1 blocking requires more tumor-infiltrating lymphocytes in the tumor microenvironment, which also indicates that pMMR tumors have limited efficacy owing to the lack of tumor-infiltrating lymphocytes (54) (Figure 1).

2.3.2 Immunotherapy in combination with chemotherapy or radiotherapy

The positive effects of standard chemotherapy on tumor immunity are mainly reflected in inducing immunogenic cell death and disrupting tumor escape strategies (21). Taxanes can elevate the activity of toll-like receptors and promote the activation of dendritic cells (21). Cyclophosphamide can deplete Treg cells, reducing the inhibition of tumor-infiltrating T cells (55). Therefore, the immune enhancement effect of chemotherapy may have a synergistic effect with immunotherapy. However, owing to its non-targeted effect, excessive chemotherapy can also lead to the depletion or dysfunction of immune cells (21).

Radiation induces tumor cell damage that releases a large amount of damage-associated molecular patterns, increasing the formation of tumor-infiltrating lymphocytes and memory response (56). $CD8^+$T cells release γ-interferon that upregulates the expression of PD-L1 in tumor cells, thereby exerting a synergistic effect with ICIs (20). In the previous research, when CTLA-4 inhibitor was added to radiation, radiosensitizing anti-CTLA-4 immunotherapy was observed in breast and CRC (20).

2.3.3 Tumor resection and immunotherapy

Compared with adjuvant therapy, neoadjuvant ICIs can induce stronger and more extensive tumor-specific T cell responses, reduce the incidence of toxicity, have better compliance, and may even achieve clinical complete remission and avoid unnecessary surgery (42). Although Jiahao Zhu et al. believed that surgery can cause a decrease in tumor antigens, and damage to blood vessels and lymph nodes in the surgical area, leading to reduced survival benefits of adjuvant ICIs (33), effective adjuvant therapy may be necessary for diminishing small residual lesions and preventing recurrence and metastasis, especially for the patients that didn't achieve pCR after surgery (57).

3 Perioperative immune checkpoint inhibition for colorectal cancer

3.1 ICIs monotherapy

The initial case report showed that two dMMR locally advanced rectal cancer (LARC) patients received PD-1 inhibitors (nivolumab) monotherapy to avoid adverse events (AEs) of chemoradiotherapy, which also enabled them to achieve pCR and clinical complete remission, and the latter adopted the observation and waiting (W&W) strategy without surgery (58). Moreover, the dMMR LACRC patients who are not eligible for chemotherapy, receiving

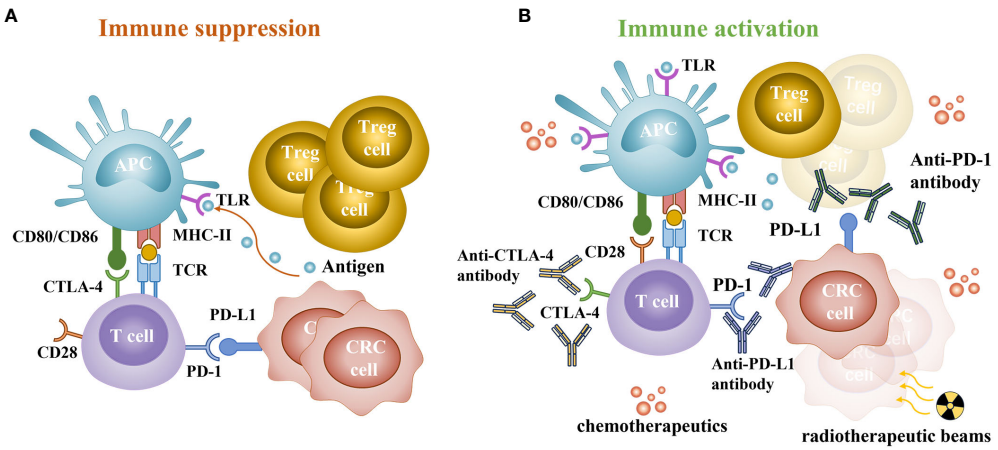

FIGURE 1
Immune status of patients with colorectal cancer. **(A)** The main way of immune suppression. CTLA-4 can competitively bind to CD80 or CD86 and inhibit activation. PD-1 is a key checkpoint for T cells, interacting with abnormally upregulated PD-L1 on cancer cells and immune cells, leading to T cell depletion and immune evasion. **(B)** The synergistic effect of chemoradiotherapy and immunotherapy. PD-1/PD-L1 and CTLA-4 checkpoint inhibitors can inhibit the negative feedback regulation of cancer cells and restore the anticancer function of T cells. Chemotherapeutics can induce immunogenic cell death and disrupt tumor escape strategies, increase the activity and quantity of toll-like receptors (TLR), promote DCs activation, deplete Treg cells, and reduce inhibition of T cells. Radiation induces tumor cell damage, releases a large number of damage-associated molecular patterns, and increases the formation and memory response of tumor-infiltrating lymphocytes.

anti-PD-1 inhibitors (pembrolizumab) monotherapy can also get pCR (59).

Further researches have also confirmed the value of ICIs in neoadjuvant therapy for CRC (Table 1). In a prospective phase 2 study (NCT04165772) (64), 12 patients with LARC received neoadjuvant PD-1 inhibitors (dostarlimab) monotherapy. Surprisingly, all patients achieved clinical complete remission, and no grade 3/4 AEs were reported. Moreover, Han, Kai, et al. (76) observed a high incidence rate (27.6%) of dMMR in 268 T4bM0 CRC patients. The pCR rate of the neoadjuvant ICIs monotherapy (pembrolizumab or nivolumab) group was significantly higher than that of the chemoradiotherapy group (70.0% *vs.* 0%). Compared with neoadjuvant chemotherapy and chemoradiotherapy, it significantly reduced the incidence of open surgery and had better disease-free survival and relatively longer overall survival. These results are also consistent with other researches (71, 72, 77, 78). Other neoadjuvant PD-1 inhibitors (toripalimab (45), sintilimab (73)) monotherapy may also have similar efficacy. A multicenter phase II study (NCT05662527) will further evaluate the efficacy and safety of neoadjuvant pembrolizumab in patients with stage I–III dMMR colon cancer (79).

Therefore, neoadjuvant monotherapy based on ICIs can significantly improve the pCR rate and avoid unnecessary surgeries, especially for those are ineligible for chemotherapy, which may translate into long-term survival benefits for dMMR LACRC, with acceptable safety and a low recurrence rate (64, 76). However, there is still a large proportion of patients who failed to achieve pCR after surgery. Effective adjuvant therapy may be necessary to reduce micro-diseases and prevent recurrence and metastasis (57). While there are limited researches on adjuvant ICIs monotherapy. Lynch syndrome is a common form of familial CRC associated with alterations in four DNA MMR genes (80). A case report shows that a Lynch syndrome patient with peritoneal metastasis received nivolumab as adjuvant therapy, achieving pCR, and no recurrence was observed during a 9-month follow-up (81). A retrospective study (75) suggests that dMMR/MSI-H LACRC patients who have received neoadjuvant immunotherapy can further improve their pCR rate to 75.9% by combining adjuvant anti-PD-1 treatment based on their postoperative efficacy. These researches indicated that adjuvant ICIs monotherapy can be a promising option for mCRC and LACRC. To further determine this advantage, a phase III clinical trial (NCT03803553) will evaluate the efficacy of adjuvant PD-I inhibitor (nivolumab) versus standard adjuvant chemotherapy in MSI-H CRC patients (75).

3.2 Immunotherapy doublet therapy

3.2.1 Immunotherapy combinations

In the NICHE study (NCT03026140) (35), early-stage dMMR colon cancer patients receiving neoadjuvant CTLA-4 inhibitor (ipilimumab) and PD-1inhibitor (nivolumab) gained better pathological responses (5). The NICHE 2 study further expanded the sample size, with a pCR rate of 67% (72/112) and 5 patients experiencing 3/4 grade AEs (37). However, this combination did not indicate significant improvement in pMMR patients (35). Similarly, compared to perioperative chemotherapy (82), combining anti-CTLA-4 (tremelimumab) and anti-PD-L1 (durvalumab) did not significantly prolong median relapse-free survival (9.7 months) and overall survival (24.5 months) in pMMR CRC patients with liver metastasis (36). Numerous studies have confirmed the efficacy and safety of immunotherapy combinations, which has promoted the NCCN guidelines (v2.2022) to recommend nivolumab ± ipilimumab or pembrolizumab as neoadjuvant treatment options for resectable dMMR/MSI-H mCRC (35, 83). But current immunotherapy combinations did not improve the efficacy of pMMR patients with early-stage CRC or mCRC significantly. Nonetheless, the safety of immunotherapy combinations has been confirmed for pMMR CRC (36, 83).

3.2.2 Chemotherapy and immunotherapy combination

Recently, two studies on immunotherapy combined with chemotherapy are underway, which will address the issue of whether the synergistic effect can also appear in perioperative therapy of LACRC. ATOMIC study (NCT02912559) (84) is exploring the efficacy of PD-L1 inhibitors (atezolizumab) combined with chemotherapy versus adjuvant chemotherapy in dMMR stage III CRC, with the primary endpoint being disease-free survival. Although the POLE EDM indicates a better response of CRC to immunotherapy plus chemotherapy, there seems to be no similar improvement in advanced CRC (43, 85). Therefore, the POLEM trial (NCT03827044) (85) aims to investigate whether adjuvant chemotherapy combined with PD-L1 inhibitor (avelumab) can improve disease-free survival in stage III dMMR/MSI-H/POLE EDM colon cancer patients.

3.2.3 Radiotherapy and immunotherapy combination

The potential synergistic effect of immunotherapy and radiotherapy has prompted extensive research to validate its efficacy in various cancers (86–89). Not limited to dMMR-mCRC, it was reported that local radiotherapy combined with PD-1 inhibitor (sintilimab) (90) or PD-L1 inhibitor (tislelizumab) (91) can overcome the immune resistance of pMMR mCRC. Several researches are ongoing to investigate whether the synergistic effect appears in LARC. Li et al. are conducting a multicenter Ib phase study to investigate the safety and efficacy of PD-1 inhibitor (sintilimab) combined with radiotherapy for MSI-H/dMMR rectal cancer (92). Another Phase II study will evaluate whether neoadjuvant anti-PD-1therapy (pembrolizumab) and radiotherapy can improve the safety and efficacy of LARC patients (93).

3.2.4 Chemoradiotherapy and immunotherapy combination

Although two researches applying PD-1 inhibitors (nivolumab (74) and pembrolizumab (65), respectively) combined with chemotherapy showed no significant improvement in pCR rate, another study on 980 LARC patients suggested that the pCR rate of

TABLE 1 Clinical trials involving perioperative immunotherapy in CRC.

Types	Identifier	Trial phase	Period	Treatment	Case	PCR (case, %)	MPR (case, %)	TRAEs ≥grade 3 (case, %)	R0 resection (case, %)	Study time	References
LARC	NCT04911517	2	Neoadjuvant	CRT + concurrent Tislelizumab	50	(13, 50)	(21, 80.7)	(2, 7.7)	(27, 100)	2021/6-2024/12	(39)
LARC	NCT04518280	NA	Neoadjuvant	SCRT→ CAPOX + Toripalimab: 65 CAPOX + Toripalimab→ SCRT→ CAPOX + Toripalimab:65	130	NA	NA	NA	NA	2021/5-2023/12	(60)
LARC	NCT05176964	2	Neoadjuvant	SCRT→ CAPOX + Tislelizumab	50	NA	NA	NA	NA	2021/12-2024/12	(61)
LARC (Stage II-III)	NCT03854799	2	Neoadjuvant	CRT with Avelumab→ TME	MSI-H:1, MSS:38, Unkown: 62	(22, 23)	(59, 61.5)	(12, 12)	NA	2019/8-2023/12	(62)
dMMR/ pMMR CC	NCT03026140	2	Neoadjuvant	Ipilimumab→ Nivolumab	dMMR:32 pMMR:30	dMMR: (22, 68.8) pMMR: (3, 10)	dMMR: (31, 96.9) pMMR: (7, 23.3)	(7, 12)	(35, 100)	2017/3-2024/12	(35)
dMMR/MSI-H CC	NCT03026140	2	Neoadjuvant	Ipilimumab→ Nivolumab	112	(72, 67)	(102, 95)	(5, 4)	NA	2017/3-2024/12	(37)
LARC	NCT05420584	2	Neoadjuvant	chemotherapy→ Tislelizumab	30	NA	NA	NA	NA	2022/11-2024/12	(63)
dMMR/MSI-H CRC	NCT03926338	2	Neoadjuvant	Toripalimab: 17 Toripalimab + Celecoxib: 17	34	(15, 88) (11, 65)	NA	(1, 3)	(34, 100)	2019/5-2024/5	(17)
dMMR RC	NCT04165772	2	Neoadjuvant	dostarlimab→ CRT	16	(12, 100)	NA	0	NA	2019/12-2025/11	(64)
dMMR/ pMMR CRC	NA	NA	Neoadjuvant	Tremelimumab + Durvalumab→ Durvalumab	pMMR:21 dMMR:2	dMMR: (2, 100) pMMR: (2, 9)	dMMR: (2, 100) pMMR: (5, 22)	(5, 22)	(17, 74)	2016/11-2019/11	(36)
LARC	NCT02921256	2	Neoadjuvant	PA: FOLFOX + NCRT + Pembrolizumab: 90 CA: FOLFOX +: 95	185	PA: (22, 31.9) CA: (20, 29.4)	NA	PA: (33, 48.2) CA:(25, 37.3)	PA: (65, 94) CA: (61, 89.4)	2016/10-2023/3	(65)
MSS/MSI-H LARC	NCT04231552	2	Neoadjuvant	SCRT→ CapeOX + Camrelizumab→ Surgery	dMMR: 1 pMMR: 28 Unknown: 1	dMMR: (1, 100) pMMR: (12, 46.2)	NA	(8, 26.7)	(27, 100)	2019/11-2022/9	(50)

(Continued)

10.3389/fimmu.2023.1269341

TABLE 1 Continued

Types	Identifier	Trial phase	Period	Treatment	Case	PCR (case, %)	MPR (case, %)	TRAEs ≥grade 3 (case, %)	R0 resection (case, %)	Study time	References
LARC	NA	3	Neoadjuvant	SCRT→ chemotherapy + Camrelizumab:37 SCRT→ chemotherapy: 61	980	(18, 49.2) (13, 21.6)	NA	(26, 26.6)	(1, 1.6) (0, 0)	2015/1-2021/12	(66)
LARC (Stage II-III)	NCT04083365	2	Neoadjuvant	CRT +Durvalumab→ Surgery	60	(19, 34.5)	NA	(4, 7.3)	NA	2019/11-2021/8	(67)
LARC	NCT03503630	2	Neoadjuvant	SCRT→FOLFOX6 + Avelumab→ TME	44	(15, 37.5)	(27, 67.5)	(31, 70.5)	NA	2018/7-2024/6	(68)
dMMR LARC	NCT04340401	2	Neoadjuvant	CapeOX + Camrelizumab→ Radiotherapy→ CapeOX→ Surgery	27	(7, 33.3)	(7, 33.3)	Lymphopenia: 24 Diarrhea: 8 Thrombocytopenia:4	NA	2020/5-2022/8	(69)
CRC	NA	NA	Neoadjuvant	PD-1:26dMMR CapeOx + PD-1 + SCRT/LCRT: 68pMMR	94	dMMR: (15, 57.7) pMMR: (24, 35.3)	(17, 65.4) (40, 58.8)	(35, 37.2)	(94, 100)	2017/1-2021/10	(70)
LARC	NA	NA	Neoadjuvant	PD-1 inhibitors or cytotoxic chemotherapy	73	(22, 59.5)	(23, 62.2)	(8, 11.0)	(38, 100)	2017/10-2021/12	(71)
dMMR/MSI-H LACRC	NA	NA	Neoadjuvant	Sintilimab	11	(10, 90.9)	(11, 100)	0	NA	2020/6-2022/6	(72)
dMMR LARC	NCT04304209	2	Neoadjuvant	Sintilimab	17	pCR:(3, 17.6) cCR: (9, 52.9)	(12, 75)	(1, 16)	NA	2016/10-2022/6	(73)
MSS/MSI-H LARC	NCT02948348	1/2	perioperative	CRT + Nivolumab→ surgery→ FOLFOX or XELOX	MSS:37, MSI-H5	MSS: (11, 30) MSI-H: (3, 60)	NA	MSS: (4, 10.3) MSH:0	NA	2017/1-2020/12	(74)
dMMR/MSI-H CRCs	NA	NA	perioperative	neoadjuvant PD-1 inhibitor: 32 perioperative PD-1 inhibitor: 22	32	(22, 75.9)	NA	0	(29, 100)	2019/6-2021/6	(75)

NA, not available; CRC, colorectal cancer; CC, colon cancer; CRT, chemoradiotherapy; pCR, pathologic complete response; MPR, major pathological response rate; cCR, clinical complete remission; TEAEs, Treatment-emergent Adverse Events; OS, Overall Survival; LARC, locally advanced rectal cancer; MSI-H/dMMR, high microsatellite instability/deficient mismatch repair; pMMR, mismatch repair-proficient; MSS, microsatellite stable; TME, total mesorectal excision.

10.3389/fimmu.2023.1269341

the SCRT with immunotherapy (PD-1 inhibitor camrelizumab) group was higher than that of the non-immunotherapy group (49.2% *vs* 21.6%) (66). The significant differences in this large-scale study manifested the effectiveness and safety of combined immunotherapy. In a phase II trial (NCT04231552) (50), patients with advanced rectal cancer received CAPOX combined with PD-1 inhibitor (camrelizumab) after SCRT and reached a higher pCR rate of 46.2% than that of the combination of PD-L1 inhibitor (avelumab) and mFOLFOX6 after SCRT (37.5%) (68). While it is worth noting that the mid-term results of a phase II trial (NCT04911517) (39) showed that in pMMR LARC patients, the combination of LCRT and PD-1 inhibitor (tislelizumab) also achieved a high pCR rate (50.0%). Therefore, despite the shorter radiotherapy time, SCRT may achieve similar efficacy as LCRT, combined with immunotherapy.

Considering that LCRT may increase toxicity and reduce tolerance of patients compared with SCRT, it remains necessary to determine the optimal combination of LARC neoadjuvant therapy. TORCH (NCT04518280) (60) explored the combination of SCRT and PD-1 inhibitor (toripalimab) for the neoadjuvant therapy of LARC. And the preliminary efficacy showed that the pCR rate and CR rate were as high as 56.2% (18/32) and 58.1% (36/62), respectively. This result suggests that SCRT combined with immunotherapy may be more advantageous. Moreover, the REGINA study (NCT04503694) (94) will investigate the efficacy of the combination of PD-1 inhibitor (Nivolumab) and chemotherapy with SCRT, while the PRIME-PR study (NCT04621370) (95) will directly compare the differences in efficacy between LCRT and SCRT in neoadjuvant immunotherapy combined with TNT.

Currently, neoadjuvant chemoradiotherapy followed by total mesorectal excision is considered the optimal treatment for LARC (74). However, recent results have shown that compared to neoadjuvant chemoradiotherapy alone (10.5%-38.0%), long-term radiation therapy (LCRT) or short-term radiation therapy (SCRT) combined with immunotherapy can significantly improve the pCR rate (37.5%-50.0%) of LARC patients without increasing the risk of AEs (96, 97). Moreover, the determination of radiotherapy strategies may further improve the safety of combination therapy.

3.2.5 Targeted therapy and immunotherapy combination

Since cyclooxygenase-2 may mediate immune escape and inflammatory response (98), applying cyclooxygenase-2 inhibitors may elevate the responsiveness of cancer cells to ICIs. To further demonstrate its synergistic effect, a phase II trial (NCT03926338) (17) discovered that PD-1 inhibitor (toripalimab) (99) combined with cyclooxygenase-2 inhibitors (celecoxib) can achieve a higher pCR rate in dMMR/MSI-H LACRC, compared with anti-PD-1 monotherapy (15 (88%) *vs* 11 (65%)). Only 1 case (3%) of grade 3/4 treatment-related AEs was observed. However, in the NICHE study (NCT03026140) (35), pMMR CRC patients who received neoadjuvant CTLA-4 inhibitor (ipilimumab) combined with PD-1 inhibitor (nivolumab) and celecoxib showed no significant improvement. Therefore, the synergistic effect of targeted therapy and immunotherapy seems to be more evident in dMMR/MSI-H LACRC, while the improvement in the efficacy of pMMR CRC is limited.

4 Conclusion

Recent studies have shown that compared with chemotherapy or chemoradiotherapy, perioperative immunotherapy-based therapies can significantly improve the pCR rate of dMMR/MSI-H CRC, without increasing AEs or postoperative complications. Meanwhile, the combination strategies are also expected to further improve the efficacy of pMMR patients, especially immunotherapy combined with chemoradiotherapy or radiotherapy. However, recent studies on immunotherapy combinations and the combination of targeted treatment and ICIs seem to have failed to achieve better results in pMMR/MSS CRC. Many promising immunotherapy-based therapies still require expanding sample size and follow-up results. Furthermore, mature biomarkers for identifying CRC patients with therapeutic responses are required. Additionally, limited toxicity of immunotherapy may be related to low doses and shorter treatment duration, while the higher pCR rate may be associated with more treatment cycles and longer treatment intervals (17, 35, 42). Therefore, further research is expected to determine the optimal therapeutic combination, treatment cycle, and dosage for different populations to coordinate the relationship between efficacy and safety (100). In addition, there are many ongoing but not yet reported studies on perioperative immunotherapy for CRC, as shown in Supplementary Table 1.

Author contributions

J-TC: Conceptualization, Investigation, Resources, Supervision, Writing – original draft, Writing – review & editing. Y-WZ: Conceptualization, Funding acquisition, Investigation, Project administration, Supervision, Writing – review & editing. T-RH: Investigation, Resources, Writing – review & editing. J-LW: Investigation, Writing – review & editing. MQ: Conceptualization, Funding acquisition, Methodology, Project administration, Resources, Supervision, Writing – review & editing.

Funding

The author(s) declare financial support was received for the research, authorship, and/or publication of this article. This study was supported by the Science and Technology Department of Sichuan Province Key Research and Development Project (grant no. 2022YFS0209) and 1.3.5 Project for Disciplines of Excellence, West China Hospital, Sichuan University (grant no. ZYJC21017).

Conflict of interest

The authors declare that the research was conducted in the absence of any commercial or financial relationships that could be construed as a potential conflict of interest.

Publisher's note

Supplementary material

The Supplementary Material for this article can be found online at: https://www.frontiersin.org/articles/10.3389/fimmu.2023.1269341/full#supplementary-material

References

1. Dekker E, Tanis PJ, Vleugels JLA, Kasi PM, Wallace MB. Colorectal cancer. *Lancet* (2019) 394(10207):1467–80. doi: 10.1016/s0140-6736(19)32319-0

2. Keum N, Giovannucci E. Global burden of colorectal cancer: emerging trends, risk factors and prevention strategies. *Nat Rev Gastroenterol Hepatol* (2019) 16 (12):713–32. doi: 10.1038/s41575-019-0189-8

3. Akimoto N, Ugai T, Zhong R, Hamada T, Fujiyoshi K, Giannakis M, et al. Rising incidence of early-onset colorectal cancer - a call to action. *Nat Rev Clin Oncol* (2021) 18(4):230–43. doi: 10.1038/s41571-020-00445-1

4. Riesco-Martinez MC, Modrego A, Espinosa-Olarte P, La Salvia A, Garcia-Carbonero R. Perioperative chemotherapy for liver metastasis of colorectal cancer: lessons learned and future perspectives. *Curr Treat Opt Oncol* (2022) 23(9):1320–37. doi: 10.1007/s11864-022-01008-5

5. Zhang X, Wu T, Cai X, Dong J, Xia C, Zhou Y, et al. Neoadjuvant immunotherapy for msi-H/dmmr locally advanced colorectal cancer: new strategies and unveiled opportunities. *Front Immunol* (2022) 13:795972. doi: 10.3389/fimmu.2022.795972

6. Matzner P, Sandbank E, Neeman E, Zmora O, Gottumukkala V, Ben-Eliyahu S. Harnessing cancer immunotherapy during the unexploited immediate perioperative period. *Nat Rev Clin Oncol* (2020) 17(5):313–26. doi: 10.1038/s41571-019-0319-9

7. Horowitz M, Neeman E, Sharon E, Ben-Eliyahu S. Exploiting the critical perioperative period to improve long-term cancer outcomes. *Nat Rev Clin Oncol* (2015) 12(4):213–26. doi: 10.1038/nrclinonc.2014.224

8. van der Bij GJ, Oosterling SJ, Beelen RH, Meijer S, Coffey JC, van Egmond M. The perioperative period is an underutilized window of therapeutic opportunity in patients with colorectal cancer. *Ann Surg* (2009) 249(5):727–34. doi: 10.1097/SLA.0b013e3181a3ddbd

9. Bahadoer RR, Dijkstra EA, van Etten B, Marijnen CAM, Putter H, Kranenbarg EM, et al. Short-course radiotherapy followed by chemotherapy before total mesorectal excision (Tme) versus preoperative chemoradiotherapy, tme, and optional adjuvant chemotherapy in locally advanced rectal cancer (Rapido): a randomised, open-label, phase 3 trial. *Lancet Oncol* (2021) 22(1):29–42. doi: 10.1016/s1470-2045(20)30555-6

10. Zhao P, Li L, Jiang X, Li Q. Mismatch repair deficiency/microsatellite instability-high as a predictor for anti-pd-1/pd-L1 immunotherapy efficacy. *J Hematol Oncol* (2019) 12(1):54. doi: 10.1186/s13045-019-0738-1

11. Du F, Liu Y. Predictive molecular markers for the treatment with immune checkpoint inhibitors in colorectal cancer. *J Clin Lab Anal* (2022) 36(1):e24141. doi: 10.1002/jcla.24141

12. Yu I, Dakwar A, Takabe K. Immunotherapy: recent advances and its future as a neoadjuvant, adjuvant, and primary treatment in colorectal cancer. *Cells* (2023) 12 (2):258. doi: 10.3390/cells12020258

13. Pawlik TM, Raut CP, Rodriguez-Bigas MA. Colorectal carcinogenesis: msi-H versus msi-L. *Dis Markers* (2004) 20(4-5):199–206. doi: 10.1155/2004/368680

14. Lin A, Zhang J, Luo P. Crosstalk between the msi status and tumor microenvironment in colorectal cancer. *Front Immunol* (2020) 11:2039. doi: 10.3389/fimmu.2020.02039

15. Lenz HJ, Van Cutsem E, Luisa Limon M, Wong KYM, Hendlisz A, Aglietta M, et al. First-line nivolumab plus low-dose ipilimumab for microsatellite instability-high/mismatch repair-deficient metastatic colorectal cancer: the phase ii checkmate 142 study. *J Clin Oncol* (2022) 40(2):161–70. doi: 10.1200/jco.21.01015

16. Andre T, Amonkar M, Norquist JM, Shiu KK, Kim TW, Jensen BV, et al. Health related quality of life in patients with microsatellite instability-high or mismatch repair deficient metastatic colorectal cancer treated with first-line pembrolizumab versus chemotherapy (Keynote-177): an open-label, randomised, phase 3 trial. *Lancet Oncol* (2021) 22(5):665–77. doi: 10.1016/s1470-2045(21)00064-4

17. Hu H, Kang L, Zhang J, Wu Z, Wang H, Huang M, et al. Neoadjuvant pd-1 blockade with toripalimab, with or without celecoxib, in mismatch repair-deficient or microsatellite instability-high, locally advanced, colorectal cancer (Picc): A single-centre, parallel-group, non-comparative, randomised, phase 2 trial. *Lancet Gastroenterol Hepatol* (2022) 7(1):38–48. doi: 10.1016/s2468-1253(21)00348-4

18. Kwon M, An M, Klempner SJ, Lee H, Kim KM, Sa JK, et al. Determinants of response and intrinsic resistance to pd-1 blockade in microsatellite instability-high gastric cancer. *Cancer Discovery* (2021) 11(9):2168–85. doi: 10.1158/2159-8290.Cd-21-0219

19. Fan A, Wang B, Wang X, Nie Y, Fan D, Zhao X, et al. Immunotherapy in colorectal cancer: current achievements and future perspective. *Int J Biol Sci* (2021) 17 (14):3837–49. doi: 10.7150/ijbs.64077

20. Sharabi AB, Lim M, DeWeese TL, Drake CG. Radiation and checkpoint blockade immunotherapy: radiosensitisation and potential mechanisms of synergy. *Lancet Oncol* (2015) 16(13):e498–509. doi: 10.1016/s1470-2045(15)00007-8

21. Yu WD, Sun G, Li J, Xu J, Wang X. Mechanisms and therapeutic potentials of cancer immunotherapy in combination with radiotherapy and/or chemotherapy. *Cancer Lett* (2019) 452:66–70. doi: 10.1016/j.canlet.2019.02.048

22. Le DT, Uram JN, Wang H, Bartlett BR, Kemberling H, Eyring AD, et al. Pd-1 blockade in tumors with mismatch-repair deficiency. *N Engl J Med* 372(26):2509–20. doi: 10.1056/NEJMoa1500596

23. Overman MJ, McDermott R, Leach JL, Lonardi S, Lenz HJ, Morse MA, et al. Nivolumab in patients with metastatic DNA mismatch repair-deficient or microsatellite instability-high colorectal cancer (Checkmate 142): an open-label, multicentre, phase 2 study. *Lancet Oncol* (2017) 18(9):1182–91. doi: 10.1016/s1470-2045(17)30422-9

24. Sahin IH, Akce M, Alese O, Shaib W, Lesinski GB, El-Rayes B, et al. Immune checkpoint inhibitors for the treatment of Msi-H/Mmr-D colorectal cancer and a perspective on resistance mechanisms. *Br J Cancer* (2019) 121(10):809–18. doi: 10.1038/s41416-019-0599-y

25. Ren Y, Miao JM, Wang YY, Fan Z, Kong XB, Yang L, et al. Oncolytic viruses combined with immune checkpoint therapy for colorectal cancer is a promising treatment option. *Front Immunol* (2022) 13:961796. doi: 10.3389/fimmu.2022.961796

26. Crupi MJF, Taha Z, Janssen TJA, Petryk J, Boulton S, Alluqmani N, et al. Oncolytic virus driven T-cell-based combination immunotherapy platform for colorectal cancer. *Front Immunol* (2022) 13:1029269. doi: 10.3389/fimmu.2022.1029269

27. Liu C, Liu R, Wang B, Lian J, Yao Y, Sun H, et al. Blocking Il-17a enhances tumor response to anti-pd-1 immunotherapy in microsatellite stable colorectal cancer. *J Immunother Cancer* (2021) 9(1). doi: 10.1136/jitc-2020-001895

28. Yuan J, Li J, Gao C, Jiang C, Xiang Z, Wu J. Immunotherapies catering to the unmet medical need of cold colorectal cancer. *Front Immunol* (2022) 13:1022190. doi: 10.3389/fimmu.2022.1022190

29. Aparicio C, Belver M, Enríquez L, Espeso F, Núñez L, Sánchez A, et al. Cell therapy for colorectal cancer: the promise of chimeric antigen receptor (Car)-T cells. *Int J Mol Sci* (2021) 22(21):11781. doi: 10.3390/ijms222111781

30. Evrard C, Tachon G, Randrian V, Karayan-Tapon L, Tougeron D. Microsatellite instability: diagnosis, heterogeneity, discordance, and clinical impact in colorectal cancer. *Cancers* (2019) 11(10):1567. doi: 10.3390/cancers11101567

31. Jin Z, Sinicrope FA. Prognostic and predictive values of mismatch repair deficiency in non-metastatic colorectal cancer. *Cancers* (2021) 13(2):300. doi: 10.3390/cancers13020300

32. Kanani A, Veen T, Søreide K. Neoadjuvant immunotherapy in primary and metastatic colorectal cancer. *Br J Surg* (2021) 108(12):1417–25. doi: 10.1093/bjs/znab342

33. Zhu J, Lian J, Xu B, Pang X, Ji S, Zhao Y, et al. Neoadjuvant immunotherapy for colorectal cancer: right regimens, right patients, right directions? *Front Immunol* (2023) 14:1120684. doi: 10.3389/fimmu.2023.1120684

34. Wu Z, Hu H, Wang C, Zhang J, Cai Y, Xie X, et al. The prognostic and predictive value of mismatch repair status in patients with locally advanced rectal cancer following neoadjuvant therapy. *Ann Trans Med* (2022) 10(8):491. doi: 10.21037/atm-22-124

35. Verschoor YL, Jvd B, Beets G, Sikorska K, Aalbers A, Av L, et al. Neoadjuvant nivolumab, ipilimumab, and celecoxib in mmr-proficient and Mmr-deficient colon cancers: final clinical analysis of the niche study. *JCO* (2022) 40(16_suppl):3511. doi: 10.1200/JCO.2022.40.16_suppl.3511

36. Kanikarla Marie P, Haymaker C, Parra ER, Kim YU, Lazcano R, Gite S, et al. Pilot clinical trial of perioperative durvalumab and tremelimumab in the treatment of resectable colorectal cancer liver metastases. *Clin Cancer Res* (2021) 27(11):3039–49. doi: 10.1158/1078-0432.Ccr-21-0163

37. Chalabi M, Verschoor YL, van den Berg J, Sikorska K, Beets G, Lent AV, et al. Neoadjuvant immune checkpoint inhibition in locally advanced mmr-deficient colon cancer: the niche-2 study. *Ann Oncol* (2022) 33(7):S1389–S. doi: 10.1016/j.annonc.2022.08.016

38. Hou W, Yi C, Zhu H. Predictive biomarkers of colon cancer immunotherapy: present and future. *Front Immunol* (2022) 13:1032314. doi: 10.3389/fimmu.2022.1032314

39. Gao J, Zhang X, Yang Z, Zhang J, Bai Z, Deng W, et al. Interim result of phase ii, prospective, single-arm trial of long-course chemoradiotherapy combined with concurrent tislelizumab in locally advanced rectal cancer. *Front Oncol* (2023) 13:1057947. doi: 10.3389/fonc.2023.1057947

40. Wu M, Huang Q, Xie Y, Wu X, Ma H, Zhang Y, et al. Improvement of the anticancer efficacy of Pd-1/Pd-L1 blockade via combination therapy and pd-L1 regulation. *J Hematol Oncol* (2022) 15(1):24. doi: 10.1186/s13045-022-01242-2

41. Hu W, Yang Y, Qi L, Chen J, Ge W, Zheng S. Subtyping of microsatellite instability-high colorectal cancer. *Cell Commun Signal CCS* (2019) 17(1):79. doi: 10.1186/s12964-019-0397-4

42. Chalabi M, Fanchi LF, Dijkstra KK, Van den Berg JG, Aalbers AG, Sikorska K, et al. Neoadjuvant immunotherapy leads to pathological responses in mmr-proficient and mmr-deficient early-stage colon cancers. *Nat Med* (2020) 26(4):566–76. doi: 10.1038/s41591-020-0805-8

43. Wen L, Chen Z, Ji X, Fong WP, Shao Q, Ren C, et al. Pathological complete response to immune checkpoint inhibitor in patients with colorectal cancer liver metastases harboring pole exonuclease domain mutation. *J Immunother Cancer* (2022) 10(7):e004487. doi: 10.1136/jitc-2022-004487

44. Ma X, Riaz N, Samstein RM, Lee M, Makarov V, Valero C, et al. Functional landscapes of pole and pold1 mutations in checkpoint blockade-dependent antitumor immunity. *Nat Genet* (2022) 54(7):996–1012. doi: 10.1038/s41588-022-01108-w

45. Qin Q, Yang K, Ma T, Wang H, Yu P, Yuan M, et al. Serial circulating tumor DNA in monitoring the effect of neoadjuvant and adjuvant immunotherapy in patients with colon cancer: case series and review of the literature. *J Immunother* (2022) 45 (8):358–62. doi: 10.1097/cji.0000000000000436

46. Wang H, Zhou Y, Zhang Y, Fang S, Zhang M, Li H, et al. Subtyping of microsatellite stability colorectal cancer reveals guanylate binding protein 2 (Gbp2) as a potential immunotherapeutic target. *J Immunother Cancer* (2022) 10(4)e004302. doi: 10.1136/jitc-2021-004302

47. Wu X, Lan X, Hu W, Zhang W, Lai X, Xu S, et al. Cmtm6 expression in M2 macrophages is a potential predictor of Pd-1/Pd-L1 inhibitor response in colorectal cancer. *Cancer Immunol Immunother* (2021) 70(11):3235–48. doi: 10.1007/s00262-021-02931-6

48. Peyraud F, Guegan JP, Bodet D, Nafia I, Fontan L, Auzanneau C, et al. Circulating L-arginine predicts the survival of cancer patients treated with immune checkpoint inhibitors. *Ann Oncol* (2022) 33(10):1041–51. doi: 10.1016/j.annonc.2022.07.001

49. Xu S, Yin W, Zhang Y, Lv Q, Yang Y, He J. Foes or friends? Bacteria enriched in the tumor microenvironment of colorectal cancer. *Cancers* (2020) 12(2):372. doi: 10.3390/cancers12020372

50. Lin Z, Cai M, Zhang P, Li G, Liu T, Li X, et al. Phase ii, single-arm trial of preoperative short-course radiotherapy followed by chemotherapy and camrelizumab in locally advanced rectal cancer. *J Immunother Cancer* (2021) 9(11):e003554. doi: 10.1136/jitc-2021-003554

51. Wang C, Chevalier D, Saluja J, Sandhu J, Lau C, Fakih M. Regorafenib and nivolumab or pembrolizumab combination and circulating tumor dna response assessment in refractory microsatellite stable colorectal cancer. *Oncologist* (2020) 25 (8):e1188–94. doi: 10.1634/theoncologist.2020-0161

52. Ramos-Casals M, Brahmer JR, Callahan MK, Flores-Chávez A, Keegan N, Khamashta MA, et al. Immune-related adverse events of checkpoint inhibitors. *Nat Rev Dis Primers* (2020) 6(1):38. doi: 10.1038/s41572-020-0160-6

53. Johdi NA, Sukor NF. Colorectal cancer immunotherapy: options and strategies. *Front Immunol* (2020) 11:1624. doi: 10.3389/fimmu.2020.01624

54. Coukos G. Neoadjuvant immune-checkpoint blockade in resectable colon cancer. *Nat Med* (2020) 26(4):473–4. doi: 10.1038/s41591-020-0826-3

55. Scurr M, Pembroke T, Bloom A, Roberts D, Thomson A, Smart K, et al. Low-dose cyclophosphamide induces antitumor T-cell responses, which associate with survival in metastatic colorectal cancer. *Clin Cancer Res* (2017) 23(22):6771–80. doi: 10.1158/1078-0432.Ccr-17-0895

56. Herrera FG, Ronet C, Ochoa de Olza M, Barras D, Crespo I, Andreatta M, et al. Low-dose radiotherapy reverses tumor immune desertification and resistance to immunotherapy. *Cancer Discovery* (2022) 12(1):108–33. doi: 10.1158/2159-8290.Cd-21-0003

57. Kuan FC, Lai CH, Ku HY, Wu CF, Hsieh MC, Liu TW, et al. The survival impact of delayed surgery and adjuvant chemotherapy on stage ii/iii rectal cancer with pathological complete response after neoadjuvant chemoradiation. *Int J Cancer* (2017) 140(7):1662–9. doi: 10.1002/ijc.30562

58. Zhang J, Cai J, Deng Y, Wang H. Complete response in patients with locally advanced rectal cancer after neoadjuvant treatment with nivolumab. *Oncoimmunology* (2019) 8(12):e1663108. doi: 10.1080/2162402x.2019.1663108

59. Demisse R, Damle N, Kim E, Gong J, Fakih M, Eng C, et al. Neoadjuvant immunotherapy-based systemic treatment in mmr-deficient or msi-high rectal cancer: case series. *J Natl Compr Cancer Netw JNCCN* (2020) 18(7):798–804. doi: 10.6004/jnccn.2020.7558

60. Wang Y, Shen L, Wan J, Zhang H, Wu R, Wang J, et al. Short-course radiotherapy combined with capox and toripalimab for the total neoadjuvant therapy of locally advanced rectal cancer: A randomized, prospective, multicentre, double-arm, phase ii trial (Torch). *BMC Cancer* (2022) 22(1):274. doi: 10.1186/s12885-022-09348-z

61. Zheng R, Wang BS, Li Z, Chi P, Xu B. Combining Chemotherapy and Tislelizumab with Preoperative Split-Course Hypofraction Radiotherapy for Locally Advanced Rectal Cancer: Study Protocol of a Prospective, Single-Arm, Phase Ii Trial. *BMJ Open* (2023) 13(3):e066976. doi: 10.1136/bmjopen-2022-066976

62. Salvatore L, Bens M, Corallo S, Bergamo F, Pellegrini I, Rasola C, et al. Phase Ii Study of Preoperative (Preop) Chemoradiotherapy (Ctrt) Plus Avelumab (Ave) in Patients (Pts) with Locally Advanced Rectal Cancer (Larc): the Avana Study. *JCO* (2021) 39(15_suppl):3511. doi: 10.1200/JCO.2021.39.15_suppl.3511

63. Fan Y, Zhu X, Xu C, Ding C, Hu J, Hong Q, et al. Neoadjuvant Arterial Embolization Chemotherapy Combined Pd-1 Inhibitor for Locally Advanced Rectal Cancer (Neci Study): a Protocol for a Phase II Study. *BMJ Open* (2023) 13(3):e069401. doi: 10.1136/bmjopen-2022-069401

64. Cercek A, Lumish M, Sinopoli J, Weiss J, Shia J, Lamendola-Essel M, et al. Pd-1 blockade in mismatch repair-deficient, locally advanced rectal cancer. *N Engl J Med* (2022) 386(25):2363–76. doi: 10.1056/NEJMoa2201445

65. Rahma OE, Yothers G, Hong TS, Russell MM, You YN, Parker W, et al. Use of total neoadjuvant therapy for locally advanced rectal cancer: initial results from the pembrolizumab arm of a phase 2 randomized clinical trial. *JAMA Oncol* (2021) 7 (8):1225–30. doi: 10.1001/jamaoncol.2021.1683

66. Zhai ML, Zhang FY, Yang JR, Zhang S, Zhao L, Lin ZY, et al. Current status of neoadjuvant therapy for locally advanced rectal cancer in Wuhan Union hospital cancer center. *Radiat Oncol (London England)* (2022) 17(1):109. doi: 10.1186/s13014-022-02081-8

67. Grassi E, Zingaretti C, Petracci E, Corbelli J, Papiani G, Banchelli I, et al. Phase II study of capecitabine-based concomitant chemoradiation followed by durvalumab as a neoadjuvant strategy in locally advanced rectal cancer: the pandora trial. *ESMO open* (2023) 8(5):101824. doi: 10.1016/j.esmoop.2023.101824

68. Shamseddine A, Zeidan Y, Bouferraa Y, Turfa R, Kattan J, Mukherji D, et al. So-30 efficacy and safety of neoadjuvant short-course radiation follow ed by mfolfox-6 plus avelumab for locally-advanced rectal adenocarcino ma: averectal study. *Ann Oncol* 32: S215. doi: 10.1016/j.annonc.2021.05.054

69. Wu AW, Li YJ, Ji DB, Zhang L, Zhang XY, Cai Y, et al. Pkuch 04 trial: total neoadjuvant chemoradiation combined with neoadjuvant pd-1 blockade for pmmr/mss locally advanced middle to low rectal cancer. *JCO* (2022) 40(16_suppl):3609.

70. Liu XZ, Xiong Z, Xiao BY, Yu GY, Li YJ, Yao YF, et al. Multicenter Real-World Study on Safety and Efficacy of Neoadjuvant Therapy in Combination with Immunotherapy for Colorectal Cancer. *Zhonghua wei chang wai ke za zhi = Chinese J Gastrointest Surg* (2022) 25 (3):219–27. doi: 10.3760/cma.j.cn441530-20220228-00070

71. Xiao BY, Zhang X, Cao TY, Li DD, Jiang W, Kong LH, et al. Neoadjuvant immunotherapy leads to major response and low recurrence in localized mismatch repair-deficient colorectal cancer. *J Natl Compr Cancer Network JNCCN* (2023) 21 (1):60–6.e5. doi: 10.6004/jnccn.2022.7060

72. Pei F, Wu J, Zhao Y, He W, Yao Q, Huang M, et al. Single-agent neoadjuvant immunotherapy with a pd-1 antibody in locally advanced mismatch repair-deficient or microsatellite instability-high colorectal cancer. *Clin Colorect Cancer* (2023) 22(1):85–91. doi: 10.1016/j.clcc.2022.11.004

73. Chen G, Jin Y, Guan WL, Zhang RX, Xiao WW, Cai PQ, et al. Neoadjuvant pd-1 blockade with sintilimab in mismatch-repair deficient, locally advanced rectal cancer: an open-label, single-centre phase 2 study. *Lancet Gastroenterol Hepatol* (2023) 8 (5):422–31. doi: 10.1016/s2468-1253(22)00439-3

74. Bando H, Tsukada Y, Inamori K, Togashi Y, Koyama S, Kotani D, et al. Preoperative chemoradiotherapy plus nivolumab before surgery in patients with microsatellite stable and microsatellite instability-high locally advanced rectal cancer. *Clin Cancer Res* (2022) 28(6):1136–46. doi: 10.1158/1078-0432.Ccr-21-3213

75. Zhang X, Yang R, Wu T, Cai X, Li G, Yu K, et al. Efficacy and safety of neoadjuvant monoimmunotherapy with pd-1 inhibitor for dmmr/msi-H locally advanced colorectal cancer: A single-center real-world study. *Front Immunol* (2022) 13:913483. doi: 10.3389/fimmu.2022.913483

76. Han K, Tang J-H, Liao L-E, Jiang W, Sui Q-Q, Xiao B-Y, et al. Neoadjuvant immune checkpoint inhibition improves organ preservation in T4bm0 colorectal cancer with mismatch repair deficiency: A retrospective observational study. *Dis Colon Rectum* (2022) 66(10):e996–e1005. doi: 10.1097/dcr.0000000000002466

77. Ludford K, Raghav K, Murphy MAB, Fleming ND, Nelson D, Lee MS, et al. Neoadjuvant pembrolizumab in localized/locally advanced solid tumors with mismatch repair deficiency. *Ann Oncol* (2021) 32:S1210–S. doi: 10.1016/j.annonc.2021.08.1703

78. Eefsen RL, Larsen JS, Klarskov LL, Altaf R, Høgdall E, Ingeholm P, et al. Therapy with pembrolizumab in treatment-naïve patients with nonmetastatic,

mismatch repair deficient colorectal cancer. *Int J Cancer* (2023) 152(10):2145–52. doi: 10.1002/ijc.34420

79. Justesen TF, Gögenur I, Tarpgaard LS, Pfeiffer P, Qvortrup C. Evaluating the efficacy and safety of neoadjuvant pembrolizumab in patients with stage I-iii mmr-deficient colon cancer: A national, multicentre, prospective, single-arm, phase ii study protocol. *BMJ Open* (2023) 13(6):e073372. doi: 10.1136/bmjopen-2023-073372

80. Boland PM, Yurgelun MB, Boland CR. Recent progress in lynch syndrome and other familial colorectal cancer syndromes. *CA: Cancer J Clin* (2018) 68(3):217–31. doi: 10.3322/caac.21448

81. Tonello M, Nappo F, Vassallo L, Di Gaetano R, Davoli C, Pizzolato E, et al. Complete pathological response of colorectal peritoneal metastases in lynch syndrome after immunotherapy case report: is a paradigm shift in cytoreductive surgery needed? *BMC Gastroenterol* (2022) 22(1):17. doi: 10.1186/s12876-021-02084-x

82. Nordlinger B, Sorbye H, Glimelius B, Poston GJ, Schlag PM, Rougier P, et al. Perioperative folfox4 chemotherapy and surgery versus surgery alone for resectable liver metastases from colorectal cancer (Eortc 40983): long-term results of a randomised, controlled, phase 3 trial. *Lancet Oncol* (2013) 14(12):1208–15. doi: 10.1016/s1470-2045(13)70447-9

83. Benson AB, Venook AP, Al-Hawary MM, Arain MA, Chen YJ, Ciombor KK, et al. Colon cancer, version 2.2021, nccn clinical practice guidelines in oncology. *J Natl Compr Cancer Network JNCCN* (2021) 19(3):329–59. doi: 10.6004/jnccn.2021.0012

84. Sinicrope FA, Ou FS, Zemla T, Nixon AB, Mody K, Levasseur A, et al. Randomized Trial of Standard Chemotherapy Alone or Combined with Atezolizumab as Adjuvant Therapy for Patients with Stage Iii Colon Cancer and Deficient Mismatch Repair (Atomic, Alliance A021502). *JCO* (2019) 37(15):e15169. doi: 10.1200/JCO.2019.37.15_suppl.e15169

85. Lau D, Kalaitzaki E, Church DN, Pandha H, Tomlinson I, Annels N, et al. Rationale and design of the polem trial: avelumab plus fluoropyrimidine-based chemotherapy as adjuvant treatment for stage iii mismatch repair deficient or pole exonuclease domain mutant colon cancer: a phase iii randomised study. *ESMO Open* (2020) 5(1):e000638. doi: 10.1136/esmoopen-2019-000638

86. Segal NH, Cercek A, Ku G, Wu AJ, Rimner A, Khalil DN, et al. Phase ii single-arm study of durvalumab and tremelimumab with concurrent radiotherapy in patients with mismatch repair-proficient metastatic colorectal cancer. *Clin Cancer Res* (2021) 27(8):2200–8. doi: 10.1158/1078-0432.Ccr-20-2474

87. McLaughlin M, Patin EC, Pedersen M, Wilkins A, Dillon MT, Melcher AA, et al. Inflammatory microenvironment remodelling by tumour cells after radiotherapy. *Nat Rev Cancer* (2020) 20(4):203–17. doi: 10.1038/s41568-020-0246-1

88. Qian JM, Schoenfeld JD. Radiotherapy and immunotherapy for head and neck cancer: current evidence and challenges. *Front Oncol* (2020) 10:608772. doi: 10.3389/fonc.2020.608772

89. Filippi AR, Fava P, Badellino S, Astrua C, Ricardi U, Quaglino P. Radiotherapy and immune checkpoints inhibitors for advanced melanoma. *Radiother Oncol* (2016) 120(1):1–12. doi: 10.1016/j.radonc.2016.06.003

90. Zhou P, Wang Y, Qin S, Han Y, Yang Y, Zhao L, et al. Abscopal effect triggered by radiation sequential mono-immunotherapy resulted in a complete remission of pmmr sigmoid colon cancer. *Front Immunol* (2023) 14:1139527. doi: 10.3389/fimmu.2023.1139527

91. Liu S, Zhang Y, Lin Y, Wang P, Pan Y. Case report: the msi-L/P-mmr metastatic rectal cancer patient who failed systemic therapy responds to anti-pd-1 immunotherapy after stereotactic body radiation-therapy. *Front Immunol* (2022) 13:981527. doi: 10.3389/fimmu.2022.981527

92. Li X, Fang C, Wang X, Yu Y, Wang Z, Qiu M. Neoadjuvant treatment of sintilimab plus hypofractionated radiotherapy for msi-H/dmmr rectal cancer: a prospective, multicenter, phase ib study. *Cancer Med* (2022) 11(23):4405–10. doi: 10.1002/cam4.4720

93. Corrò C, Buchs NC, Tihy M, Durham-Faivre A, Bichard P, Frossard JL, et al. Study protocol of a phase ii study to evaluate safety and efficacy of neo-adjuvant pembrolizumab and radiotherapy in localized rectal cancer. *BMC Cancer* (2022) 22(1):772. doi: 10.1186/s12885-022-09820-w

94. Bregni G, Senti C, Reina EA, Gkolfakis P, Moretti L, Veron A, et al. 505tip regina: A phase ii trial of neoadjuvant regorafenib (Rego) in c ombination with nivolumab (Nivo) and short-course radiotherapy (Scrt) in intermediate-risk, stage ii-iii rectal cancer (Rc). *Ann Oncol* 32:S579. doi: 10.1016/j.annonc.2021.08.1024

95. Hanna CR, O'Cathail SM, Graham JS, Saunders M, Samuel L, Harrison M, et al. Durvalumab (Medi 4736) in combination with extended neoadjuvant regimens in rectal cancer: A study protocol of a randomised phase ii trial (Prime-rt). *Radiat Oncol (London England)* (2021) 16(1):163. doi: 10.1186/s13014-021-01888-1

96. Chen L, Yang X, Zhang Y, Liu J, Jiang Q, Ji F, et al. Survival outcomes analysis according to mismatch repair status in locally advanced rectal cancer patients treated with neoadjuvant chemoradiotherapy. *Front Oncol* (2022) 12:920916. doi: 10.3389/fonc.2022.920916

97. Cercek A, Roxburgh CSD, Strombom P, Smith JJ, Temple LKF, Nash GM, et al. Adoption of total neoadjuvant therapy for locally advanced rectal cancer. *JAMA Oncol* (2018) 4(6):e180071. doi: 10.1001/jamaoncol.2018.0071

98. Hashemi Goradel N, Najafi M, Salehi E, Farhood B, Mortezaee K. Cyclooxygenase-2 in cancer: a review. *J Cell Physiol* (2019) 234(5):5683–99. doi: 10.1002/jcp.27411

99. Keam SJ. Toripalimab: first global approval. *Drugs* (2019) 79(5):573–8. doi: 10.1007/s40265-019-01076-2

100. Kang MK. Implications of recent neoadjuvant clinical trials on the future practice of radiotherapy in locally advanced rectal cancer. *World J Gastroenterol* (2023) 29(6):1011–25. doi: 10.3748/wjg.v29.i6.1011

Frontiers in Immunology

Explores novel approaches and diagnoses to treat immune disorders.

The official journal of the International Union of Immunological Societies (IUIS) and the most cited in its field, leading the way for research across basic, translational and clinical immunology.

Discover the latest Research Topics

See more →

Frontiers

Avenue du Tribunal-Fédéral 34
1005 Lausanne, Switzerland
frontiersin.org

Contact us

+41 (0)21 510 17 00
frontiersin.org/about/contact